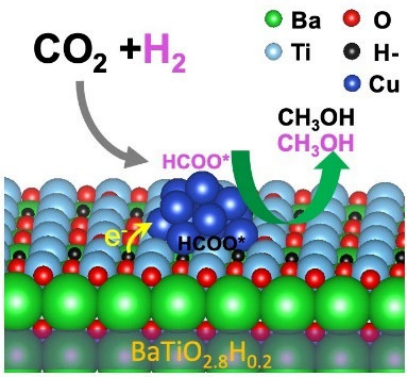


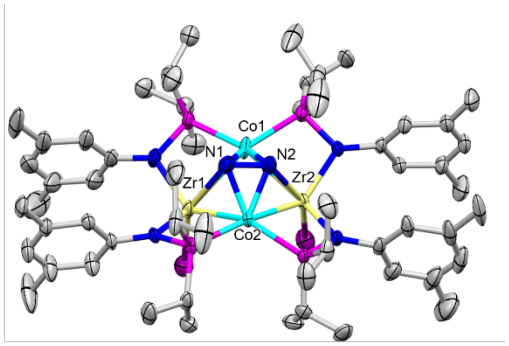


U.S. DEPARTMENT OF ENERGY | Office of Science

# 2024 Catalysis Science PI Meeting

# *Advancing Catalysis for Sustainability*

**Hilton Rockville Hotel & Executive Meeting Center**
**Rockville, MD**
**November 18 – 20, 2024**

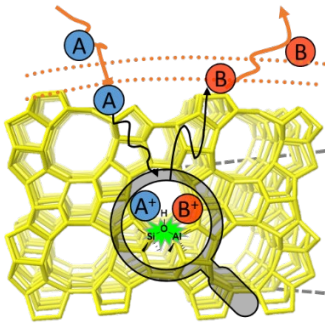


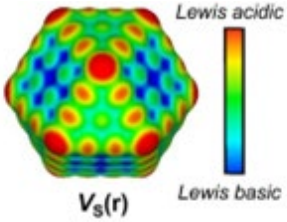


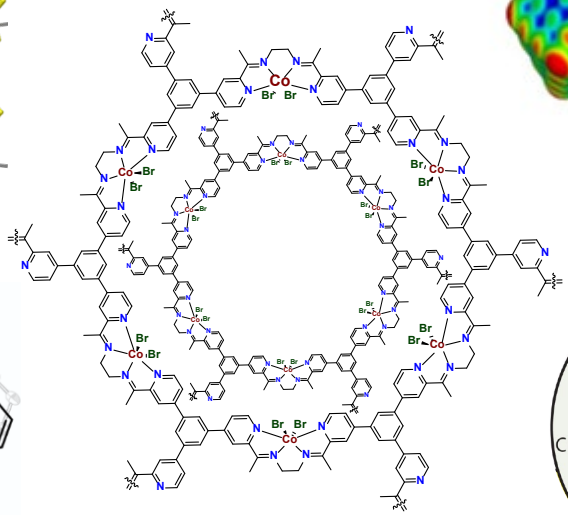

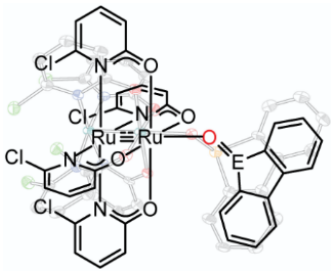


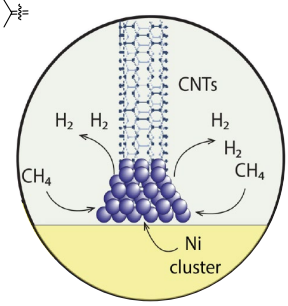

Program and Abstracts for the

# 2024 BES Catalysis Science Research PI Meeting:
# "Advancing Catalysis for Sustainability"


Hilton Rockville Hotel & Executive Meeting Center
Rockville, MD
November 18 - 20, 2024

The research grants and contracts described in this document are supported by the U.S. Department of Energy, Office of Science/Basic Energy Sciences, as part of the Catalysis Science Program within the Chemical Sciences, Geosciences and Biosciences Division

## FOREWORD

The 2024 Catalysis Science Research PI Meeting is sponsored by the Division of Chemical Sciences, Geosciences and Biosciences, Office of Basic Energy Sciences (BES), U.S. Department of Energy. It is held on November 18-20, 2024, at the Hilton Rockville Hotel in Rockville, Maryland. The purposes of this meeting are to discuss recent advances in the chemical, physical, and biological bases of catalysis science, to foster exchange of ideas and cooperation among BES/Catalysis Science Program PIs, and to discuss the new science challenges and opportunities recently emerging in catalytic technologies for energy production and use.

Catalysis research activities within BES emphasize fundamental research aimed at understanding reaction mechanisms and, ultimately, controlling the chemical conversion of natural and artificial feedstocks to useful energy carriers. The long-term goals of this research are to discover fundamental scientific principles, and to produce insightful approaches for the prediction of catalyst structure-reactivity behavior. Such knowledge, integrated with advances in chemical and materials synthesis, *in-situ* and *operando* analytical instrumentation, chemical kinetics and dynamics measurements, and computational chemistry methods, will allow the control of chemical reactions along desired pathways. This new knowledge will impact the efficiency of conversion of a variety of feedstocks into fuels, chemicals, or materials, while minimizing the impact to the environment.

The purpose of this meeting is to highlight the fundamental advances in catalysis science of relevance to the energy, economic and environmental future of the U.S. This year's meeting theme "*Advancing Catalysis for Sustainability*" emphasizes emerging opportunities and approaches in fundamental science for sustainable catalytic processes. The plenary session focused on accelerating catalysis research and featured three talks and a panel discussion spanning topics such as artificial intelligence, autonomous experimentation, and the transition from fundamental to applied catalysis research. Additionally, this year's program includes six talks from projects awarded through the "Clean Energy & Manufacturing" directed FOA, three Early Career Awardees bringing fresh and unique approaches to sustainability in catalysis, as well as 15 oral and 58 poster presentations by BES/Catalysis Science PIs.

Special thanks to the program investigators and their students, postdocs, and collaborators for their dedication to the continuous success and visibility of the BES/Catalysis Science Program. We also thank the Oak Ridge Institute for Science and Education staff for the logistical and web support of the meeting. Finally, very special thanks to Raul Miranda[1] for his longstanding and continuing contributions to the BES/Catalysis Science Program, now through his role as Team Lead for Chemical Transformations in the BES/Chemical Sciences, Geosciences and Biosciences Division.

Carrie Farberow[1,2], Eric Wiedner[1,3], Viviane Schwartz[1], and Chris Bradley[1]
[1]Catalysis Science Program, Office of Basic Energy Sciences, US Department of Energy
[2]National Renewable Energy Laboratory
[3]Pacific Northwest National Laboratory

**2024 Catalysis Science PI Meeting**

*'Advancing Catalysis for Sustainability'*

November 18th – 20th, 2024

**Program Chairs:** Carrie Farberow and Eric Wiedner

**Monday, November 18**

**OPENING SESSION**

8:30-9:00 am Welcoming Remarks and Program Updates
**Viviane Schwartz and Chris Bradley**, DOE/BES/Catalysis Science Program

9:00-9:10 am Welcome from Meeting Chairs
**Carrie Farberow**, National Renewable Energy Laboratory and **Eric Wiedner**, Pacific Northwest National Laboratory

**PI SESSION I**

Session Chair: **Steven Tait**, Indiana University Bloomington

9:10 – 9:45 am *Creating Well-Defined Gold/Metal-Oxide Interfaces for Selective Oxidation Catalysis Using ALD*
**Francisco Zaera**, University of California – Riverside

9:45 – 10:20 am *Understanding Dynamic Activation of Single-atom Catalysts in the Reaction Environment*
**Zdenek Dohnalek**, Pacific Northwest National Laboratory

10:20 – 10:35 am Break

10:35 – 11:10 am *Mechanistic Insights into the Active Sites in Cu/ceria for $CO_2$ Hydrogenation to Methanol*
**Yuanyuan Li,** Oak Ridge National Laboratory

11:10 – 11:45 am *Lewis Acids and Bases in Metal-Free Catalysis*
**Clemens Krempner,** Texas Tech University

11:45 – 12:20 am *Cooperative Bond Activation with Unusual Redox States of Aluminum*
**Neal Mankad,** University of Illinois Chicago

12:20 – 1:30 pm **Working Lunch**

**POSTER SESSION I**

1:30 – 3:15 pm

3:15 – 3:30 pm Break

**CEM AWARDS SESSION I**

Session Chair: **Líney Árnadóttir**, Oregon State University

3:30 – 3:55 pm *Design of New Catalysts for the Generation of Clean $H_2$ from Liquid Organic Hydrogen Carriers*
**Andreas Heyden**, University of South Carolina

3:55 – 4:20 pm *Direct Coupling of $CO_2$ and Alkene to Produce Unsaturated Carboxylic Acid: A Mechanistic Study*
**Bin Wang**, University of Oklahoma

4:20 – 4:45 pm *Comparing Interfacial Proton-Electron Transfer Across the Molecules-to-Materials Design Continuum*
**James McKone**, University of Pittsburgh

4:45 – 5:00 pm Break

**CEM AWARDS SESSION II**

Session Chair: **Manos Mavrikakis**, University of Wisconsin – Madison

5:00 – 5:25 pm *Cross-Scale Modulation of Electrocatalysts for Hydroxide Exchange Membrane Water Electrolysis*
**Sen Zhang**, University of Virginia

5:25 – 5:50 pm *Ambient Temperature Electrocatalytic Alkane Dehydrogenation: Considerations from Atomic-Scale to Device-Scale*
**Brian Tackett**, Purdue University

5:50 – 6:15 pm *Nitrides of Earth-abundant Metals as Catalytic Supports for Water Electrolysis*
**Jingguang Chen**, Columbia University and Brookhaven National Laboratory

6:15 **Dinner (on your own)**

**Tuesday, November 19**

**PI SESSION II**

Session Chair: **Kelsey Stoerzinger**, University of Minnesota

8:30 – 9:05 am *Engaging Molecular Radicals for Super-Reducing Solid-State Photocatalysis*
**Philip Milner**, Cornell University

9:05 – 9:40 am *Electrocatalysis on Heteroatom-doped Carbon ($CN_X$) Catalysts: Beyond Oxygen Reduction Reaction*
**Umit Ozkan**, The Ohio State University

9:40 – 10:15 am *Artificial Intelligence for Accelerating Catalytic Materials Discovery*
**Hongliang Xin**, Virginia Tech

10:15 – 10:30 am Break

10:30 am – 11:05 pm *Optimizing Electrocatalytic Hydrogen Evolution or Selective $CO_2$ Reduction at Transition Metal Hydrides*
**Jenny Yang**, University of California – Irvine

**EARLY CAREER AWARDEE SESSION**

Session Chair: **Sara Thoi**, Johns Hopkins University

11:05 – 11:25 am *Tuning Electrocatalytic Reduction of Plasma Pre-Activated $CO_2$ Toward Multicarbon Products*
**Lea Winter,** Yale University

11:25 – 11:45 am *Enzyme-like Porous Catalysts for Upgrading Biomass Feedstocks*
**Andy Nguyen,** University of Illinois Chicago

11:45 – 12:05 am *Insights into the Catalysts Originating from Phosphine-Modified Co(II) Hydroformylation Precatalysts*
**Matthew Chambers,** Louisiana State University

12:05 – 1:30 pm **Working Lunch**

**POSTER SESSION II**

1:30 – 3:15 pm

3:15 – 3:30 pm Break

**PLENARY SESSION – Accelerating Catalysis Research**

Session Chair: **Eric Wiedner**, Pacific Northwest National Laboratory

3:30 – 4:00 pm *Accelerating Heterogeneous Catalyst Development Cycle for Net Zero Applications*
**Cory Phillips**, Program Director, Catalysis & Reaction Engineering, ARPA–E

4:00 – 4:30 pm *Initial Lessons Learned in Developing an Integrated Platform to Predict Degradation of Catalysts for Sustainable Conversion of Alternate Feedstocks to Fuels and Chemicals*
**Simon Bare**, SLAC National Accelerator Laboratory

4:30 – 4:40 pm *AI for Multidisciplinary Exploration and Discovery (AIMED) Workshop on Heterogenous Catalysis*
**Hongliang Xin**, Virginia Tech

4:40 – 4:55 pm Break

4:55 – 5:45 pm Panel – *Accelerating Catalysis Research*
*Panelists*: **Cory Phillips**, Program Director, Catalysis & Reaction Engineering, ARPA–E; **Simon Bare**, SLAC National Accelerator Laboratory; **Hongliang Xin**, Virginia Tech
*Moderator:* **Carrie Farberow**, National Renewable Energy Laboratory

5:45 **Dinner (on your own)**

**Wednesday, November 28**

8:30-8:50 am BES Update
**Gail McLean**, Division Director, DOE/BES/Chemical Science, Geosciences and Biosciences Division

**PI SESSION III**

Session Chair: **Matthew Conley**, University of California – Riverside

8:50 – 9:25 am *Mechanocatalytic Redox Reactions over Reducible Metal Oxides*
**Carsten Sievers**, Georgia Institute of Technology

9:25 – 10:00 am *Catalytic Hydrocarbon Functionalization at Activated Surface Organometallic Sites*
**Aaron Sadow**, Ames Laboratory

10:00 – 10:35 am *Catalytic Upcycling and Deconstruction of Polyolefins by C–H Bond Functionalization and C–C Bond Cleavage*
**John Hartwig**, Lawrence Berkeley National Laboratory

10:35 – 10:50 am Break

## PI SESSION IV

Session Chair: **Friederike Jentoft**, University of Massachusetts Amherst

10:50 – 11:25 am *Unveiling the Active Site using Integrated Computational XANES Simulations and Mechanistic Studies*
**Cong Liu**, Argonne National Laboratory

11:25 – 12:00 am *Effect of Pt Nuclearity on $H_2$ Activation and Selective Hydrogenation*
**Ayman Karim**, Virginia Tech

12:00 – 12:35 pm *Connecting Structure to Catalytic Function in Bimetallic Alloys*
**Jesse Bond**, Syracuse University

## CLOSING SESSION

12:35 – 12:40 pm Final Remarks
**Carrie Farberow, Eric Wiedner, Viviane Schwartz, and Chris Bradley**

12:40 pm Adjourn

# TABLE OF CONTENTS

# ABSTRACTS

# ORAL PRESENTATION ABSTRACTS

# Creating Well-Defined Gold/Metal-Oxide Interfaces for Selective Oxidation Catalysis Using ALD

Francisco Zaera
Department of Chemistry and UCR Center for Catalysis, University of California, Riverside, CA 92521, USA

## Presentation Abstract

As the chemistry of solids is in most instances determined by the nature of their surfaces, control over the nature of surface sites during preparation is critical to the design of materials for specific applications. This is a difficult task, especially when complex multicomponent atomic ensembles are required. In this presentation we illustrate how atomic layer deposition (ALD) may be used, in combination with synthetic methods for the growth of gold nanoparticles, to prepare such sites. We will describe the development of prototypical surface sites comprised of a well-defined silica supports (SBA-15, which contains 1D mesopores with a narrow size distribution), titania thin films, and gold nanoparticles, as that combination has proven to offer some unique and useful surface chemistry for low-temperature catalysis. The resulting materials have been characterized using a surface-science approach, relying on the use of adsorption-desorption isotherms together with electron microscopy and a variety of spectroscopic techniques, including IR, NMR, XPS, EPR, and Visible-UV absorption. They have then been tested for the promotion of catalytic reactions, specifically for the low-temperature oxidation of carbon monoxide and biomass feedstocks (5-

**Grant Number: DE-SC0023119**
**Grant Title: Selective Oxidation of Oxygenates with Well-Defined Gold-Based Surface Catalytic Sites**

## RECENT PROGRESS

In the first three-year period of this project (of which the second year has just ended), we have been developing the required synthetic routes for catalyst preparation and establishing the procedures for the kinetic studies of the catalytic selective oxidation to be promoted with our newly designed catalysts.

### *ALD of $TiO_2$ Films Inside the Pores of SBA-15.*

Capitalizing on our previous experience growing thin oxide films on porous materials using ALD, in this project we have deposited $TiO_2$ films of different thicknesses on SBA-15 using tetrakis(dimethylamido)titanium (TDMAT) and water to produce new mixed-oxide surface sites in a controlled fashion and characterized them using a variety of techniques. Figure 1 provides a summary of the results obtained from $N_2$ adsorption-desorption isothermal measurements on the grown $TiO_2$ films as a function of the number of ALD cycles used. As expected, the pore diameter is monotonically reduced with

increasing number of cycles, at a $TiO_2$ film growth rate of ~1.15 ± 0.05 Å/cycle; the pore total volume and surface area follow similar trends as well (Figure 1-right). Particularly noteworthy is the fact that the pore size distribution retains its narrow nature throughout the titania deposition, an indication of the uniform nature of the grown film. We learned an important lesson from these studies, and that is that the deposition conditions need to be tuned carefully to obtain complete and uniform film growth; incomplete deposition manifests itself as a bimodal pore distribution, whereas over-exposures to the ALD precursor or poor pumping causes CVD-type deposition and leads to pore plugging and to the associated losses in pore surface area and pore volume. Mass transport plays a crucial role in determining the quality of the final films, which is why here we propose to develop a fluidized bed reactor to replace our current batch reactor approach. The redox properties of the titania films were subsequently characterized as a function of thickness, that is, the number of ALD cycles used. $^{29}$Si CP/MAS NMR was employed to identify the nature of the surface species that form in the initial stages of deposition, and infrared absorption spectroscopy was used to follow the transition from silica to titania surfaces. The reducibility of the titania sites by CO and $H_2$ was studied *ex situ* using EPR and *in situ* with ambient-pressure X-ray photoelectron spectroscopy (XPS). It was determined that the titania ALD films are amorphous, initially constructed out of tetrahedral rather than hexagonal units, and they easier to reduce (reversibly) than crystalline titania. A gradual transition in the nature of the surface was observed, with unique mixed Si–O–Ti sites forming during the first few ALD cycles and a more typical titania surface progressively developing as the film grows in thickness.

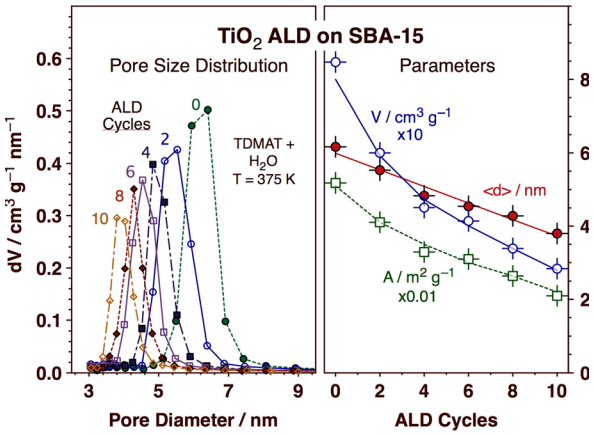


**Fig. 1.** Structural data for SBA-15 covered with titania ALD films, extracted from adsorption-desorption isothermal measurements, as a function of the number of ALD cycles used. Left: Set of pore-size distribution curves. Right: Pore average diameters <d>, pore volumes V, and specific areas A.

***Size Control of Au NPs Deposited on Silica Surfaces.***

In parallel, we have developed a methodology for depositing Au NPs on silica with small and tunable diameters and narrow size distributions. Our protocol relies on the pre-functionalization of the surface with amine groups, which are tethered to surface silanol groups using APTES. The added amine groups act as new nucleation centers for the Au ions, well dispersed throughout the surface. It was found that the critical step to control particle size is the subsequent calcination step, at which time the metal sinters as the organic matter is removed from the surface. We demonstrated that by controlling the calcination temperature and time it is possible to adjust the Au NP average size from less than 2 nm to approximately 6 nm (Figure 2), the range that we believe is the most critical to tune the catalytic properties. In the future, we aim to map out the parameter space for such size control, which includes not only temperature and time but also the amount of

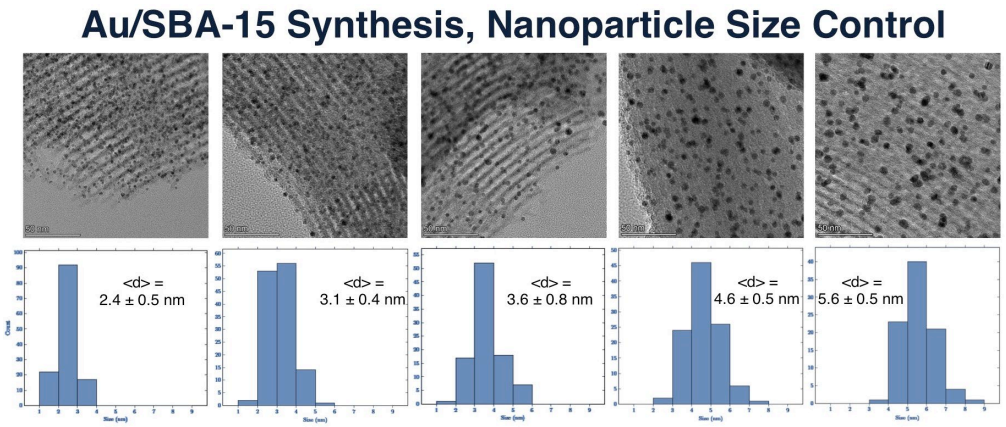


**Fig. 2**. TEM images and Au NP particle size distributions for Au/SBA-15 catalysts prepared via impregnation of SBA-15 with Au salts after pre-treatment with APTES to create amine surface nucleation sites. The NP size was controlled by adjusting the time and temperature of the subsequent calcination step.

APTES used in the derivatization step, using a variety of spectroscopies, with focus on IR (to detect and quantify the propylamine tethered moieties). A similar approach with alternative amine-containing derivatization agents will also be explored to expand its use to other oxides.

***Identification of Sites at the Au/$TiO_2$ Interface.***

We have combined the use of ALD for the growth of titania films with the addition of Au NPs in order to prepare the type of oxidation catalysts targeted by this project. The resulting solids, which were made by either depositing Au on the titania films or growing the titania films on Au/SBA-15 catalysts, were fully characterized. The physical properties of both titania and Au phases were found to be similar in all catalysts except for the thickness of the former, which was varied by using one to four ALD cycles. However, it was found that if the titania film is deposited after the Au nanoparticles, it partially covers the metal surface and reduces the catalytic activity (compared with the case where the Au is deposited last). In those samples, XPS data showed a large fraction of partially-positively-charged Au atoms ($Au^{\partial+}$), and titration of surface sites with CO and infrared absorption spectroscopy detection identified a large fraction of low-coordination Ti sites ($Ti_{4c}$), with a surface coverage that increased with titania film thickness (Figure 3).

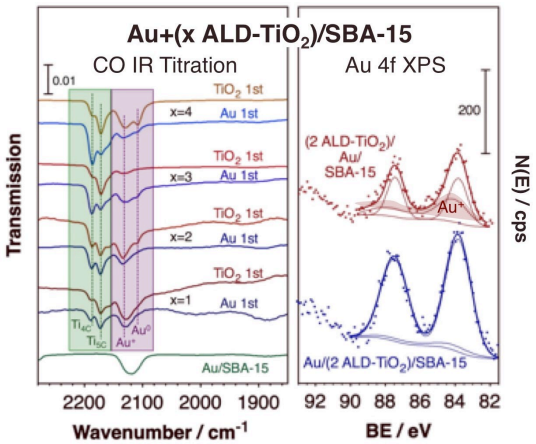


**Fig. 3**. CO-IR titration (left) and Au 4f XPS (right) spectra from catalysts made via ALD of $TiO_2$ films and Au NPs on SBA-15 in both possible orders (titania or Au NPs first). Unique $Ti_{4c}$ and $Au^{\partial+}$ interface sites were identified.

***Rate Enhancing Effect of Titania Films on Au-Based Oxidation Catalysts.***

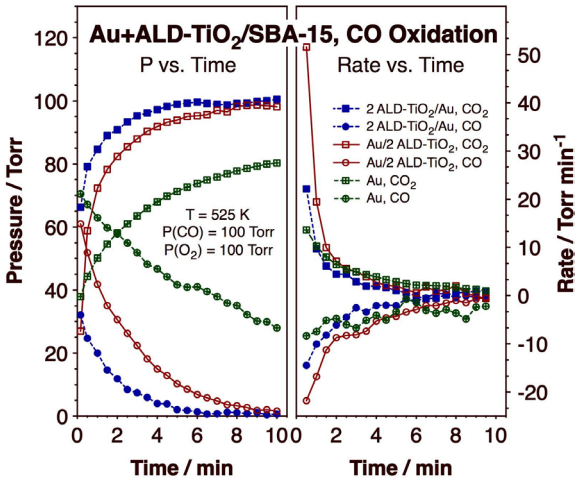


**Fig. 4.** Kinetics of CO oxidation with $O_2$ promoted by the (2 ALD-$TiO_2$)/Au/SBA-15 and Au/(2 ALD-$TiO_2$)/SBA-15 catalysts. Left: CO and $CO_2$ pressures (in a batch reactor) versus time. Right: Corresponding reaction rates.

The promotional effect of the titania films on the catalytic oxidation of CO was demonstrated next. A synergy between the Au and $TiO_2$ phases was identified as it relates to the bonding and conversion of CO, the tuning of which could be controlled by varying the synthetic parameters. An example of the results from the kinetic measurements of this reaction are shown in Figure 4, in this case for titania films made by using 2 ALD cycles and Au NPs approximately 6 nm in diameter. One important conclusion from this work is that the order of the deposition matters: adding the titania films after depositing the Au NPs leads to a partial covering of the surface of the metal and to a reduction of catalytic activity. On the other hand, new sites are produced that may exhibit unique behavior for the oxidation of organic feedstocks. This is a point worth exploring in more detail.

***Selective Oxidation of 5-HMF Using Au/$TiO_2$ Catalysts.***

Preliminary data illustrating the feasibility of promoting the room-temperature selective oxidation of 5-HMF with molecular oxygen using Au/$TiO_2$ catalysts have also been acquired recently (Figure 5). Full conversion was achieved in a few hours, with high selectivity toward the production of HFCA. It is worth noting that our experiments were carried out at atmospheric pressures; with only a few exceptions, most previous work has attained similar activity and selectivity only at high pressures. In these experiments $^1$H NMR was used to analyze the composition of the reaction mixture, but we plan to add high-pressure liquid chromatography (HPLC) detection to expedite the data acquisition. We have previously worked with HPLC to study the conversion of glycerol, and other laboratories have used HPLC for research with HMF and related molecules.

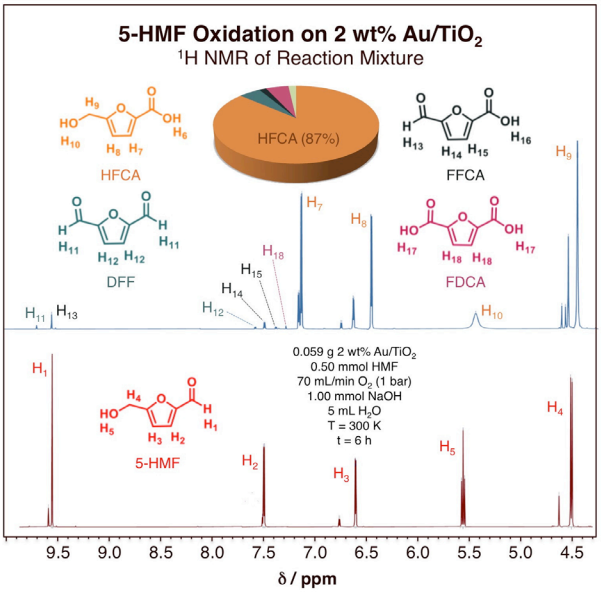


**Fig. 5.** $^1$H NMR analysis of the reaction mixture after the room-temperature oxidation of 5-HMF with $O_2$ using a homemade 2 wt% Au/$TiO_2$ catalyst.

**Publications Acknowledging this Grant in 2021-2024**

*(I) Intellectually led by this grant*

1. Xiangdong Qin, Wang Ke, Yovanny Vazquez, Ilkeun Lee, and Francisco Zaera, CO Oxidation Catalyzed by Au Dispersed on SBA-15 modified with $TiO_2$ Films Grown via Atomic-Layer-Deposition (ALD), *Catalysts* **2023**, *13(7)*, 1106 (12 pages). DOI: 10.3390/catal13071106. INVITED: Special Issue, "Advances in Catalytic Oxidation of Methane and Carbon Monoxide II".
2. Wang Ke, Xiangdong Qin, Robert M. Palomino, Juan Pablo Simonovis, Sanjaya D. Senanayake, José A. Rodriguez, Francisco Zaera, Redox Properties of $TiO_2$ Thin Films Grown on Mesoporous Silica by Atomic Layer Deposition (ALD), *J. Phys. Chem. Lett.* **2023**, *14*, 4696-4703. DOI: 10.1021/acs.jpclett.3c00834.
3. Hao Yan, Mingyue Zhao, Yueqiang Cao, Xin Zhou, Yibin Liu, Xiaobo Chen, Xiang Feng, Xuezhi Duan, Francisco Zaera, Xinggui Zhou, and Chaohe Yang, Crystal-Facet-Dependent Electron Sink Effect for Enhanced Selective Oxidation of Polyols at the Secondary Hydroxyl Position, *J. Catal.* **2024**, *431*, 115401 (11 pages). DOI: 10.1016/j.jcat.2024.115401.
4. Wang Ke, Xiangdong Qin, Yovanny Vazquez, Ilkeun Lee and Francisco Zaera, Direct Characterization of Interface Sites in $Au/TiO_2$ Catalysts Prepared Using Atomic Layer Deposition, *Chem Catal.* B2024, *4(5)*, 100977 (19 Pages). DOI: 10.1016/j.checat.2024.100977.

*(II) Jointly funded by this grant and other grants with intellectual leadership by other funding sources*

5. Letícia F. Rasteiro, Md Abdul Motin, Luiz H. Vieira, Elisabete M. Assaf, Francisco Zaera, Growth of $ZrO_2$ films on Mesoporous Silica Sieve via Atomic Layer Deposition (ALD), *Thin Solid Films* **2023**, *768*, 139716 (6 pages). DOI: 10.1016/j.tsf.2023.139716.

Zdenek Dohnalek

## Understanding dynamic activation of single-atom catalysts in the reaction environment

Marcus A. Sharp, Christopher J. Lee, Benjamin A. Jackson, Hoan K. K. Nguyen, Mausumi Mahapatra, Simone Raugei, Líney Árnadóttir, Mal-Soon Lee, Bruce D. Kay, and Zdenek Dohnálek
Pacific Northwest National Laboratory, Physical and Computational Sciences Directorate, and Institute for Integrated Catalysis

### Presentation Abstract

Surface science provides a unique platform for studies of atomically precise catalysts, exploring their dynamically evolving structure and associated activity. These precisely defined systems, often homotopic, are crucial for validating theoretical methods and uncovering structure-activity relationships in more complex environments. A combination of high-resolution imaging, spectroscopic characterization, reactivity measurements, and density functional calculations were utilized to attain mechanistic insights into surface structure, adsorbate binding, diffusion, clustering, and product formation. The presented studies focus on Pd and Rh single-atom catalysts supported on $Fe_3O_4(001)$, revealing their temperature and coverage-dependent behavior and stability. We show that $H_2$ dissociates heterolytically on such single-atom centers. Further, formic acid, which deprotonates to surface formate and hydroxyl species, is employed as a model to follow the dehydration and dehydrogenation reaction channels. We demonstrate that trace amounts of Rh adatoms cause a shift from the dehydration pathway yielding CO on bare $Fe_3O_4(001)$ to dehydrogenation yielding $CO_2$ on $Rh_{ad}$-$Fe_3O_4(001)$. As Rh adatoms are highly unstable, we further studied the Rh stabilized substitutionally in octahedral iron sites within the $Fe_3O_4(001)$ surfaces that are present on high surface area catalysts. There we show that $Rh_{oct}$ is transiently activated by surface hydroxyls and converted to Rh adatoms as the catalytically active species that are only present during the reaction. Studies of such dynamic processes are of critical importance for the future design of catalysts with maximum activity and selectivity.

**FWP 47319: Advancing key catalytic reaction steps for achieving carbon neutrality**

**PI:** Johannes Lercher
**Co-PIs:** Aaron M. Appel, Liney Arnadottir (Oregon State U.), David A. Dixon (U. Alabama), John L. Fulton, Bojana Ginovska, Jian Zhi Hu, Abhijeet Karkamkar, Bruce D. Kay, Greg A. Kimmel, Libor Kovarik, Mal-Soon Lee, John C. Linehan, Zbynek Novotny, Gregory K. Schenter, Wendy J. Shaw, János Szanyi, Ba Tran, Huamin Wang, Yong Wang (Washington State U.), Nancy Washton, Eric S. Wiedner

Yuanyuan Li

**Mechanistic Insights into the Active Sites in Cu/ceria for $CO_2$ Hydrogenation to Methanol**

Yuanyuan Li[a], Haohong Song[b], Yang He[a], Kinga Unocic [c], Jorge Perez-Aguilar[d], Jiyun Hong[d], Adam S. Hoffman[d], Jorge Moncada Vivas[e], Yang He[a], Sanjaya Senanayake[e], Simon Bare[d], De-en Jiang[b, f], Zili Wu[a, c]
[a] Chemical Sciences Division, Oak Ridge National Laboratory
[b] Interdisciplinary Materials Science, Vanderbilt University
[c] Center for Nanophase Materials Sciences, Oak Ridge National Laboratory
[d] Stanford Synchrotron Radiation Lightsource, SLAC National Accelerator Laboratory
[e] Chemistry Division, Brookhaven National Laboratory
[f] Department of Chemical and Biomolecular Engineering, Vanderbilt University,

**Presentation Abstract**

$CO_2$ hydrogenation to methanol has been studied for decades but little has been revealed about the nature of the active sites in metal/support systems due to the challenges of determining the active structures of catalysts under high-pressure reaction conditions. In this work, by designing and combining multiple in situ and operando techniques including conventional and high energy resolution fluorescence detected X-ray absorption spectroscopy, environmental electron microscopy, ambient pressure X-ray photoelectron spectroscopy and IR spectroscopy, we study the dynamic evolution and working status of catalytic sites in a model system - Cu/ceria in $CO_2$ hydrogenation. The combined experimental results and density functional theory (DFT) calculations determine that the active Cu-$Ce^{3+}$ pair is responsible for the formation of methanol. The formation of this pair involves the fast reduction of Cu and gradual transformation of $Ce^{4+}$ to active $Ce^{3+}$ sites, which, most likely, interact with active carbonate intermediates. The Cu-$Ce^{3+}$ interaction in this pair is weak under the reaction condition and can be easily disturbed by the reducing and oxidizing reactants, leading to the dynamic changes at the interface and the conversion of reactants to methanol. In addition, the results reveal that high pressure reactions have strict requirements on active sites, which, if not well designed, will be covered and strongly interact with adsorbates or lead to the formation of byproducts. The results obtained from this work provides guidance for designing efficient catalysts for methanol synthesis from $CO_2$ hydrogenation, and the methods developed in this work can be of general use to reveal active structures/sites for high pressure reactions.

Research was supported by the U.S. Department of Energy, Office of Science, Basic Energy Sciences, Chemical Sciences, Geosciences, and Biosciences Division, Catalysis Science Program. This research is part of FWP ERKCC96: Fundamentals of Catalysis and Chemical Transformations.

Clemens Krempner

## Lewis Acids and Bases in Metal-Free Catalysis

Elin Sarkissian, Jacob Culvyhouse, Shipra Garg, Adelia J.A Aquino, Hans Lischka, Clemens Krempner*
Department of Chemistry & Biochemistry, Texas Tech University, Lubbock, Texas, 79409.

### Presentation Abstract

Herein, we report the design and application of new "inverse" Frustrated Lewis Pairs (FLPs) composed of organosuperbases and tri- and tetraborylated Lewis acids. These conceptually new systems catalyze the selective metal-free hydrogenation of a range of aromatic aldehydes to primary alcohols under mild conditions and with low catalyst loadings. The experimental results and mechanistic studies support the notion that these multiple boron center containing Lewis acids act cooperatively in activating both molecular hydrogen and the carbonyl substrate. In addition, we report the discovery of a new catalytic transformation, in which organic superbases catalyze highly selective Sb-C bond formation reactions. For example, reactions of catalytic amounts of various superbases with $Sb(C_6F_5)_3$ and weakly acidic terminal alkynes and heteroaromatic compounds, respectively, gave rise to the formation of a wide range of new tris(arylalkinyl)stibines and tris(heteroaryl)stibines in good to excellent yields. Even the significantly less electron-deficient stibines, $Ph_2SbC_6F_5$ and $PhSb(C_6F_5)_2$ smoothly underwent base-catalyzed exchange reaction with terminal alkynes to generate the stibines $PhSb(C{\equiv}CPh)_2$, and $Ph_2Sb(C{\equiv}C\text{-}Ar\text{-}X)$. Kinetic studies of this new catalytic process showed the empirical rate law to be of first-order dependence with respect to the base catalyst, alkyne, and stibine suggesting σ-bond metathesis to be the most probable reaction mechanism.

**USDOE DE-SC0019094**
**Frustrated Lewis Pairs as Transition Metal-Free Catalysts for the Hydrogenation of Organic Substrates, $CO_2$ and CO.**

**Graduate students:** Jacob Culvyhouse, Elin Sarkissian, Shipra Garg, Ryan Perry, Chamila Manankandayalage
**Collaborators:** Hans Lischka, Adelia J. A. Aquino

## RECENT PROGRESS

***Polyborylated Lewis acids in Frustrated Lewis Pair (FLP) catalyzed hydrogenations of aldehydes.***

The primary objective of this project was to understand cooperative FLP catalysis, e.g. the combination of two or more distinct Lewis acidic centers into a single molecule to catalyze hydrogenation reactions that are facilitated by cooperative interactions with the two or even more catalytically active centers. To confirm our hypothesis, we synthesized the borylated Lewis acids **1**-**4** (Scheme 1).

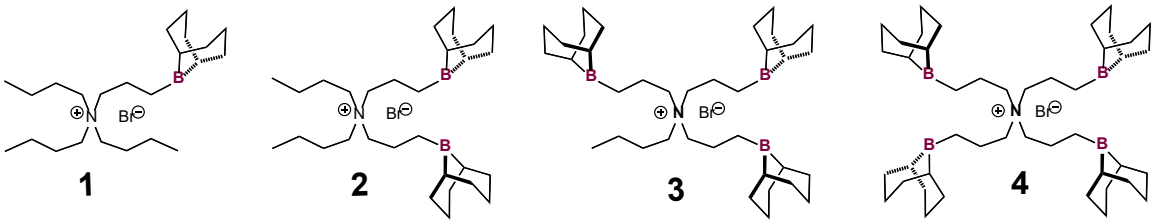


**Scheme 1.** Selected borylated Lewis acids for FLP-catalyzed hydrogenations.

We then combined tetraborylated Lewis acid **4** with a range of bases of different basicities to investigated the ability of these new FLPs to catalyze the hydrogenation of polar unsaturated organic substrates (Table 1). In fact, combinations of **4** with the strong organic bases $\mathbf{P_1}$, $\mathbf{P_2}$**-Et,** and **G** readily hydrogenated benzylidene aniline and acetophenone to N-phenyl-benzylamine and 1-phenyl-ethanol, respectively, while the weaker bases PMP and DBU were inactive (80 or 85 bar $H_2$ at 60°C in THF). When 3,4,5-trimethoxybenzaldehyde was used as the substrate, all bases in combination with **4** proved to be highly active FLP catalysts in quantitatively generating the respective alcohol.

In optimizing the reaction conditions for a substrate scope, we found that at 60°C, 85 bar hydrogen pressure and with a very low catalyst loading of 0.5 mol% of **4** and 1 mol% of the bases $\mathbf{P_2}$**-Et**, $\mathbf{P_1}$ or **G**, hydrogenation of 3,4,5-trimethoxybenzaldehyde was quantitative after 7 hours. Reducing the $H_2$-pressure from 85 bar to 50 bar under otherwise identical conditions reduced the product yields to about 65-75% after 7 hours, while increasing reaction time to 24 hours resulted in full conversion. Under the optimized conditions, the most robust catalyst systems **4**/$\mathbf{P_1}$, **4**/**G** and also **4**/**DBU** showed excellent activities in selectively hydrogenating a wide range of substituted aromatic and heteroaromatic aldehydes to their corresponding benzylic alcohols.

In addition, the performance of the borylated Lewis acids **1**-**4** (Table 2) in combination with $\mathbf{P_1}$ as base components to catalyze the hydrogenation of 3,4,5-trimethoxybenzaldehyde to 3,4,5-trimethoxybenzyl alcohol was tested (Table 2). The catalyst loading of the individual FLPs was adjusted such that in every catalytic run four equivalents of Lewis acidic boron centers per 100 equivalents of aldehyde with 1 mol% of base were realized. Notably, the FLPs **4**/$\mathbf{P_1}$ and **3**/$\mathbf{P_1}$ showed the expected high activities, while the mono- and diborylated Lewis acids **1** and **2** did not show any noticeable activity regardless of the conditions applied.

**Table 1.** Screening of Frustrated Lewis Pairs (FLPs) for the catalytic hydrogenation of benzylidene aniline, acetophenone and 3,4,5-trimethoxybenzaldehyde.

**Bases**

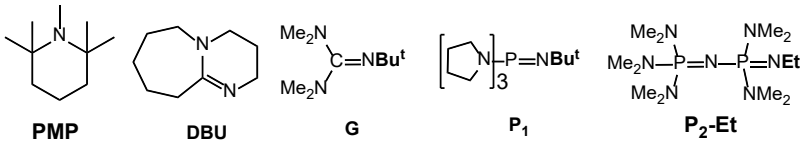


| Acid/base | Acid/base [mol%] | substrate | $p_{H2}$ [bar] | T [°C] | t [hrs.] | conv. [%] |
|---|---|---|---|---|---|---|
| **4/P$_2$-Et** | 2/2 | benzylidene aniline | 85 | 60 | 7 | >99 |
| **4/P$_1$** | 2/2 | benzylidene aniline | 85 | 60 | 7 | >99 |
| **4/G** | 2/2 | benzylidene aniline | 85 | 60 | 7 | >99 |
| **4/DBU** | 2/2 | benzylidene aniline | 85 | 60 | 7 | 0 |
| **4/PMP** | 2/2 | benzylidene aniline | 85 | 60 | 7 | 0 |
| **4/P$_2$-Et** | 2/2 | acetophenone | 80 | 60 | 24 | >99 |
| **4/P$_1$** | 2/2 | acetophenone | 80 | 60 | 24 | >99 |
| **4/G** | 2/2 | acetophenone | 80 | 60 | 24 | >99 |
| **4/DBU** | 2/2 | acetophenone | 80 | 60 | 24 | 0 |
| **4/PMP** | 2/2 | acetophenone | 80 | 60 | 24 | 0 |
| **4/P$_2$-Et** | 1/2 | 3,4,5-trimethoxybenzaldehyde | 50 | 60 | 7 | >99 |
| **4/P$_1$** | 1/2 | 3,4,5-trimethoxybenzaldehyde | 50 | 60 | 7 | >99 |
| **4/G** | 1/2 | 3,4,5-trimethoxybenzaldehyde | 50 | 60 | 7 | >99 |
| **4/DBU** | 1/2 | 3,4,5-trimethoxybenzaldehyde | 50 | 60 | 7 | >99 |
| **4/PMP** | 1/2 | 3,4,5-trimethoxybenzaldehyde | 50 | 60 | 7 | >99 |

**Table 2.** FLP-catalyzed hydrogenation of 3,4,5-trimethoxybenzaldehyde to 3,4,5-trimethoxybenzyl alcohol with selected Lewis acids and bases in THF.

| Entry | Acid | Base | Acid/base [mol%] | $p_{H2}$ [bar] | T [°C] | t [hrs.] | Conv. [%] |
|---|---|---|---|---|---|---|---|
| 1 | **1** | **P$_1$** | 2/1 | 85 | 60 | 14 | 0 |
| 2 | **2** | **P$_1$** | 1/1 | 85 | 60 | 14 | <10 |
| 3 | **3** | **P$_1$** | 0.7/1 | 85 | 60 | 14 | 99 |
| 4 | **3** | **P$_1$** | 0.7/1 | 85 | 60 | 7 | 70 |
| 5 | **3** | **P$_1$** | 0.5/1 | 85 | 60 | 7 | 40 |
| 6 | **4** | **P$_1$** | 0.5/1 | 85 | 60 | 7 | 99 |
| 7 | **4** | **P$_1$** | 0.5/1 | 50 | 60 | 7 | 70 |
| 8 | **4** | **P$_1$** | 0.5/1 | 85 | 25 | 7 | 30 |

We hypothesize that the superior activity of tetraborylated **4** in combination with suitable bases is the result of a cooperative activation of both $H_2$ and the substrate through more than two boron centers. DFT calculations on the mechanism of these hydrogenation reactions seem to support the notion that tetraborylated **4** as well as triborylated **3** act cooperatively in activating both molecular hydrogen and the carbonyl substrate.

***Organic superbase-catalyzed formation of antimony-carbon bonds.***
We investigated the ability of $Sb(C_6F_5)_3$ (**5**) to serve as a weak Lewis acid component in FLP catalysis. $Sb(C_6F_5)_3$ when combined with bulky organic superbases did not engage in the heterolytic hydrogen cleavage nor in catalytic hydrogenations. Instead, we discovered that the organosuperbases **$P_2$-Et**, **$P_2$-Bu$^t$** and **$P_4$-Bu$^t$** catalyzed the quantitative conversion of $Sb(C_6F_5)_3$ (**5**) to stibine **2** at 25°C in less than 15 minutes (Figure 1). With the weaker base **$P_1$**, the reaction was complete in less than 24 hours, while guanidine (**G)** because of its significantly lower basicity showed only 64% conversion after 24 hours.

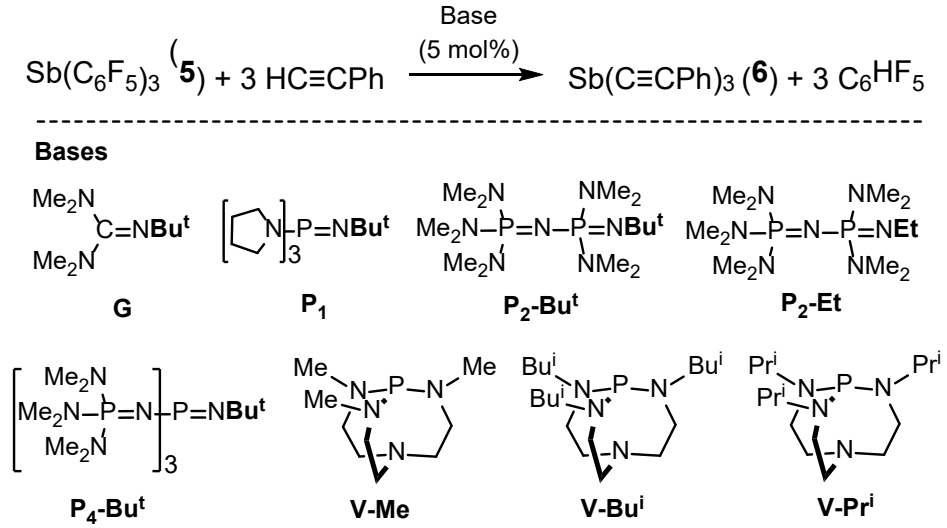


| Base | p$K_a$ | t [min] | Conv. [%] |
|---|---|---|---|
| **G** | 24 | 15 | 7 |
| **$P_1$** | 28 | 15 | 65 |
| **V-Me** | 33 | 15 | 69 |
| **V-Bu$^i$** | 34 | 15 | 73 |
| **V-Pr$^i$** | 34 | 15 | 73 |
| **$P_2$-Et** | 34 | 15 | >99 |
| **$P_2$-Bu$^t$** | 33 | 15 | >99 |
| **$P_4$-Bu$^t$** | 42 | 15 | >99 |

**Figure 1.** Screening of organic superbases for the catalytic conversion of **5** to **6**.

We extended this novel base-catalyzed Sb-C bond formation process to the selective synthesis of a range of new tris(arylethinyl)stibines (**7**) and so far unknown stibines with heterocyclic substituents (**8**-**10**) (Scheme 2). Efforts were undertaken to synthesize the unknown tris(fluorenyl)stibine, $Sb(C_{13}H_9)_3$. Instead, when three equiv. of fluorene were treated with $Sb(C_6F_5)_3$ (**5**) under base catalysis, bis(fluorenyl)stibine **12** was formed as the sole product. Reaction of one equiv. of fluorene with **5** selectively provided mono-substituted stibine **11** in good yields.

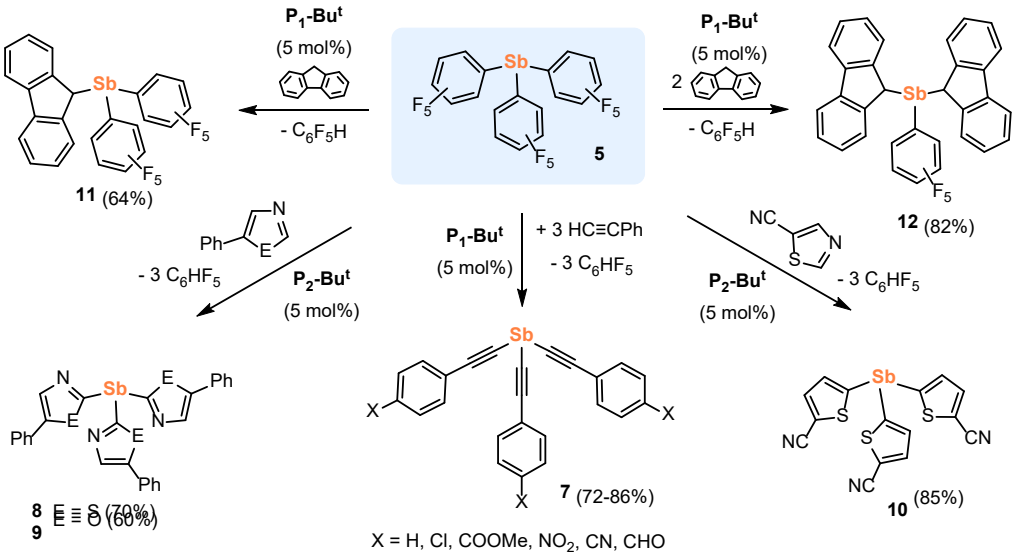


**Scheme 2.** Scope of the organic superbase-catalyzed Sb-C bond formation reaction.

To gain mechanistic insights into the base-catalyzed Sb-C bond-formation event, kinetic measurements of the model reaction: $Ph_2SbC_6F_5$ + PhC≡CH + $P_1$-$Bu^t$ → $Ph_2SbC{\equiv}CPh$ + $C_6HF_5$ + $P_1$-$Bu^t$ were performed using $^{19}F$ NMR spectroscopy. The results suggest the empirical rate law to exhibit an approximately first-order dependence on **$P_1$-$Bu^t$** (cat.), PhC≡CH, and $Ph_2SbC_6F_5$ (Figure 2a–c). Deuterium isotope studies show that the reaction exhibits a KIE ($k_H/k_D$) of 1.2 (Figure 2d) suggesting the C-H bond activation of the alkyne to be involved in the operative turnover-limiting step. Computations support the experimental reaction conditions with a pathway proposed to proceed via a concerted σ-bond metathesis transition state, where the base catalyst activates the Sb-$C_6F_5$ bond sequence through secondary bond interactions (pnictogen bonding).

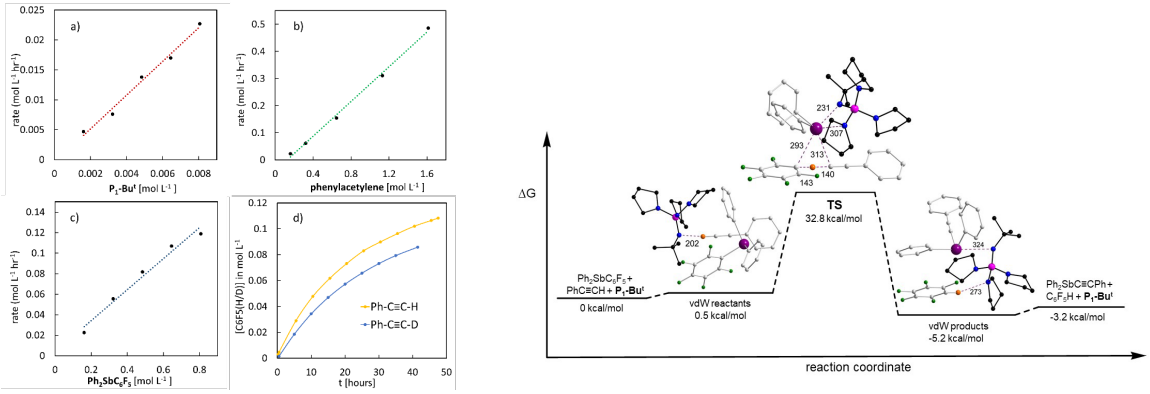


**Figure 2**. left) Plot of initial reaction rate $\delta p/\delta t$ against the concentration of a) **$P_1$-$Bu^t$**, b) PhC≡CH, c) $Ph_2SbC_6F_5$, and d) Plot of concentration of $C_6F_5H/D$ vs time for the **$P_1$-$Bu^t$** catalyzed reaction of $Ph_2SbC_6F_5$ with PhC≡CH; right) Computed free energy profile (kcal/mol) and optimized structure of the transition state (TS).

**Publications Acknowledging this Grant in 2021-2024**

*(I) Intellectually led by this grant*


1. Culvyhouse, J.; Unruh, D. K.; Lischka, H.; Aquino, A. J. A.; Krempner, C. Facile Access to Organostibines via Selective Organic Superbase Catalyzed Antimony-Carbon Protonolysis. *Angew. Chem. Int. Ed.* **2024**, *63*, e202407822.
2. Mummadi, S.; Krempner, C. Triphenylborane in Metal-Free Catalysis. *Molecules* **2023**, *28*, 1340-57.
3. Manankandayalage, C. P.; Unruh, D. K.; Perry, R.; Krempner, C. 1,8-Dihydroxy Naphthalene - A New Building Block for the Self-Assembly with Boronic Acids and 4,4-Bipyridine to Stable Host–Guest Complexes with Aromatic Hydrocarbons. *Molecules* **2023**, *28*, 5394-5407.
4. Manankandayalage, C.; Katakam, N.; Unruh, D. K.; Aquino, A. A.; Krempner, C. "Inverse" Intramolecular Frustrated Lewis Pair Mediated Activation and Cleavage of Carbon Dioxide. *Chem. Commun.* **2022**, *58*, 9385-9388.
5. Manankandayalage, C.; Unruh, D. K.; Krempner, C. Carbon monoxide bond cleavage mediated by an intramolecular frustrated Lewis pair: access to new B/N heterocycles via selective incorporation of single carbon atoms. *Chem. Commun.* **2021**, *57*, 12528-12531.
6. Garg, S.: Unruh, D. K.; Krempner, C. Synthesis, Structures and Catalytic Activity of Some BINOL Based Boronates and Boronium Salts. *Dalton Trans.* **2021**, *50*, 5044-5049.
7. Manankandayalage, C.; Unruh, D. K.; Krempner, C. Small Molecule Activation with Intramolecular "Inverse" Frustrated Lewis Pairs. *Chem. Eur. J.* **2021**, 27, 6263-6273.
8. Garg, S.; Unruh, D. K.; Krempner, C. Zirconium and hafnium polyhedral oligosilsesqui-oxane complexes - green homogeneous catalysts in the formation of bio-derived ethers via a MPV/etherification reaction cascade. *Catal. Science & Technol.* **2021**, *11*, 211-218.

Neal P. Mankad

## Cooperative Bond Activation with Unusual Redox States of Aluminum

Neal P. Mankad
Department of Chemistry, University of Illinois Chicago

### Presentation Abstract

We recently discovered that complexes with Al-Fp linkages [Fp = $FeCp(CO)_2$] have anomalously weak Al-Fe bonds susceptible to reversible homolytic cleavage at ambient conditions. These spontaneous bond scission processes give rise to frustrated radical pairs (FRPs) consisting of Al-containing radicals paired with Fp· that are capable of cooperative bond activation. Depending on the nature of the ligand sphere supporting the Al site, the Al-containing radical can either be a redox non-innocent $Al^{III}$/L· assembly or feature a *bona fide*, mononuclear $Al^{II}$ site. In either case, the Al-containing radicals have biphilic nature, allowing them to activate inert reactants including $CO_2$ and promote dramatic levels of coordination induced bond weakening of C-C, C-O, N-H, and O-H bonds. The ability to access Al-containing radicals at ambient conditions has enabled us to map reactivity patterns of such intermediates for the first time. Translating these reactivity observations into catalytic transformations is being pursued using an approach that combines computational predictions and data science.

## DE-SC0021055: Earth-abundant catalysts for carbonylation reactions that involve heterometallic mechanisms or radical intermediates

**Postdocs:** Daniel Kim, Soumen Sinhababu
**Students:** Maxim Radzhabov, Roushan Singh, Supundrika Subasinghe, Pinku Tung

### RECENT PROGRESS

***Cu-catalyzed carbonylation reactions***

In an extension of previous research on Cu-catalyzed carbonylation reactions of alkyl halides under thermal conditions (Cheng et al., *Acc. Chem. Res.* **2021**), here we have developed Cu-catalyzed carbonylation reactions under photochemical conditions. First, we reported (Tung et al., *J. Am. Chem. Soc.* **2023**; Figure 1) that simple salts such as CuCl or $CuBr{\cdot}SMe_2$ act as pre-catalysts for oxocarbonylative dimerization of alkyl halides to form aliphatic acid anhydrides under CO pressure (6 atm) and blue light (390 nm) irradiation. Abundant bases such as NaOH or $K_2CO_3$ readily serve as the oxygen source in this transformation. The simplest anhydride, acetic anhydride, is an important commodity chemical and was produced in high yield and good selectivity from methyl iodide under these conditions. Mechanistic studies revealed that, under the photochemical conditions, the soluble pre-catalysts convert to Cu nanoparticles that promote the reaction by heterogeneous catalysis. Second, we reported (Tung et al., *Org. Lett.* **2024**; Figure 2) the fluorocarbonylative variant of this transformation by replacing the oxygen base with

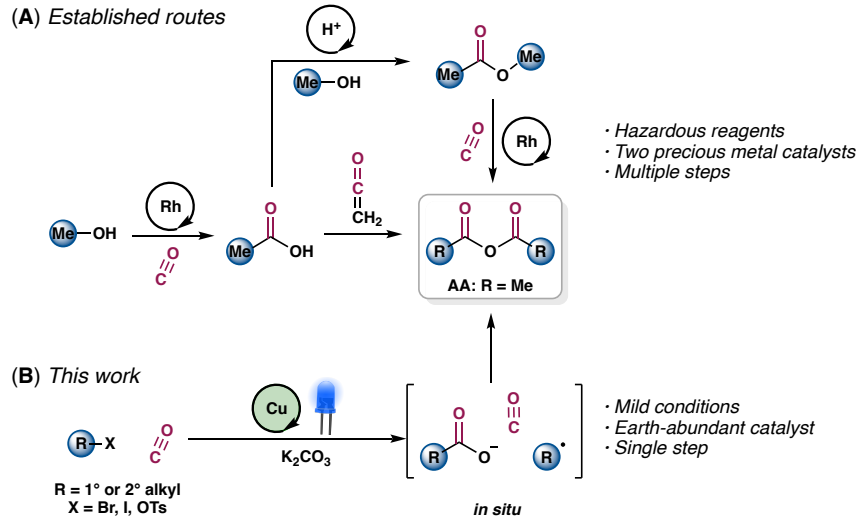


*Figure 1. Light-mediated aliphatic anhydride synthesis by Cu-catalyzed carbonylation.*

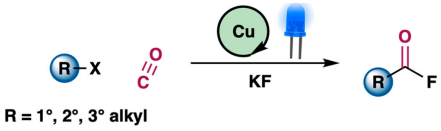


*Figure 2. Cu-catalyzed fluorocarbonylation to generate acyl fluorides.*

KF. Various alkyl halides were converted to the corresponding acyl fluorides with good efficiency. In the same study, for certain reactants bearing remote phenyl substituents, tandem fluorocarbonylation and Friedel-Crafts cyclization to form $\alpha$-tetralone structures was observed. The $\alpha$-tetralone core structure is an important motif in medicinally active compounds and natural products. Once again, mechanistic studies indicated a heterogeneous catalysis modality with Cu nanoparticles being formed *in situ* from the soluble pre-catalysts. Commercially available Cu nanoparticles were also found to be catalytically active.

### *Design of Al/Fe heterobinuclear catalysts*

Compared to Cu (0.006%), Al (8.23%) and Fe (5.63%) have significantly higher abundance in the earth's crust. Motivated by maximizing sustainability of future catalytic technologies, we have engaged in fundamental studies mapping reaction chemistry of Al/Fe heterobinuclear complexes and establishing design rules for rational catalyst design. In our initial work (Sinhababu et al., *J. Am. Chem. Soc.* **2022**), we discovered that

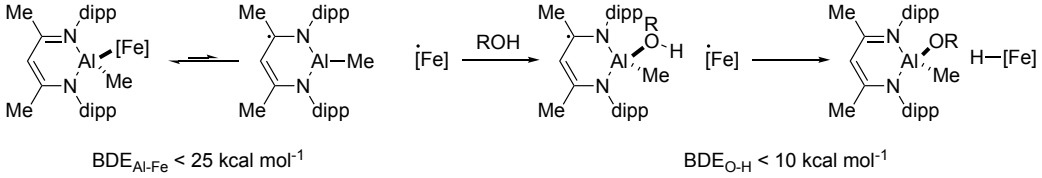


*Figure 3. Coordination-induced bond weakening by an Al-containing radical intermediate.*

a complex with an [Al]–FeCp(CO)$_2$ linkage features a weak Al–Fe bond that undergoes reversible homolysis at ambient conditions, giving rise to a pair of radical intermediates capable of cooperative bond activation. The Al-containing radical, while formally in the rare Al$^{II}$ oxidation state, was found to be redox non-innocent and instead presents as an Al$^{III}$ Lewis acid bound to a ligand-centered radical. In subsequent work (Sinhababu et al., *Nat. Commun.* **2024**; Figure 3), we showed that this unusual Al-containing radical is capable of dramatic coordination-induced bond weakening (CIBW), for example lowering the O–H bond dissociation energy (BDE) of water to < 10 kcal mol$^{-1}$ upon

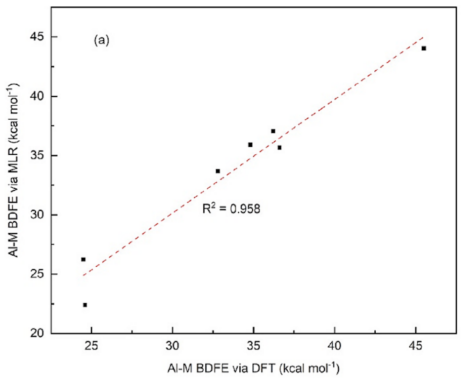


$$\text{Al-M BDFE}(\text{kcal mol}^{-1}) = 109.4 + 41.4E^{\circ} + 2.03pK_a - 0.89[\%V_{bur}(\mathbf{1\text{-}M})]$$

*Figure 4. Multivariate linear regression analysis of Al–M bond strengths.*

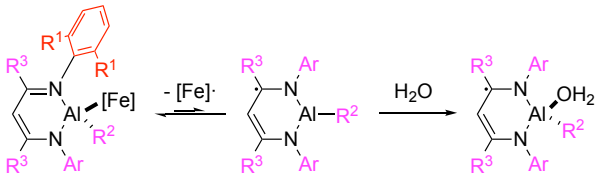


*Figure 5. In-progress modeling of Al-Fe bond strength and Al Lewis acidity as functions of $R^1$, $R^2$, and $R^3$ variations.*

coordination. We have also observed evidence for CIBW of N–H, C–O (Sinhababu et al., *Organometallics* **2022**), and C–C bonds (Singh et al., unpublished).

Although the observations described above were strictly stoichiometric reactions, our long-term goal is to develop catalytic processes (e.g. carbonylation reactions) involving Al/Fe cooperation and CIBW by Al-containing radicals. Our approach is to use computational predictions combined with data science to bring forth design rules and enable rational catalyst synthesis. In our initial report (Subasinghe et al., *Polyhedron* **2023**; Figure 4), we uncovered the factors controlling Al–M BDEs for a series of complexes with M = Cr, Mo, W, Mn, Fe, Ru, and Co by calculating the predicted bond strengths and then employing multivariate linear regression analysis with thermodynamic descriptors such as M–H p$K_a$, reduction potential, and steric volume. A comprehensive follow-up study currently in progress (Subasinghe et al., *Organometallics*, in revision; Figure 5) extends this approach to describe both Al–Fe BDE and Lewis acidity of the Al-containing radical as functions of variations in ligand structure. Upon completion of this study, we expect to have a global model reporting how to tune BDE and Lewis acidity independently such that catalytic turnover is facilitated.

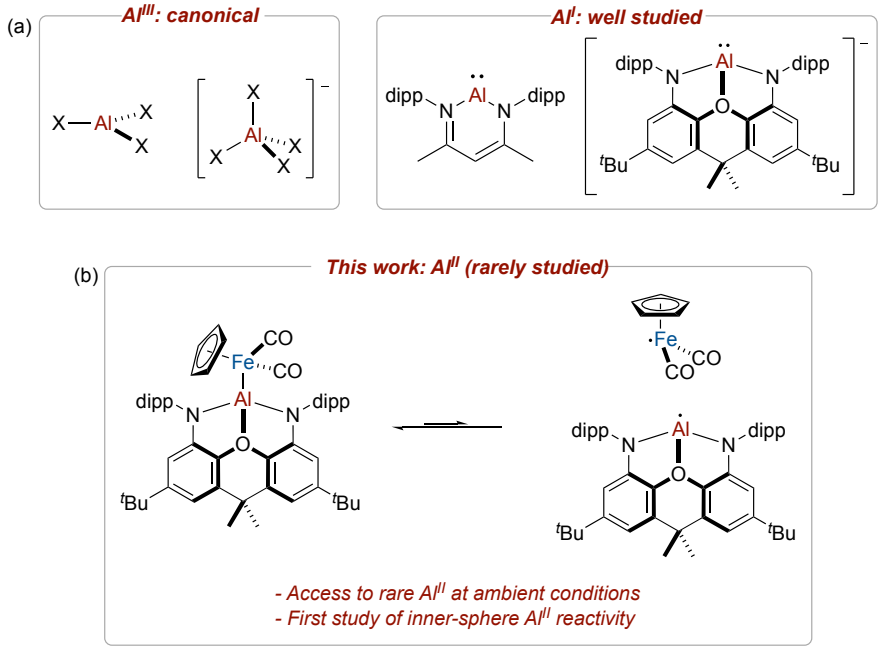


*Figure 6. Unpublished system enabling the first study of $Al^{II}$ reaction chemistry.*

Lastly, in unpublished work (Singh et al., in preparation; Figure 6), we have discovered a redox innocent Al/Fe system that engages in cooperative bond activation using a *bona fide* Al-centered radical. To our knowledge, this is the first study of inner-sphere reactivity of any mononuclear $Al^{II}$

compound, as previously this oxidation state was observed only in dialane ($X_2Al–AlX_2$) form or found to do only outer-sphere electron transfer. Upon publication, therefore, this study will represent a landmark in the chemistry of earth's most abundant metal. Furthermore, it will add a new class of compounds to our library of potential catalysts.

**Publications Acknowledging this Grant in 2021-2024**

***(I) Intellectually led by this grant***


1. Singh, R. P.; Mankad, N. P. Frustrated Al/M Heterobimetallic Complexes (M = Cr, Mo, W) That Exhibit Both Lewis and Radical Pair Behavior. *Inorg. Chem.* **2024**, *ASAP*, https://doi.org/10.1021/acs.inorgchem.4c03276.
2. Subasinghe, S. M. S.; Mankad, N. P. Lessons from Recent Theoretical Treatments of Al–M Bonds (M = Fe, Cu, Ag, Au) That Capture $CO_2$. *Dalton Trans.* **2024**, *53* (33), 13709–13715. https://doi.org/10.1039/D4DT02018A.
3. Sinhababu, S.; Singh, R. P.; Radzhabov, M. R.; Kumawat, J.; Ess, D. H.; Mankad, N. P. Coordination-Induced O-H/N-H Bond Weakening by a Redox Non-Innocent, Aluminum-Containing Radical. *Nat Commun* **2024**, *15* (1), 1315. https://doi.org/10.1038/s41467-024-45721-1.
4. Tung, P.; Mankad, N. P. Photochemical Synthesis of Acyl Fluorides Using Copper-Catalyzed Fluorocarbonylation of Alkyl Iodides. *Org. Lett.* **2024**, *26* (15), 3299–3303. https://doi.org/10.1021/acs.orglett.4c00967.
5. Subasinghe, S. M. S.; Mankad, N. P. Predictive Models for Metal–Metal Bond Dissociation Free Energies between Aluminum(III) and a Series of Transition Metal Carbonyls. *Polyhedron* **2023**, *245*, 116637. https://doi.org/10.1016/j.poly.2023.116637.
6. Singh, R. P.; Sinhababu, S.; Mankad, N. P. Aluminum-Containing Heterobimetallic Complexes as Versatile Platforms for Homogeneous Catalysis. *ACS Catal.* **2023**, *13* (19), 12519–12542. https://doi.org/10/gtq9z6.
7. Tung, P.; Mankad, N. P. Light-Mediated Synthesis of Aliphatic Anhydrides by Cu-Catalyzed Carbonylation of Alkyl Halides. *J. Am. Chem. Soc.* **2023**, *145* (17), 9423–9427. https://doi.org/10.1021/jacs.3c01224.
8. Radzhabov, M. R.; Mankad, N. P. Activation of Robust Bonds by Carbonyl Complexes of Mn, Fe and Co. *Chem. Commun.* **2023**, *59* (80), 11932–11946. https://doi.org/10.1039/D3CC03078D.
9. Radzhabov, M. R.; Mankad, N. P. Fe-Promoted C–F Activation of Aryl Fluorides Enables Heck-Type Coupling with Alkenes and One-Pot Synthesis of Indenes. *Organometallics* **2023**, *42* (15), 2111–2121. https://doi.org/10.1021/acs.organomet.3c00256.
10. Tung, P.; Mankad, N. P. Cu-Catalyzed C–C Bond Formation with CO; Topics in Organometallic Chemistry; Springer: Berlin, Heidelberg; **2023**; pp 1–21. https://doi.org/10.1007/3418_2023_84.
11. Sinhababu, S.; Mankad, N. P. Diverse Thermal and Photochemical Reactivity of an Al–Fe Bonded Heterobimetallic Complex. *Organometallics* **2022**, *41* (15), 1917–1921. https://doi.org/10/gq2xdg.

12. Sinhababu, S.; Radzhabov, M. R.; Telser, J.; Mankad, N. P. Cooperative Activation of $CO_2$ and Epoxide by a Heterobinuclear Al–Fe Complex via Radical Pair Mechanisms. *J. Am. Chem. Soc.* **2022**, *144* (7), 3210–3221. https://doi.org/10/gsthps.
13. Sinhababu, S.; Lakliang, Y.; Mankad, N. P. Recent Advances in Cooperative Activation of $CO_2$ and $N_2O$ by Bimetallic Coordination Complexes or Binuclear Reaction Pathways. *Dalton Transactions* **2022**, *51* (16), 6129–6147. https://doi.org/10.1039/D2DT00210H.
14. Radzhabov, M.; Mankad, N. Cobalt-Catalyzed (E)-β-Selective Hydrogermylation of Terminal Alkynes. *Organic Letters* **2021**, *23* (8), 3221–3226. https://doi.org/10.1021/acs.orglett.1c00928.
15. Yu, H. C.; Telser, J.; Mankad, N. P. Synthesis and Characterization of Heteromultinuclear Ni/M Clusters (M = Fe, Ru, W) Including a Paramagnetic (NHC)Ni-WCp*$(CO)_3$Heterobinuclear Complex. *Organometallics* **2021**, *40* (13), 2123–2132. https://doi.org/10.1021/acs.organomet.1c00263.

***(II) Jointly funded by this grant and other grants with intellectual leadership by other funding sources***

16. Tung, P.; Schuhmacher, A.; Schilling, P. E.; Bode, J. W.; Mankad, N. P. Preparation of Potassium Acyltrifluoroborates (KATs) from Carboxylic Acids by Copper-Catalyzed Borylation of Mixed Anhydrides. *Angewandte Chemie International Edition* **2021**, *61* (7), e202114513. https://doi.org/10.1002/anie.202114513.
17. Cheng, L. J.; Mankad, N. P. Copper-Catalyzed Carbonylative Coupling of Alkyl Halides. *Accounts of Chemical Research* **2021**, *54* (9), 2261–2274. https://doi.org/10.1021/acs.accounts.1c00115.

Andreas Heyden

## Design of New Catalysts for the Generation of Clean $H_2$ from Liquid Organic Hydrogen Carriers

Donna A. Chen[1], Andreas Heyden[2], Kevin Huang[3], Jochen Lauterbach[2], John R. Monnier[2], John M. Tengco[2]
University of South Carolina, Columbia, SC, Department of: Chemistry and Biochemistry[1], Chemical Engineering[2], Mechanical Engineering[3]

### Presentation Abstract

This project focuses on the design and evaluation of new catalysts for the reversible storage of $H_2$ through the hydrogenation-dehydrogenation of liquid organic hydrogen carriers (LOHC). The methylcyclohexane (MCH)-toluene pair has shown promise as LOHC system, but a major problem is that catalytic dehydrogenation is endothermic and not always reversible due to side reactions. Bimetallic Ni- and Pt-based catalysts have been studied for the dehydrogenation of MCH, in which a second metal (Cu, Sn) is added to prevent undesirable C-C bond breaking reactions that lead to coking and deactivation.

Pt catalysts on different metal oxide supports were investigated to understand the role of the support in preventing deactivation. Furthermore, experiments on single-crystal have been conducted in which the composition, morphology and structure of the model catalysts can be characterized on an atomic scale before and after the reaction. Microkinetic modeling studies of different Pt and Ni surfaces demonstrate that during MCH dehydrogenation, coking is favored on stepped surfaces but not on (111) surfaces. Controlled synthesis of bimetallic Cu on Ni catalysts was carried out by galvanic displacement and electroless deposition; it was found that the presence of Cu increased catalyst activity, with the highest TOF achieved at the highest Cu concentrations. In order to achieve high conversions at the moderate temperatures (250-300 °C) that favor high selectivity to toluene, a membrane reactor is being designed in which an electrochemically driven solid acid-membrane (cesium diphosphate) is used to control the rate of $H_2$ diffusion out of the system.

**DE-SC0023376:** Design of New Catalysts for the Generation of Clean $H_2$ from Liquid Organic Hydrogen Carriers: Dehydrogenation of Methylcyclohexane on Bimetallic Catalysts

**PIs:** Donna A. Chen, Andreas Heyden, Kevin Huang, Jochen Lauterbach, John R. Monnier, and John M. Tengco
**Postdoctoral associates:** Ali S. Ahsen, Minal Gupta, Fangliang Li, Azadah Menrani, Md. Fakhruddin Patwary, Thossaporn Osnree, and Yanjiao Yi
Research Associates: Wenqiang Wu and Salai Ammal
**Students:** Musbau Gbadamosi, Patrick Holcombe, Mengxiong Qiao, Bhawana Rayamajhi, Kaveh Shiarati, Kangkang Zhang, and Haiying Zhou

## RECENT PROGRESS

### *Role of Support in Deactivation of Pt Catalysts*

The MCH dehydrogenation activities of 5%wt Pt catalysts as a function of support ($SiO_2$, $\gamma$-$Al_2O_3$, $TiO_2$, $ZrO_2$) were compared at 300 °C (Fig. 1). The Pt/$\gamma$-$Al_2O_3$ catalyst has the highest conversion and excellent long-term stability over 20 hours on stream while the other catalysts deactivate over time. Pt/$\gamma$-$Al_2O_3$ is also the only catalyst for which single-atom species can be observed in the electron microscopy images. Toluene selectivities for all catalysts were $\geq$99.9%. Furthermore, activity can be restored for Pt/$SiO_2$ after re-reducing the catalyst in $H_2$ at 300 °C, which suggests that the deactivation is due to the formation of soft coke. In addition to the fouling of the Pt surface, there is also evidence that deactivation occurs via blocking of the pores in the support. A four-channel reactor system has been constructed for high-throughput screening of Pt catalysts on metal oxide and mixed metal oxide supports; interestingly, Pt on a single-phase $CeTi_{0.05}O_x$ support was identified to have comparable to the best Pt/$\gamma$-$Al_2O_3$ catalyst and is much more active than Pt on either pure oxide support.

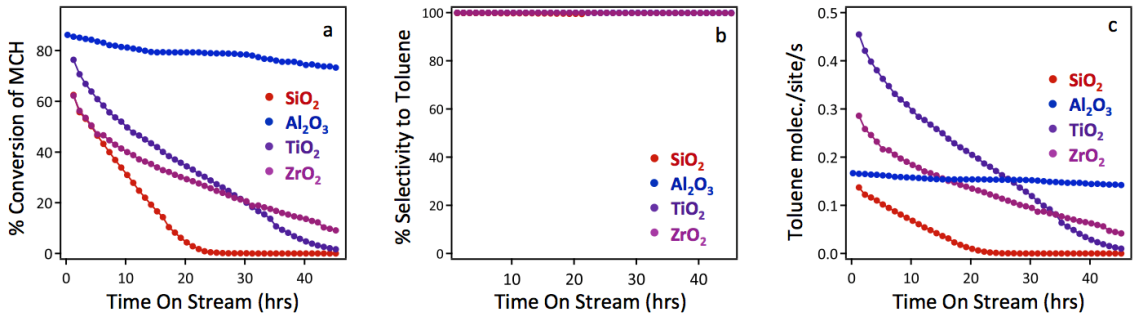


**Fig. 1**: Activities for 5% wt Pt catalysts on various oxide supports at 10% MCH/He and 300 °C.

### *Single Crystal Studies*

A custom-designed microreactor system coupled to the ultrahigh vacuum (UHV) chamber was constructed. The single-crystal model surfaces have ~10,000 fewer active sites than conventional catalysts on high surface area supports, and therefore the system was designed to operate in recirculation mode, where the reactant gas makes multiple passes over the catalyst to increase concentration before detection. MCH dehydrogenation was studied on Pt surfaces with different types of active sites: Pt(111), 2 ML Pt particles on non-interacting highly-oriented pyrolytic graphite (HOPG), and 2 ML Pt particles on a $TiO_2$(110). For 2 ML of Pt/HOPG particle heights were 12.2 Å$\pm$3.2 Å with a particle density of $3.6 \times 10^{12}/cm^2$, and for Pt/$TiO_2$, smaller particles were formed with a higher particle density of $6.0 \times 10^{12}/cm^2$ due to the stronger particle-support interactions. Turnover frequencies (TOFs) for dehydrogenation of 2.5% MCH/Ar to toluene at 300 °C were compared with the total number of active sites based on temperature programmed desorption experiments for CO, assuming that one CO adsorbs per Pt atom. The TOF on Pt(111) ($2 \times 10^{-2}$ $s^{-1}$) is four times lower than that on Pt/HOPG, and this behavior is attributed to the greater number of highly active undercoordinated sites on the Pt clusters on HOPG compared to Pt(111). Since the Pt particles on $TiO_2$ are smaller than on HOPG, Pt/$TiO_2$ should have a greater number of undercoordinated sites, but Pt/$TiO_2$ has a TOF comparable to Pt(111) and lower than Pt/HOPG. It is proposed that strong metal support interaction (SMSI) occurs upon heating these surfaces under MCH reaction conditions, which is a reducing environment due to the production of $H_2$;

specifically, $TiO_x$ (x<2) from the support migrates onto the surface of the Pt particles and potentially blocks active sites. This hypothesis is supported by the post-reaction XPS experiment that shows a significant loss in Pt signal after reaction.

***Microkinetic Modeling***

The reaction mechanism of MCH dehydrogenation to toluene was investigated using a combination of DFT and microkinetic modeling techniques on three Pt surface models: Pt(111), Pt(100), and Pt(211). This reaction network involves 6 consecutive dehydrogenation steps, and we identified a total of 41 intermediate species and 104 elementary reactions for each surface model. The structures of all intermediate species and transition states (TSs) corresponding to the elementary reactions were optimized using the PBE+D3 functional, followed by BEEF-vdW single point calculations, providing an ensemble of 2000 energies describing the DFT functional uncertainty. Next, we performed a microkinetic analysis employing a continuous stirred tank reactor (CSTR) model to identify the intrinsic catalytic activity, dominant reaction mechanism, and rate-controlling steps for the conversion of MCH to toluene. A CSTR simulation at 10% MCH conversion (T=573 K, and $P_{MCH}$=0.1 bar, $P_{inert}$=0.9 bar) was carried out for all 2000 BEEF-vdW functionals. In agreement with experiments, we found that the more open (100) and (211) stepped surfaces are more active than the close packed Pt(111) facet. However, the Pt(111) surfaces possesses a kinetic barrier that is more than 1 eV larger than for the more open surfaces for C-C bond cleavage and coke formation, i.e., if the activity of Pt(111) can be considered adequate, then selective poisoning of the more open surface facets can lead to a stable and selectivity catalyst for the dehydrogenation of MCH. Similar calculations were also carried out for the Ni surfaces that we find to be 1-3 orders of magnitude less active than the Pt catalysts. Interestingly, C-C bond cleavage and coke precursor formation is thermodynamically not favorable on Ni(111) while it is rapid on the more open Ni surfaces. Thus, similar to Pt, coke-resistance requires blocking the more open, stepped Ni sites, perhaps by an inactive metal like Sn or Cu.

***Synthesis of Ni-Cu/$SiO_2$ Catalysts***

The controlled synthesis of Cu on $Ni/SiO_2$ has been carried out by galvanic displacement (GD) and electroless deposition (ED) to ensure that well-mixed, exclusively bimetallic particles are formed and to allow surface compositions to be systematically varied over the full composition space. Cu on $Ni/SiO_2$ GD catalysts were prepared by exposing a 5% $Ni/SiO_2$ base catalyst to a solution of $Cu(NO_3)_2$ to spontaneously reduce $Cu^{2+}$ while metallic Ni at the surface of the particles is oxidized. Cu loadings ranging from 0.1-0.8% wt% were achieved by varying exposure time, concentration and temperature, but a maximum of 0.8% Cu was reached when the surface of the Ni particles was completely covered by Cu. STEM imaging and EDX mapping confirm bimetallic catalyst formation and excellent association between Cu and Ni (Fig. 2); there is also no particle sintering or segregation of the metals during MCH reaction. In contrast, $CuNi/SiO_2$ catalysts prepared by conventional co-dry impregnation (co-DI) has compositions that varied with particle size. Activities of the Cu-Ni catalysts were evaluated for MCH reaction at 400 °C with the TOFs calculated from the active sites determined by pulsed $H_2$ chemisorption. The GD catalyst with the highest Cu loading had the best TOF (0.13 $s^{-1}$ at 1.7% Cu), which more than twice the TOF of the co-DI catalyst with the same Cu loading. Since greater Cu loading results in improved activity, CuNi catalysts were also prepared by ED of $Cu^{2+}$ on $Ni/SiO_2$ in the presence of hydrazine as reducing agent, and again the highest Cu loading resulted in the highest activity. Studies are

currently underway to synthesize Ni on Cu catalysts by ED in order to prepare surfaces with higher concentrations of Cu.

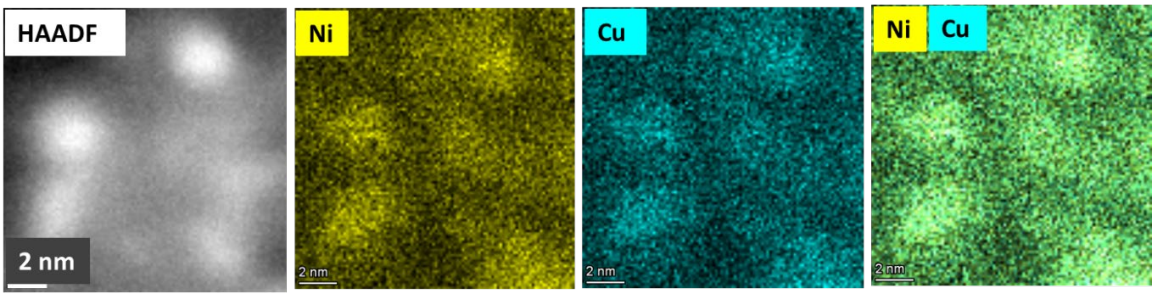


**Fig. 2**: EDX mapping of 0.76% Cu, 4.35% Ni/$SiO_2$ by GD.

***Development of the Electrochemical Hydrogen Pump***

An electrochemical hydrogen pump (EHP) had been constructed for selectively transporting hydrogen out of the reactor under electrochemical control (Fig. 3). The membrane developed for this pump is the solid acid $CsH_2PO_4$ (CDP) which exhibits super-protonic conductivity in the temperature regime for the MCH dehydrogenation (250-300 °C) and is the only solid oxide membrane that can operate at these low temperatures. CDP membrane has the disadvantage of requiring high humidity for operation (20-38% water), but our studies have shown that MCH dehydrogenation activity does not diminish even for water concentrations as high as 38%. Furthermore, the addition of hydrophilic $SnO_2$ to form a CDP:$SnO_2$ (4:1) composite electrolyte increased the stability for ionic conductivity at lower water partial pressures. A Pt/C catalyst was used for the hydrogen oxidation reaction, and the testing this CPD:$SnO_2$-based membrane electrode assembly (MEA) in a symmetrical cell demonstrated that the diffusion of hydrogen gas

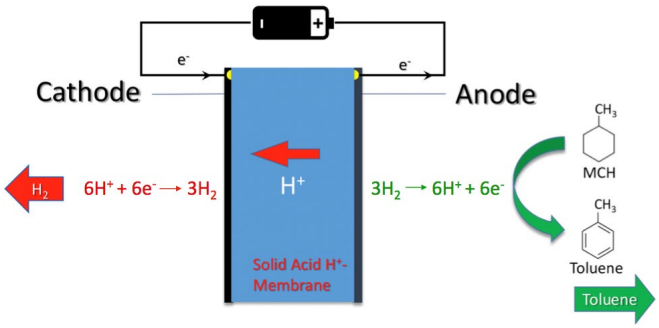


**Fig. 3**. Working principle of the electrochemical hydrogen pump.

across the membrane could be electrochemically controlled. Currently, the MEA is being tested for hydrogen transport out of the anode cell in which the Pd/C catalyst is used for both the dehydrogenation of MCH to toluene and hydrogen, and the electrochemical hydrogen oxidation reaction.

**Publications Acknowledging this Grant in 2021-2024**

***(I)*** *Intellectually led by this grant:*

1. Szaro, N. A.; Bello, M.; Fricke, C.; Bamidele, O.; Heyden, A.* Benchmarking the Accuracy of Density Functional Theory Against the Random Phase Approximation for the Ethane Dehydrogenation Network on Pt(111) *J. Phys. Chem. Lett*. **2023**, *14*, 10769-10778.

2. Li, F.; Ahsen A. S.; Ammal, S. C.; Qiao, M.; Maddumapatabandi, T. D.; Beniwal, S.; Heyden, A., and Chen, D. A.* Characterizing the Surface Compositions of Supported Bimetallic PtSn Clusters: Effects of Cluster-Support Interactions and Surface Adsorbates. *Surf. Sci.* **2024**, in press.

3. Gupta, M.; Zhang, K.; and Huang, K.* $SnO_2$ as a New Conductivity Stabilizer for $CsH_2PO_4$ (CDP) Protonic Conductor. *J. Electrochem. Soc.* **2024**, under review.

Bin Wang

# Direct Coupling of $CO_2$ and Alkene to Produce Unsaturated Carboxylic Acid: A Mechanistic Study

Bin Wang
University of Oklahoma, Norman

## Presentation Abstract

Direct coupling of $CO_2$ and ethylene towards acrylic acid and its derivatives is a valuable approach using $CO_2$ to introduce the carboxylic group as a C1 feedstock. Acrylic acid and its derivatives are building-block molecules for manufacturing adhesive products and acrylate-related polymers. Transition metal-based molecular catalysts have been investigated for decades but with limited success because of the challenge for activation of the two chemically distinct molecules, catalyzing the C-C coupling step, stabilization of bulky transition states, and release of the product by beta-hydrogen transfer and metal-oxygen bond cleavage. It is valuable to explore heterogeneous catalysts for this reaction, leveraging the versatile active sites in heterogenous catalysts that can be tuned by changing the metal centers, local coordination, support, and solvents. In this contribution, we employed density functional theory (DFT) calculations and ab initio molecular dynamics (AIMD) simulations to design heterogeneous catalysts for the direct coupling of $CO_2$ and $C_2H_4$ using two different catalysts, atomically dispersed metal centers in zeolite and nitrogen-doped graphene. We selected metal centers (or metal dimer centers) that can adsorb and activate $CO_2$ and ethylene in a comparable manner and facilitate the C-C coupling and hydrogen transfer. Some fundamental issues have been identified such as the balance between these two elementary steps, which is further determined by the stability of intermediate (metallactone) and the electronic structure of the metal centers. We further propose different approaches to mitigate the challenge with an emphasis on lowering the activation barrier of the hydrogen-transfer within the metallactone.

**Grant Number:** DE-SC0023448
**Grant Title:** Computational design of heterogeneous catalysts for coupling $CO_2$ and ethylene to manufacture acrylic acid derivatives

**Postdoc(s):** Zaheer Masood, Na Zhang
**Student(s):** Quy Nguyen

## RECENT PROGRESS

**A. Atomically dispersed metal active sites at graphene edges**.

**1. C-C Coupling over metal monomer active sites.** The active site configuration (Fig.1) is structurally mimicking general designs of the homogeneous catalyst with the transition-metal active site anchored to pyridine/phosphine-based ligands, taking advantages of their well-defined multifunctional properties in catalyzing the reaction.

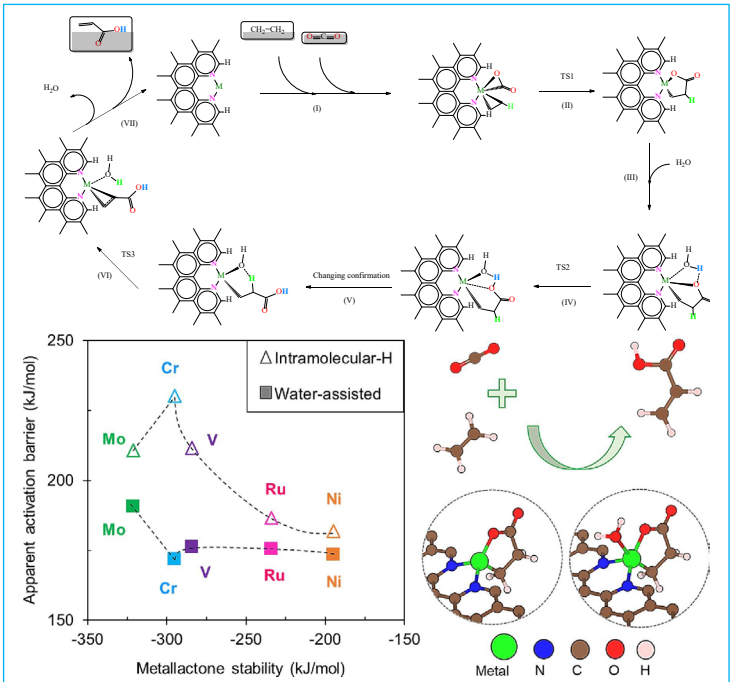


Figure 1. Schematic of the active sites and reaction pathways of $CO_2$-ethylene coupling. The calculated activation barriers over representing metals and key surface intermediate are shown at the bottom panel.

There are three key steps of the reaction on the heterogeneous catalysts, which include: i) the co-adsorption of $CO_2$ and $C_2H_4$ on the active site of catalysts; ii) the C-C coupling of adsorbed reactants to form the metallactone intermediate; and iii) hydrogen transfer and the release of free molecule of the acrylic acid product. A family of catalysts was created by screening a vast range of metal dopants to find the most potential candidates.

The coordination of metal centers was observed with pronounced roles in the activity of catalyst at each elementary step. For instance, the catalysts doped with metal active sites showing higher coordination numbers were observed with better co-activation of $CO_2$ and $C_2H_4$ in the 1:1 molar stoichiometry and the more stable metallactone intermediate. However, the metal centers with higher coordination number are also associated with a more stable metallactone intermediate, which corresponds to a higher activation barrier of the hydrogen transfer and the whole catalytic cycle. The metal center with a balance in either the strength of reactants co-adsorption or the relative stability of intermediates have thus been suggested to improve the activity and selectivity of reaction compared to competitive processes. In all cases, we find that the intramolecular β-H transfer within the metallactone intermediate forming acrylic acid is the rate-determining step due to the highly strained ring of transition state.

To tackle the challenge, we proposed to use water as a "proton-exchanger" to alter the intramolecular β-H transfer by sequential steps of ring-opening, conformation changing, and protonation (Fig. 1). Accordingly, the DFT-based activation barriers are significantly reduced. A few promising active sites embedded in the graphene-based catalysts has been proposed for direct coupling of $CO_2$ and $C_2H_4$ under heterogeneous catalysis.

**2. Coupling reaction on $N_3M$-$MN_3$ dimer anchored on graphene defects site.** As the reaction involves activation of two chemically distinct reactants, we designed $N_3M$-$MN_3$ dual active sites embedded in graphene for achieving a synergistic effect to couple $CO_2$-$C_2H_4$ and hydrogen transfer. We found that on β-H transfer is the rate-limiting step on Ir, Pd, Zn, Cu, Ru and Os dimers. In contrast, C-C coupling step is rate limiting on Rh, Ni and Co dimers. We are in the process of analyzing dimers incorporating different metals.

**B. Active sites embedded in the MFI zeolite for the direct coupling.**

**1. Coupling over single atom centers in MFI.** Zeolite-based catalysts (Fig. 2) were screened based on the thermodynamic free energy profile and classified into three groups. The first group of catalysts do not favor metallactone formation; it either dissociates during geometry optimization into *CO and *$C_2H_4$ or this step requires positive free energy. In the second group of active sites, β–H transfer is the rate-limiting step with significant reaction energy. In the third group of metals, the free energy profiles are downhill (all steps possess negative reaction free energies). These active sites include Sc, Y, Cr, Mo, W, Mn, Tc and Re. This group of metals seems to be promising for this reaction and was further investigated for kinetic studies. The calculated activation barriers for β–H transfer are between 120 and 189 kJ/mol.

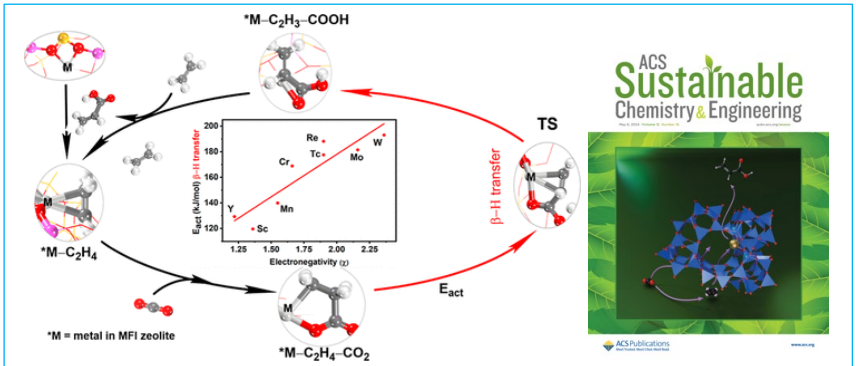


Figure 2. Schematic of the reaction pathway of $CO_2$-ethylene coupling over metal-exchanged zeolite.

Among the catalysts screened here, the Sc-MFI is the most promising one. We thus extend our work toward carboxylation of longer alkenes with $CO_2$ to form unsaturated acids. Functionalization of C=C double in longer alkenes with $CO_2$ has several important applications like copolymer synthesis and functionalization of plastics that possess a small amount of C=C double bonds, the latter of which leads to facile decomposition and upcycling of the plastics. In this work we used butene as a representative alkene and Sc-exchanged MFI zeolite as catalysts. We employed DFT calculations for $CO_2$-butene coupling on Sc-exchanged MFI zeolites and investigated the carboxylation of 1-butene and 2-butene (as representative alkene) with $CO_2$ on Sc-exchanged MFI zeolites using DFT calculations. We find that the carboxylation of alkenes is rate-limited by the β-H transfer. We examined carboxylation at the C1 and C2 positions of 1-butene and cis and trans isomers for 2-butene. Based on activation barriers of β-H transfer, our results demonstrated that Sc-MFI zeolite preferably carboxylates at the terminal position of butene. In the case of non-terminal butene, carboxylation of the trans isomer is more favorable than the cis isomer. Furthermore, we demonstrated that the energy of degenerate orbitals of C, O, and H atoms (involved in β-H transfer) in the metallactone ring can serve as a descriptor for activation energy of β-H transfer.

**2. Coupling on atomically dispersed M-O-M di-atomic sites in MFI zeolites**. In this study we designed a heterogeneous catalyst with multifunctional active sites, M-O-M in MFI zeolite, which was expected to synergistically bind and activate $C_2H_4$ and $CO_2$. In this M-O-M active site, metals (M) are low-coordinated metal sites for binding $C_2H_4$ and $CO_2$; the bridge O (from M-O-M) is a Lewis base site for hydrogen abstraction. The local

confinement also plays a role to stabilize the intermediates and transition states. This unique active site was expected to govern an alternate mechanism, different than the reaction mechanism on single atom active site that we discussed above. Mono-atomic sites mechanism has few limitations of the reaction mechanism — the formation of a five-membered metallactone ring and a high activation barrier for β–H transfer. In this study we investigated reaction mechanism of $CO_2$-$C_2H_4$ coupling on M-O-M diatomic active site in MFI zeolite (M = Zn, Cd, Ag, and Pd), following an alternate mechanism that avoids the formation of a metallactone ring, hence avoiding β–H transfer. In this mechanism, the M-O-M diatomic active site cleaves the C-H bond heterolytically (formation of $*C_2H_3$ and M-O<u>H</u>-M) followed by facilitating C-C coupling of $*C_2H_3$ with $CO_2$ (insertion of $CO_2$ into M-C bond) assisted by the adjacent metal center (formation of $*C_2H_3COO$). Transfer of cleaved hydrogen back to $*C_2H_3COO$ completes the catalytic cycle by forming adsorbed acrylic acid. We demonstrated that changing metal in M-O-M diatomic active sites can regulate C-H cleavage, C-C coupling, and proton transfer steps independently and has the potential to divert reaction mechanisms toward pathways different from the pathways on homogeneous catalysts, opening new routes toward $CO_2$-$C_2H_4$ coupling.

**Publications Acknowledging this Grant in 2021-2024**

*(I) Intellectually led by this grant*


1. Nguyen, Q. P.; Masood, Z.; Wang, B. Mechanistic study of direct coupling of CO2 and C2H4 over atomically dispersed metal at graphene edges. *Chemical Engineering Journal* **2024**, *488*, 150922. DOI: 10.1016/j.cej.2024.150922.

2. Masood, Z.; Nguyen, Q. P.; Wang, B. Computational Design of Metal-Exchanged MFI Zeolites for Coupling CO2-Ethylene to Form Acrylic Acid. *ACS Sustainable Chemistry & Engineering* **2024**, *12* (18), 6960-6968. DOI: 10.1021/acssuschemeng.3c08535.
   Selected as cover of the journal issue


*(II) Jointly funded by this grant and other grants with intellectual leadership by other funding sources*

N/A

James R. McKone

## Comparing Interfacial Proton-Electron Transfer Across the Molecules-to-Materials Design Continuum

James R. McKone, Univ. of Pittsburgh
Giannis Mpourmpakis, Univ. of Pittsburgh & National Technical Univ. of Athens
Ellen Matson, Univ. of Rochester
Veronica Augustyn, North Carolina State Univ.
Ethan Crumlin, Lawrence Berkeley National Laboratory

### Presentation Abstract

Our research team is developing fundamental scientific insights directed at advancing carbon-neutral hydrogen technologies. The focus of our interdisciplinary research program is on critically comparing the chemistry of tungsten polyoxometalate (POM) compounds and nanoparticulate tungsten oxides toward reactions involving proton-coupled electron transfer (PCET). Of relevance to the DOE BES Catalysis Science program, these studies are oriented around electrocatalytic hydrogenations of organic model compounds like TEMPO and azobenzene as well as the oxygen reduction reaction. This presentation will summarize our approach and highlight recent results demonstrating that the dynamics (i.e., kinetic and transport processes) of PCET can vary dramatically even between W-based POMs and extended $WO_x$ nanomaterials that exhibit broadly similar structure and redox thermochemistry. These results subvert the prevailing view of molecular polyoxometalates as atomically precise models of extended oxides and motivate interesting questions about the extent to which POMs or POM-derived solid catalysts exhibit unique physicochemical properties that cannot be replicated in extended oxides, or vice versa.

**DE-SC0023465: From Molecules to Materials: Understanding Hydrogen Activation and Transfer in Metal Oxides**

**PIs:**
(as listed on cover page)

**Postdoc(s):**
Payman Sharifi Abdar, University of Pittsburgh
Haoyi Li, Lawrence Berkeley National Laboratory
Hyunguk Kwon, University of Pittsburgh
Kyung-Eun You, University of Pittsburgh
Noah Holzapfel, North Carolina State University
Zhou Lu, University of Rochester

**Student(s):**
Shreya Thakkar, University of Pittsburgh
Evan Miu, University of Pittsburgh
Andreas Towarnicky, University of Pittsburgh
Mona Abdelgaid, University of Pittsburgh
Michael Spencer, North Carolina State University
Saeed Saeed, North Carolina State University
Eric Schreiber, University of Rochester
Kathryn Proe, University of Rochester

## RECENT PROGRESS

### *Unveiling the Surface Chemistry of $WO_x$ mediated hydrogen spillover*

In a study lead by Crumlin and Mpourmpakis, we have carried out the first measurements of the dynamic surface chemistry accompanying thermochemical hydrogen spillover on $Pt/WO_3$ composites (**Figure 1**) using *operando* ambient pressure XPS. Experiments and calculations suggest the surface chemistry evolves along at least three separate pathways over various temperature ranges. At temperatures between 25 and 50 °C, hydrogen spillover predominates, resulting in the formation of $W^V$ states. At temperatures between 50 and 150 °C, the average oxidation state of W increases slightly, which we attribute to destabilization of spilt-over H atoms in the near surface of the oxide. At temperatures above 150 °C, we observe a significant increase in the prevalence of $W^{IV}$ states attributable to the formation of oxygen vacancies presaging bulk reduction of $WO_3$ to sub-oxide phases.

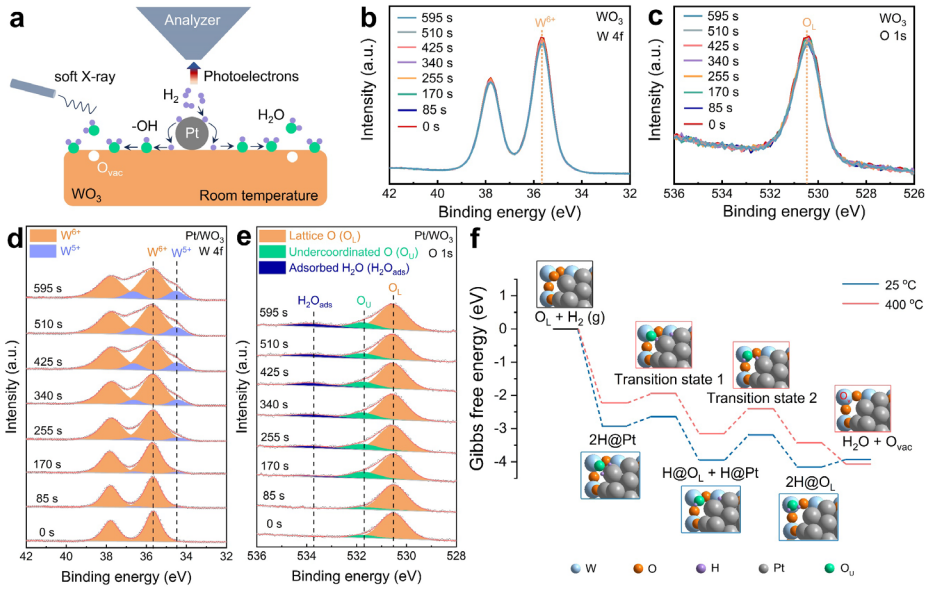


**Figure 1.** Highlights from experimental (AP-XPS) and computational investigation of the surface chemistry of $Pt/H_xWO_3$ composites as they undergo gas-solid hydrogen spillover.

### *Comparative studies of H-H and H-N bond formation on polyoxotungstate clusters*

Matson and McKone collaborated to execute a study (**Figure 2**) aimed at mapping the thermochemistry of nonaqueous PCET using the canonical Keggin polyoxotungstate cluster $[PW_{12}O_{40}]^{4-}$ ($PW_{12}$). Voltammetric measurements were carried out in the presence of organic acids with pKa values from 5 to 40 , which afforded estimates to be made of the relevant hydrogen bond dissociation free energies in the range of 40–50 kcal $mol^{-1}$ for the reduce, protonated cluster. This makes the $H_2PW_{12}$ cluster very similar to $H_2$ in terms of the thermodynamic reactivity of its H equivalents. Indeed, further measurements were made demonstrating that the $PW_{12}$ cluster slowly evolves $H_2$ even after the addition of a single equivalent of protons and electrons, implying the compound engages in bimolecular H-H coupling at low driving force. Notably, addition of azobenzene instead to the reduced, protonated cluster rapidly generates hydrazobenzene, the partial hydrogenation product, with no evidence for further reduction to aniline even in the presence of a large excess of acid and reducing equivalents.

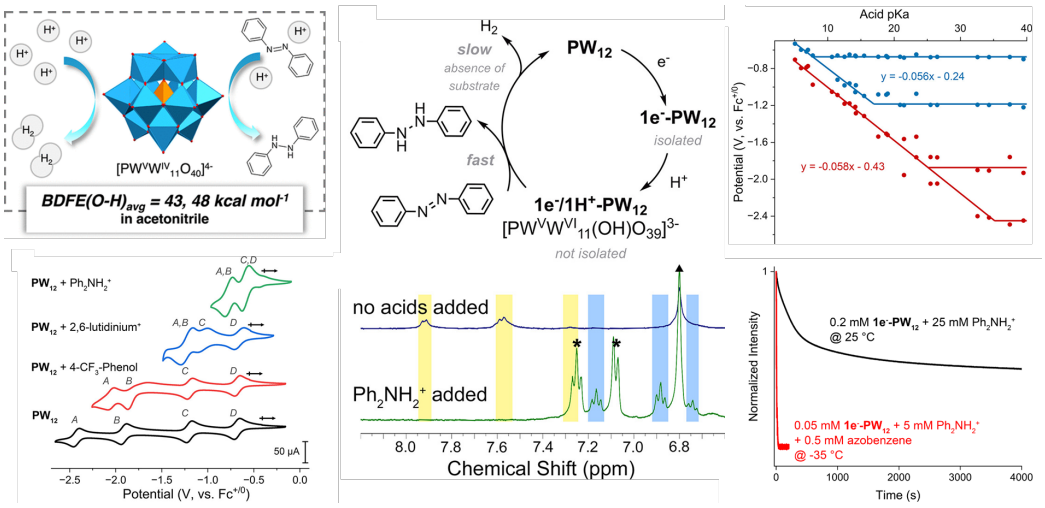


**Figure 2.** Highlights from experimental studies of nonaqueous PCET thermochemistry of a Keggin $PW_{12}$ cluster and its ability to mediate H-H and H-N bond formation.

## *Coupling proton insertion with molecular hydrogenation in colloidal systems*

Of relevance to the development of oxide-based catalysts for slurry-type catalytic hydrogenations, Augustyn, McKone, and Crumlin collaborated on a study aimed at understanding the formation of $H_xWO_3$ through aqueous solution-phase hydrogen spillover (**Figure 3**). Using a Pt catalyst and phosphinic acid ($H_3PO_2$) as a unique chemical reductant, we directly observed the formation of $H_xWO_3$ using *in-situ* optical spectroscopy and X-ray diffraction measurements. The reduction was observed to proceed in two distinct steps, each of which conformed well to a classical model describing the nucleation and propagation of phase-boundaries in the solid state. Further measurements were made to demonstrate the ability to hydrogenate TEMPO, a common model H acceptor, which resulted in rapid and complete removal of H atoms from $H_xWO_3$. This two-step spillover-hydrogenation sequence amounts to net hydrogen transfer that is catalytic in Pt and $WO_3$

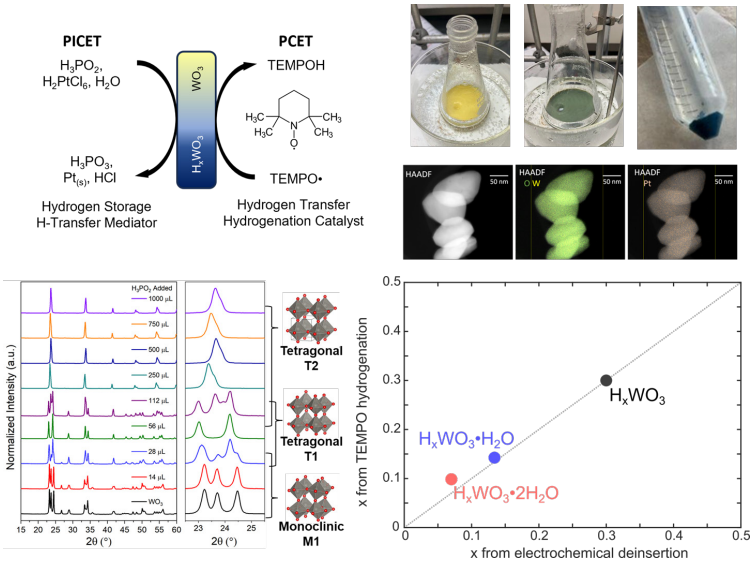


**Figure 3.** Highlights from experimental investigations of Pt/$H_xWO_3 \cdot nH_2O$ composites as colloidal hydrogen transfer mediators.

surface sites and stoichiometric in bulk $WO_3$. Notably, hydrated phases of $WO_3$ were found to accept markedly smaller amounts of hydrogen than the anhydrous phase under otherwise identical conditions—work is ongoing to understand whether this difference is attributable to thermodynamics or kinetic/transport limitations in the system.

### *Coupling proton insertion with molecular hydrogenation in electrochemical systems*

In a separate and closely related study, McKone and Augustyn have developed a chemical reaction platform that we call *electrochemical looping hydrogenation* (**Figure 4**). In this system, electrocatalytic water electrolysis is coupled with molecular hydrogenation in a two-step sequence, with $H_xWO_3$ acting as a hydrogen transfer mediator. This reaction system has been successfully implemented in continuous and recirculated configurations, and the latter has been used to characterize the kinetics of proton-electron transfer from $H_xWO_3$ to hydroxy-TEMPO in aqueous and nonaqueous conditions. Notably, the rate of H-transfer was found to be identical for hydrogenations carried out in water and in toluene, which strongly implicates a mechanism involving neutral hydrogen-atom transfer (HAT).

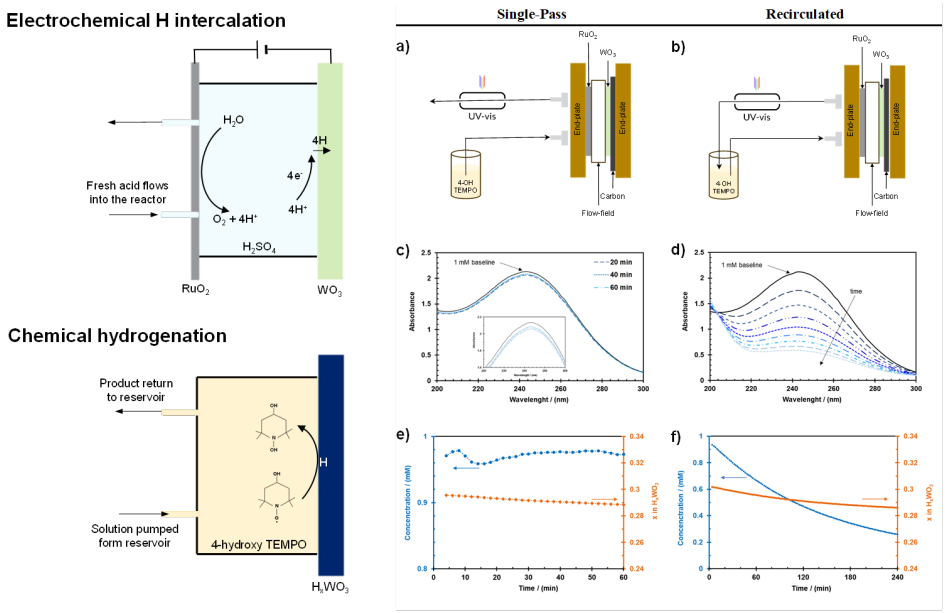


**Figure 4.** Highlights from experimental work demonstrating the concept of electrochemical looping hydrogenation using $H_xWO_3$ bronze phases as an inorganic solid-state H-transfer mediator.

### *Bridging the Molecules-to-Materials design continuum with carbon-supported clusters*

Finally, in work-in-progress led by McKone and Matson (**Figure 5**), we have used straightforward wet impregnation methods to anchor the polyoxotungstate cluster $W_{10}O_{32}^{4-}$ onto conductive carbon supports. Additional thermal treatments of these POM/C composites results in aerobic oxidation of the organic counterions, yielding first molecular-scale aggregates with limited long-range order and then ultra-fine $WO_3$ nanoparticles. These POM/C and $WO_x$/C composites can be characterized with respect to their reactivity toward electrocatalytic PCET using rotating-disk electrode voltammetry, thereby enabling direct apples-to-apples comparisons between molecular and extended oxides. Catalytic activity towards the oxygen reduction reaction was found to increase as the POM was

decomposed into the bulk oxide, implying that some feature of the surface chemistry or bulk electronic structure of the extended solid is integral to the catalytic mechanism.

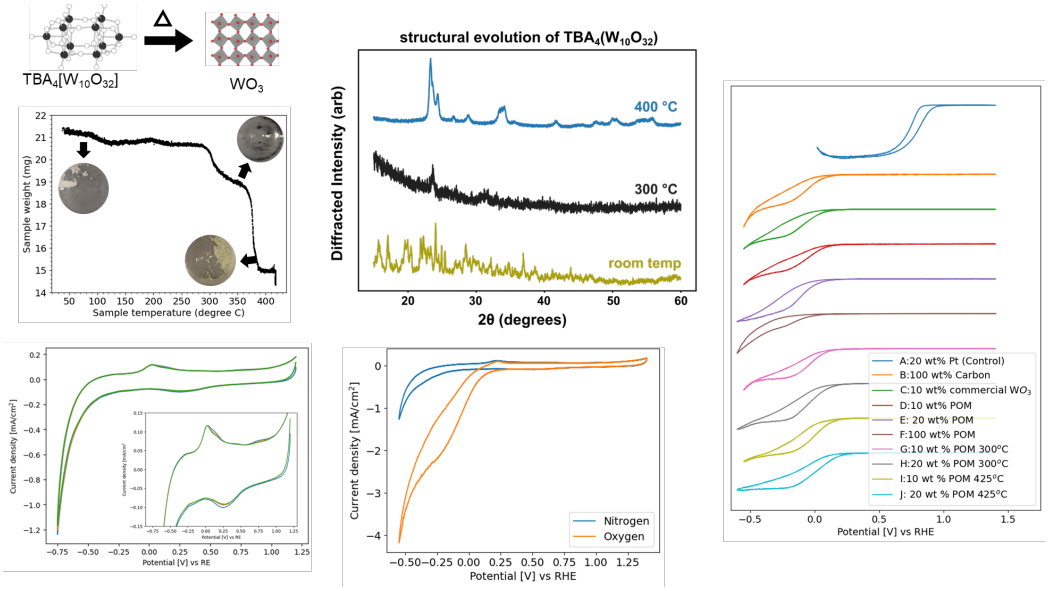


**Figure 5.** Highlights from work in progress on electrocatalytic oxygen reduction using carbon-supported polyoxotungstates before and after aerobic thermal treatments to convert them into amorphous and crystalline $WO_x$ nanoparticles.

## Publications Acknowledging this Grant in 2021-2024

*(I) Intellectually led by this grant*

- Miu, E.V.; McKone, J.R.; Mpourmpakis, G.; Global and Local Connectivities Describe Hydrogen Intercalation in Metal Oxides*; Phys. Rev. Lett.* ***2023***, 131, 108001.
- Proe, K. R.; Schreiber, E.; Matson, E. M.; Proton-coupled electron transfer at the surface of polyoxovanadate-alkoxide clusters*; Acc. Chem. Res.* **2023**, *12,* 1602–1612.
- Schreiber, E.; Brennessel, W. W.; Matson, E. M.; Regioselectivity of H-atom uptake at the surface of reduced polyoxovanadate clusters; *Chem. Sci.* **2023**, *14*, 1386-1396.
- Lu, Z.; Cooney, S.; McKone, J.; Matson, E. Selective Hydrogenation of Azobenzene to Hydrazobenzene via Proton-Coupled Electron Transfer from a Polyoxotungstate Cluster *JACS Au* **2024**, 4, 1310–1314.
- Li, H.; Abdelgaid, M.; Paudel, J.; Holzapfel, N.; Augustyn, V.; McKone, J.; Mpourmpakis, G.; Crumlin, E. *Operando* Unveiling of Hydrogen Spillover Mechanisms on Tungsten Oxide Surfaces **2024**, *under revision.*
- Holzapfel, N.; Chagnot, M.; Sharifi Abdar, P.; Paudel, J.; Crumlin, E.; McKone, J.; Augustyn, V. Solution-Phase Synthesis of Platinum-Decorated Hydrogen Tungsten Bronzes for Hydrogen Atom Transfer from Oxides to Molecules **2024**, *under revision.*

*(II) Jointly funded by this grant and other grants with intellectual leadership by other funding sources*

- Spencer, M.A.; Holzapfel, N.P.; You, K-E.; Mpourmapkis, G.; Augustyn, V. Participation of electrochemical inserted protons in the hydrogen evolution reaction on tungsten oxides *Chem Sci*. **2024**, 15, 5385–5402.

## Cross-Scale Modulation of Electrocatalysts for Hydroxide Exchange Membrane Water Electrolysis

Sen Zhang
Department of Chemistry, University of Virginia

### Presentation Abstract

Crucial to sustainable energy future is the ability to manipulate important chemical reactions for the production and conversion of clean hydrogen ($H_2$) fuel and renewable carbon-based chemicals through the development of advanced catalysts. Well-defined nanocrystals with atomically precise surfaces and interfaces allow us to bridge the knowledge gap between conventional single-crystal bulk materials and powder catalysts to achieve a new and in-depth understanding of structure-catalytic property relationships. In this presentation, I will first highlight how the surfaces and interfaces of nano- and sub-nano catalysts can be precisely controlled at the atomic level to optimize catalytic performance in the oxygen evolution reaction (OER) and hydrogen evolution reaction (HER), both of which are integral to water electrolyzers. I will also emphasize how modulating nanocrystal-ionomer interfaces can enhance integration of catalysts into hydroxide exchange membrane water electrolyzers (HEMELs). This integrated approach, combining controlled synthesis across scales, in-situ structural characterization, and theoretical modeling for catalyst design, will be discusses.

**DE-SC0023443: Fundamental Studies of Catalytic Sites and Catalyst/Membrane Integrations for Advanced Hydroxide Exchange Membrane Electrolyzers**

**PIs:** *Sen Zhang, T. Brent Gunnoe, Charles Machan, Huiyuan Zhu, William A. Goddard III, Jingguang G. Chen, Yushan Yan*
**Postdocs:** *Macarena Alférez, Yizhen Chen, Qiang Gao, Soonho Kwon, Sameeta Sahoo, Wenjuan Shi, Zhenhua Xie*
**Students:** *Chris Chapman, Elizabeth Johnson, Mollie Morrow, Charles Musgrave, Daniel Musikanth, Nathaniel Nichols, Alexandra Oliveira, William Porter, Chris Webber, Chenxin Yang, Yuanqi Liu*
**Affiliations(s):** *Division of Chemistry and Chemical Engineering, California Institute of Technology; Department of Chemical Engineering, Columbia University; Department of Chemical and Biomolecular Engineering, University of Delaware*

### RECENT PROGRESS

#### *OER catalyst development*

PGM-free OER electrocatalyst is critical to the development of advanced HEMELs. Three types of OER electrocatalysts have been developed for this project.

[1] Single atom catalysts with well-defined and modulated coordination structures have been studied by the Zhang and Goddard groups. The design of advanced electrocatalysts is often hindered by uncertainties in identifying and controlling the active surfaces and catalytic centers within heterogeneous materials. We developed single-site Co catalysts, substitutionally doped into surface-controlled $TiO_2$ anatase nanocrystals, for the enhanced OER (Fig. 1). Grand canonical quantum mechanics (GC-QM) calculations reveal that the kinetics of the OER, following an adsorbate evolution mechanism, is markedly influenced by the coordination environment of Co. The simulations suggest significantly higher turnover frequencies when Co is doped into the {001} surfaces of $TiO_2$ compared to the {101} surfaces. Consistent with the computational findings, experimental results show that Co-doped $TiO_2$ nanoplates with selectively exposed {001} surfaces exhibit enhanced current densities and turnover frequencies compared to $TiO_2$ nanobipyramids with {101} surfaces. This study highlights the synergy between theoretical calculations and precision synthesis in the development of more effective catalysts.

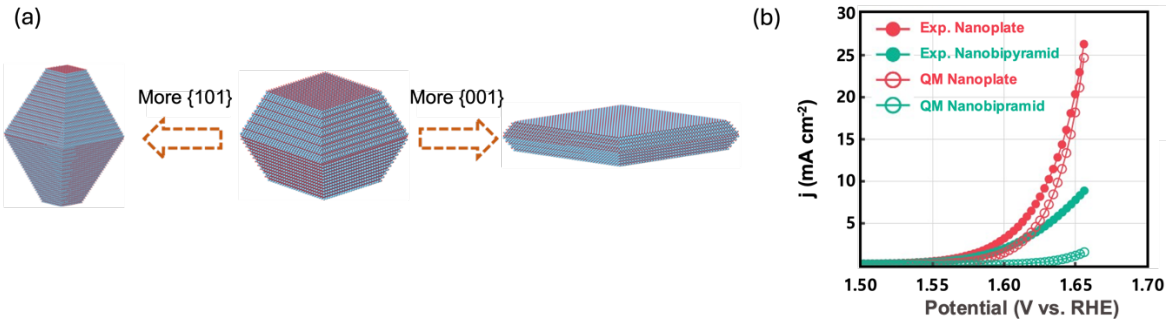


Figure 1. (a) $TiO_2$ nanocrystals with controlled surface facet exposure (more {001} in nanoplates and more {101} in nanobipyramids). (b) Experimental OER current density comparison with theoretical results obtained from GCQM calculations.

[2] Low nuclearity nanocluster catalysts have been studied by the Zhang, Chen, Yan, and Goddard groups. The NiFeOOH nanoclusters hosted on $TiO_2$ brookite nanorods were synthesized by the Zhang group. As shown in Fig. 2a and b, the unique NiFeOOH/$TiO_2$ heterostructure makes NiFeOOH, an active catalytic component for the OER, stabilized in the surface of $TiO_2$ nanorods in a form of small nanoclusters (~1 nm) to maximize their active surface area. The NiFeOOH/$TiO_2$ exhibited encouraging OER activity and durability in rotating disk electrode (RDE) testing condition, superior to pure NiFeOOH. To understand the atomic structure of NiFeOOH/$TiO_2$ under the OER condition, *in situ* X-ray absorption spectroscopy (XAS) measurements were conducted at the Ni and Fe K-edges on NiFeOOH/$TiO_2$ ($Ni_xFe_y$, x/y=1/3 and 3/1) catalysts, as well as monometallic $FeO_x/TiO_2$ and $NiO_x/TiO_2$ catalysts by the Chen group. The catalysts were tested at various conditions: open circuit potential (OCP), and at 1.3, 1.52, 1.55, 1.6, and 1.7 V vs. RHE. The Fe and Ni oxidation states under OER potentials were found to be sensitive to Ni/Fe ratio. The NiFeOOH/$TiO_2$ ($Ni_xFe_y$, x/y=3/1) catalyst with the better performance was found to show enhanced Fe-Ti interaction when the potential becomes more positive. With the revealed atomic structure, the Goddard group conducted Grand Canonical Quantum Mechanics (GCQM) calculation to understand the reaction mechanism as well as the $TiO_2$-NiFeOOH interfacial effect on the OER kinetics. The Yan group implemented the NiFeOOH/$TiO_2$ OER catalyst at the anode of a single-cell HEMEL.

The assembled HEMEL delivered a low cell voltage (~1.7 V) at 500 mA $cm^{-2}$ in 1 M KOH electrolyte at 60 °C with a low decay rate of 0.17 mV $h^{-1}$, as shown in Fig. 2c and d.

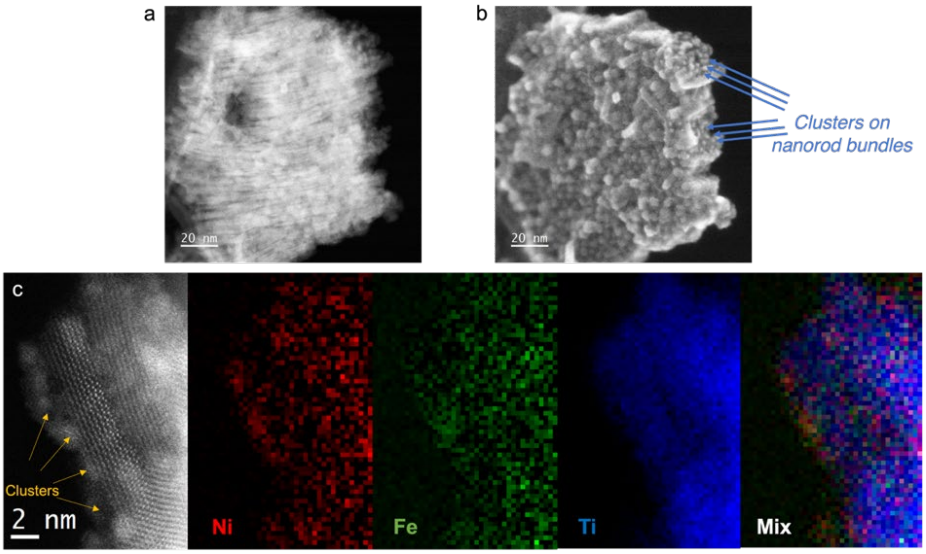


Figure 2. STEM HAADF image (a), STEM secondary electron (SE) image (b), and STEM electron energy loss spectroscopy (EELS) elemental mapping (c) of NiFeOOH-$TiO_2$ after stability test. The nanorods form assembled superstructures with porous channels.

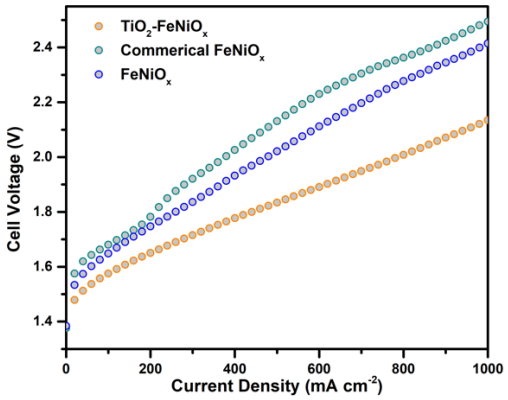


Figure 3. LSVs of Pure-water HEMELs with NiFeOOH-$TiO_2$ OER catalyst and $NiFeO_x$ OER catalyst.

[3] Building on our strategy to use bis-*N*-donor capping arene ligands to make carbon-supported electrocatalysts for water oxidation, we seek to make related ligands that are dianionic. We anticipate that strongly donating dianionic ligands will enhance catalyst stability and reduce over potential for water oxidation. Gunnoe has achieved initial success isolating the proligand shown in Fig. 4. After isolation of new transition metal complexes (initially, we are targeting Fe, Co and Ni complexes), we will study homogeneous electrocatalytic water oxidation as well as new carbon-supported materials for OER. Goddard has provided calculations that indicate that covalent attachment of capping arene Co complexes to carbon materials should reduce the activation barrier for rate limiting

O–O bond formation during catalytic OER. Further, their calculations predict sites of covalent attachment that will optimize catalytic activity. To test these predictions, Gunnoe has been working to synthesize amine containing capping arene ligands that can be covalently bonding to carbon materials through diazonium grafting. Gunnoe has recently isolated 6-$^{NO2}$FP, which is a precursor to reduction to form an amine.

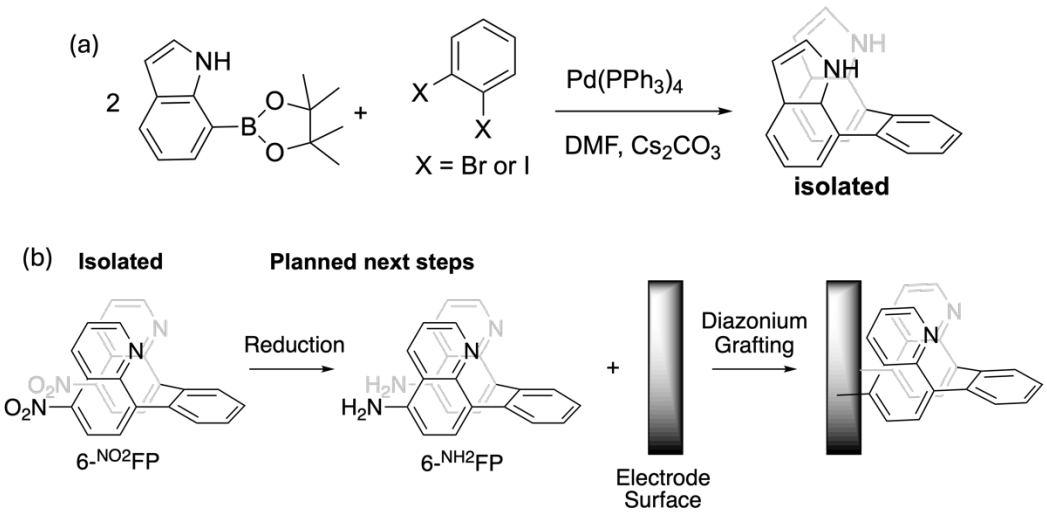


Figure 4. (a) Isolation of new capping arene ligand has been accomplished. (b) Isolation of new capping arene ligand with nitro functionality as a precursor to covalent attachment to electrode surfaces.

### *HER catalyst development*

The first focus of our study is to elucidate the coordination and interfacial effects that enable the further minimization of PGM loading for the HER in HEMELs. The second focus is to develop strategies to improve PGM-free HER catalyst efficiency.

[1] The Chen group led a study of developing mono-layer Pt and Au on transition metal nitrides (TMNs) supports. TMNs are a class of electrocatalyst support materials similar to transition metal carbides (TMCs) with the advantage of avoiding the issues arising from surface deposits of graphitic carbon during synthesis. We explored the feasibility of using TMN-supported Pt and Au as alkaline HER electrocatalysts. TMN of Ti, V, Ta, Mo and W were synthesized by reacting the corresponding films in the flow of ammonia gas at 850 °C for 10 hours. Monolayer coverage of Pt or Au was deposited onto the TMN films using physical vapor deposition in a UHV system equipped with XPS to verify surface compositions. Results from the preliminary study established a volcano-like trend between the electrochemical HER activity and hydrogen binding energy (HBE) calculated from DFT for well-characterized thin films of TMNs and TMN-supported catalysts. Pt/TiN was found to be the most active among the metal-modified TMN thin films.

[2] Pt nanoparticles supported on 2-dimensional (2D) $Ce_2O_3$ nanosheets were studied by the Zhang, Chen, and Goddard groups (**Fig. 5**). The creation of metal-metal oxide interfaces is an important approach to fine-tuning catalyst properties through strong interfacial interactions. The interfaces between Pt and $CeO_x$ are found to improve Pt surface energetics for the HER within an alkaline

electrolyte. The Pt-$CeO_x$ interfaces are formed by depositing size-controlled Pt nanoparticles onto a carbon support already coated with ultrathin $CeO_x$ nanosheets. This interface structure facilitates substantial electron transfer from Pt to $CeO_x$, resulting in decreased hydrogen binding energies on Pt surfaces, and water dissociation for the HER, as predicted by the DFT calculations. Electrochemical testing indicates that both Pt specific activity and mass activity are improved by a factor of 2 to 3 following the formation of Pt-$CeO_x$ interfaces. This study underscores the significance and potential of harnessing robust interfacial effects to enhance electrocatalytic reactions.

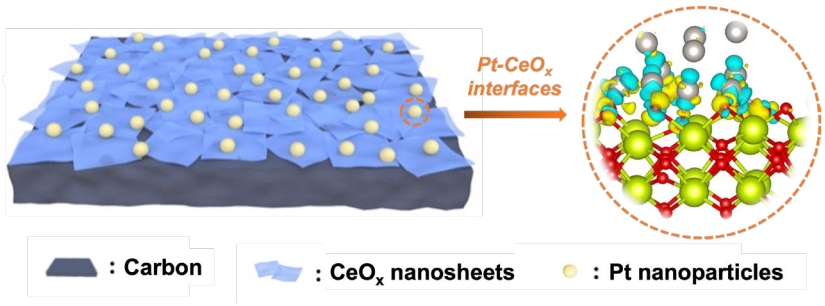


Figure 5. Schematic illustration of Pt-CeOx interfacial effect, which enables effective electron transfer from Pt to CeOx, leading to lowered hydrogen binding energies on Pt surfaces and promoting water dissociation for the HER within an alkaline electrolyte.

[3] Co and Ni corroles HER catalysts were studied by the Machan group (Fig. 6). Corroles are a ring-truncated version of porphyrin and as a result are trianionic supports, rather than dianionic. In the initial stages of this project, we have synthesized and isolated 5,10,15-tris(pentafluorophenyl)corrole (tfpc), as well as the corresponding Co(III) complex with a triphenylphosphine ligand. Currently, we are testing deposition conditions with this compound for the HER, as well as using nucleophilic aromatic substitution with primary amines (n-butylamine) to functionalize the fluorophenyl rings. This will allow us to test the conditions required for covalent attachment strategies, as well as model the effect of covalent attachment on catalytic activity. As a point of comparison, we have also synthesized and isolated a series of metal phthalocyanines (Mn-Cu), which are a dianionic ligand framework. For heterogenized molecular catalysts, Machan and Zhu groups are working together to immobilize these complexes onto carbon through covalent binding to make heterogeneous materials for the HER.

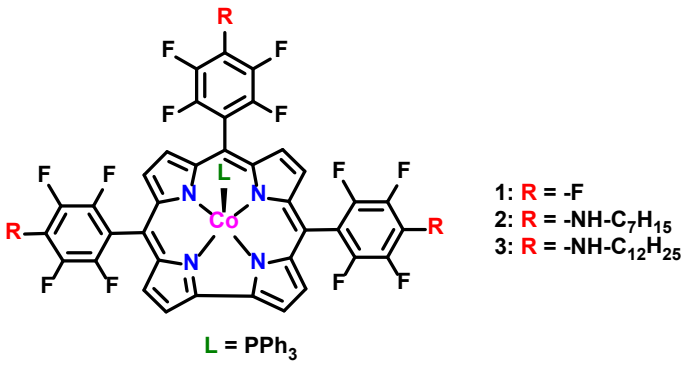

Figure 6. Cobalt corroles studied as bifunctional catalysts for water splitting at pH 14.

**Publications Acknowledging this Grant in 2021-2024**

*(I) Intellectually led by this grant*


1. Shen-Wei Yu, Soonho Kwon, Yizhen Chen, Zhenhua Xie, Xiner Lu, Kai He, Sooyeon Hwang, Jingguang G. Chen,* William A. Goddard III,* and Sen Zhang*, "Construction of a Pt-CeOx Interface for the Electrocatalytic Hydrogen Evolution Reaction", *Advanced Functional Materials* **2024**, *34*, 2402966.
2. Lei Shi, Huiyuan Zhu*, "Transition-metal nitrides: Pioneering a new era in the hydrogen evolution reaction", *Chem Catalysis* **2024**, *4*, 100919.
3. Qiang Gao, Xue Han, Yuanqi Liu, Huiyuan Zhu*, "Electrifying Energy and Chemical Transformations with Single-Atom Alloy Nanoparticle Catalysts", *ACS Catalysis* **2024**, *14*, 6045–6061.
4. Weijie Zhang, Sen Zhang, "Catalysts: Combinatorial heterogeneous catalysis", Encyclopedia of Condensed Matter Physics,Elsevier B.V., 2023, DOI: 10.1016/B978-0-323-90800-9.00201-8.
5. Weijie Zhang, Sen Zhang, "Catalysts: Materials", Encyclopedia of Condensed Matter Physics , Elsevier B.V., 2023, DOI: 10.1016/B978-0-323-90800-9.00202-X.
6. Sameeta Sahoo, Elizabeth K. Johnson, Xiangru Wei, Sen Zhang, and Charles W. Machan*, "Exploring the Role of Polymer Interactions During Water Electrolysis under Basic Conditions with Bifunctional Cobalt Corroles ", *Energy Advance* **2024**, *3*, 2280-2286


*(II) Jointly funded by this grant and other grants with intellectual leadership by other funding sources*


7. William N. Porter, Kevin K. Turaczy, Marcus Yu, Hansen Mou, and Jingguang G. Chen*, "Transition metal nitride catalysts for selective conversion of oxygen-containing molecules ", *Chemical Science* **2024**, *15*, 6622-6642.

8. Chang Liu, Wonil Jung, Sungho Jeon, Grayson Johnson, Zixiao Shi, Langqiu Xiao, Shengsong Yang, Cheng-Yu Chen, Jun Xu, Cherie R. Kagan, **Sen Zhang**, David A. Muller, Eric A. Stach, Christopher B. Murray,* Thomas E. Mallouk*, "Stabilizing alkaline fuel cells with a Nb-doped brookite $TiO_2$ cathode support", *Cell Reports Physical Science* **2024**, *5*, 102090.

## Brian M. Tackett

### Ambient Temperature Electrocatalytic Alkane Dehydrogenation: Considerations from Atomic-Scale to Device-Scale

B. M. Tackett (Lead PI), B. W. Boudouris, R. P. Gounder, J. P. Greeley, J. T. Miller,
Purdue University, Chemical Engineering

### Presentation Abstract

Electrocatalytic dehydrogenation of light alkanes to alkenes has potential to drastically decarbonize production of olefins, which are among the most ubiquitous industrial chemical building blocks. Achieving this vision will require fundamental developments of the electrocatalytic process from the atomic scale to the device scale. Our team has recently made significant progress on both fronts, which will be discussed in this presentation. At the atomic scale, we combined state-of-the-art electrochemical mass spectrometry with density functional theory calculations to paint a vivid picture of propane activation at the Pt electrode in acidic aqueous electrolyte at room temperature. We found a maximum fractional coverage of 0.15 C/$Pt_{atom}$ at 0.30 V vs RHE, and we revealed the identity of the surface adsorbate to be deeply dehydrogenated, but surprisingly maintained an intact C3 backbone, enabling reversible desorption. At the device scale, gas diffusion electrodes are required for continuous alkane electrolysis, due to their low solubility in aqueous electrolytes. We developed a new gas diffusion electrode configuration that overcomes the most significant challenges for the most commonly used carbon-based and PTFE-based gas diffusion layers (GDLs). Specifically, we made the first self-conductive, hydrophobic, all-polymer GDL by coating a commercial PTFE membrane with a porous conductive polymer. This enabled excellent resistance to electrolyte flooding, with commercially relevant current densities sustained over more than 20 hours. These new insights and innovations are critical for achieving low-temperature alkane dehydrogenation, which will lay the foundation more broadly for decarbonized electrochemical manufacturing.

### *DE SC0023257*: Low-Temperature Electrocatalytic Manufacturing of Essential Chemical Building Blocks

**Postdoc(s):** Ashmita Biswas, Sanghyun Ahn, Viswanath Pasumarthi
**Student(s):** Ashutosh Bhadouria, Brandon Bolton, Joseph Heil, Hwiyoon Noh, Hyunki Yeo, Ryoh-Suke Sekiya, Enes Akyildiz, Hyunki Yeo, Durvesh Parab, Wei-Ling Huang

### RECENT PROGRESS

#### *Propane Activation on Pt Electrodes at Room Temperature: Quantification of Adsorbate Identity and Coverage*

The rise in shale gas availability in North America over the past 15 years has dramatically increased the use of light alkanes, especially ethane and propane, as chemical feedstocks to make higher value products. Paraffinic C—H bond activation of these molecules, therefore, represents the first chemical processing step needed to produce many chemical goods, such as olefins, alcohols, oxygenates, and polymers. In 2019 alone, global annual production capacities for ethylene and propylene reached 185 and 130 million metric tons, respectively, while global market demand for propylene oxide is forecasted to grow by ~6% from an estimated 10 million metric tons in 2023. Traditionally, thermal reactors are used to activate these light alkanes, and for the case of propane,

thermal catalytic processes have been commercialized. However, thermal C—H bond activation is energy- and carbon-intensive, and non-oxidative catalytic propane activation suffers from coking, requiring frequent oxidative regeneration. These factors result in thermal propane dehydrogenation having a high carbon footprint of 1.5 kg $CO_2$ equivalent ($CO_2e$) per kg. Lowering the operating temperature for C—H bond activation of light alkanes could alleviate these issues but will inherently lead to a decrease in conversion and reaction rate for these endothermic routes. Alternatively, an electrochemical pathway can enable C—H bond activation at room temperature and ambient conditions, using electrochemical potential as the reaction driving force. Furthermore, combining an electrochemical process with increasingly available renewable energy can drastically reduce carbon emissions and help transition to a decarbonized chemical industry.

Enabling such an electrocatalytic process first requires an understanding of propane adsorption at an electrocatalyst. Past work on electrochemical alkane activation focused on total oxidation for hydrocarbon fuel cells, which successfully demonstrated activation of neutral, non-polar hydrocarbon species on electrocatalysts in aqueous, acidic environments. The studies relied on either potentio-dynamic or galvano-dynamic experiments to oxidize adsorbed species, which provided some insights about the amount and identity of adsorbates via charge analysis. Typically, product quantification was performed off-line, if at all, which limited understanding of the nature of adsorbed species. Early electrochemical mass spectrometry studies enabled more detailed analysis of adsorbate identity, but the focus remained on total oxidation, favoring higher temperatures and strongly acidic electrolytes, with little insights into activation processes that could benefit chemical manufacturing. More recently, a new chip-based electrochemical mass spectrometer (ECMS) system enabled operando detection of gaseous products derived from methane, ethane, and butane, which were activated via electrocatalytic oxidation sweeps at room temperature. The works showed that Pt adsorbs these species, with similar trends to those presented in prior literature, and demonstrated the utility of the ECMS to enable real-time, quantitative measurement of desorbed gaseous species produced during alkane activation. Herein, we use a similar approach to discover critical insights about the nature of propane adsorption and activation on Pt electrodes at room temperature. Specifically, we rely on features of the chip-based ECMS that enable real-time (~1s response) product quantification with 100% collection efficiency to closely couple charge passed with speciation of desorbed products. The chip interface also facilitates reactant gas pulse/purge procedures, detailed in prior work, that are analogous to temperature programmed reaction/desorption experiments in thermal catalysis.

In this work, we combine ECMS and density functional theory (DFT) calculations to answer the following questions: (i) Under what conditions does propane adsorb on Pt? (ii) What is the fractional coverage of propane-derived adsorbate species? and (iii)

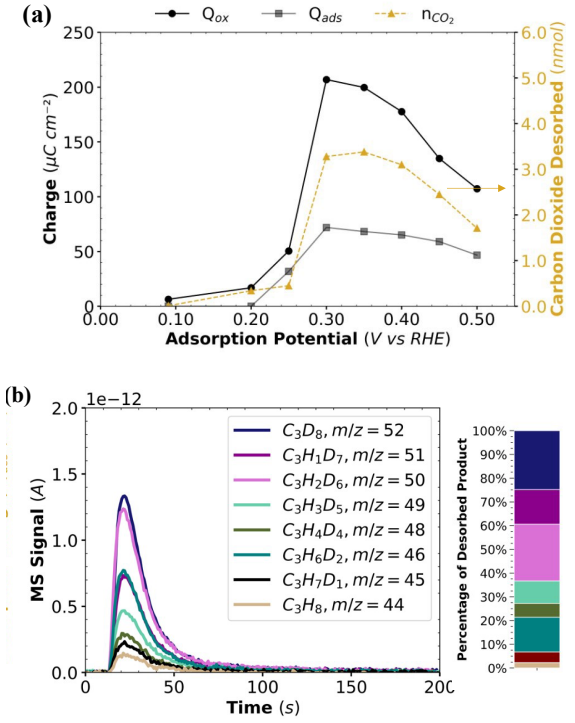


**Figure 1.** (a) Extent of propane adsorption on Pt in 1.0 M $HClO_4$ at room temperature, using three independent measurement techhniques enabled by electrochemical mass spectrometry. (b) Speciation of products desorbed from Pt following propane adsorption during a deuterium exchange. The majority of products have at least 6 H replaced by D.

What does the propane-derived adsorbate look like? We find that at 20 °C, in 1 M $HClO_4$ saturated with 100% propane at 1 atm, Pt can adsorb propane with a maximum coverage of 0.15 $C/Pt_{atom}$ (0.05 propane/$Pt_{atom}$) at 0.30 V vs RHE. The degree of adsorption is strongly dependent on $H^*$ coverage, yielding greater propane coverage at potentials that favor $H^*$ oxidation (**Figure 1**). Potentiodynamic sequences were used to determine the degree of dehydrogenation of surface species, revealing deeply dehydrogenated adsorbates that surprisingly tend to not break C—C bonds. We confirm the distribution of dehydrogenated adsorbates with a deuterium exchange experiment, revealing that C3 adsorbates with eight and six hydrogens removed, respectively, are the most abundant surface species (**Figure 1**). This result was rationalized with DFT calculations that reveal accessible energetics for deep dehydrogenation on Pt sites. Further, activation energies for C—C and C—H bond breaking of deeply dehydrogenated species were compared to reveal kinetic favorability for C—H bond activation. The methodology and insights from this work provide a framework to study and optimize room temperature electrocatalytic reactions of light alkanes to enable decarbonized chemical manufacturing.

***Conducting Polymer Transforms Hydrophobic Porous Membranes into Robust Gas Diffusion Layers in Electrocatalytic Applications***

The demand for sustainable chemical production is rapidly increasing as carbon-emission regulations tighten. At the same time, the rapid global influx of solar and wind energy facilitates decarbonized chemical synthesis routes via electrification. In particular, electrochemical manufacturing is a promising way to produce valuable chemical commodities, powered by renewable energy. A substantial fraction of these envisioned decarbonized electrochemical pathways involve gaseous reactants, which require electrodes that incorporate gas diffusion layers (GDLs) in continuous flowing electrolyzers to mitigate low solubility and the slow diffusion of reactants. The most prominent example of this technology in recent work is for the electrochemical $CO_2$ reduction reaction (CO2RR), where GDLs enable conversion of $CO_2$ into high-value products at much greater current densities, compared to standard electrodes in batch cells. This is achieved by porous channels in the GDL transporting reactants from a gas stream to continuously replenish $CO_2$ in the aqueous phase near the electrode-electrolyte interface. Critically, the GDL also acts as a conductive current collector to facilitate electron transfer through the external circuit, making porous carbon paper the traditional GDL material of choice. The major challenge for this technology, however, is to prevent the liquid electrolyte from filling the gas channels and increasing mass transport resistance of gaseous reactant to the electrocatalyst surface – this is known as flooding in the GDL. This often causes undesired side reactions, and it decreases energy efficiency. In traditional carbon-based GDLs, flooding tends to occur at high reaction rates after several hours of operation, posing a critical barrier to desired performance for industrial chemicals manufacturing.

Recently, porous polytetrafluoroethylene (PTFE) membranes were used to replace carbon-based GDLs, taking advantage of the chemical stability and inherent hydrophobicity of PTFE. Due to the non-conductive nature of PTFE, magnetron sputtering of metal layers was required in previous work to impart conductivity, and this strategy showed enhanced catalytic performance and improved stability in CO2RR when the metal layer was catalytically suitable for the desired reaction. Despite these advances, the typical preparation method of sputtering metal with a thickness of 300 – 500 nm results in complications and drawbacks for general use in electrochemical devices. Most significantly, this configuration impedes progress for CO2RR and other decarbonized electrochemical reactions, due to its severe limitation on electrocatalyst composition and morphology. Rational design of electrocatalysts, relying on structure-function relationships, has resulted in improved performances that employ various metal and alloy particles with a range of sizes, compositions, morphologies, and preferentially exposed facets. But exploiting these concepts in the current configuration of porous PTFE GDL is essentially impossible when

conductivity is established by a sputtered contiguous metal film. Thus, enabling the best catalyst performance in combination with the robust and hydrophobic porous PTFE GDL requires a non-metal conductive layer, which will not contribute to the reaction, is compatible with any electrocatalyst motif, and maintains desired gas diffusion properties. To achieve this, we designed a new GDL structure composed of a porous conductive polymer layer assembled on a microporous PTFE layer in the first demonstration of a self-conductive PTFE-based all-polymer GDL. We selected poly(3,4-ethylenedioxythiophene) (PEDOT) as the conductive layer, to add electrical conductivity, while maintaining the original properties of the PTFE GDL.

In this work, we first synthesized PEDOT doped with $PF_6^-$ (PEDOT:$PF_6$) on commercial PTFE membranes to form a thin, porous, and electrically conductive layer via electropolymerization, resulting in a PEDOT-coated PTFE (PEDOT-PTFE) GDL. The self-conductive GDL was then evaluated in a continuous flowing electrolyzer, with CO2RR as a probe reaction. The CO2RR performance of nanoparticle electrocatalysts assembled in this configuration was evaluated in acidic, neutral, and alkaline electrolytes. Importantly, PEDOT-PTFE GDLs showed comparable results with those of the commercial carbon-based GDL, Sigracet 22bb, during short-term testing. Lastly, CO2RR stability tests were executed at industrially relevant current densities (i.e., –200 mA·cm$^{-2}$), in which PEDOT-PTFE GDLs exhibited remarkable resistance to electrolyte flooding compared to the carbon-based GDL in all electrolytes tested (**Figure 2)**. These results highlight that the PEDOT layer imparts sufficient electrical conductivity to enable reaction on electrocatalyst nanoparticles, while maintaining the best properties of robust porous PTFE. Thus, PEDOT-PTFE can be widely used for any gas-fed electrocatalytic reactions requiring the application of a GDL, while providing better stability than carbon-based GDLs.

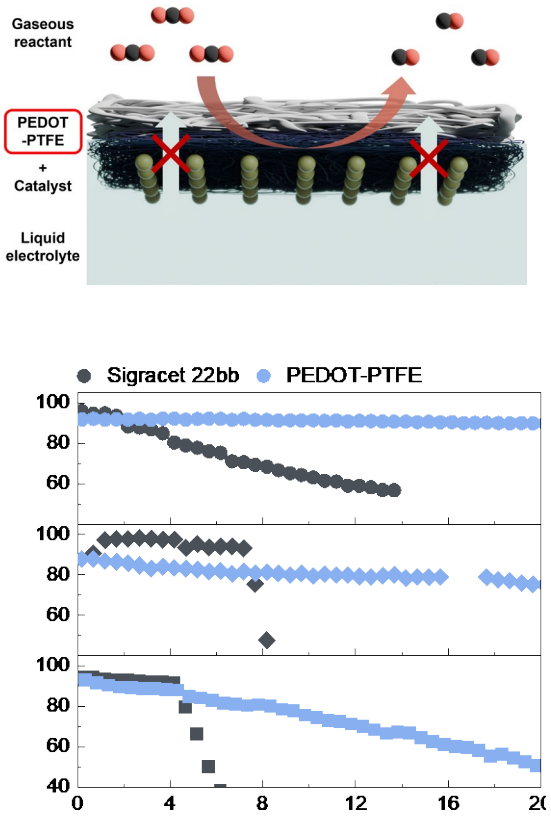


**Figure 2.** (top) Schematic diagram of self-conductive hydrophobic PEDOT-PTFE gas diffusion electrode that is compatible with any metal electrocatalyst. (bottom) Stability testing of conventional carbon-based GDL (Sigracet 22bb) compared to PEDOT-PTFE for electrocatalytic $CO_2$ reduction reaction with 1 mg cm$^{-2}$ Ag nanoparticle catalyst layer.

## Publications Acknowledging this Grant in 2021-2024


(I) 1. Bhadouria, A.; Heil, J. N.; Parab, D. E.; Greeley, J. P.; Tackett, B. M. "Propane Activation on Pt Electrodes at Room Temperature: Quantification of Adsorbate Coverage and Identity." *J. Amer. Chem. Soc.* **2024,** *Under review.*

(I) 2. Noh, H.; Yeo, Y.; Boudouris, B. W.; Tackett, B. M.. "Conducting Polymer Transforms Hydrophobic Porous Membranes into Robust Gas Diffusion Layers in Electrochemical Applications." *Energy Environ. Sci.* **2024,** *Under review.*

(II) 3. Bolton, B. K., Chovatiya, A., Russell, C. K., Daya, R., Trandal, D. S., Wei, L. Reddy, G. K., Kamasamudram, K., Miller, J. T., Schneider, W. F., Gounder R., "Mechanistic Insights into $NH_3$ Oxidation Rate and Selectivity Hysteresis on Pt/$Al_2O_3$ Catalysts." *ACS Catalysis.* **2024**, *Under review.*

Jingguang Chen

## Nitrides of Earth-abundant Metals as Cost-effective Catalysts for Water Electrolysis

Jingguang Chen, Ping Liu, Jose Rodriguez, Peter Khalifah, Kotaro Sasaki, Yugang Zhang
Chemistry Division, Brookhaven National Laboratory

### Presentation Abstract

Hydrogen production by water electrolysis represents the most promising pathway to achieve the DOE Hydrogen Shot objective: "Reduce the cost of clean hydrogen by 80% to $1 per 1 kilogram in 1 decade". Water electrolysis occurs through two half-cell reactions: the hydrogen evolution reaction (HER) at the cathode and oxygen evolution reaction (OER) at the anode. Electrolyzers based on polymer membranes to separate the cathode and anode have advantages of simplicity of operation, and current practical membrane electrolyzers utilize acidic electrolytes because of the availability and reliability of acidic membranes. However, one limiting challenge in acidic HER and OER is the need for stable Pt-group metal (PGM) electrocatalysts, but the high costs and scarcity of these materials make it difficult to meet the DOE targets for cost-effective $H_2$ production.

In the current project we attempt to reduce the cost of catalysts using nitrides of Earth-abundant metals (EAM). The PIs of this proposal have published pioneering work showing that EAM-nitrides can exhibit HER/OER activities comparable to those of PGM catalysts in acidic electrolytes. At present, key knowledge gaps for advancing metal nitride-based electrocatalysts are a lack of fundamental understanding of the following: (1) the correlation between catalyst composition and HER/OER activity; (2) the long-term electrocatalytic stability in acidic electrolyte; (3) the nature of active sites under HER/OER conditions; and (4) reaction mechanisms and descriptors controlling the HER/OER activity and stability.

**Grant or FWP Number:** BNL-CO-060
**Grant Title:** Nitrides of Earth-abundant Metals as Cost-effective Catalysts for Water Electrolysis

**PI:** Lead PI: Jingguang Chen (BNL & Columbia University)
**Postdocs:** Xue Han, Tianyou Mou, Sinwoo Kang, Wenjie Liao
**Students:** Daniela Bushiri, Kevin Turaczy, Wenhao Liu, Dario Lewczyk
**Affiliations:** BNL, Columbia University, Stony Brook University

### RECENT PROGRESS

***Theoretical Prediction and Experimental Verification of IrOx Supported on Titanium Nitride for Acidic Oxygen Evolution Reaction***

Activity, stability, and material cost are three critical factors when designing acid oxygen evolution reaction (OER) electrocatalysts for practical applications. To date, iridium oxide ($IrO_x$)-based materials are the best acidic OER electrocatalysts that can meet the stability requirement under harsh operating conditions. However, high costs and scarcity of Ir limit large-scale applications of $IrO_x$. Therefore, it is imperative to discover

OER electrocatalysts with reduced Ir loading while maintaining their catalytic activity and stability in the acid environment.

Depositing Ir-based materials on a support is a promising method to reduce the overall Ir loading and tune the Ir-support interactions to enhance the OER performance. Transition metal nitrides have been recently identified as promising support materials for electrocatalysts due to their high electrical conductivity and low costs. Particularly, titanium nitride (TiN) holds the merits of metal-like conductivity and excellent resistance to acidic oxidation, making it a promising support for Ir. Several studies have been reported for Ir oxides deposit on TiN in the form of $IrO_2$@Ir/TiN (60 wt. % of Ir on TiN), $IrO_2$@Ir/TiN (40 wt. % of Ir on TiN) and $IrO_2$/TiN. However, these reported electrocatalysts contained a high content of Ir, and their electrocatalytic stability was rather low (<10 hours at 10 mA $cm^{-2}$). Meanwhile, a comprehensive understanding, coupled with theoretical calculations and *in situ* characterization, of the structure-activity-stability correlation to advance the OER performance of TiN-supported Ir and $IrO_x$, remains unclear.

In our study, we develop a framework for designing active and stable materials for acidic OER based on density functional theory (DFT) predictions and proof-of-concept experimental verification of thin films and nanoparticles. A partially oxidized Ir ($IrO_x$) overlayer on a TiN support was selected for DFT calculations to reduce the Ir loading to a few monolayers while maintaining a similar number of active sites. In addition, such a model system also allows direct verification by experimental studies, as recently demonstrated for nitride-supported Pt for the hydrogen evolution reaction. Using the binding energy of *OH (* denotes adsorbed intermediates) as the OER reactivity descriptor for $IrO_x$/TiN, the OER activity was found to be improved by increasing the Ir coverage from one to three monolayers (MLs), and the trend was confirmed by the experimentally synthesized $IrO_x$/TiN film model catalysts. For practical applications, the promising thin film results were extended to powder-based catalysts with $IrO_x$ deposited on TiN nanoparticles ($IrO_x$/TiN NPs). The $IrO_x$/TiN NPs exhibited excellent acidic OER performance, requiring a minimum overpotential of 293 mV at 10 mA $cm^{-2}$ and long-term stability of 250 hours with neglect degradation. The mass activity of $IrO_x$/TiN with a reduced Ir loading of 40 $\mu g_{Ir}$ $cm^{-2}$ achieved 270.8 A $g_{Ir}^{-1}$, significantly higher than the benchmark commercial $IrO_2$ (C-$IrO_2$). When further integrated into a proton exchange membrane water electrolyzer (PEMWE) cell with the $IrO_x$/TiN catalyst at a low Ir loading of 0.2 mg $cm^{-2}$, only 1.69 V was required to achieve a current density of 1 A $cm^{-2}$, lower than that using C-$IrO_2$ (above 1.8 V). *In situ* X-ray absorption spectroscopy (XAS) characterization further revealed the transition of Ir to $IrO_x$ under OER conditions, as well as the presence of the Ir-Ti bond to highlight the interaction between $IrO_x$ and TiN. According to the DFT results, the direct Ir-Ti bonding tuned the binding strength of *OH on the $IrO_x$ layer, leading to a higher OER activity than bulk $IrO_2$ while still maintaining high stability under the acidic OER condition. Overall, DFT calculations of the overlayer models predict an overpotential trend of 1ML > 2ML > 3ML $IrO_x$ over the TiN substrate, which is then verified by experiments over TiN thin films with the corresponding coverages of $IrO_x$. These findings provide guidance to prepare the nanoparticle catalysts for more practical and commercial applications, and $IrO_x$/TiN NPs show a better catalytic performance toward acidic OER than C-$IrO_2$. More importantly, this study highlights the importance of integrating theoretical prediction and experimental studies of well-

characterized thin film catalysts to facilitate the development of commercially viable powder-based nanoparticle OER catalysts with enhanced activity and promising stability.

***Trends in Electrocatalytic Stability and Hydrogen Evolution Activity of Pt Supported on Transition Metal Nitrides***

As a high energy density fuel and a key component in wide-ranging commercial applications, hydrogen fulfills a critical role in modern society. Despite ongoing efforts to promote the production of green hydrogen, it continues to be produced predominantly through carbon-intensive processes such as steam methane reforming. Utilizing electricity to produce $CO_2$-free $H_2$ creates opportunities for storing excess energy from renewable sources as a transportable, energy-dense fuel and reducing the environmental footprint of chemical processes requiring $H_2$. Efforts towards economical production of green $H_2$ has made the hydrogen evolution reaction (HER) from water electrolysis one of the most studied electrochemical reactions.

The commercial sector is dominated by alkaline water electrolyzers, proton exchange membrane (PEM) electrolyzers, and solid oxide electrolysis cells. Of these, the PEM electrolyzer remains popular for large-scale applications due to the availability of high-performance Nafion™ membranes as well as operation at near ambient temperature conditions, ease of cell design, and high load flexibility for grid balancing. These advantages enable PEM electrolyzers to achieve high current densities and hydrogen purities while offering flexibility across wide ranging applications and scales. However, this technology is still hindered by its high cost of operation partially due to its dependency on scarce platinum (Pt) group metal electrocatalysts. Pt is the benchmark material for HER catalysis in PEM electrolyzers. However, due to its high cost and sensitivity to poisoning by trace impurities in the feed water, the search for more robust and abundant alternatives continues to garner significant interest.

By incorporating carbon and nitrogen atoms into the interstitial sites of earth-abundant transition metals, the resulting transition metal carbides (TMCs) and nitrides (TMNs) show unique catalytic properties. For example, TMCs such as $Mo_2C$ and WC have shown bulk electronic properties similar to Pt, resulting in competitive HER activity. In addition, these TMCs have also been found to synergize with Pt to enhance HER activity with a decreased Pt loading. Previous experimental work and density functional theory (DFT) calculations of metal-modified TMC thin films have established trends for HER activity in both acidic and alkaline conditions. Consistent with the Sabatier's principle, Pt-modified TMCs showed the highest HER activity because their surfaces neither too strongly nor weakly bind to hydrogen. However, synthesizing clean and high surface area TMCs, which requires reactions with hydrocarbons at high temperatures, can be challenging due to the accumulation of graphitic surface carbon. This accumulation can prevent the direct interaction between Pt and TMC, thus reducing catalyst activity.

TMNs are a similar class of materials as TMCs, but they avoid the accumulation of surface carbon because extra surface nitrogen atoms recombine to desorb as molecular $N_2$ at the TMN synthesis temperatures. Like TMCs, these materials also demonstrate unique catalytic properties and synergistic interactions with Pt. Studies have found Pt-modified WN and NbN to exhibit Pt-like HER activity, and Pt/TiN has been shown to have higher methanol oxidation activity than bulk Pt metal. However, a systematic understanding of the general trends in the electrochemical stability and activity of TMN-based electrocatalysts is lacking at present.

In our study we investigated the trend in the stability of TMN thin films (TiN, VN, $Ta_3N_5$, MoN, and WN) over a wide range of applied potentials and pH values, which revealed that all of these TMNs should be stable under the conditions of acidic HER. Further studies were performed to determine the relationship between the acidic HER activity and hydrogen binding energy (HBE) for TMNs and metal-modified TMNs to determine whether HBE is a useful descriptor for TMN-based electrocatalysts. TMN thin films were prepared and modified with one monolayer (ML) of Pt and gold (Au) to study the synergistic effects of these precious metals with the TMN substrates under electrochemical conditions using linear sweep voltammetry. The results were compared to DFT calculations to establish a trend between HER activity and HBE values. Powder catalysts were studied to investigate how the trend can be extended to more commercially applicable powder catalysts, while X-ray absorption spectroscopy (XAS) was utilized to characterize the powder catalysts under *in-situ* electrocatalytic conditions.

**Publications Acknowledging this Grant in 2021-2024**


1. H. Mou, J.J. Jeong, B. Lamichhane, S. Kattel, Z. Zhuang, J.H Lee, Q. Chang and J.G. Chen, "Trends in Electrocatalytic Activity and Stability of Transition Metal Nitrides", *Chem Catalysis*, 4 (2024) 100867.
2. X. Han, T. Mou, A. Islam, S. Kang, Q. Chang, Z. Xie, X. Zhao, K. Sasaki, J.A. Rodriguez, P. Liu, and J.G. Chen, "Theoretical Prediction and Experimental Verification of IrOx Sup-ported on Titanium Nitride for Acidic Oxygen Evolution Reaction", *Journal of the American Chemical Society,* 146 (2024) 16499-16510.
3. T. Mou, D.A. Bushiri, D.V. Esposito, J.G. Chen, and P. Liu, "Rationalizing Acidic Oxygen Evolution Reaction over $IrO_2$: Essential Role of Hydronium Cation", *Angewandte Chemie International Edition*, 63 (2024) e202409526.
4. X. Zhao, H. Cheng, X. Chen, Q. Zhang, C. Li, J. Xie, N. Marinkovic, L. Ma, J.-C. Zheng, and K. Sasaki, "Multiple Metal-nitrogen Bonds Synergistically Boosting the Activity and Durability of High-Entropy Alloy Electrocatalyst*", Journal of American Chemical Society*, 146 (2024) 3010-3022.
5. W.N. Porter, H.A. Mera, W. Liao, Z. Lin, P. Liu, J.R. Kitchin and J.G. Chen, "Controlling Bond Scission Pathways of Isopropanol on Fe- and Pt-Modified Mo2N Model Surfaces and Powder Catalysts", *ACS Catalysis*, 14 (2024) 1653-1662.
6. D.A. Bushiri, A.F. Baxter, L. Odunjo, D.V. Fraga-Alvarez, Y. Yuan, J.G. Chen and D.V. Esposito, "Oxide Encapsulated Ruthenium Oxide Catalysts for Selective Oxygen Evolution in Unbuffered pH Neutral Seawater", *ACS Applied Energy Materials,* 7 (2024) 5479-5489.
7. V. Mehar, E. Huang, R. Shi, N. Rui, R. Rosales, I. Waluyo, A. Hunt, P. Liu and J.A. Rodriguez, "Microscopic investigation of $H_2$ reduced $CuO_x$/Cu(111) and ZnO/$CuO_x$/Cu(111) inverse catalysts: STM, AP-XPS and DFT studies", *ACS Catalysis,* 13 (2023) 9857-9870.
8. K. Turaczy, W. Liao, H. Mou, N.N. Nichols, P. Liu and J.G. Chen, "Correlating hydrogen binding energy with HER activity of Pt and Pd modified-$Mo_2N$ surfaces", *ACS Catalysis*, 13 (2023) 14268-14276.

Phillip J. Milner

## Engaging Molecular Radicals for Super-Reducing Solid-State Photocatalysis

Phillip Milner[1], Andrew Musser[1], Jianheng Ling[1], Amy Vonder Haar[1], Kiser Colley[1], Juno Kim[1], Jaehwan Kim[1], Katrina Doherty[1], Yujing Wang
[1]Department of Chemistry and Chemical Biology, Cornell University, Ithaca, NY, 14850

### Presentation Abstract

Transforming recalcitrant halogenated molecules such as chloroarene persistent organic pollutants (POPs) and halogenated greenhouse gases (GHGs) is an important but challenging component of environmental remediation efforts. Combining electricity and light (electrophotocatalysis, EPC) is an exciting approach to access the deeply reducing potentials required for single electron transfer to these inert molecules, yet EPC is held back by the poor stability and mechanistic ambiguity of current homogeneous systems. Supported by the DOE, we have explored whether the incorporation of EPCs into redox-active polymeric materials can improve their stability and lead to enhanced catalysis and altered selectivity. In this talk, we will discuss how we have successfully incorporated perylene diimides into redox-active polymers to produce the first known heterogeneous EPCs. Critically, we also provide the first concrete evidence that these catalysts operate via pre-complexation with chloroarene substrates, decoupling their catalytic activity from lifetime effects of traditional photocatalysts. Building upon these findings, we identify iminoimides as a new class of even more deeply reducing catalysts, providing promise for the reductive upconversion of inert halogenated compounds.

**Grant or FWP Number: DE-SC0024199**

**PI(s):** Phillip Milner, Andrew Musser
**Postdoc(s):** Juno Kim
**Student(s):** Jianheng Ling, Amy Vonder Haar, Kiser Colley, Jaehwan Kim, Katrina Doherty, Yujing Wang

## RECENT PROGRESS

***Development of the first deeply reducing, electrophotocatalytically active perylene diimide polymers that can reduce chloroarenes with high efficiency***

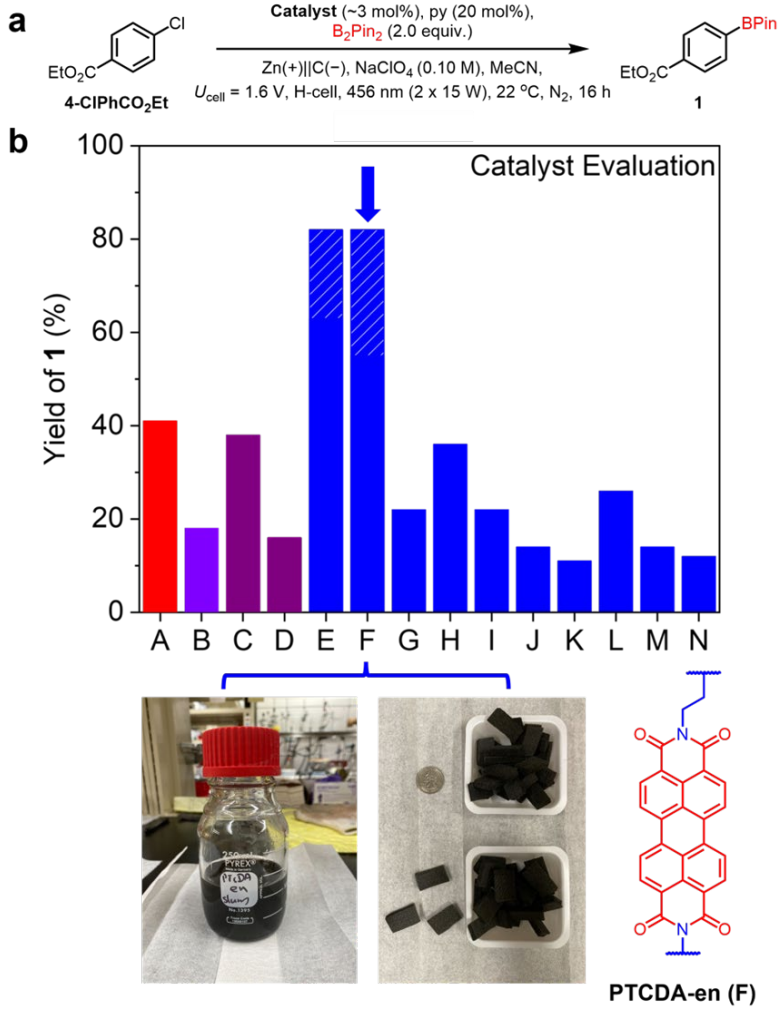


***First mechanistic insight that electrophotocatalysis proceeds via pre-complexation***

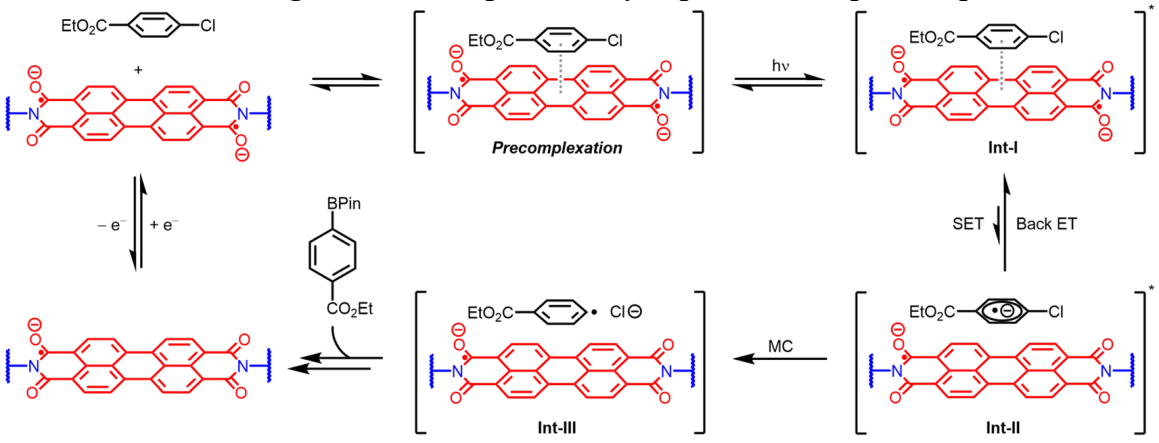

## *Identification of iminoimides as potent reductive electrophotocatalysts*

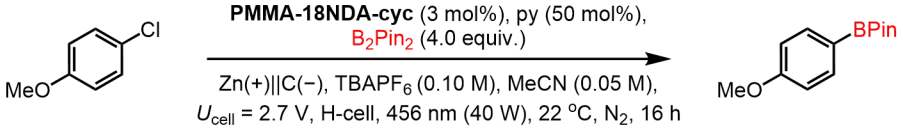


| Entry | Variation | Conversion (%) | NMR Yield (%) |
|---|---|---|---|
| **1** | **None** | **100** | **56** |
| 2 | No PMMA-18NDA-cyc | <5 | 0 |
| 3 | No light | <5 | 0 |
| 4 | No applied voltage | 0 | 0 |

## *Reductant-free generation of catalytically active radical anions*

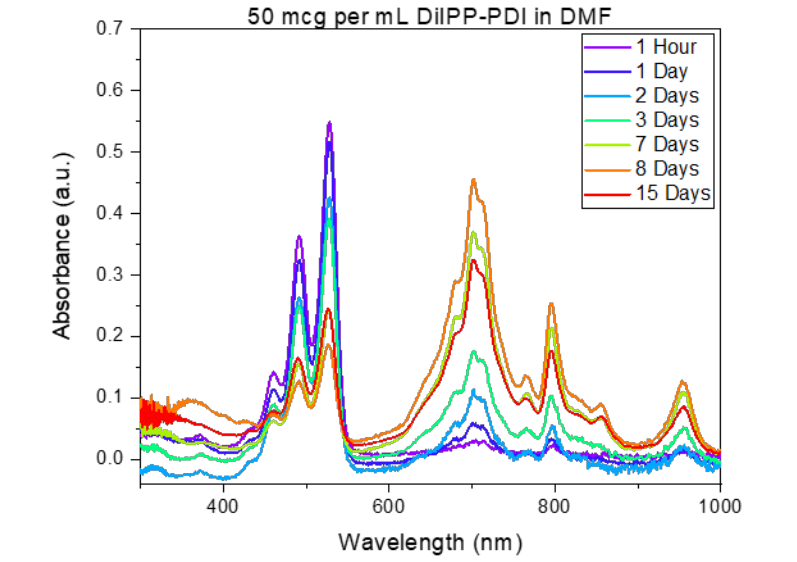

***Unraveling photophysical pathways in MOFs relevant to catalysis***

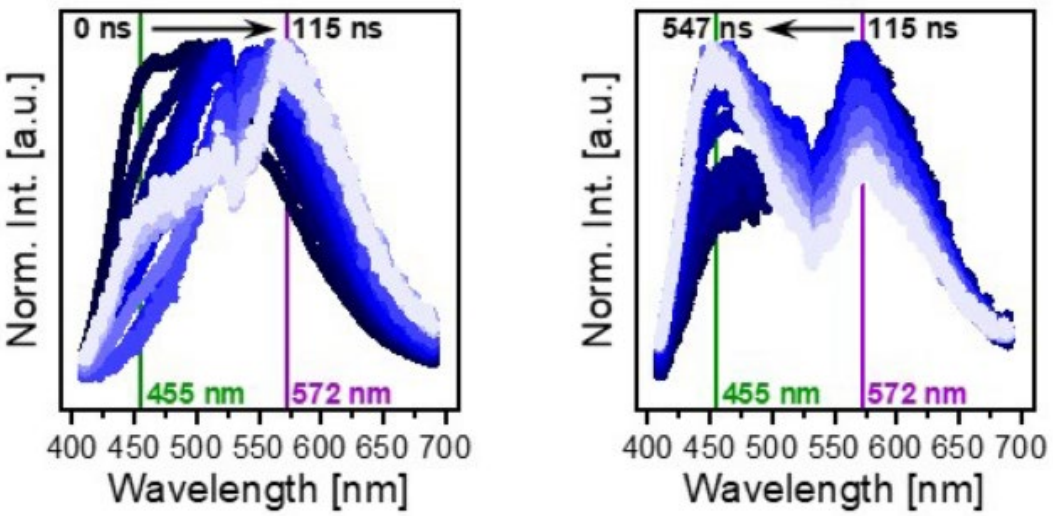


**Publications Acknowledging this Grant in 2021-2024** (project started in 2023)

*(I) Intellectually led by this grant*

1) Griffin, S. N.; Bain, D. C.; Halder, A.; Tsangari, S.; Milner, P. J.; Musser, A. J. Unveiling Long-Lived Dual Emission in a Tetraphenylethylene-Based Metal–Organic Framework. *MRS Commun.* **2024**, *Accepted.*
2) Kim, J.; Ling, J.; Lai, Y.; Milner, P. J. Redox-Active Organic Materials: From Energy Storage to Redox Catalysis. *ACS Mater. Au*, **2024**, *4*, 258–273. *Invited submission to the "Rising Stars in Materials Science" special issue.*
3) Ling, J.; Vonder Haar, A. L.; Colley, K. Z.; Kim, J.; Musser, A. J.; Milner, P. J. Polymer Connectivity Governs Electrophotocatalytic Activity in the Solid State. *Submitted to Nat. Chem.*

*(II) Jointly funded by this grant and other grants with intellectual leadership by other funding sources*

1) Bayu I. Z. Ahmad, Kiser Z. Colley, Andrew J. Musser, Phillip J. Milner*. A Fully Light-Driven Approach to Separate Carbon Dioxide from Emission Streams. *Submitted to Nature.*

Umit S. Ozkan

# Electrocatalysis on Heteroatom-doped Carbon (CNx) Catalysts: Beyond Oxygen Reduction Reaction

Umit S. Ozkan[1], Dishari Basu[1], Niharika Vennala[1], Anant Sohale[1], Aravind Asthagiri[1], Anne Co[2]
[1]Department of Chemical and Biomolecular Engineering, The Ohio State University
[2]Department of Chemistry and Biochemistry, The Ohio State University

## Presentation Abstract

Heteroatom-doped carbon nanostructures (CNx) have been studied extensively for electrocatalytic Oxygen Reduction Reaction (ORR) in PEM fuel cells due to their economic viability over precious metal-based catalysts. Recently, we have shown that CNx catalysts are also active for anodic reactions such as Oxygen Evolution Reaction (OER) and Bromine Evolution Reaction (BER). In this reporting period, we have focused on expanding the electrocatalytic applications of CNx beyond ORR and enhancing the ORR activity of CNx. We have demonstrated an enhancement in ORR activity of CNx by facile electrochemical bromine incorporation using BER and anodic activation using OER. We investigated this enhancement effect using a series of characterization techniques such as XPS, Raman, and NEXAFS. Our results show that post BER enhancement effect likely stems from an increase in pyridinic N content and favorable charge distribution on carbon adjacent to it. In the quest of exploring various electrocatalytic applications of CNx, we have found CNx to be highly active for electrocatalytic Iodide Oxidation Reaction (IOR) in acidic medium. We have also found an interesting application of CNx, removal of p-nitrophenol (a USEPA priority pollutant) using low temperature electrochemical hydrogenation. Further advancing our studies to explore the nature of active sites of CNx for ORR, we also investigated the $CO_2$ poisoning of CNx catalysts for ORR. Using a combination of electrochemical measurements, NAP-XPS and DFT studies we have found that poisoning effect of $CO_2$ for ORR was likely due to $HCO_3$ and $CO_3$ species on various CNx sites. Thus, our work is aimed at gaining a fundamental insight into the multifunctional electrocatalytic activity of CNx for various reactions such ORR, halogen evolution and electrochemical hydrogenation, via characterization techniques, molecular probes and DFT studies.

**Grant Number:** DE-FG02-07ER15896; **Grant Title:** Fundamental studies of the multifunctional electrocatalysis on heteroatom-doped carbon (CNx) catalysts
**PIs:** Umit Ozkan (PI), Aravind Asthagiri (Co-PI), Anne Co (Co-PI)
**Students :** Dishari Basu, Niharika Vennala, Anant Sohale

## RECENT PROGRESS

### *Effect of electrochemical BER treatment on ORR:*

It was found that the ORR performance was significantly enhanced after an electrochemical BER treatment. Experiments at different potentials, different HBr concentrations as well as by simply

soaking the catalyst in HBr were carried out. Figure 1 shows that the ORR enhancement is not observed in case of soaking of the catalyst in HBr without electrochemical treatment and or in case of potential treatment without the $Br^-$ ions. There was no enhancement effect with the potential treatment below the thermodynamic BER potential in the presence of HBr, either. It is only seen post 1.07V potential treatment (BER thermodynamic potential) in HBr. This indicates that electrochemical BER treatment is essential for the enhancement of ORR.

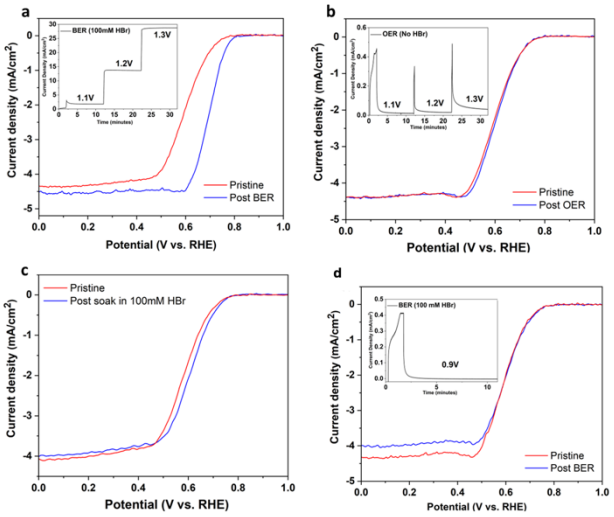


*Figure 1: . Cathodic polarization plots collected at 1000 rpm in $O_2$-saturated 0.1 M $HClO_4$ (10 mV/s, 800 µg catalyst/$cm^2_{Geometric}$) over a) CNx pre- and post-BER up to 1.3 V with 100 mM HBr and b) CNx pre and post potential application up to 1.3 V without HBr c) CNx pre- and post- 100 mM HBr soaking without potential application d) CNx pre- and post- anodic potential hold at 0.9V for 10 mins in 100mM HBr*

Figure 2 shows N1s XPS data indicating an increase in pyridinic-N post BER. Pyridinic N are considered as the markers for active sites for ORR [1]. Br 3d XPS spectra was used to study the interaction of bromine with CNx. Bromine is incorporated into CNx through strong C-Br ionic bonds and charge transfer complexes with carbon which could also be responsible for the enhancement of ORR. NEXAFS N K-edge analysis performed in collaboration with scientists from Stanford synchrotron Radiation Lightsource (SSRL) showed the distortion in the structure of the CNx attributing to the defects, supported by the Raman data. Additionally, NEXAFS C-K edge data of post BER-ORR samples showed increase in oxygenated carbon compared to pristine ORR, suggesting the possibility of α-carbons adjacent to pyridinic nitrogen being responsible for enhancement of ORR.

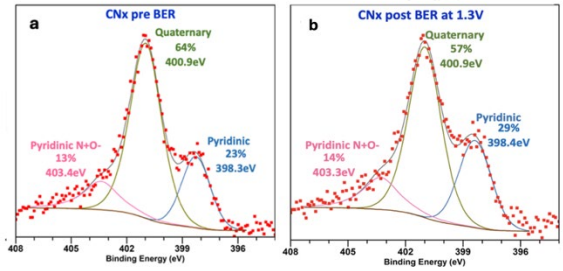


*Figure 2: Post-treatment N1s spectra for CNx subjected to: a) ORR (control sample)b) ORR followed by BER at 1.3V for 10 minutes with 100 mM HBr in the electrolyte*

***Effect of OER treatment on ORR :***

In this work we have studied the effect of anodic potential treatment over 1.23 V (OER) on ORR. The effect could be enhancement or degradation of ORR depending on the potential up to which OER anodic sweep is given and treatment time. The anodic potentials play a very key role in influencing the ORR. Additionally, the effect of potential hold time at various potentials and corresponding effect on ORR were examined. At higher anodic potentials, there is a degradation effect of ORR. The possible reasons for this behavior through increasing potential and time were investigated with the aid of spectroscopy techniques, such as XPS, Raman and NEXAFS.

### *Electrocatalytic Iodide Oxidation Reaction (IOR) on CNx catalyst:*

In our study, we have explored CNx as a catalyst for iodide oxidation reaction (IOR) in acidic medium. The redox potential for $I^-/I_{2(s)}$ is around 0.54 V[2]. CNx has shown good activity for IOR with negligible overpotential and significant anodic currents at different molarities of HI (supply of iodide species ) in the electrolyte. Figure 3 demonstrates the increase in IOR current with increase in supply of iodide ions indicating that the current is due to reaction associated with the iodide species. The control experiments on bare glassy carbon were performed, showing that the reaction was indeed due to electrocatalytic reaction on CNx. Additionally, CNx catalyst post IOR is analyzed to study iodine species formed due anodic potential treatment in HI.

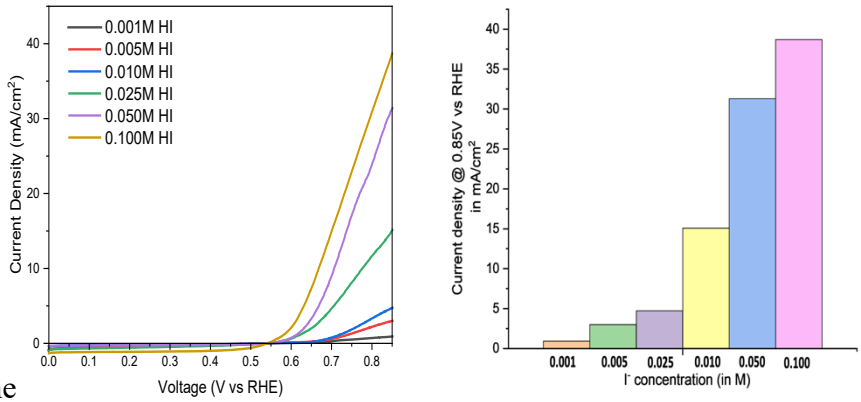


*Figure 3:a)Plots of capacitance-corrected LSV sweeps up to 0.85Vvs Reversible Hydrogen Electrode (RHE) at different HI molarities in an electrolyte of 0.1 M $HClO_4$. (At 1000 rpm, 10 mV/s) b) Current density @0.85 at different HI molarities*

UV analysis indicates the presence of molecular iodine on CNx post IOR with a broad peak at around 460nm [3] whereas the pristine CNx has no trace of this peak. XPS analysis of I 3d region also indicates the presence of the molecular iodine on IOR-treated CNx. This analysis signifies the possible formation of molecular iodine post electrochemical iodide oxidation reaction. Further investigation on the active sites and the electrochemistry of iodine species on CNx are part of the future plans.

### *Exploring the use of CNx for electrocatalytic hydrogenation of aromatics*

Electrochemical hydrogenation of organic compounds is an area which has been explored as a greener and safer alternative to conventional thermal hydrogenation reactions[4]. P-nitrophenol is a carcinogenic ground water contaminant and has been designated as a “priority pollutant” by USEPA[5]. Our preliminary results indicate that CNx shows considerable activity for removal of p-nitrophenol by electrochemical hydrogenation in acidic medium, without the use of any reducing agents such as $NaBH_4$ or external high-pressure hydrogen gas, even at room temperature and atmospheric pressures. There are many challenges for the low temperature electrocatalytic hydrogenation of these compounds especially from the competitive hydrogen evolution reaction (HER) at reducing voltages. Further studies are needed to optimize and improve the catalytic activity and explore the active sites of CNx for electrochemical hydrogenation reactions

***Investigation of $CO_2$ poisoning of CNx for ORR: An Experimental and DFT study***

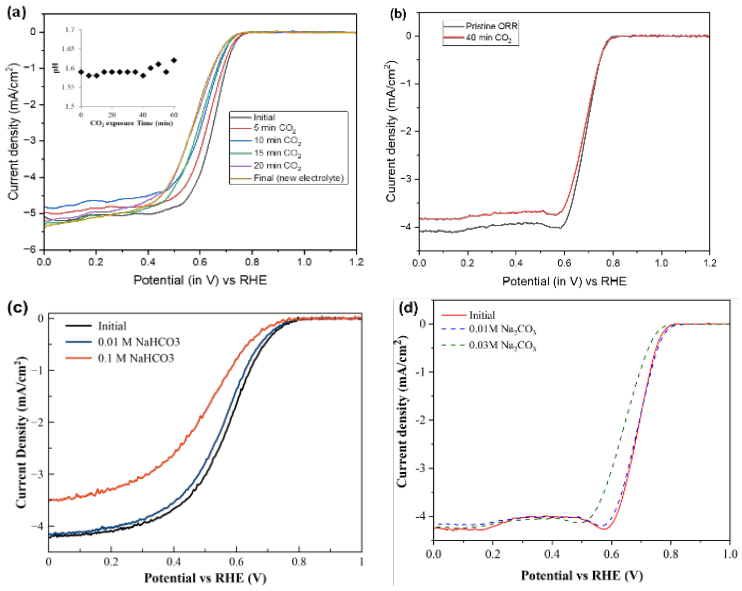


*Figure 5: Polarization curves for ORR in 0.1 M $HClO_4$ ($O_2$ saturated, 1000 rpm, 10 mV/s and 800 $\mu g_{catalyst}$ /$cm^2_{geometric}$) (a) bubbling $CO_2$ through electrolyte (b) gas phase exposure to dry $CO_2$ (c) addition of bicarbonate (d) addition of carbonate*

We have shown CNx to be resistant to common poisons such as CO, $H_2S$, and CN for ORR[6, 7], making it important to find new poison probes. This study aims to investigate the active sites of heteroatom-doped carbon nanostructures (CNx) for ORR with $CO_2$ as a poison probe. A combined experimental-DFT study was used to investigate the species responsible for this poisoning effect on CNx. Bubbling $CO_2$ in the electrolyte showed poisoning effect of ORR on CNx whereas gas phase exposure to dry $CO_2$ did not (Figure 5 a-b). Moreover, addition of bicarbonate ($HCO_3$) and carbonate ($CO_3$) salts to the electrolyte also showed similar poisoning effect (Figure 5 c-d) suggesting that $HCO_3$ and $CO_3$ could be the poisoning species. NAP-XPS measurements indicated a reduced adsorption of $O_2$ on $CO_2$-poisoned-CNx or diminished access to the all the same sites as pristine CNx. DFT calculations predicted that $HCO_3$ is favored adjacent to the N species on several CNx site models and $CO_3$ is favored on pyrrolic sites. These $HCO_3$ species were believed to block and delay the initial step of ORR on several sites such as armchair, zigzag, and basal quaternary. This study suggests the possibility of new ORR active sites on CNx.

**References:**


1. Mamtani, K.; Jain, D.; Dogu, D.; Gustin, V.; Gunduz, S.; Co, A. C.; Ozkan, U. S., Insights into oxygen reduction reaction (ORR) and oxygen evolution reaction (OER) active sites for nitrogen-doped carbon nanostructures (CNx) in acidic media. *Applied Catalysis B: Environmental* **2018,** *220*, 88-97.

2. Atkins, P. W.; De Paula, J.; Keeler, J., *Atkins' physical chemistry*. Oxford university press: 2023.

3. Kljubin, V.; Kljubina, K.; Makovetskaya, K., Determination of free iodine concentration in an X-ray contrast agent. *Optics and Spectroscopy* **2016,** *120*, 546-550.

4. Akhade, S. A.; Singh, N.; Gutiérrez, O. Y.; Lopez-Ruiz, J.; Wang, H.; Holladay, J. D.; Liu, Y.; Karkamkar, A.; Weber, R. S.; Padmaperuma, A. B., Electrocatalytic hydrogenation of biomass-derived organics: a review. *Chemical reviews* **2020,** *120* (20), 11370-11419.

5. Liu, J.; Li, J.; Meng, R.; Jian, P.; Wang, L., Silver nanoparticles-decorated-Co3O4 porous sheets as efficient catalysts for the liquid-phase hydrogenation reduction of p-Nitrophenol. *Journal of colloid and interface science* **2019,** *551*, 261-269.

6. von Deak, D.; Singh, D.; King, J. C.; Ozkan, U. S., Use of carbon monoxide and cyanide to probe the active sites on nitrogen-doped carbon catalysts for oxygen reduction. *Applied Catalysis B: Environmental* **2012,** *113*, 126-133.

7. Singh, D.; Mamtani, K.; Bruening, C. R.; Miller, J. T.; Ozkan, U. S., Use of H2S to probe the active sites in FeNC catalysts for the oxygen reduction reaction (ORR) in acidic media. *Acs Catalysis* **2014,** *4* (10), 3454-3462.

## Publications Acknowledging this Grant in 2021-2024:

### Intellectually led by this grant

1. Jain, D.; Hightower, J.; Basu, D.; Gustin, V.; Zhang, Q.; Co, A. C.; Asthagiri, A.; Ozkan, U. S. Highly Active Nitrogen – Doped Carbon Nanostructures as Electrocatalysts for Bromine Evolution Reaction: A Combined Experimental and DFT Study. *Journal of Catalysis* **2022**, *413*, 1005–1016.
2. Rao, A., Gustin, V., Hightower, J., Gunduz, G., Basu, D., Khalifa, Y., Sohale, A., Co, A.C., Asthagiri, A., and Ozkan, U.S. "$CO_2$ Poisoning of $CN_x$ for the Oxygen Reduction Reaction," Journal of Physical Chemistry, C. (in review).
3. Basu, D., Vennala, N., Sohale, A., McFarlane, P., Nordlund, D., Gunduz, G., Co, A.C., Asthagiri, A., Ozkan, U.S., "Effect of electrochemical bromide doping on the performance of nitrogen-doped carbon nanostructures for oxygen reduction reaction," *Applied Catalysis B*. (in review)
4. Basu, D., Vennala, N., Sohale, A., Nordlund, D., Gunduz, G., Co, A.C., Asthagiri, A., Ozkan, U.S., "Effect of anodic treatment of CNx for ORR activity," *Energy and Fuels* (in review)
5. Zhang, Q., Rao, A., Ozkan, U.S., Asthagiri, A., "Phosphate Poisoning Mechanism on CNx Oxygen Reduction Reaction Catalysts under Acidic Conditions," *Energy and Fuels* (in review)

### Jointly funded by this grant and other grants with intellectual leadership by other funding sources

1) Kim, J.; Gunduz, S.; Co, A.C.; Ozkan, U.S.; Electrochemical exsolution of metal nanoparticles from perovskite oxide upon electrolysis. *Applied Catalysis B: Environmental* **2024**, *344*, p.123603.
2) Kim, J.; Kim, Y. J.; Ferree, M.; Gunduz, S.; Co, A. C.; Kim, M.; Ozkan, U. S. In-Situ Exsolution of Bimetallic CoFe Nanoparticles on (La,Sr)$FeO_3$ Perovskite: Its Effect on Electrocatalytic Oxidative Coupling of Methane. *Applied Catalysis B: Environmental* **2023**, *321*, 122026.
3) Kim, J.; Ferree, M.; Gunduz, S.; Co, A. C.; Ozkan, U. S. $Sr_2Fe_2$–$XMoXO_6$ Double Perovskites as Electrocatalysts for Oxidative Dehydrogenation of Ethane: Effect of B-Site Stoichiometry. *Electrochimica Acta* **2023**, *461*, 142633.
4) Kim, J.; Ferree, M.; Gunduz, S.; Millet, J. M.; Aouine, M.; Co, A. C.; Ozkan, U. S. Electrocatalytic Oxidative Coupling of Methane on NiFe Exsolved Perovskite Anode: Effect of Water. *ChemCatChem* **2023**, *15* (7), e202201336.
5) Kim, J.; Deka, D. J.; Gunduz, S.; Co, A. C.; Ozkan, U. S. Synergy between the Proton Conducting and a Mixed Electronic and Oxygen Ionic Conducting Phases in a Composite Anode for Electrocatalytic Propane ODH. *Applied Catalysis A: General* **2023**, *658*, 119169.
6) Ferree, M.; Gunduz, S.; Kim, J.; LaRosa, R.; Khalifa, Y.; Co, A. C.; Ozkan, U. S. Enhanced $N_2$ Activation on a Composite $Co_3Mo_3N$ Nitride and $La_{0.6}Sr_{0.4}Co_{0.2}Fe_{0.8}O_3$ Perovskite Cathode for High-Temperature Electrochemical Ammonia Synthesis. *ACS Sustainable Chem. Eng.* **2023**, *11* (13), 5007–5013.
7) Kim, J.; Ferree, M.; Gunduz, S.; Millet, J.-M. M.; Aouine, M.; Co, A. C.; Ozkan, U. S. Exsolution of Nanoparticles on A-Site-Deficient Lanthanum Ferrite Perovskites: Its Effect on Co-Electrolysis of $CO_2$ and $H_2O$. *J. Mater. Chem. A* **2022**, *10* (5), 2483–2495.
8) Gunduz, S.; Deka, D. J.; Ferree, M.; Kim, J.; Millet, J.-M. M.; Co, A. C.; Ozkan, U. S. Composite Cathodes with Oxide and Nitride Phases for High-Temperature Electrocatalytic Ammonia Production from Nitrogen and Water. *ECS Adv.* **2022**, *1* (1), 014501.
9) Gunduz, S.; Deka, D. J.; Kim, J.; Wilson, M.; Warren, M.; Ozkan, U. S. Incident-Angle Dependent *Operando* XAS Cell Design: Investigation of the Electrochemical Cells under Operating Conditions at Various Incidence Angles. *RSC Adv.* **2021**, *11* (12), 6456–6463.
10) Deka, D. J.; Kim, J.; Gunduz, S.; Aouine, M.; Millet, J.-M. M.; Co, A. C.; Ozkan, U. S. Investigation of Hetero-Phases Grown via in-Situ Exsolution on a Ni-Doped (La,Sr)FeO3 Cathode and the Resultant Activity Enhancement in CO2 Reduction. *Applied Catalysis B: Environmental* **2021**, *286*, 119917.
11) Deka, D. J.; Kim, J.; Gunduz, S.; Jain, D.; Shi, Y.; Miller, J. T.; Co, A. C.; Ozkan, U. S. Coke Formation during High-Temperature CO2 Electrolysis over AFeO3 (A = La/Sr) Cathode: Effect of A-Site Metal Segregation. *Applied Catalysis B: Environmental* **2021**, *283*, 119642.

Hongliang Xin

## Artificial Intelligence for Accelerating Catalytic Materials Discovery

Hongliang Xin
**Department of Chemical Engineering, Virginia Polytechnic Institute and State University**

**Presentation Abstract**

In the pursuit of sustainable energy and chemical transformations, the discovery of novel catalytic materials remains a critical challenge. The advent of artificial intelligence (AI) offers unprecedented opportunities to accelerate this process by advancing theory through data-driven learning, providing a pathway to identify catalysts with optimal properties. This talk will explore how AI, particularly machine learning (ML), can enhance our understanding of catalytic processes, using ammonia chemistry as a specific case to illustrate the integration of theory with data and tools. By leveraging physics-based principles, such as linear adsorption-energy scaling and Brønsted-Evans-Polanyi (BEP) relationships, AI enables the prediction of catalytic behavior in complex nanostructured materials. This approach moves beyond traditional trial-and-error methods and addresses the high computational cost of brute-force simulations. We will discuss how AI unifies catalysis theory by learning from data, transforming it into a predictive and scalable framework that drives sustainable innovation. Finally, we will introduce the emerging concept of agentic catalysis, where semi-autonomous AI agents optimize experimental and computational workflows, accelerating catalytic materials research. By learning from data and integrating domain knowledge, these agents offer a promising future for advancing catalysis science.

**DE-SC0023323: Interpretable Deep Learning of Interfacial Electrokinetics**

**Student(s):** Yang Huang (Dartmouth), Shih-Han Wang, Hemanth Pillai (FHI), Minxi Lin

## RECENT PROGRESS

***Unifying Theory of Electronic Descriptors of Metal Surfaces upon Perturbation***

We present a unifying theory for predicting electronic descriptors (e.g., the $d$-band center $\varepsilon_d$) of transition and noble metal surfaces by interpretable deep learning. Distinct from black-box machine learning models, fundamental insights into underlying physical processes can be obtained without sacrificing prediction accuracy. In addition to the charge transfer, strain, and ligand effects in the conventional wisdom, we identified orbital resonance in $d$-electron hopping as a crucial factor that modulates the shape of the $d$-state distribution, thereby shifting $\varepsilon_d$ of a $d$-metal site upon perturbation. Our findings reveal the promise of machine learning in advancing domain knowledge, paving the way toward theory-guided, data-driven design of materials beyond brute-force screening.

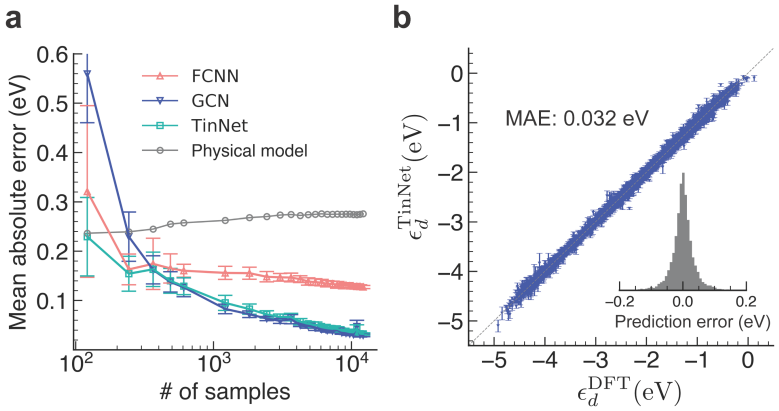


*Fig. 1: (a) The learning curves of FCNN, GCN, and TinNet models for the ϵd prediction of d-metal sites in a diverse set of d-metal catalysts. The physics-based model is also shown for comparison with data-driven deep learning models. The error bar corresponds to the standard deviation of the error estimates from nested 10-fold cross-validation. MAE represents the mean absolute error. (b) The parity plot between the DFT-calculated and TinNet-predicted ϵd along with the histogram of prediction errors.*

***Origin of unique electronic structures of single-atom alloys unraveled by interpretable deep learning***

We uncover the origin of unique electronic structures of single-atom alloys (SAAs) by interpretable deep learning. The approach integrates tight-binding moment theory with graph neural networks to accurately describe the local electronic structure of transition and noble metal sites upon perturbation. We emphasize the complex interplay of interatomic orbital coupling and on-site orbital resonance, which shapes the d-band characteristics of an active site, shedding light on the origin of free-atom-like d-states that are often observed in SAAs involving $d^{10}$ metal hosts. This theory-infused neural network approach significantly enhances our understanding of the electronic properties of single-site catalytic materials beyond traditional theories.

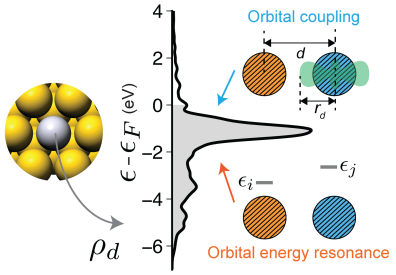

***Unraveling Reactivity Origin of Oxygen Reduction at High-Entropy Alloy Electrocatalysts with a Computational and Data-Driven Approach***

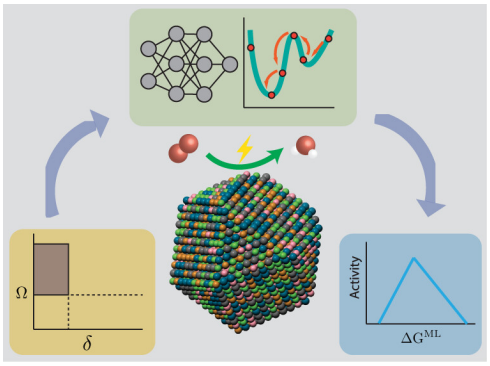


High-entropy alloys (HEAs), characterized as compositionally complex solid solutions with five or more metal elements, have emerged as a novel class of catalytic materials with unique attributes. Because of the remarkable diversity of multielement sites or site ensembles stabilized by configurational entropy, human exploration of the multidimensional design space of HEAs presents a formidable challenge, necessitating an efficient, computational and data-driven strategy over traditional trial-and-error experimentation or physics-based modeling. Leveraging deep learning interatomic potentials for large-scale molecular simulations and pretrained machine learning models of surface reactivity, our approach effectively rationalizes the enhanced activity of a previously synthesized PdCuPtNiCo HEA nanoparticle system for electrochemical oxygen reduction, as corroborated by experimental observations. We contend that this framework deepens our fundamental understanding of the surface reactivity of high-entropy materials and fosters the accelerated development and synthesis of monodisperse HEA nanoparticles as a versatile material platform for catalyzing sustainable chemical and energy transformations.

***Explainable AI for Optimizing Oxygen Reduction on Pt Monolayer Core–Shell Catalysts***

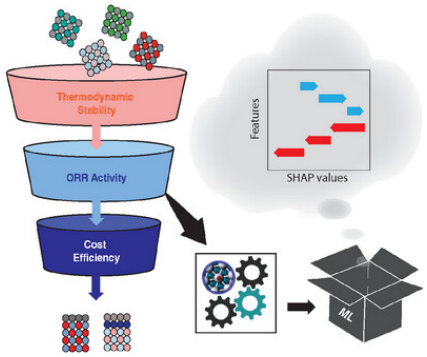


As a subfield of artificial intelligence (AI), machine learning (ML) has emerged as a versatile tool in accelerating catalytic materials discovery because of its ability to find complex patterns in high-dimensional data. While the intricacy of cutting-edge ML models, such as deep learning, makes them powerful, it also renders decision-making processes challenging to explain. Recent advances in explainable AI technologies, which aim to make the inner workings of ML models understandable to humans, have considerably increased our capacity to gain insights from data. In this study, taking the oxygen reduction reaction (ORR) on {111}-oriented Pt monolayer core–shell catalysts as an example, we show how the recently developed theory-infused neural network (TinNet) algorithm enables a rapid search for optimal site motifs with the chemisorption energy of hydroxyl (OH) as a single descriptor, revealing the underlying physical factors that govern the variations in site reactivity. By exploring a broad design space of Pt monolayer core–shell alloys (~17,000 candidates) that were generated from ~1500 thermodynamically stable bulk structures in existing material databases, we identified novel alloy systems along with previously known catalysts in the goldilocks zone of reactivity properties. SHAP

(SHapley Additive exPlanations) analysis reveals the important role of adsorbate resonance energies that originate from s–p-band interactions in chemical bonding at metal surfaces. Extracting physical insights into surface reactivity with explainable AI opens up new design pathways for optimizing catalytic performance beyond active sites.

***Bridging the complexity gap in computational heterogeneous catalysis with machine learning***

Heterogeneous catalysis underpins a wide variety of industrial processes including energy conversion, chemical manufacturing and environmental remediation. Significant advances in computational modelling towards understanding the nature of active sites and elementary reaction steps have occurred over the past few decades. The complexity gap between theory and experiment, however, remains overwhelming largely due to the limiting length and timescales of ab initio simulations, which severely impede the discovery of high-performance catalytic materials. This Review summarizes recent developments and applications of machine learning to narrow and, optimistically, bridge the gap created by the dynamic, mechanistic and chemostructural complexities inherent to the reactive interfaces of practical relevance. We foresee the prospects and challenges of machine learning for the automated design of sustainable catalytic technologies within a data-centric ecosystem that coevolves with computational and data sciences.

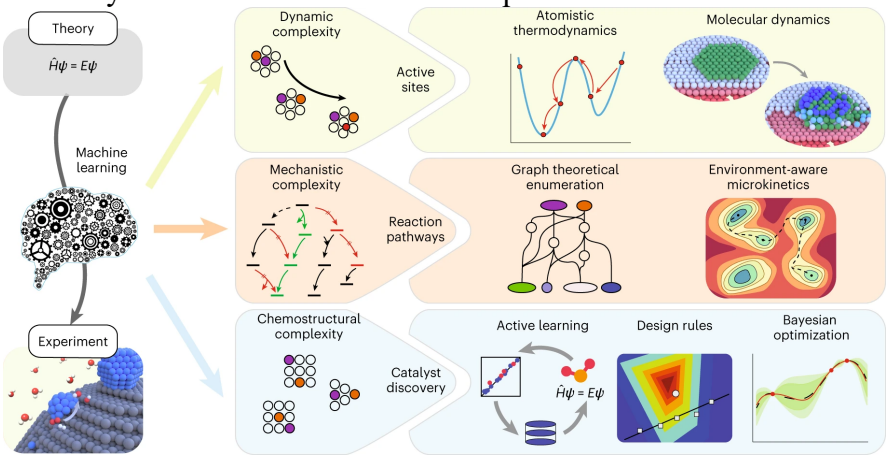


*Fig. 2: The dynamic, mechanistic and chemostructural complexities of operando catalytic systems pose grand challenges in revealing the nature of active sites, unravelling reaction pathways and ultimately accelerating catalyst discovery.*

***Interpretable Machine Learning for Catalytic Materials Design toward Sustainability***

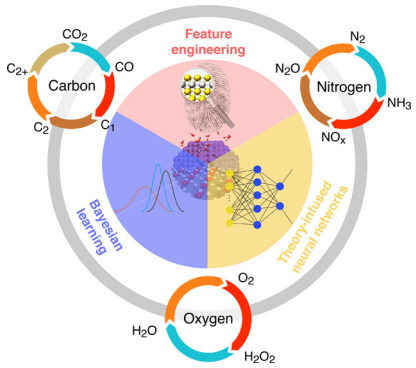


Finding catalytic materials with optimal properties for sustainable chemical and energy transformations is one of the pressing challenges facing our society today. Traditionally, the discovery of catalysts or the philosopher's stone of alchemists relies on a trial-and-error approach with physicochemical intuition. Decades-long advances in science and engineering, particularly in quantum chemistry and computing infrastructures, popularize a paradigm of computational science for materials discovery. However, the brute-force search through a vast chemical space is hampered by its formidable cost. In recent years, machine learning (ML) has emerged as a promising approach to streamline the design of active sites by learning from data. As ML is increasingly employed to make predictions in practical settings, the demand for domain interpretability is surging. Therefore, it is of great importance to provide an in-depth review of our efforts in tackling this challenging issue in computational heterogeneous catalysis.

In this Account, we present an interpretable ML framework for accelerating catalytic materials design, particularly in driving sustainable carbon, nitrogen, and oxygen cycles. By leveraging the linear adsorption-energy scaling and Brønsted–Evans–Polanyi (BEP) relationships, catalytic outcomes (i.e., activity, selectivity, and stability) of a multistep reaction can often be mapped onto one or two kinetics-informed descriptors. One type of descriptor of great importance is the adsorption energies of representative species at active site motifs that can be computed from quantum-chemical simulations. To complement such a descriptor-based design strategy, we delineate our endeavors in incorporating domain knowledge into a data-driven ML workflow. We demonstrate that the major drawbacks of black-box ML algorithms, e.g., poor explainability, can be largely circumvented by employing (1) physics-inspired feature engineering, (2) Bayesian statistical learning, and (3) theory-infused deep neural networks. The framework drastically facilitates the design of heterogeneous metal-based catalysts, some of which have been experimentally verified for an array of sustainable chemistries. We offer some remarks on the existing challenges, opportunities, and future directions of interpretable ML in predicting catalytic materials and, more importantly, on advancing catalysis theory beyond conventional wisdom. We envision that this Account will attract more researchers' attention to develop highly accurate, easily explainable, and trustworthy materials design strategies, facilitating the transition to the data science paradigm for sustainability through catalysis.

**Publications Acknowledging this Grant in 2021-2024**

*(I) Intellectually led by this grant*

1. *Huang, Y.; Wang, S.-H.; Kamanuru, M.; Achenie, L. E. K.; Kitchin, J. R.; Xin, H. Unifying Theory of Electronic Descriptors of Metal Surfaces upon Perturbation. Phys. Rev. B.* ***2024****, 110 (12), L121404. https://doi.org/10.1103/physrevb.110.l121404.*
2. *Huang, Y.; Wang, S.-H.; Achenie, L. E. K.; Choudhary, K.; Xin, H. Origin of Unique Electronic Structures of Single-Atom Alloys Unraveled by Interpretable Deep Learning. J. Chem. Phys.* ***2024****, 161. https://doi.org/10.1063/5.0232141*
3. *Huang, Y.; Wang, S.-H.; Wang, X.; Omidvar, N.; Achenie, L. E. K.; Skrabalak, S. E.; Xin, H. Unraveling Reactivity Origin of Oxygen Reduction at High-Entropy Alloy Electrocatalysts with a Computational and Data-Driven Approach. J. Phys. Chem. C Nanomater. Interfaces* ***2024****, 128 (27), 11183–11189. https://doi.org/10.1021/acs.jpcc.4c01630.*
4. *Omidvar, N.; Wang, S.-H.; Huang, Y.; Pillai, H. S.; Athawale, A.; Wang, S.; Achenie, L. E. K.; Xin, H. Explainable AI for Optimizing Oxygen Reduction on Pt Monolayer Core–Shell Catalysts. Electrochem. Sci. Adv.* ***2024****, n/a (n/a), e202300028. https://doi.org/10.1002/elsa.202300028.*
5. *Mou, T.; Pillai, H. S.; Wang, S.; Wan, M.; Han, X.; Schweitzer, N. M.; Che, F.; Xin, H. Bridging the Complexity Gap in Computational Heterogeneous Catalysis with Machine Learning. Nature Catalysis* ***2023****, 6 (2), 122–136. https://doi.org/10.1038/s41929-023-00911-w.*

*(II) Jointly funded by this grant and other grants with intellectual leadership by other funding sources*

1. *Xin, H.; Mou, T.; Pillai, H. S.; Wang, S.-H.; Huang, Y. Interpretable Machine Learning for Catalytic Materials Design toward Sustainability. Acc. Mater. Res.* ***2024****, 5 (1), 22–34. https://doi.org/10.1021/accountsmr.3c00131.*

Jenny Y. Yang

# Optimizing Electrocatalytic Hydrogen Evolution or Selective $CO_2$ Reduction at Transition Metal Hydrides

Jenny Y. Yang
University of California, Irvine

Fuel forming reactions such as the hydrogen evolution reaction (HER) and $CO_2$ reduction (CO2R) are vital to transitioning to a carbon neutral economy. Metal hydride intermediates are ubiquitous in these catalytic and electrocatalytic processes. Guiding metal hydride reactivity is important for achieving selective, kinetically fast, and low overpotential reductions. Our work has focused on understanding kinetic and thermodynamic aspects for controlling these reactive hydride species in an effort to design more selective electrocatalysts that operate at low overpotentials. Key to our approach is understanding the free energy changes and rate of discrete steps of catalysis through isolation of proposed intermediates. These include the application of transition metal hydricity, or free energy of hydride release.

Our work describes how hydricity values can be applied to optimize HER and CO2R catalysis. This framework provided general guidelines for achieving selective $CO_2$ reduction to formate ($HCO_2^-$) in the presence of protons. Kinetic information on steps in the proposed catalytic cycle of HER and CO2R catalysts were evaluated to identify potential rate determining steps. Hydricity values were also used to design an electrocatalyst for the interconversion between $CO_2$ and $HCO_2^-$ at low overpotentials.

Almost all reductive reactions employ classic metal hydrides, where the electrons and proton are co-located on the metal center. However, these require very reducing potentials to generate strong enough hydride donors for reduction. In contrast, formate dehydrogenase (FDH) generates a competent hydride donor at more mild potentials, through bidirectional hydride transfer, where the proton and electrons of the hydride are not collocated. We have explored some bio-inspired architectures to better understand bidirectional hydride transfer. More recently, we have focused our efforts to translate the thermal $CO_2$ hydrogenation activity of homogeneous catalysts, which also proceeds through metal hydrides, to electrocatalysis.

**Grant or FWP Number: New Synthetic Strategies for Electrocatalytic C1 Reduction at Mild Potentials**

**Postdoc(s):** Kelsey Collins (Scientist, AFRL)
**Student(s):** Faith Flinkingshelt, Elise Payong, Andrew Cypcar, Tyler Kerr (PD, UCLA), Sarah Wang (Analyst, RMI), Alissa Matus (Prof., Cypress College)

## RECENT PROGRESS

### *Translating Homogeneous Hydrogenation Activity to Electrochemical Reduction*

**Scheme 1**. Proposed mechanisms for $CO_2$ hydrogenation and electrocatalytic reduction by $[Co(dmpe)_2(H)]^{2+}$.[30]

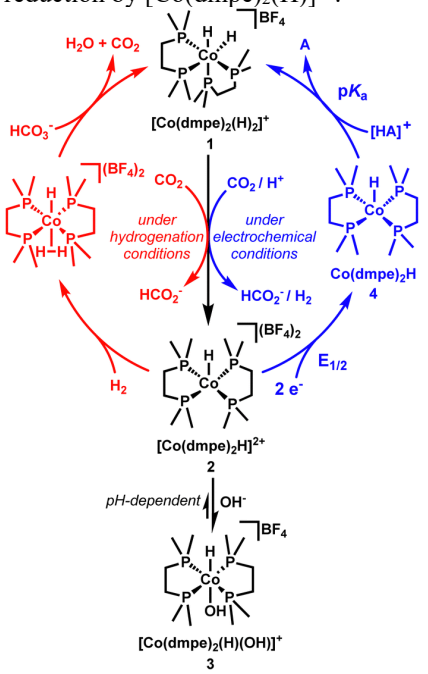


A molecular $CO_2$ hydrogenation catalyst, $[Co(dmpe)_2(H)]^{2+}$ (**2**) (dmpe = 1,2-bis(dimethylphosphino)ethane) was explored for electrocatalytic $CO_2$ reduction under aqueous conditions. This catalyst exhibits one of highest activities for $CO_2$ hydrogenation to $HCO_2^-$ by a first-row transition metal in water.[1-3] The proposed hydrogenation mechanism is depicted in red in **Scheme 1**. To obtain the electrochemical potential and pH requirements to generate the metal hydride intermediate, we measured the p$K_a$ and reduction potential shown in blue in **Scheme 1.**[4]

Controlled potential electrolysis (CPE) experiments were performed using a 0.2 M sodium carbonate solution saturated with $CO_2$ from pH 7-9, resulting in mixed $H_2/HCO_2^-$ selectivity. The highest faradaic yield for $HCO_2^-$ was 54% at pH 7.8. At other pH conditions, the Faradaic efficiency for $H_2$ is higher than that of formate. To understand the pH-dependent product selectivity, we performed stoichiometric studies with the isolated metal hydride intermediate. In summary, the ligation of the $OH^-$ after hydride transfer results in a pH-dependent hydricity of the donor.[1-3] As a result, the free energy of $H_2$ evolution is always favorable, even at higher pH value, leading to mixed product selectivity. These studies initiated our motivation to investigate this topic further and determine general guidelines (if they exist) on how hydrogenation activity in homogeneous catalysts translates to electrochemical activity.

### *Isolation of Proposed Catalytic Intermediates for $CO_2$ Hydrogenation*

Ru(MACHO)$L_3$ (L = neutral or anionic ligands) complexes are also among the most active and stable catalysts for the hydrogenation of $CO_2$ to $CH_3OH$, with up to $10^3$ turnovers.[5-7] Our studies have focused on isolating or characterizing the active hydride donor in the catalytic cycle so that it's reactivity can be studied independently and hydricity evaluated for application in an electrocatalytic reduction. Despite extensive studies on Ru(MACHO) derivatives as a hydrogenation catalyst, the proposed active hydride donor, Ru(MACHO)(CO)$H_2$, had never been isolated or fully characterized. Under hydrogenation conditions, the resting state catalyst Ru(MACHO(CO)HCl forms the hydride donor via $H_2$

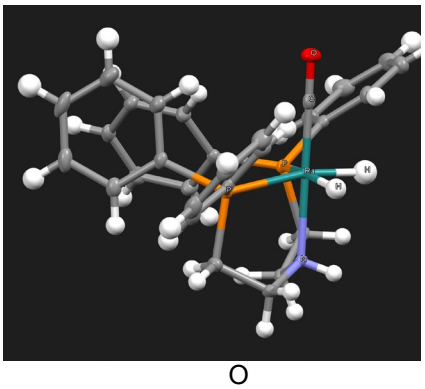


**Figure 1**. Preliminary single crystal X-ray structure of cis-Ru(Macho)(CO)$H_2$, a proposed active catalytic intermediate involved in $CO_2$ hydrogenation.

and a base. We have chemically accessed the dihydride using the hydride donor $LiEt_3BH$ and characterized the product by $^1H$ and $^{31}P$ NMR spectroscopy and single crystal X-ray analysis (**Figure 1**). The dihydride intermediate, which reduces $CO_2$ and the methylester/formamide has always been proposed as a trans-dihydride complex, with the pincer ligand coordinated in a meridional fashion. However, the initial product we isolated has the two hydrides cis to each other, with the MACHO ligand coordinated in a facial geometry (**Figure 1**). The hydrides were found in the X-ray data difference map, and the $^1H/^{31}P$ NMR spectra also support the dihydride formulation. Using separate conditions, we have also generated the trans hydride isomer. We find both dihydrides reacts quantitatively to reduce $CO_2$ to form formate, indicating they are both strong hydride donors. We initiated a collaboration with Dr. John Linehan and Dr. Aaron Appel at PNNL to examine potential intermediates using high-pressure NMR spectroscopy under hydrogenation conditions.

**Publications Acknowledging this Grant in 2021-2024**

*(I) Intellectually led by this grant*

1. Matus, A.; Cypcar, A.; Trevino, R.; Linehan, J.; Appel, A. M.; Yang, J. Y. Characterizing the Structure and Properties of a Ru(macho) Dihydride Complex. *in preparation*
2. Wang, X. S.; Yang, J. Y.; Electrocatalytic Reduction of N2O and Mechanistic Insights Using a Platinum CO2 Reduction Electrocatalyst. *in preparation*
3. Kerr, T.; Ziller, J. W.; Yang, J. Y., Proton-Induced Oxidation and Dimerization of a Tungsten Bisdithiolene Complex. *in preparation*
4. Cypcar, A.; Yang, J. Y. Controlling Hydrogen Evolution and CO2 Reduction at Transition Metal Hydrides. *Acc. Chem. Res., accepted*
   Invited to special issue *Upgrading C1 Feedstocks to Value-Added Chemicals and Fuels Using Molecular Systems*
5. Wang, X. S.; Yang, J. Y., Translating Aqueous CO2 Hydrogenation Activity to Electrocatalytic Reduction with a Homogeneous Cobalt Catalyst. *Chem. Commun.,* **2023**, *59*, 338-341.
6. Shafaat, H. S.*; Yang, J. Y.*, Uniting biological and chemical strategies for selective CO2 reduction, *Nature Catalysis*, **2021**, *4*, 928-933.
   Invited Perspective in special Focus Issue *CO2 Reimagined*

**References**

(1) Burgess, S. A.; Appel, A. M.; Linehan, J. C.; Wiedner, E. S. Changing the Mechanism for CO2 Hydrogenation Using Solvent-Dependent Thermodynamics. *Angewandte Chemie International Edition* **2017**, *56* (47), 15002-15005, https://doi.org/10.1002/anie.201709319. DOI: https://doi.org/10.1002/anie.201709319 (acccessed 2022/12/19).
(2) Jeletic, M. S.; Mock, M. T.; Appel, A. M.; Linehan, J. C. A Cobalt-Based Catalyst for the Hydrogenation of CO2 under Ambient Conditions. *J. Am. Chem. Soc.* **2013**, *135* (31), 11533-11536. DOI: 10.1021/ja406601v.
(3) Jeletic, M. S.; Helm, M. L.; Hulley, E. B.; Mock, M. T.; Appel, A. M.; Linehan, J. C. A Cobalt Hydride Catalyst for the Hydrogenation of CO2: Pathways for Catalysis and Deactivation. *ACS Catalysis* **2014**, *4* (10), 3755-3762. DOI: 10.1021/cs5009927.

(4) Wang, X. S.; Yang, J. Y. Translating aqueous CO2 hydrogenation activity to electrocatalytic reduction with a homogeneous cobalt catalyst. *Chemical Communications* **2023**, 10.1039/D2CC05473F. DOI: 10.1039/D2CC05473F.
(5) Kar, S.; Goeppert, A.; Prakash, G. K. S. Integrated CO2 Capture and Conversion to Formate and Methanol: Connecting Two Threads. *Acc. Chem. Res.* **2019**, *52* (10), 2892-2903. DOI: 10.1021/acs.accounts.9b00324.
(6) Sen, R.; Goeppert, A.; Surya Prakash, G. K. Homogeneous Hydrogenation of CO2 and CO to Methanol: The Renaissance of Low-Temperature Catalysis in the Context of the Methanol Economy. *Angewandte Chemie International Edition* **2022**, *61* (42), e202207278. DOI: https://doi.org/10.1002/anie.202207278.
(7) Kar, S.; Sen, R.; Kothandaraman, J.; Goeppert, A.; Chowdhury, R.; Munoz, S. B.; Haiges, R.; Prakash, G. K. S. Mechanistic Insights into Ruthenium-Pincer-Catalyzed Amine-Assisted Homogeneous Hydrogenation of CO2 to Methanol. *J. Am. Chem. Soc.* **2019**, *141* (7), 3160-3170. DOI: 10.1021/jacs.8b12763.

# Tuning Electrocatalytic Reduction of Plasma Pre-Activated $CO_2$ Toward Multicarbon Products

Lea R. Winter
Department of Chemical and Environmental Engineering, Yale University

## Presentation Abstract

Upgrading $CO_2$ to chemicals and fuels represents a scalable strategy for mitigating climate change. Electrochemical conversion of $CO_2$ with water under mild conditions that are compatible with renewable energy could provide a low-carbon approach compared to alternatives that require $H_2$ or high temperature and pressure. However, electrocatalytic $CO_2$ reduction with $H_2O$ ($CO_2R$) is rate-limited by the $CO_2$ or CO activation step. This limitation also constrains catalyst design to favor $CO_2$/CO activation at the expense of tuning catalytic pathways toward high-value multicarbon products. Nonthermal plasma has accomplished $CO_2$ conversion at atmospheric pressure, but the non-selective nature of plasma makes it challenging to control the subsequent conversion to valuable products.

This project focuses on unlocking new electrocatalyst design spaces for multicarbon product generation using $CO_2$/CO pre-activation with nonthermal plasma. By applying nonthermal plasma in $CO_2R$ for the first time as an approach that is outside the conventional scope of catalyst development, we may help solve outstanding challenges in electrocatalytic $CO_2$ upgrading to high-value products. This strategy could potentially decouple reactant/intermediate activation and product formation using plasma pre-activation, opening a wider design space for electrocatalysts optimized for selective product generation further along the reaction pathway. Based on coupling plasma with electrocatalysts across a novel engineered interface, we are discovering new reaction pathways and catalyst design strategies for electrocatalytic reduction of pre-activated $CO_2$ to $C_{3+}$ products.

**Enzyme-like porous catalysts for upgrading biomass feedstocks**

Andy I. Nguyen
Department of Chemistry, University of Illinois Chicago

## Presentation Abstract

Biomass is the largest source of renewable carbon, and the ability to refine it into valuable products could significantly reduce petroleum usage. Catalysts for biomass upgrading should ideally allow for the use of green reagents and produce desired products with high selectivity. Enzymes outperform current synthetic catalysts on efficiency and selectivity due to their advanced multifunctional active sites, but they are fragile and costly. To achieve efficient catalysis with increased durability and recyclability, there has been a longstanding interest in combining the key features of enzymes with solid-state materials to create enzyme-like heterogeneous catalysts. However, the laborious and time-intensive design, synthesis, optimization, and characterization of enzyme-mimicking materials has impeded progress. Our proposal aims to circumvent these challenges by leveraging recently described peptide frameworks, which are crystalline porous solid-state materials spontaneously generated from peptide self-assembly. Like enzyme active sites, the pores within these materials have multiple unique functional groups that are permutable, enabling rapid synthesis of elaborate catalyst variants. This proposal will evolve these scaffolds to enhance the sustainability and efficiency of catalytic processes for the aerobic oxidation of lignin and polyol deoxygenation. Furthermore, the crystallinity of these peptide frameworks provides a unique opportunity to routinely obtain high-resolution structural data that informs the rational design of next-generation catalysts. The expected outcomes of this research are more efficient catalysts for upgrading biomass, versatile tools to precisely manipulate multiple noncovalent interactions, and fundamental structure-activity knowledge for enzyme-like catalyst design.

# Insights into the Catalysts Originating from Phosphine-Modified Co(II) Hydroformylation Precatalysts

Matthew B. Chambers
Louisiana State University, Department of Chemistry

## Presentation Abstract

This work aims to advance the development of base metal catalysts and our understanding of how precatalysts of intermediate oxidation states can yield active carbonylation catalysts under reducing conditions. Recently, a Co(II) hydro-formylation precatalyst, [Co(acac)(bisphosphine)]$BF_4$, was reported. This system was found to be indefinitely stable, produce minimal side products, and have a rate within an order of magnitude of commercially relevant Rh catalysts under mild conditions for Co (140ºC and 30 bar). This spurred immense interest in Co(II) precatalyst, which led to conflicting claims that the cationic Co(II) precatalyst was not active for hydroformylation. We have disambiguated these reports and identified a key discrepancy that arose from the [Co(acac)(bisphosphine)]$BF_4$ material being poorly characterized. We have since developed a reliable calibrated ESI-MS characterization method for the Co(II) precatalyst. We have optimized the synthesis to remove impurities and characterize the material more completely. Under mild hydroformylation conditions, we confirmed the viability of catalysis and achieved aldehyde yields greater than the original report. In this work, we are now developing this novel Co(II) precatalyst by targeting *in-situ* spectroscopic evidence for the nature of the catalytic state. In this presentation, the parameters that impact the activation of the precatalyst will be discussed to identify true catalytically relevant conditions for spectroscopic studies. Additionally, we have expanded the ancillary ligand scope to include trisphosphine ligands. These ligands afford substantially more stable precatalysts and more reliable catalytic performance while using comparable conditions. Such ligands are unprecedented for hydroformylation catalysis and stand to provide key insights into the role of the ligand field in the formation and activity of the catalytic state.

Simon R Bare

## Integrated Platform to Predict Degradation of Catalysts for Sustainable Conversion of Alternate Feedstocks to Fuels and Chemicals

[1,11]Simon R Bare, [2]Anastassia Alexandrova, [3,11]Matteo Cargnello, [4]Phillip Christopher, [5]Ashley Head, [1]Sarah Hesse, [1,10]Adam S. Hoffman, [6]Matthew Kanan, [7]Shyam Kattel, [8]Ambarish Kulkarni, [9]Robert Rallo, [10]Robert Rioux, [1]Christopher J. Tassone, [11]Kirsten Winther, [5]Judith Yang

[1]SSRL, SLAC National Accelerator Laboratory, [2]Department of Chemistry and Biochemistry, UCLA, [3]Department of Chemical Engineering, Stanford University, [4]Department of Chemical Engineering, UC Santa Barbara, [5]Center for Functional Nanomaterials, Brookhaven National Laboratory, [6]Department of Chemistry, Stanford University, [7]Department of Physics, Central Florida University, [8]Department of Chemical Engineering, UC Davis, [9]ACMDD, PNNL, [10]Department of Chemical Engineering, Penn State University, [11]SUNCAT, SLAC National Accelerator Laboratory

### Presentation Abstract

Imagine a scenario where one could predict catalyst degradation early in the discovery process. This is perhaps the most effective way to add commercial value and relevance to early-stage efforts. One of the most relevant mechanisms of catalyst degradation is the non-reversible phenomenon of sintering. During sintering, supported metal nanoparticles grow with consequent decrease in active surface area, overall activity and/or selectivity. No current theories can consider the full complexity of catalyst sintering during industrial use and at present there is no unified framework predictive of long-term degradation of industrial catalysts by sintering. This project uses data science as a unifying platform to connect reactivity data, a suite of relevant *in-situ* and *operando* characterization, and computational chemistry to develop a platform that predicts long term catalyst performance from short term measurements. The presentation will provide an update on the excellent progress of the project after one year of operation.

**The work was supported by the Division of Chemical Sciences, Geosciences, and Biosciences, Office of Basic Energy Sciences, US Department of Energy (DOE) as part of the Accelerate Innovations in Emerging Technologies initiative. FWP 101064.**

**Postdoc(s):** [1]Anastassiya Khan, [1]Donjae Shin, [1]Zhihengyu Chen, [3]Jake Heinlein, [2]Yonghyuk Lee, [5]Xiaobo Chen, [4]Seunghwa Hong, [8]Anshuman Kumar, [4]Selin Bac, [5]Sabrina Gericke, [7]Sourav Ghoshal
**Student(s):** [6]Kesha Tamakuwala, [4]Emily Schroeder, [10]Zayne Weber, [6]Robert Kennedy,

## RECENT PROGRESS

### *Catalyst synthesis, testing and characterization*

The synthesis teams have collaborated to develop a shared online database of all synthesized samples, giving each one a unique code to prevent any ambiguity as to what samples are being tested. Many samples have been shipped to various institutions for characterization via a suite of complementary methods.

At UCSB, reactivity analysis and associated characterization of a series of catalysts with varying Rh wt% (0.1-5%) on rutile $TiO_2$ prepared via incipient wetness have been completed. This analysis suggests that there exist surface sites on rutile $TiO_2$ that provide excellent stability for Rh single atoms, even at 500°C under close to equilibrium RWGS conditions. Alternatively, $CH_4$ formation sites on Rh nanoparticles rapidly lose their reactivity. The rate of loss of reactivity seems to correlate with initial Rh nanoparticle size.
Initial $CO_2$ conversion experimentation has been performed for Rh deposited on shaped anatase $TiO_2$ particles to understand how the support influences reactivity evolution.
At Stanford, nanoparticles of Rh/$TiO_2$ (rutile) have been synthesized and their catalytic activity as a function of Rh weight loading and pretreatment conditions. Varying the RhNP weight loading (0.1%, 0.25%, 0.5%) while maintaining the total mass of Rh in the reactor showed, with decreasing weight loading, trends of decreasing rates of methanation and delayed onset of the RWGS reaction.

Initial $CO_2$ conversion also decreases with decreased weight loading, but all samples reached the same steady-state conversion after several hours under reaction. Varying the gas composition during the pretreatment procedure (5% $O_2$ in Ar, 20% $H_2$ in Ar, pure Ar) revealed the $O_2$ pretreatment is necessary for methanation to occur. Varying the reaction temperature shows methanation preferentially occurring at lower temperatures.

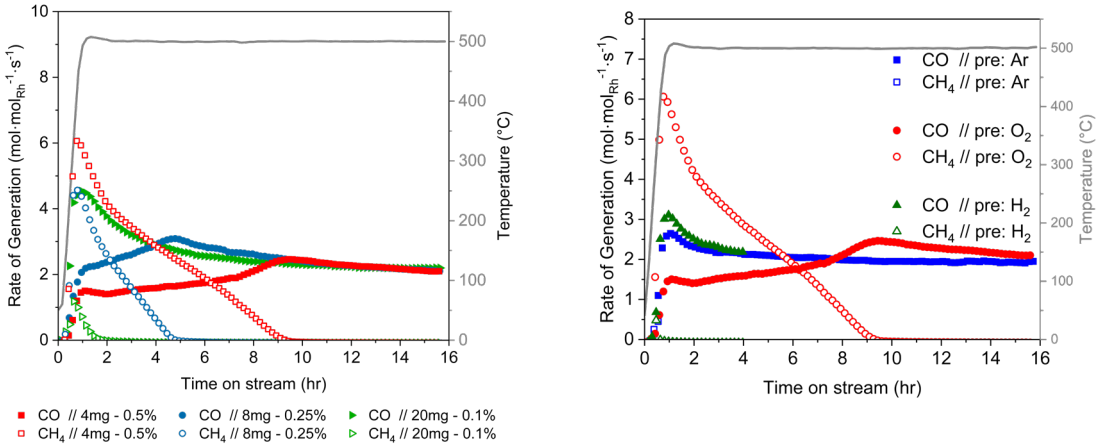


***Figure 1:*** *(left) summary of rates of generation of the products CO and $CH_4$ for different weight loadings (0.1%, 0.25%, 0.5%) of RhNPs on rutile $TiO_2$, with different masses of catalyst loaded (20 mg, 8 mg, and 4 mg respectively) to ensure constant total mass of Rh in the reactor (0.02 mg) for each test. (right) summary of rates of generation of CO and $CH_4$ for a 0.5% RhNP on rutile $TiO_2$ sample exposed to different pretreatment gas compositions (pure Ar, 5% $O_2$ in Ar, and 20% $H_2$ in Ar) for the 400 °C, 30-minute pretreatment prior to the reaction under RWGS conditions.*

A Python-based analysis tool has been developed that standardizes the format and key parameters for reactor testing results that gets shared with the machine learning teams. This was a lengthy and critical step that will allow us to rapidly collect the raw testing data for sharing with the ML groups.

At SSRL, the $Rh/TiO_2$ (rutile) samples have been characterized via operando XAS, SAXS, and WAXS tracking the Rh oxidation state (XAS), the Rh local coordination (XAS), the Rh nanoparticle size (XAS + SAXS), and variations in the $TiO_2$ support (WAXS) as a function of time on stream based upon: i) Rh metal loading (0.1-5 wt% Rh), ii) initial Rh starting species or nanoparticle, iii) pretreatment atmosphere, iv) RWGS reaction temperature, and v) dilution ratio of the $Rh/TiO_2$ catalyst to $SiO_2$ diluent.

The SAXS results characterizing the Rh particle size as a function of temperature and time on stream have been shared with PNNL machine learning team to help train a model that predicts Rh particle size distribution as a function of temperature and time.

XAS analysis show that increasing Rh metal loading leads to the formation of small Rh oxide clusters after the oxidation pre-treat, while WAXS analysis results showing the transformation from anatase to rutile is inhibited by the loading of Rh. Both scattering and spectroscopy results showing that the heat generated from methanation reaction is accelerate the sintering of Rh and impacting the selectivity to RWGS. To improve reactivity quantification at the beamline an Agilent 490 micro gas chromatography (uGC) apparatus has been installed and a method for reactant and product separation has been developed. The uGC allows for quantitative product analysis during the operando XAS and X-ray scattering measurements as well as SSRL-based reactor testing between beamtimes.

At SLAC, packed bed reactor to aid in generating RWGS time on stream data for the machine learning teams has been constructed, benchmarked, and is operational. Reactor experiments run at SLSC mirror conditions that are proposed to the Stanford (Cargnello) or UCSB (Christopher) teams from the SSRL machine learning suggestions, to test for variations in measurements due to institution reactor differences. Many datasets have been contributed to the machine learning teams dataset.

At the CFN at BNL, in-situ ETEM experiments on pure anatase $TiO_2$ supports under RWGS reaction conditions have been performed to investigate surface facet-dependent reaction dynamics. The results have been correlated with theory, APXPS measurements, and activity measurements to understand which facets are the most active and how activity can be increased through oxygen vacancy formation.

Also, in-situ ETEM experiments with 1 wt% Rh on anatase $TiO_2$ supports under various gases have been conducted ($O_2$, $CO_2$, and CO). These data will be correlated with APXPS and FTIR spectroscopy measurements under various gases ($O_2$, $CO_2$, and CO). Preliminary results are consistent with titania overlayer growth and $RhTiO_x$ formation seen in ETEM.

At Penn State University, chemisorption surface areas after reduction and oxidation treatments of rhodium nanoparticle coated rutile nanoparticles haven been measutred. Material showed a repetitive pattern of Rh being inaccessible after reduction and then being accessible after oxidation. This coverage by the support material agrees with what was reported in the literature for other catalytic materials and systems. These results suggest that oxidation may restore degraded catalysts back to full catalytic capabilities

For the testing at PSU, Reactor #1 has been built out and has been undergoing testing and validation in order to be able to begin running catalytic materials under reaction conditions. Reactor #1 is expected to become operational November 2024. Reactor #2 is under construction using best building practices learned from reactor #1. It is expected to become operational November 2024.
At Stanford, a reactor made of SiC tubing and an alumina sheathed internal thermocouple has been fabricated for testing at elevated temperatures up to 750°C and pressure of 10 bar, to minimize RWGS activity contributions from the background. Using this equipment high activity and selectivity of dispersed carbonate catalysts ($M_2CO_3/Al_2O_3$, M= K, Na) in this intermediate temperature and pressure RWGS regime, as well as excellent stability at <600°C has been demonstrated.

***Theory***
At UC Davis, machine learning interatomic potentials (MLIPs) have been trained using first-principles DFT data on Rh-doped alumina in cluster and cationic configurations to investigate deactivation mechanisms in these systems (Figure 2). Two different MLIP architectures: MACE and NEP were benchmarked. The results demonstrate that MACE significantly outperforms NEP in predicting energies and forces, with both the root mean squared error (RMSE) and mean absolute error (MAE) being more than an order of magnitude lower.
To ensure reliable performance across diverse configurations an active learning protocol has been implemented, refining the model by focusing on challenging configurations. Using an uncertainty quantification metric, the MACE model was iteratively trained through NVT molecular dynamics (MD) simulations in LAMMPS, followed by DFT single-point energy (SPE) calculations on randomly sampled MD configurations. Configurations with uncertainties exceeding a threshold (0.3 eV/Å) were added to the initial training set, and the model was retrained until convergence. Finally, to streamline this iterative process, we developed an in-house automated software solution—Dynamic Refinement and Iterative Validation Exploration Software for Chemicals and Materials (DRIVES-CheM). Employing DRIVES-CheM to obtain the optimized MACE parameters, metadynamics calculations were performed to investigate catalytic deactivation mechanisms in doped alumina surfaces. Significant differences in the energy barriers for different locations of Rh were observed.

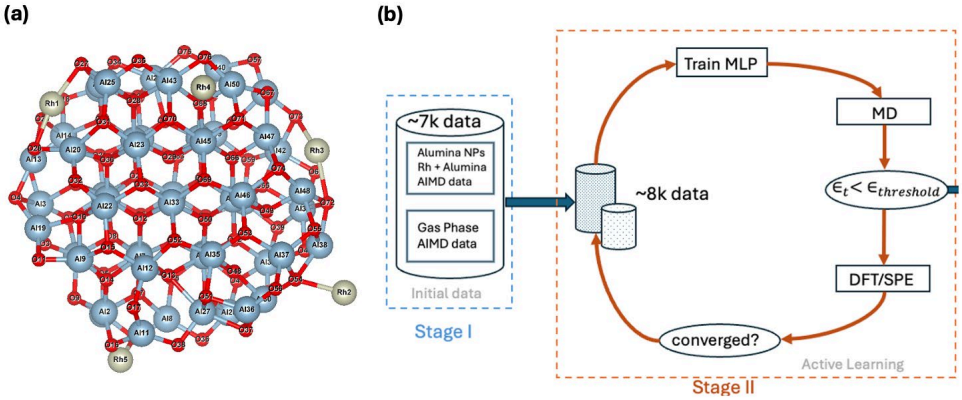


Figure 2. (a) Atomistic models capture the wide diversity of Rh environments for $Rh/Al_2O_3$ systems. (b) Automated protocols to train machine learning potentials for predicting catalyst deactivation.

The theoretical work at the University of Central Florida is focused on the DFT calculations of thermodynamic and kinetic stability of Rh single-atom catalysts supported on rutile and anatase $TiO_2$ at experimental conditions. The thermodynamics stability of Rh single-atom catalyst supported on rutile $TiO_2$ as a function of OH surface coverage (with and without O/OH

vacancies) at experimental temperatures and pressures and coverage of H and CO has been calculated.

At UCLA, the accelerated surface structure determination for $TiO_2$ has been performed utilizing machine-learning potential under reductive conditions. The iterative training of the MACE model, an equivariant message-passing graph tensor network that encodes many-body atomic geometry information at each layer, was completed for the rutile and anatase $TiO_2$ surfaces using an active-learning workflow.

A total of 1,615 DFT single-point calculations were performed during this active learning process to refine the training structures, requiring 18,365.3 node hours. The final converged training set includes 1,804 configurations and 973,020 force components. The out-of-sample root mean square errors (RMSEs) of the final converged MACE model are below 4 meV/atom for energy predictions and 178 eV/Å for force predictions.

Extensive MACE-based samplings, conducted through the grand canonical genetic algorithm (GCGA) in our in-house code GOCIA, explored the configurational space of $TiO_2$ surfaces. Figure 3 (left): Calculated surface phase diagram. Samplings identified stable surface reconstructions under reductive conditions, revealing both known and previously unreported reconstructions. A reconstructed surface (termed as $TiO_{1.69}$) featuring a shear plane—known as Wadsley defects—emerges as the most stable structure below the oxygen-poor limit. This reorganization, by transforming corner-sharing octahedra into edge-sharing ones, reduces the system's free energy and accommodates excess titanium interstitials, preventing crystal collapse.The outermost titanium atoms occupy non-lattice sites, forming vertically oriented $TiO_5$ polyhedra with apical oxygen vacancies, resulting in coordinatively unsaturated titanium sites. These sites may act as active binding locations for catalysts or reactive adsorbates, potentially affecting catalytic activity and electronic properties.

Figure 3(right): Layer-decomposed density of states (DOS). Spin-polarized mid-gap states, mainly originating from $Ti^{3+}$ polarons in the up-spin channel near the surface, play a key role in surface reconstructions of reduced $TiO_2$. These states, derived from Ti 3*d* orbitals, decrease in intensity with depth, indicating a concentration of polarons at the surface with gradual delocalization into subsurface layers.
A small gap state in the down-spin channel suggests defect-related interactions between $Ti^{3+}$ and $Ti^{4+}$, possibly influencing magnetic and transport properties. The total DOS shows Ti 3*d* states dominating near the Fermi level, enhancing electron charge carriers and contributing to improved surface conductivity—a property advantageous for electron transfer in catalytic applications involving reduced $TiO_2$.

Supported by TEM characterization, we aim to demonstrate experimental verification of theoretically identified reduced rutile reconstructions. Further investigations into comparative reductions on different orientations of anatase surfaces will be conducted.

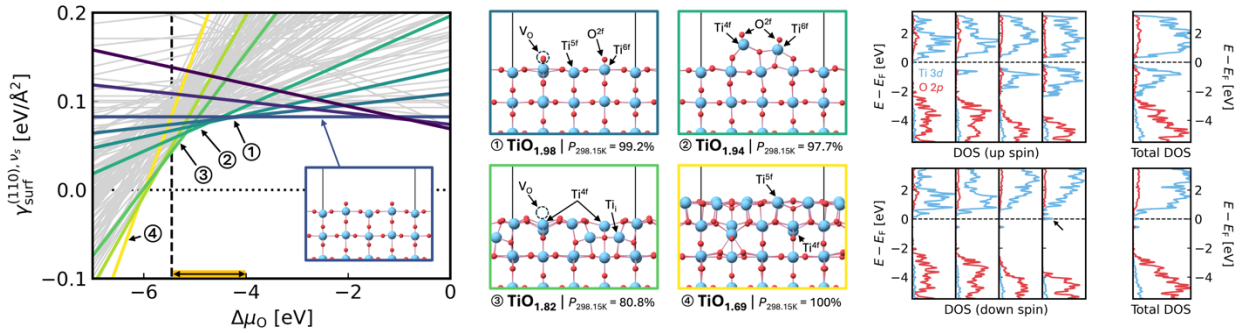


*Figure 3 (left) The surface free energies, $\gamma_{surf}^{(110),\nu_s}$, are plotted as a function of the oxygen chemical potential, $\Delta\mu_O$, for all grand-canonically sampled rutile $TiO_2$(110). The lowest surface energy structures are indicated by colored solid lines. The vertical dashed line marks the O-poor limit. The atomic structure of the conventional stoichiometric is shown as an inset. Titanium and oxygen atoms are depicted as large cyan and small red spheres, respectively. (middle) Four representative, most stable surfaces under reductive conditions are also illustrated. The Boltzmann probability at room T ($P_{273.15K}$) of each structure among all sampled configurations with the same stoichiometries is also indicated. (right) The layer-decomposed density of states (DOS) for up-spin and down-spin components, from left to right, shows the transition from bulk to surface.*

***Machine Learning***

At SLAC, an active learning algorithm based on Bayesian optimization to drive experimental selection through uncertainty sampling has been developed. The algorithm is applied to efficiently acquire RWGS performance data from several synthesis and testing locations (UCSB, Stanford & SLAC). The model iteratively suggesting experimental input and is retrained on new data. A Gaussian Process Regression model is used that accepts continuous as well as categorial input features which is needed to handle synthesis/testing input parameters (temperature, Rh weight loading, etc.) as well as location parameters (synthesis method & testing location).

In collaboration with experimental groups (UCSB, Stanford & SLAC) a data structure for RWSG synthesis and testing has been developed and used to track ML model input and output, as well as an extensive list of testing conditions and results that will be used to build sophisticated models moving forward.

A pipeline for feature engineering using an interpretable ML model has been developed. In the pipeline, SHAP analysis is performed to quantify the importance of the synthesis/testing input features using the trained Gaussian Process Regression model. Based on the calculated feature importance, relevant input features are additionally identified besides input parameters (temperature, Rh weight loading, and synthesis method, etc.) that were considered in the first round of data generation.

At PNNL Data pipelines are being developed to include new experimental data types: DRIFTS and SAXS/XAS. A prototype web application framework to provide access to the ACCELERATE data repository has been developed. The components of the web application include: (i) Data packager to facilitate data annotation and to create AI-ready data archives. (ii) Cloud-based automated ingestion and indexing pipeline for the information provided through the Data Packager module, and (iii) Data Query module to retrieve information from the repository based on the metadata schema. This module will provide a data access interface to the AI agents that are being developed in the project.

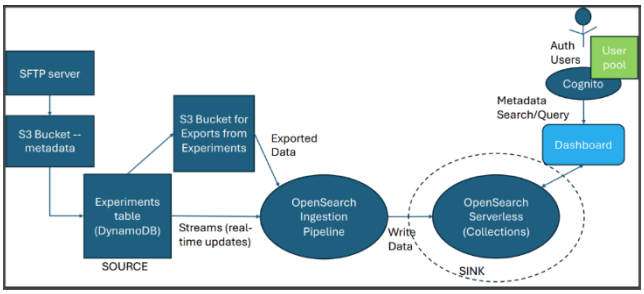


A sintering model is being developed. Extensions and improvements to the catalyst sintering model: Development of a hierarchical probabilistic model structure to learn shared model parameters across process control decisions (i.e., temperature, initial particle size). Until now our model has not generalized across experimental conditions, but this will be necessary for the experimental design component. Using SAXS data at different temperatures, we are training the hybrid model in a Bayesian framework and predict average catalyst radius under different temperature conditions – this will be used in the optimal experimental design loop to recommend temperatures that lead to minimal change in average particle size over long operating times.

Multimodal data integration is underway**.** Current work focuses on two primary data modalities: static images and movies (time evolution of TEM images). Also, an algorithm has been developed to identify nanoparticles in TEM images and compute their size and distribution. and position of nanoparticles over time. The analysis algorithm facilitates the capture of statistical features that describe the time evolution of single nanoparticles or nanoparticle populations. The example below depicts the change of the size of the tracked nanoparticle over time.

The preliminary design of an interpretable AI framework for catalyst degradation (DECAI: Degradation Estimation for Catalyst using AI) has been developed The goal of this framework will be to provide a single point of access to the data and models generated by the project as well as to existing data and knowledge on catalysis. The current framework includes prototype implementations of two generic agent teams: (i) *Information Retrieval Team*: Specialized set of agents to search the web and retrieve relevant information from literature. Sources of data include: Arxiv, Semantic Scholar, Google Scholar as well as specialized web-search engines. We plan to extend this agent to include a query interface to OSTI. (ii) *Data Retrieval Team*: Specialized agent that uses the OPTIMADE (Open Databases integration for Materials Design) interface to access a number of materials databases (e.g., the Materials Project, NOMAD, Matterverse, etc.).

## Publications Acknowledging this Grant in 2021-2024

Several manuscripts are in varying stages of preparation.

## Mechanocatalytic Redox Reactions over Reducible Metal Oxides

Carsten Sievers, AJ Medford
Georgia Institute of Technology, School of Chemical & Biomolecular Engineering

### Presentation Abstract

Mechanochemical processes use mechanical collisions in a ball mill or similar device to drive chemical reactions. The collisions can create transient surface sites with extraordinary catalytic activity and hot spots that are characterized by rapid local temperature rises followed by dissipation of heat to the environment. In addition, mechanical forces can create intimate contact between two solids, so that the conversion of a solid reactant over a solid catalyst becomes viable.

This contribution focuses on mechanocatalytic reactions involving reducible transition metal oxides. When milled in an Ar purge stream, $MoO_3$ is reduced to $MoO_2$. DFT models illustrate that this reaction occurs at high index surfaces that are commonly formed during milling. During subsequent milling of reduced $MoO_x$ in an argon stream saturated with water, hydrogen is observed in the effluent gas indicating that water splitting occurs. Active oxygen species can be used effectively in mechanocatalytic oxidative cracking of poly(ethylene). When milled with $Fe_2O_3$, the polymer is partially oxidized in random positions of the backbone. The newly added functional groups facilitate cleavage of adjacent C-C bonds.

## DE-SC0016486: Selective Oxidation of Methane over Lewis Acidic and Redox‐Active Catalysts under Transient Conditions

**PI:** Carsten Sievers, Andrew J. Medford (co-PI)
**Postdoc(s):** Dr. Letícia Rasteiro (contributing but funded by a fellowship)
**Student(s):** Van Son Nguyen, Neung-Kyung Yu

### RECENT PROGRESS

#### *The Role of Metastable Surfaces in Mechanochemical Reduction of Molybdenum Oxide*

In this study, we combined experimental results with density functional theory (DFT) calculations to explain the mechanocatalytic reduction of $MoO_3$. The experimental setup used a ball mill with a flow of inert gas (Ar) to mechanochemically reduce $MoO_3$ to $MoO_2$. The degree of reduction was measured using a combination of techniques,

including X-ray diffraction (XRD), X-ray absorption spectroscopy (XAS), and mass spectrometry. These methods provided complementary insights into the structural and chemical changes occurring during the mechanocatalytic process, confirming that $Mo^{6+}$ was reduced to $Mo^{4+}$ with a conversion of around 60% after 60 minutes when milled at 30 Hz. We used DFT to show that the reduction of the most stable $MoO_3$ surfaces involves significant thermochemical barriers that are insurmountable even at elevated temperatures that may occur during milling. However, investigation of higher index facets and defects revealed that high-energy metastable sites are highly reactive and capable of undergoing spontaneous reduction even at room temperature (Figure 1). The formation of these metastable sites is only possible due to the scale of surface fracture energies, which can drive the formation of sites that are not thermally accessible. These metastable sites offer a unique level of reactivity compared to conventional catalytic sites. This novel result, recently published in JACS Au, represents one of the first atomic-scale investigations into the molecular-scale phenomena that underlie mechanochemical processes, advancing our understanding of how mechanical forces operate in catalysis.

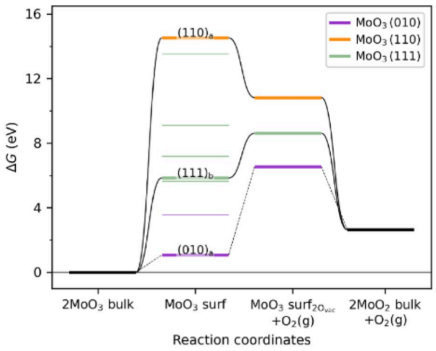


**Figure 1:** Free energy diagram for reduction of $MoO_3$ based on the most stable surface ((010)) and several high-energy meta-stable defect sites that could be created through mechanical fracture ((111) and (110)).

### *Mechanochemical Water Splitting on $MoO_2$*

Building upon this foundational work on mechanochemical reduction, we hypothesized that MoOx is reoxidized by milling in a humidified gas stream via mechanochemical water splitting. This approach could provide advantages in scalability and capital intensity as compared to solar-thermal and electrochemical routes.

To test this hypothesis, 1 g of $MoO_3$ was mechanochemically reduced by milling with a 20 mm steel ball at 30 Hz for 90 min under a flow of Ar. Then, the feed was switched to humidified Ar. After 90 min of milling under the same conditions, a new molybdenum oxide phase was observed by XRD followed by progressive amorphization at longer milling times. (Figure 2). The phase is attributed to $Mo_4O_{11}$, which contains Mo with an average oxidation state of +5.5. XANES confirmed the partial reoxidation of $MoO_x$ on the same time scale with an average oxidation state of +5.9 after 90 min.

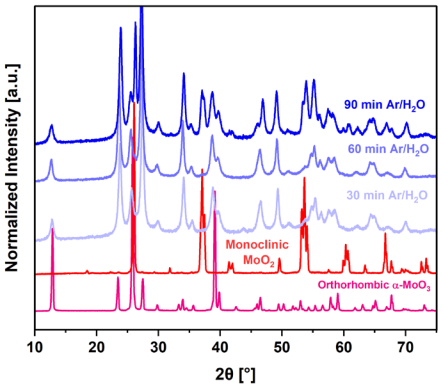


**Figure 2:** X-ray diffractograms of $MoO_x$ after milling in a flow of humid argon.

Online MS analysis of the molar flow rates of $H_2$ and $H_2O$ in the effluent stream showed that the production of $H_2$ increased during the 90 min as the $Mo_4O_{11}$ phase was formed (Figure 3). This observation is in line with a gradual depletion of oxygen vacancies that can be reoxidized. Hydrogen formation rapidly ceased when the ball mill was turned off. Since mechanochemical reduction of $MoO_3$ and reoxidation with water occur during different stages of the process, separation of the products is facilitated significantly.

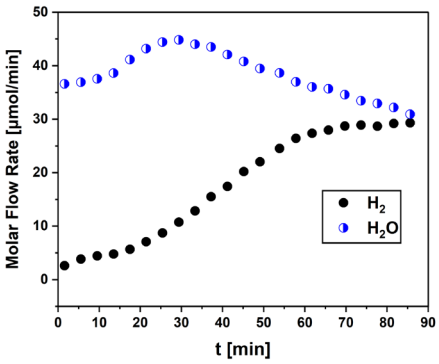


**Figure 3:** Molar flow rates of $H_2$ and water during milling of $MoO_x$ at 30 Hz in a stream of humified Ar.

### *Mechanocatalytic Oxidative Cracking of Poly(ethylene) via a Heterogeneous Fenton Process*

Mechanochemistry offers unique opportunities to process solid feedstocks like waste plastics. However, cracking of poly(olefin)s under mild conditions is thermodynamically limited under mild conditions. To overcome this challenge, we focused on oxidative cracking of poly(ethylene) by ball milling it with a Fenton system consisting of $Fe_2O_3$ and hydrogen peroxide (30 wt.% in water) in a stainless-steel vessel with stainless-steel balls. Fourier-transform infrared (FTIR) spectroscopy showed that the commercial mid density poly(ethylene) (MDPE) sample contained oxygen based functional groups due the presence of stabilizers (Figure 4a). However, when MDPE was milled with hydrogen peroxide and 5-10 wt% $Fe_2O_3$ there was a clear increase in the intensity of the bands corresponding to C=O stretching vibration. $^{13}$C-NMR analysis confirmed the presence of alcohol and carbonyl-containing groups, especially in samples with the higher $Fe_2O_3$ concentration. This result shows that parts of the polymer backbone were oxidized, which presumably occurs in random positions. The oxidation likely begins with the formation of secondary alcohols, which are further oxidized to ketones. These ketones are much more susceptible to C-C bond cleave and may be further oxidized to esters via Baeyer–Villiger oxidation followed by hydrolysis of these esters.

C–C bond scission was illustrated by high-temperature gel permeation chromatography (HT-GPC). The virgin MDPE showed a monomodal weight distribution ($M_w$ = 5876 g/mol), while the samples milled with $Fe_2O_3$ and hydrogen peroxide contained species with much lower molecular weight (Figure 4b). In case of the sample milled with 10 wt% $Fe_2O_3$ these presented products with 6-30 carbon atoms with a yield of 38%. This work was recently published in ACS Sustainable Chemistry & Engineering.

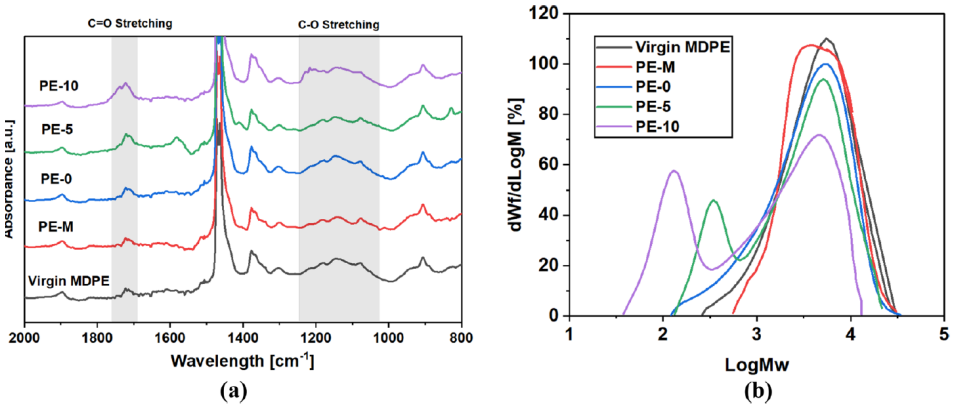


**Figure 4:** (a) FTIR spectra and (b) molecular weight distribution (MWD) determined by HT-GPC for the virgin MDPE and samples milled solely mechanically (M) or with hydrogen peroxide and 0 wt.% (PE-0), 5 wt.% (PE-5), and 10 wt.% (PE-10) of $Fe_2O_3$ catalyst.

**Publications Acknowledging this Grant in 2021-2024**

*(I) Intellectually led by this grant*


1. Lyu, Y.; Jocz, J. N.; Xu, R.; Williams, O. C.; Sievers, C., Selective Oxidation of Methane to Methanol over Ceria-Zirconia Supported Mono and Bimetallic Transition Metal Oxide Catalysts. *ChemCatChem* **2021**, *13*, 2832– 2842.
2. Lyu, Y.; Xu, R.; Williams, O. C.; Wang, Z.; Sievers, C., Reaction Paths of Methane Activation and Oxidation of Surface Intermediates over Nio on Ceria-Zirconia Catalysts Studied by in-Situ Ftir Spectroscopy. *J. Catal.* **2021**, *404*, 334-347.
3. Williams, O. C.; Sievers, C., Active Oxygen Species in Heterogeneously Catalyzed Oxidation Reactions. *Appl. Catal. A: Gen.* **2021**, *614*, 118057.
4. Jocz, J. N.; Lyu, Y.; Hare, B. J.; Sievers, C., Characterization of Surface Species During Benzene Hydroxylation over a Nio-Ceria-Zirconia Catalyst. *Langmuir* **2022**, *38*, 458–471.
5. Nguyen, V. S.; Chang, Y.; Phillips, E. V.; DeWitt, J. A.; Sievers, C., Mechanocatalytic Oxidative Cracking of Poly(Ethylene) Via a Heterogeneous Fenton Process. *ACS Sustainable Chem. Eng.* **2023**, *11*, 7617–7623.
6. Yu, N.-K.; Rasteiro, L. F.; Nguyen, V. S.; Gołąbek, K. M.; Sievers, C.; Medford, A. J., Evaluating the role of metastable surfaces in mechanochemical reduction of molybdenum oxide. *JACS Au*, accepted.


*(II) Jointly funded by this grant and other grants with intellectual leadership by other funding sources*


7. Najmi, S.; So, J.; Stavitski, E.; McDermott, W. P.; Lyu, Y.; Burt, S. P.; Hermans, I.; Sholl, D. S.; Sievers, C., In-Situ IR Spectroscopy Study of Reactions of $C_3$ Oxygenates on Heteroatom (Sn, Mo, and W) Doped Bea Zeolites and the Effect of Co-Adsorbed Water *ChemCatChem* **2021**, *13*, 445– 458.

8. Chang, Y.; Nguyen, V. S.; Hergesell, A. H.; Seitzinger, C. L.; Meisner, J.; Vollmer, I.; Schork, F. J.; Sievers, C. Thermodynamic Limits of the Depolymerization of Poly(olefin)s Using Mechanochemistry. *RSC Mechanochemistry* **2024,** *1*, 504-513.
9. Chang, Y.; Blanton, S. J.; Andraos, R.; Nguyen, V. S.; Liotta, C. L.; Schork, F. J.; Sievers, C. Kinetic Phenomena in Mechanochemical Depolymerization of Poly (styrene). *ACS Sustainable Chem. Eng.* **2024,** *12*, 178-191.
10. Kim, H.; Yu, N.-K.; Tian, N.; Medford, A. J. Assessing exchange-correlation functionals for heterogeneous catalysis of nitrogen species. *J. Phys. Chem. C* **2024,** *128*, 11159-11175.

Aaron D. Sadow

**Catalytic Hydrocarbon Functionalization at Activated Surface Organometallic Sites**

Aaron D. Sadow, Long Qi, Frédéric A. Perras, Takeshi Kobayashi, Damien B. Culver
Ames National Laboratory, Chemical and Biological Sciences Division

**Presentation Abstract**

The mission of the Ames Lab collaborative Program in Catalysis Science is to enable efficient and selective transformations by developing new catalytic principles for uniting the best features of homogeneous and heterogeneous catalysis in 3D environments. We pursue this mission through synthesis of well-defined catalytic sites in the pores of silicon oxide materials as supports, characterize the structures of the sites and the materials using advanced solid-state NMR spectroscopy, elemental analysis, infrared and X-ray adsorption spectroscopy, and electron microscopy, and study the catalysts using reactivity and kinetic measurements. Although C-H activation in homogeneous $d^0$ and $f^n d^0$ metal compounds is well established, hydrocarbon functionalization catalysis using these systems are limited. The Ames National Lab catalysis program has pursued catalytic C–H borylation and C–H alumination using surface-supported organometallic and pseudo-organometallic precursors that are activated by their grafting at Brønsted acid sites in confined environments in micropores of aluminosilicate zeolites and/or by reaction with organoaluminum Lewis acid activators. The effects of confinement can be found by comparing sites grafted in zeolites to those on external facing surfaces, as observed from dynamic behavior in solid-state NMR, regioselectivity of hydrocarbon functionalization products, the grafting and reactivity of organolanthanide sites, and the response of organometallic sites to organoaluminum activators.

**AL-03-380-011: Homogeneous and Interfacial Catalysis in 3D Controlled Environments**

**Scientists:** Dr. Yuting Li, Dr. Scott Southern
**Postdoc(s):** Dr. Mita Halder, Dr. Praveen Kumar, Dr. Marco Mais
**Student(s):** Sayak Banerjee, Puranjan Chatterjee, Austin Thompson, Danish Khan

John F. Hartwig

## Catalytic Upcycling and Deconstruction of Polyolefins by C–H Bond Functionalization and C–C Bond Cleavage

John F. Hartwig, Alex T. Bell, Ji Su,
R.J. Conk, Steven Hanna, Jake X. Shi, Nicodemo R. Ciccia

Division of Chemical Sciences, Lawrence Berkeley National Laboratory
Department of Chemistry, University of California, Berkeley

Every year, we generate 500 billion pounds of new plastics. Most of this material is used in low-value, single use applications of polyethylene, polypropylene, and to a lesser degree polyethylene terephthalate. Determining how to enable polyolefins to be used for higher value applications, how to imbue these materials with functional groups that could facilitate recycling, and how to install functionality that can trigger deconstruction are current topics in the growing field of catalytic polyolefin upcycling. In this seminar, I will present our results on polyolefin functionalization, including reactions that involve cooperative catalysis leading to the deconstruction of ethylene and polypropylene to just one or two products in high demand. Preliminary results on tuning the selectivity of the process for higher olefins and extending the lifetime of the catalyst will be presented

**Grant or FWP Number: DOE-DE-AC02-05CH11231 (LBL Catalysis and Chemical Transformations Program on Harnessing Complexity for Catalyst Efficiency)**

**Student(s):** R.J. Conk, Steven Hanna, Jake X. Shi, Nicodemo R. Ciccia

**RECENT PROGRESS (See the extended abstract for this FWP)**

**Publications for this Presentation Acknowledging this Grant in 2021-2024**

*(I) Intellectually led by this grant*

(1) Conk, R. J.; Hanna, S.; Shi, J. X.; Yang, J.; Ciccia, N. R.; Qi, L.; Bloomer, B. J.; Heuvel, S.; Wills, T.; Su, J.; et al. Catalytic deconstruction of waste polyethylene with ethylene to form propylene. *Science* **2022**, *377* (6614), 1561-1566. DOI: doi:10.1126/science.add1088.
(2) Conk, R. J.; Stahler, J. F.; Shi, J. X.; Yang, J.; Lefton, N. G.; Brunn, J. N.; Bell, A. T.; Hartwig, J. F. Polyolefin waste to light olefins with ethylene and base-metal heterogeneous catalysts. *Science* **2024**, *385* (6715), 1322-1327. DOI: doi:10.1126/science.adq7316.
(3) Chen, L.; Malollari, K. G.; Uliana, A.; Sanchez, D.; Messersmith, P. B.; Hartwig, J. F. Selective, Catalytic Oxidations of C–H Bonds in Polyethylenes Produce Functional Materials with Enhanced Adhesion. *Chem* **2021**, *7* (1), 137-145. DOI: 10.1016/j.chempr.2020.11.020 (acccessed 2021/01/15).
(4) Chen, L.; Malollari, K. G.; Uliana, A.; Hartwig, J. F. Ruthenium-Catalyzed, Chemoselective and Regioselective Oxidation of Polyisobutene. *J. Am. Chem. Soc.* **2021**, *143* (12), 4531-4535. DOI: 10.1021/jacs.1c00125.

Cong Liu

**Unveiling the Active Site using Integrated Computational XANES Simulations and Mechanistic Studies**

Yu Lim Kim, Jackie Hall, Jiayi Xu, David M. Kaphan, Max Delferro, A. Jeremy Kropf, and Cong Liu

Chemical Sciences and Engineering Division, Argonne National Laboratory, Lemont, IL 60439 USA

Identifying the structure of the catalyst is a key element of theory guided rational catalyst design. Understanding active site heterogeneity is a major challenge in heterogeneous catalysis. X-ray absorption spectroscopy (XAS) is a powerful tool to probe catalyst structure. Further, in situ spectroscopic characterization (e.g., X-ray absorption spectroscopy (XAS)) is an effective technique to study supported catalysts under realistic reaction conditions. While often overlooked as a simple reporter of formal oxidation state, X-ray Absorption Near Edge Spectroscopy (XANES) data contain additional key information on the bonding configuration and electronic environment of the metal atom(s). However, the density and convolution of information in XANES spectra compared to extended X-ray absorption fine structure (EXAFS) spectra makes the analysis of the former is more challenging. Certain bonding interactions that are key to catalysis, such as metal-hydride and second shell coordination interactions, or systems that are highly heterogeneous with an ensemble of catalytic sites, are challenging to interpret directly from experimental spectra. Computational spectroscopy simulations (e.g., XANES simulations) offer a powerful technique for interpreting experimental spectra, providing a one-to-one correspondence between a molecular structure and spectral features. Moreover, the response from this technique is dominated by the sites with the highest numerical density. However, the overall activity is dominated by the sites with the highest turnover frequencies, not necessarily those with the highest density. Thus, a systematic mechanistic study is required to identify the true active site. Our catalysis program has developed an integrated strategy combining in situ XAS measurement, computational XANES and mechanistic study that is effective in identifying the catalyst active site. Our recent work on a supported organovanadium catalyst has demonstrated that when in situ and computational XANES analyses are combined with systematic mechanistic simulations, the most active catalytic site in dynamic and disordered catalyst systems can be identified. In addition, the catalyst structure identification for oxidatively grafted Ni sites over $LiMn_2O_4$ and $Li_2Mn_2O_4$ supports using XANES simulation and the study if its catalytic mechanism will be discussed. In addition, this approach elucidates the subtle changes of XANES spectra upon lithiation in the catalyst support by investigating the electronic structures of Ni and its coordination environments. Finally, a systematic reaction mechanistic study was carried out over homologous Fe, Co, Ni and Cu sites for the hydrogenation of cyclohexene.

Ayman M. Karim

## Effect of Pt Nuclearity on $H_2$ Activation and Selective Hydrogenation

Sara Haidar[1], Hung-Ling-Yu[1], Md Raian Yousuf[1], Salman Khan[2], Dionisios G. Vlachos[2], Ayman M. Karim[1]

[1] Department of Chemical Engineering, Virginia Polytechnic Institute and State University
[2] Department of Chemical and Biomolecular Engineering, University of Delaware

### Presentation Abstract

The ability to activate hydrogen is important for many reactions including hydrogenation, hydrogenolysis, hydrodeoxygenation, hydroformylation, etc. Given the interest in maximizing the use of precious metals used for these reactions in the form of subnanometer clusters and single atoms, understanding the effect of metal nuclearity on the activation of $H_2$ and selective hydrogenation is crucial. Additionally, understanding the effect of the support on the Pt electronic properties is equally important. Using a combination of microcalorimetry, in-situ/operando infrared, Raman and X-ray absorption spectroscopies, we quantified the electron density on Pt, the binding of adsorbates, H/D exchange, and hydrogenation of $C_2H_4$ and $C_2H_2$ on different sized Pt clusters on $Al_2O_3$, $TiO_2$ and $CeO_2$. The results show a strong effect of the support leading to different trends as a function of cluster of size. In particular, the Pt supported on $CeO_2$ showed a bidirectional metal-support interaction where the different cluster sizes exhibited different $\%Ce^{3+}$ and electron density on Pt resulting in orders of magnitude volcano-type dependence of the $C_2H_4$ hydrogenation rate on size. The activity/selectivity of acetylene hydrogenation to ethylene will be presented and the consequences of the metal support interactions will be discussed.

**DE-SC0022144: Molecularly Tailored Subnanometer Hydrogenation Catalysts**

**PI:** Ayman M. Karim **co-PI:** Dionisios G. Vlachos
**Postdoc(s):** Salman Khan
**Student(s):** Sara Haidar, Hung-Ling-Yu, Md Raian Yousuf

### RECENT PROGRESS

#### *Dynamics of Cluster Size Dependent Pt-$CeO_2$ Interactions*

The properties of different size Pt clusters supported on $CeO_2$ were investigated using infrared spectroscopy, Raman spectroscopy and X-ray absorption spectroscopy. Figure 1a-c shows aberration-corrected scanning transmission electron microscopy images of $Pt/CeO_2$. The average Pt size was obtained by reduction at different temperatures of 200, 300 and 500 °C resulting in 0.8, 1.0 and 1.5 nm average diameter Pt clusters. The model fits of the EXAFS spectra in Figure 1d-e showed average Pt first shell coordination

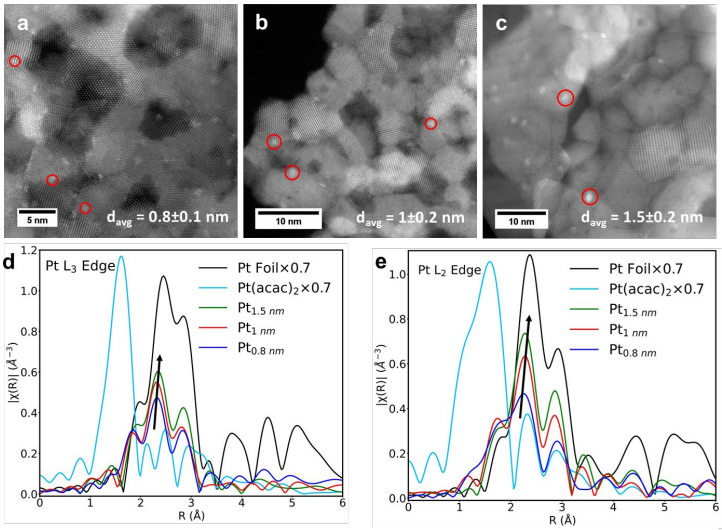


*Figure 1: AC-HAADF-STEM images of 0.8% Pt/$CeO_2$ after reduction at (a) 200 °C, (b) 300 °C, and (c) 500 °C for 2 hours under 10% $H_2$ flow with balance He.$L_3$ (d) and $L_2$ (e) $k^2$-weighted R-space data for the 0.8% Pt/$CeO_2$ reduced at 200, 300, and 500 °C (0.8, 1.0, and 1.5 nm Pt).*

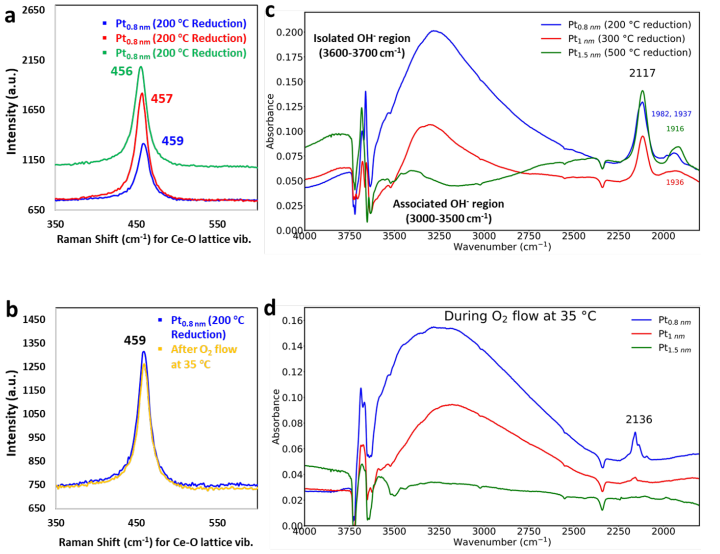


*Figure 2: In situ Raman spectra for Ce-O lattice vibration (a and b) and in situ DRIFTS spectra of $Ce^{3+}$ region and surface-adsorbed OH- groups (c and d) collected at 35 °C after reduction at 200, 300, and 500 °C followed by cooling to 35 °C under $N_2$ flow then exposed to 10% $O_2$.*

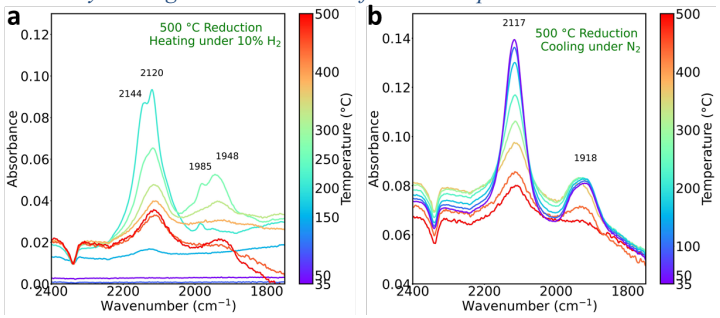


*Figure 3: Infrared spectra during heating in $H_2$ and cooling in $N_2$ for the 1.5 nm Pt/$CeO_2$.*

numbers of 4.8, 5.8 and 8.1 consistent with the average diameters from STEM. The higher the reduction temperature of the catalysts resulted in more reduction of the $CeO_2$ as shown by the red shift of the Ce-O Raman peak in Figure 2a. However, the intensity of the $Ce^{3+}$ infrared peak at ~2117 $cm^{-1}$ suggests that the concentration of $Ce^{3+}$ on the surface could be different from the bulk information obtained by Raman spectroscopy. The surface sensitivity of infrared spectroscopy can be seen when the catalysts are exposed to a flow of $O_2$. The $Ce^{3+}$ peak is completely consumed due to filling of the vacancies for the 1.5 nm Pt catalyst while there clearly remain some $Ce^{3+}$ on the 0.8 nm Pt catalyst. X-ray photoelectron spectroscopy confirmed the consumption of $Ce^{3+}$ (not shown). In contrast to IR and XPS, the consumption of $Ce^{3+}$ is completely invisible to Raman since it is a bulk technique.

The results in Figures 1-2 indicate that the Pt cluster size affects the $CeO_2$ reducibility and $Ce^{3+}$ concentration on the surface vs. in the bulk. Specifically, the amount of surface $Ce^{3+}$ appears to be affected by temperature as shown in Figure 3. The $Ce^{3+}$ peak is shown to increase with temperature during reduction, but then diffusion in the bulk starts around 200 °C. Surprisingly, during the cool

down the $Ce^{3+}$ peak increases again. We note that these changes were dependent on temperature and resulted in different final peak intensities on the catalysts with different Pt sizes as shown in Figure 2c. Furthermore, the ability to activate $O_2$ and refill the surface vacancies is also dependent on the Pt cluster size where the largest clusters are more active. This dynamic interplay between the properties of Pt and $CeO_2$ is also seen in the electronic properties of Pt, where Pt was more electron deficient on the sample with the lowest reduction extent of $CeO_2$ (reduced at 200 °C, 0.8 nm Pt clusters). This is shown by the higher Pt $L_2$ XANES white line intensity (Figure 4) for the smaller size clusters. The effect of the support on metal nanoparticles has been considered mainly as a metal oxide affecting the metal clusters. However, our results show that the interaction is bidirectional and the support properties are also modified by the metal clusters. Additionally, the bi-directional interaction is dependent on the size of the Pt clusters and can lead to different overall catalyst properties.

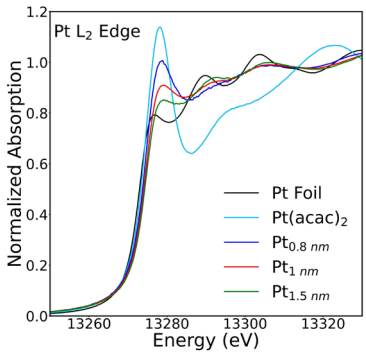


*Figure 4: Pt $L_2$ XANES spectra for the Pt/$CeO_2$ catalysts.*

### *Tuning the Metal Support Interaction for Enhanced $C_2H_4$ Hydrogenation on Pt*

The properties of supported Pt clusters are affected by their size and the size dependent metal-support interaction. To determine the effect on the catalytic properties, we investigated the activity of the catalysts for hydrogenation of ethylene. The activity was strongly dependent on the size of the clusters as shown in Figure 5. The Pt single atoms showed the lowest activity. The activity on the 0.8 nm clusters increased by more than 3 orders of magnitude then dropped significantly as the average size increased to 1.0 and 1.5 nm. It is important to note that the size distributions of these catalysts do overlap, and yet despite this, the activity is clearly different in terms of turn over frequency (TOF) and apparent activation energy ($E_{app}$). The results indicate a strong structure sensitivity that depends on the geometric and electronic properties of the Pt clusters. Specifically, in addition to having the lowest Pt-Pt coordination, the XANES results in Figure 4 indicate that the 0.8 nm clusters are the most electron deficient compared to the larger sizes. To demonstrate the importance of the electronic properties, specifically the electron density on Pt, we oxidized the 1.5 nm Pt clusters at room temperature to fill the surface oxygen vacancies then reduced the catalyst at 100 °C to reduce the Pt without significantly reducing the $CeO_2$ surface (labelled low Ov). Figure 6 shows the effect of this treatment on the infrared $Ce^{3+}$ peak and the white line intensity in the Pt $L_3$ and $L_2$ spectra. The room temperature oxidation followed by 100 °C reduction led to reduction of the $Ce^{3+}$ peak and an increase in the white line intensity in the $L_2$ XANES spectrum indicating the

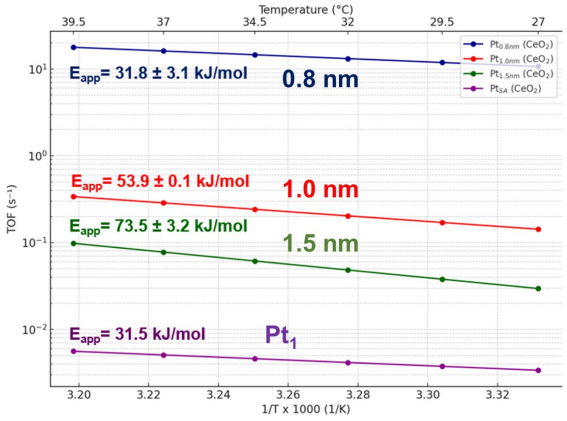


*Figure 5: Arrhenius plots of $C_2H_4$ hydrogenation on Pt/$CeO_2$ at 0.5 kPa $C_2H_4$ and 5 kPa $H_2$.*

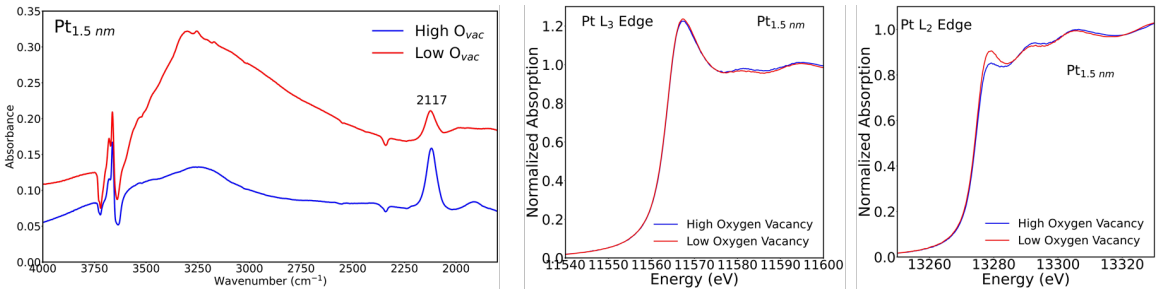


*Figure 6: Infrared spectra (a) and Pt $L_{3,2}$ XANES spectra for the 1.5 nm Pt/$CeO_2$ after reduction at 500 °C (red) and followed by oxidation in 10% $O_2$ at room temperature and reduction at 100 °C. All spectra were collected at room temperature.*

lower concentration of oxygen vacancies resulted in lower electron density on Pt. Furthermore, the increase in $L_2$ white line intensity while that at the $L_3$ remaining unchanged indicates that the increase in unoccupied d states is solely of $5d_{3/2}$ character. The lower electron density on Pt and change in the ratio of unoccupied d states ($h_{5/2}/h_{3/2}$) was not expected since the $h_{5/2}/h_{3/2}$ ratio has been considered constant (~14) for Pt metal. The results indicate that the properties of the support have a significant effect on the electronic structure of Pt clusters. We note that the Pt-Pt coordination number in those two states was unchanged (8.1 vs. 8.0, not shown), therefore, eliminating the possibility of a change in the size of the clusters. However, a change in the structure/shape cannot be ruled out. Nevertheless, the activity for ethylene hydrogenation was significantly higher after the oxidation/reduction treatment. The lower electron density on Pt (and lower $h_{5/2}/h_{3/2}$ ratio) led to a 2-3x increase in TOF and a lower $E_{app}$ (44 vs. 74 kJ/mol) as shown in Figure 7. The results show the importance of the size and the electronic properties of Pt on reactivity. More importantly, our results show the importance of understanding the effect of the Pt nuclearity and electronic structure on reactivity. Ongoing work is focused on investigating the effects of %$Ce^{3+}$, electron density and $h_{5/2}/h_{3/2}$ ratio on binding with adsorbates and their correlation with reactivity.

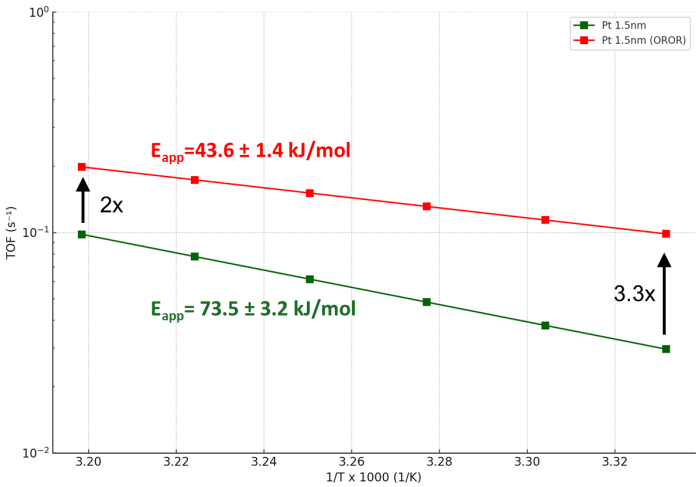


*Figure 7: Effect of pretreatment on the activity for ethylene hydrogenation on 1.5nm Pt/$CeO_2$ after reduction at 500 C (green) and after reduction at 500C followed by oxidation at room temperature and reduction at 100C (red).*

**Publications Acknowledging this Grant in 2021-2024**

*Please classify your publications into two categories according to the source of support for the work published:*

*(I) Intellectually led by this grant*

*a. Reversible Temperature-Induced Shape Transition of Pt Nanoparticles Supported on $Al_2O_3$, ACS Nano (revision submitted)*

*b. Yan, G.; Vlachos, D.G.; ACS Catalysis **2023** 13 (16), 10602-10614*

*c. <u>three more papers</u> in preparation*

*(II) Jointly funded by this grant and other grants with intellectual leadership by other funding sources*

***a.*** Li, Q.; Yan, G.; Vlachos D.G.; *ACS Catalysis, **2024**, 14, 2, 886–896*

## Connecting Structure to Catalytic Function in Bimetallic Alloys

Jesse Q. Bond
Department of Biomedical and Chemical Engineering
Syracuse University
Syracuse, NY 13244

### Presentation Abstract

At the reactor scale, multi-metallic "alloy" catalysts often perform differently from their single-component analogs comprised of the constituent metals in isolation. Alloys often deliver improved activity, selectivity, and/or stability; as such, combining metals is a common strategy for tuning the performance of a catalytic reactor. Although gains from alloying are frequently apparent, the nanoscale impacts of combining metals are numerous and complex. They may include simple geometric effects like site-blocking and ensemble disruption. They may also include fundamental changes to the composition, coordination environment, and electron density of the active site. As experimentalists, we observe convolutions of these effects, and it is challenging to resolve the specific aspect of alloy formation that underlies an observed perturbation in catalyst performance. A frustrating and longstanding challenge in the study of alloy catalysts is the difficulty of characterizing and titrating active sites under reaction conditions. This is a fundamental problem: if one can neither describe nor count active sites, one cannot define a turnover frequency. Consequently, meaningful activity descriptions for alloy catalysts are lacking. This makes it difficult to understand how changes in alloy composition and structure impact reactivity, which stymies rational design. Here, we consider rates of CO methanation over Pt and $Pt_xSn_y$ measured using steady state and transient methods. We correlate activity with spectroscopic characterization and various techniques for active site titration. We conclude that trace Sn addition (without intermetallic formation) has geometric impacts that have no influence on intrinsic activity but are detrimental to reactor scale performance. In contrast, high Sn loadings often drive intermetallic formation, which is accompanied by a near-complete loss of activity that appears to result from the loss of Pt-Pt site pairs.

**Connecting Surface Structure with Activity for Alloy Catalysts under Working Conditions: DESC0022071**

**PI:** Jesse Bond
**Postdoc(s):** None
**Student(s):** Robson Schuarca, Yaqin Tang, Mohammed Tahseen Islam
**Affiliations(s):** Syracuse University

## RECENT PROGRESS

A recent emphasis of this project has been on the use of transient methods, such as SSITKA, to provide information about active surface areas for $Pt_xSn_y$ catalysts as well as time scales for the catalytic cycle under methanation conditions (i.e., under CO and $H_2$). These efforts have been paired with FTIR spectroscopy to interrogate CO coordination on various alloy surfaces and to understand how CO binding changes with Sn-enrichment. We have transitioned to the analysis of carbonyl hydrogenation over $Pt_xSn_y$ surfaces as this is historically reported to be a system where hydrogenation rates are promoted by oxophilic metals, like Sn. Here, we observe complex impacts of alloy formation. Trace Sn-doping benefits macroscopic rates of carbonyl hydrogenation, whereas significant Sn-enrichment hinders the reaction. Work in these areas is ongoing and aimed at understanding differences observed with variations in metal composition.

## Publications Acknowledging this Grant in 2021-2024

*(I) Intellectually led by this grant*

*(II) Jointly funded by this grant and other grants with intellectual leadership by other funding sources*

1. He, W.; Potts, D.S.; Zhang, Z.; Liu, B.; Schuarca, R.L.; Hwang, S.J. Bond, J.W., Flaherty, D.W., and Cybulskis, V.J., "Lewis acidity and substituent effects influence aldehyde enolization and C–C coupling in beta zeolites," Journal of Catalysis, 2023, 427, 115105.

# NATIONAL LABORATORIES ABSTRACTS

Aaron D. Sadow

## Uniform catalytic environments at the interface: characterization of sites and distributions, catalytic activity and reaction mechanisms

Takeshi Kobayashi, Frédéric A. Perras, Long Qi, Damien Culver, Aaron D. Sadow
Ames National Laboratory, Chemical and Biological Sciences Division, Iowa State University, Ames, IA 50011-3111

### Presentation Abstract

The mission of the Ames Lab collaborative Program in Catalysis Science is to enable efficient and selective transformations by developing new catalytic principles for uniting the best features of homogeneous and heterogeneous catalysis in 3D environments. The overarching goal of this fundamental research is to synthesize and study highly uniform solid catalysts that mediate the difficult carbon-oxygen and carbon-hydrogen bond cleavage reactions, which are needed to utilize bioderived feedstocks and abundant hydrocarbons for chemical synthesis. To this end our research team combines expertise in mesoporous and nanostructured catalyst synthesis, organometallic chemistry, kinetics and mechanisms of catalytic reactions, and solid-state (SS)NMR, including the ultrasensitive dynamic nuclear polarization (DNP) technique. Uniform materials are essential because their spectroscopic features characterize the most important and most pertinent species and functionality for affecting the overall catalytic properties, thus facilitating the rational improvement of catalysts. Unfortunately, catalytic species operating at the solid-liquid interface rarely approach the ideal homogeneity (sometimes) epitomized by chemistry in a single phase. To address this gap, our team combines advanced materials synthesis and surface organometallic chemistry with cutting-edge NMR spectroscopic methods to construct uniform organometallic catalytic sites, distributed evenly in the uniform environments created by pores of hierarchical functionalized mesoporous materials. These species represent several classes of catalysts commonly applied in hydrogenations and hydrodeoxygenations of oxygenates or in C-H bond activations, which are nonetheless currently limited. Using the uniform materials and operando spectroscopy, we elucidate molecular-level mechanisms, including those involved in complex reaction networks, and then ameliorate the features that constrain catalytic performance.

### AL-03-380-011: Homogeneous and Interfacial Catalysis in 3D Controlled Environments

**Scientists:** Dr. Yuting Li, Dr. Scott Southern
**Postdoc(s):** Dr. Mita Halder, Dr. Praveen Kumar, Dr. Marco Mais
**Student(s):** Sayak Banerjee, Puranjan Chatterjee, Austin Thompson, Danish Khan

**Publications Acknowledging this Grant in 2021-2024**
***Source of support for the work published***
**(I)** ***Intellectually led by this grant*** 2021 [1-7] 2022[8-18] 2023 [19-23] 2024 [24-26]

**(II)** ***Jointly funded by this grant and other grants with intellectual leadership by other funding sources*** 2021 [27-33] 2022[34-40] 2023 [41-49] 2024 [50-59]

## RECENT PROGRESS

***Lanthanum Borohydride Catalyzed C-H Borylation of Hydrocarbons.*** The borylation of benzene is catalyzed by lanthanum borohydride grafted on $HY_{30}$ or $SiO_2/Al_2O_3$, but not by lanthanum borohydride grafted on silica or alumina. We have studied the grafting of lanthanum borohydride in the faujasite zeolite $HY_{30}$ in detail using solid-state NMR spectroscopy, DRIFTS, EXAFS, and microscopy. In addition, scandium borohydride grafts analogously on $HY_{30}$, and solid-state $^{45}Sc$ NMR spectroscopy, along with analysis of the effect of dynamics on apparent structures reveal unique behavior of these sites in the micropores of the zeolite. In these studies, the external surface of $HY_{30}$ was capped with $Ph_3Si$ moieties to favor grafting in the micropores and block grafting on the external surface. First, grafting of $Ln(BH_4)_3(THF)_3$ with $Ph_3Si$-$HY_{30}$ results in a species that has the constitution $O_{surface}$–$Ln(BH_4)_2(THF)_2$, and $H_2$, $BH_3$, and THF are eliminated. Although $Ln(BH_4)_3(THF)_3$ is to large to directly enter the micropores, DFT calculations estimate that $La(BH_4)_3(THF)_2$, having dissociated one THF from its precursor is more stable in the supercage of the zeolite than the tris(THF) starting material. Moreover, the five-coordinate trigonal bipyramidal geometry allows the complex to enter and freely move in the micropores. Analysis of the grafted materials by scanning transmission electron microscopy – energy dispersive X-ray spectroscopy (STEM-EDS) revealed that La grafts throughout the material, and its grafting is not localized on the external surface or concentrated at the surface of the zeolite particles. Remarkably, the scandium analogue was shown to form a monopodal interaction with the pore, yielding the species ≡Si(≡Al)–O–$Sc(BH_4)_2(THF)_2$ which hops between the two neigboring ≡SiO(=Al)OSi≡; in contrast La binds to both O in its lowest energy structure. These conformations are revealed by SSNMR distance measurements matched to DFT-calculated chemical shifts and quantum mechanical molecular dynamics calculations. The material $La(BH_4)_2(THF)_{2.5}$-$Ph_3Si$-$HY_{30}$ gives ca. 50 turnovers to phenylpinacolborane (7%) as catalyst for the reaction of pinacolborane and benzene, while the scandium analogue gives higher yield (8%) but lower turnovers.

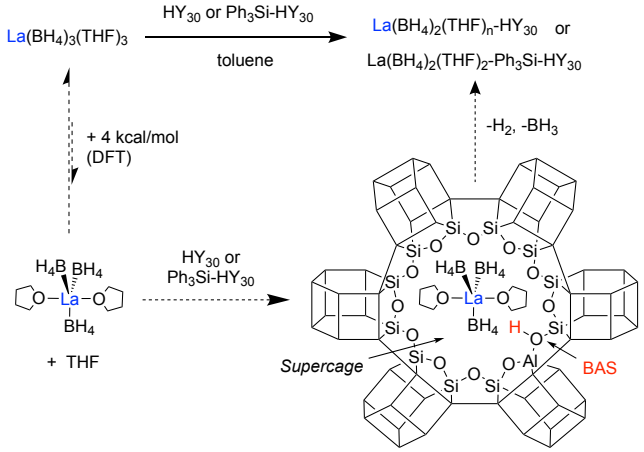


**Fig. 1.** Proposed mechanism for grafting $La(BH_4)_3(THF)_3$ in the micropores of $HY_{30}$.

Because the $BH_4$ ligand appeared to be displaced during catalysis, and the remaining THF ligands could deactivate the Ln center, we investigated activators that could displace $BH_4$ and THF. $AlMe_3$ was promising in this regard, and treatment of $La(BH_4)_2(THF)_{2.5}$-$Ph_3Si$-$HY_{30}$ with $AlMe_3$ affords a material that gives over 100 turnovers in benzene borylation (~21% yield). Solid-state NMR and EXAFS indicate that THF has dissociated from La, and one $AlMe_3$ is coordinated to the La center in the activated catalyst. The rate of benzene borylation, however, is surprisingly similar with the aluminum-activated material and its precursor (given the more than 3-fold increase in yield). Kinetic analysis reveal that the rate of HBpin decomposition, the side reaction that affects yield, is inhibited in $La(BH_4)_2AlMe_3$-$Ph_3Si$-$HY_{30}$. Moreover, the rate is first order for HBpin decomposition, whereas PhBpin formation is zero-order. Using knowledge of the rate constants and reaction orders, the turnovers and yields can be increased to >300 and 45%, respectively, by keeping the HBpin concentration low. There is an addition affect of $AlMe_3$. $La(BH_4)_2(THF)_2$-$SiO_2$ is inactive for CH borylation; however, treatment with $AlMe_3$ yields a material that is catalytically active by replacing THF and creating a more electrophilic lanthanum site. La inside of the zeolite is not activated by $AlMe_3$ in this manner; instead the intrapore site shows similar activity before and after alkylaluminum treatment. We attribute this affect to confinement of $O_{surface}$–$Ln(BH_4)_2(THF)_2$, which destabilized THF and $BH_3$ coordination, leading to highly active sites without additional Lewis acid activation by adduct formation. The non-confined analogue requires $AlMe_3$ to enable THF dissociation and catalyst activation.

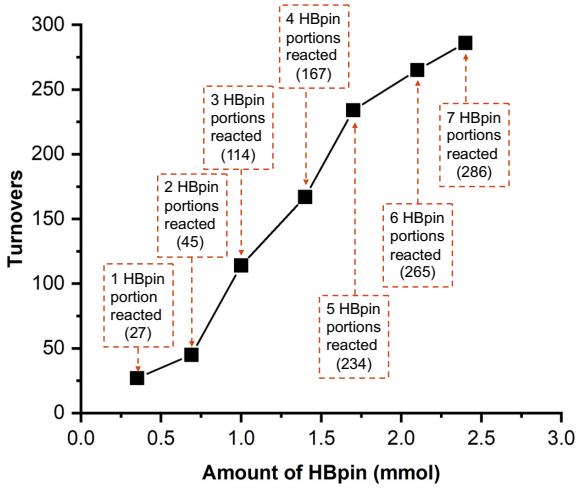


**Fig. 2.** Portion-wise addition of HBpin leads to high turnovers and higher PhBpin yield.

***Advancement of Solid-State NMR to Characterize Uniform Catalytic Sites.*** Catalytic activity and selectivity are intimately tied to the atomistic structure and configuration of the pre-catalytic, and active, sites dispersed on the surfaces of support materials. We are developing new approaches that are based on sensitivity-enhanced NMR spectroscopy ($^1H$ detection under fast MAS and dynamic nuclear polarization, DNP) to move beyond determining bonding networks, to also determine the 3D configurations of sites, their orientations on the support, and how these factors influence catalysis. Using NMR dipolar interactions-based methods, we triangulate the positions of atoms and their relative positions on the support to determine 3D structures. To date, these approaches have made the critical assumption that SOMC species can be described as single-sites and a single set of interatomic distances, but this is not necessarily the case due to the disordered nature of oxide surfaces. We performed a comprehensive study of these distance geometry methods in the presence of site heterogeneity and found that indeed NMR distance measurements can differentiate very different structures, but may fail to distinguish similar conformers.

For instance, we modulated the podality, and thus bonding angle, of a Zr metallocene complex supported onto γ-$Al_2O_3$ treated at temperatures ranging from 400 to 1000 °C. We found that we were unable to distinguish the individual conformers but instead that the fitted bonding angle appeared to be a smooth function of the treatment temperature, a measure of the mono and bipodal site ratio.

The success of these methods relies on the installation of NMR-active nuclei on the surface of the support, such as $^{27}Al$, $^{29}Si$, and $^{17}O$. $^{17}O$ is particularly interesting as it yields a unique signature for the site bonded to the metal center. Enriching silica, and other oxide supports, in $^{17}O$ is nevertheless laborious and expensive. Using *in situ* $^{17}O$ NMR, we discovered that the surface silanols of silica spontaneously exchanged with $^{17}OH_2$, enabling the facile selective labeling of silica surfaces for 3D structure determination and studies of grafting reactions.

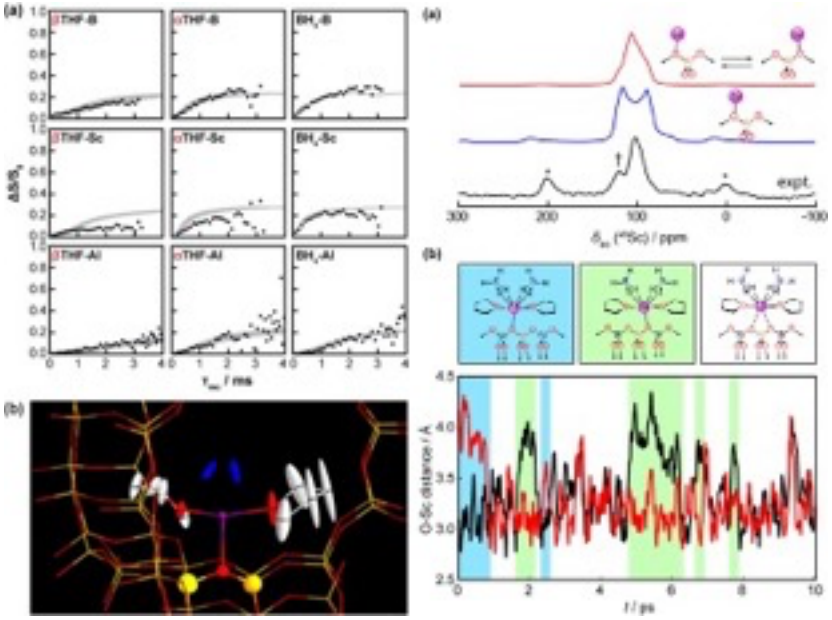

**Fig. 3.** (left) NMR-based distance measurements (top) were used to determine the 3D structure of $Sc(BH_4)_2(THF)_2/Y_{30}$ (bottom). (right) 45Sc NMR spectra (top) of this species display motional narrowing that is explained by the fluctuations in the largely ionic support-Sc bonding (bottom).

We applied these methods to understand the unique catalytic activity observed for C-H borylation when $Ln(BH_4)_3THF_n$ is grafted onto a zeolitic support. The same complex is inactive when grafted to silica. Using $^{1}H$-detected distance measurements we could determine the site's geometry and that it was coordinated at a Brønsted acid site location. The dipolar coupling, and $^{45}Sc$ NMR, experiments revealed this site to be particularly dynamic. Molecular dynamics simulations revealed that the weak, ionic, $SiOAl^{-}\cdots Sc^{+}$ interaction led to a highly fluxional and electropositive species, more prone to activation. In a separate study of Ln amidinate complexes, we discovered that fluxional, undercoordinated, complexes can be generated using confinement, potentially opening the door to new and unique catalysis.

Owing to the enhanced catalysis observed in zeolite-supported single sites, we aimed to finally solve the debate regarding the structure of the acid sites on amorphous silica alumina. The literature on the topic is divided into two camps that hypothesize that the sites are either very dilute zeolitic acid sites (SiO(H)Al), or the less active pseudo-bridging silanols (PBS, Si-OH···Al). Using reverse H/D exchange of the most active acid sites using $C_6H_6$ on an otherwise perdeuterated catalyst, we could selectively detect the Brønsted sites

in amorphous silica-alumina for the first time and further measure their distance to a nearest Al center. These proved to be identical to the distances measured in zeolites, confirming once and for all that amorphous silica-alumina catalysts share the same active sites as zeolites. Increasing their concentration is expected to also benefit the design of metal catalysts supported at acidic sites for enhanced activity.

***Metal-Support Cooperativity for C–O hydrogenolysis.*** Heterogeneous catalysts with single-site metal active sites have the potential to perform catalytic transformations with maximal metal atom utilization, and with selectivities that can be tuned by systematic variation of the coordination environment, similar to molecular catalysts. Catalyst stability is conferred when strong coordination results from embedding metal centers in the support, but this type of bonding can also reduce reactivity in multistep catalytic transformations due to the limited availability of binding sites for reactants. The trade-off between stability and reactivity can be mitigated when the support provides additional binding sites to assist in the chemisorption and activation of the reactants. Catalysts with single-site first-row transition metals are promising performance in selective catalytic hydrogenation. Still, they are less reported for more complex reactions for instance C–O hydrogenolysis. First-row transition metals with single electron redox cycles can be active for selective C–O hydrogenolysis of oxygenated hydrocarbons when leveraging the cooperativity with the support that is the redox and chemically non-innocent. We recently reported that a single-site, well-defined Fe catalyst supported on non-innocent nitrogen-doped carbons (N-Cs) can catalyze C–O bond hydrogenolysis of aryl alcohols and ethers at as low as 170 °C. Microscopic, spectroscopic, and computational studies reveal that the Fe sites in the as-synthesized catalysts are predominantly penta-coordinated $N_4Fe^{III}(OH)$. In the presence of $H_2$ under reaction temperature, the hydroxyl ligand is lost when $N_4Fe^{III}OH$ is reduced to $N_4Fe^{II}$. Alcoholic substrates react to the tetra-coordinated $Fe^{II}$ sites through homolytic cleavage of the O-H bond and re-oxidation to $Fe^{III}$. In this course, one electron is transferred to the support and is localized by adjacent additional graphitic nitrogen atoms, together with the formation of a new C-H bond involving a carbon atom in the N-C support. Overall, support-mediated redox and chemical processes with a non-innocent support were successfully demonstrated for a chemical transformation involving reactant binding and multiple bond activations in a single catalytic turnover, which is analogous to the behavior of chemically- and redox-non-innocent ligands in molecular catalysts based on first-row transition metal ions. Such processes are common in upgrading renewable feedstocks such as biomass and $CO_2$. Better understanding of metal-support cooperativity can generate more effective catalyst designs and applications, with base metals as substitutes for classic precious metal-based catalysts.

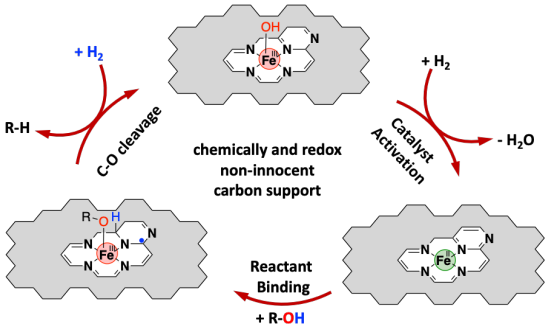


**Fig. 4**. Proposed chemical and redox non-innocence of an extended N-doped carbon support, which promotes homolytic O-H bond cleavage of alcohols at atomically-dispersed $Fe^{II}$ sites. One-electron oxidation of $Fe^{II}$ to $Fe^{III}$ is accompanied by free radical generation at carbon, stabilized by adjacent N.

**Awards or leadership activities during 2021-2024 calendar years**

Frédéric Perras: DOE Early Career Award (2020)
Long Qi: Great Plains Catalysis Society Meeting organizing committee (2020, 2022)
Aaron Sadow: Director of Institute for Cooperative Upcycling of Plastics (iCOUP) DOE-EFRC (2020-2028)
Aaron Sadow: Great Plains Catalysis Society Meeting organizing committee (2022)
Aaron Sadow: Trapp Innovation Award (2022)
Frédéric Perras: Recognized as an emerging researcher by the Journal of Physical Chemistry (2023)
Frédéric Perras: Awarded the Caldarelli Prize in Magnetic Resonance (2023)
Aaron Sadow: AAAS Fellow (2023)
Aaron Sadow: David C. Henderson Endowed Professor
Frédéric Perras: Early-Career and Emerging Researchers in Physical Chemistry (2023)
Frédéric Perras: Emerging Investigators (2024)
Frédéric Perras: New Voices in Magnetic Resonance (2023)

**Publications Acknowledging this Grant in 2021-2024**


(1) Patnaik, S.; Kanbur, U.; Ellern, A.; Sadow, A. D. Hydrosilane σ-Adduct Intermediates in an Adaptive Zinc-Catalyzed Cross-dehydrocoupling of Si−H and O−H Bonds. *Chem. Eur. J.* **2021**, *27* (40), 10428-10436, 10.1002/chem.202101146. DOI: 10.1002/chem.202101146.

(2) Naik, P. J.; Chatterjee, P.; Chen, S.; Huang, W.; Slowing, I. I. Regulating the Catalytic Activity of Pd Nanoparticles by Confinement in Ordered Mesoporous Supports. *ChemCatChem* **2021**, *13* (2), 539-542, 10.1002/cctc.202001594. DOI: 10.1002/cctc.202001594.

(3) Eedugurala, N.; Wang, Z.; Kanbur, U.; Ellern, A.; Pruski, M.; Sadow, A. D. Synthesis and Characterization of Tris(oxazolinyl)borato Copper(II) and Copper(I) Complexes. *Helv. Chim. Acta* **2021**, *104* (2), e2000209, 10.1002/hlca.202000209. DOI: 10.1002/hlca.202000209.

(4) Boteju, K. C.; Venkatesh, A.; Chu, Y.-Y.; Wan, S.; Ellern, A.; Rossini, A. J.; Sadow, A. D. Ancillary Steric Effects on the Activation of SiH Bonds in Arylsilazido Rare-Earth Compounds. *Organometallics* **2021**, *40* (11), 1654-1669. DOI: 10.1021/acs.organomet.1c00162.

(5) Perras, F. A.; Paterson, A. L.; Syed, Z. H.; Kropf, A. J.; Kaphan, D. M.; Delferro, M.; Pruski, M. Revealing the Configuration and Conformation of Surface Organometallic Catalysts with DNP-Enhanced NMR. *J. Phys. Chem. C* **2021**, *125* (24), 13433-13442. DOI: 10.1021/acs.jpcc.1c03176.

(6) Chen, J.; Qi, L.; Zhang, B.; Chen, M.; Kobayashi, T.; Bao, Z.; Yang, Q.; Ren, Q.; Huang, W.; Zhang, Z. Tandem Synthesis of Tetrahydroquinolines and Identification of the Reaction Network by Operando NMR. *Catal. Sci. Technol.* **2021**, *11* (13), 4332-4341, 10.1039/D1CY00418B. DOI: 10.1039/D1CY00418B.

(7) Naik, P. J.; An, Y.; Sedinkin, S. L.; Masching, H.; Freppon, D.; Smith, E. A.; Venditti, V.; Slowing, I. I. Non-Innocent Role of the Ceria Support in Pd-Catalyzed

Halophenol Hydrodehalogenation. *ACS Catal.* **2021**, 10553-10564. DOI: 10.1021/acscatal.1c02716.
(8) Li, Y.; Kanbur, U.; Cui, J.; Wang, G.; Kobayashi, T.; Sadow, A. D.; Qi, L. Supported Lanthanum Borohydride Catalyzes CH Borylation Inside Zeolite Micropores. *Angew. Chem. Int. Ed.* **2022**, *61*, e202117394, /10.1002/anie.202117394. DOI: 10.1002/anie.202117394.
(9) Perras, F. A.; Kanbur, U.; Paterson, A. L.; Chatterjee, P.; Slowing, I. I.; Sadow, A. D. Determining the Three-Dimensional Structures of Silica-Supported Metal Complexes from the Ground Up. *Inorg. Chem.* **2022**, *61* (2), 1067-1078. DOI: 10.1021/acs.inorgchem.1c03200.
(10) Chatterjee, P.; Wang, H.; Manzano, J. S.; Kanbur, U.; Sadow, A. D.; Slowing, I. I. Surface Ligands Enhance the Catalytic Activity of Supported Au Nanoparticles for the Aerobic α-Oxidation of Amines to Amides. *Catal. Sci. Technol.* **2022**, *12* (6), 1922-1933, 10.1039/D1CY02121D. DOI: 10.1039/D1CY02121D.
(11) Cui, J.; Chatterjee, P.; Slowing, I. I.; Kobayashi, T. In Situ $^{29}$Si Solid-State NMR Study of Grafting of Organoalkoxysilanes to Mesoporous Silica Nanoparticles. *Microporous Mesoporous Mater.* **2022**, *339*, 112019. DOI: 10.1016/j.micromeso.2022.112019.
(12) Lin, Y.; Nie, R.; Li, Y.; Wu, X.; Yu, J.; Xie, S.; Shen, Y.; Mao, S.; Chen, Y.; Lu, D.; et al. Highly Efficient and Anti-poisoning Single-atom Cobalt Catalyst for Selective Hydrogenation of Nitroarenes. *Nano Res.* **2022**. DOI: 10.1007/s12274-022-4294-6.
(13) Luo, Z.; Yin, Z.; Yu, J.; Yan, Y.; Hu, B.; Nie, R.; Kolln, A. F.; Wu, X.; Behera, R. K.; Chen, M.; et al. General Synthetic Strategy to Ordered Mesoporous Carbon Catalysts with Single-Atom Metal Sites for Electrochemical $CO_2$ Reduction. *Small* **2022**, *18* (16), 2107799, 10.1002/smll.202107799. DOI: 10.1002/smll.202107799.
(14) Hu, H.; Nie, Y.; Tao, Y.; Huang, W.; Qi, L.; Nie, R. Metal-free Carbocatalyst for Room Temperature Acceptorless Dehydrogenation of N-Heterocycles. *Sci. Adv.* **2022**, *8* (4), eabl9478. DOI: 10.1126/sciadv.abl9478.
(15) Chu, Y.-Y.; Lolinco, A.; Eedugurala, N.; Ellern, A.; Windus, T. L.; Sadow, A. D. Reversible Ligand Protonation in Noninnocent Constrained-Geometry-Like Group 4 Complexes. *Organometallics* **2022**, *41* (2), 141-154. DOI: 10.1021/acs.organomet.1c00612.
(16) Cunningham, J.; Perras, F. A. INTERFACES. A Program for Determining the 3D Structures of Surfaces Sites Using NMR Data. *J. Magn. Reson. Open* **2022**, *12-13*, 100066. DOI: 10.1016/j.jmro.2022.100066.
(17) Kobayashi, T.; Liu, D.-J.; Perras, F. A. Spatial Arrangement of Dynamic Surface Species from Solid-state NMR and Machine Learning-accelerated MD Simulations. *Chem. Commun.* **2022**, *58* (100), 13939-13942, 10.1039/D2CC05861H. DOI: 10.1039/D2CC05861H.
(18) Yin, Z.; Yu, J.; Xie, Z.; Yu, S.-W.; Zhang, L.; Akauola, T.; Chen, J. G.; Huang, W.; Qi, L.; Zhang, S. Hybrid Catalyst Coupling Single-Atom Ni and Nanoscale Cu for Efficient CO2 Electroreduction to Ethylene. *J. Am. Chem. Soc.* **2022**, *144* (45), 20931-20938. DOI: 10.1021/jacs.2c09773.
(19) Naik, P. J.; Kunal, P.; Liu, D.-J.; Evans, J. W.; Slowing, I. I. Efficient Transfer Hydrodehalogenation of Halophenols Catalyzed by Pd Supported on Ceria. *Appl. Catal., A* **2023**, *650*, 119007. DOI: 10.1016/j.apcata.2022.119007.

(20) Perras, F. A.; Arroyave, A.; Southern, S. A.; Lamb, J. V.; Li, Y.; LaPointe, A.; Delferro, M. Double-resonance $^{17}$O NMR Experiments Reveal Unique Configurational Information for Surface Organometallic Complexes. *Chem. Commun.* **2023**, *59* (31), 4604-4607, 10.1039/D3CC00899A. DOI: 10.1039/D3CC00899A.
(21) Perras, F. A.; Culver, D. B. On the Uuse of NMR Distance Measurements for Assessing Surface Site Homogeneity. *Dalton Trans.* **2023**, *52* (48), 18502-18512, 10.1039/D3DT03201A. DOI: 10.1039/D3DT03201A.
(22) Salvia, W. S.; Zhao, T. Y.; Chatterjee, P.; Huang, W.; Perras, F. A. Are the Brønsted Acid Sites in Amorphous Silica–Alumina Bridging? *Chem. Commun.* **2023**, *59* (94), 13962-13965, 10.1039/D3CC04237E. DOI: 10.1039/D3CC04237E.
(23) Shekar, S. C.; Perras, F. A. Multiplex Detection of Multiple-Quantum/Single-Quantum NMR Correlation Spectra. *J. Phys. Chem. C* **2023**, *127* (15), 7352-7359. DOI: 10.1021/acs.jpcc.3c00857.
(24) Luo, Z.; Li, L.; Nguyen, V. T.; Kanbur, U.; Li, Y.; Zhang, J.; Nie, R.; Biswas, A.; Bud'ko, S. L.; Oh, J.; et al. Catalytic Hydrogenolysis by Atomically Dispersed Iron Sites Embedded in Chemically and Redox Non-innocent N-Doped Carbon. *J. Am. Chem. Soc.* **2024**, *146* (12), 8618-8629. DOI: 10.1021/jacs.4c00741.
(25) Yu, J.; Yan, Y.; Lin, Y.; Liu, H.; Li, Y.; Xie, S.; Sun, S.; Liu, F.; Zhang, Z.; Li, W.; et al. Improved High-Current-Density Hydrogen Evolution Reaction Kinetics on Single-Atom Co Embedded in an Order Pore-Structured Nitrogen Assembly Carbon Support. *Nanoscale Horiz.* **2024**, 10.1039/D4NH00299G. DOI: 10.1039/D4NH00299G.
(26) Agarwal, A.; Mais, M.; Perras, F. A. Selective 17O-labeling of Silica. *Chem. Commun.* **2024**, *60* (84), 12189-12192, 10.1039/D4CC04584J. DOI: 10.1039/D4CC04584J.
(27) Perras, F. A.; Paterson, A. L. High Field Solid-State NMR of Challenging Nuclei in Inorganic Systems. In *Reference Module in Chemistry, Molecular Sciences and Chemical Engineering*, Elsevier, 2021.
(28) Matsuki, Y.; Kobayashi, T.; Fukazawa, J.; Perras, F. A.; Pruski, M.; Fujiwara, T. Efficiency Analysis of Helium-cooled MAS DNP: Case Studies of Surface-modified Nanoparticles and Homogeneous Small-molecule Solutions. *Phys. Chem. Chem. Phys.* **2021**, *23* (8), 4919-4926, 10.1039/D0CP05658H. DOI: 10.1039/D0CP05658H.
(29) Sluiter, J. B.; Michel, K. P.; Addison, B.; Zeng, Y.; Michener, W.; Paterson, A. L.; Perras, F. A.; Wolfrum, E. J. Direct Determination of Cellulosic Glucan Content in Starch-containing Samples. *Cellulose* **2021**, *28* (4), 1989-2002. DOI: 10.1007/s10570-020-03652-2.
(30) Paterson, A. L.; Liu, D.-J.; Kanbur, U.; Sadow, A. D.; Perras, F. A. Observing the Three-Dimensional Dynamics of Supported Metal Complexes. *Inorg. Chem. Front.* **2021**, *8* (6), 1416-1431, 10.1039/D0QI01241F. DOI: 10.1039/D0QI01241F.
(31) Zhang, J.; Mason, A. H.; Wang, Y.; Motta, A.; Kobayashi, T.; Pruski, M.; Gao, Y.; Marks, T. J. Beyond the Active Site. Cp*$ZrMe_3$/Sulfated Alumina-Catalyzed Olefin Polymerization Tacticity via Catalyst···Surface Ion-Pairing. *ChemCatChem* **2021**, *13* (11), 2564-2569, 10.1002/cctc.202100406. DOI: 10.1002/cctc.202100406 (acccessed 2021/08/03).
(32) Chen, M.; Yan, Y.; Gebre, M.; Ordonez, C.; Liu, F.; Qi, L.; Lamkins, A.; Jing, D.; Dolge, K.; Zhang, B.; et al. Thermal Unequilibrium of PdSn Intermetallic

Nanocatalysts: From In Situ Tailored Synthesis to Unexpected Hydrogenation Selectivity. *Angew. Chem. Int. Ed.* **2021**, *60* (33), 18309-18317, 10.1002/anie.202106515. DOI: 10.1002/anie.202106515 (acccessed 2021/08/03).
(33) Li, G.; Wang, B.; Kobayashi, T.; Pruski, M.; Resasco, D. E. Optimizing the Surface Distribution of Acid Sites for Cooperative Catalysis in Condensation Reactions Promoted by Water. *Chem. Catal.* **2021**, *1* (5), 1065-1087. DOI: 10.1016/j.checat.2021.08.005.
(34) Gao, J.; Dorn, R. W.; Laurent, G. P.; Perras, F. A.; Rossini, A. J.; Conley, M. P. A Heterogeneous Palladium Catalyst for the Polymerization of Olefins Prepared by Halide Abstraction Using Surface $R_3Si^+$ Species. *Angew. Chem. Int. Ed.* **2022**, *61* (20), e202117279, 10.1002/anie.202117279. DOI: 10.1002/anie.202117279.
(35) Fought, E. L.; Han, Y.; Windus, T. L.; Slowing, I. I.; Kobayashi, T.; Evans, J. W. Modeling of Linear Nanopores in a-$SiO_2$ Tuning Pore Surface Structure. *Microporous Mesoporous Mater.* **2022**, *341*, 112077. DOI: 10.1016/j.micromeso.2022.112077.
(36) Luo, S.; Wang, T.; Qi, L.; Tompsett, G. A.; Timko, M. T.; Auerbach, S. M.; Fan, W. Titrating Controlled Defects into Si-LTA Zeolite Crystals Using Multiple Organic Structure-Directing Agents. *Chem. Mater.* **2022**, *34* (4), 1789-1799. DOI: 10.1021/acs.chemmater.1c04036.
(37) Crandall, Z.; Basemann, K.; Qi, L.; Windus, T. L. Rxn Rover: Automation of Chemical Reactions with User-friendly, Modular Software. *React. Chem. Eng.* **2022**, *7* (2), 416-428, 10.1039/D1RE00265A. DOI: 10.1039/D1RE00265A.
(38) Fan, J.; Suo, X.; Wang, T.; Wang, Z.; Do-Thanh, C.-L.; Mahurin, S. M.; Kobayashi, T.; Yang, Z.; Dai, S. Mechanochemistry-driven Phase Transformation of Crystalline Covalent Triazine Frameworks Assisted by Alkaline Molten Salts. *J. Mater. Chem. A* **2022**, *10* (27), 14310-14315, 10.1039/D2TA02117J. DOI: 10.1039/D2TA02117J.
(39) Fan, J.; Wang, T.; Chen, H.; Wang, Z.; Thapaliya, B. P.; Kobayashi, T.; Yuan, Y.; Popovs, I.; Yang, Z.; Dai, S. Mechanochemistry-Driven Construction of Aza-fused π-Conjugated Networks Toward Enhanced Energy Storage. *Adv. Func. Mater.* **2022**, 2202669, 10.1002/adfm.202202669. DOI: 10.1002/adfm.202202669.
(40) Deshpande, N.; Chen, J.-Y.; Kobayashi, T.; Cho, E. H.; Pineault, H.; Lin, L.-C.; Brunelli, N. A. Investigating the Impact of Micropore Volume of Aminosilica Functionalized SBA-15 on Catalytic Activity for Amine-catalyzed Reactions. *J. Catal.* **2022**, *414*, 356-364. DOI: 10.1016/j.jcat.2022.09.016.
(41) An, Y.; Chatterjee, P.; Naik, P.; Banerjee, S.; Huang, W.; Slowing, I. I.; Venditti, V. Hydrogen Spillover and Substrate–support Hydrogen Bonding Mediate Hydrogenation of Phenol Catalyzed by Palladium on Reducible Metal Oxides. *Chem. Sci.* **2023**, *14* (48), 14166-14175, 10.1039/D3SC02913A. DOI: 10.1039/D3SC02913A.
(42) Chu, Y.-Y.; García Alejo, A.; Bud'ko, S. L.; Boteju, K.; Patnaik, S.; Ellern, A.; Pérez García, M.; Sadow, A. D. Structure and Magnetic Properties of Homoleptic Trivalent Tris(alkyl)lanthanides. *Inorg. Chem.* **2023**, *62* (30), 11751-11760. DOI: 10.1021/acs.inorgchem.3c00435.
(43) Drabo, P.; Fischer, M.; Emondts, M.; Hamm, J.; Engelke, M.; Simonis, M.; Qi, L.; Scott, S. L.; Palkovits, R.; Delidovich, I. Solvent Effects on Catalytic Activity and

Selectivity in Amine-Catalyzed d-Fructose Isomerization. *J. Catal.* **2023**, *418*, 13-21. DOI: 10.1016/j.jcat.2022.12.029.
(44) Hafezisefat, P.; Qi, L.; Brown, R. C. Lignin Depolymerization and Esterification with Carboxylic Acids to Produce Phenyl Esters. *ACS Sustainable Chem. Eng.* **2023**, *11* (48), 17053-17060. DOI: 10.1021/acssuschemeng.3c05221.
(45) Kanbur, U.; Paterson, A. L.; Rodriguez, J.; Kocen, A. L.; Yappert, R.; Hackler, R. A.; Wang, Y.-Y.; Peters, B.; Delferro, M.; LaPointe, A. M.; et al. Zirconium-Catalyzed C–H Alumination of Polyolefins, Paraffins, and Methane. *J. Am. Chem. Soc.* **2023**, *145* (5), 2901-2910. DOI: 10.1021/jacs.2c11056.
(46) Lai, Q.; Mason, A. H.; Agarwal, A.; Edenfield, W. C.; Zhang, X.; Kobayashi, T.; Kratish, Y.; Marks, T. J. Rapid Polyolefin Hydrogenolysis by a Single-Site Organo-Tantalum Catalyst on a Super-Acidic Support: Structure and Mechanism. *Angew. Chem. Int. Ed.* **2023**, *62* (50), e202312546. DOI: 10.1002/anie.202312546.
(47) Li, M.; Qiu, L.; Popovs, I.; Yang, W.; Ivanov, A. S.; Kobayashi, T.; Thapaliya, B. P.; Moitra, D.; Yu, X.; Wu, Z.; et al. Construction of Boron- and Nitrogen-Enriched Nanoporous π-Conjugated Networks Towards Enhanced Hydrogen Activation. *Angew. Chem. Int. Ed.* **2023**, *62* (28), e202302684. DOI: 10.1002/anie.202302684.
(48) Staples, O.; Ferrandon, M. S.; Laurent, G. P.; Kanbur, U.; Kropf, A. J.; Gau, M. R.; Carroll, P. J.; McCullough, K.; Sorsche, D.; Perras, F. A.; et al. Silica Supported Organometallic $Ir^{I}$ Complexes Enable Efficient Catalytic Methane Borylation. *J. Am. Chem. Soc.* **2023**, *145* (14), 7992-8000. DOI: 10.1021/jacs.2c13612.
(49) Wei, X.; Johnson, G.; Ye, Y.; Cui, M.; Yu, S.-W.; Ran, Y.; Cai, J.; Liu, Z.; Chen, X.; Gao, W.; et al. Surfactants Used in Colloidal Synthesis Modulate Ni Nanoparticle Surface Evolution for Selective $CO_2$ Hydrogenation. *J. Am. Chem. Soc.* **2023**, *145* (26), 14298-14306. DOI: 10.1021/jacs.3c02739.
(50) Southern, S. A.; Li, Y.; Liu, D.-J.; Sadow, A. D.; Qi, L.; Perras, F. A. Enhanced Activity from Coordinatively Unsaturated and Dynamic Zeolite-Bound Organoscandium Species. *ACS Catal.* **2024**, *14*, 9440-9451. DOI: 10.1021/acscatal.4c00678.
(51) Shaw, W. J.; Kidder, M. K.; Bare, S. R.; Delferro, M.; Morris, J. R.; Toma, F. M.; Senanayake, S. D.; Autrey, T.; Biddinger, E. J.; Boettcher, S.; et al. A US Perspective on Closing the Carbon Cycle to Defossilize Difficult-to-Electrify Segments of our Economy. *Nat. Rev. Chem.* **2024**, *8* (5), 376-400. DOI: 10.1038/s41570-024-00587-1.
(52) Wang, T.; Luo, S.; Shah, M.; Qi, L.; Tompsett, G. A.; Timko, M. T.; Auerbach, S. M.; Fan, W. Removing Fluoride from Double Four-Membered Rings Yielding Defect-Free Zeolites under Mild Conditions Using Ozone. *Chem. Mater.* **2024**, *36* (2), 870-880. DOI: 10.1021/acs.chemmater.3c02695.
(53) An, L.; Yao, Y.; Hall, T. B.; Zhao, F.; Qi, L. Agile Synthesis and Automated, High-throughput Evaluation of Diglycolamides for Liquid–liquid Extraction of Rare-earth Elements. *Green Chem.* **2024**, 10.1039/D4GC01146E. DOI: 10.1039/D4GC01146E.
(54) Del Rose, T.; Li, Y.; Qi, L.; Hlova, I. Z. Mechanochemical Extraction of Lithium from α-Spodumene at Low Temperatures. In *Rare Metal Technology 2024*, Cham, 2024; Forsberg, K., Ouchi, T., Azimi, G., Alam, S., Neelameggham, N. R., Baba, A. A., Peng, H., Karamalidis, A., Eds.; Springer Nature Switzerland: pp 141-149. DOI: 10.1007/978-3-031-50236-1_15.

(55) Edenfield, W. C.; Mason, A. H.; Lai, Q.; Agarwal, A.; Kobayashi, T.; Kratish, Y.; Marks, T. J. Rapid Polyolefin Plastic Hydrogenolysis Mediated by Single-Site Heterogeneous Electrophilic/Cationic Organo-group IV Catalysts. *ACS Catal.* **2024**, *14* (1), 554-565. DOI: 10.1021/acscatal.3c05161.
(56) Uchagawkar, A.; Ramanathan, A.; Zhu, H.; Chen, L.; Hu, Y.; Douglas, J.; Mais, M.; Kobayashi, T.; Subramaniam, B. Insights into Dopant-Mediated Tuning of Silica-Supported Mo Metal Centers for Enhanced Olefin Metathesis. *ACS Catal.* **2024**, *14* (11), 8317-8329. DOI: 10.1021/acscatal.4c01700.
(57) Southern, S. A.; Thompson, A.; Sadow, A. D.; Perras, F. A. Size Matters: Altering the Metal-Surface Coordination in Micropores Via Structural Confinement Effects. *Inorg. Chem. Front.* **2024**, 10.1039/D4QI01261E. DOI: 10.1039/D4QI01261E.
(58) Jiménez, J. D.; Lustemberg, P. G.; Danielis, M.; Fernández-Villanueva, E.; Hwang, S.; Waluyo, I.; Hunt, A.; Wierzbicki, D.; Zhang, J.; Qi, L.; et al. From Methane to Methanol: Pd-iC-CeO2 Catalysts Engineered for High Selectivity via Mechanochemical Synthesis. *J. Am. Chem. Soc.* **2024**, *146* (38), 25986-25999. DOI: 10.1021/jacs.4c04815.
(59) Zhang, Y.; Qi, L.; Li, Y.; Yang, T.; Meira, D. M.; Dun, C.; Hu, H.; Chen, H.; Xu, S.; Urban, J. J.; et al. Mechanism and Kinetics of Ethanol–Acetaldehyde Conversion to 1,3-Butadiene over Isolated Lewis Acid La Sites in Silanol Nests in Dealuminated Beta Zeolite. *ACS Catal.* **2024**, *14* (20), 15204-15220. DOI: 10.1021/acscatal.4c03935.

Max Delferro

## Unveiling the Active Site using Integrated Computational XANES Simulations and Mechanistic Studies

**Principal Investigators**: Max Delferro (Lead PI), David M. Kaphan, Cong Liu, A. Jeremy Kropf
**Additional Argonne Staff:** Magali Ferrandon
**Postdocs:** Jackie Hall, Yu Lim Kim, Uddhav Kanbur, Joshua DeMuth, Kaixi Deng, Meaghan Bruening

Chemical Sciences and Engineering Division, Argonne National Laboratory, Lemont, IL 60439 USA

Chemisorption of organometallic complexes on inorganic supports is a powerful strategy for developing heterogeneous, single-site, *homogeneous-in-function* catalysts. Typical support materials, most commonly silica ($SiO_2$) and alumina ($Al_2O_3$), play a crucial role in stabilizing reaction intermediates and site-isolating reactive species throughout the catalytic cycle; however, the inert nature of these catalyst supports precludes direct modulation or augmentation of catalytic processes by manipulation of the support akin to electronic ligand design and "redox non-innocence" in homogeneous catalysis. Thus, the overarching goal of the Catalysis Science Program at Argonne is to understand though a combination of experimentation, computation, and X-ray characterization, how catalytic processes can be controlled through modulation of the electronic interactions between supported organometallic catalysts and non-traditional or non-innocent surfaces. Our experimental efforts have focused on two themes, the understanding of complex, multi-component active sites for which surface effects are central to the promotion of catalysis, and the investigation of Li-ion battery cathodes as tunable, "redox non-innocent" catalyst supports. For the first task, we have synthesized well-defined, organozirconium, organoiridium, and organoruthenium catalysts on high-surface area silicon nitride, silica, and sulfated zirconia, respectively, for the dehydrogenation of alkanes and selective hydrofunctionalization of alkenes. In a second task we explored the role of reductive surface lithiation in an organochromium catalyst for ethylene polymerization/oligomerization, and a suppored copper species that efficiently catalyzed oxidative C-C bond formation. The chemisorption of the molecular complex $Cr(CH_2SiMe_3)_4$ on anatase titania nanoparticles as well as on a silica support led to the bipodal complexes $Cr/TiO_2$ and $Cr/SiO_2$, respectively. Subsequent reductive lithium intercalation with n-butyllithium results in the formation of lower valent $Cr^{2+}$ species $Cr/Li_xTiO_2$ and $Cr/Li/SiO_2$. These materials have been shown to catalyze the upgrading of olefins, such as ethylene and isoprene, with high selectivity towards trimerization vs polymerization and stereoselection, respectively, depending on the lithiation content. In addition, organocopper grafted on $Li_xMn_2O_4$ is catalytically active for the oxidative coupling of terminal alkynes, with steady-state reaction rate data of oxidative propyne dimerization, indicating that intercalative redox tuning of the support provides increased catalytic performance and transfers the reaction from kinetic regime where reoxidation of surface Mn sites is rate controlling in the delithiated state, to a regime of rate limiting substrate activation at high lithiation states.

**FWP59066: Selective Upgrading of Alkenes via Organometallic-Support Electronic Interactions**

**Principal Investigators**: Max Delferro (Lead PI), David M. Kaphan, Cong Liu, A. Jeremy Kropf
**Additional Argonne Staff:** Magali Ferrandon
**Postdocs:** Jackie Hall, Yu Lim Kim, Uddhav Kanbur, Joshua DeMuth, Kaixi Deng, Meaghan Bruening
**Affiliations:** Chemical Sciences and Engineering Division, Argonne National Laboratory, Lemont, IL 60439

## RECENT PROGRESS

***Surface Organometallic Catalysts on Non-Traditional Supports for the C-H Activation of Alkanes.*** The discovery of generalizable approaches to rational catalyst design is one of the core challenges at the heart of modern heterogeneous catalysis research. Our approach to this problem involves integrated experimental, computational and spectroscopic investigation of well-defined active sites on non-traditional catalyst support surfaces to capture and understand catalyst metal-surface stereoelectronic communication, and to discover new strategies to leverage these interactions to manipulate and enhance the behavior of catalysts. In an encouraging preliminary, we have determined the surface structure of a supported organozirconium complex on silicon nitride ($Zr/Si_3N_4$) using an array of analytic and spectroscopic techniques, including ICP-OES, DRIFTS, SSNMR and XAS, and found the nitride surface to dramatically enhance activity in catalytic dehydrogenation. Specifically, the homoleptic tetrabenzylzirconium was grafted on mesoporous $Si_3N_4$, yielding atomically-disperse pentacoordinated zirconium dibenzyl sites bounded to three surface nitrogen (Figure 1a). This pre-catalyst material was assessed for non-oxidative dehydrogenation of propane (PDH) in comparison to the analogous organozirconium precursor grafted on silica ($Zr/SiO_2$) in a plug flow reactor between 450 °C and 550 °C. At the lower

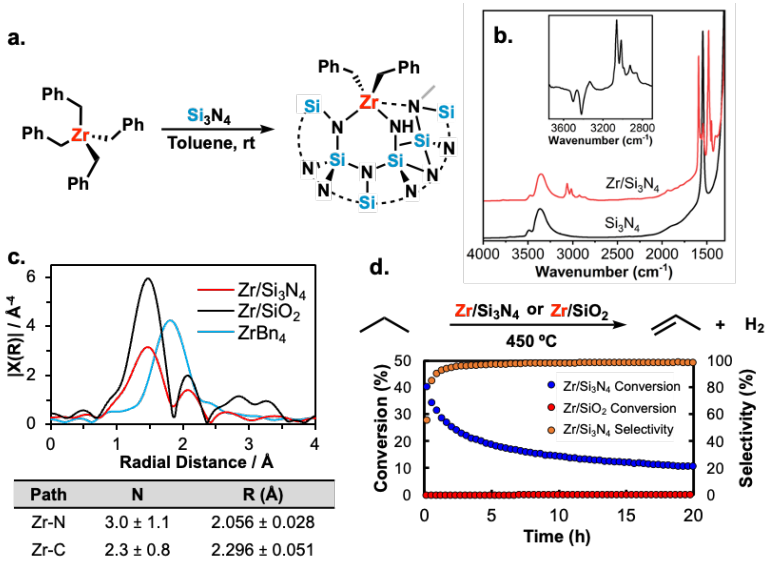


| Path | N | R (Å) |
|---|---|---|
| Zr-N | 3.0 ± 1.1 | 2.056 ± 0.028 |
| Zr-C | 2.3 ± 0.8 | 2.296 ± 0.051 |

**Figure 1**. a) Grafting of $ZrBn_4$ on *m*-$Si_3N4$; b) DRIFTS spectra of *m*-$Si_3N_4$ and $Zr/Si_3N_4$; c) EXAFS spectra ($k^3$-weighted, k = 3−11 $Å^{-1}$) $Zr/Si_3N_4$, $Zr/SiO_2$, and $ZrBn_4$ coordination number (N) and bond distance (R); d) $Zr/Si_3N_4$ PDH conversion (blue) and selectivity (orange), vs $Zr/SiO_2$ conversion (red). 2.0 mol % propane in Ar, 5 mL/min.

temperature, initial burst of reactivity with low selectivity was observed, plausibly associated with formation of transient hydride species, followed by exceptional activity with selectivity >95% for the generation of propene and slow deactivation over 72 hours on stream (conversion and selectivity of 25% and 95% at 2 h; 19% and 97% at 5 h; 10% and 99% at 24h; and 5% and 99% at 72h). The $Zr/SiO_2$ analogue exhibited negligible activity (conversion < 0.1 %) under the same reaction conditions (Figure 1d). Increasing the temperature to 550 °C, a similar profile was obtained for $Zr/Si_3N_4$, with an initial activity of 2.96 $mol_{propene}$ $mol_{Zr}^{-1}$ $h^{-1}$ and selectivity for propene reaching >95% for the duration of 68 h on stream with negligible coke formation, while the $Zr/SiO_2$ only showed minimal improvement in conversion respect the run at 450 °C (from 0.1% to 0.27%). The forward rate constant for the dehydrogenation (*kf*) for $Zr/Si_3N_4$ was determined to be 234 $mol_{propene}$ $mol_{metal}^{-1}$ $h^{-1}$ $bar^{-1}$ at 550 °C, exceeding the most active SOMC catalysts on $SiO_2$ by 4-fold (Ga = 52.7, Cr = 45.3, Co = 33.8, and V = 11.2 $mol_{propene}$ $mol_{metal}^{-1}$ $h^{-1}$ $bar^{-1}$ at 550 °C), with comparable or greater selectivity to propylene, further validating the enhancement in catalytic performance engendered by the nitride support. Moreover, a preliminary computational analysis by DFT was performed to investigate differences in energetics of the putative key C-H activation mechanism between the two catalytic systems ($Zr/Si_3N_4$ *vs* $Zr/SiO_2$). The computed barriers for the heterolytic C-H bond activation across the Zr-N single bond and Zr=N imido were found to be 37.6 kcal/mol and 40.4 kcal/mol, respectively, with the energetics of the process being exergonic (ΔG = -6.5 kcal/mol). Note that the isomerization of the Zr on $Si_3N_4$ model to form the imido structure was found to be slightly favored (ΔG = -2.3 kcal/mol), with a net $\Delta\Delta G^{\ddagger}$ = 0.5 kcal/mol for propane activation between the two possible species. Thus, both pathways are potentially catalytically relevant given the range of possible local geometries on the amorphous surface. In contrast, heterolytic bond activation at a similar $Zr/SiO_2$ site was calculated to have a significantly higher activation barrier ($\Delta G^{\ddagger}$ = 60.0 kcal/mol) and was highly endergonic (ΔG = 44.6 kcal/mol).

***Organochromium Olefin Oligomerization and Polymerization Enabled by Surface Lithiation.*** The development of heterogeneous catalysts for selective ethylene oligomerization operating via the oxidative cyclization mechanism is challenging. Several prominent homogeneous systems for ethylene oligomerization involving metallacycles have been developed (e.g., Phillips systems) and are mainly comprised of a redox-active transition metal complex (e.g., chromium) and an alkylating agent (e.g., $AlR_3$). Typically, the activation of these complexes leads to the formation of lower valent species capable of coordinating and oxidatively adding two ethylene molecules to form a metallacyclopentene intermediate. We have recently developed an activator-free system by leveraging the electronic properties of traditional inorganic supports (Figure 2). Chromium on

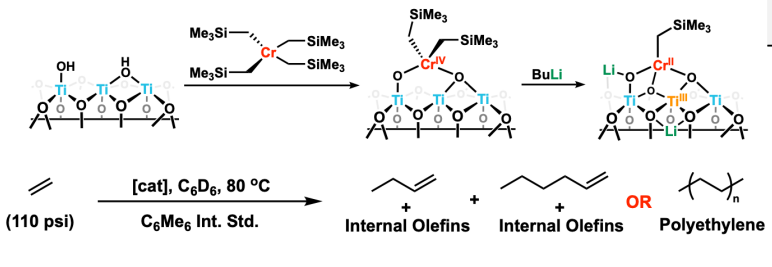


| Catalyst | Polymer | Oligomer (C4/C6) | Initial rate (mol / mol Cr $s^{-1}$ x $10^{-3}$) | Turnovers (17h) |
|---|---|---|---|---|
| $Cr/TiO_2$ | ✓ | N/A | 1221 | 3358 |
| $Cr/Li_{0.005}TiO_2$ | ✓ | N/A | 105 | 1703 |
| $Cr/Li_{0.01}TiO_2$ | ✓ | N/A | 98.2 | 822 |
| $Cr/Li_{0.1}TiO_2$ | N/A | ✓ (48/52) | 5.45 | 67 |
| $Cr/Li_{0.6}TiO_2$ | N/A | ✓ (20/80) | 5.85 | 143 |

**Figure 2**. Reaction diagrams for the synthesis of supported single-site Cr catalysts on $TiO_2$ and $Li_xTiO_2$ and their performances in ethylene polymerization/oligomerization.

lithium titanium oxide ($Cr/Li_xTiO_2$) mediates the formation of hexenes from ethylene with selectivity up to 80%, sustained over long reaction times (~72 h). The reduced chromium catalyst is obtained either by lithiation of a titania-supported chromium complex using n-butyllithium, or directly by a reductive grafting step involving the immobilization of a chromium complex onto lithium-intercalated titanium oxide. Extensive spectroscopic characterization of the chromium materials has been conducted, including XPS, XAS, EPR and DRIFTs, all of which suggest reduced chromium species. Kinetic studies on the $Cr/Li_xTiO_2$/ethylene system revealed a first order dependence on chromium and second order dependence on ethylene, consistent with the oxidative cyclization mechanism. Lithium incorporation in the anatase titania support has also been varied to provide a range of materials $Cr/Li_xTiO_2$ ($0.05 < x < 0.6$) and their reactivity toward ethylene oligomerization has been studied. At low lithium intercalation levels ($x < 0.1$) exclusive polymerization was observed while a crossover to oligomerization occurs at higher lithium loadings ($x > 0.1$).

Furthermore, in a follow-up study, we discovered that the same approach to electronic manipulation of the surface chromium species by post-synthetic lithiation could be used to generate exceptionally active catalysts for diene polymerization with unique control of selectivity. The parent $Cr/SiO_2$ complex is a moderately active catalyst for isoprene polymerization, affording 92% selectivity for *trans*-1,4 insertion, while no appreciable activity was detected on the titania supported analogue. In contrast, global lithiation of the catalyst surface with BuLi results in a single component catalyst that is at least an order of magnitude more active for both oxide surfaces, and the dominant insertion selectivity is inverted, affording >80% *cis*-1,4 selectivity. The nature of the reduced Cr surface species was further probed in this report with *in situ* DRIFTS CO treatment, which revealed the presence of a highly electron rich, low valent Cr site, which is slowly converted to a Cr $\eta^1$-acyl complex upon insertion of the alkyl group into the Cr bound carbonyl.

***Intercalative Redox Tuning for $Cu/Li_xMn_2O_4$ Catalyzed Oxidative Alkyne Coupling.*** Understanding the relationship between the catalytic active site and surface in supported heterogenous catalysts can allow for predicting structure-property relationships and new strategies for catalyst design. Previously, we have demonstrated that reduction of $LiMn_2O_4$ by lithium intercalation led to systematic increases in the activity of supported Ni catalysts for cyclohexene hydrogenation. Here, the influence of support lithiation on the electronic properties of Cu species supported on $Li_xMn_2O_4$ is investigated to further understand this capability for tuning catalytic proficiency. $Li_xMn_2O_4$ with various degrees of lithiation ($x = 0, 0.1, 0.3, 0.7, 1.0, 2.0$) was prepared by reaction of $MnO_2$ with n-BuLi at room temperature in benzene. Cu was then added by addition of copper mesityl ($Mes_xCu_x$, $x = 4,5$) to a suspension of $Li_xMn_2O_4$ benzene at room temperature (Figure 3a) and the resultant materials were evaluated as catalyst for the oxidative homocoupling of alkynes. Results of reaction of phenylacetylene (23 °C, benzene, in air) revealed that $Cu/MnO_2$ and

$Cu/LiMn_2O_4$ were both competent as catalysts for the coupling reaction whereas bare $MnO_2$ and $Mes_xCu_x$ supported on $SiO_2$ provided no measurable activity, signifying the vital interaction of Cu with the $Li_xMn_2O_4$ support. Additionally, $Cu/Li_xMn_2O_4$, although showing initially lower activity than $Cu/MnO_2$, displayed stable reaction rates until complete substrate conversion unlike $Cu/MnO_2$ which exhibited rates that decelerated quickly during reaction, indicating a role of the surface redox state on the catalytic properties of the supported Cu. Characterization of Cu and Mn oxidation state by XAS revealed a systematic decrease in Mn oxidation state with increasing lithiation, and $Cu/MnO_2$ being close to completely $Cu^{2+}$, with evidence of reduced Cu environments increasing with lithiation, while $Cu^{2+}$ remains the dominant formal oxidation state, with the exception of the fully lithiated $Cu/Li_2Mn_2O_4$, which appears to be fully converted to $Cu^+$ (Figure 3b). Additional

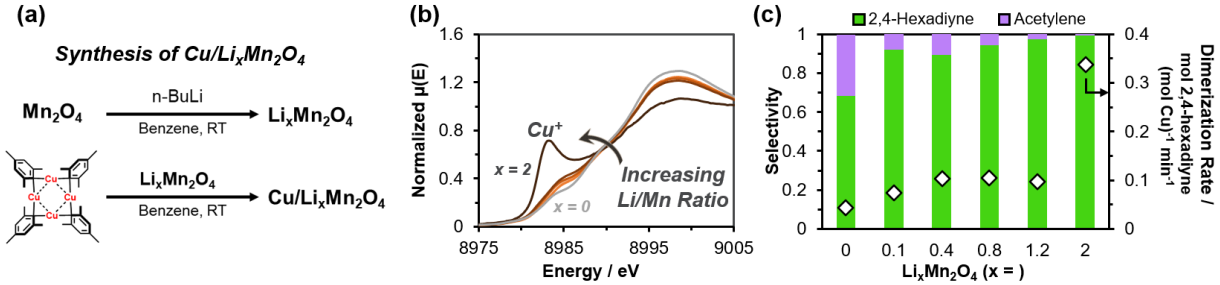


**Figure 3.** (a) Schematic representing the synthesis procedure for $Cu/Li_xMn_2O_4$. (b) Cu K-edge X-ray absorption near edge structure (XANES) of $Cu/Li_xMn_2O_4$ with increasing Li (x = #) content. (c) Results of the oxidative coupling of propyne over $Cu/Li_xMn_2O_4$ with various Li (x = #) concentrations indicating the rate of dimerization and product selectivity.

mechanistic experiments performed on the oxidative coupling of propyne in a flow reactor (200 °C, $C_3:O_2$ = 1, 24 h) revealed that increasing reductive lithiation not only increases the turnover rate of dimerization to 2,4-hexadiyne, but also leads to improved selectivity over deleterious acetylene formation from oxygen transfer and C-C fragmentation (Figure 3c). This study revealed a crossover in rate controlling transition state from reoxidation of the surface remove from the Cu site for the lower lithiation materials to propyne activation at the highest lithiation state.

## Publications Acknowledging this Grant in 2021-2024

***Work at Argonne funded solely by this FWP with Argonne as the lead institution:***


1. Kanbur, U.; Hall, J. N.; Kropf, A. J.; Delferro, M.; Kaphan, D. Heterogeneous Organochromium Catalysts for Stereoselective Isoprene Polymerization. *Organometallics* **2024**, ASAP. DOI: 10.1021/acs.organomet.4c00245.

2. Hall, J. N.; Chapovetsky, A.; Ferrandon, M. S.; Kim, Y. L.; Kanbur, U.; McCullough, K. E.; Liu, C.; Kropf, A. J.; Delferro, M.; Kaphan, D. M. Intercalative Redox Tuning for $Cu/Li_xMn_2O_4$-Catalyzed Oxidative Alkyne Coupling. *ACS Catal.* **2024**, *14* (14), 11051-11064. DOI: 10.1021/acscatal.4c02491

3. DeMuth, J. C.; Kim, Y. L.; Hall, J. N.; Syed, Z. H.; Deng, K.; Perras, F. A.; Ferrandon, M. S.; Kropf, A. J.; Liu, C.; Kaphan, D. M.; Delferro, M. Silicon Nitride Surface Enabled Propane

Dehydrogenation Catalyzed by Supported Organozirconium. *J. Am. Chem. Soc.* **2024**, *146*, 14404–14409. DOI: 10.1021/jacs.4c02776.

4. Kanbur, U.; Hall, J. N.; Kim, Y. L.; Niklas, J.; Poluektov, O. G.; Liu, C.; Kropf, A. J.; Delferro, M.; Kaphan, D. M. Supported Organochromium Ethylene Oligomerization Enabled by Surface Lithiation. *ACS Catal.* **2024**, *14* (11), 8640-8651. DOI: 10.1021/acscatal.4c01672
5. Xu, J.; Patel, P.; Kropf, A. J.; Kaphan, D.; Delferro, M.; Liu, C. Theoretical Investigation of the Hydrogenation of Cyclohexene Catalyzed by Supported Single-Atom Sites on Redox Non-Innocent $LiMn_2O_4$ and $Li_2Mn_2O_4$ Surfaces. *J. Phys. Chem. C* **2024**, *128* (12), 4946-4957. DOI: 10.1021/acs.jpcc.4c00284
6. Xu, J.; Lund, C.; Patel, P.; Kim, Y. L.; Liu, C. Recent Advances on Computational Modeling of Supported Single-Atom and Cluster Catalysts: Characterization, Catalyst–Support Interaction, and Active Site Heterogeneity. *Catalysts* **2024**, *14* (4), 224. DOI: 10.3390/catal14040224
7. Hall, J. N.; Chapovetsky, A.; Kanbur, U.; Kim, Y.; McCullough, K.; Syed, Z.; Johnson, C.; Ferrandon, M.; Liu, C.; Kropf, A. J.; Delferro, M.; Kaphan, D. M. Oxidative Grafting for Catalyst Synthesis in Surface Organometallic Chemistry. *ACS Appl. Mater. Interfaces* **2023**, *15* (46), 53498-53514. DOI: 10.1021/acsami.3c12656.
8. Kanbur, U.; Witzke, R. J.; Xu, J.; Ferrandon, M. S.; Goetjen, T. A.; Kropf, A. J.; Perras, F. A.; Liu, C.; Tilley, T. D.; Kaphan, D. M.; Delferro, M. Supported Electrophilic Organoruthenium Catalyst for the Hydrosilylation of Olefins. *ACS Catal.* **2023**, *13* (20), 13383-13394. DOI: 10.1021/acscatal.3c03399.
9. Hall, J. N.; Kropf, A. J.; Kanbur, U.; Dogan, F.; Byron, C.; Wen, J.; Delferro, M.; Kaphan, D. M. Structural and reactive evolution of oxidatively grafted Pd catalysts on $MnO_2$ for the low-temperature oxidation of CO. *Chem. Commun.* **2023**, *59* (45), 6861-6864. DOI: 10.1039/D3CC01094E.
10. Staples, O.; Ferrandon, M. S.; Laurent, G. P.; Kanbur, U.; Kropf, A. J.; Gau, M. R.; Carroll, P. J.; McCullough, K.; Sorsche, D.; Perras, F. A.; Delferro, M.; Kaphan, D. M.; Mindiola, D. J. Silica Supported Organometallic $Ir^{I}$ Complexes Enable Efficient Catalytic Methane Borylation. *J. Am. Chem. Soc.* **2023**, *145* (14), 7992-8000. DOI: 10.1021/jacs.2c13612.
11. Chapovetsky, A.; Kennedy, R. M.; Witzke, R.; Wegener, E. C.; Dogan, F.; Patel, P.; Ferrandon, M.; Niklas, J.; Poluektov, O. G.; Rui, N.; Senanayake, S. D.; Rodriguez, J. A.; Zaluzec, N. J.; Yu, L.; Wen, J.; Johnson, C.; Jenks, C. J.; Kropf, A. J.; Liu, C.; Delferro, M.; Kaphan, D. M. Lithium-Ion Battery Materials as Tunable, "Redox Non-Innocent" Catalyst Supports. *ACS Catal.* **2022**, *12*, 7233-7242. DOI: 10.1021/acscatal.2c00935.
12. Patel, P.; Lu, Z.; Jafari, M. G.; Hernandez-Prieto, C.; Zatsepin, P.; Mindiola, D. J.; Kaphan, D. M.; Delferro, M.; Kropf, A. J.; Liu, C. Integrated Experimental and Computational K-Edge X-ray Absorption Near-Edge Structure Analysis of Vanadium Catalysts. *J. Phys. Chem. C* **2022**, *126*, 11949-11962. DOI: 10.1021/acs.jpcc.2c02049.

13. Patel, P.; Wells, R. H.; Kaphan, D. M.; Delferro, M.; Skodje, R. T.; Liu, C., Computational Investigation of the Role of Active Site Heterogeneity for a Supported Organovanadium(III) Hydrogenation Catalyst. *ACS Catal.* **2021**, *11*, 1-16. DOI: 10.1021/acscatal.1c00688).

***Intellectual Property:***

14. US Patent US20220126277 A1. Lithium-ion battery cathode and anode materials as tunable and dynamically responsive support materials for single site heterogeneous catalysis. Kaphan, D.; Delferro, M.; Chapovetsky, A.; Jenks, C. J.; Johnson, C. S.

15. US Patent US20220040677A1. Multimetallic catalysts for methanation of carbon dioxide and dry reforming of methane. Ferrandon, M.; Celik, G.; Delferro, M.

16. US Patent App. 18/372,509, 2024. Selective and long-lived single component heterogeneous ethylene trimerization catalysts enabled by surface lithiation. Kaphan, D.; Delferro, M.; Kanbur, U.; Liu, C.

17. US Patent App. 18/617,601, 2024. Support enabled propane dehydrogenation for organozirconium on silicon nitride. Kaphan, D.; Delferro, M.; DeMuth, J.

***Work at Argonne funded by this FWP with Argonne not the lead institution**:*

18. Shaw, W. J.; Kidder, M. K.; Bare, S. R.; Delferro, M.; Morris, J. R.; Toma, F. M.; Senanayake, S. D. et al. A US perspective on closing the carbon cycle to defossilize difficult-to-electrify segments of our economy. *Nat. Rev. Chem.* **2024**, *8*, 376-400. DOI: 10.1038/s41570-024-00587-1.

19. Hall, J. N.; Vicchio, S. P.; Kropf, A. J.; Delferro, M.; Bollini, P. Can the Rate of a Catalytic Turnover Be Altered by Ligands in the Absence of Direct Binding Interactions? *J. Am. Chem. Soc.* **2024**, *146*, 12113-12129. DOI: 10.1021/jacs.4c01978.

20. Byron, C.; Ferrandon, M. S.; Kropf, A. J.; Delferro, M.; Teplyakov, A. V. Surface Basic Site Effect on Boron-Promoted Platinum Catalysts for Dry Reforming of Methane. *J. Phys. Chem. C* **2023**, *127* (50), 24137–24148. DOI: 10.1021/acs.jpcc.3c05724.

21. Azina Rahmani, A.; Sultanov, M. A.; Kamiru-White, K.; Shultz-Johnson, L. R.; Butkus, B. E.; Xie, S.; Liu, F.; Nguyen, D. T. H.; Wilson-Faubert, N.; Nazemi, A.; Banerjee, P.; Zhai, L.; Delferro, M.; Wen, J.; Jurca, T. Ultrathin Atomic Layer Deposited $Al_2O_3$ Overcoat Stabilizes $Al_2O_3$-Pt/Ni-foam Hydrogenation Catalysts. *ACS Appl. Mater. Interfaces* **2023**, *15* (37), 43756-43766. DOI: 10.1021/acsami.3c08545.

22. An, S.; Patel, P.; Liu, C.; Skodje, R. Active Site Engineering via Optimizing Heterogeneous Support Structure for Single Atom Catalysis. *J. Phys. Chem. C* **2023**, *127*, 16901-16913. DOI: 10.1021/acs.jpcc.3c03915.

23. Xu, J.; Patel, P.; Liu, D.-J.; Xu, T.; Liu, C. Understanding the Dynamic Evolution of Atomically Dispersed Cu Catalyst for $CO_2$ Electrochemical Conversion Using Integrated XANES Analysis and Mechanistic Studies. *J. Catal.* **2023**, *425*, 296-305. DOI: 10.1016/j.jcat.2023.06.020.

24. Barrios-Vargas, L. J.; Abeynayake, N. S.; Secrist, C.; Le, N.; Webster, C. E.; Donnadieu, B.; Kaphan, D. M.; Roy, A.; Ibarra, I. A.; Montiel-Palma, V. Homogeneous versus MOF-supported catalysis: A direct comparison of catalytic hydroboration at Ni tripodal $P_3E$ (E = Si, Ge) complexes. *Dalton Trans.* **2023**, *52*, 8883-8892. DOI: 10.1039/D3DT01328F.

25. Hall, J. N.; Kropf, A. J.; Delferro, M.; Bollini, P. Kinetic and X-ray Absorption Spectroscopic Analysis of Catalytic Redox Cycles over Highly Uniform Polymetal Oxo Clusters. *ACS Catal.* **2023**, *13* (8), 5406-5427. DOI: 10.1021/acscatal.2c06023.

26. Bukowski, B. C.; Purdy, S. C.; Wegener, E. C.; Wu, Z.; Kropf, A. J.; Zhang, G.; Miller, J. T.; Greeley, J. Intermetallic alloy structure–activity descriptors derived from inelastic X-ray scattering. *Phys. Chem. Chem. Phys.* **2023**, *25* (16), 11216-11226. DOI: 10.1039/D3CP00330B.

27. Perras, F. A.; Arroyave, A.; Southern, S. A.; Lamb, J. V.; Li, Y.; LaPointe, A.; Delferro, M. Double-resonance $^{17}O$ NMR experiments reveal unique configurational information for surface organometallic complexes. *Chem. Commun.* **2023**, *59* (31), 4604-4607. DOI: 10.1039/D3CC00899A.

28. Zhu, Y.; Mukherjee, D.; Helgert, T. R.; Nguyen, S. T. (Catecholate)$Cu^{I}_2$-Displayed Porous Organic Polymers as Efficient Heterogeneous Catalysts for the Mild and Selective Aerobic Oxidation of Alcohols. *CCS Chemistry* **2023**, *5* (2), 445-454. DOI: 10.31635/ccschem.022.202101765.

29. Jafari, M.G.; Fehn, D.; Reinholdt, A.; Hernandez-Prieto, C.; Patel, P.; Gau, M. R.; Carroll, P. J.; Krzystek, J.; Liu, C.; Ozarowski, A.; Telser, J.; Delferro, M.; Meyer, K.; Mindiola, D. J. Tale of Three Molecular Nitrides: Mononuclear Vanadium (V) and (IV) Nitrides As Well As a Mixed-Valence Trivanadium Nitride Having a $V_3N_4$ Double-Diamond Core. *J. Am. Chem. Soc.* **2022**, *144*, 10201-102019. DOI: 10.1021/jacs.2c00276.

30. An, S.; Patel, P.; Liu, C.; Skodje, R. T. Computational Aspects of Single-Molecule Kinetics for Coupled Catalytic Cycles: A Spectral Analysis. *J. Phys. Chem. A* **2022**, *126*, 3783-3796. DOI: 10.1021/acs.jpca.2c02153.

31. Ferrandon, M. S.; Byron, C.; Celik, G.; Zhang, Y.; Ni, C.; Sloppy, J.; McCormick, R. A.; Booksh, K.; Teplyakov, A. V.; Delferro, M. Grafted Nickel-Promoter Catalysts for Dry Reforming of Methane Identified through High-Throughput Experimentation. *Appl. Catal., A* **2022**, *629*, 118379. DOI: 10.1016/j.apcata.2021.118379.

32. Wells, R.; An, S.; Patel, P.; Liu, C.; Skodje, R. T. Single Molecule Kinetics of Styrene Hydrogenation on Silica Supported Vanadium: The Role of Disorder for One-Atom Catalysts. *J. Phys. Chem. C* **2021**, *125*, 37, 20286–20300. DOI: 10.1021/acs.jpcc.1c04759.

33. Jafari, M. G.; Park, Y.; Pudasaini, B.; Kurogi, T.; Carroll, P. J.; Kaphan, D. M.; Kropf, J.; Delferro, M.; Baik, M.-H.; Mindiola, D. J. Phosphorus-Atom Transfer from Phosphaethynolate to an Alkylidyne. *Angew. Chem., Int. Ed.* **2021**, *60*, 24411-24417.DOI: 10.1002/anie.202107475.

34. Kou, J.; Zhu Chen, J.; Gao, J.; Zhang, X.; Zhu, J.; Ghosh, A.; Liu, W.; Kropf, A. J.; Zemlyanov, D.; Ma, R.; Guo, X.; Datye, A. K.; Zhang, G.; Guo, L.; Miller, J. T. Structural and Catalytic Properties of Isolated $Pt^{2+}$ Sites in Platinum Phosphide ($PtP_2$). *ACS Catal.* **2021**, *11*, 13496-13509.DOI: 10.1021/acscatal.1c03970.

35. Kaphan, D. M.; Brereton, K. R.; Klet, R. C.; Witzke, R. J.; Miller, A. J. M.; Mulfort, K. L.; Delferro, M.; Tiede, D. M., Photocatalytic Transfer Hydrogenation in Water: Insight into Mechanism and Catalyst Speciation. *Organometallics* **2021**, *40*, 1482-1491. DOI: 10.1021/acs.organomet.1c00133.

36. Liu, P.; Zhang, Y.; Liu, C.; Emery, J. D.; Das, A.; Bedzyk, M. J.; Hock, A. S.; Martinson, A. B. F. Thermal Atomic Layer Deposition of Gold: Mechanistic Insights, Nucleation, and Epitaxy. *ACS Appl. Mater. Interfaces* **2021**, *13*(7), 9091–9100. DOI: 10.1021/acsami.0c17943.

37. Perras, F. A.; Paterson, A. L.; Syed, Z. H.; Kropf, A. J.; Kaphan, D. M.; Delferro, M.; Pruski, M., Revealing the Configuration and Conformation of Surface Organometallic Catalysts with DNP-Enhanced NMR. *J. Phys. Chem. C* **2021**, *125*, 13433-13442. DOI: 10.1021/acs.jpcc.1c03176.

38. Wang, J.; Lu, Y.; Liu, L.; Yu, L.; Yang, C.; Delferro, M.; Hoffman, A. S.; Bare, S. R.; Karim, A. M.; Xin, H., Catalytic CO Oxidation on $MgAl_2O_4$-Supported Iridium Single Atoms: Ligand Configuration and Site Geometry. *J. Phys. Chem. C* **2021**, *125*, 11380-11390. DOI: 10.1021/acs.jpcc.1c02287.

39. Robison, L.; Gong, X.; Evans, A. M.; Son, F. A.; Wang, X.; Redfern, L. R.; Wasson, M. C.; Syed, Z. H.; Chen, Z.; Idrees, K. B.; Islamoglu, T.; Delferro, M.; Dichtel, W. R.; Coudert, F.-X.; Gianneschi, N. C.; Farha, O. K., Transient Catenation in a Zirconium-Based Metal-Organic Framework and Its Effect on Mechanical Stability and Sorption Properties. *J. Am. Chem. Soc.* **2021**, *143*, 1503-1512. DOI: 10.1021/jacs.0c1126

José A Rodriguez

## Catalysis for Advanced Fuel Synthesis and High Value Chemicals

José A. Rodriguez, Ping Liu, Sanjaya D. Senanayake, Jingguang Chen and Michael G. White
Brookhaven National Laboratory, Chemistry Department

### Presentation Abstract

This program pursues an understanding of catalysis for fuels synthesis and energy-related chemical conversions by elucidating catalytically important properties of well-defined surfaces, surface films, powders and nanostructures. It is divided into three thrusts with a coordinated effort across overall themes, including the development of characterization techniques (*in-situ* time-resolved X-ray difraction, X-ray absorption spectroscopy, and photoemission) at the National Synchrotron Light Source II. Computational tools are also developed for a basic understanding of catalytic reactions. Thrust 1, Catalysis for C1 Chemistry, addresses the conversion and manipulation of C-H and C-O bonds with an emphasis on the transformation of methane into valuable chemicals and the production of alcohols through the hydrogenation of $CO_2$. Thrust 2, Multi-carbon products via tandem reactions of $CO_2$ and alkanes, uses tandem reactions to convert $CO_2$ and light alkanes into multi-carbon products and to transform $CO_2$ into carbon nanofibers. Thrust 3, Nanostructured Interfaces for Catalysis, uses novel approaches to prepare and characterize metal and metal compound nanostructures, including cluster deposition and imaging to advance the understanding of supported nanocatalysts. The catalytic properties of metal-oxide, metal-carbide and metal-sulfide interfaces are investigated in a systemathic way. Emphasis is placed on understanding basic principles of surface reactivity.

**FWP-BNL-CO040: Catalysis for Advanced Fuel Synthesis and Energy, Conversion of C-O and C-H bonds**

**Co-PIs:** Ping Liu, Sanjaya Senanayake, Jingguang Chen, and Michael G. White
**Postdoc(s):** Irene Barba-Nieto, Vikram Mehar, Erwei Huang, Juan Jimenez, Arephin Islam, Prabhakar Kasala, Wenjie Liao, Yong Yuan.
**Student(s):** Yi Tian, Hong Zhang, Kaixi Deng, Luolin Shi, Jason Wang, Yuxi Wang, An Nguyen
**Affiliations(s):** All the students are from SUNY Stony Brook, most of them (6) from the Department of Chemistry, and one from the Materials Science Department

## RECENT PROGRESS

C1 chemistry involves the conversion of molecules that contain one carbon atom into valuable products. C1 chemistry is expected to become a major area of interest for the transportation fuel and chemical industries in the relatively near future. In general, the feedstocks for C1 chemistry include natural gas (mostly methane), carbon monoxide, carbon dioxide, methanol and synthesis gas (a mixture of carbon monoxide and hydrogen). Thus, a fundamental understanding of the conversion of C-O and C-H bonds is essential for controlling C1 chemistry. The Catalysis Group at BNL has been quite active in this area. The systems under investigation involved pure metal catalysts or catalysts that contained compounds of metals with light elements (C, N, O, S). We have developed and applied synchrotron-based techniques for *in-situ* characterization (AP-XPS, XRD, PDF, XAS) to understand catalyst function in operating environments. Theoretical methods for catalytic science have also been advanced (optimized KMC, reaction network analysis). In the last year (Sept 2023- October 2024 time period), this program has led research published in 64 articles and collaborated on 25 additional articles led by external collaborators. During the last year, major research achievements are:

**Thrust 1:**

- In a full collaboration with Thrusts 2 and 3, we have investigated the performance of nanostructures of Co or Fe dispersed on ceria and indium oxide with the aim of accomplishing selective activations of $CO_2$ and light alkanes.
- Studied the properties of ceria- and indium oxide-based catalysts that lead to high selectivity (>80%) in the synthesis of methanol from $CO_2$ hydrogenation.
- Studied the role of bimetallic bonding in alloy catalysts with a high selectivity towards methanol or methane formation during $CO_2$ hydrogenation.
- Examined processes that combine photo and thermal approaches in the valorization of $CO_2$.
- Evaluated the MTM activity and selectivity of Rh single active site catalysts dispersed on ceria.
- Evaluated MTM on mechanically milled $Pd/CeO_2$ catalysts in a high-pressure flow reactor in liquid-solid-gas environment coupled to in situ XANES measurements.
- Tested C-Pd(111) and $CeO_2$-C-Pd(111) for MTM using AP-XPS. Understand role of interfacial C in tuning selective partial oxidation of C-H bonds.
- Developed synchrotron-based tools for transient studies in C1 catalysis.
- Developed machine learning models to describe complex catalysis, ready for extraction of effective descriptors, effective prediction of catalytic behaviors and enhanced understanding of reaction mechanism.
- Developed theoretical models to capture the complexity of catalysts and chemical environments by combining DFT and KMC simulations, working toward bridging the material and pressure gap.

**Thrust 2:**

- Continued to investigate the effects of promoters for converting $CO_2$ into solid carbon materials.
- Developed tandem reaction strategies to convert biogas ($CO_2$ + $CH_4$) into carbon nanofibers.
- Continued to study the hydroformylation reaction mechanism and use it to design improved catalysts with isolated sites.

**Thrust 3:**

- Continued the preparation of model catalysts involving nanostructures of MgO dispersed on late transition metals {Pd(111), Pt(111), Cu(111) and Au(111)}. The activity of the new catalysts for the valorization of $CO_2$ and $CH_4$ will be tested in Thrust 1.
- Studied the intrinsic activity of $CsO_x$ nanostructures for $CO_2$ conversion into olefins and aromatics.
- Investigations of alkali and metal oxide promoters on metal cluster catalysts for improving $CO_2$ conversion to methanol and higher alcohols.
- Continued method development to bridge the material-gap and pressure-gap between theoretical modeling and experiment, aiming to enhance the understanding of experimental observations and facilitate the design of improved nanostructured catalysts.
- Investigations of well-defined Co, Fe and Co-Fe alloy catalysts to optimize the growth of carbon nanofibers (CNF) from CO via the Boudouard reaction ($2CO \rightarrow CO + C$). This work is in support of activities in Thrust 2.

Below are examples of the research done during the 2023-2024 period:

**A. Dynamic nature of inverse oxide/metal catalysts and a high selectivity for $CO_2$ to methanol production.**

Our studies show that a powder catalyst generated by the deposition of ceria nanoparticles (5% wt) on copper oxide displays high activity, selectivity (> 80%), and stability for the $CO_2 \rightarrow CH_3OH$ conversion [Moncada et al, *ACS Catal.,* **2023**, *13,* 15248-15258]. The evolution of this system under reaction conditions was studied using a combination of environmental transmission electron microscopy (E-TEM), in-situ x-ray absorption spectroscopy (XAS) and time-resolved x-ray diffraction (TR-XRD). The in-situ studies pointed to a full conversion of CuO into metallic copper with a complete transformation of $Ce^{4+}$ into $Ce^{3+}$. Images of E-TEM (Figure 1) showed drastic changes in the morphology of the catalyst when it was exposed to $H_2$, $CO_2$, and $CO_2/H_2$ mixtures. Under a $CO_2/H_2$ feed, there was a redispersion of the ceria particles that was detected by E-TEM (Figure 1) and in-situ TR-XRD. These morphological changes

were made possible by the inverse oxide/metal configuration and facilitate the binding and selective conversion of $CO_2$ to methanol. Static models for catalysts structure have a limited validity and are not useful for an efficient design or optimization of catalysts. The changes in composition and morphology seen in this study for the 5%$CeO_x$/Cu system under different reaction conditions illustrate how dynamic can be the behavior of an inverse oxide/metal catalysts during $CO_2$ hydrogenation. Small nanoparticles of an oxide on top of a metal substrate can adapt their structure and oxidation state in response to reactant molecules ($CO_2$, $H_2$, $CO_2/H_2$) in extreme ways not seen for a bulk oxide or a conventional metal on oxide configuration. This special behavior opens new approaches for the design of highly efficient catalysts for the trapping and conversion of $CO_2$ [Moncada et al, *ACS Catal.*, **2023**, *13*, 15248-15258; Deng et al, *ACS Catal.* **2024**, *14*, 11832-11844].

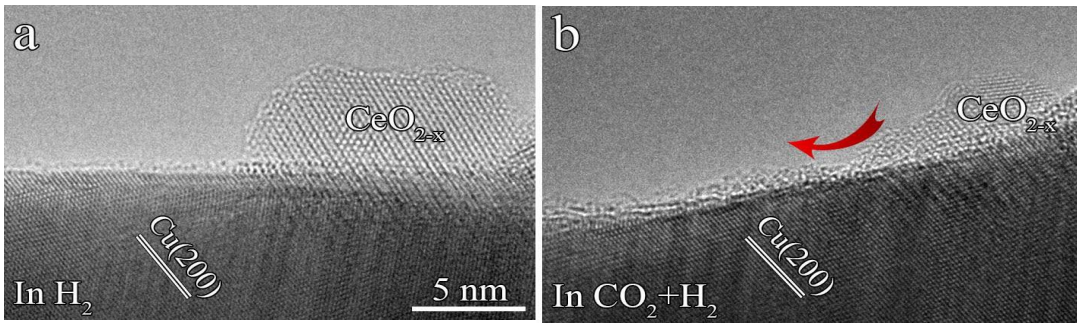


**Figure 1** Environmental TEM images for a ceria nanoparticle under $H_2$ (a:) and $CO_2/H_2$ (b) environments. The ceria nanoparticle changed its morphology to react with $CO_2$.

## B. Magnesium Oxide Nanoclusters: A Non-expensive and Sustainable Solution for the Efficient Conversion of Methane through C-C Coupling

Bulk MgO is a common catalyst used for the activation of $CH_4$ and C-C coupling, but it operates at high temperatures (>700 K) and suffers rapid deactivation by carbon deposition. In contrast, MgO nanostructures embedded in copper oxide ($Cu_2O$), Figure 2, can activate $CH_4$ at 300 K and achieve C-C coupling without deactivation at a relatively low temperature (500 K) [Islam et al, *ACS Nano* **2024**, *18*, 41, 28371–28381]. To explore $CH_4$ activation on MgO-Cu catalysts, we studied the MgO/$Cu_2O$/Cu(111) system using scanning tunneling microscopy (STM) and ambient-pressure X-ray photoelectron spectroscopy (AP-XPS). These techniques revealed the morphology and chemical characteristics of the catalyst: Small nanostructures (0.2-0.5 nm wide, 0.4-0.6 Å high) of MgO were immersed in the rows and channels of a $Cu_2O$ film (Figure 2b,c). These nanostructures were able to activate methane at room temperature, dissociating this molecule into $CH_x$ and H, with minimal carbon deposition (Figure 2d). DFT studies showed that methane activation is driven by electron transfer from copper to MgO, with smaller $Mg_2O_2$ clusters offering stronger binding and lower activation barriers for C-H bond dissociation. $Mg_3O_3$ clusters promote C-C coupling due to weaker *$CH_3$ binding, facilitating ethane formation. Catalytic tests showed that MgO/$CuO_x$/Cu(111) converts methane into ethane (and ethylene) at 500 K with large activity, comparable to highly expensive Pt/$SiO_2$ catalysts but without the problem of

carbon deactivation, highlighting the importance of MgO unit size in methane conversion [Islam et al, *ACS Nano* **2024**, *18*, 41, 28371–28381].

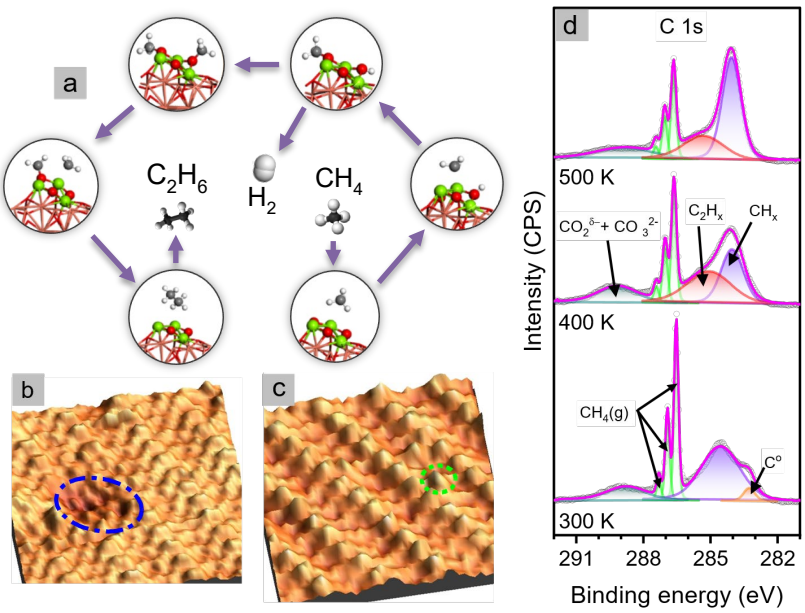


**Figure 2.** DFT calculated reaction scheme (a), STM images (b,c), and XPS spectra (d) for the activation and conversion of $CH_4$ to $C_2H_6$ on MgO nanoclusters dispersed on copper oxide. Methane is activated at room temperature.

## C. Adatom Mediated Cluster-Support Interactions

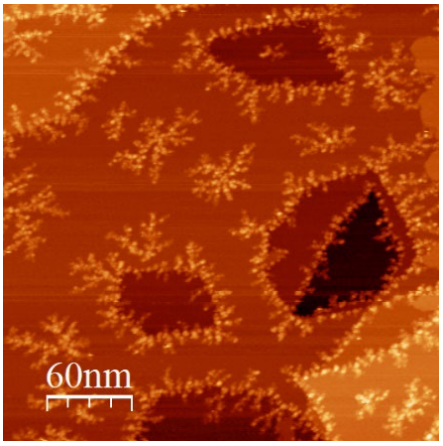


**Figure 3** STM image showing a reconstructed Cu(111) surface after the deposition of small $Ti_3O_5$ clusters.

Differences in aggregation and reconstruction of the Cu surface after the deposition of small $Ti_3O_5$ and $Ti_3O_6$ clusters can be attributed to the strength of Cu adatom binding to the clusters [Wang et al, *J. Phys. Chem. C*, **2024**, *128*, 17153]. The $Ti_3O_5$ and $Ti_3O_6$ clusters were deposited onto a Cu(111) surface using mass-selected cluster deposition. STM images showed complex morphologies (Figure 3). Holes were created in the Cu surface are a result of Cu adatoms detaching from the steps and binding to the cluster aggregates. DFT calculations showed that interactions between the isolated clusters and the Cu surface cannot account for the differences observed in cluster aggregation and surface reconstruction. Instead, the calculations show that the binding of Cu adatoms to the clusters is energetically favorable. These interactions are likely responsible for the formation of pits and isolated Cu islands [Wang et al, *J. Phys. Chem. C*, **2024**, *128*, 17153].

### D. Selective Methane to Methanol Conversion with $H_2O_2$ on a Mechano-Chemically Prepared Pd-iC-$CeO_2$ Catalyst

Conversion of methane to methanol with 100% selectivity was demonstrated in aqueous hydrogen peroxide ($H_2O_2$) solution on a mechano-chemically prepared palladium–interlayer carbon–ceria catalyst (Pd–iC–$CeO_2$) [Jimenez et al, *J. Am. Chem. Soc.* **2024**, 25986–25999]. A selectivity of 100% was observed under mild conditions: 0.5 M (1.7 wt%) $H_2O_2$, 75°C, 20 atm (20% $CH_4$, balance argon). The catalyst and chemistry were characterized under reaction conditions using ATR-IR, XANES, NEXAFS, and $^1$H-NMR. The palladium-based catalyst for the methane to methanol (MtM) conversion was prepared by a straightforward mechanochemical synthesis that resulted in a palladium–interlayer carbon–ceria (Pd–iC–$CeO_2$) material that incorporated an active interfacial carbon (iC) layer. This interfacial carbon (iC) was essential for balancing the activation of the oxidant agent ($H_2O_2$) and methane to achieve ideal product selectivity. In the absence of the iC layer, the Pd–$CeO_2$ system showed no selectivity towards methanol at 75°C, and predominantly produced carbon dioxide at 110 °C. Solvent-mediated quantum chemical (DFT) calculations provided mechanistic insights including that the iC layer favors a reaction pathway wherein methane activation is the limiting step and MeOH formation is facile [Jimenez et al, *J. Am. Chem. Soc.* **2024**, 25986–25999].

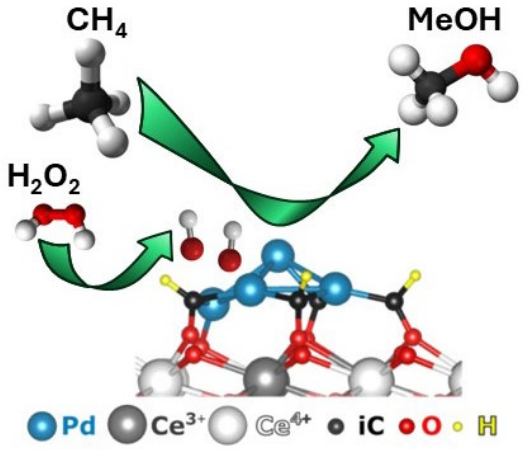


**Figure 4** Methane to methanol in one step over a Pd–iC–$CeO_2$ catalyst.

### E. $CO_2$ Fixation into Carbon Nanofibres using Electrochemical–Thermochemical Tandem Catalysis

Carbon dioxide fixation into value-added carbon nanofibres (CNF) for longer-term storage is a promising avenue for achieving net-negative carbon emissions. However, directly converting $CO_2$ to CNF via thermocatalytic approaches faces thermodynamic constraints, while electrocatalytic methods typically lead to amorphous carbon with limited yields or require energy-intensive conditions (>720 °C). Research at Thrust 2 has validated an electrocatalytic–thermocatalytic tandem strategy for CNF production by integrating the co-electrolysis of $CO_2$ and water into syngas (CO and $H_2$) with a subsequent thermochemical process at relatively mild conditions (370–450 °C, 1 atm), yielding CNFs (Figure 5) at a high production rate (average 2.5 $g_{carbon}\ g_{metals}^{-1}\ h^{-1}$). The composition of a FeCo alloy was optimized to enhance the dissociative activation of syngas and favor C-C bond formation to yield CNFs. This tandem strategy opens a door to leverage renewable energy for decarbonizing $CO_2$ into valuable solid carbon products while producing renewable $H_2$ [Xie et al, *Nature Catal.* **2024**, *7*, 98-2024].

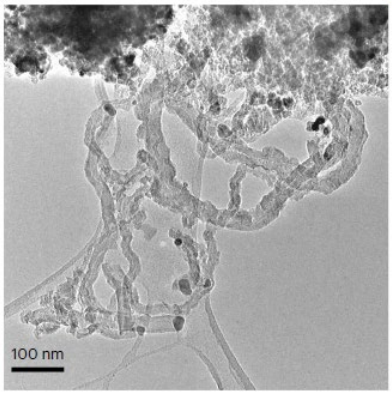


**Figure 5** TEM of CNFs

## Publications for this grant (Sept 2023- October 2024)

In the sept 2023- October 2024 period, 18 articles have been published with this FWP as the main driver or the main provider of ideas, with nearly half of them published in high impact journals including *Nature Catalysis* (1), the *Journal of the American Chemical Society* (1), *Angew. Chemie In Ed* (1), *ACS Nano* (2), *ACS Catalysis* (2) and *J. Phys. Chem. Lett.* (1). In addition, there are 13 articles in which this FWP has made a minor contribution. Graduate Students, postdoctoral fellows and PIs funded under this FWP are highlighted.

### FY 2024 Journal Publications:

**Thrust 1:**

- **Publications intellectually led by this FWP**
- Tuning Oxide Morphology to Improve Activity and Selectivity for the Selective Conversion of Carbon Dioxide to Methanol, J. Moncada, X. Chen, K. Deng, Y. Wang, W. Xu, N. Marinkovic, G. Zhou, A. Martinez-Arias and J.A. Rodriguez, *ACS Catal.*, **2023**, *13*, 15248-15258. https://doi.org/10.1021/acscatal.3c04222
- Screening of Cu-based catalysts for selective methane to methanol conversion, E. Huang, P. Liu , *J. Phys. Chem. C,* **2024**, *128*, 7876–7883. https://doi.org/10.1021/acs.jpcc.4c01179
- $CO_2$ hydrogenation over rhodium cluster catalyst nucleated within a manganese oxide framework. S. Xiang, J.D. Jiménez, L.F. Posada, S.J.B. Rubio, H.S. Khanna, S.Hwang, S., D. Leshchev, S.L. Suib, A.I. Frenkel, S.D. Senanayake, *Applied Catal. A: General*, **2024**, *683*, 119845. https://doi.org/10.1016/J.APCATA.2024.119845
- A US perspective on closing the carbon cycle to defossilize difficult-to-electrify segments of our economy, W.J. Shaw, M.K. Kidder, S.R. Bare, M. Delferro, J.R. Morris, F.M. Toma, S.D. Senanayake, T. Autrey, E.J. Biddinger, S. Boettcher, M.E. Bowden, P.F. Britt, R.C. Brown, R.M. Bullock, J. G. Chen, C. Daniel, P.K. Dorhout, R.A. Efroymson, K.J. Gaffney, J.A. Rodriguez, P. Liu … K.S. Walton, *Nature Reviews Chem.*, **2024**, *8*, 376–400. https://doi.org/10.1038/s41570-024-00587-1
- $CsO_x$ Nanostructures on Au(111): Morphology- and Size-dependent Activity for the Water–Gas Shift Reaction, R. Shi, P.J. Ramirez, R. Rosales, M. Mahapatra, N. Rui, and J.A. Rodriguez, *J. Phys. Chem. C*, **2024**, 128, 3260-3268. https://doi.org/10.1021/acs.jpcc.3c08190
- MgO Nanostructures on Cu(111): Understanding Size- and Morphology-Dependent $CO_2$ Binding and Hydrogenation, K.P. Reddy, A. Islam, Y. Tian, H. Lin, D. Kim, A. Hunt, I. Waluyo, and J.A. Rodriguez, *J. Phys. Chem. C*. **2024**, *128*, 7149-7158. https://doi.org/10.1021/acs.jpcc.4c02049
- The Surface Chemistry of Methanol on Pd(111) and H–Pd(111) Surfaces: C–O Bond Cleavage and the Effects of Metal Hydride Formation. J. Kim, H. Lim, H., Y. Tian, L. Piliai, A. Hunt, I. Waluyo, S. D. Senanayake, and J.A. Rodriguez, *J. Phys. Chem. Lett.*, **2024**, *15*, 6209–6215. https://doi.org/10.1021/acs.jpclett.4c01134
- Observing Chemical and Morphological Changes in a Cu@$TiO_x$ Core@Shell Catalyst: Impact of Reversible Metal-Oxide Interactions on CO2 Activation and Hydrogenation, K. Deng, X. Chen, J. Moncada, K.L. Salvatore, N. Rui, W. Xu, S. Xiang, N. Marinkovic, A. Frenkel, G. Zhou, S. Wong, and J.A, Rodriguez, *ACS Catal.*, **2024**, *14*, 11832-11844. https://pubs.acs.org/doi/full/10.1021/acscatal.4c02694

- From Methane to Methanol: Pd-ic-$CeO_2$ Catalysts Engineered for High Selectivity via Mechanochemical Synthesis, J.J. Jimenez, P.G. Lustemberg, M. Danielis, E. Fernandez-Villanueva, S. Hwang, I. Waluyo, A. Hunt, D. Wierzbicki, J. Zhang, L. Qi. A. Trovarelli, J.A. Rodriguez, S. Colussi, M.V. Ganduglia-Pirovano, and S.D. Senanayake, *J. Am. Chem. Soc.* **2024**, *146*, 25986-25999. https://pubs.acs.org/doi/10.1021/jacs.4c04815
- Low-Temperature Activation and Coupling of Methane on MgO Nanostructures Embedded in $Cu_2O$/Cu(111). A. Islam, E. Huang. Y. Tian, P.J. Ramirez, K.P. Reddy, H. Lim, N. White, A. Hunt, I. Waluyo, P. Liu, and J.A. Rodriguez, *ACS Nano*, *18*, 28371-28381. https://pubs.acs.org/doi/full/10.1021/acsnano.4c10811

- **Collaborative Publications**

- Morphology dependent reactivity of $CsO_x$ nanostructures on Au(111): binding and hydrogenation of $CO_2$ to HCOOH, V. Mehar, W. Liao, M. Mahapatra, R. Shi, H. Lim, I. Barba-Nieto, A. Hunt, I. Waluyo, P. Liu, J. A. Rodriguez , *ACS Nano,* **2023**, *17*, 22990-22998. https://doi.org/10.1021/acsnano.3c08324 (led by Thrust 3, this thrust helped with the theoretical studies).
- Active sites of atomically dispersed Pt supported on Gd-doped ceria with improved low temperature performance for CO oxidation. Y. Li, H. Wang, H. Song, N. Rui, M. Kottwitz, M., S. D. Senanayake, R.G. Nuzzo, Z. Wu, D. Jiang, and A.I. Frenkel, *Chemical Science*, **2023,** *14*, 12582–12588. https://doi.org/10.1039/D3SC03988A (provided XPS characterization).
- Directing $CO_2$ electroreduction pathways for selective C2 product formation using single-site doped copper catalysts, Z. Li, P. Wang, X. Lyu, V.K.R. Kondapalli, S. Xiang, J.D. Jimenez, L. Ma, T. Ito, T. Zhang, J. Raj, Y. Fang, Y. Bai, J. Li, A. Serov, V. Shanov, A.I. Frenkel, S.D. Senanayake, S. Yang, T.P. Senftle, and J. Wu, (2024). *Nature Chemical Engineering*, **2024**, *1*, 159–169. https://doi.org/10.1038/s44286-023-00018-w (provided XAS characterization).
- $LaCeO_x$ coupled N-doped graphene/Ru single-atoms as a binary-site catalyst for efficient hydrogen evolution based on hydrogen spillover. V. Dao, H. Choi, S. Yadav, J.D. Jiménez, C. Kim, T. van Nguyen, K. Chen, K., P. Uthirakumar, Q. van Le, S.D. Senanayake, H.Y. Kim, and I.-H. Lee, *Applied Catalysis B: Environmental*, **2024**, *343*, 123452. https://doi.org/https:// doi.org/10.1016/ j.apcatb.2023.123452 (provided help with the characterization).
- Controlling bond scission pathways of isopropanol on Fe- and Pt-modified $Mo_2N$ model surfaces and powder catalysts, W. Porter, H. Mera, W. Liao, Z. Lin, P. Liu, J. Kitchin, and J. G. Chen, *ACS Catal.* **2024**, *14*, 1653-1662. https://doi.org/10.1021/acscatal.3c04700 (provided theoretical studies).
- Direct Observation of Twin van der Waals Molecular Chains, S. Fang, P. Zahl, X. Wang, P. Liu, D. Stacchiola, and Y.H. Hu, *J. Phys. Chem. Lett.* **2023**, *14*, 10710-10716. https://doi.org/10.1021/ acs.jpclett.3c02914 (provided theoretical studies).
- Role of Atomicity and Interface on $InO_x$-$TiO_2$ Composites: Thermo-Photo Valorization of $CO_2$, R. Sayago-Charro, I. Barba-Nieto, U. Caudillo-Flores, A. Tolosana-Moranchel, J.A. Rodriguez, M. Fernandez-Garcia, and A. Kubacka, *ACS. Appl. Mater. Interfaces* **2024**, https://doi.org/10.1021/acsami.4c04803 (provided help with the XAS characterization).

**Thrust 2:**

- **Publications intellectually led by this FWP**

- Converting Carbon Dioxide into Carbon Nanotubes by Reacting with Ethane, Y. Yuan, E. Huang, S. Hwang, P. Liu and J.G. Chen, *Angew. Chem. Int. Ed*, **2024**, *63*, e202404047. https://doi.org/10.1002/anie.202404047
- $CO_2$ fixation into carbon nanofibers using electrochemical-thermochemical tandem catalysis, Z. Xie, E. Huang, S. Garg, S. Hwang, P. Liu and J.G. Chen, *Nature Catal.*, **2024**, 7. 98-109. https://doi.org/10.1038/s41929-023-01085-1
- Comparison of Direct and $CO_2$-Oxidative Dehydrogenation of Propane, Y. Yuan, W.N. Porter and J.G. Chen, *Trends in Chemistry*, **2023**, *5*, 840-852. https://doi.org/10.1016/j.trechm.2023.09.001

- **Collaborative Publications**

- Tandem Reactors and Reactions for $CO_2$ Conversion, S. Garg, Z, Xie and J.G. Chen, *Nature Chemical Engineering*, **2024**, *1*, 139-1487. https://doi.org/10.1038/s44286-023-00020-2 (provided intellectual discussions)
- Role of $H_2O$ in catalytic conversion of C1 molecules, L. Jiang, K. Li, W.N. Porter, H. Wang, G. Li and J.G. Chen, *J. Am. Chem. Soc.*, **2024**, 146, 2857-2875. https://doi.org/10.1021/jacs.3c13374 (provided intellectual discussions)
- $CO_2$-Mediated Oxidative Dehydrogenation of Propane Enabled by Pt-Based Bimetallic Catalysts, P. Zhai, Z. Xie, E. Huang, D.R. Aireddy, H. Yu, D.A. Cullen, P. Liu, J.G. Chen and K. Ding, *Chem*, 9 (2023) 3268-3285. https://doi.org/10.1016/j.chempr.2023.07.002 (provided theoretical support and intellectual discussions)

**Thrust 3:**

- **Publications intellectually led by this FWP**

- Morphology dependent reactivity of $CsO_x$ nanostructures on Au(111): binding and hydrogenation of $CO_2$ to HCOOH, V. Mehar, W. Liao, M. Mahapatra, R. Shi, H. Lim, I. Barba-Nieto, A. Hunt, I. Waluyo, P. Liu, J. A. Rodriguez , *ACS Nano,* **2023**, *17*, 22990-22998. https://doi.org/10.1021/acsnano.3c08324.
- Revealing Intermetallic Active Sites of PtNi Nanocatalysts for Reverse Water Gas Shift Reaction, H. Li, H. Zhang, X. Wang, R. Nuzzo, A. Frenkel, P. Liu, D. Gersappe, *J. Phys. Chem. C, 2023,* 127, 22067-22075
- Aggregation of Size-Selected Oxide Clusters Deposited onto Au(111), J. Wang, M. Toledo Rozycki, X. Tong and M. G. White, *Langmuir* **2023**, 39, 13481–13492. https://doi.org/ 10.1021/acs.langmuir.3c01220.
- Composition-Dependent Reconstructions of Titanium Oxide Clusters and Cu(111) Support via Cluster-Adatom Interactions, J. Wang, L. Shi, X. Tong, and M.G. White, *J. Phys. Chem. C*, **2024**, *128*, 17153-17164. https://pubs.acs.org/doi/10.1021/acs.jpcc.4c04803
- Understanding the Morphology and Chemical Activity of Model $ZrO_x$/Au(111) Catalysts for $CO_2$ Hydrogenation, Y. Tian, H. Lim, J. Kim, A. Hunt, I. Waluyo, S.D.

Senanayake, and J.A. Rodriguez, *Surf. Sci*. **2024**, *750*, 122590. https://www.sciencedirect.com/science/article/pii/S0039602824001419

- **Collaborative Publications**

- $CsO_x$ Nanostructures on Au(111): Morphology- and Size-dependent Activity for the Water–Gas Shift Reaction, R. Shi, P.J. Ramirez, R. Rosales, M. Mahapatra, N. Rui, and J.A. Rodriguez, *J. Phys. Chem. C*, **2024**, 128, 3260-3268. https://doi.org/10.1021/acs.jpcc.3c08190 (led by Thrust 1, this thrust helped with the STM studies).
- MgO Nanostructures on Cu(111): Understanding Size- and Morphology-Dependent $CO_2$ Binding and Hydrogenation, K.P. Reddy, A. Islam, Y. Tian, H. Lin, D. Kim, A. Hunt, I. Waluyo, and J.A. Rodriguez, *J. Phys. Chem. C*. **2024**, *128*, 7149-7158. https://doi.org/10.1021/acs.jpcc.4c02049 (led by Thrust 1, this thrust helped with the STM studies).
- Mechanism of Stoichiometrically Governed Titanium Oxide Brownian Tree Formation on Stepped Au(111), R. Lavroff, J. Wang, M. G. White, P. Sautet and A. Anastassia, *J. Phys. Chem. C*, **2023**, *127*, 8030-8040. https://doi.org/10.26434/chemrxiv-2023-2gt6z (provided experimental studies and intellectual discussions).
- Momentum-Resolved Exciton Coupling and Valley Polarization Dynamics in Monolayer $WS_2$, A. Kunin, S. Chernov, J. Bakalis, Z. Li, S. Cheng, Z. H. Withers, M. G. White, G. Schönhense, X. Du, R. K. Kawakami, and T. K. Allison, *Phys. Rev. Lett.* **2023**, *130*, 046202. https://doi.org/10.1103/ PhysRevLett.130.046202 (provided intellectual discussions).
- Determination of the interfacial energy between graphene nanoplatelets and deuterated or hydrogenated polystyrene, Y. Lin, X. Liu, G. Onghai, A. Raut, Y. Fang, Y. Yin, S. Fu, H. Fang, K. Feng, X. Wang, P. Liu, T. Li, J. Sokolov, M. Rafailovich, *Macromolecules,* **2023**, *56*, 8039-8046. https://doi.org/10.1021/acs.macromol.3c00982 (provided theoretical studies).
- Low-Temperature Activation and Coupling of Methane on MgO Nanostructures Embedded in $Cu_2O$/Cu(111). A. Islam, E. Huang. Y. Tian, P.J. Ramirez, K.P. Reddy, H. Lim, N. White, A. Hunt, I. Waluyo, P. Liu, and J.A. Rodriguez, *ACS Nano*, *18*, 28371-28381. https://pubs.acs.org/doi/full/10.1021/acsnano.4c10811(led by Thrust 1, this thrust helped with the STM studies).

**Catalysis Program at Lawrence Berkeley National Laboratory:**
**Harnessing Complexity for Catalytic Efficiency**

John F. Hartwig (Program leader), Polly L. Arnold, Alexis T. Bell, Robert G. Bergman (Affiliate), Shannon Boettcher (New program member), Neil Razdan (New faculty), Kenneth N. Raymond (Affiliate), Miquel B. Salmeron, T. Don Tilley, F. Dean Toste, Peidong Yang

Chemical Sciences Division, Lawrence Berkeley National Laboratory

**Presentation Abstract**

The LBNL Catalysis Program seeks to reveal foundational principles for the creation of new catalysts, realization of new processes, and creation of new approaches to learn how catalysts operate. The overarching theme of the current research is to reveal and exploit complexity inherent in, or designed to be a part of, catalytic systems that operate with high rates and selectivity. The types of catalysts and catalytic reactions studied in the current Catalysis Program, and the classes of mechanisms by which the catalysts react, are broad in scope, but converge on several themes that constitute the three subtasks. These three subtasks are organized by layers of complexity. The first subtask focuses on catalytic systems in which two components, one the active site and one the supramolecular confines of that site, work cooperatively to change the course of the catalytic transformation; the second seeks to establish principles by which secondary interactions near a catalytic active site lead to enhanced activity and selectivity in catalytic reactions.; the third subtask attempts to create new catalytic systems that involve multiple catalytic sites that work cooperatively and to reveal those that convert from one to another, often by *in situ* and *in operando* conditions. Each of these subtasks directly addresses PROs in workshop reports on catalysis and cross-cutting themes of the BES CSGB division.

**FWP Number: CH030201**

**FWP Title: Program in Catalysis and Chemical Transformations – Harnessing Complexity for Catalytic Efficiency**

**Graduate Students:** Alghannam, Afnan; Brown, Gretchen; Carter, Robert; Colton, David; Conk, RJ; Craescu, Cristina; Elissiry, Luke; Feijoo, Julian; Fitzgerald, Madeline; Gusman, Maria Fonseca; Heafner, Elizabeth; Hernandez, Matt; Herrera, Gabe; Joyner, Isaac; Lara, Jaden; Maddi, Vincent; Manske, Jenna; Martinez, Jose; Pan, Judy; Rothweiler, Aila; See, Matthew; Shan, Yu; Shi, Ethan; Singh, Gurjot; Wang, Tianle; Xie, Yuanzhe; Xu, Nicole.

**Postdocs:** Chae, Sudong; Forbes, Katherine; Jaugstetter, Maximillian; Syed, Zoha; Treacy, Sean; Wong, Anthony.

**Affiliates:** Park, Jeong; Su, Ji; Yang, Ji.

## RECENT PROGRESS

### Subtask 1. Catalysis in Confined Spaces

Subtask 1 focuses on conducting catalysis in confined environments with themes that are connected by their relationships between synthetic and natural confined spaces. This focus was initiated by work on catalysis within supramolecular nanovessels, which has been a long-standing research topic of the LBNL Catalysis Program. Now, this work on confined environments has motivated research on catalysis in a broader range of confined spaces, including fully synthetic alternative supramolecular cages, the ordered layers on nanostructured catalysts, semi-synthetic active sites and artificial metalloenzymes with synthetic cofactors within mutated protein hosts, and natural metalloenzymes mutated to enable understanding of subtle divergences in reactivity.

### 1.1 Host-Mediated Electrochemical Processes and Tunable Electrochemical Entropy through Solvent Ordering by a Supramolecular Host

Over the last decade, **Toste, Raymond, Bergman** have demonstrated that the microenvironments within a highly anionic supramolecular $M_4L_6$ catalyst host (Fig. 1.1) can impart catalytic rate accelerations of more than a million-fold and product selectivities not otherwise observed. The encapsulation of small molecules within the $M_4L_6$ hosts is primarily driven by entropy, and recent terahertz spectroscopy findings revealed that water molecules encapsulated in the host cavity exhibit a high degree of organization, resembling amorphous ice. The encapsulation process involves displacing numerous solvent molecules, leading to a substantial increase in overall entropy. The entropic changes in this system are influenced not only by solvent reorganization but also by alteration in degrees of freedom, akin to phase changes observed in certain materials.

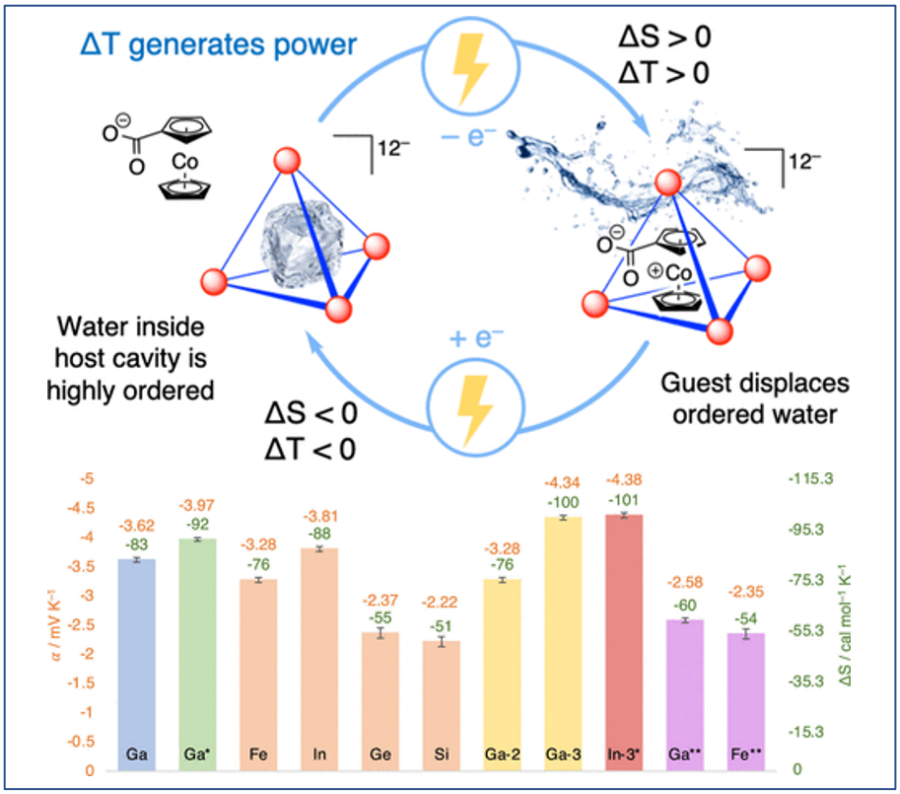


Fig. 1.1 Redox entropy of cobaltacenium carboxylic acid in the presence of various $M_4L_6$ hosts.

The **Toste, Bergman, Raymond** team has recently demonstrated an electrochemically controlled guest (cobaltacenium carboxylic acid) encapsulation process with $M_4L_6$ hosts, aiming to create a systems with large and reversible molar entropic changes suitable for thermally regenerative electrochemical cycles (TRECs), suitable for thermogalvanic waste-heat harvesting and electrochemical cooling, among other potential applications. One such system showed that an electrochemical $Ga_4L_6$ host-guest system undergoes one-electron oxidation with an entropic change of 3.62 $mV \cdot K^{-1}$ or a reaction entropy ($\Delta S$) of 83.5 cal $mol^{-1} \cdot K^{-1}$. This value represents a nearly four-fold increase over the state-of-the-art TREC electrolyte, potassium ferricyanide.[83] Upon encapsulation of a guest, water molecules that structurally resemble amorphous ice are displaced from the host cavity, leveraging a change in the degrees of freedom and ordering of the solvent rather than the solvation of the redox-active species to increase entropy.

The $M_4L_6$ hosts can also be structurally varied at the metal vertices, the linker and end groups of the bridging ligand, offering a wide range of entropic changes and rational optimization of the system's $\Delta S$, showing a range of −51 to −101 cal $mol^{-1}$ $K^{-1}$ (−2.2 to −4.4 mV $K^{-1}$) depending on ligand and metal vertex modifications, demonstrating the potential for rational design of high-entropy electrolytes and a new strategy to overcome theoretical limits on ion solvation reorganization entropy. By leveraging this synthetic diversification, it becomes possible to explore encapsulation entropy in unprecedented ways and optimize the thermodynamics of the system.

Xia, K.; Rajan, A.; Surendranath, Y.; Bergman, R. G.; Raymond, K. N.; Toste, F. D., Tunable Electrochemical Entropy through Solvent Ordering by a Supramolecular Host. *J. Am. Chem. Soc.* **2023**, *145*, 25463-25470. DOI 10.1021/jacs.3c10145

### 1.2 Non-Natural Zinc Hydride Active Site in Carbonic Anhydrase Variants Catalyzes the Reduction of Dialkyl Ketones with High Enantioselectivity

Human carbonic anhydrase II (hCAII) naturally catalyzes the reaction between two achiral molecules—water and carbon dioxide—to yield the achiral product carbonic acid through a zinc hydroxide intermediate. The **Hartwig** group, in collaboration with Douglas Clark, have previously shown that a non-natural zinc hydride, instead of a hydroxide, can be generated in this enzyme to create a catalyst for the reduction of aryl ketones (Fig. 1.2). High enantioselectivities indicate that the reactions occur at the cofactor in the enzyme active site. These mechanistic data provide strong evidence that the process involves a mononuclear zinc-hydride, despite the instability of terminal hydrides on electropositive metals in protic environments. Thus, monomeric hydrides, even on electropositive metals, might be employed as catalytic intermediates in enzymatic processes, thereby bridging a gap between molecular catalysis and biocatalysis.

Dialkyl ketones are a more challenging substrate to reduce, and the enantioselective reduction of dialkyl ketones with two alkyl groups that are similar in size and electronic properties is a particularly challenging transformation to achieve with high activity and selectivity. Though carbonic anhydrase confers no chirality during its natural function of hydration and dehydration of carbonic acid, we have now shown that hCAII, as well as a double mutant of it, catalyzes the enantioselective reduction of dialkyl ketones with high yields and enantioselectivities, even when the two alkyl groups are similar in size. We also show that variants of hCAII catalyze the site-selective reduction of one ketone over the other in an unsymmetrical aliphatic diketone. Computational docking of a dialkyl ketone to variants of hCAII containing the zinc hydride provided insights into the origins of the reactivity of various substrates and the high enantioselectivity of the transformations and show how a confined environment can control the enantioselectivity of an abiological intermediate (Fig. 1.3).

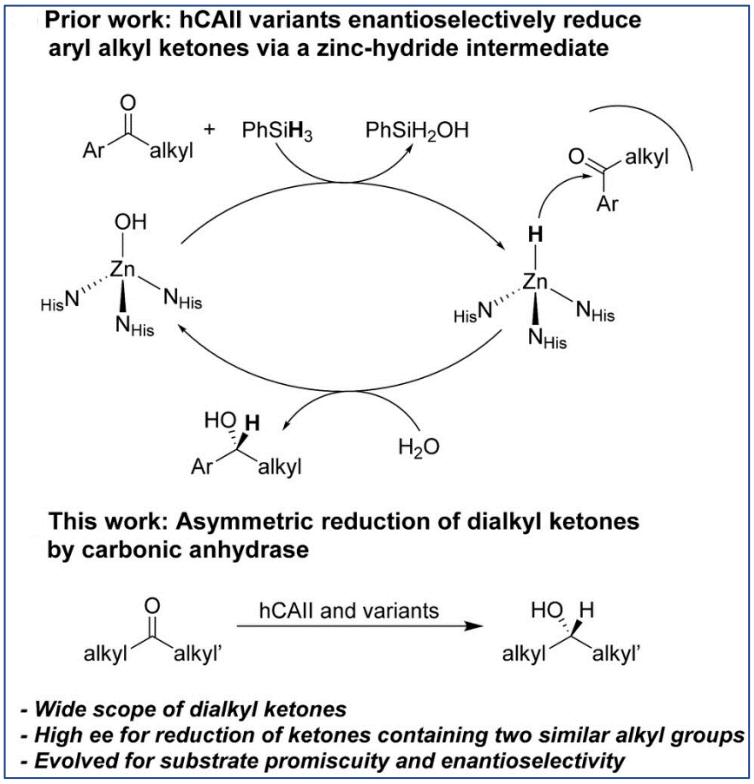


Fig. 1.2 Enantioselective reduction of ketones through an unnatural zinc-hydride in hCAII enzyme variants.

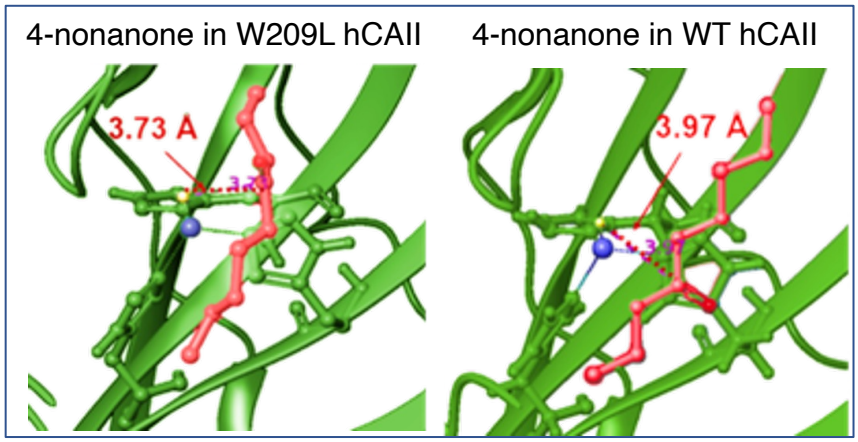


Fig. 1.3. Reorientation of 4-nonanone dialkyl ketone substrate with respect to the Zn-H through enzyme residue mutations for high selectivity.

Chen, R.; Kayrouz, C. S.; McAmis, E.; Clark, D. S.; Hartwig, J. F., Carbonic Anhydrase Variants Catalyze the Reduction of Dialkyl Ketones with High Enantioselectivity. *Angew. Chem. Int. Ed.* **2024**. *63*, e202407111. DOI 10.1002/anie.202407111.

### 1.3 Nanometer-Resolved Observation of Electrochemical Microenvironment Formation at Nanoparticle–Ligand interfaces for Copper-Catalyzed $CO_2$ Reduction

While microenvironments at the surfaces of electrocatalysts can strongly influence the rates and selectivity of catalytic reactions, the structure of these reactive microenvironments remain understudied, especially in the context of confinement created by local fields. Inspired by the work

on nanovessels and enzymes in this subtask, **Yang** and his collaborators have begun to investigate the impact of reactive microenvironments on catalyst activity and selectivity through a focus on Nanoparticle-Ordered-Ligand Interlayer (NOLI) structures formed by the detachment of surface-bonded ligands under electrochemical bias.

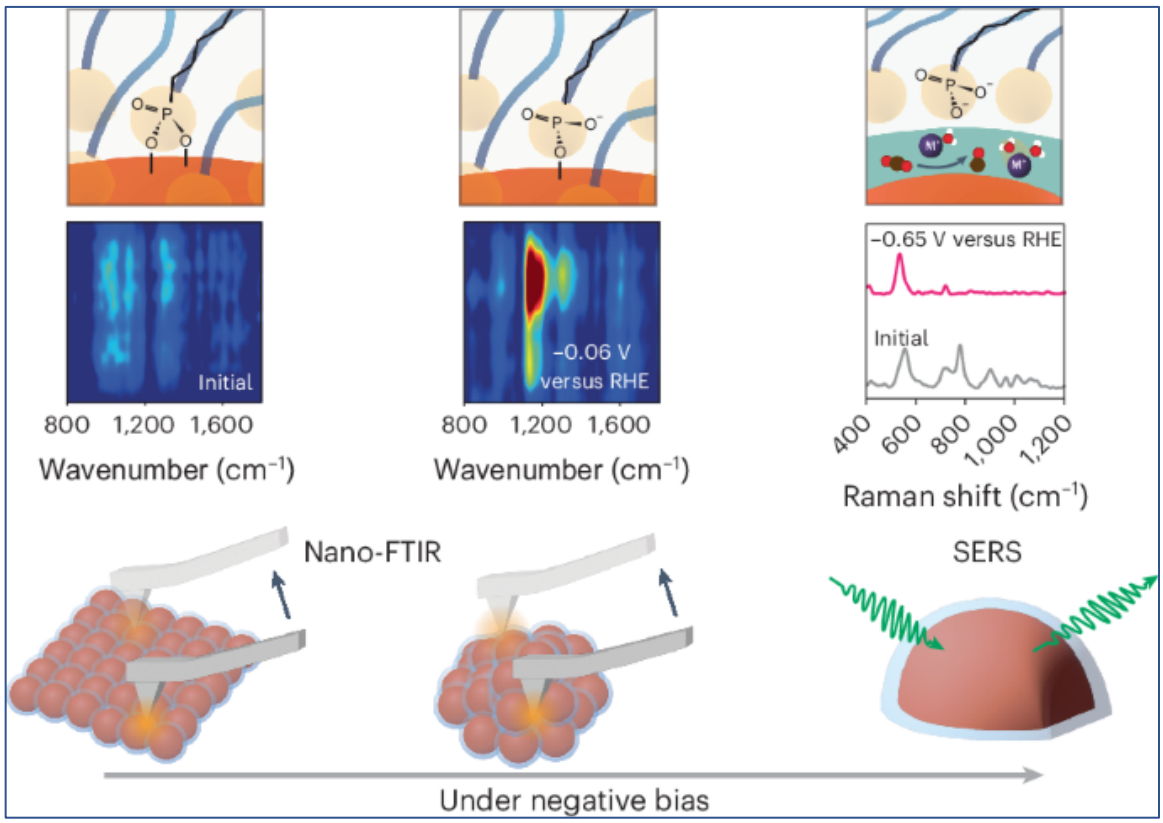


Fig. 1.4. *In situ* infrared nanospectroscopy and surface-enhanced Raman spectroscopy for interrogation of the NOLI under applied bias.

The dynamic response of surface ligands on nanoparticles (NPs) to external stimuli critically determines the functionality of NP–ligand systems. The NOLI microenvironment is highly active and selective for CO2-to-CO conversion by copper NPs. However, the lack of in situ characterization techniques with high spatial resolution hampers a comprehensive molecular-level understanding of the mechanism of interlayer formation. We have now utilized *in situ* infrared nanospectroscopy and surface-enhanced Raman spectroscopy, unveiling an electrochemical bias-induced, consecutive bond cleavage mechanism of surface ligands leading to formation of the NP-ordered-ligand interlayer (Fig 1.4). This real-time molecular insight will further influence the design of confined localized fields in multiple catalytic systems. Moreover, the demonstrated capability of capturing nanometer-resolved, dynamic molecular-scale events holds promise for the advancement of using controlled local molecular behavior to achieve desired functionalities across multiple research domains in nanoscience.

Shan, Y.; Zhao, X.; Fonseca Guzman, M.; Jana, A.; Chen, S.; Yu, S.; Ng, K. C.; Roh, I.; Chen, H.; Altoe, V.; Gilbert Corder, S. N.; Bechtel, H. A.; Qian, J.; Salmeron, M. B.; Yang, P., Nanometre-Resolved Observation of Electrochemical Microenvironment Formation at the Nanoparticle–Ligand Interface. *Nat. Catal.* **2024**. 7, 422–431. DOI 10.1038/s41929-024-01119-2.

**Subtask 2. Catalysis Driven by Secondary Interactions**

Subtask 2 focuses on the creation of multi-functional single-site catalysts that draw concepts from Subtask 1 for transformations crucial to efficient use of feedstocks, such as additions to alkenes, reductions of carbon dioxide, utilization of biomass sources, and functionalization of hydrocarbons. This subtask ranges from sites containing a single metal center in which interactions beyond the core of this active site (from directional hydrogen bonds to ionic interactions and weaker dispersion interactions) to active sites containing multiple metals in which interactions between metals, in addition to the interactions of the ligands, influence catalysis. Thus, the research in this subtask, together, will reveal principles to control both homogeneous and heterogeneous catalysis through a series of non-covalent interactions and through both direct and distant metal-metal interactions.

**2.1 Metal–Metal Redox Exchange between $Co_4O_4$ and Mn(II) to Produce Heterometallic Manganese–Cobalt Oxo Cubanes through "Dangler" Intermediates**

The **Tilley** group has demonstrated the ability to use cobalt-oxo cubanes $Co_4O_4(OAc)_4(Pyr)_4$ as a functional mimic of the OEC's manganese cubane cluster. To continue expanding the accessible oxidation chemistry of these synthetic cubanes, it will be important to define the role of metals beyond cobalt and to investigate cooperative effects by which heterometallic interactions influence reactivity by relaying electronic and chemical effects through the tetrametallic framework. Furthermore, pendent metals bound to heterocubanes are components of well-known active sites in enzymes like the OEC that mediate difficult chemical transformations. Investigations into the specific role of these metal ions, sometimes referred to as "danglers", have been hindered by a paucity of rational synthetic routes to appropriate model structures. For this purpose, they have undertaken development of rational synthetic routes to oxo-cubane structures with predetermined compositions.

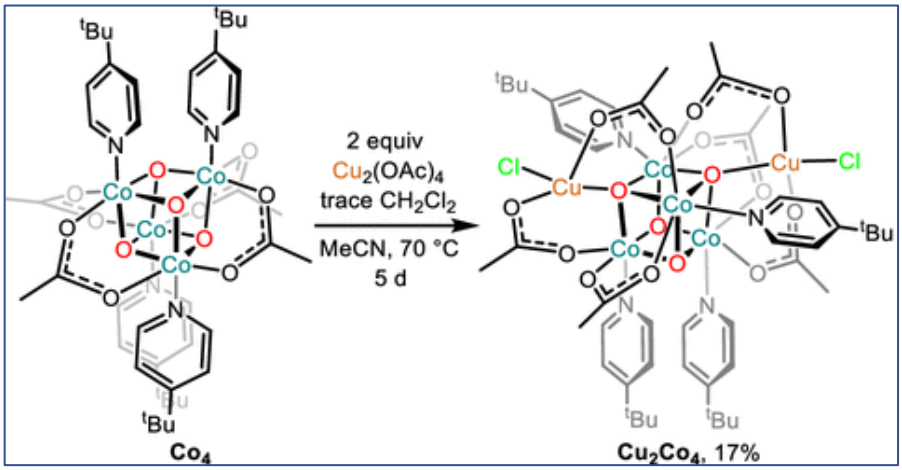


Fig. 2.1. Synthesis of dicopper "dangler" $Co_4O_4$ cubane.

To generate pendent metal ions bonded to an oxo cubane through a carboxylate bridge, the cubane $Co_4(\mu_3\text{-}O)_4(OAc)_4(t\text{-}Bupy)_4$ was exposed to various metal acetate complexes. Reaction with $Cu(OAc)_2$ gave the structurally characterized dicopper dangler $Cu_2Co_4(\mu_4\text{-}O)_2(\mu_3\text{-}O)_2(OAc)_6(Cl)_2(t\text{-}Bupy)_4$ (Fig 2.1). In contrast, the analogous reaction with $Mn(OAc)_2$ produced the $Mn^{IV}$-containing cubane cation $[MnCo_3(\mu_3\text{-}O)_4(OAc)_4(t\text{-}Bupy)_4]^+$ by way of a metal–metal exchange that gives Co(II) and Co(III) byproducts (Fig 2.2). Additionally, reaction of the formally Co(IV) cubane complex $[Co_4(\mu_3\text{-}O)_4(OAc)_4(t\text{-}Bupy)_4]^+$ with Mn(II) gave the corresponding Mn-containing cubane in 80% yield. A mechanistic examination of the related metal–metal exchange reaction between $Co_4(\mu_3\text{-}O)_4(OBz)_4(py)_4$ and $[Mn(acac)_2(py)_2][PF_6]$ by UV–vis spectroscopy provided support for a process involving rate-determining association of the reactants and electron

transfer through a μ-oxo bridge in the adduct intermediate. The rates of exchange correlate with the donor strength of the pyridine and benzoate ligand substituents of the cubane; more electron-donating pyridine ligands accelerate metal–metal exchange. However, both electron-donating and -withdrawing benzoate ligands can accelerate exchange. These experiments suggest that the basicity of the cubane oxo ligands promotes metal–metal exchange reactivity. The redox potentials of the Mn and cubane starting materials, along with isotopic labeling studies suggest an inner-sphere electron-transfer mechanism in a dangler intermediate.

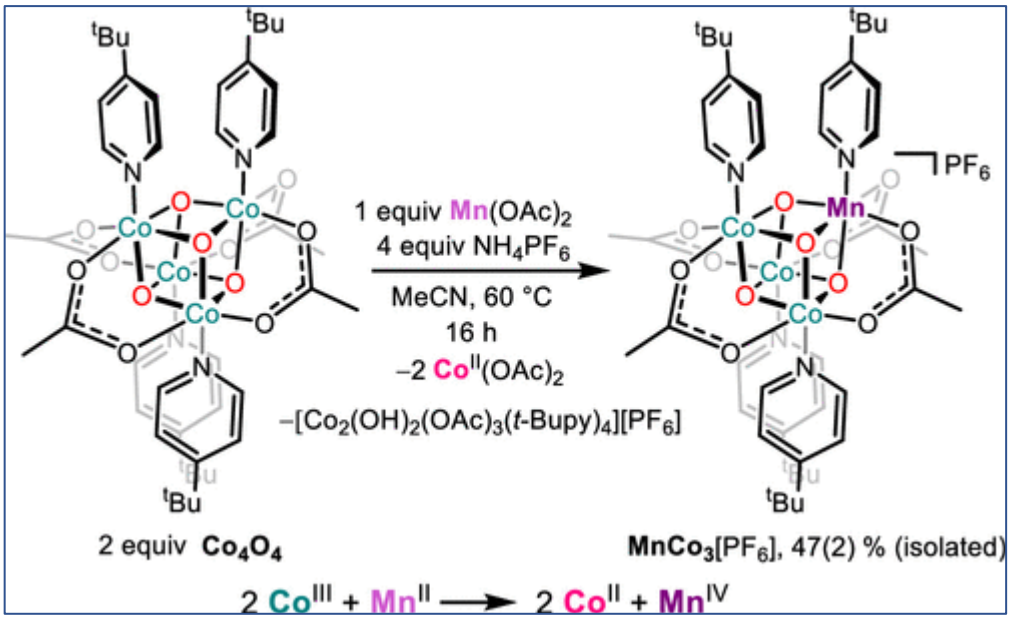


Fig. 2.2. Metal–Metal redox exchange reaching between $Co_4$ and $Mn(OAc)_2$ with the corresponding formal redox equation.

Wheeler, T. A.; Tilley, T. D., Metal-Metal Redox Exchange to Produce Heterometallic Manganese-Cobalt Oxo Cubanes via a "Dangler" Intermediate. *J. Am. Chem. Soc.* **2024**, *146*, 20279-20290. DOI 10.1021/jacs.4c05367.

**2.2 Control of metallacycle sterics in the catalytic dinitrogen reduction to either secondary or tertiary amines by lanthanide, actinide, and group 4 metal complexes.**

The low-energy conversion of atmospheric dinitrogen to amines is a grand challenge and could bring food and energy justice to many. For decades, chemists targeting homogeneous catalysts for this, citing biology as inspiration, have focused on electron-rich d-block complexes. The range of d-block metal complexes that can catalyze dinitrogen reduction to ammonia or tris(silyl) amines under ambient conditions has increased recently but lacks electropositive metal complexes, such as those of the f-block, which lack filled d-orbitals that would support classical binding modes of $N_2$. The **Arnold** group has now identified numerous examples of lanthanide, actinide, and group 4 metals that can catalyze the reduction of dinitrogen to not only tertiary amines but significantly to secondary silyl amines as well.

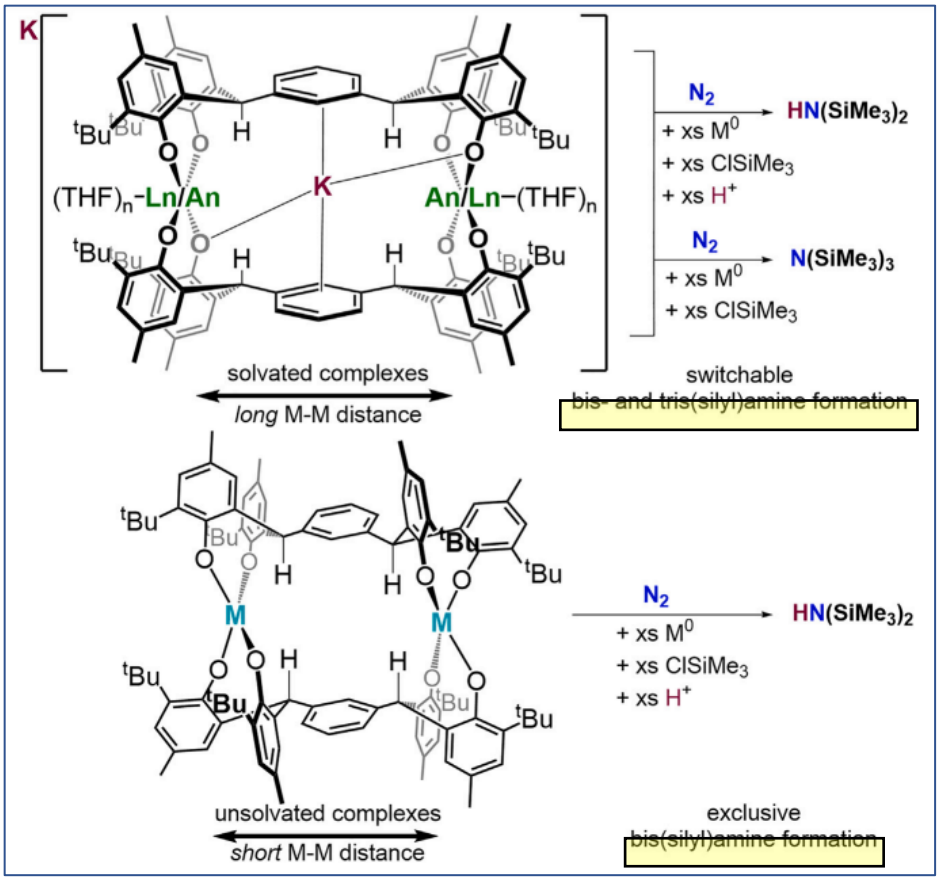


Fig. 2.3. Catalytic dinitrogen reduction by (top) lanthanide and uranium metallacycle cavities with larger metal-metal distances and (bottom) titanium and zirconium metallacycle cavities with shorter metal-metal distances.

The formation of this truly unusual amine product is controlled by the metallacycle sterics. The group 4 complexes featuring small cavities are most selective for bis(silyl)amine, while lanthanide complexes and a solvent-ligated uranium(IV) complex, all featuring larger cavities and greater metal-metal distances, can also accommodate the more conventionally observed tris(silyl)amine product (Fig 2.3). These results offer new catalytic applications for earth-abundant and plentiful titanium and members of the lanthanides that are also less toxic than many base metals used in catalysis. Further work on this growing project now includes evaluation and comparison of reactivity with mononucleating ligands, rather than binucleating ligand systems which create the metallacycle cavity and impart steric control, as well as monodentate phenolic ligands. The breadth of dinitrogen reduction activity we have now observed across the lanthanide and group 4 metals and in conjunction with ligand geometries and functionality underscores the extent to which these metals have been under-explored and underutilized in the transformation of difficult substrates.

Wong, A.; Lam, F. Y. T.; Hernandez, M.; Lara, J.; Trinh, T. M.; Kelly, R. P.; Ochiai, T.; Rao, G.; Britt, R. D.; Kaltsoyannis, N.; Arnold, P.L., Catalytic Dinitrogen Conversion to Amines by Lanthanide and Group IV Catalysts. *Chem. Catal.* **2024**, 100964. DOI 10.1016/j.checat.2024.100964.

**2.3 Combined Experimental and Theoretical Studies of Distorted (≡Si-O)$_3$Ti-OH Sites on Amorphous Silica and Their Effect on Cyclohexene Epoxidation.**

Silica supported metal cations, such as titanium, are widely used as catalysts in industrially relevant process, and Ti/$SiO_2$ in particular is active for the catalytic, gas-phase epoxidation of

cyclohexene to cyclohexene oxide with $H_2O_2$. The **Bell** group, with Head-Gordon, recently published two articles which together first present experimental and theoretical evidence for distorted ≡Ti–OH groups supported on amorphous $SiO_2$ and examines the influence of distortion on the strength of adsorption of polar molecules and secondly elaborates the effects of ≡Ti–OH site distortion on the kinetics and mechanism of the catalylsis (Fig. 2.4).

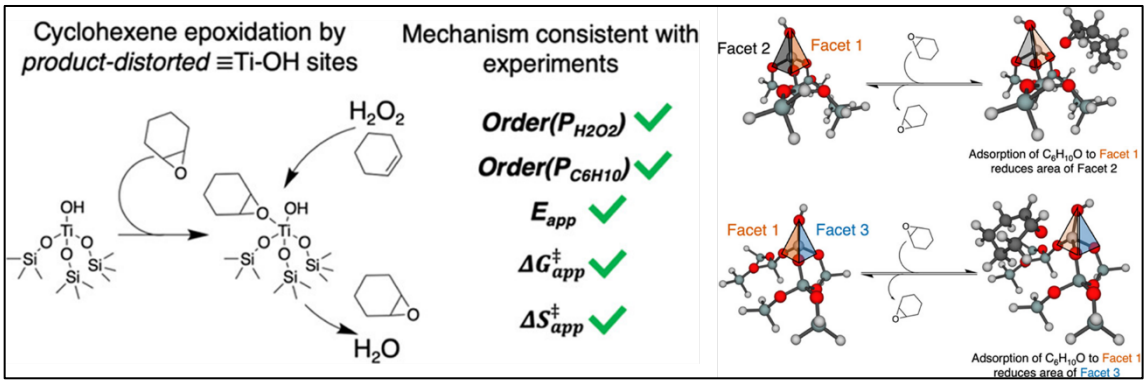


Fig. 2.4. Epoxidation of cyclohexene by product-distorted $(\equiv Si\text{-}O)_3Ti\text{-}OH$ Sites on amorphous silica through an experimentally- and theoretically-validated mechanism.

For the theoretical part of this effort, we developed a model for isolated ≡Si–OH or ≡Ti–OH groups on the surface of amorphous silica. The ≡M–OH group is represented by a small cluster, the properties of which are described by high-level density functional theory (DFT), whereas the large amorphous silica surroundings are represented by molecular mechanics (MM). The QM/MM model was validated by demonstrating that the predicted enthalpy of adsorption for polar molecules on ≡Si–OH groups agrees satisfactorily with both experimentally measured values determined by microcalorimetry and adduct-adsorption isotherms measured by infrared spectroscopy. QM/MM calculations made with our model revealed that the enthalpy of adsorption is proportional to the area of the triangular O–Ti–O facets of the ≡Ti–OH group to which polar molecules are bound and can be correlated with ≡Ti–OH site facet areas deduced from X-ray absorption spectroscopy (XAS/EXAFS) measurements.

We next utilized the experimentally validated computational method to calculate enthalpies of adsorption and transition states along the well-established mechanism for the catalytic cycle and put forward a steady-state microkinetic model (MKM) to investigate the effects of distortion on predicted kinetic observables (apparent activation energy, $E_a$, and reaction orders) and to establish whether the mechanism is consistent with observed kinetics. We show that adsorption of epoxide product to one facet of the tetrahedral ≡Ti–OH site significantly reduces the facet area on the opposite side. We show that these reduced-area facets can catalyze the epoxidation of cyclohexene, while epoxide remains co-adsorbed to the other side, which we find is the dominant path toward production of epoxide. This mechanism shows quantitative agreement between experiments and our predictions and also illustrates the key role of adsorbates in influencing the degree of distortion of ≡Ti–OH sites, in addition to the amorphous support itself.

Leonhardt, B. E.; Head-Gordon, M.; Bell, A. T., The Effects of ≡Ti–OH Site Distortion and Product Adsorption on the Mechanism and Kinetics of Cyclohexene Epoxidation over $Ti/SiO_2$. *ACS Catal.* **2024**, *14*, 3049−3064. DOI 10.1021/acscatal.3c06073.

Leonhardt, B. E.; Shen, H.; Head-Gordon, M.; Bell, A. T., Experimental and Theoretical Evidence for Distorted Tetrahedral ≡Ti−OH Sites Supported on Amorphous Silica and Their Effect on the Adsorption of Polar Molecules. *J. Phys. Chem. C* **2024**, *128*, 129–145. DOI 10.1021/acs.jpcc.3c07027.

**Subtask 3. Catalysis from Multisite Cooperativity and Evolution**

Subtask 3 focuses on catalytic systems involving multiple catalytic sites and systems working in concert, thereby complementing the multi-functional sites of Subtask 2. This research also includes catalysts that change shape, composition, and oxidation state during catalysis; deep analysis of these changes by special tools designed for *operando* measurements at the ALS; tandem catalytic processes that transform substrates through sequential steps to value-added products; and multiple homogeneous and heterogeneous catalysts that cleave and form carbon-carbon bonds selectively under mild conditions. This theme of catalytic transformations made possible by multi-site systems gained increased prominence during the prior funding cycle to become a dedicated subtask during the past three years. At the same time, several of the lines of research involving multiple metals in molecular and heterogeneous systems fall on a continuum spanning multiple metals within one site acting cooperatively (Subtask 2) and multiple metals serving different roles (an active site with a nearby Lewis acid, for example) to achieve a transformation (Subtask 3). This continuum emphasizes how the concepts of one subtask often influence the research conducted in another subtask.

**3.1 Cooperative, Multicatalytic Systems for the Deconstruction of Polyolefins to Feedstocks**

Despite the success of **Hartwig, Bell** and **Su** using multiple catalysts to deconstruct polyethylene (PE) to propene in yields up to 85% (*Science* **2022**), this DIE process requires at least one homogeneous catalyst in the sequence, thereby limiting its ultimate practicality, and it does not catalyze the DIE of polypropylene (PP). Thus, Hartwig, Bell and collaborator Su have worked to improve the published DIE of PE by developing heterogeneous catalysts for each step that work in concert and to expand this methodology to polypropylene, which accounts for an additional 21% of waste plastic or 1500 MT of waste material that could be valorized into propylene and isobutylene by DIE. Isobutylene is a valuable commodity chemical, used as a monomer, feedstock, and precursor to high-octane gasoline.

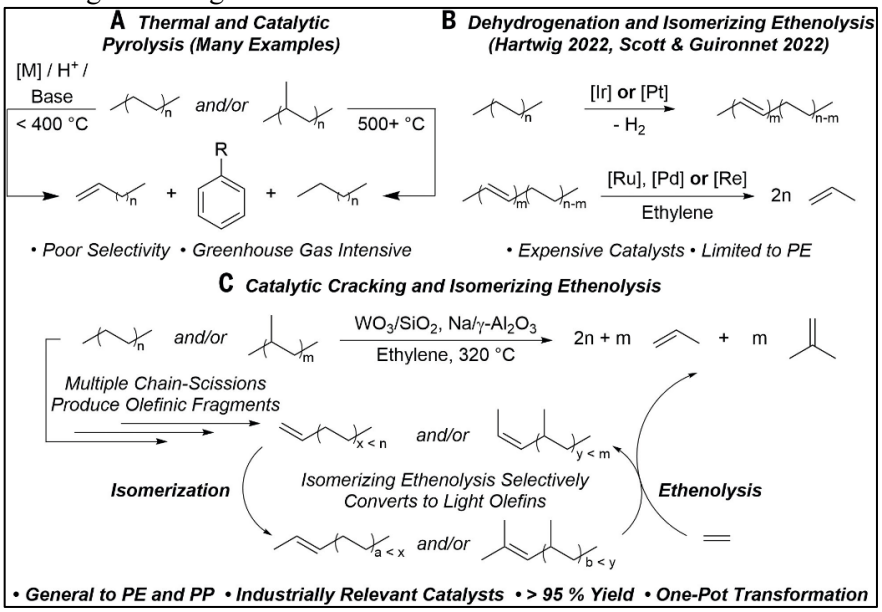


Fig. 3.1. (A) Previous work on the application of thermal and catalytic cracking for the chemical recycling of polyolefins. (B) Previous work applying a strategy of dehydrogenation and tandem isomerizing ethenolysis to affect conversion of PE to propylene. (C) Current work on the combination of catalytic cracking and isomerizing ethenolysis to yield olefins from PE and PP.

In a recent publication in *Science*, we show that the simple combination of tungsten oxide on silica and sodium on gamma-alumina transforms PE, PP, or a mixture of the two, including

postconsumer forms of these materials, to propylene or a mixture of propylene and isobutylene without the need for dehydrogenation of the starting polyolefins (Fig. 3.1). This process occurs with a combination comprising tungsten oxide on silica ($WO_3/SiO_2$) and sodium metal on gamma-phase alumina ($Na/\gamma\text{-}Al_2O_3$), initiated by catalytic cracking by the W- or Na-containing catalysts, which then convert PE to propylene and and PP to a combination of propylene and isobutylene, respectively, with >90% yield in 90 min at 320 °C on a 1-g scale. The reaction proceeds at this temperature because it appears to be initiated by catalytic cleavage of the C–C bonds of the alkane chains to generate alkenes.

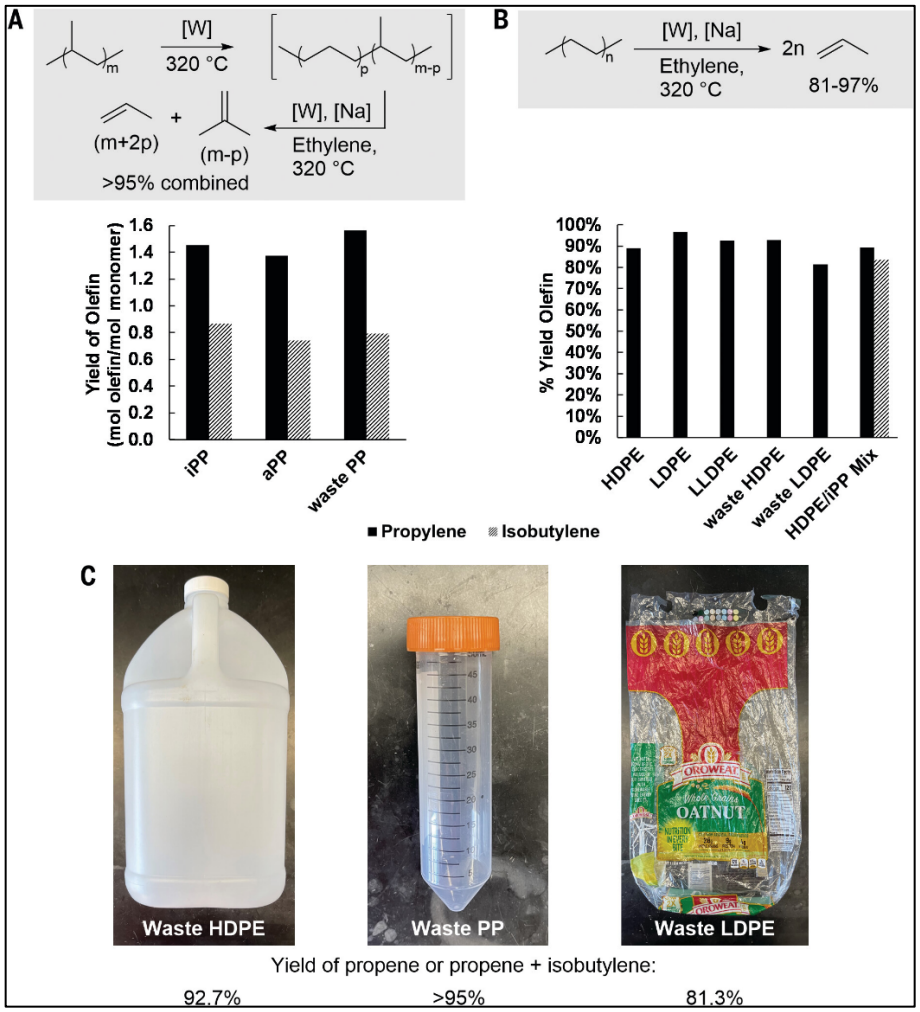


Fig. 3.2. Experiments on the tandem catalytic cracking and isomerizing ethenolysis of polyolefins (CIE).

The results of this work demonstrate the feasibility of deconstructing the two largest-volume plastics PE and PP to form products that are feedstock materials for the chemical industry using inexpensive, heterogeneous catalysts. Although deeper assessment is required to establish the economic feasibility of increasing this reaction to commercial scales, we believe that this study may yield further methods for recovering feedstock propylene and isobutylene from PE and PP, which can again be cycled through chemical industries.

Conk, R. J.; Stahler, J. F.; Shi, J. X.; Yang, J.; Lefton, N. G.; Brunn, J. N.; Bell, A. T.; Hartwig, J. F., Polyolefin Waste to Light Olefins with Ethylene and Base-Metal Heterogeneous Catalysts. *Science* **2024**. *385*, 1322-1327. DOI 10.1126/science.adq7316.

### 3.2 Chemoenzymatic Hydroaminomethylation of Olefins to Form Linear Primary Amines

Methods that form amines from feedstock chemicals are an important component of industrial chemistry. Many methods for the synthesis of amines yield mixtures of primary, secondary, and tertiary amines, necessitating costly downstream separations. The **Hartwig** group has recently published a chemoenzymatic approach to hydroaminomethylation that addresses these challenges by combining a homogeneous rhodium-catalyzed hydroformylation of alkenes by $H_2$ and CO with an enzymatic transamination catalyzed by an ω-transaminase from *Vibrio fluvialis* (VfTA). This sequential chemoenzymatic hydroaminomethylation reaction converts olefins to amines with high regioselectivity and chemoselectivity for the linear primary amine, across a series of olefins with varying structures (Fig. 3.3).

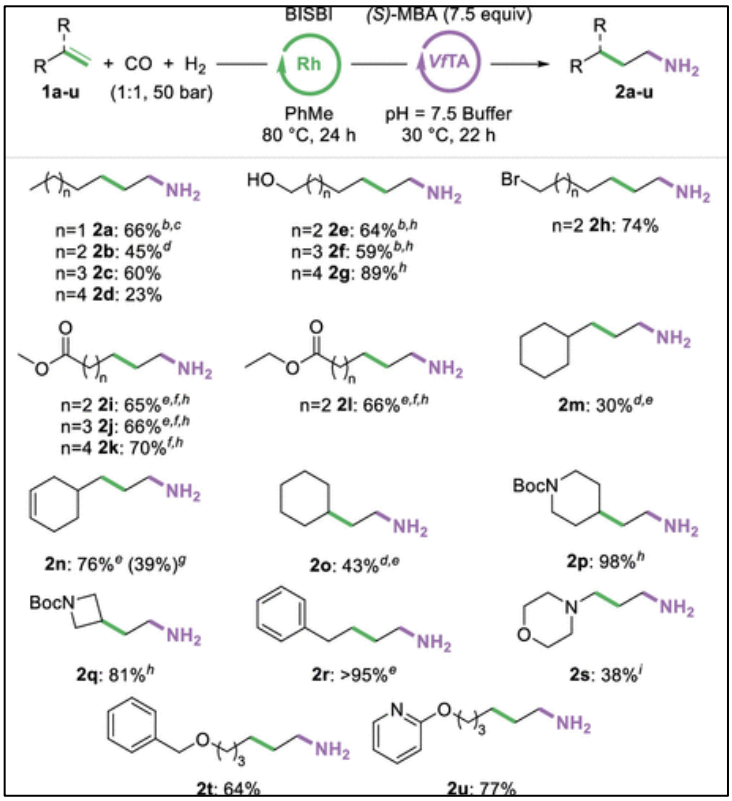


Fig 3.3. Chemo-enzymatic hydroaminomethylation of alkenes through a sequential process.

In collaboration with Douglas Clark, active-site mutation of wildtype VfTA successfully yielded enzyme variants with increased activity for the formation of primary amines from long-chain aldehydes. Furthermore, we reported progress toward a tandem process that incorporates a biocatalytic cascade utilizing ammonium salts as a terminal nitrogen source through the recycling of an intermediate amine donor, the amino acid alanine, which is required for the transaminase enzyme (Fig. 3.4). This study illustrates the potential to combine chemo- and biocatalytic reactions in both tandem and sequential processes to produce valuable materials from readily available feedstocks (alkenes, $H_2$, CO, and ammonium), with selectivities that have not been achieved with transition-metal catalysts.

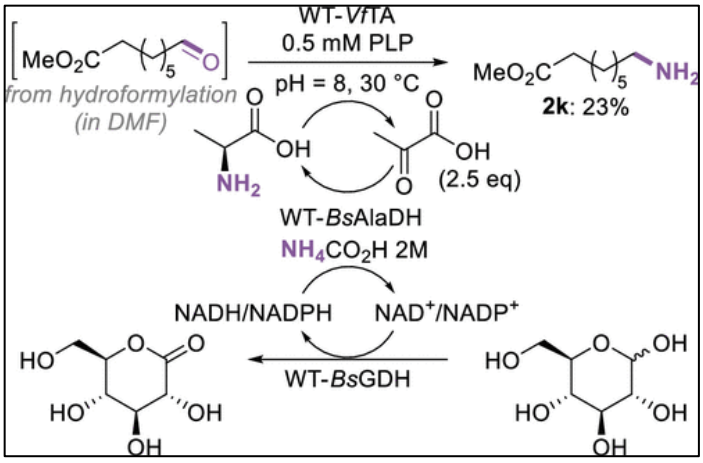


Fig. 3.4 Alanine recycling cascade for the transamination of linear aldehydes.

Manske, J. L.; Nicolai, J.; Bloomer, B. J.; Clark, D. S.; Hartwig, J. F., A Chemoenzymatic Hydroaminomethylation Strategy for the Selective Synthesis of Linear Primary Amines from Olefins by Sequential and Tandem Processes. *ACS Catal.* **2024**, *14*, 14356–14362. DOI 10.1021/acscatal.4c03770.

### 3.3 *Operando* HERFD X-ray Absorption Spectroscopy of Evolving Cu Nanoparticle Electrocatalysts for the $CO_2$ Reduction Reaction

The **Yang** group has recently shown that Cu nanoparticles that catalyze the electrochemical reduction of $CO_2$ evolve into nanograins that become more active. This strongly suggests that the surface density of active sites on nanoparticle catalysts might be further increased by using smaller building blocks. However, only recently have techniques emerged that enable sensitive spectroscopic data collection to distinguish catalytically relevant surface sites from the underlying bulk material under applied potential in the presence of an electrolyte layer. We have recently demonstrated that *operando* high-energy-resolution fluorescence detected X-ray absorption spectroscopy (HERFD-XAS) is a powerful spectroscopic method which offers critical surface chemistry insights in $CO_2$ electroreduction with sub-electronvolt energy resolution using hard X-rays.

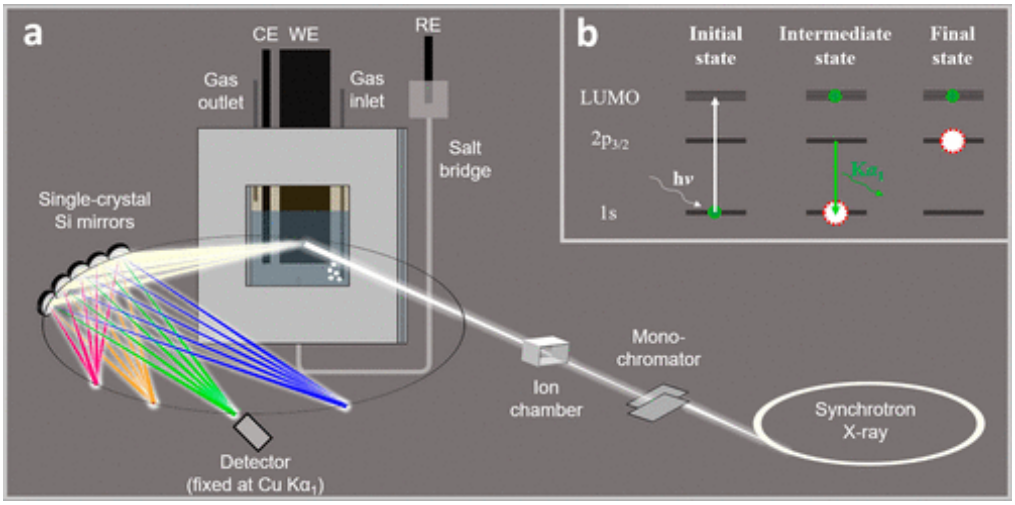


Fig. 3.5. Schematic depicting *operando* HERFD-XAS experiments during electrochemical $CO_2$ reduction.

Combined with the high surface area-to-volume ratio of 5 nm copper nanoparticles, operando HERFD-XAS has allowed us to observe, with clear evidence, the breaking of chemical bonds in a ligand desorption process between the surface ligands and the Cu surfaces of nanoparticles occurring under electrochemical potentials relevant for the $CO_2$ reduction reaction ($CO_2RR$). In addition, the dynamic evolution of oxidation state and coordination number throughout the operation of the nanocatalyst can be continuously tracked by this HERFD-XAS method. With these results in hand, undercoordinated metallic copper nanograins are proposed to be the real active sites in the $CO_2RR$ with these systems. This work emphasizes the importance of HERFD-XAS compared to routine XAS in catalyst characterization and mechanism exploration, especially in the complicated electrochemical $CO_2RR$. We foresee that this research should enable the design of both next-generation molecular complexes as building blocks to generate active sites for selective $CO_2$ reduction and catalyst activities that are precisely correlated to the nature of the active sites, rather than the structure of the underlying, inactive bulk

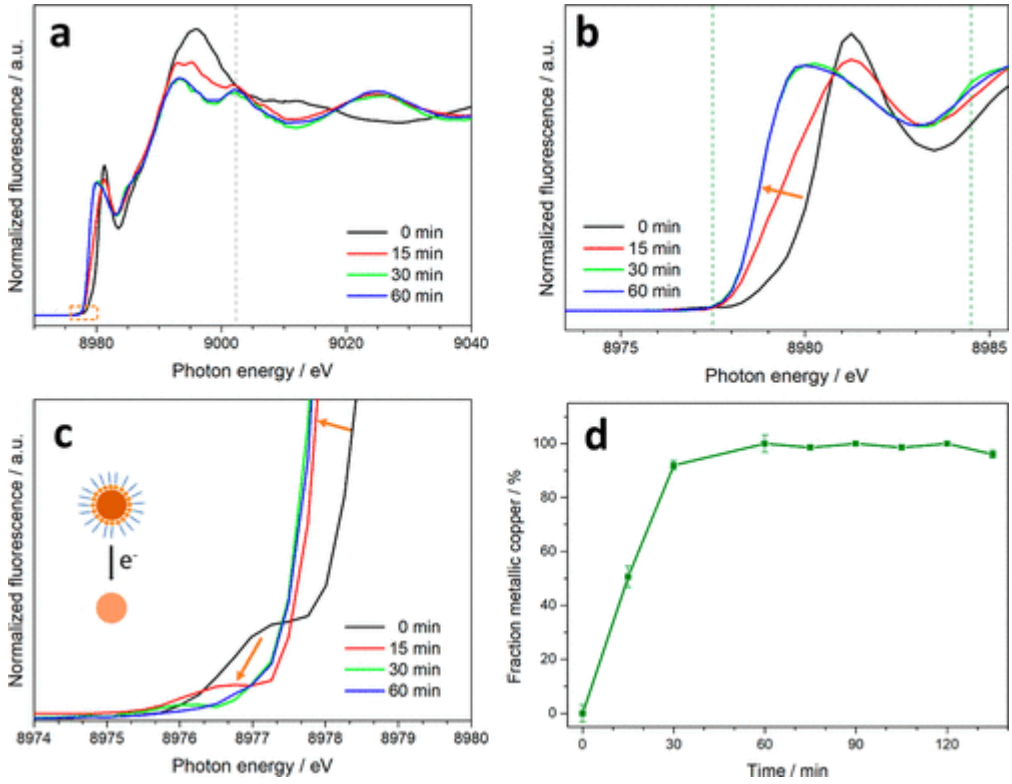


Fig. 3.6. *Operando* HERFD-XANES characterization. (a) Overview of the XANES region showing the changing spectra with time. The dashed line shows the metallic feature around 9002 eV. (b) Magnification of the edge region showing reduction from Cu2O to metallic Cu. The dashed green vertical lines indicate the linear combination fitting range. (c) Magnification of the ligand feature near 8977.2 eV, showing its fast decrease and eventual disappearance. (d) Results of the linear combination fitting, showing that the oxide catalyst is significantly reduced after just 30 min and fully metallic after 60 min of operation.

Feijóo, J.; Yang, Y.; Fonseca Guzman, M.; Vargas, A.; Chen, C.; Pollock, C.; Yang, P., *Operando* High-Energy-Resolution X-ray Spectroscopy of Evolving Cu Nanoparticle Electrocatalysts for $CO_2$ Reduction. *J. Am. Chem. Soc.* **2023**, *145* (37), 20208–20213. DOI 10.1021/jacs.3c08182.

**FY 2024 Journal Publications:**

**A. Publications that were solely supported by this FWP, and those in collaboration with others that are based on research that is intellectually led by the FWP and advances one or more of the FWP's objectives.**

Blue font: PIs of this FWP; green font: students and postdocs supported by the FWP; red font: PIs of other BES-supported research FWPs at LBNL.

**2023**


Chen, H.; Falling, L.; Kersell, H.; Zhao, X.; Nemsak, S.; Hunt, A.; Waluyo, I.; Ogasawara, H.; Bell, A.; Salmeron, M., Elucidating the Active Phases of CoOx Films on Au(111) in the CO Oxidation Reaction. *Nat. Commun.* **2023**, 6889. DOI 10.1038/s41467-023-42301-7.

Chen, L.; Song, Z.; Zhang, S.; Chang, C.-K.; Chuang, Y.-C.; Peng, X.; Dun, C.; Urban, J. J.; Guo, J.; Chen, J.-L.; Prendergast, D.; Salmeron, M.; Somorjai, G. A.; Su, J., Ternary NiMo-Bi Liquid Alloy Catalyst for Efficient Hydrogen Production from Methane Pyrolysis. *Science* **2023**, *381* (6660), 867-861. DOI 10.1126/science.adh8872.

Feijóo, J.; Yang, Y.; Fonseca Guzman, M.; Vargas, A.; Chen, C.; Pollock, C.; Yang, P., *Operando* High-Energy-Resolution X-ray Spectroscopy of Evolving Cu Nanoparticle Electrocatalysts for $CO_2$ Reduction. *J. Am. Chem. Soc.* **2023**, *145* (37), 20208–20213. DOI 10.1021/jacs.3c08182.

Kissman, E. N.; Neugebauer, M. E.; Sumida, K. H.; Swenson, C. V.; Sambold, N. A.; Marchand, J. A.; Millar, D. C.; Chang, M. C. Y., Biocatalytic Control of Site-Selectivity and Chang Length-Selectivity in Radical Amino Acid Halogenases. *Proc. Natl. Acad. Sci.* **2023**, 120 (12), e2214512120. DOI 10.1073/pnas.2214512120.

Kynman, A. E.; Christodoulou, S.; Ouellette, E. T.; Peterson, A.; Kelly, S.; Maron, L.; Arnold, P. L., Photocatalytic Dechlorination of Unactivated Chlorocarbons Including PVC Using Organolanthanide Complexes. *Chem. Commun.* **2023**, *50*, 10924-10927. DOI 10.1039/D3CC02906A.

Ma, S.; Hartwig, J.F. Progression of Hydroamination Catalyzed by Late Transition-Metal Complexes from Activated to Unactivated Alkenes. *Acc. Chem. Res.* **2023**, *56*, 1565-1577. DOI 10.1021/acs.accounts.3c00141.

Rios, P.; See, M. S.; Handford, R. C.; Cooper, J. K.; Tilley, T. D., Tetracopper σ-Bound μ-Acetylide and -Diyne Units Stabilized by a Naphthyridine-based Dinucleating Ligand. *Angew. Chem. Int. Ed.* **2023**, e202310307. DOI 10.1002/anie.202310307.

Xia, K.; Rajan, A.; Surendranath, Y.; Bergman, R. G.; Raymond, K. N.; Toste, F. D., Tunable Electrochemical Entropy through Solvent Ordering by a Supramolecular Host. *J. Am. Chem. Soc.* **2023**, *145*, 25463-25470. DOI 10.1021/jacs.3c10145


**2024**


Chen, P.-C.; Gao, M.; McCandler, C. A.; Song, C.; Jin, J.; Yang, Y.; Maulana, A. L.; Persson, K. A.; Yang, P., Complete Miscibility of Immiscible Elements at the Nanometre Scale. *Nat. Nanotechnol.* **2024**. DOI 10.1038/s41565-024-01626-0.

Chen, R.; Kayrouz, C. S.; McAmis, E.; Clark, D. S.; Hartwig, J. F., Carbonic Anhydrase Variants Catalyze the Reduction of Dialkyl Ketones with High Enantioselectivity. *Angew. Chem. Int. Ed.* **2024**. *63*, e202407111. DOI 10.1002/anie.202407111.

Conk, R. J.; Stahler, J. F.; Shi, J. X.; Yang, J.; Lefton, N. G.; Brunn, J. N.; Bell, A. T.; Hartwig, J. F., Polyolefin Waste to Light Olefins with Ethylene and Base-Metal Heterogeneous Catalysts. *Science* **2024**. *385*, 1322-1327. DOI 10.1126/science.adq7316.

Lefton, N. G.; Bell, A. T., Effects of Structure on the Activity, Selectivity, and Stability of Pt-Sn-DeAlBEA for Propane Dehydrogenation. *ACS Catal.* **2024**. *14*, 3986–4000. DOI 10.1021/acscatal.3c06047.

Leonhardt, B. E.; Head-Gordon, M.; Bell, A. T., The Effects of ≡Ti–OH Site Distortion and Product Adsorption on the Mechanism and Kinetics of Cyclohexene Epoxidation over $Ti/SiO_2$. *ACS Catal*. **2024**, *14*, 3049−3064. DOI 10.1021/acscatal.3c06073.

Leonhardt, B. E.; Shen, H.; Head-Gordon, M.; Bell, A. T., Experimental and Theoretical Evidence for Distorted Tetrahedral ≡Ti−OH Sites Supported on Amorphous Silica and Their Effect on the Adsorption of Polar Molecules. *J. Phys. Chem. C* **2024**, *128*, 129–145. DOI 10.1021/acs.jpcc.3c07027.

Manske, J. L.; Nicolai, J.; Bloomer, B. J.; Clark, D. S.; Hartwig, J. F., A Chemoenzymatic Hydroaminomethylation Strategy for the Selective Synthesis of Linear Primary Amines from Olefins by Sequential and Tandem Processes. *ACS Catal.* **2024**, *14*, 14356–14362. DOI 10.1021/acscatal.4c03770.

Ríos, P.; See, M. S.; Gonzalez, O.; Handford, R. C.; Nicolay, A.; Rao, G.; Britt, R. D.; Bediako, D. K; Tilley, T. D., Iron Homo- and Heterobimetallic Complexes Supported by a Symmetrical Dinucleating Ligand. *Chem. Commun.* **2024**, *60*, 8912-8915. DOI 10.1039/d4cc02155j.

Rutkauskaite, R.; Zhang, X.; Woodward, A.W.; Liu, Y.; Herrera, G.; Purkis, J.M.; Woodall, S.D.; Sarsfield, M.; Schreckenbach, G.; Natrajan, L.S.; Arnold P. L., The Effect of Ancillary Ligands on Hydrocarbon C-H Bond Functionalization by Uranyl Photocatalysts. *Chem. Sci.* **2024, 15,** 6965–6978. DOI 10.1039/d4sc01310g.

See, M. S.; Ríos, P.; Tilley, T. D., Diborane Reductions of $CO_2$ and $CS_2$ Mediated by Dicopper μ-Boryl Complexes of a Robust Bis(Phosphino)-1,8-Napthyridine Ligand. *Organometallics* **2024**. DOI: 10.1021/acs.organomet.4c00122

Shan, Y.; Zhao, X.; Fonseca Guzman, M.; Jana, A.; Chen, S.; Yu, S.; Ng, K. C.; Roh, I.; Chen, H.; Altoe, V.; Gilbert Corder, S. N.; Bechtel, H. A.; Qian, J.; Salmeron, M. B.; Yang, P., Nanometre-Resolved Observation of Electrochemical Microenvironment Formation at the Nanoparticle–Ligand Interface. *Nat. Catal.* **2024**. 7, 422–431. DOI 10.1038/s41929-024-01119-2.

Treacy, S. M.; Smith, A. L.; Bergman, R. G.; Raymond, K. N.; Toste, F. D., Supramolecular-Catalyzed Cascade Reduction of Azaarenes Interogated via Data Science. *J. Am. Chem. Soc.* **2024,** *146.* DOI 10.1021/jacs.4c11482.

Wheeler, T. A.; Tilley, T. D., Metal-Metal Redox Exchange to Produce Heterometallic Manganese-Cobalt Oxo Cubanes via a "Dangler" Intermediate. *J. Am. Chem. Soc.* **2024**, *146*, 20279-20290. DOI 10.1021/jacs.4c05367.

Wong, A.; Lam, F. Y. T.; Hernandez, M.; Lara, J.; Trinh, T. M.; Kelly, R. P.; Ochiai, T.; Rao, G.; Britt, R. D.; Kaltsoyannis, N.; Arnold, P.L., Catalytic Dinitrogen Conversion to Amines by Lanthanide and Group IV Catalysts. *Chem. Catal.* **2024**, 100964. DOI 10.1016/j.checat.2024.100964.

Yang Y.; Shi C.; Feijóo J.; Jin J.; Chen C.; Han Y.; Yang P., Dynamic Evolution of Copper Nanowires during CO2 Reduction Probed by Operando Electrochemical 4D-STEM and X-ray Spectroscopy. *J. Am. Chem. Soc*. **2024**, 146, 23398–23405. DOI: 10.1021/jacs.4c06480

Zhang, Y.: Qi, L.; Nozik, D.; Dun, C.; Urban, J.; Bell, A. T., Mechanism and Kinetics of Propane and n-Butane Dehydrogenation over Isolated and Nested ≡SiOZn–OH Sites Grafted onto Silanol Nests of Dealuminated Beta Zeolite. *ACS Catal.* **2024**, *14*, 2787–2804. DOI 10.1021/acscatal.3c05605.

**B. Other publications based on research receiving support from this FWP.**

**2023**

Kanbur, U.; Witzke, R. J.; Xu, J.; Ferrandon, M. S.; Goetjen, T. A.; Kropf, A. J.; Perras, F. A.; Liu, C.; Tilley, T. D.; Kaphan, D. M.; Delferro, M., Supported Electrophilic Organoruthenium Catalyst for the Hydrosilylation of Olefins. *ACS Catal.* **2023**, 13, 20, 13383–13394. DOI 10.1021/acscatal.3c03399. *statement requested 10/2/23*.

Yang, Y.; Feijóo, J.; Li, Q.; Krumov, M.; Merkens, S.; Salvo, G. D.; Chuvilin, A.; Jin, J.; Huang, H.; Pollock, C. J.; Salmeron, M. B.; Wang, C.; Muller, D. A.; Abruña, H. D.; Yang, P., *Operando* Methods: A New Era of Electrochemistry. *Curr. Opin. Electrochem.* **2023**, *42,* 101403. DOI 10.1016/j.coelec.2023.101403. *requested statement from Miquel.*

**2024**

Chen. Y.; Zhang, R.; Chen, Z; Xhen, Z.; Liao, J.; Song, X.; Liang, X.; Wang, Y.; Dong, J.; Singh, C. V.; Wang, D.; Toste, F. D.; Li, Y.; Zhao, J., Heterogeneous Single-Atom-Site Catalyst Enables Chemoselective Carbene N-H Bond Insertions. *J. Am. Chem. Soc.* **2024**, *146*, 10847-10856. DOI 10.1021/jacs.4c01408. *Discussion, analysis, and writing of this manuscript (F.D.T.) was supported by the U.S. Department of Energy.*

Ewing, P. M. D. A.; Majhi, P. K.; Prentice, C.; Young, C. M.; van Rees, K.; Arnold, P. L.; Zysman-Colman, E.; Smith, A. D. α-Phenylthioaldehydes for the Effective Generation of Acyl Azolium and Azolium Enolate Intermediates. *Chem. Sci.* **2024**, *15*, 9369-9375. DOI: 10.1039/D3SC06879J. *Discussion, analysis, and writing of this manuscript (PLA) was supported by the U.S. Department of Energy.*

Dombrowski, J. P.; Kalendra, V.; Ziegler, M. S.; Lakshmi, K. V.; Bell, A. T.; Tilley, T. D., M–Ge–Si Thermolytic Molecular Precursors and Models for Germanium-Doped Transition Metal Sites on Silica. *Dalton Trans.* **2024**, 53, 7340-7349. DOI 10.1039/D4DT00644E.

Katzer, N. J.; Kaur, M.; Sen, A.; Nimaiyar, R.; Autschbach, J.; Arnold, P. L.; Hintermair, U. Tetraphenylpentalenide Organolanthanide Complexes. *Chem. Commun.* **2024**, *60*, 9749-9752. DOI: 10.1039/d4cc02570a. *Discussion, analysis, and writing of this manuscript (PLA) was supported by the U.S. Department of Energy.*

**Program Publications List (2020-2023)**

**A. Publications that were solely supported by this FWP, and those in collaboration with others that are based on research that is intellectually led by the FWP and advances one or more of the FWP's objectives.**

**2020**


Amit, E.; Dery, S.; Kim, S.; Roy, A.; Hu, Q.; Toste, F. D.; Gross, E., Electrochemical Deposition of N-heterocyclic Carbene Monolayers on Metal Surfaces. *Nat. Commun.* **2020**, *11* (1), 5714. DOI 10.1038/s41467-020-19500-7.

Amtawong, J.; Skjelstad, B. B.; Balcells, D.; Tilley, T. D., Concerted Proton-Electron Transfer Reactivity of an Oxidized $Co_4O_4$ Cubane. *Inorg. Chem.* **2020**, *59* (20), 15553–15560. DOI 10.1021/acs.inorgchem.0c02625.

Arnold, P. L.; Ochiai, T.; Lam, F. Y. T.; Kelly, R. P.; Seymour, M. L.; Maron, L., Metallacyclic Actinide Catalysts for Dinitrogen Conversion to Ammonia and Secondary Amines. *Nat. Chem.* **2020**, *12* (7), 654–659. DOI 10.1038/s41557-020-0457-9.

Chen, C.; Li, Y.; Yu, S.; Louisia, S.; Jin, J.; Li, M.; Ross, M. B.; Yang, P., Cu-Ag Tandem Catalysts for High-Rate $CO_2$ Electrolysis toward Multicarbons. *Joule* **2020**, *4* (8), 1688–1699. DOI 10.1016/j.joule.2020.07.009.

Derrick, J. S.; Loipersberger, M.; Chatterjee, R.; Iovan, D. A.; Smith, P. T.; Chakarawet, K.; Yano, J.; Long, J. R.; Head-Gordon, M.; Chang, C. J., Metal–Ligand Cooperativity via Exchange Coupling Promotes Iron- Catalyzed Electrochemical $CO_2$ Reduction at Low Overpotentials. *J. Am. Chem. Soc.* **2020**, *142* (48), 20489–20501. DOI 10.1021/jacs.0c10664.

Desnoyer, A. N.; Nicolay, A.; Rios, P.; Ziegler, M. S.; Tilley, T. D., Bimetallics in a Nutshell: Complexes Supported by Chelating Naphthyridine-Based Ligands. *Acc. Chem. Res.* **2020**, *53* (9), 1944–1956. DOI 10.1021/acs.accounts.0c00382.

Kim, D.; Yu, S.; Zheng, F.; Roh, I.; Li, Y.; Louisia, S.; Qi, Z.; Somorjai, G. A.; Frei, H.; Wang, L.-W.; Yang, P., Selective $CO_2$ Electrocatalysis at the Pseudocapacitive Nanoparticle/Ordered-Ligand Interlayer. *Nat. Energy* **2020**, *5* (12), 1032–1042. DOI 10.1038/s41560-020-00730-4.

Koshy, D. M.; Johnson, G. R.; Bustillo, K. C.; Bell, A. T., Scanning Nanobeam Diffraction and Energy Dispersive Spectroscopy Characterization of Characterization of a Model Mn-Promoted Co/Al2O3 Nanosphere Catalyst for Fischer–Tropsch Synthesis. *ACS Catal.* **2020**, *10*, 12071–12079. DOI 10.1021/acscatal.0c02546.

Nicolay, A.; Ziegler M. S.; Rochlitz, L.; Tilley, T. D., Low-Valent Iron and Cobalt Complexes Supported by a Rigid Xanthene-Based Disilylamido Ligand. *Polyhedron* **2020**, *180*, 114420. DOI 10.1016/j.poly.2020.114420.

Qi, L; Zhang, Y.; Conrad, M. A.; Russell, C. K.; Miller, J: Bell, A. T., Ethanol Conversion to Butadiene over Isolated Zinc and Yttrium Sites Grafted onto Dealuminated Beta Zeolite. *J. Am. Chem. Soc.* **2020** *142*, 14674–14687. DOI 10.1021/jacs.0c06906.

Qi, Z.; Chen, L.; Zhang, S.; Su, J.; Somorjai, G. A., A Mini Review of Cobalt-Based Nanocatalyst in Fischer-Tropsch Synthesis. *Appl. Catal. A-Gen.* **2020**, *602*, 117701. DOI 10.1016/j.apcata.2020.117701.

Qiu, Y.; Hartwig, J. F., Mechanism of Ni-Catalyzed Oxidations of Unactivated C($sp^3$)–H Bonds. *J. Am. Chem. Soc.* **2020**, *142* (45), 19239–19248. DOI 10.1021/jacs.0c09157.

Xi, Y.; Su, B.; Qi, X.; Pedram, S.; Liu, P.; Hartwig, J. F., Application of Trimethylgermanyl-Substituted Bisphosphine Ligands with Enhanced Dispersion Interactions to Copper-Catalyzed Hydroboration of Disubstituted Alkenes. *J. Am. Chem. Soc.* **2020**, *142*, 18213–18222. DOI 10.1021/jacs.0c08746.

Morimoto, M.; Bierschenk, S. M., Xia, K. T.; Bergman, R. G.; Raymond, K. N.; Toste, F. D. Advances in Supramolecular Host-Mediated Reactivity *Nat. Catal.* **2020**, *3*, 969-984. DOI 10.1038/s41929-020-00528-3.

Zee, D. Z.; Nippe, M.; King, A. E.; Chang, C. J.; Long, J. R., Tuning Second Coordination Sphere Interactions in Polypyridyl–Iron Complexes to Achieve Selective Electrocatalytic Reduction of Carbon Dioxide to Carbon Monoxide. *Inorg. Chem.* **2020**, *59* (7), 5206–5217. DOI 10.1021/acs.inorgchem.0c00455.

Zhang, B.; Chen, C.; Chuang, W.; Chen, S.; Yang, P. Size Transformation of $Au_{22}(SG)_{18}$ Nanocluster and its Surface Sensitive Dynamics, *J. Am. Chem. Soc.* **2020**, *142*, 11514–11520. DOI: 10.1021/jacs.0c03919.

**2021**

Amtawong, J.; Skjelstad, B. B.; Handford, R. C.; Suslick, B. A.; Balcells, D.; Tilley, T. D., C–H Activation by $RuCo_3O_4$ Oxo Cubanes: Effects of Oxyl Radical Character and Metal–Metal Cooperativity. *J. Am. Chem. Soc.* **2021**, *143* (31), 12108–12119. DOI 10.1021/jacs.1c04069.

Chen, C.; Li, Y.; Yang, P., Address the "Alkalinity Problem" in $CO_2$ Electrolysis with Catalyst Design and Translation. *Joule* **2021**, *5* (4), 737–742. DOI 10.1016/j.joule.2021.02.008.

Chen, L.; Malollari, K. G.; Uliana, A.; Sanchez, D.; Messersmith, P. B.; Hartwig, J. F., Selective, Catalytic Oxidations of C-H Bonds in Polyethylenes Produce Functional Materials with Enhanced Adhesion. *Chem.* **2021**, *7* (1), 137–145. DOI 10.1016/j.chempr.2020.11.020.

Chen, L.; Qi, Z.; Peng, X.; Chen, J.-L.; Pao, C.-W.; Zhang, X.; Dun, C.; Young, M.; Prendergast, D.; Urban, J. J.; Guo, J.; Somorjai, G. A.; Su, J., Insights into the Mechanism of Methanol Steam Reforming Tandem Reaction over $CeO_2$ Supported Single-Site Catalysts. *J. Am. Chem. Soc.* **2021**, *143* (31), 12074–12081. DOI 10.1021/jacs.1c03895.

Chen, S.; Li, M.; Yu, S.; Louisia, S.; Chuang, W.; Gao, M.; Chen, C.; Jin, J.; Salmeron, M. B.; Yang, P., Ligand Removal of Au25 Nanoclusters by Thermal and Electrochemical Treatments for Selective $CO_2$ Electroreduction to CO. *J. Chem. Phys.* **2021**, *155* (5), 051101. DOI 10.1063/5.0059363.

Dery, S.; Mehlman, H.; Hale, L.; Carmiel-Kostan, M.; Yemini, R.; Ben-Tzvi, T.; Noked, M.; Toste, F. D.; Gross, E., Site-Independent Hydrogenation Reactions on Oxide-Supported Au Nanoparticles Facilitated by Intraparticle Hydrogen Atom Diffusion. *ACS Catal.* **2021**, *11* (15), 9875–9884. DOI 10.1021/acscatal.1c01987.

Desnoyer, A. N.; Nicolay, A.; Ziegler, M. S.; Lakshmi, K. V.; Cundari, T. R.; Tilley, T. D., A Dicopper Nitrenoid by Oxidation of a CuICuI Core: Synthesis, Electronic Structure, and Reactivity. *J. Am. Chem. Soc.* **2021**, *143* (18), 7135–7143. DOI 10.1021/jacs.1c02235.

Dombrowski, J. P.; Ziegler, M. S.; Phadke, N.; Mansoor, E.; Levine, D. S.; Head-Gordon, M.; Bell, A. T.; Tilley, T. D., Siloxyaluminate and Siloxygallate Complexes as Models for Framework and Partially-Hydrolyzed Framework Sites in Zeolites and Zeotypes. *Chem. Eur. J.* **2021**, *27* (1), 307–315. DOI 10.1002/chem.202002926.

Fuentes, M. A.; Gava, R.; Saper, N. I.; Romero, E.; Caballero, A.; Hartwig, J. F.; Pérez, P. J., Copper-Catalyzed Dehydrogenative Amidation of Light Alkanes. *Angew. Chem. Int. Ed.* **2021**, *60* (34), 18467–18471. DOI 10.1002/anie.202104737.

Ji, P.; Park, J.; Gu, Y.; Clark, D. S.; Hartwig, J. F., Abiotic Reduction of Ketones with Silanes Catalysed by Carbonic Anhydrase Through an Enzymatic Zinc Hydride. *Nat. Chem.* **2021**, *13* (4), 312–318. DOI 10.1038/s41557-020-00633-7.

Li, M.; Zhang, B.; Cheng, T.; Yu, S.; Louisia, S.; Chen, C.; Chen, S.; Cestellos-Blanco, S.; Goddard, W. A.; Yang, P., Sulfur-Doped Graphene Anchoring of Ultrafine Au25 Nanoclusters for Electrocatalysis. *Nano Res.* **2021**. DOI 10.1007/s12274-021-3561-2.

Liu, G.; Lee, M.; Kwon, S.; Zeng, G.; Eichhorn, J.; Buckley, A. K.; Toste, F. D.; Goddard, W. A.; Toma, F. M., $CO_2$ Reduction on Pure Cu Produces only $H_2$ after Subsurface O is Depleted: Theory and Experiment. *Proc. Natl. Acad. Sci. U.S.A.* **2021**, *118* (23), e2012649118. DOI 10.1073/pnas.2012649118.

Nicolay, A.; Héron, J.; Shin, C.; Kuramarohit, S.; Ziegler, M. S.; Balcells, D.; Tilley, T. D., Unsymmetrical Naphthyridine-Based Dicopper(I) Complexes: Synthesis, Stability, and Carbon–Hydrogen Bond Activations. *Organometallics* **2021**, *40* (12), 1866–1873. DOI 10.1021/acs.organomet.1c00188.

Nozik, D.; Tinga, F. M. P.; Bell, A. T., Propane Dehydrogenation and Cracking over Zn/H-MFI Prepared by Solid-State Ion Exchange of ZnCl. *ACS Catal.* **2021**, *11*, 23, 14489–14506. DOI 1021/acscatal.1c03641.

Phadke, N. M.; Mansoor, E.; Head-Gordon, M.; Bell, A. T., Mechanism and Kinetics of Light Alkane Dehydrogenation and Cracking over Isolated Ga Species in Ga/H-MFI. *ACS Catal.* **2021**, 11, 2062–2075. DOI 10.1021/acscatal.0c04906.

Qi, L; Babucci, M.; Zhang, Y.; Lund, A.; Liu, L.; Li, J.; Chen, Y.; Hoffman, A. S.; Bare, S. R.; Han, Y.; Gates, B. C.; Bell, A. T., Propane Dehydrogenation Catalyzed by Isolated Pt Atoms in ≡SiOZn−OH Nests in Dealuminated Zeolite Beta. *J. Am. Chem. Soc.* **2021** *143*, 21364–21378. DOI 10.1021/jacs.1c10261.

Qi, Z.; Chen, L.; Zhang, S.; Su, J.; Somorjai, G. A., Mechanism of Methanol Decomposition over Single-Site Pt1/$CeO_2$ Catalyst: A DRIFTS Study. *J. Am. Chem. Soc.* **2021**, *143* (1), 60–64. DOI 10.1021/jacs.0c10728.

Salmeron, M.; Eren, B., High-Pressure Scanning Tunneling Spectroscopy. *Chem. Rev.* **2021**, *121* (2), 962–1006. DOI 10.1021/acs.chemrev.0c00429.

Smith, P. T.; Benke, B. P.; An, L.; Kim, Y.; Kim, K.; Chang, C., A Supramolecular Porous Organic Cage Platform Promotes Electrochemical Hydrogen Evolution from Water Catalyzed by Cobalt Porphyrins. *ChemElectroChem* **2021**, *8* (9), 1653–1657. DOI 10.1002/celc.202100331.

Suslick, B. A.; Tilley, T. D., Olefin Hydroarylation Catalyzed by a Single-Component Cobalt(-I) Complex. *Org. Lett.* **2021**, *23* (4), 1495–1499. DOI 10.1021/acs.orglett.1c00258.

Van der Mynsbrugge, J.; Bell, A. T., Challenges for the Theoretical Description of the Mechanism and Kinetics of Reactions Catalyzed by Zeolites. *J. Catal.* **2021**, *404*, 832–849. DOI 10.1016/j.jcat.2021.08.048.

Witzke, R. J.; Hait, D.; Head-Gordon, M.; Tilley, T. D., Two-Coordinate Iron(I) Complexes on the Edge of Stability: Influence of Dispersion and Steric Effects. *Organometallics* **2021**, *40* (11), 1758–1764. DOI 10.1021/acs.organomet.1c00218.

Wuttig, A.; Derrick, J. S.; Loipersberger, M.; Snider, A.; Head-Gordon, M.; Chang, C. J.; Toste, F. D., Controlled Single-Electron Transfer via Metal–Ligand Cooperativity Drives Divergent Nickel-Electrocatalyzed Radical Pathways. *J. Am. Chem. Soc.* **2021**, *143* (18), 6990–7001. DOI 10.1021/jacs.1c01487.

Yu, S.; Kim, D.; Qi, Z.; Louisia, S.; Li, Y.; Somorjai, G. A.; Yang, P., Nanoparticle Assembly Induced Ligand Interactions for Enhanced Electrocatalytic $CO_2$ Conversion. *J. Am. Chem. Soc.* **2021**, *143*, 19919–19927. DOI 10.1021/jacs.1c09777.

Zhang, Y.; Qi, L.; Lund, A.; Lu, P.; Bell, A. T., Mechanism and Kinetics of Acetone Conversion to Isobutene over Isolated Hf Sites Grafted to Silicalite-1 and $SiO_2$. *J. Am. Chem. Soc.* **2021**, *143* (22), 8352–8366. DOI 10.1021/jacs.1c01315.

Wuttig, A.; Toste, F. D. The Interface is a Tunable Dimension in Electricity-Driven Organic Synthesis. *Nat. Sci.* **2021**, e20210036. DOI 10.1001/ntls.20210036.

**2022**


Amtawong, J.; Nguyen, A.I.; Tilley, T. D., Mechanistic Aspects of Cobalt Oxo Cubane Clusters in Oxidation Chemistry. *J. Am. Chem. Soc.* **2022**, *144* (32), 1475–1492. DOI 10.1021/jacs.1c11445.

Bell, A. T., Insights into the Mechanism and Kinetics of Propene Oxidation and Ammoxidation over Bismuth Molybdate Catalysts Derived from Experiments and Theory. *J. Catal.* **2022**, *408*, 436–452. DOI 10.1016/j.jcat.2021.05.009.

Bierschenk, S. M.; Pan, J. Y.; Settineri, N. S.; Warzok, U.; Bergman, R. G.; Raymond, K. N.; Toste, F. D., Impact of Host Flexibility on Selectivity in a Supramolecular-Host-Catalyzed Enantioselective aza-Darzens Reacton. *J. Am. Chem. Soc.* **2022**, *144* (25), 11425–11433. DOI 10.1021/jacs.2c04182.

Chen, C., Yu, S., Yang, Y., Louisia, S., Roh, I., Jin, J., Chen, S., Chen, P.-C., Shan, Y.; Yang, P., Exploration of the Bio-Analogous Asymmetric C-C Coupling Mechanism in Tandem $CO_2$ Electroreduction. *Nature Catal.* **2022**, (5), 878–887. DOI 10.1038/s41929-022-00844-w.

Chen, L.; Hou, K.; Verma, P.; Qi, Z.; Zhang, S.; Liu, Y.; Guo, J.; Stavila, V.; Allendorf, M.; Zheng L.; Salmeron, M.; Prendergast, D.; Su, J.; Somorjai, G., Reversible Dehydrogenation and Rehydrogenation of Cyclohexane and Methyl-Cyclohexane by Single Site Platinum Catalyst. *Nat. Commun.* **2022**, 13, 1092. DOI 10.1038/s41467-022-28607-y.

Conk, R. J.; Hanna, S.; Shi, J. X.; Yang, J.; Ciccia, N. R.; Qi, L.; Bloomer, B. J.; Heuvel, S.; Wills, T.; Su, J.; Bell, A. T.; Hartwig, J. F., Catalytic Deconstruction of Waste Polyethylene with Ethylene to Form Propylene. *Science* **2022**, *377*, 1561–1566. DOI 10.1126/science.add1088.

De La Torre, P.; Derrick, J. S.; Snider, A.; Smith, P. T.; Loipersberger, M.; Head-Gordon, M.; Chang, C. J., Exchange Coupling Determines Metal-Dependent Efficiency for Iron- and Cobalt-Catalyzed Photochemical $CO_2$ Reduction. *ACS Catal.* **2022**, *12* (14), 8484–8493. DOI 10.1021/acscatal.2c02072.

Derrick, J. S.; Loipersberger, M.; Nistanaki, S. K.; Rothweiler, A. V.; Head-Gordon, M.; Nichols, E. M.; Chang, C. J., Templating Bicarbonate in the Second Coordination Sphere Enhances Electrochemical $CO_2$ Reduction Catalyzed by Iron Porphyrins. *J. Am. Chem. Soc.* **2022**, *144* (26), 11656–11663. DOI 10.1021/jacs.2c02972.

Hanna, S.; Bloomer, B.; Ciccia, N. R.; Butcher, T. W.; Conk, R. J.; Hartwig, J. F., Contra-Thermodynamic Olefin Isomerization by Chain-Walking Hydroboration and Dehydroboration. *Org. Lett.* **2022**, *24* (4), 1005–1010. DOI 10.1021/acs.orglett.1c03124.

Kynman, A. E.; Elghanayan, L. K.; Desnoyer, A. N.; Yang, Y.; Sévery, L.; Di Giuseppe, A.; Tilley, T. D.; Maron, L.; Arnold, P.L., Controlled Monodefluorination and Alkylation of $C(sp^3)$–F Bonds by Lanthanide Photocatalysts: Importance of Metal–Ligand Cooperativity. *Chem. Sci.* **2022**, *13*, 14090–14100. DOI 10.1039/D2SC04192H.

Loipersberger, M.; Derrick, J. S.; Chang, C. J.; Head-Gordon, M., Deciphering Distinct Overpotential-Dependent Pathways for Electrochemical $CO_2$ Reduction Catalyzed by an Iron–Terpyridine Complex. *Inorg. Chem.* **2022**, *61* (18), 6919–6933. DOI 10.1021/acs.inorgchem.2c00279.

Louisia, S.; Kim, D.; Li, Y.; Gao, M.; Yu, S.; Roh, I.; Yang, P., The Presence and Role of the Intermediary CO Reservoir in Heterogeneous Electroreduction of $CO_2$. *Proc. Natl. Acad. Sci. U.S.A.* **2022**, *119* (18), e2201922119. DOI 10.1073/pnas.2201922119.

Ma, S.; Xi, Y.; Fan, H.; Roediger, S.; Hartwig, J. F., Enantioselective Hydroamination of Unactivated Terminal Alkenes. *Chem* **2022**, *8* (2), 532–542. DOI 10.1016/j.chempr.2021.12.005.

Narouz, M. R.; De La Torre, P.; An, L.; Chang, C. J., Multifunctional Charge and Hydrogen-Bond Effects of Second-Sphere Imidazolium Pendants Promote Capture and Electrochemical

Reduction of $CO_2$ in Water Catalyzed by Iron Porphyrins. *Angew. Chem. Int. Ed.* **2022**, *61* (37), e202207666. DOI 10.1002/anie.202207666.

Neugebauer, M.E.; Kissman, E.N.; Marchand, J.A.; Pelton, J.G.; Sambold, N.A.; Millar, D.C.; Chang, M.C.Y., Conversion of a Radical Hydroxylase Into a Halogenase Through Reaction Pathway Engineering. *Nat. Chem. Biol.* **2022**, *18* (2), 1171–179. DOI 10.1038/s41589-021-00944-x.

Nguyen, Q. N. N.; Xia, K. T.; Zhang, Y.; Chen, N.; Morimoto, M.; Pei, X.; Ha, Y.; Guo, J.; Yang, W.; Wang, L.-P.; Bergman, R. G.; Raymond, K. N.; Toste, F. D.; Tantillo, D. J., The Source of Rate Acceleration for Carbocation Cyclization in Biomimetic Supramolecular Cages. *J. Am. Chem. Soc.* **2022**, *144* (25), 11413–11424. DOI 10.1021/jacs.2c04179.

Nozik, D.; Bell, A. T., Role of $Ga^{3+}$ Sites in Ethene Oligomerization over Ga/H-MFI. *ACS Catal.* **2022**, 12, 14173–14184. DOI 10.1021/acscatal.2c03357.

Piesch, M.; Nicolay, A.; Haimerl, M.; Seidl, M.; Balázs, G.; Tilley, T. D.; Scheer, M., Binding, Release and Functionalization of Intact Pnictogen Tetrahedra Coordinated to Dicopper Complexes. *Chem. Eur. J.* **2022**, *28* (45), e202201144. DOI 10.1002/chem.20220114.

Qi, L; Zhang, Y.; Babucci, M.; Chen, C.; Lu, P.; Li, J.; Dun, C.; Hoffman, A. S.; Urban, J. J.; Tsapatsis, M.; Bare, S. R.; Han, Y.; Gates, B. C.; Bell, A. T., Dehydrogenation of Propane and n-Butane Catalyzed by Isolated $PtZn_4$ Sites Supported on Self-Pillared Zeolite Pentasil Nanosheets. *ACS Catal.* **2022**, *12*, 11177–11189. DOI 10.1021/acscatal.2c01631.

Ríos, P.; See, M. S.; Handford, R. C.; Teat, S. J.; Tilley, T. D., Robust dicopper(I) μ-boryl Complexes Supported by a Dinucleating Naphthyridine-Based Ligand. *Chem. Sci.* **2022**, *13* (22), 6619–6625. DOI 10.1039/D2SC00848C.

Yang, S.; Zhao, X.; Lu, Y.-H.; Barnard, E.; Yang, P.; Baskin, A.; Lawson, J. W.; Prendergast, D.; Salmeron, M., The Nature of the Electrical Double Layer on Suspended Graphene Electrodes. *J. Am. Chem. Soc.* **2022**, *144* (29), 13327–13333. DOI 10.1021/jacs.2c03344.

Yang, Y.; Roh, I.; Louisia, S.; Chen, C.; Jin, J.; Yu, S.; Salmeron, M.; Wang, C.; Yang, P., *Operando* Resonant Soft X-ray Scattering Studies of Chemical Environment and Interparticle Dynamics of Cu Nanocatalysts for $CO_2$ Electroreduction. *J. Am. Chem. Soc.* **2022**, *144* (20), 8927–8931. DOI 10.1021/jacs.2c03662.

Yu, S.; Louisia, S.; Yang, P., The Interactive Dynamics of Nanocatalyst Structure and Microenvironment during Electrochemical $CO_2$ Conversion. *J. Am. Chem. Soc. Au* **2022**, *2* (3), 562–572. DOI 10.1021/jacsau.1c00562.

Zhang, Y.; Qi, L.; Leonhardt, B.; Bell, A. T., Mechanism and Kinetics of n-Butane Dehydrogenation to 1,3-Butadiene Catalyzed by Isolated Pt Sites Grafted into SiOZn-OH Nests in Dealuminated Zeolite Beta. *ACS Catal.* **2022**, 12, 3333–3345. DOI 10.1021/acscatal.2c00059.

**2023**

An, L.; De La Torre, P.; Smith, P. T.; Narouz, M. R.; Chang, C. J., Synergistic Porosity and Charge Effects in a Supramolecular Porphyrin Cage Promote Efficient Photocatalytic $CO_2$ Reduction. *Angew. Chem. Int. Ed.* **2023**, *62* (5), e202209396. DOI 10.1002/anie.202209396.

Bloomer, B.J.; Natoli, S.N.; Garcia-Borràs, M.; Pereira, J.H.; Hu, D.B.; Adams, P.D.; Houk, K.N.; Clark, D.S.; Hartwig, J.F., Mechanistic and Structural Characterization of an Iridium-Containing Cytochrome Reveals Kinetically Relevant Cofactor Dynamics. *Nat. Cat.* **2023**, *6*, 39–51. DOI 10.1038/s41929-022-00899-9.

Chen, L.; Song, Z.; Zhang, S.; Chang, C.-K.; Chuang, Y.-C.; Peng, X.; Dun, C.; Urban, J.J.; Guo, J.; Chen, J.-L.; Prendergast, D.; Salmeron, M.; Somorjai, G.A.; Su, J., Ternary NiMo-Bi Liquid Alloy Catalyst for Efficient Hydrogen Production from Methane Pyrolysis, *Science*, **2023**, 381 6660 867-861, DOI 10.1126/science.adh8872.

Chen, P.; Chen, C.; Yang, Y.; Maulana, A. L.; Jin,J.; Feijóo, J.; Yang, P., The Chemical and Structural Evolution of AgCu Catalysts in Electrochemical $CO_2$ Reduction. *J. Am. Chem. Soc.* **2023,** 145, 10116–10125. DOI 10.1021/jacs.3c00467

Kynman, A. E.; Christodoulou, S.; Ouellette, E. T.; Peterson, A.; Kelly, S.; Maron, L.; Arnold, P. L. Photocatalytic Dechlorination of Unactivated Chlorocarbons Including PVC Using Organolanthanide Complexes. *Chem. Commun.* **2023**, Advance Article, DOI 10.1039/D3CC02906A

Ma, S.; Fan, H.; Day, C.S.; Xi, Y.; Hartwig, J.H., Remote Hydroamination of Disubstituted Alkenes by a Combination of Isomerization and Regioselective N–H Addition. *J. Am. Chem. Soc.* **2023**, *145* (7), 3875–3881. DOI 10.1021/jacs.2c13054.

Qi, L.; Das, S.; Zhang, Y.; Nozik, D.; Gates, B. C.; Bell, A. T., Ethene Hydroformylation Catalyzed by Rhodium Dispersed with Zinc or Cobalt in Silanol Nests of Dealuminated Zeolite Beta. *J. Am. Chem. Soc.* **2023**, 145, 2911–2929. DOI 10.1021/jacs.2c11075.

Xu, L.; Lechner, B.A.J.; Je, L.; Somorjai, G.A.; Salmeron, M.; Mavrikakis, M., Formation of Active Sites on Transition-Metal Surfaces under Catalytic Reactive Conditions. *Science* **2023,** 380, 70–76. DOI 10.1126/science.add0089.

Yang, Y.; Louisia, S.; Yu, S.; Jin, J.; Roh, I.; Chen, C.; Guzman, M. V. F.; Feijoo, J.; Chen, P.; Pollock, C. J.; Huang, X.; Wang, H.; Shao, Y.; Wang, C.; Muller, D. A.; Abruña, H. D.; Yang, P., *Operando* Studies Reveal Active Cu Nanograins for $CO_2$ Electroreduction. *Nature* **2023,** 614, 262. DOI 10.1038/s41586-022-05540-0.

Yang, Y.; Tsun, J.; Jin, J.; Feijóo, J.; Roh, I.; Louisia, S.; Yu, S.; Guzman, M.F.; Chen, C.; Muller, D.; Abruña, H.; Yang, P., *Operando* Electrochemical Liquid-Cell STEM (EC-STEM) Studies of Evolving Cu Nanocatalysts for $CO_2$ Electroreduction. *ACS Sustain. Chem. Eng.* **2023** 11, 4119–4124. DOI 10.1021/acssuschemeng.2c06542.

**B. Other publications reporting research receiving support from this FWP.**

**2020**

Cowie, B. E.; Douair, I.; Maron, L.; Love, J. B.; Arnold, P. L., Selective oxo Ligand Functionalisation and Substitution Reactivity in an oxo/Catecholate-Bridged $U^{IV}/U^{IV}$ Pacman Complex. *Chem. Sci.* **2020**, *11* (27), 7144–7157. DOI 10.1039/d0sc02297g. *Additional discussion, analysis, and writing of this manuscript (P.L.A.) was supported by the U.S. Department of Energy (DOE).*

Dovera, C. M.; Grintera, D. C., Yima, C. M.; Muryn, C. A.; Bluhm, H.; Salmeron, M.; Thornton, G. Orientation of Acetic Acid Hydrogen Bonded to $TiO_2$(110). *Surface Sci.* **2020,** 699, 121628. DOI 10.1016/j.susc.2020.121628. *FWP supported Salmeron's contributions.*

Janvelyan, N; van Spronsen, M.A.; Wu, C.H.; Qi, Z.; Montemore, M. N.; Shan, J.; Zakharov, D.N.; Xu, F.; Boscoboinik, A.; Salmeron, M.B.; Stach, E.; Flyztani-Stephanopoulos, M.; Biener, J.; Friend, C. M., Stabilization of a Nanoporous NiCu Catalyst for Non-oxidative Ethanol Dehydrogenation. *Cat. Sci. & Tech*. **2020**. *Materials characterization and catalysis experiments.*

O'Connor, R.; van Spronsen, M.A.; Egle, T.; Xu, F.; Kersell, H. R.; Oliver-Meseguer, J.; Karatok, M.; Salmeron, M.; Madix, R. J.; Friend, C.M., Hydrogen Migration at Restructuring Palladium–Silver Oxide Boundaries Dramatically Enhances Reduction Rate of Silver Oxide. *Nat. Commun*. **2020**, 11, 1844. DOI 10.1038/s41467-020-15536-x. *Acknowledges DOE -BES Award No. DE-SC0012573, and ALS facilities.*

Xi, Y.; Ma, S.; Hartwig, J. F., Catalytic Asymmetric Addition of an Amine N-H bond Across Internal Alkenes. *Nature* **2020**, *588* (7837), 254–260. DOI 10.1038/s41586-020-2919-z. *The*

*development of the catalytic system and reagent and the mechanistic studies were supported by DOE. The application to asymmetric hydroamination was supported by NIH.*

Zhang, S.; Chen, L.; Qi, Z.; Zhuo, L.; Chen, J.-L.; Pao, C.-W.; Su, J.; Somorjai, G. A., Insights into the Mechanism of n-Hexane Reforming over a Single-Site Platinum Catalyst. *J. Am. Chem. Soc.* **2020**, *142* (39), 16533–16537. DOI 10.1021/jacs.0c07911. *Catalysis synthesis and characterization was fund in part by DOE (Bell).*

**2021**

Arnold, P. L.; Halliday, C. J. V.; Puig-Urrea, L.; Nichol, G. S., Instantaneous and Phosphine-Catalyzed Arene Binding and Reduction by U(III) Complexes. *Inorg. Chem.* **2021**, *60* (6), 4162–4170. DOI 10.1021/acs.inorgchem.1c00327. *Additional discussion, analysis, and writing of this manuscript (P.L.A.) was supported by the U.S. Department of Energy (DOE).*

Day, C. S.; Fawcett, A.; Chatterjee, R.; Hartwig, J. F., Mechanistic Investigation of the Iron-Catalyzed Azidation of Alkyl C($sp^3$)−H Bonds with Zhdankin's $\lambda^3$ Azidoiodane. *J. Am. Chem. Soc.* **2021**, *143* (39), 16184–16196. DOI 10.1021/jacs.1c07330. *The Catalysis program supported the EPR work.*

Dejesus, J. F.; Kerr, R. W. F.; Penchoff, D. A.; Carroll, X. B.; Peterson, C. C.; Arnold, P. L.; Jenkins, D. M., Actinide Tetra-n-Heterocyclic Carbene 'Sandwiches'. *Chem. Sci.* **2021**, *12* (22), 7882–7887. DOI 10.1039/D1SC01007G. *Additional discussion, analysis, and writing of this manuscript (P.L.A.) was supported by the U.S. Department of Energy (DOE).*

Gray, S. J.; Brown, K.; Francis, L. Y. T.; Garden, J. A.; Arnold, P. L., Dinuclear Ce(IV) Aryloxides: Highly Active Catalysts for Anhydride/Epoxide Ring-Opening Copolymerization. *Organometallics* **2021**, *40* (7), 948–958. DOI 10.1021/acs.organomet.1c00055. *Additional discussion, analysis, and writing of this manuscript (P.L.A.) was supported by the U.S. Department of Energy (DOE).*

Kerr, R. W. F.; Ewing, P. M. D. A.; Raman, S. K.; Smith, A. D.; Williams, C.K.; Arnold, P. L., Ultrarapid Cerium(III)–NHC Catalysts for High Molar Mass Cyclic Polylactide. *ACS Catal.* **2021**, *11* (3), 1563–1569. DOI 10.1021/acscatal.0c04858. *Additional discussion, analysis, and writing of this manuscript (P.L.A.) was supported by the U.S. Department of Energy (DOE).*

Lu, P.; Ghosh, S.; Dorneles De Mello, M.; Kamaluddin, H. S.; Li, X.; Kumar, G.; Duan, X.; Abeykoon, M.; Boscoboinik, J. A.; Qi, L.; Dai, H.; Luo, T.; Al-Thabaiti, S.; Narasimharao, K.; Khan, Z.; Rimer, J. D.; Bell, A. T.; Dauenhauer, P.; Mkhoyan, K. A.; Tsapatsis, M., Few-Unit-Cell MFI Zeolite Synthesized Using a Simple Di-Quaternary Ammonium Structure-Directing Agent. *Angew. Chem. Int. Ed.* **2021**, *60* (35), 19214–19221. DOI 10.1002/anie.202104574. *The Catalysis program supported Q.L.'s efforts in conducting reactions using the materials synthesized at Johns Hopkins University and A.T.B.'s effort on supervising this phase of the research and editing the paper.*

Mao, Y.; Loipersberger, M.; Kron, K. J.; Derrick, J. S.; Chang, C. J.; Sharada, S. M.; Head-Gordon, M., Consistent Inclusion of Continuum Solvation in Energy Decomposition Analysis: Theory and Application to Molecular $CO_2$ Reduction Catalysts. *Chem. Sci.* **2021**, *12* (4), 1398–1414. DOI 10.1039/d0sc05327a. *Synthetic compounds were provided to the collaboration with support from the DOE.*

Sakamoto, S.; Butcher, T. W.; Yang, J. L.; Hartwig, J. F., gem-Difluoroallylation of Aryl Halides and Pseudo Halides with Difluoroallylboron Reagents in High Regioselectivity. *Angew. Chem. Int. Ed.* **2021**, *60* (49), 25746–25752. DOI 10.1002/anie.202111476. *The FWP supported the work performed in the Program's Catalysis Facility.*

Zhao, J.; Ji, S.; Guo, C.; Li, H.; Dong, J.; Dong, J.; Guo, P.; Wang, D.; Li, Y.; Toste, F. D., A Heterogeneous Iridium Single-Atom-Site Catalyst for Highly Regioselective Carbenoid O-H Bond Insertion. *Nat. Catal.* **2021**, *4* (6), 523–531. DOI 10.1038/s41929-021-00637-7.

*Additional discussion, analysis, and writing of this manuscript (F.D.T.) was supported by the U.S. Department of Energy (DOE).*

**2022**

Aljama, H.; Head-Gordon, M.; Bell, A., Assessing the Stability of Pd-Exchanged Sites in Zeolites with the Aid of a High Throughput Quantum Chemistry Workflow. *Nat. Commun.* **2022**, *13* (1), 2910. DOI 10.1038/s41467-022-29505-z. *The Catalysis program supported A.T.B.'s efforts in conceptualizing the project, developing the methodology, data analysis, supervising the research and editing the paper.*

Berg, I.; Einav, A.; Hale, L.; Toste, F. D.; Gross, E., N-Heterocyclic Carbene Nanolayer for Copper Film Oxidation Mitigation. *Angew. Chem. Int. Ed.* **2022**, *61* (25), e202201093. DOI 10.1002/anie.202201093. *Synthesis of ligands (L.H.) and discussion, analysis, and writing of this manuscript (L.H. & F.D.T.) was supported by the U.S. Department of Energy (DOE).*

Cestellos-Blanco, S.; Louisia, S.; Ross, M. B.; Li, Y.; Soland, N. E.; Detomasi, T. C.; Spradlin, J. N. C.; Nomura, D. K.; Yang, P., Toward Abiotic Sugar Synthesis from $CO_2$ Electrolysis. *Joule* **2022**, *6* (10), 2304–2323. DOI 10.1016/j.joule.2022.08.007. *The Catalysis program contributed to experimental design, $CO_2$ reduction experiments and manuscript development.*

**2023**

Kurandina, D.; Huang, B.; Xu, W.; Hanikel, A. D.; Storoscio, G. D.; Wang, K.; Gagliardi, L.; Toste, F. D.; Yaghi, O. M., Porous Crystalline Nitrone-Linked Covalent Organic Framework. *Angew. Chem. Int. Ed.* **2023**, e202307674. DOI 10.1002/anie.202307674. *Synthesis of ligands (B.H.) and discussion, analysis, and writing of this manuscript (B.H. & F.D.T.) was supported by the U.S. Department of Energy.*

**Zili Wu**

**FWP ERKCC96: Fundamentals of Catalysis and Chemical Transformations**

**PIs:** Miaofang Chi, Sheng Dai, Vanda Glezakou, Stephan Irle, De-en Jiang (Vanderbilt University), Yuanyuan Li, Felipe Polo-Garzon, Zili Wu (lead PI), Zhenzhen Yang

**Postdoc(s):** Zhuoran Gan, Joshua Orege, Hailing Yu (UTK), Junyan Zhang,

**Student(s):** Kevin Siniard (UTK), Haohong Song (Vanderbilt University), Yiming Chen (Vanderbilt University)

**Affiliation (s):** Oak Ridge National Laboratory

## RECENT PROGRESS

The overarching goal of this program is *to understand how to control the catalytic activity, selectivity and stability in the activation and conversion of C=O and C-H bonds, and C-C coupling reactions based on $C_1$ molecules through tuning the local environment around the active sites on the surface and at the metal-oxide interfaces involving complex oxides.* To address our program overarching goal and the science challenges in converting $C_1$ feedstocks ($CO_2$, $CH_4$) into coupling products, we organize our research into two thrusts and a theory crosscutting thrust. Thrust 1 aims to understand how to efficiently activate C=O bond and promote C-C coupling in $CO_2$ hydrogenation through tuning the geometric and electronic local structures of supported metal catalysts. Thrust 2 aims to mechanistically understand how to efficiently activate both C=O and C-H bonds in $CO_2$ and $CH_4$ and promote C-C coupling through tuning the configurational entropic (via high entropy oxides) and electronic local environment of active centers on the surfaces and at the interfaces of defined catalysts. The Crosscutting Thrust pursues to use advanced theory and simulation enhanced through artificial intelligence and machine learning to establish general principles on how to control C-C coupling reaction pathways and delineate the dynamic role of catalysts and supports in complex reactive environments.

In the following, we summarize our past research accomplishments into two sections: **Part 1**. tuning local environment of catalytic sites to impact hydrogenation reactions including $CO_2$ and other model unsaturated compounds, and **Part 2**. tuning local environment of catalytic sites to impact C-H and C=O bond activation and conversion in methane combustion and dry reforming of methane (DRM).

### Part 1. Tuning local environment of catalytic sites to impact hydrogenation reactions

*A. Controlling local electronic environment to enhance hydrogenation catalysis from anion sites tuning*

*A1. $N_2$ hydrogenation and acetylene semi-hydrogenation over $BaTiO_{2.5}H_{0.5}$* To reveal the role of lattice hydrides in hydrogenation reactions, we used first-principles density functional theory (DFT), coupled with microkinetic modeling, to investigate the reaction mechanisms of ammonia synthesis and acetylene semi-hydrogenation on a prototypical perovskite oxyhydride (POH), $BaTiO_{2.5}H_{0.5}$ (BTOH).[23,43] Taking acetylene hydrogenation as an example, two different mechanisms are examined on a representative surface of BTOH under the reaction conditions.[43] Although both are based on the Horiuti-Polanyi mechanism, the way that $H_2$ is activated is different. In mechanism a, a lattice hydride H atom and then a surface adsorbed H atom

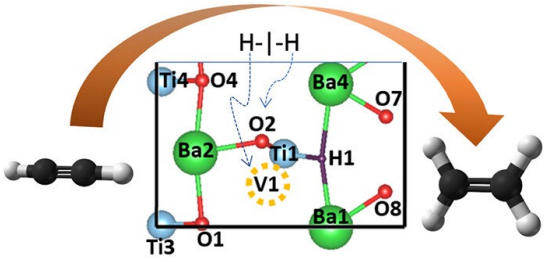


**Fig 1.** Mechanistic overview of acetylene hydrogenation over a BTOH surface.

sequentially hydrogenate the adsorbed acetylene. In mechanism b, two lattice hydride H atoms from the BTOH sequentially hydrogenate the adsorbed acetylene. In both mechanisms, the H atoms are replenished from gas phase $H_2$ dissociation (**Fig 1**). A selectivity analysis for the temperature range of 373 – 673 K shows that the product observed is essentially only ethylene. This work shows the potential of using lattice hydrides for selective hydrogenation, further demonstrated for $CO_2$ hydrogenation to methanol below.

*A2. $CO_2$ hydrogenation to methanol promoted by lattice hydrides* Based upon our DFT studies of hydrogenation reactions over BTOH illustrated above, we utilized POH as a support for Cu NPs in $CO_2$ hydrogenation to understand the catalytic role of lattice hydrides. We found that the yield to methanol on $Cu/BaTiO_{2.8}H_{0.2}$ is about 3 times over $Cu/BaTiO_3$ under the same reaction condition with similar selectivity to methanol.[49] The contrast suggests that significant roles are played by the support hydrides in the reaction. Temperature programmed reaction and isotopic labelling studies indicate that $BaTiO_{2.8}H_{0.2}$ surface hydride species follow a Mars van Krevelen mechanism in $CO_2$ hydrogenation, promoting methanol production (**Fig 2**). High-pressure steady-state isotopic transient kinetic analysis (SSITKA) studies suggest that $Cu/BaTiO_{2.8}H_{0.2}$ possesses both a higher density and more active and selective sites for methanol production compared to $Cu/BaTiO_3$. An operando high-pressure diffuse reflectance infrared spectroscopy (DRIFTS)-SSITKA study shows that formate species are the major surface intermediates over both catalysts, and the subsequent hydrogenation steps of formate are likely rate-limiting. However, the catalytic reactivity of $Cu/BaTiO_{2.8}H_{0.2}$ towards the formate species is much higher than $Cu/BaTiO_3$, likely due to the altered electronic structure of interface Cu sites by the hydrides in the support as validated by density functional theory (DFT) calculations. We are currently explore the role of lattice hydrides for promoting $CO_2$ hydrogenation to C-C coupling products.

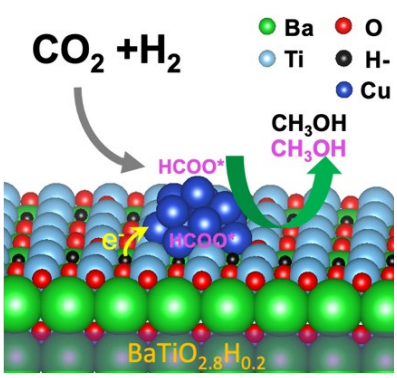


**Fig 2.** The operation of both surface hydrogen and lattice hydrogen in hydrogenating $CO_2$ to methanol over $Cu/BaTiO_{2.8}H_{0.2}$.

*B. Dynamic local interfacial sites for selective $CO_2$ hydrogenation to methanol*

The reaction of $CO_2$ hydrogenation to methanol has been intensively studied with the attempt to design active catalysts with high methanol selectivity. However, due to the high-pressure reaction condition, currently, there is still little knowledge on the nature of active sites, making it difficult to rationally design efficient catalysts. To reveal the status of working catalysts under high pressure reaction conditions, we combined multiple *in situ* and *operando* techniques including conventional and high energy resolution fluorescence detected X-ray absorption spectroscopy, environment electron microscopy, ambient pressure X-ray photoelectron spectroscopy, neutron and IR spectroscopy to study a model system - Cu/ceria in $CO_2$ hydrogenation. The combined results showed the correlated methanol formation with the increase of $Ce^{3+}$ species which was associated with the reaction intermediate carbonates/formates. Neighboring with this $Ce^{3+}$ species was the interfacial Cu sites, which weakly but dynamically interacted with ceria support under the reaction. Such dynamicity, most likely, was driven by the adsorption of reactants/intermediates and favors the formation of methanol (**Fig. 3**). This work provides insights into the nature of local active center/sites for the formation of methanol from $CO_2$ hydrogenation and methodologies for studying catalysts under realistic high pressure reaction conditions. With these, active structures/sites can be rationally designed for high pressure catalytic reactions beyond $CO_2$ hydrogenation.

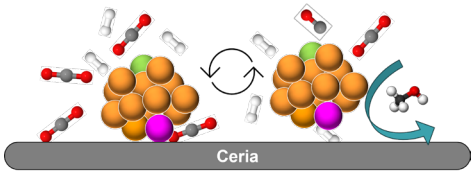


**Fig 3.** A schematic showing the catalytic behavior of Cu/ceria for the reaction of $CO_2$ hydrogenation to methanol. Magenta ball represents accessible Cu site near active $Ce^{3+}$ site and the green ball represents the accessible Cu site that is relatively electron rich and away from ceria support (unpublished work).

*C. Stable and selective $CO_2$ hydrogenation from cation sites tuning of high entropy oxides (HEOs)*

Utilizing the configurational entropic (it refers to the number of ways that atoms or molecules pack together in the host matrix. More disorder of a system and higher randomness of a structure with a lower Gibbs free energy can contribute to the stability of host structure at high temperatures ($\Delta G = H - T\Delta S$)) stabilization effect in HEOs, we showed that exsoluted metal species (surface segregated out of the bulk of the HEO) are extremely stably under demanding hydrogenation conditions such as reverse water gas shift reaction (RWGS). Shown in **Fig 4**, CuFeCoNi alloy particles can be exsoluted from the HEO ($Zr_{0.5}(NiFeCuMnCo)_{0.5}O_x$) bulk structure upon 600°C $H_2$ treatment and dissolved back in the structure upon 550°C in air.[60] The entropic confinement effect from the HEO matrix endorses stable performance of the metal alloy for $CO_2$ hydrogenation selectively to CO at 400°C over 500hr, in sharp contrast to the severe deactivation by the ternary doped $Zr_{0.5}(MnCu)_{0.5}O_x$ catalyst within 40hr. A similarly stabilization effect was also found in the RWGS reaction at 500°C over another HEO system ($Co_3MnNiCuZnOx$).[67] This unique entropic confinement effect will be capitalized to stabilize metal sites under harsh reaction conditions including C-C coupling reaction in $CO_2$ hydrogenation at elevated pressures, and in the high temperature DRM reaction.

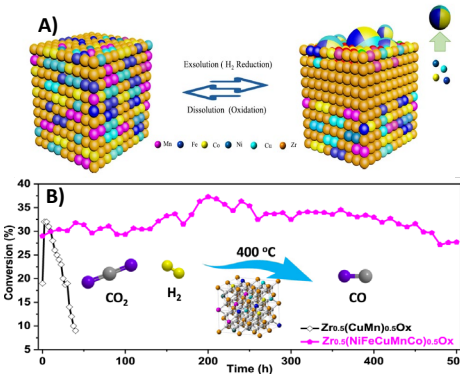


**Fig 4.** A) schematics of the intelligent behavior of HEOs; B) stable performance of HEO-derived catalyst in RWGS reaction.

*D. $H_2$ activation and hydrogenation with heterogeneous Frustrated Lewis Pairs (FLPs)*

Hydrogenation reactions promoted by earth-abundant non-metal catalysts under mild conditions is an attractive and challenging subject. In our recent work (Chen *et al.*),[4] sterically hindered Lewis acid ("B" center) and Lewis base ("N" center) sites were anchored within the rigid lattice of highly crystalline hexagonal boron nitride (h-BN) scaffolds to form the so-called FLPs (**Fig 5**). The active sites were created via precision defect regulation during the molten-salt-involved ($NaNH_2$ and $NaBH_4$) h-BN construction procedure. The as-afforded h-BN scaffolds achieved highly efficient $H_2/D_2$ activation and dissociation under ambient pressure via FLP-like behavior. Attractive catalytic efficiency in styrene hydrogenation reaction over the FLP BN catalyst far surpassed the current heterogeneous analogues such as bulk BN where little defects are present, underscoring the importance of precision regulation of the defect types in the h-BN skeleton. Extension of this concept was recently advanced by the construction of B- and N-enriched nanoporous π-conjugated networks (BN-NCNs) FLPs which also showed promising hydrogenation performances in both gas phase hydrogenation of acetylene and liquid phase styrene hydrogenation.[31] These results provide a promising approach to construct metal-free heterogeneous catalysts toward various hydrogenation reactions and potentially for the hydrogenation of $CO_2$.

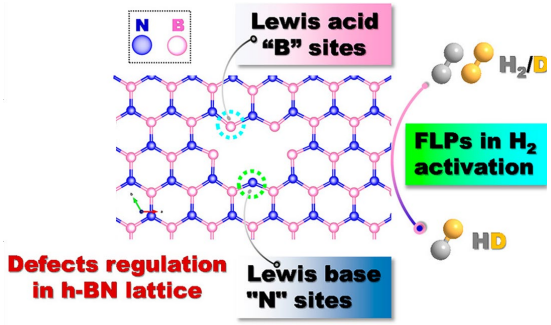


**Fig 5.** FLP sites created in BN with excellent capacity in activating $H_2$ and catalyzing hydrogenation reactions including $CO_2$.

**Part 2. Tuning local environment of catalytic sites to impact C-H and C=O activation**

*A. Boosting the C-H activation capability of single atoms by tailoring the local coordination environment*

Catalytic methane combustion is of importance not only for efficient energy production but also for reducing methane emission and removal of atmospheric methane. For this reaction, the challenge is the designing of active structures with reduced usage of critical element Pd. The goal of this work is to address the challeng and reveal how the local electronic structure and atomic structure of Pd atoms can be tuned to enhance C-H bond activation and thus methane combustion. We hypothesized that the strong interaction between Pd single atoms and ceria support needs to be manipulated for efficient C-H activation and methane conversion. In one study,[44] we broke the strong Pd single atom-ceria support interaction by introducing defects on the surface of ceria support. The introduction of defects was achieved by a simple thermal pretreatment to ceria prior to Pd deposition. According to XAS, XPS and IR results, the activated Pd single atom at this site had oxygen-deficient local structure and elongated interacting distance with ceria. These features facilitated the efficient conversion of methane compared to regular Pd SAs (**Fig. 6**). In another study,[55] to disturb the stable Pd single atom-ceria support geometry, we tuned the distances of neighboring Pd single atoms, which was achieved by modifying the local electron density of Pd single atom sites on ceria support. We found that paring Pd single atom sites and controlling their interatomic distances could help further improve the C-H bond activation capability (**Fig. 6**). Specifically, our results showed that the turnover frequency (TOF) of the $Pd_2$ structure with the Pd-Pd distance of 2.99 Å was higher than that of the $Pd_2$ structure with the Pd-Pd distance of 2.75 Å. The TOF is at least 26 times that of ceria supported Pd single atoms, and 4 times that of ceria supported PdO nanoparticles. The concept of tuning metal size in the range of single atoms to clusters could be exploited in $CO_2$ hydrogenation to construct metal sites with different local environments to tune both activity and selectivity.

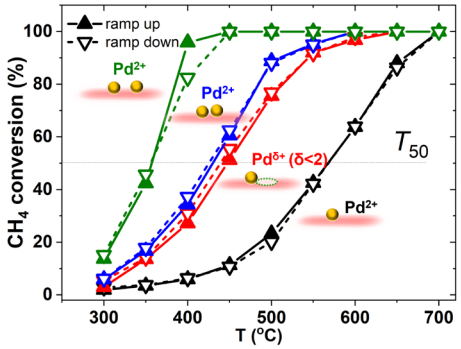


**Fig 6.** Temperature dependent methane conversion over ceria supported different Pd structures from Pd SAC to dimers.

*B. Controlling C-H bond activation via tuning the cation sites in complex oxides*

Understanding how the change of cations in complex oxides impacts the ability in C-H bond activation can help to develop more efficient $CH_4$ conversion catalysts. However, the surface reconstruction of complex oxides made it complicated due to dynamic behavior in surface composition changes of the oxides under difference conditions. Our latest work[20] presents a detailed kinetic analysis of catalytic $CH_4$ combustion over a set of seven perovskites ($SrTiO_3$, $SrZrO_3$, $SrFeO_3$, $LaFeO_3$, $LaInO_3$, $LaCoO_3$, $LaMnO_3$) with various surface terminations (**Fig 7**). Steady-state isotopic transient kinetic analysis was employed to measure turnover frequency (TOF) and density of surface intermediates (*N*) under operando conditions. Top surface characterization elucidated performance-structure relationships between near-monolayer surface composition and intrinsic reactivity of the catalysts. In general, surface reconstruction is shown as a tool to tune TOF and *N* to improve reaction rates, a concept that could be

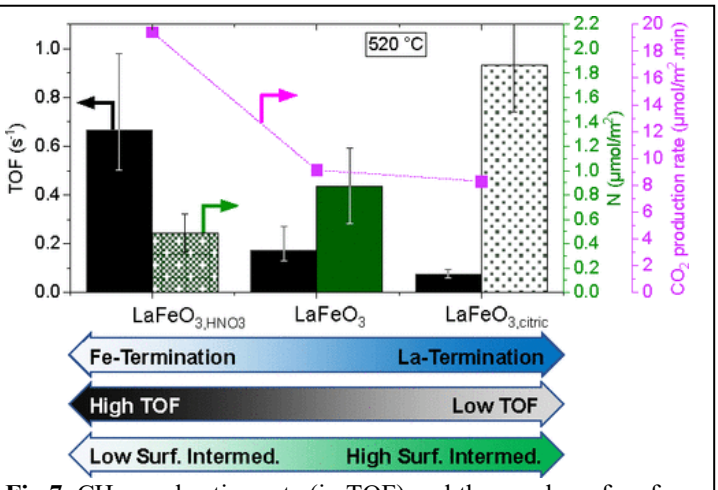


**Fig 7**. $CH_4$ combustion rate (in TOF) and the number of surface intermediates as well as $CO_2$ production rate vary several times over the same $LaFeO_3$ perovskite but with varying surface composition through different chemical treatments.

utilized in our future studies of HEOs for DRM and $CO_2$ hydrogenation.

*C. Achieving stable activity in dry reforming of methane (DRM) via tuning metal-support interactions*

Two major challenges in DRM are metal sintering and coke formation under harsh reaction conditions. We postulate that both challenges can be addressed via tuning metal-support interactions and utilized two approaches: harnessing the confinement of active sites in zeolite supports, or leveraging the moderate configurational entropy of a solid oxide solution. Both approaches can stabilize active sites (clusters or nanoparticles) to limit sintering. Limiting sintering of active sites can also decelerate coking.

In the first approach, through a solid-state grinding protocol, we anchor highly dispersed $Ni^{2+}$ sites onto dealuminated Beta (dBeta) zeolite support. Dealumination of the Beta zeolite created Al-vacancies where Ni can be substituted. Notably, the dispersion and Ni-zeolite interaction can be precisely controlled by adjusting the airflow during calcination, allowing for tunable metal dispersion ranging from NPs to isolated sites within the framework. By combining *in situ* XAS and *ab initio* simulations, it is elucidated that the efficient removal of byproducts during catalyst synthesis conduced to strengthened Ni-Si interactions that suppress coking and sintering after 100 h of time-on-stream (TOS) during DRM at 650 °C.[56] A combination of IR spectroscopy, XAS, and microscopy allowed us to characterize the dispersion of the synthesized Ni species and their interaction with the support. Structure-performance correlations demonstrated that the finely tuned synthesis method leads to catalysts with significantly enhanced stability during DRM. Interestingly, transient isotopic kinetic studies showed that metallic Ni sites in NPs have higher TOF than those on dispersed sites (clusters), explaining the observed macroscopic conversion of reactants (**Fig 8**). This work constructs fundamental understanding regarding the implication of facile synthesis protocols on metal-support interaction in zeolite-supported Ni sites, and it lays needed foundations on how these interactions can be tuned for outstanding DRM performance.

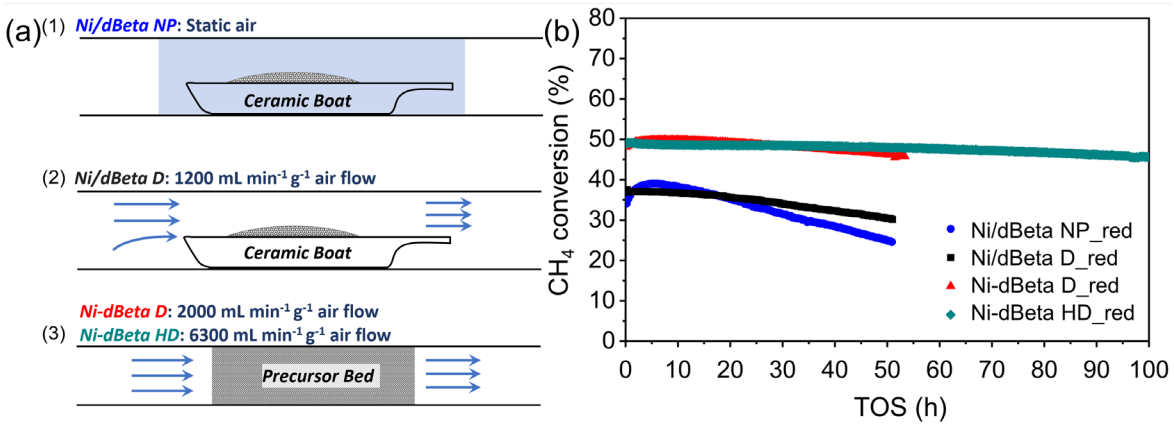


**Fig 8.** (A) Different flow conditions for removal of synthesis byproducts lead to (B) different stability during DRM at 650 °C of Ni/dBeta catalysts.

In the second approach, we envisioned a solid oxide solution catalyst where 4 elements were included ($NiMgCuZnO_x$). The four components of the solid solution were chosen based on the following considerations: Ni-Mg based catalysts are promising combinations in DRM; Cu and Zn are metal dopants to enhance activation of $CO_2$, inhibit $CH_4$ decomposition, and improve carbon deposition resistance; Ni, Mg, Cu and Zn possess similar ionic radii, which facilitates the formation of a homogeneous solid solution and aids the structural stability of the catalyst. An equimolar precursor mixture of Ni, Mg, Cu and Zn salts was deployed to provide a system with moderate configurational entropy, allowing for the moderate exsolution of active sites. Exsolution of NiCu bimetallic active sites occurred under the reductive DRM conditions due to their redox nature, different from Mg and Zn. Interestingly, the coke/surface interactions are sufficiently weak to promote continuous detachment of coke from the surface, thus preventing catalyst

deactivation. The catalyst exhibited remarkably stable performance during DRM at 800 °C, showing minimal deactivation for 120 h of TOS. The approach presented here shows tuned stability of a solid solution to exsolute tightly anchored nanoparticles that provide stable active sites for DRM (**Fig 9).**

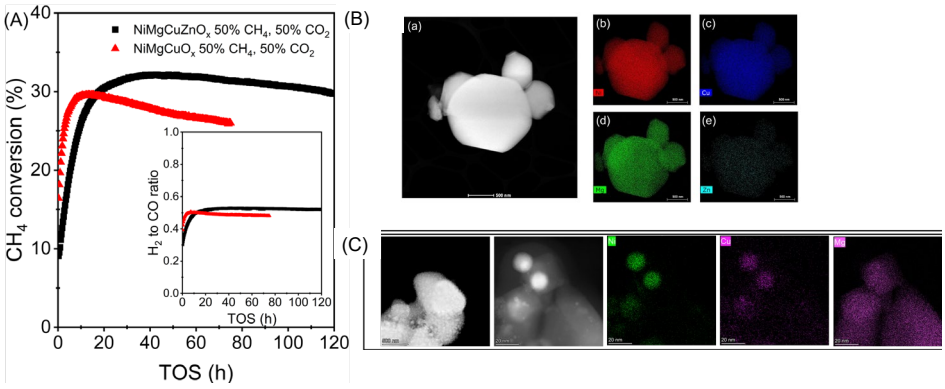


**Fig 9.** (A) 4-component solid solution (NiMgCuZnOx) shows greater stability during DRM at 800 °C when compared with 3-component counterpart. (B) As-synthesized solid solution shows homogeneous distribution of metals. (C) Spent catalyst after DRM shows exsoluted NiCu nanoparticles. (unpublished work)

*D. Revealing surface composition/reconstruction of HEOs with advanced electron microscopy*

It remains a challenge in understanding the surface composition and structure of HEOs. Taking advantage of the advanced STEM imaging and spectroscopy techniques in combination with DFT, we recently investigated the atomic-scale structural and chemical responses of a model HEO (CeYLaHfTiZrOx) to different high-temperature redox environments.[50] The HEO particle bulk shows pseudorandom two-phase structure with a significant ability to accommodate oxygen vacancies, whereas the surface and subsurface layers exhibit dynamic elemental and structural reconstructions under different gas environments (shown in **Fig 10** as an example of the pristine HEO). The atomic arrangements and elemental distributions revealed in this study can serve as direct structural inputs for DFT calculations and guide the design of more efficient catalysts to take advantage of the dynamic surface structure of HEOs, which will be employed as a unique approach in our research in studying the structure of complex oxide-based catalysts.

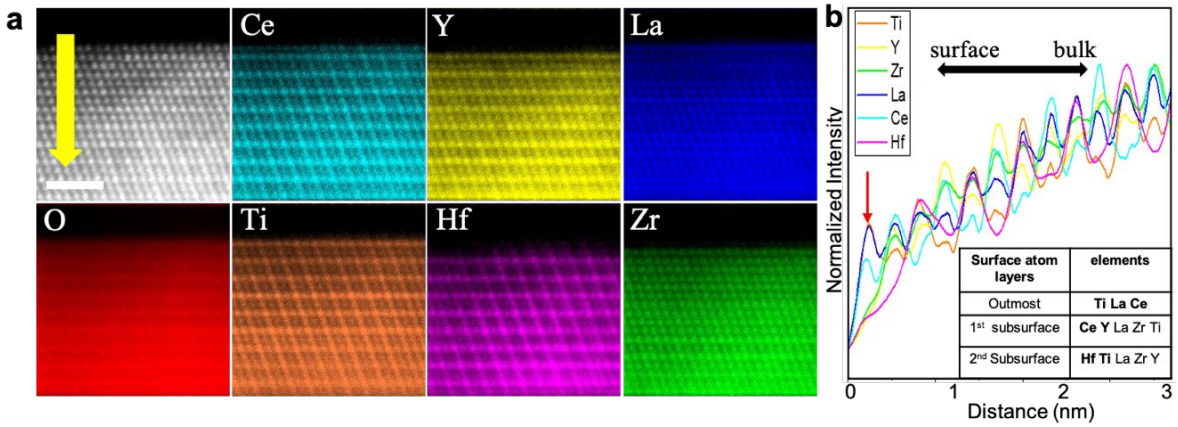


**Fig 10.** Atomic STEM analysis of the surface crystal structure and elemental distribution of a pristine HEO particle. a) HAADF-STEM analysis at the very edge of the particle in [110] zone axis and corresponding atomic STEM-EDX maps of Ce, Y, La, Hf, Ti and Zr. b) Line profiles of the EDX maps across the surface atom layers as indicated by the yellow arrow. Scale bar 2nm.

**Publications Acknowledging this Grant (ERKCC96) in 2021 –2024 (total –88)**

***(I) Intellectually led by this grant (total – 56 )***


(1) Blum, T.; Graves, J.; Zachman, M. J.; Polo-Garzon, F.; Wu, Z.; Kannan, R.; Pan, X.; Chi, M. Machine Learning Method Reveals Hidden Strong Metal-Support Interaction in Microscopy Datasets. *Small Methods* **2021**, *n/a* (n/a), 2100035, https://doi.org/10.1002/smtd.202100035.
(2) Chen, H.; Wang, W.; Yang, Z.; Suo, X.; Lu, Z.; Xiao, W.; Dai, S. Alkaline salt-promoted construction of hydrophilic and nitrogen deficient graphitic carbon nitride with highly improved photocatalytic efficiency. *J. Mater. Chem. A* **2021**, *9* (8), 4700-4706, 10.1039/D1TA00524C.
(3) Chen, H.; Yang, Z.; Peng, H.; Jie, K.; Li, P.; Ding, S.; Guo, W.; Suo, X.; Liu, J.; Yan, R.; et al. A bifunctional zeolitic porous liquid with incompatible Lewis pairs for antagonistic cascade catalysis. *Chem* **2021**, *7* (12), 3340-3358. DOI: https://doi.org/10.1016/j.chempr.2021.08.022.
(4) Chen, H.; Yang, Z.; Wang, X.; Polo-Garzon, F.; Halstenberg, P. W.; Wang, T.; Suo, X.; Yang, S.-Z.; Meyer, H. M.; Wu, Z.; et al. Photoinduced Strong Metal–Support Interaction for Enhanced Catalysis. *J. Amer. Chem. Soc.* **2021**, *143* (23), 8521-8526. DOI: 10.1021/jacs.0c12817.
(5) Leng, Y.; Zhang, Z.; Chen, H.; Du, S.; Liu, J.; Nie, S.; Dong, Y.; Zhang, P.; Dai, S. Overcoming the phase separation within high-entropy metal carbide by poly(ionic liquid)s. *Chem. Commun.* **2021**, *57* (30), 3676-3679. DOI: 10.1039/D1CC00497B.
(6) Liu, T.; Jiang, D.-e. Understanding the interaction between carboxylates and coinage metals from first principles. *The Journal of Chemical Physics* **2021**, *155* (3), 034301. DOI: 10.1063/5.0053045.
(7) Okejiri, F.; Yang, Z.; Chen, H.; Do-Thanh, C.-L.; Wang, T.; Yang, S.; Dai, S. Ultrasound-driven fabrication of high-entropy alloy nanocatalysts promoted by alcoholic ionic liquids. *Nano Research* **2021**. DOI: 10.1007/s12274-021-3760-x.
(8) Polo-Garzon, F.; Blum, T. F.; Bao, Z.; Wang, K.; Fung, V.; Huang, Z.; Bickel, E. E.; Jiang, D.-e.; Chi, M.; Wu, Z. In Situ Strong Metal–Support Interaction (SMSI) Affects Catalytic Alcohol Conversion. *ACS Catal.* **2021**, *11* (4), 1938-1945. DOI: 10.1021/acscatal.0c05324.
(9) Sun, Y.; Dai, S. High-entropy catalysts: Supremacy of diversity. *Chem Catalysis* **2021**, *1* (3), 490-492. DOI: https://doi.org/10.1016/j.checat.2021.06.019.
(10) Sun, Y.; Dai, S. High-entropy materials for catalysis: A new frontier. *Science Advances* **2021**, *7* (20), eabg1600. DOI: 10.1126/sciadv.abg1600.
(11) Wang, S.; Wu, Z.; Dai, S.; Jiang, D.-e. Deep Learning Accelerated Determination of Hydride Locations in Metal Nanoclusters. *Angew. Chem. Int. Ed.* **2021**, *60* (22), 12289-12292, DOI: https://doi.org/10.1002/anie.202100407.
(12) Wang, S.; Liu, T.; Jiang, D.-e. Locating Hydrides in Ligand-Protected Copper Nanoclusters by Deep Learning. *ACS Appl. Mater. Inter.* **2021**, *13* (45), 53468-53474. DOI: 10.1021/acsami.1c14618.
(13) Wang, X.; Li, M.; Wu, Z. In situ spectroscopic insights into the redox and acid-base properties of ceria catalysts. *Chin. J. Catal.* **2021**, *42* (12), 2122-2140. DOI: https://doi.org/10.1016/S1872-2067(21)63806-8.
(14) Yang, W.; Gong, J.; Wang, X.; Bao, Z.; Guo, Y.; Wu, Z. A Review on the Impact of SO2 on the Oxidation of NO, Hydrocarbons, and CO in Diesel Emission Control Catalysis. *ACS Catal.* **2021**, *11* (20), 12446-12468. DOI: 10.1021/acscatal.1c03013.
(15) Bao, Z.; Fung, V.; Moon, J.; Hood, Z.; Rochow, M.; Kammert, J.; Polo-Garzon, F.; Wu, Z. Revealing the interplay between "intelligent behavior" and surface reconstruction of non-precious metal doped SrTiO3 catalysts during methane combustion. *Catal. Today* **2022**, *416*, 113672. DOI: https://doi.org/10.1016/j.cattod.2022.03.012.
(16) Chen, B.; Xu, Y.; Xiong, C.; Rickard, S.; Boscoboinik, J. A.; Jiang, D.-e.; Kidder, M.; Savara, A. Mechanism for Acetone and Crotonaldehyde Production during Steam Reforming of Ethanol over La0.7Sr0.3MnO3–x Perovskite: Evidence for a Shared C4 Aldol Addition Intermediate. *ACS Catal.* **2022**, *12* (8), 4358-4374. DOI: 10.1021/acscatal.2c00650.

(17) Chen, H.; Xiong, C.; Moon, J.; Ivanov, A. S.; Lin, W.; Wang, T.; Fu, J.; Jiang, D.-e.; Wu, Z.; Yang, Z.; et al. Defect-Regulated Frustrated-Lewis-Pair Behavior of Boron Nitride in Ambient Pressure Hydrogen Activation. *J. Amer. Chem. Soc.* **2022**, *144* (24), 10688-10693. DOI: 10.1021/jacs.2c00343.
(18) Okejiri, F.; Fan, J.; Huang, Z.; Siniard, K. M.; Chi, M.; Polo-Garzon, F.; Yang, Z.; Dai, S. Ultrasound-mediated synthesis of nanoporous fluorite-structured high-entropy oxides toward noble metal stabilization. *iScience* **2022**, *25* (5), 104214. DOI: https://doi.org/10.1016/j.isci.2022.104214.
(19) Peng, H.; Dong, T.; Yang, S.; Chen, H.; Yang, Z.; Liu, W.; He, C.; Wu, P.; Tian, J.; Peng, Y.; et al. Intra-crystalline mesoporous zeolite encapsulation-derived thermally robust metal nanocatalyst in deep oxidation of light alkanes. *Nat. Commun.* **2022**, *13* (1), 295. DOI: 10.1038/s41467-021-27828-x.
(20) Polo-Garzon, F.; Fung, V.; Zhang, J.; Bao, Z.; Meyer, H. M.; Kidder, M.; Wu, Z. CH4 Activation over Perovskite Catalysts: True Density and Reactivity of Active Sites. *ACS Catal.* **2022**, 11845-11853. DOI: 10.1021/acscatal.2c03239.
(21) Sun, Y.; Wu, T.; Bao, Z.; Moon, J.; Huang, Z.; Chen, Z.; Chen, H.; Li, M.; Yang, Z.; Chi, M.; et al. Defect Engineering of Ceria Nanocrystals for Enhanced Catalysis via a High-Entropy Oxide Strategy. *ACS Centr. Sci.* **2022**, *8* (8), 1081-1090. DOI: 10.1021/acscentsci.2c00340.
(22) Sun, Y.; Polo-Garzon, F.; Bao, Z.; Moon, J.; Huang, Z.; Chen, H.; Chen, Z.; Yang, Z.; Chi, M.; Wu, Z.; et al. Manipulating Copper Dispersion on Ceria for Enhanced Catalysis: A Nanocrystal-Based Atom-Trapping Strategy. *Advanced Science* **2022**, *9* (8), 2104749, DOI: https://doi.org/10.1002/advs.202104749.
(23) Wang, K.; Wu, Z.; Jiang, D.-e. Ammonia synthesis on BaTiO2.5H0.5: computational insights into the role of hydrides. *Physical Chemistry Chemical Physics* **2022**, *24* (3), 1496-1502, 10.1039/D1CP05055A. DOI: 10.1039/D1CP05055A.
(24) Xiong, C.; Dai, S.; Wu, Z.; Jiang, D.-e. Single Atoms Anchored in Hexagonal Boron Nitride for Propane Dehydrogenation from First Principles. *ChemCatChem* **2022**, *14* (9), e202200133. DOI: https://doi.org/10.1002/cctc.202200133.
(25) Zachman, M. J.; Fung, V.; Polo-Garzon, F.; Cao, S.; Moon, J.; Huang, Z.; Jiang, D.-e.; Wu, Z.; Chi, M. Measuring and directing charge transfer in heterogenous catalysts. *Nat. Commun.* **2022**, *13* (1), 3253. DOI: 10.1038/s41467-022-30923-2.
(26) Chen, B.; Rickard, S.; Bao, Z.; Wu, Z.; Kidder, M. K.; Savara, A. Evidence of redox cycling as a sub-mechanism in hydrogen production during ethanol steam reforming over La0.7Sr0.3MnO3-x perovskite oxide catalysts. *Applied Surface Science* **2023**, *617*, 156603. DOI: https://doi.org/10.1016/j.apsusc.2023.156603.
(27) Chen, H.; Jiang, D.-e.; Yang, Z.; Dai, S. Engineering Nanostructured Interfaces of Hexagonal Boron Nitride-Based Materials for Enhanced Catalysis. *Acc. Chem. Res.* **2023**, *56* (1), 52-65. DOI: 10.1021/acs.accounts.2c00564.
(28) Fung, V.; Hu, G.; Wu, Z.; Jiang, D.-e. Hydrogen-mediated polarity compensation on the (110) surface terminations of ABO3 perovskites. *The Journal of Chemical Physics* **2023**, *159* (17), 174706. DOI: 10.1063/5.0161435.
(29) Fung, V.; Janik, M.; Crossley, S.; Chin, Y.-H. C.; Savara, A. Toward Understanding and Controlling Organic Reactions on Metal Oxide Catalysts. *J. Phys. Chem. C* **2023**, *127* (28), 13451-13465. DOI: 10.1021/acs.jpcc.3c02470.
(30) He, Y.; Zhang, J.; Polo-Garzon, F.; Wu, Z. Adsorbate-Induced Strong Metal–Support Interactions: Implications for Catalyst Design. *J. Phys. Chem. Lett.* **2023**, *14* (2), 524-534. DOI: 10.1021/acs.jpclett.2c03391.
(31) Li, M.; Qiu, L.; Popovs, I.; Yang, W.; Ivanov, A. S.; Kobayashi, T.; Thapaliya, B. P.; Moitra, D.; Yu, X.; Wu, Z.; et al. Construction of Boron- and Nitrogen-Enriched Nanoporous π-Conjugated Networks Towards Enhanced Hydrogen Activation. *Angew. Chem. Int. Ed.* **2023**, *62* (28), e202302684. DOI: https://doi.org/10.1002/anie.202302684.
(32) Li, M.; Zhang, T.; Yang, S.-Z.; Sun, Y.; Zhang, J.; Polo-Garzon, F.; Siniard, K. M.; Yu, X.; Wu, Z.; Driscoll, D. M.; et al. Mechanochemistry-Induced Strong Metal–Support Interactions Construction toward Enhanced Hydrogenation. *ACS Catal.* **2023**, 6114-6125. DOI: 10.1021/acscatal.2c05730.

(33) Li, Y.; Wang, H.; Song, H.; Rui, N.; Kottwitz, M.; Senanayake, S. D.; Nuzzo, R. G.; Wu, Z.; Jiang, D.-e.; Frenkel, A. I. Active sites of atomically dispersed Pt supported on Gd-doped ceria with improved low temperature performance for CO oxidation. *Chem. Sci.* **2023**, *14* (44), 12582-12588. DOI: 10.1039/D3SC03988A.
(34) Li, Y.; Wu, Z. A review of in situ/operando studies of heterogeneous catalytic hydrogenation of CO2 to methanol. *Catal. Today* **2023**, 114029. DOI: https://doi.org/10.1016/j.cattod.2023.02.006.
(35) Moon, J.; Cheng, Y.; Wu, Z.; Ramirez-Cuesta, A. J. Neutron Scattering (NS) Spectroscopy. In *Springer Handbook of Advanced Catalyst Characterization*, Wachs, I. E., Bañares, M. A. Eds.; Springer International Publishing, 2023; pp 493-516.
(36) Moon, J.; Li, M.; Ramirez-Cuesta, A. J.; Wu, Z. Raman Spectroscopy. In *Springer Handbook of Advanced Catalyst Characterization*, Wachs, I. E., Bañares, M. A. Eds.; Springer International Publishing, 2023; pp 75-110.
(37) Polo-Garzon, F. Case Study: Calorimetry. In *Springer Handbook of Advanced Catalyst Characterization*, Wachs, I. E., Bañares, M. A. Eds.; Springer International Publishing, 2023; pp 1061-1069.
(38) Savara, A. Derivation of an Adsorption Isotherm, Chemical Potential, and Entropy for 2D Gas Adsorbates with Packing Exclusions and Attractive Interactions. *J. Phys. Chem. C* **2023**, *127* (28), 13573-13581. DOI: 10.1021/acs.jpcc.3c00497.
(39) Siniard, K. M.; Li, M.; Yang, S.-Z.; Zhang, J.; Polo-Garzon, F.; Wu, Z.; Yang, Z.; Dai, S. Ultrasonication-Induced Strong Metal-Support Interaction Construction in Water Towards Enhanced Catalysis. *Angew. Chem. Int. Ed.* **2023**, *62* (20), e202214322, DOI: https://doi.org/10.1002/anie.202214322.
(40) Sun, F.; Tang, Q.; Jiang, D.-e. Atomically Precise Metal Nanoclusters as Electrocatalysts. In *Atomically Precise Nanochemistry*, 2023; pp 195-225.
(41) Sun, Y.; Yang, Z.; Dai, S. Nonclassical Strong Metal–Support Interactions for Enhanced Catalysis. *J. Phys. Chem. Lett.* **2023**, *14* (9), 2364-2377. DOI: 10.1021/acs.jpclett.2c03915.
(42) Vuong, V.-Q.; Lee, K. H.; Savara, A. A.; Fung, V.; Irle, S. Toward Quantum Chemical Free Energy Simulations of Platinum Nanoparticles on Titania Support. *J. Chem. Theory Comput.* **2023**, DOI: 10.1021/acs.jctc.3c00661.
(43) Wang Romero, K.; Polo-Garzon, F.; Wu, Z.; Savara, A.; Jiang, D.-e. Acetylene Semi-Hydrogenation on a Perovskite Oxyhydride Surface: Insights from First Principles and Microkinetic Modeling. *ACS Catal.* **2023**, *13*, 9213-9221. DOI: 10.1021/acscatal.3c01983.
(44) Yang, W.; Polo-Garzon, F.; Zhou, H.; Huang, Z.; Chi, M.; Meyer Iii, H.; Yu, X.; Li, Y.; Wu, Z. Boosting the Activity of Pd Single Atoms by Tuning Their Local Environment on Ceria for Methane Combustion. *Angew. Chem. Int. Ed.* **2023**, *62* (5), e202217323. DOI: https://doi.org/10.1002/anie.202217323.
(45) Yang, W.; Kim, M.-Y.; Polo-Garzon, F.; Gong, J.; Jiang, X.; Huang, Z.; Chi, M.; Yu, X.; Wang, X.; Guo, Y.; et al. CH4 combustion over a commercial Pd/CeO2-ZrO2 three-way catalyst: Impact of thermal aging and sulfur exposure. *Chemical Engineering Journal* **2023**, *451*, 138930. DOI: https://doi.org/10.1016/j.cej.2022.138930.
(46) Yu, X.; Cheng, Y.; Li, Y.; Polo-Garzon, F.; Liu, J.; Mamontov, E.; Li, M.; Lennon, D.; Parker, S. F.; Ramirez-Cuesta, A. J.; et al. Neutron Scattering Studies of Heterogeneous Catalysis. *Chemical Reviews* **2023**, *123* (13), 8638-8700. DOI: 10.1021/acs.chemrev.3c00101.
(47) Zhang, J.; Wu, Z.; Polo-Garzon, F. Recent Developments in Revealing the Impact of Complex Metal Oxide Reconstruction on Catalysis. *ACS Catal.* **2023**, *13* (23), 15393-15403. DOI: 10.1021/acscatal.3c03297.
(48) Fung, V.; Janik, M.; Crossley, S.; Chin, Y.-H. C.; Savara, A. Unimolecular and bimolecular reactions of organic intermediates on metal oxide catalysts: an update. *Catalysis Reviews* **2024**. DOI: 10.1080/01614940.2024.2354699.
(49) He, Y.; Li, Y.; Lei, M.; Polo-Garzon, F.; Perez-Aguilar, J.; Bare, S. R.; Formo, E.; Kim, H.; Daemen, L.; Cheng, Y.; et al. Significant Roles of Surface Hydrides in Enhancing the Performance of

Cu/BaTiO2.8H0.2 Catalyst for CO2 Hydrogenation to Methanol. *Angew. Chem. Int. Ed.* **2024**, *63* (1), e202313389. DOI: https://doi.org/10.1002/anie.202313389.
(50) Huang, Z.; Wang, L.; Li, T.; Venkatraman, K.; He, Y.; Polo-Garzon, F.; Smith, J.; Du, Y.; Hu, L.; Wu, Z.; et al. Atomic Scale Responses of High Entropy Oxides to Redox Environments. *Nano Lett.* **2024**, DOI: 10.1021/acs.nanolett.1024c02985. DOI: 10.1021/acs.nanolett.4c02985.
(51) Li, M.; Michael Siniard, K.; Driscoll, D. M.; Ivanov, A. S.; Lu, X.; Chen, H.; Zhang, J.; Polo-Garzon, F.; Yang, Z.; Dai, S. Stabilization and manipulation of highly concentrated copper single atoms by high entropy oxides. *J. Catal.* **2024**, *437*, 115645. DOI: https://doi.org/10.1016/j.jcat.2024.115645.
(52) Siniard, K. M.; Li, M.; Cai, Y.; Zhang, J.; Polo-Garzon, F.; Driscoll, D. M.; Ivanov, A. S.; Lu, X.; Chen, H.; Li, Y.; et al. Precision Structure Engineering of High-Entropy Oxides under Ambient Conditions. *ACS Catal.* **2024**, *14* (19), 14807-14818. DOI: 10.1021/acscatal.4c03349.
(53) Wang, H.; Choi, H.; Shimogawa, R.; Li, Y.; Zhang, L.; Kim, H. Y.; Frenkel, A. I. Unravelling the origin of reaction-driven aggregation and fragmentation of atomically dispersed Pt catalyst on ceria support. *Nanoscale* **2024**, *16* (31), 14716-14721. DOI: 10.1039/D4NR01396D.
(54) Xiang, G.; Chen, H.; Yi, C.; Liu, Z.; Dai, S. Oxygen vacancy-regulated atomic dispersed Au on CeFeOx for preferential oxidation of CO in H2-rich stream. *Chemical Engineering Journal* **2024**, *479*, 147775. DOI: https://doi.org/10.1016/j.cej.2023.147775.
(55) Yang, W., H. Song, L. Zhang, J. Zhang, F. Polo-Garzon, H. Wang, H. Meyer III, D.-e. Jiang, Z. Wu, and Y. Li, Active Palladium Structures on Ceria Obtained by Tuning Pd−Pd Distance for Efficient Methane Combustion. *ACS Catalysis*, **2024**. DOI: 10.1021/acscatal.4c04985
(56) Zhang, J.; Li, Y.; Song, H.; Zhang, L.; Wu, Y.; He, Y.; Ma, L.; Hong, J.; Tayal, A.; Marinkovic, N.; et al. Tuning Metal-Support Interactions in Nickel-Zeolite Catalysts Leads to Enhanced Stability during Dry Reforming of Methane. *Nat. Commun.* **2024**, DOI: 10.1038/s41467-41024-50729-41468.

***(II) Jointly funded by this grant and other grants with intellectual leadership by other funding sources (total - 32)***

(57) Chen, Y.; Rana, R.; Sours, T.; Vila, F. D.; Cao, S.; Blum, T.; Hong, J.; Hoffman, A. S.; Fang, C.-Y.; Huang, Z.; et al. A Theory-Guided X-ray Absorption Spectroscopy Approach for Identifying Active Sites in Atomically Dispersed Transition-Metal Catalysts. *J. Amer. Chem. Soc.* **2021**, *143* (48), 20144-20156. DOI: 10.1021/jacs.1c07116.
(58) Gao, W.; Elnabawy, A. O.; Hood, Z. D.; Shi, Y.; Wang, X.; Roling, L. T.; Pan, X.; Mavrikakis, M.; Xia, Y.; Chi, M. Atomistic insights into the nucleation and growth of platinum on palladium nanocrystals. *Nat. Commun.* **2021**, *12* (1), 3215. DOI: 10.1038/s41467-021-23290-x.
(59) He, X.; Walter, M.; Jiang, D.-e. Understanding Superatomic Ag Nanohydrides. *Small* **2021**, 2004808. DOI: https://doi.org/10.1002/smll.202004808.
(60) Hou, S.; Ma, X.; Shu, Y.; Bao, J.; Zhang, Q.; Chen, M.; Zhang, P.; Dai, S. Self-regeneration of supported transition metals by a high entropy-driven principle. *Nat. Commun.* **2021**, *12* (1), 5917. DOI: 10.1038/s41467-021-26160-8.
(61) Hutama, A. S.; Marlina, L. A.; Chou, C.-P.; Irle, S.; Hofer, T. S. Development of Density-Functional Tight-Binding Parameters for the Molecular Dynamics Simulation of Zirconia, Yttria, and Yttria-Stabilized Zirconia. *ACS Omega* **2021**, *6* (31), 20530-20548. DOI: 10.1021/acsomega.1c02411.
(62) Lawson, S.; Farsad, A.; Adebayo, B.; Newport, K.; Schueddig, K.; Lowrey, E.; Polo-Garzon, F.; Rezaei, F.; Rownaghi, A. A. A Novel Method of 3D Printing High-Loaded Oxide/H-ZSM-5 Catalyst Monoliths for Carbon Dioxide Reduction in Tandem with Propane Dehydrogenation. *Advanced Sustainable Systems* **2021**, *5* (3), 2000257. DOI: https://doi.org/10.1002/adsu.202000257.
(63) Liu, X.; Li, B.; Han, G.; Liu, X.; Cao, Z.; Jiang, D.-e.; Sun, Y. Electrocatalytic synthesis of heterocycles from biomass-derived furfuryl alcohols. *Nat. Commun.* **2021**, *12* (1), 1868. DOI: 10.1038/s41467-021-22157-5.
(64) Moon, J.; Cheng, Y.; Daemen, L.; Novak, E.; Ramirez-Cuesta, A. J.; Wu, Z. On the Structural Transformation of Ni/BaH2 During a N2-H2 Chemical Looping Process for Ammonia Synthesis: A Joint

In Situ Inelastic Neutron Scattering and First-Principles Simulation Study. *Topic Catal.* **2021**, *64*, 685-692. DOI: 10.1007/s11244-021-01445-w.
(65) Wang, Z.; Rong, J.; Lv, J.; Chong, R.; Zhang, L.; Wang, L.; Chang, Z.; Wang, X. Chelation-mediated in-situ formation of ultrathin cobalt (oxy)hydroxides on hematite photoanode towards enhanced photoelectrochemical water oxidation. *J. Energy Chem.* **2021**, *56*, 152-161. DOI: https://doi.org/10.1016/j.jechem.2020.08.009.
(66) Xu, X.; Wang, X.; Jiang, D.-e. Band Gap as a Novel Descriptor for the Reactivity of 2D Titanium Dioxide and its Supported Pt Single Atom for Methane Activation. *J. Phys. Chem. Lett.* **2021**, *12* (10), 2484-2488. DOI: 10.1021/acs.jpclett.1c00318.
(67) Zhao, J.; Bao, J.; Yang, S.; Niu, Q.; Xie, R.; Zhang, Q.; Chen, M.; Zhang, P.; Dai, S. Exsolution–Dissolution of Supported Metals on High-Entropy Co3MnNiCuZnOx: Toward Sintering-Resistant Catalysis. *ACS Catal.* **2021**, *11* (19), 12247-12257. DOI: 10.1021/acscatal.1c03228.
(68) Zhu, M.; Tian, P.; Cao, X.; Chen, J.; Pu, T.; Shi, B.; Xu, J.; Moon, J.; Wu, Z.; Han, Y.-F. Vacancy engineering of the nickel-based catalysts for enhanced CO2 methanation. *Appl. Catal. B: Environ.* **2021**, *282*, 119561. DOI: https://doi.org/10.1016/j.apcatb.2020.119561.
(69) Zhu, X.; Gao, Y.; Wang, X.; Haribal, V.; Liu, J.; Neal, L. M.; Bao, Z.; Wu, Z.; Wang, H.; Li, F. A tailored multi-functional catalyst for ultra-efficient styrene production under a cyclic redox scheme. *Nat. Commun.* **2021**, *12* (1), 1329. DOI: 10.1038/s41467-021-21374-2.
(70) Chen, Y.; Rana, R.; Huang, Z.; Vila, F. D.; Sours, T.; Perez-Aguilar, J. E.; Zhao, X.; Hong, J.; Hoffman, A. S.; Li, X.; et al. Atomically Dispersed Platinum in Surface and Subsurface Sites on MgO Have Contrasting Catalytic Properties for CO Oxidation. *J. Phys. Chem. Lett.* **2022**, *13* (17), 3896-3903. DOI: 10.1021/acs.jpclett.2c00667.
(71) Fadaeerayeni, S.; Yu, X.; Sarnello, E.; Bao, Z.; Jiang, X.; Unocic, R. R.; Fang, L.; Wu, Z.; Li, T.; Xiang, Y. Ammonia-Assisted Light Alkane Anti-coke Reforming on Isolated ReOx Sites in Zeolite. *ACS Catal.* **2022**, *12* (5), 3165-3172. DOI: 10.1021/acscatal.2c00230.
(72) Gao, Z.-H.; Wei, K.; Wu, T.; Dong, J.; Jiang, D.-e.; Sun, S.; Wang, L.-S. A Heteroleptic Gold Hydride Nanocluster for Efficient and Selective Electrocatalytic Reduction of CO2 to CO. *J. Amer. Chem. Soc.* **2022**, *144* (12), 5258-5262. DOI: 10.1021/jacs.2c00725.
(73) Iftikhar, S.; Martin, W.; Gao, Y.; Yu, X.; Wang, I.; Wu, Z.; Li, F. LaNixFe1−xO3 as flexible oxygen or carbon carriers for tunable syngas production and CO2 utilization. *Catal. Today* **2022**. DOI: https://doi.org/10.1016/j.cattod.2022.07.022.
(74) Li, W.; Nie, X.; Yang, H.; Wang, X.; Polo-Garzon, F.; Wu, Z.; Zhu, J.; Wang, J.; Liu, Y.; Shi, C.; et al. Crystallographic dependence of CO2 hydrogenation pathways over HCP-Co and FCC-Co catalysts. *Appl. Catal. B: Environ.* **2022**, *315*, 121529. DOI: https://doi.org/10.1016/j.apcatb.2022.121529.
(75) Li, Y.; Song, Y.; Zhang, X.; Liu, T.; Xu, T.; Wang, H.; Jiang, D.-e.; Jin, R. Atomically Precise Au42 Nanorods with Longitudinal Excitons for an Intense Photothermal Effect. *J. Amer. Chem. Soc.* **2022**, *144* (27), 12381-12389. DOI: 10.1021/jacs.2c03948.
(76) Song, S.; Yang, K.; Zhang, P.; Wu, Z.; Li, J.; Su, H.; Dai, S.; Xu, C.; Li, Z.; Liu, J.; et al. Silicalite-1 Stabilizes Zn-Hydride Species for Efficient Propane Dehydrogenation. *ACS Catal.* **2022**, *12* (10), 5997-6006. DOI: 10.1021/acscatal.2c00928.
(77) Wang, H.; Rui, N.; Senanayake, S. D.; Zhang, L.; Li, Y.; Frenkel, A. I. Tuning the Placement of Pt "Single Atoms" on a Mixed CeO2–TiO2 Support. *J. Phys. Chem. C* **2022**, *126* (38), 16187-16193. DOI: 10.1021/acs.jpcc.2c05198.
(78) Xie, H.; Xie, X.; Hu, G.; Prabhakaran, V.; Saha, S.; Gonzalez-Lopez, L.; Phakatkar, A. H.; Hong, M.; Wu, M.; Shahbazian-Yassar, R.; et al. Ta–TiOx nanoparticles as radical scavengers to improve the durability of Fe–N–C oxygen reduction catalysts. *Nat. Energy* **2022**, *7* (3), 281-289. DOI: 10.1038/s41560-022-00988-w.
(79) Deng, Q.; Peng, H.; Yang, Z.; Wang, T.; Wang, J.; Zeng, Z.; Dai, S. A one-pot synthesis of high-density biofuels through bifunctional mesoporous zeolite-encapsulated Pd catalysts. *Appl. Catal. B: Environ.* **2023**, *337*, 122982. DOI: https://doi.org/10.1016/j.apcatb.2023.122982.

(80) He, X.; Ding, Y.; Huang, Z.; Liu, M.; Chi, M.; Wu, Z.; Segre, C. U.; Song, C.; Wang, X.; Guo, X. Engineering a Self-Grown TiO2/Ti-MOF Heterojunction with Selectively Anchored High-Density Pt Single-Atomic Cocatalysts for Efficient Visible-Light-Driven Hydrogen Evolution. *Angew. Chem. Int. Ed.* **2023**, *n/a* (n/a), e202217439. DOI: https://doi.org/10.1002/anie.202217439.
(81) Wang, H.; Shimogawa, R.; Zhang, L.; Ma, L.; Ehrlich, S. N.; Marinkovic, N.; Li, Y.; Frenkel, A. I. Migration and aggregation of Pt atoms on metal oxide-supported ceria nanodomes control reverse water gas shift reaction activity. *Communications Chemistry* **2023**, *6* (1), 264. DOI: 10.1038/s42004-023-01064-4.
(82) Yu, X.; Moon, J.; Cheng, Y.; Daemen, L.; Liu, J.; Kim, S. W.; Kumar, A.; Chi, M.; Fung, V.; Ramirez-Cuesta, A. J.; et al. In Situ Neutron Scattering Study of the Structure Dynamics of the Ru/Ca2N:e– Catalyst in Ammonia Synthesis. *Chem. Mater.* **2023**, *35* (6), 2456-2462. DOI: 10.1021/acs.chemmater.2c03599.
(83) Zhang, M.; Duan, X.; Gao, Y.; Zhang, S.; Lu, X.; Luo, K.; Ye, J.; Wang, X.; Niu, Q.; Zhang, P.; et al. Tuning Oxygen Vacancies in Oxides by Configurational Entropy. *ACS Appl. Mater. Inter.* **2023**, *15* (39), 45774-45789. DOI: 10.1021/acsami.3c07268.
(84) Zhao, X.; Wang, Y.; Chen, X.; Yu, X.; Li, W.; Zhang, S.; Meng, X.; Zhao, Z.-M.; Dong, T.; Anderson, A.; et al. Sustainable bioplastics derived from renewable natural resources for food packaging. *Matter* **2023**, *6* (1), 97-127. DOI: https://doi.org/10.1016/j.matt.2022.11.006.
(85) Chen, Y.; Rana, R.; Zhang, Y.; Hoffman, A. S.; Huang, Z.; Yang, B.; Vila, F. D.; Perez-Aguilar, J. E.; Hong, J.; Li, X.; et al. Dynamic structural evolution of MgO-supported palladium catalysts: from metal to metal oxide nanoparticles to surface then subsurface atomically dispersed cations. *Chem. Sci.* **2024**, *15* (17), 6454-6464, 10.1039/D4SC00035H. DOI: 10.1039/D4SC00035H.
(86) Han, T.; Li, Y.; Wu, T.; Meira, D. M.; Xiang, S.; Cao, Y.; Lee, I.; Zhou, X.-G.; Jiang, D.-e.; Frenkel, A. I.; et al. Remote Activation of H–H Bonds by Platinum in Dilute Alloy Catalysts. *ACS Catal.* **2024**, *14* (9), 7157-7165. DOI: 10.1021/acscatal.4c00886.
(87) Huang, Z.; Li, T.; Li, B.; Dong, Q.; Smith, J.; Li, S.; Xu, L.; Wang, G.; Chi, M.; Hu, L. Tailoring Local Chemical Ordering via Elemental Tuning in High-Entropy Alloys. *J. Amer. Chem. Soc.* **2024**, *146* (3), 2167-2173. DOI: 10.1021/jacs.3c12048.
(88) Polo-Garzon, F.; Wu, Z.; Li, Y.; Zhang, J.; Yu, X.; Toups, E.; Lopez-Honorato, E.; Damron, J. T.; Foster, J. C.; Cheng, Y.; et al. Low-temperature dechlorination of polyvinyl chloride (PVC) for production of H2 and carbon materials using liquid metal catalysts. *Science Advances* **2024**, *10* (30), eadm9963. DOI: 10.1126/sciadv.adm9963.

Johannes A. Lercher

**Advancing Key Catalytic Reaction Steps for Achieving Carbon Neutrality**

**PI:** Johannes A. Lercher

**Subtask PIs:** Aaron M. Appel, Liney Arnadottir (Oregon State U.), Zdenek Dohnálek, Sungmin Kim, Wendy J. Shaw, Ba Tran, Yong Wang, Eric S. Wiedner

**CoPIs:** David A. Dixon (U. Alabama), John L. Fulton, Bojana Ginovska, Jian Zi Hu, Abhi J. Karkamkar, Bruce D. Kay, Konstantin Khivantsev, Greg A. Kimmel, Libor Kovarik, ThuyThanh D. Le, Mal Soon Lee, John C. Linehan, Zbynek Novotny, Simone Raugei, Udishnu Sanyal, Gregory K. Schenter, Honghong Shi, Janos Szanyi, Huamin Wang, Nancy M. Washton

**Presentation Abstract**

The central goal of this Basic Energy Sciences (BES) Catalysis Sciences research program is to bridge *heterogeneous catalysis, homogeneous catalysis and surface science* in designing catalytic pathways. It is focused on advancing knowledge based design of catalytic reactions by tailoring active centers and the covalently and weakly bound environment. Emphasizing the rate acceleration of C-C and C-H bond formation and C-O bond cleavage, the program employs both acid-base and metal-based sites. It is structured in two central tasks: (i) design the intrinsic reactivity of catalytic sites and their environments via chemical specificity, nuclearity, and state, including spatial constraints and functionalization, and (ii) to enhance the reactivity by adjusting the excess chemical potential of substrates and intermediates via solvents and external electric potential. These tasks are interconnected by a crosscutting subtask, which integrates computational catalysis to lead and complement experimental efforts. We aim to achieve three goals. The *first goal* is to delineate how mobile and bound functionalities of catalytic sites influence the thermodynamics of initial and the transition states. Our *second goal* is to expand the unilateral description of the impact of the catalyst on the substrate toward quantifying their mutual impact including also solvents, and external electric potential. The *third goal* is aspirational and focuses on developing a set of tools to derive common quantifiable parameters to enable rapid kinetic and computational modeling, considering both the adapting thermodynamic states of catalysts and reactants.

**FWP 47319: Advancing key catalytic reaction steps for achieving carbon neutrality**

**PI:** Johannes Lercher

**Co-PIs:** Aaron M. Appel, Liney Arnadottir (Oregon State U.), David A. Dixon (U. Alabama), Zdenek Dohnalek, John L. Fulton, Bojana Ginovska, Jian Zi Hu, Abhi J. Karkamkar, Bruce D. Kay, Konstantin Khivantsev, Sungmin Kim, Greg A. Kimmel, Libor Kovarik, ThuyThanh D. Le, Mal Soon Lee, Johannes A. Lercher, John C. Linehan, Zbynek Novotny, Simone Raugei, Udishnu Sanyal, Gregory K. Schenter, Wendy J. Shaw, Honghong Shi, Janos Szanyi, Ba L. Tran, Huamin Wang, Yong Wang, Nancy M. Washton, Eric S. Wiedner

## RECENT PROGRESS

***Insights into acetic acid binding and ketene formation on anatase.*** Understanding the adsorption and reactivity of carboxylic acids on oxide surfaces is of great interest in catalysis for biomass upgrading via ketonization, a carbon-carbon coupling reaction. Formate, the simplest carboxylate, is one of the key intermediates in $CO_2$ hydrogenation. We investigated acetic acid[1] adsorption and reaction on anatase $TiO_2$(101) using scanning tunneling microscopy (STM), infrared reflection-absorption spectroscopy (IRRAS), temperature-programmed desorption (TPD), and density functional theory (DFT) calculations. In the studies of acetic acid, we identified two surface intermediates: (1) dissociated, bidentate acetate with an associated bridging hydroxyl, and (2) molecular, monodentate acetic acid (Figure 1). Hydroxyl species play a critical role in the diffusion of acetate species, as established by AIMD simulations of propanol dimer and trimer formation and MD (TD-DFT) XANES spectra simulations, which show how changes in the pre-edge are related to changes in the symmetry of the Al T-site due to the propanol interactions. The coexistence of ordered phases with increasing monolayer (ML) saturation coverages consisting of (1) pure acetate (0.5 ML), (2) mixed acetate/acetic acid (0.67 ML), (3) mixed acetate/acetic acid (1.0 ML), and (4) pure acetic acid demonstrates similar energetics for both acetate and acetic acid species.

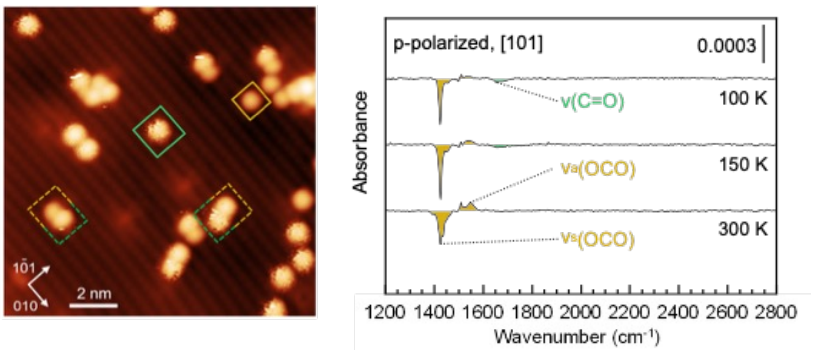


Figure 1. Left: STM images after the adsorption of 0.04 ML of acetic acid on anatase $TiO_2$(101) at 80 K. Isolated and paired features are observed due to a mixture of monomers and hydrogen-bonded dimers in the gas phase. Smooth (orange) species are assigned to bidentate acetate and fuzzy (green) molecularly bound acetic acid. Right: P-polarized IRRAS spectra from 0.27 ML of $CD_3COOD$ adsorbed on anatase $TiO_2$(101) at 100 K exhibit vibrational signatures of both deprotonated acetate (orange) and molecularly bound acetic acid (green).

Under ultra-high-vacuum conditions, monodentate acetic acid and bidentate acetate were observed below room temperature, while only bidentate acetate was observed up to 575 K. The deprotonation of acetic acid produces water at 280 K. In contrast, further decomposition of bidentate acetate produces ketene and acetic acid at 645 K. This model study provided insight into the stability and reactivity of carboxylic acid surface-bound intermediates, relevant to ketonization for biomass upgrading.

***$ZnO_x$ on $TiO_2$: Effects of $TiO_2$ facets on catalytic activity of acetone to isobutene.*** C-C coupling of carbonyl compounds cooperated with self-deoxygenation form chemicals with more carbon and fewer oxygen atoms, which provides a strategy for increasing energy density in upgrading abundant biomass-derived feedstocks. Catalysts, such as $Zn_xTi_yO_z$ and $Zn_xZr_yO_z$, with balanced Lewis acidity and basicity from the close interaction of Zn and Ti or Zr sites, are well suited for efficient conversion of oxygenates, such as acetone, to hydrocarbons, such as isobutene. However, these mixed metal oxides present a high degree of structural heterogeneity, making it difficult to study the nature of active sites at the molecular level. Here, we leverage our well-defined faceted $TiO_2$ nanocrystals with further addition of second metal oxides that have well-controlled structures to determine mechanistic aspects in deoxygenation and C-C coupling reactions. Specifically,

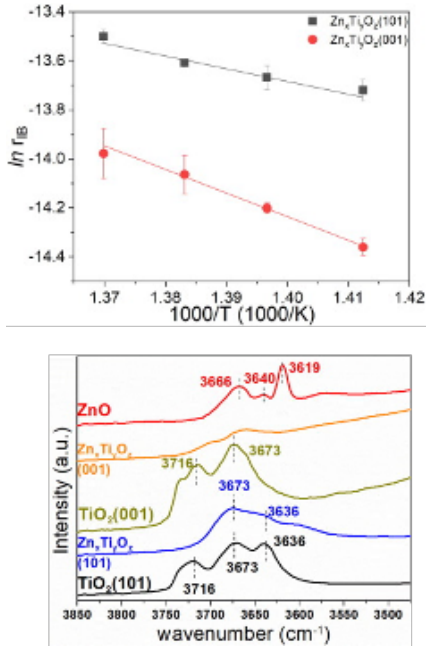


Figure 2. (a) Temperature dependence of measured isobutene formation rate over $Zn_xTi_yO_z$ catalysts. (b) DRIFTS-OH of $TiO_2$, $Zn_xTi_yO_z$, and ZnO.

anatase $TiO_2$(101) and (001) were synthesized and $Zn_xTi_yO_z$ samples with uniformly dispersed $ZnO_x$ were prepared by liquid-phase chemical grafting. The obtained materials were evaluated for acetone-to-isobutene reactions and characterized for their physicochemical properties. It was found (Figure 2) that over $TiO_2$(001), both terminal and bridging hydroxyls were readily titrated by Zn deposition, whereas a substantial number of bridging hydroxyls on $TiO_2$(101) remained. Although a dominant Zn-O-terminated surface was obtained on two $Zn_xTi_yO_z$ samples, bridging hydroxyls with greater H–D exchange reactivity were observed on $Zn_xTi_yO_z$(101) compared with $Zn_xTi_yO_z$(001). The bridging hydroxyls showing rapid proton transfer efficiently stabilize a transition state of diacetone alcohol intramolecular rearrangement for isobutene production as opposed to diacetone alcohol dehydration.

***Tuning the coordination environment of single atoms: the effects of bulk and surface Mo doping on $CO_2$ hydrogenation over Pd/anatase-$TiO_2$.*** We investigated how doping anatase $TiO_2$ with Mo affects supported Pd catalysts, differentiating the roles of bulk and surface Mo species. Mo was either added to the hydrolysis solution (to form $TiO_2$) or impregnated onto $TiO_2$ in a second step. For the former, most Mo atoms are expected to be in the $TiO_2$ bulk and for the latter, most Mo are expected to stay on the $TiO_2$ surface. The CO production (rWGS) rate (left panel of Figure 3) per total Pd increases with bulk Mo (red) concentration until 0.8 wt% and then decreases. In contrast, surface Mo (blue) doping does not significantly alter the rWGS rate. STEM images reveal that the average size of Pd particles on bulk Mo-doped $TiO_2$ is smaller than the ones on non-doped Pd/$TiO_2$. As a result, the former has a two-fold fraction of peripheral active sites, accounting for the two-fold per-total-Pd rWGS rate.

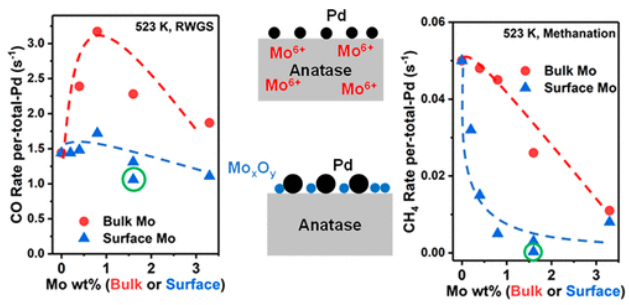


Figure 3. Effects of Mo doping on anatase $TiO_2$ on the kinetics of $CO_2$ hydrogenation over supported 2% Pd at 250 °C. Variations in the per-total-Pd CO (rWGS) (left) and $CH_4$ (methanation) (right) production rates with Mo concentration.

The $CH_4$ production (right panel of Figure 3) rate per total Pd decreases significantly with increasing Mo concentration. This effect is more prominent with surface than bulk Mo, implying that it is a short-range effect. The results of our combined kinetic and spectroscopy (FTIR, XAS, XPS) data demonstrated two effects of Mo doping on Pd/$TiO_2$ catalysts: (1) an electronic effect related to increased electron density on Pd, which weakens *CO and *H adsorption and thus suppresses $CO_2$ methanation, and (2) a structural effect related to increased Pd dispersion, which increases the fraction of peripheral Pd sites and thus promotes the rWGS. The higher surface reducibility is expected to facilitate cleavage of the Pd–O interface, thus creating

the active form of peripheral sites under reaction conditions. The ability of bulk $Mo^{6+}$ substitution to help maintain Pd dispersion enhances catalyst stability.

***Atomistically defined sulfide clusters in zeolites as active centers for alkene hydrogenation.***

Supercages of faujasite-type zeolites serve as robust scaffolds for stabilizing dinuclear ($Mo_2S_4$) and tetranuclear ($Mo_4S_4$) molybdenum sulfide clusters. Both clusters have one unpaired electron per Mo atom and show identical catalytic activity per sulfide cluster. The clusters bind hydrogen as hydride on Mo atoms. Introducing $Ni^{2+}$ and $Co^{2+}$ into the zeolite matrix led to a new type of dimeric cluster (Figure 4). The activation of $H_2$ is strongly influenced by the presence of the second transition metal. Unlike monometallic $Mo_2S_4$ clusters, the bimetallic transition metal sulfide clusters bind hydrogen as –SH groups on the bridging sulfur atoms. DFT calculations also show that the formation of –SH via dissociative adsorption of $H_2$ is thermodynamically and kinetically favorable in the bimetallic clusters. Ethene hydrogenation is concluded to proceed via an Eley-Rideal type mechanism, wherein physisorbed ethene reacts with the dissociatively adsorbed hydrogen to form ethane. While maintaining the apparent activation energy, the overall turnover frequency of ethene hydrogenation is at least three times higher on the bimetallic clusters. This higher rate is attributed to the heterolytic $H_2$ adsorption and the associated higher concentration of H*.

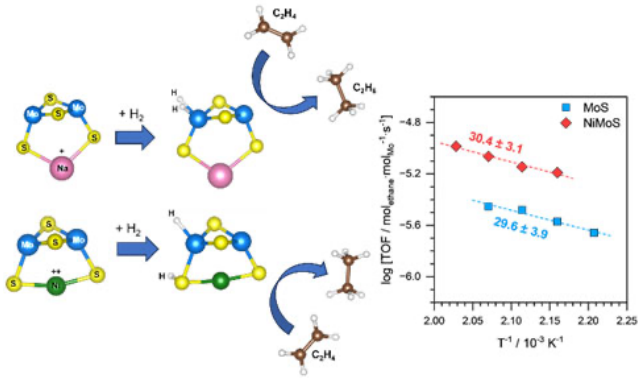


Figure 4. A schematic representation of dissociative adsorption of $H_2$ on (a) monometallic MoS as hydrides and (b) bimetallic NiMoS forming –SH groups, followed by hydrogenation of ethene to ethane. (b) Arrhenius plots on representative MoS and NiMoS catalysts. The dashed lines are linear fits, and the reported numbers are apparent activation energies in $kJ \cdot mol^{-1}$.

***Controlling nuclearity and geometry at Cu(I) active sites for unactivated alkene hydrogenation.***

We incorporated proximal and remote steric bulk for the isolation of an elusive CuH monomer in our effort for rational design of monodentate *N*-heterocyclic carbene (NHC). Detailed QM/MM simulations have been performed to understand the role of steric properties of the NHC ligands on short-distance contacts and solvation to disfavor $Cu_2H_2$ dimer formation. The linear (NHC)CuH monomer can insert unactivated cyclic internal alkenes, and the linear Cu-alkyl complexes do not undergo hydrogenolysis to regenerate CuH (Figure 5). We have now achieved reactivity with $H_2$ at a trigonal planar Cu-alkyl complex supported by a newly designed biscarbene ligand, retaining similar proximal and remote steric bulk, to release cyclopentyl and regenerate the Cu-H species (Figure 5). These observations have led to

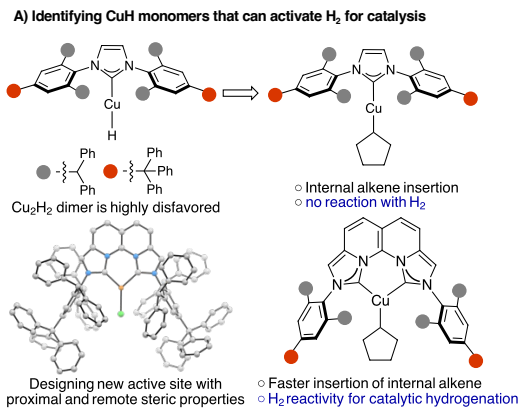


Figure 5. Designing new ligands that contain proximal and remote steric bulk to control nuclearity for isolating transient Cu-H monomers. The resulting linear and trigonal planar Cu(I)-alkyl complexes, from alkene insertion into the Cu-H bond, display unexpected contrast toward $H_2$ for catalytic alkene hydrogenation.

preliminary studies of CuH-catalyzed hydrogenation of unactivated terminal and internal alkenes.

***Impact of charge both adjacent to and remote from the active site on the reactivity.*** Previous work showed that positioning a positive charge in the protein scaffold close to the active site of $[Rh(P^{Et}_2N^{gly}P^{Et}_2)_2]^+$ in an artificial enzyme could enhance the catalytic activity. We continue to investigate the mechanistic effect of charge on the catalytic activity by introducing negatively charged residues in the secondary and outer coordination spheres. We found that placing a negative charge in the secondary or outer coordination sphere can reduce the activity by as much as two times. Adding a positive charge to the negatively charged variants in the secondary coordination sphere restores the catalytic activity, negating the effect of the negative charge (Figure 6). Using vibrational and NMR spectroscopy, we observed minimal changes in the electronic density at the rhodium center of a series of either positive or negatively charged functional groups in the secondary sphere (Figure 6, inset). These data demonstrate that the enhancement in the catalytic activity is likely not due to modulation of the electronic structure, and the interdependence of the positive and negative charges is more consistent with a role such as $CO_2$ positioning.

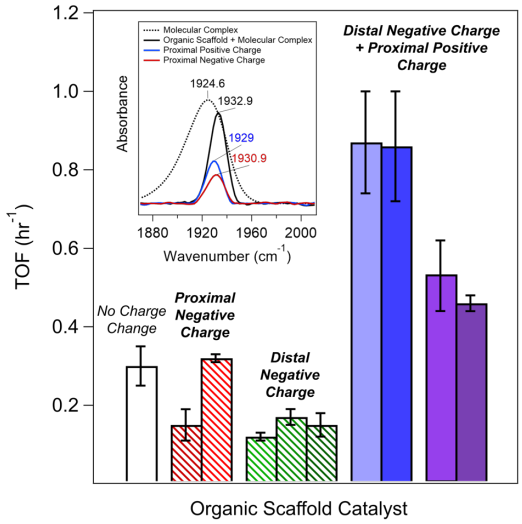


Figure 6. Negatively charged functional groups in the secondary or outer coordination spheres for the hydrogenation of $CO_2$ to formate can slow activity, as hypothesized. (Inset) Fourier transform IR spectra for a series of variants with negative or positive charge indicate that the electronic properties at the metal stay the same.

***Ionic environment in zeolite pores enhancing the reactivity for the C–O elimination reaction in alcohol dehydration.*** The strongly ionic environment in zeolite crystallites, arising from hydrated hydronium ions and the negatively charged aluminum tetrahedra, stabilizes the cationic transition state, thereby decreasing the reaction barrier and enhancing the reaction rate. The ionic strength influences the reaction rate in the dehydration of substituted cyclic alcohols of 4-methylcyclohexanol and cis-2-methylcyclohexanol following the E1 (stepwise) and E2 (concerted) C–O elimination mechanisms (Figure 7). The dehydration rate responds to the ionic strength and is independent of the C–O elimination mechanism. The strong repulsions when the void space between neighboring hydronium ions falls below the critical distance of 0.4 nm for H-MFI leads to the reorganization of the ion pairs in the pore, leading to a volcano-like variation in the reaction rate versus the ionic strength. We conclude that the negative impact of a high density of hydrated hydronium ions results

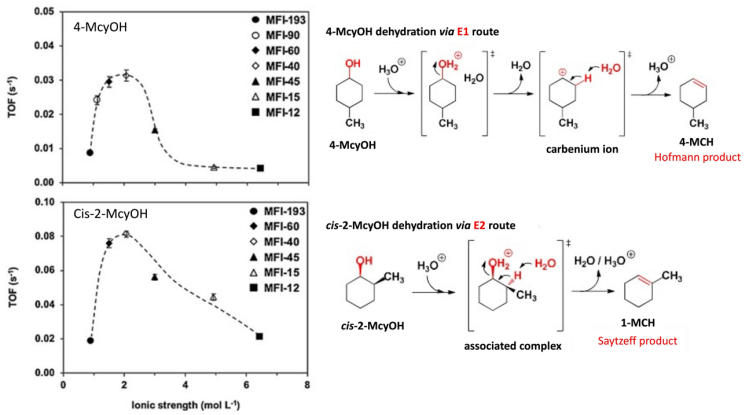


Figure 7. Dehydration mechanisms of 4-methylcyclohexanol (E1, stepwise) and cis-2-methylcyclohexanol (E2, concerted), and the turnover frequency of dehydration as a function of the ionic strength.

from the required local reorganization and the enhanced charge separation.

***Effects of the open-circuit potential (OCP) and $H_3O^+$ at the metal surface and outer Helmholtz plane on free-energy barrier for hydrogenolysis.***

The OCP established by the quasi-equilibrated electrode reaction of $H_2$ and hydrated $H_3O^+$ has significant effect on reactivity. For the hydrogenolysis of benzylic alcohol on Pd/C, the reaction follows a pathway of protonated benzyl alcohol dehydration to a benzylic carbenium ion, followed by a hydride addition to form toluene. The dehydration of protonated benzyl alcohol is kinetically relevant, as it is enhanced at a lower pH, i.e., the hydrogenolysis rate increases by 2–3 orders of magnitude as the pH decreases from 7 to 0.6. The OCP stabilizes all cationic species in the elementary steps. The initial state (benzyl alcohol oxonium ion) is less stabilized than the dehydration transition state and the product (benzylic carbenium), thus lowering the free-energy barrier of the rate-determining step (Figure 8).

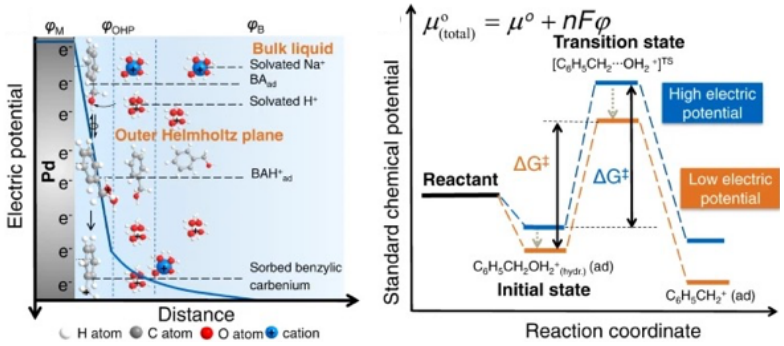


Figure 8. The reaction steps of benzyl alcohol hydrogenolysis between the Pd surface and the Helmholtz plane with the potential profiles as a function of distance from the Pd surface. Standard chemical potential profiles of the initial and transition states under low and high electric potentials.

***Development of realistic computational slab models for complex oxides.***

Oxides containing ferromagnetic elements, such as Fe, Ni, and Co, present unique challenges in modeling metal oxide surfaces, and are attracting a growing interest for their potential application to catalytic processes with improved performance. We investigated computational $Fe_3O_4$ slab structures based on experimental structures, proposed computational models, and developed a strategic slab relaxation procedure to identify a stable minima. The slab configuration dictates the overall slab dipoles and the effect of the total slab multiplicity, all of which affect the surface energetics, electron structure, active site, and, predicted reactivity. Figure 9 shows three different slab configurations for reconstructed $Fe_3O_4$ surfaces: tetrahedral and octahedral termination from previous work and our proposed symmetric configuration. In our calculations, the symmetric slab structure has the lowest dipole moment but could require more oxide layers to describe the bulk structure between the two surfaces properly. The method of obtaining these slab structures affects both the total energy and stability, but minor relaxations can significantly affect the total energy of the system, leading to misleading trends in reactivity.

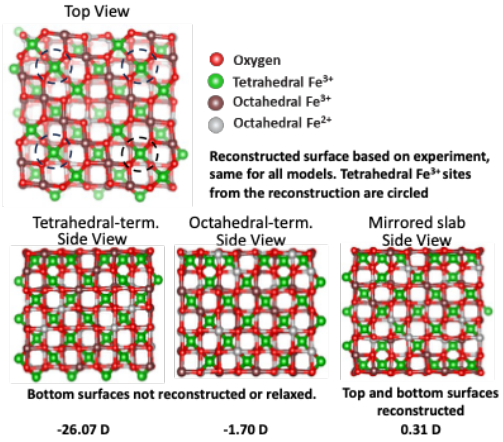


Figure 9. Three different minima slab configurations for a reconstructed $Fe_3O_4$ surface and their dipole moments in the Z-direction. The octahedral-terminated and mirrored slabs have lower dipole moments in the Z-direction.

**Publications Acknowledging this Grant in 2021-2024**

## *Intellectually led by this grant*

### 2021


1. Allec, S. I.; Nguyen, M. T.; Rousseau, R.; Glezakou, V. A., The Role of Sub-Surface Hydrogen on $Co_2$ Reduction and Dynamics on Ni(110): An Ab Initio Molecular Dynamics Study. *J. Chem. Phys.* **2021**, *155*, 044702. http://dx.doi.org/10.1063/5.0048894
2. Chen, F.; Shetty, M.; Wang, M.; Shi, H.; Liu, Y. S.; Camaioni, D. M.; Gutierrez, O. Y.; Lercher, J. A., Differences in Mechanism and Rate of Zeolite-Catalyzed Cyclohexanol Dehydration in Apolar and Aqueous Phase. *ACS Catal.* **2021**, *11*, 2879-2888. http://dx.doi.org/10.1021/acscatal.0c05674
3. Chen, L.; Kovarik, L.; Szanyi, J., Temperature-Dependent Communication between $Pt/Al_2o_3$ Catalysts and Anatase $Tio_2$ Dilutant: The Effects of Metal Migration and Carbon Transfer on the Reverse Water–Gas Shift Reaction. *ACS Catal.* **2021**, *11*, 12058-12067. http://dx.doi.org/10.1021/acscatal.1c03133
4. Chen, L.; Smith, R. S.; Kay, B. D.; Dohnalek, Z., Formation of Gas-Phase Allyl Radicals from Glycerol on Rutile $Tio_2$(110). *J. Phys. Chem. C* **2021**, *125*, 7227-7239. http://dx.doi.org/10.1021/acs.jpcc.1c00991
5. Chen, L.; Unocic, R. R.; Hoffman, A. S.; Hong, J.; Braga, A. H.; Bao, Z.; Bare, S. R.; Szanyi, J., Unlocking the Catalytic Potential of $Tio_2$-Supported Pt Single Atoms for the Reverse Water–Gas Shift Reaction by Altering Their Chemical Environment. *JACS Au* **2021**. http://dx.doi.org/10.1021/jacsau.1c00111
6. Doudin, N.; Collinge, G.; Gurunathan, P. K.; Lee, M.-S.; Glezakou, V.-A.; Rousseau, R.; Dohnálek, Z., Creating Self-Assembled Arrays of Mono-Oxo $(Moo_3)_1$ Species on $Tio_2$(101) Via Deposition and Decomposition of $(Moo_3)_N$ Oligomers. *Proc. Natl. Acad. Sci. U.S.A.* **2021**, *118*, e2017703118. http://dx.doi.org/10.1073/pnas.2017703118
7. Doudin, N.; Collinge, G.; Persaud, R. R.; Gurunathan, P. K.; Lee, M.-S.; Glezakou, V. A.; Dixon, D. A.; Rousseau, R.; Dohnalek, Z., Binding and Stability of Mgo Monomers on Anatase $Tio_2$(101). *J. Chem. Phys.* **2021**, *154*, 204703. http://dx.doi.org/10.1063/5.0047521
8. Grifoni, E.; Piccini, G.; Lercher, J. A.; Glezakou, V.-A.; Rousseau, R.; Parrinello, M., Confinement Effects and Acid Strength in Zeolites. *Nat. Commun.* **2021**, *12*, 2630. http://dx.doi.org/10.1038/s41467-021-22936-0
9. Jaegers, N. R.; Wang, Y.; Hu, J. Z.; Wachs, I. E., Impact of Hydration on Supported $V_2o_5/Tio_2$ Catalysts as Explored by Magnetic Resonance Spectroscopy. *J. Phys. Chem. C* **2021**, *125*, 16766-16775. http://dx.doi.org/10.1021/acs.jpcc.1c04150
10. Khivantsev, K.; Jaegers, N. R.; Kwak, J.-H.; Szanyi, J.; Kovarik, L., Precise Identification and Characterization of Catalytically Active Sites on the Surface of Γ-Alumina. *Angew. Chem. Int. Ed.* **2021**, *60*, 17522-17530. http://dx.doi.org/10.1002/anie.202102106
11. Kovarik, L.; Bowden, M.; Szanyi, J., High Temperature Transition Aluminas in Δ-$Al_2o_3$/Θ-$Al_2o_3$ Stability Range: Review. *J. Catal.* **2021**, *393*, 357-368. http://dx.doi.org/https://doi.org/10.1016/j.jcat.2020.10.009
12. Laureanti, J. A.; Su, Q.; Shaw, W. J., A Protein Scaffold Enables Hydrogen Evolution for a Ni-Bisdiphosphine Complex. *Dalton Trans.* **2021**, *50*, 15754-15759. http://dx.doi.org/10.1039/D1DT03295J

13. Lee, I.; Lee, M.-S.; Tao, L.; Ikuno, T.; Khare, R.; Jentys, A.; Huthwelker, T.; Borca, C. N.; Kalinko, A.; Gutiérrez, O. Y.; Govind, N.; Fulton, J. L.; Hu, J. Z.; Glezakou, V.-A.; Rousseau, R.; Sanchez-Sanchez, M.; Lercher, J. A., Activity of Cu–Al–Oxo Extra-Framework Clusters for Selective Methane Oxidation on Cu-Exchanged Zeolites. *JACS Au* **2021**, *1*, 1412-1421. http://dx.doi.org/10.1021/jacsau.1c00196
14. Lin, F.; Wang, H.; Zhao, Y.; Fu, J.; Mei, D.; Jaegers, N. R.; Gao, F.; Wang, Y., Elucidation of Active Sites in Aldol Condensation of Acetone over Single-Facet Dominant Anatase Tio2 (101) and (001) Catalysts. *JACS Au* **2021**, *1*, 41-52. http://dx.doi.org/10.1021/jacsau.0c00028
15. Liu, Y.; Cheng, G.; Baráth, E.; Shi, H.; Lercher, J. A., Alkylation of Lignin-Derived Aromatic Oxygenates with Cyclic Alcohols on Acidic Zeolites. *Appl. Catal. B* **2021**, *281*, 119424. http://dx.doi.org/10.1016/j.apcatb.2020.119424
16. Lu, Y.; Zhang, Z.; Wang, H.; Wang, Y., Toward Efficient Single-Atom Catalysts for Renewable Fuels and Chemicals Production from Biomass and $Co_2$. *Appl. Catal. B: Environ.* **2021**, *292*, 120162. http://dx.doi.org/10.1016/j.apcatb.2021.120162
17. Mayberry, D. D.; Linehan, J. C.; Appel, A. M., Designing Catalytic Systems Using Binary Solvent Mixtures: Impact of Mole Fraction of Water on Hydride Transfer. *lnorg. Chem.* **2021**, *60*, 17132-17140. http://dx.doi.org/10.1021/acs.inorgchem.1c02397
18. Milaković, L.; Hintermeier, P. H.; Liu, Y.; Baráth, E.; Lercher, J. A., Influence of Intracrystalline Ionic Strength in Mfi Zeolites on Aqueous Phase Dehydration of Methylcyclohexanols. *Angew. Chem. Int. Ed.* **2021**, *60*, 1-6. http://dx.doi.org/10.1002/anie.202107947
19. Peng, G.; Xu, L.; Glezakou, V.-A.; Mavrikakis, M., Mechanism of Methanol Synthesis on Ni(110). *Catal. Sci. Technol.* **2021**, *11*, 3279-3294. http://dx.doi.org/10.1039/D1CY00107H
20. Persaud, R. R.; Fang, Z.; Zall, C. M.; Appel, A. M.; Dixon, D. A., Computational Study of Triphosphine-Ligated Cu(I) Catalysts for Hydrogenation of $Co_2$ to Formate. *J. Phys. Chem. A* **2021**, *125*, 6600-6610. http://dx.doi.org/10.1021/acs.jpca.1c04050
21. Speelman, A. L.; Tran, B. L.; Erickson, J. D.; Vasiliu, M.; Dixon, D. A.; Bullock, R. M., Accelerating the Insertion Reactions of (Nhc)Cu–H Via Remote Ligand Functionalization. *Chem. Sci. J.* **2021**, *12*, 11495-11505. http://dx.doi.org/10.1039/D1SC01911B
22. Sudduth, B.; Yun, D. M.; Sun, J. M.; Wang, Y., Facet-Dependent Selectivity of $Ceo_2$ Nanoparticles in 2-Propanol Conversion. *J. Catal.* **2021**, *404*, 96-108. http://dx.doi.org/10.1016/j.jcat.2021.09.009
23. Wiedner, E. S.; Preston, A. Z.; Helm, M. L.; Appel, A. M., Thermodynamic Trends for Reduction of Co by Molecular Complexes. *Organometallics* **2021**, *40*, 2039-2050. http://dx.doi.org/10.1021/acs.organomet.1c00178
24. Wu, Y.; Gao, F.; Wang, H.; Kovarik, L.; Sudduth, B.; Wang, Y., Probing Acid–Base Properties of Anatase Tio2 Nanoparticles with Dominant {001} and {101} Facets Using Methanol Chemisorption and Surface Reactions. *J. Phys. Chem. C* **2021**, *125*, 3988-4000. http://dx.doi.org/10.1021/acs.jpcc.0c11107
25. Xin, H.; Liu, Y.; Hu, C.; Lercher, J. A., Electronic Impact of $Ni_2p$ Nanoparticle Size on Hydrogenation Rates. *J. Catal.* **2021**, *401*, 129-136. http://dx.doi.org/10.1016/j.jcat.2021.07.017
26. Xu, S.; Jaegers, N. R.; Hu, W.; Kwak, J. H.; Bao, X.; Sun, J.; Wang, Y.; Hu, J. Z., High-Field One-Dimensional and Two-Dimensional $^{27}$al Magic-Angle Spinning Nuclear Magnetic Resonance Study of Θ-, Δ-, and Γ-$Al_2o_3$ Dominated Aluminum Oxides: Toward Understanding

the Al Sites in Γ-$Al_2o_3$. *ACS Omega* **2021**, *6*, 4090-4099. http://dx.doi.org/10.1021/acsomega.0c06163
27. Yang, G.; Maliekkal, V.; Chen, X.; Eckstein, S.; Shi, H.; Camaioni, D. M.; Baráth, E.; Haller, G. L.; Liu, Y.; Neurock, M.; Lercher, J. A., Rate Enhancement of Phenol Hydrogenation on Pt by Hydronium Ions in the Aqueous Phase. *J. Catal.* **2021**, *404*, 579-593. http://dx.doi.org/10.1016/j.jcat.2021.11.003
28. Yik, E.; Hibbitts, D.; Wang, H.; Iglesia, E., Hydrogenation and Cs Bond Activation Pathways in Thiophene and Tetrahydrothiophene Reactions on Sulfur-Passivated Surfaces of Ru, Pt, and Re Nanoparticles. *Appl. Catal. B: Environ.* **2021**, *291*, 119797. http://dx.doi.org/10.1016/j.apcatb.2020.119797
29. Zhu, Y. F.; Yuk, S. F.; Zheng, J.; Nguyen, M. T.; Lee, M. S.; Szanyi, J.; Kovarik, L.; Zhu, Z. H.; Balasubramanian, M.; Glezakou, V. A.; Fulton, J. L.; Lercher, J. A.; Rousseau, R.; Gutierrez, O. Y., Environment of Metal-O-Fe Bonds Enabling High Activity in $Co_2$ Reduction on Single Metal Atoms and on Supported Nanoparticles. *J. Am. Chem. Soc.* **2021**, *143*, 5540-5549. http://dx.doi.org/10.1021/jacs.1c02276
30. Deng, F.; Huang, J.; Ember, E. E.; Achterhold, K.; Dierolf, M.; Jentys, A.; Liu, Y.; Pfeiffer, F.; Lercher, J. A., On the Mechanism of Catalytic Decarboxylation of Carboxylic Acids on Carbon-Supported Palladium Hydride. *ACS Catal.* **2021**, 14625-14634. http://dx.doi.org/10.1021/acscatal.1c03869
31. Dey, A.; Houle, F. A.; Lubner, C. E.; Sevilla, M.; Shaw, W. J., Introduction to (Photo)Electrocatalysis for Renewable Energy. *Chem. Commun.* **2021**, *57*, 1540-1542. http://dx.doi.org/10.1039/D0CC90530E
32. Giustra, Z. X.; Chen, G.; Vasiliu, M.; Karkamkar, A.; Autrey, T.; Dixon, D. A.; Liu, S.-Y., A Comparison of Hydrogen Release Kinetics from 5- and 6-Membered 1,2-Bn-Cycloalkanes. *RSC Adv.* **2021**, *11*, 34132-34136. http://dx.doi.org/10.1039/D1RA07477F
33. Khivantsev, K.; Jaegers, N. R.; Aleksandrov, H. A.; Kovarik, L.; Derewinski, M. A.; Wang, Y.; Vayssilov, G. N.; Szanyi, J., Biomimetic Co Oxidation Below −100 °C by a Nitrate-Containing Metal-Free Microporous System. *Nat. Commun.* **2021**, *12*, 6033. http://dx.doi.org/10.1038/s41467-021-26157-3
34. Kim, Y.; Collinge, G.; Lee, M.-S.; Khivantsev, K.; Cho, S. J.; Glezakou, V.-A.; Rousseau, R.; Szanyi, J.; Kwak, J. H., Surface Density Dependent Catalytic Activity of Single Palladium Atoms Supported on Ceria. *Angew. Chem. Int. Ed.* **2021**, *60*, 22769-22775. http://dx.doi.org/10.1002/anie.202105750
35. Li, H.; Guo, D.; Ulumuddin, N.; Jaegers, N. R.; Sun, J.; Peng, B.; McEwen, J.-S.; Hu, J.; Wang, Y., Elucidating the Cooperative Roles of Water and Lewis Acid–Base Pairs in Cascade C–C Coupling and Self-Deoxygenation Reactions. *JACS Au* **2021**, *1*, 1471-1487. http://dx.doi.org/10.1021/jacsau.1c00218
36. Petrik, N. G.; Wang, Y.; Wen, B.; Wu, Y.; Ma, R.; Dahal, A.; Gao, F.; Rousseau, R.; Wang, Y.; Kimmel, G. A.; Selloni, A.; Dohnálek, Z., Conversion of Formic Acid on Single- and Nano-Crystalline Anatase $Tio_2$(101). *J. Phys. Chem. C* **2021**, *125*, 7686-7700. http://dx.doi.org/10.1021/acs.jpcc.1c00571
37. Pfriem, N.; Liu, Y.; Zahn, F.; Shi, H.; Haller, G. L.; Lercher, J. A., Impact of the Local Concentration of Hydronium Ions at Tungstate Surfaces for Acid-Catalyzed Alcohol Dehydration. *J. Am. Chem. Soc.* **2021**, *143*, 20133-20143. http://dx.doi.org/10.1021/jacs.1c07203
38. Yao, Y.; Wu, X.; Chen, B.; Tu, Z.; Gutiérrez, O. Y.; Cui, Y.; Wang, J.; Huang, J.; Xu, Y.; Sun, H.; Chen, H.; Yan, Z.; Mei, D.; Zhao, Y.; Lercher, J. A., Copper-Based Catalysts Confined

in Carbon Nanocage Reactors for Condensed Ester Hydrogenation: Tuning Copper Species by Confined $Sio_2$ and Methanol Resistance. *ACS Sustain. Chem. Eng.* **2021**, *9*, 16270-16280. http://dx.doi.org/10.1021/acssuschemeng.1c05526

**2022**

1. Carroll, T. G.; Ryan, D. E.; Erickson, J. D.; Bullock, R. M.; Tran, B. L., Isolation of a Cu–H Monomer Enabled by Remote Steric Substitution of a N-Heterocyclic Carbene Ligand: Stoichiometric Insertion and Catalytic Hydroboration of Internal Alkenes. *J. Am. Chem. Soc.* **2022**, *144*, 13865-13873. http://dx.doi.org/10.1021/jacs.2c05376
2. Chalek, C. L.; Gole, J. L.; Dixon, D. A., Excited Electronic State Cross Sections for Group 3 Halide and Oxide Production: Evaluating Relative Excited-State Quantum Yields. *J. Phys. Chem. A* **2022**, *126*, 3427-3432. http://dx.doi.org/10.1021/acs.jpca.2c01780
3. Confer, M. P.; Qu, T.; Rupar, P. A.; Dixon, D. A., Composite Correlated Molecular Orbital Theory Calculations of Ring Strain for Use in Predicting Polymerization Reactions. *ChemPhysChem* **2022**, *23*, e202200133. http://dx.doi.org/10.1002/cphc.202200133
4. Devore, T. C.; Wang, H.; Winstead, C. B.; Gole, J. L.; Hu, Y.; Dixon, D. A., Electronically Excited Complex Formation in Magnesium Cluster–Halogen Atom Reactions. *J. Phys. Chem. A* **2022**, *126*, 1848-1860. http://dx.doi.org/10.1021/acs.jpca.2c00196
5. Gole, J. L.; Chalek, C. L.; Mason, M. M.; de Melo, G. F.; Vasiliu, M.; Dixon, D. A., Observation of Selectively Populated Monohalide Excited States from the Reactions of Group 3 Metal (Sc, Y, and La) Monomers and Dimers with Halogen-Containing Molecules. *J. Phys. Chem. A* **2022**, *126*, 3403-3426. http://dx.doi.org/10.1021/acs.jpca.2c01779
6. Kadam, S. A.; Hwang, A.; Iglesia, E., Consequences of Intrapore Liquids on Reactivity, Selectivity, and Stability for Aldol Condensation Reactions on Anatase $Tio_2$ Catalysts. *ChemCatChem* **2022**, *14*, e202200059. http://dx.doi.org/10.1002/cctc.202200059
7. Khare, R.; Weindl, R.; Jentys, A.; Reuter, K.; Shi, H.; Lercher, J. A., Di- and Tetrameric Molybdenum Sulfide Clusters Activate and Stabilize Dihydrogen as Hydrides. *J. Am. Chem. Soc.* **2022**, *2*, 613-622. http://dx.doi.org/10.1021/jacsau.1c00507
8. Li, H.; Hurlock, M. J.; Sudduth, B.; Li, J.; Sun, J.; Zhang, Q.; Wang, Y., Acetone to Isobutene Conversion on $Zn_xti_yo_z$: Effects of $Tio_2$ Facet. *J. Catal.* **2022**, *410*, 236-245. http://dx.doi.org/10.1016/j.jcat.2022.03.031
9. Meyer, L. C.; Sanyal, U.; Stoerzinger, K. A.; Koh, K.; Fulton, J. L.; Camaioni, D. M.; Gutierrez, O. Y.; Lercher, J. A., Influence of the Molecular Structure on the Electrocatalytic Hydrogenation of Carbonyl Groups and $H_2$ Evolution on Pd. *ACS Catal.* **2022**, *12*, 11910-11917. http://dx.doi.org/10.1021/acscatal.2c03207
10. Schmid, J.; Wang, M.; Gutiérrez, O. Y.; Bullock, R. M.; Camaioni, D. M.; Lercher, J. A., Controlling Reaction Routes in Noble-Metal-Catalyzed Conversion of Aryl Ethers. *Angew. Chem. Int. Ed.* **2022**, *61*, e202203172. http://dx.doi.org/10.1002/anie.202203172
11. Sharp, M. A.; Lee, C. J.; Mahapatra, M.; Smith, R. S.; Kay, B. D.; Dohnálek, Z., Preparation and Characterization of Model Homotopic Catalysts: Rh Adatoms, Nanoparticles, and Mixed Oxide Surfaces on $Fe_3o_4$(001). *J. Phys. Chem. C* **2022**, *126*, 14448-14459. http://dx.doi.org/10.1021/acs.jpcc.2c03426
12. Sudduth, B.; Sun, J.; Wang, Y., Chemical Grafting of Highly Dispersed $Vox/Ceo_2$ for Increased Catalytic Activity in Methanol Oxidative Dehydrogenation. *Catal. Lett.* **2022**, *152*, 2980-2992. http://dx.doi.org/10.1007/s10562-021-03862-8

13. Tao, L.; Lee, I.; Khare, R.; Jentys, A.; Fulton, J. L.; Sanchez-Sanchez, M.; Lercher, J. A., Speciation of Cu-Oxo Clusters in Ferrierite for Selective Oxidation of Methane to Methanol. *Chem. Mater.* **2022**, *34*, 4355-4363. http://dx.doi.org/10.1021/acs.chemmater.1c04249
14. Vasiliu, M.; Edwards, K. C.; Tapu, D.; Castillo, C. E.; Stein, T. H.; Craciun, R.; Arduengo, A. J.; Dixon, D. A., Bond Dissociation Energies of Carbene–Carbene and Carbene–Main Group Adducts. *J. Phys. Chem. A* **2022**, *126*, 2658-2669. http://dx.doi.org/10.1021/acs.jpca.2c00921
15. Bramley, G. A.; Nguyen, M.-T.; Glezakou, V.-A.; Rousseau, R.; Skylaris, C.-K., Understanding Adsorption of Organics on Pt(111) in the Aqueous Phase: Insights from Dft Based Implicit Solvent and Statistical Thermodynamics Models. *J. Chem. Theory Comput.* **2022**, *18*, 1849-1861. http://dx.doi.org/10.1021/acs.jctc.1c00894
16. Chen, L.; Kovarik, L.; Meira, D.; Szanyi, J., Differentiating and Understanding the Effects of Bulk and Surface Mo Doping on $Co_2$ Hydrogenation over Pd/Anatase-$Tio_2$. *ACS Catal.* **2022**, *12*, 13492-13500. http://dx.doi.org/10.1021/acscatal.2c03181
17. Chen, L.; Meyer, L. C.; Kovarik, L.; Meira, D.; Pereira-Hernandez, X. I.; Shi, H.; Khivantsev, K.; Gutiérrez, O. Y.; Szanyi, J., Disordered, Sub-Nanometer Ru Structures on $Ceo_2$ Are Highly Efficient and Selective Catalysts in Polymer Upcycling by Hydrogenolysis. *ACS Catal.* **2022**, *12*, 4618-4627. http://dx.doi.org/10.1021/acscatal.2c00684
18. Chen, L.; Zhu, Y.; Meyer, L. C.; Hale, L. V.; Le, T. T.; Karkamkar, A.; Lercher, J. A.; Gutiérrez, O. Y.; Szanyi, J., Effect of Reaction Conditions on the Hydrogenolysis of Polypropylene and Polyethylene into Gas and Liquid Alkanes. *React. Chem. Eng.* **2022**, *7*, 844-854. http://dx.doi.org/10.1039/D1RE00431J
19. Cheng, G.; Zhang, W.; Jentys, A.; Ember, E. E.; Gutiérrez, O. Y.; Liu, Y.; Lercher, J. A., Importance of Interface Open Circuit Potential on Aqueous Hydrogenolytic Reduction of Benzyl Alcohol over Pd/C. *Nat. Commun.* **2022**, *13*, 7967. http://dx.doi.org/10.1038/s41467-022-35554-1
20. García-Vargas, C. E.; Collinge, G.; Yun, D.; Lee, M.-S.; Muravev, V.; Su, Y.-Q.; Pereira-Hernández, X. I.; Jiang, D.; Glezakou, V.-A.; Hensen, E. J. M.; Rousseau, R.; Datye, A. K.; Wang, Y., Activation of Lattice and Adatom Oxygen by Highly Stable Ceria-Supported Cu Single Atoms. *ACS Catal.* **2022**, *12*, 13649-13662. http://dx.doi.org/10.1021/acscatal.2c04001
21. Genc, A.; Kovarik, L.; Fraser, H. L., A Deep Learning Approach for Semantic Segmentation of Unbalanced Data in Electron Tomography of Catalytic Materials. *Sci. Rep.* **2022**, *12*, 16267. http://dx.doi.org/10.1038/s41598-022-16429-3
22. Grakovich, P. N.; Allayarov, S. R.; Confer, M. P.; Kalinin, L. A.; Frolov, I. A.; Rudneva, T. N.; Ivanov, L. F.; Dixon, D. A., Infrared Laser Ablation of Poly(Vinylidene Fluoride): The Loss of Hf. *J. Fluorine Chem.* **2022**, *255-256*, 109947. http://dx.doi.org/10.1016/j.jfluchem.2022.109947
23. Hu, W.; Jaegers, N. R.; Winkelman, A. D.; Murali, S.; Mueller, K. T.; Wang, Y.; Hu, J. Z., Modelling Complex Molecular Interactions in Catalytic Materials for Energy Storage and Conversion in Nuclear Magnetic Resonance. *Front. Catal.* **2022**, *2*, 935174. http://dx.doi.org/10.3389/fctls.2022.935174
24. Khivantsev, K.; Jaegers, N. R.; Kovarik, L.; Derewinski, M. A.; Kwak, J. H.; Szanyi, J., On the Nature of Extra-Framework Aluminum Species and Improved Catalytic Properties in Steamed Zeolites. *Molecules* **2022**, *27*, Art. No. 2352. http://dx.doi.org/10.3390/molecules27072352

25. Li, X.; Pereira-Hernandez, X. I.; Chen, Y. Z.; Xu, J.; Zhao, J. K.; Pao, C. W.; Fang, C. Y.; Zeng, J.; Wang, Y.; Gates, B. C.; Liu, J. Y., Functional $Ceo_x$ Nanoglues for Robust Atomically Dispersed Catalysts. *Nature* **2022**, *611*, 284-288. http://dx.doi.org/10.1038/s41586-022-05251-6
26. Makoś, M. Z.; Gurunathan, P. K.; Raugei, S.; Kowalski, K.; Glezakou, V.-A.; Rousseau, R., Modeling Absolute Redox Potentials of Ferrocene in the Condensed Phase. *J. Phys. Chem. Lett.* **2022**, *13*, 10005-10010. http://dx.doi.org/10.1021/acs.jpclett.2c02447
27. Milakovic, L.; Liu, Y.; Barath, E.; Lercher, J. A., Dehydration of Fatty Alcohols on Zirconia Supported Tungstate Catalysts. *Catal. Sci. Technol.* **2022**, *12*, 6084-6091. http://dx.doi.org/10.1039/d2cy00785a
28. Ni, L.; Khare, R.; Bermejo-Deval, R.; Zhao, R.; Tao, L.; Liu, Y.; Lercher, J. A., Highly Active and Selective Sites for Propane Dehydrogenation in Zeolite Ga-Bea. *J. Am. Chem. Soc.* **2022**, *144*, 12347-12356. http://dx.doi.org/10.1021/jacs.2c03810
29. Piccini, G. M.; Lee, M. S.; Yuk, S. F.; Zhang, D. F.; Collinge, G.; Kollias, L.; Nguyen, M. T.; Glezakou, V. A.; Rousseau, R., Ab Initio Molecular Dynamics with Enhanced Sampling in Heterogeneous Catalysis. *Catal. Sci. Technol.* **2022**, *12*, 12-37. http://dx.doi.org/10.1039/d1cy01329g
30. Vij, A.; Wilson, W. W.; Haiges, R.; Edwards, K. C.; Dixon, D. A.; Christe, K. O., Fluoro-Nitrogen Cations. *Angew. Chem. Int. Ed.* **2022**, *61*, e202116565. http://dx.doi.org/https://doi.org/10.1002/anie.202116565
31. Yu, I. K. M.; Deng, F. L.; Chen, X.; Cheng, G. H.; Liu, Y.; Zhang, W.; Lercher, J. A., Impact of Hydronium Ions on the Pd-Catalyzed Furfural Hydrogenation. *Nat. Commun.* **2022**, *13*. http://dx.doi.org/10.1038/s41467-022-34608-8
32. Zhao, R.; Haller, G. L.; Lercher, J. A., Alkene Adsorption and Cracking on Acidic Zeolites – a Gradual Process of Understanding. *Microporous and Mesoporous Mat.* **2022**, *358*, 112390. http://dx.doi.org/10.1016/j.micromeso.2022.112390

**2023**

1. Duda, D. P.; Dixon, D. A., Triphenylphosphine─Closed-Shell Metal Cation Interactions. *J. Phys. Chem. A* **2023**, *127*, 9985-9994. http://dx.doi.org/10.1021/acs.jpca.3c06388
2. Edwards, K. C.; Vasiliu, M.; Maxwell, J. W.; Castillo, C. E.; Marion, D. M.; Craciun, R.; Hall, J. F.; Tapu, D.; Dixon, D. A., Nhc Carbene–Metal Complex Ligand Binding Energies. *J. Phys. Chem. A* **2023**, *127*, 10838-10850. http://dx.doi.org/10.1021/acs.jpca.3c06409
3. Galan, B. R.; Bigelow, J. O.; Dougherty, W. G.; Kassel, W. S.; Hulley, E. B.; Helm, M. L.; Rakowski DuBois, M.; Appel, A. M.; Linehan, J. C., Operando Mechanistic Studies of $Co_2$ Hydrogenation by Ruthenium Complexes Using High-Pressure Nmr Spectroscopy. *ACS Catal.* **2023**, *13*, 15611-15619. http://dx.doi.org/10.1021/acscatal.3c03908
4. Ginovska, B.; Gutiérrez, O. Y.; Karkamkar, A.; Lee, M.-S.; Lercher, J. A.; Liu, Y.; Raugei, S.; Rousseau, R.; Shaw, W. J., Bioinspired Catalyst Design Principles: Progress in Emulating Properties of Enzymes in Synthetic Catalysts. *ACS Catal.* **2023**, *13*, 11883-11901. http://dx.doi.org/10.1021/acscatal.3c00320
5. Gole, J. L.; Dixon, D. A., Supersonically Expanded Sodium Metal-Dilute Halogen Gas Interactions. The Importance of Reaction Populated and Energy Storing Reservoir States and Population Inversion Created Amplification in $Na_2$. *J. Chem. Phys.* **2023**, *159*, 244301. http://dx.doi.org/10.1063/5.0179613

6. Hu, Y.; Fang, Z.; Vasiliu, M.; Dixon, D. A., Computational Study of Dehydration and Dehydrogenation of Ethanol on $(TiO_2)_N$ (N = 2–4) Nanoclusters. *J. Phys. Chem. A* **2023**, *127*, 3614-3624. http://dx.doi.org/10.1021/acs.jpca.3c00776
7. Kim, S.; Jaegers, N. R.; Hu, W.; Hu, J. Z.; Chen, F.; Liu, Q.; Camaioni, D. M.; Derewinski, M. A.; Gutiérrez, O. Y.; Liu, Y.; Lercher, J. A., Impact of the Environment of Bea-Type Zeolites for Sorption of Water and Cyclohexanol. *J. Phys. Chem. C* **2023**, *427*, 23390-23399. http://dx.doi.org/10.1021/acs.jpcc.3c05405
8. Lin, F.; Hu, W.; Jaegers, N. R.; Gao, F.; Hu, J. Z.; Wang, H.; Wang, Y., Elucidation of the Roles of Water on the Reactivity of Surface Intermediates in Carboxylic Acid Ketonization on $TiO_2$. *J. Am. Chem. Soc.* **2023**, *145*, 99-109. http://dx.doi.org/10.1021/jacs.2c08511
9. Liu, Q.; Pfriem, N.; Cheng, G.; Baráth, E.; Liu, Y.; Lercher, J. A., Maximum Impact of Ionic Strength on Acid-Catalyzed Reaction Rates Induced by a Zeolite Microporous Environment. *Angew. Chem. Int. Ed.* **2023**, *62*, e202208693. http://dx.doi.org/10.1002/anie.202208693
10. Ma, R. Z.; O'Connor, C. R.; Collinge, G.; Allec, S. I.; Lee, M. S.; Dohnalek, Z., The Role of Surface Hydroxyls in the Mobility of Carboxylates on Surfaces: Dynamics of Acetate on Anatase $TiO_2$(101). *J. Phys. Chem. Lett.* **2023**, *14*, 2542-2550. http://dx.doi.org/10.1021/acs.jpclett.3c00175
11. O'Connor, C. R.; Ma, R.; Collinge, G.; Lee, M.-S.; Kimmel, G. A.; Dohnálek, Z., Insights into Acetic Acid Binding and Ketene Formation on Anatase $TiO_2$(101). *Top. Catal.* **2023**, *66*, 1087-1101. http://dx.doi.org/10.1007/s11244-023-01828-1
12. Patrick, E. A.; Bowden, M. E.; Erickson, J. D.; Bullock, R. M.; Tran, B. L., Single-Crystal to Single-Crystal Transformations: Stepwise $Co_2$ Insertions into Bridging Hydrides of $[(Nhc)Cuh]_2$ Complexes. *Angew. Chem. Int. Ed.* **2023**, *62*, e202304648. http://dx.doi.org/10.1002/anie.202304648
13. Rupprechter, G.; Dohnalek, Z.; Volpe, A. F., Preface to "from Coadsorption and Catalysis at Solid Surfaces to Liquid-Solid Interfaces in Theory and Experiment, Published in Honor of Professor Robert K. Grasselli, Irsee Ix Symposium Kloster Irsee, Germany 16-19 June 2022 (Irsee Ix)". *Top. Catal.* **2023**, *66*, 1071-1072. http://dx.doi.org/10.1007/s11244-023-01858-9
14. Tian, J.; Collinge, G.; Yuk, S. F.; Lin, J.; Glezakou, V.-A.; Lee, M.-S.; Wang, Y.; Rousseau, R., Dynamically Formed Active Sites on Liquid Boron Oxide for Selective Oxidative Dehydrogenation of Propane. *ACS Catal.* **2023**, *13*, 8219-8236. http://dx.doi.org/10.1021/acscatal.3c01759
15. Tran, B. L.; Erickson, J. D.; Speelman, A. L.; Bullock, R. M., Mechanistic Studies of Carbonyl Allylation Mediated by (Nhc)Cuh: Isoprene Insertion, Allylation, and B-Hydride Elimination. *lnorg. Chem.* **2023**, *62*, 342-352. http://dx.doi.org/10.1021/acs.inorgchem.2c03402
16. Chen, L.; Allec, S. I.; Nguyen, M.-T.; Kovarik, L.; Hoffman, A. S.; Hong, J.; Meira, D.; Shi, H.; Bare, S. R.; Glezakou, V.-A.; Rousseau, R.; Szanyi, J., Dynamic Evolution of Palladium Single Atoms on Anatase Titania Support Determines the Reverse Water–Gas Shift Activity. *J. Am. Chem. Soc.* **2023**, *145*, 10847-10860. http://dx.doi.org/10.1021/jacs.3c02326
17. Chen, L.; Moreira, J. B.; Meyer, L. C.; Szanyi, J., Efficient and Selective Dual-Pathway Polyolefin Hydro-Conversion over Unexpectedly Bifunctional M/$TiO_2$-Anatase Catalysts. *Appl. Catal. B: Environ.* **2023**, *335*, 122897. http://dx.doi.org/10.1016/j.apcatb.2023.122897

18. Jaegers, N.; Washton, N. M.; Wang, Y.; Hu, J. Z. *High-Field Nuclear Magnetic Resonance (Nmr) Spectroscopy* in *Springer Handbook of Advanced Catalyst Characterization*; Wachs, I. E., Bañares, M. A., Eds.; Springer International Publishing: Cham, 2023; pp 757-785.
19. Möbs, M.; Dixon, D. A.; de Melo, G. F.; Vasiliu, M.; Graubner, T.; Christe, K. O.; Kraus, F., The Crucial Role of $Sb_2f_{10}$ in the Chemical Synthesis of $F_2$. *Angew. Chem. Int. Ed.* **2023**, *62*, e202307218. http://dx.doi.org/10.1002/anie.202307218
20. Wang, Y.; Chen, X.; Shi, H.; Lercher, J. A., Catalytic Reforming of Methane with $H_2s$ Via Dynamically Stabilized Sulfur on Transition Metal Oxides and Sulfides. *Nat. Catal.* **2023**, *6*, 204-214. http://dx.doi.org/10.1038/s41929-023-00922-7
21. Zhang, R.; Wang, Y.; Gaspard, P.; Kruse, N., The Oscillating Fischer-Tropsch Reaction. *Science* **2023**, *382*, 99-103. http://dx.doi.org/10.1126/science.adh8463
22. Zhang, Z.; Tian, J.; Lu, Y.; Yang, S.; Jiang, D.; Huang, W.; Li, Y.; Hong, J.; Hoffman, A. S.; Bare, S. R.; Engelhard, M. H.; Datye, A. K.; Wang, Y., Memory-Dictated Dynamics of Single-Atom Pt on $Ceo_2$ for Co Oxidation. *Nat. Commun.* **2023**, *14*, 2664. http://dx.doi.org/10.1038/s41467-023-37776-3
23. Zhao, R.; Khare, R.; Zhang, Y.; Sanchez-Sanchez, M.; Bermejo-Deval, R.; Liu, Y.; Lercher, J. A., Promotion of Adsorptive and Catalytic Properties of Zeolitic Brønsted Acid Sites by Proximal Extra-Framework $Si(Oh)_X$ Groups. *Nat. Catal.* **2023**, *6*, 68-79. http://dx.doi.org/10.1038/s41929-022-00906-z

**2024**

1. Kim, S.; Lee, M.-S.; Camaioni, D. M.; Gutiérrez, O. Y.; Glezakou, V.-A.; Govind, N.; Huthwelker, T.; Zhao, R.; Rousseau, R.; Fulton, J. L.; Lercher, J. A., Self-Organization of 1-Propanol at H-Zsm-5 Brønsted Acid Sites. *JACS Au* **2023**, *3*, 2487-2497. http://dx.doi.org/10.1021/jacsau.3c00259
2. Chen, L.; Meira, D.; Kovarik, L.; Szanyi, J., Hydrogen Spillover Is Regulating Minority Rh1 Active Sites on Tio2 in Room-Temperature Ethylene Hydrogenation. *ACS Catal.* **2024**, *14*, 7369-7380. http://dx.doi.org/10.1021/acscatal.4c00482
3. Chirila, A.; Hu, Y.; Linehan, J. C.; Dixon, D. A.; Wiedner, E. S., Thermodynamic and Kinetic Activity Descriptors for the Catalytic Hydrogenation of Ketones. *J. Am. Chem. Soc.* **2024**, *146*, 6866-6879. http://dx.doi.org/10.1021/jacs.3c13876
4. Dong, Z.; Mukhtar, A.; Ludwig, T.; Akhade, S. A.; Hu, W.; Hu, J. Z.; Grubel, K.; Engelhard, M.; Wood, B. C.; Autrey, T.; Lin, H., Silver-Decorated Palladium on Carbon Catalyst for Enhanced Ammonium Formate Dehydrogenation. *Catalysis Science & Technology* **2024**, *14*, 449-463. http://dx.doi.org/10.1039/D3CY01057K
5. Duda, D. P.; Edwards, K. C.; Dixon, D. A., Phosphine Versus Carbene Metal Interactions: Bond Energies. *Inorg. Chem.* **2024**, *63*, 14525-14538. http://dx.doi.org/10.1021/acs.inorgchem.4c01796
6. Kim, S.; Chen, F.; Camaioni, D. M.; Derewinski, M. A.; Gutiérrez, O. Y.; Liu, Y.; Lercher, J. A., Confined Ionic Environments Tailoring the Reactivity of Molecules in the Micropores of Bea-Type Zeolite. *J. Am. Chem. Soc.* **2024**. http://dx.doi.org/10.1021/jacs.4c03405
7. Kovarik, L.; Bowden, M.; Khivantsev, K.; Kwak, J. H.; Szanyi, J., Structural Complexity of $\Gamma$-$Al_2o_3$: The Nature of Vacancy Ordering and the Structure of Complex Antiphase Boundaries. *Acta Mater.* **2024**, *266*, 119639. http://dx.doi.org/10.1016/j.actamat.2023.119639

8. Lee, C. J.; Sharp, M. A.; Jackson, B. A.; Mahapatra, M.; Raugei, S.; Árnadóttir, L.; Lee, M.-S.; Kay, B. D.; Dohnálek, Z., Dynamic Activation of Single-Atom Catalysts by Reaction Intermediates: Conversion of Formic Acid on Rh/Fe3o4(001). *ACS Catal.* **2024**, 15396-15406. http://dx.doi.org/10.1021/acscatal.4c03582
9. Lu, Y. B.; Lin, F.; Zhang, Z. H.; Thompson, C.; Zhu, Y. F.; Doudin, N.; Kovarik, L.; Vargos, C. E. G.; Jiang, D.; Fulton, J. L.; Wu, Y. Q.; Gao, F.; Dohnalek, Z.; Karim, A. M.; Wang, H. M.; Wang, Y., Enhancing Activity and Stability of Pd-on-Tio<Sub>2</Sub> Single-Atom Catalyst for Low-Temperature Co Oxidation through <I>in Situ</I> Local Environment Tailoring. *J. Am. Chem. Soc.* **2024**, *146*, 28141-28152. http://dx.doi.org/10.1021/jacs.4c07861
10. Tran, B. L.; Erickson, J. D., Insertion Reactions and Structural Studies of $[(Nhc)Cuh]_2$ with Nitrogen-Based Substrates. *Polyhedron* **2024**, *249*, 116811. http://dx.doi.org/10.1016/j.poly.2023.116811
11. Tran, B. L.; Fuller, J. T.; Erickson, J. D.; Ginovska, B.; Raugei, S., Direct Observation of B-Alkynyl Eliminations from Unstrained Propargylic Alkoxide Cu(<Sc>I</Sc>) Complexes by C-C Bond Cleavage. *Chem. Sci. J.* **2024**, 9. http://dx.doi.org/10.1039/d4sc02982h
12. Trevino, R. E.; Fuller, J. T.; Reid, D. J.; Laureanti, J. A.; Ginovska, B.; Linehan, J. C.; Shaw, W. J., Understanding the Role of Negative Charge in the Scaffold of an Artificial Enzyme for $Co_2$ Hydrogenation on Catalysis. *JBIC Journal of Biological Inorganic Chemistry* **2024**, *29*, 625-638. http://dx.doi.org/10.1007/s00775-024-02070-0
13. Zhang, J.; Hu, W.; Li, Y.; Savoy, A.; Sun, J.; Chi, T. Y.; Wang, Y., Advances in the Catalytic Production of Acrylonitrile. *Chem Catal.* **2024**, *4*, 100825. http://dx.doi.org/10.1016/j.checat.2023.100825
14. Zhu, Y.; Luo, R.; Shi, H.; Koh, K.; Kovarik, L.; Fulton, J. L.; Lercher, J. A.; Zhao, Z.-J.; Gong, J.; Gutiérrez, O. Y., Formation of (Rh–Fe)–$Feo_x$ Complex Sites Enables Methanol Synthesis from $Co_2$. *ACS Catal.* **2024**, *14*, 10031-10039. http://dx.doi.org/10.1021/acscatal.4c00339
15. Mahapatra, M.; Sharp, M. A.; Lee, C. J.; Zhu, Y.; Gutiérrez, O. Y.; Kay, B. D.; Dohnálek, Z., The Evolution of Model Rh/Fe3o4(001) Catalysts in Hydrogen Environments. *Surf. Sci.* **2025**, *751*, 122617. http://dx.doi.org/10.1016/j.susc.2024.122617
16. Zhang, J.; Hu, W.; Qian, B.; Li, H.; Sudduth, B.; Engelhard, M.; Zhang, L.; Hu, J.; Sun, J.; Zhang, C.; He, H.; Wang, Y., Tuning Hydrogenation Chemistry of Pd-Based Heterogeneous Catalysts by Introducing Homogeneous-Like Ligands. *Nat. Commun.* **2023**, *14*, 3944. http://dx.doi.org/10.1038/s41467-023-39478-2
17. Aigner, M.; Van Daele, S.; Minoux, D.; Nesterenko, N.; Zhao, R.; Baumgärtl, M.; Khare, R.; Jentys, A.; Schroeder, C.; Sanchez-Sanchez, M.; Lercher, J. A., Direct Methane Utilization through Benzene Dehydroalkylation Catalyzed by $Co^{2+}$ Sites in Zsm-5 Intersections. *J. Catal.* **2024**, *438*, 115686. http://dx.doi.org/10.1016/j.jcat.2024.115686
18. Chen, H.; Iyer, J.; Liu, Y.; Krebs, S.; Deng, F.; Jentys, A.; Searles, D. J.; Haider, M. A.; Khare, R.; Lercher, J. A., Mechanism of Electrocatalytic $H_2$ Evolution, Carbonyl Hydrogenation, and Carbon–Carbon Coupling on Cu. *J. Am. Chem. Soc.* **2024**, *146*, 13949-13961. http://dx.doi.org/10.1021/jacs.4c01911
19. Jang, S.; Gun Oh, D.; Kim, H.; Hyun Kim, K.; Khivantsev, K.; Kovarik, L.; Hun Kwak, J., Controlling the Phase Transformation of Alumina for Enhanced Stability and Catalytic Properties. *Angew. Chem. Int. Ed.* **2024**, *63*, e202400270. http://dx.doi.org/https://doi.org/10.1002/anie.202400270

20. Li, H.; Pang, J.; Hu, W.; Caballero, V.; Sun, J.; Tan, M.; Hu, J. Z.; Ni, Y.; Wang, Y., Confined Dual Lewis Acid Centers for Selective Cascade C–C Coupling and Deoxygenation. *Chem. Sci. J.* **2024**. http://dx.doi.org/10.1039/D3SC06921D
21. Palermo, A. P.; Zhang, S.; Okrut, A.; Schöttle, C.; Grosso-Giordano, N. A.; Runnebaum, R. C.; Edwards, K. C.; Guan, E.; Ertler, D.; Solovyov, A.; Kistler, J. D.; Aydin, C.; Lu, J.; Busygin, I.; Dixon, D. A.; Gates, B. C.; Katz, A., Remotely Bonded Bridging Dioxygen Ligands Enhance Hydrogen Transfer in a Silica-Supported Tetrairidium Cluster Catalyst. *J. Am. Chem. Soc.* **2024**, *146*, 3773-3784. http://dx.doi.org/10.1021/jacs.3c10660
22. Pennington, M.; Edwards, K. C.; Qu, F.; Dixon, D. A.; Rupar, P. A., Detection of the Bict State in a Borafluorene with High Stokes Shift Fluorescence. *Organometallics* **2024**, *43*, 998-1004. http://dx.doi.org/10.1021/acs.organomet.4c00042
23. Shaw, W. J.; Kidder, M. K.; Bare, S. R.; Delferro, M.; Morris, J. R.; Toma, F. M.; Senanayake, S. D.; Autrey, T.; Biddinger, E. J.; Boettcher, S.; Bowden, M. E.; Britt, P. F.; Brown, R. C.; Bullock, R. M.; Chen, J. G.; Daniel, C.; Dorhout, P. K.; Efroymson, R. A.; Gaffney, K. J.; Gagliardi, L.; Harper, A. S.; Heldebrant, D. J.; Luca, O. R.; Lyubovsky, M.; Male, J. L.; Miller, D. J.; Prozorov, T.; Rallo, R.; Rana, R.; Rioux, R. M.; Sadow, A. D.; Schaidle, J. A.; Schulte, L. A.; Tarpeh, W. A.; Vlachos, D. G.; Vogt, B. D.; Weber, R. S.; Yang, J. Y.; Arenholz, E.; Helms, B. A.; Huang, W.; Jordahl, J. L.; Karakaya, C.; Kian, K.; Kothandaraman, J.; Lercher, J.; Liu, P.; Malhotra, D.; Mueller, K. T.; O'Brien, C. P.; Palomino, R. M.; Qi, L.; Rodriguez, J. A.; Rousseau, R.; Russell, J. C.; Sarazen, M. L.; Sholl, D. S.; Smith, E. A.; Stevens, M. B.; Surendranath, Y.; Tassone, C. J.; Tran, B.; Tumas, W.; Walton, K. S., A Us Perspective on Closing the Carbon Cycle to Defossilize Difficult-to-Electrify Segments of Our Economy. *Nat. Rev. Chem.* **2024**, *8*, 376-400. http://dx.doi.org/10.1038/s41570-024-00587-1
24. Wang, Y.; Zhao, W.; Chen, X.; Ji, Y.; Zhu, X.; Chen, X.; Mei, D.; Shi, H.; Lercher, J. A., Methane–$H_2S$ Reforming Catalyzed by Carbon and Metal Sulfide Stabilized Sulfur Dimers. *J. Am. Chem. Soc.* **2024**, *146*, 8630-8640. http://dx.doi.org/10.1021/jacs.4c00738
25. Xie, S.; Wang, C.; Hu, W.; Hu, J. Z.; Wang, Y.; Dong, Z.; Intan, N. N.; Pfaendtner, J.; Lin, H., Chemical Recycling of Post-Consumer Polyester Wastes Using a Tertiary Amine Organocatalyst. *Cell Rep.* **2024**, *5*, 102145. http://dx.doi.org/10.1016/j.xcrp.2024.102145
26. Yuan, Z.; Huang, L.; Liu, Y.; Sun, Y.; Wang, G.; Li, X.; Lercher, J. A.; Zhang, Z., Synergy of Oxygen Vacancies and Base Sites for Transfer Hydrogenation of Nitroarenes on Ceria Nanorods. *Angew. Chem. Int. Ed.* **2024**, *63*, e202317339. http://dx.doi.org/10.1002/anie.202317339

*Jointly funded by this grant and other grants with intellectual leadership by other funding sources*

**2021**


1. Cheng, G. H.; Jentys, A.; Gutierrez, O. Y.; Liu, Y.; Chin, Y. H.; Lercher, J. A., Critical Role of Solvent-Modulated Hydrogen-Binding Strength in the Catalytic Hydrogenation of Benzaldehyde on Palladium. *Nat. Catal.* **2021**, *4*, 976-985. http://dx.doi.org/10.1038/s41929-021-00701-2
2. Chu, Y.; Sanyal, U.; Li, X. S.; Qiu, Y.; Song, M.; Engelhard, M. H.; Davidson, S. D.; Koh, K.; Meyer, L. C.; Zheng, J.; Xie, X.; Li, D.; Liu, J.; Gutiérrez, O. Y.; Wang, Y.; Shao, Y., Tuning Proton Transfer and Catalytic Properties in Triple Junction Nanostructured Catalysts. *Nano Energy* **2021**, *86*, 106046. http://dx.doi.org/https://doi.org/10.1016/j.nanoen.2021.106046
3. Galhardo, T. S.; Braga, A. H.; Arpini, B. H.; Szanyi, J.; Gonçalves, R. V.; Zornio, B. F.; Miranda, C. R.; Rossi, L. M., Optimizing Active Sites for High Co Selectivity During $Co_2$ Hydrogenation over Supported Nickel Catalysts. *J. Am. Chem. Soc.* **2021**, *143*, 4268-4280. http://dx.doi.org/10.1021/jacs.0c12689
4. Hensley, A. J. R.; Collinge, G.; Wang, Y.; McEwen, J. S., Guiding the Design of Oxidation-Resistant Fe-Based Single Atom Alloy Catalysts with Insights from Configurational Space. *J. Chem. Phys.* **2021**, *154*, 174709. http://dx.doi.org/10.1063/5.0048698
5. Lai, J.-K.; Jaegers, N. R.; Lis, B. M.; Guo, M.; Ford, M. E.; Walter, E.; Wang, Y.; Hu, J. Z.; Wachs, I. E., Structure–Activity Relationships of Hydrothermally Aged Titania-Supported Vanadium–Tungsten Oxide Catalysts for Scr of Nox Missions with $Nh_3$. *ACS Catal.* **2021**, *11*, 12096-12111. http://dx.doi.org/10.1021/acscatal.1c02130
6. Lee, C. J.; Sharp, M. A.; Smith, R. S.; Kay, B. D.; Dohnálek, Z., Adsorption of Ethane, Ethene, and Ethyne on Reconstructed $Fe_3O_4$(001). *Surf. Sci.* **2021**, *714*, 121932. http://dx.doi.org/10.1016/j.susc.2021.121932
7. Maluf, N. E. C.; Braga, A. H.; Gothe, M. L.; Borges, L. R.; Alves, G. A. S.; Goncalves, R. V.; Szanyi, J.; Vidinha, P.; Rossi, L. M., Zeolitic-Imidazolate Framework Derived Intermetallic Nickel Zinc Carbide Material as a Selective Catalyst for $Co_2$ to Co Reduction at High Pressure. *Eur. J. Inorg. Chem.* **2021**, *2021*, 4521-4529. http://dx.doi.org/10.1002/ejic.202100530
8. Pfriem, N.; Hintermeier, P. H.; Eckstein, S.; Kim, S.; Liu, Q.; Shi, H.; Milakovic, L.; Liu, Y.; Haller, G. L.; Baráth, E.; Liu, Y.; Lercher, J. A., Role of the Ionic Environment in Enhancing the Activity of Reacting Molecules in Zeolite Pores. *Science* **2021**, *372*, 952-957. http://dx.doi.org/10.1126/science.abh3418
9. Sanyal, U.; Yuk, S. F.; Koh, K.; Lee, M. S.; Stoerzinger, K.; Zhang, D.; Meyer, L. C.; Lopez-Ruiz, J. A.; Karkamkar, A.; Holladay, J. D.; Camaioni, D. M.; Nguyen, M. T.; Glezakou, V. A.; Rousseau, R.; Gutiérrez, O. Y.; Lercher, J. A., Hydrogen Bonding Enhances the Electrochemical Hydrogenation of Benzaldehyde in the Aqueous Phase. *Angew. Chem. Int. Ed.* **2021**, *60*, 290-296. http://dx.doi.org/10.1002/anie.202008178
10. Shaimukhametova, I. F.; Bogdanova, S. A.; Allayarov, S. R.; Dixon, D. A., Influence of Irradiation with Helium Ions on the Surface Properties of Kynar Polyvinylidene Fluoride. *High Energ. Chem.* **2021**, *55*, 502-506. http://dx.doi.org/10.1134/s0018143921060126
11. Shetty, M.; Wang, H.; Chen, F.; Jaegers, N.; Liu, Y.; Camaioni, D. M.; Gutiérrez, O. Y.; Lercher, J. A., Directing the Rate-Enhancement for Hydronium Ion Catalyzed Dehydration Via

Organization of Alkanols in Nanoscopic Confinements. *Angew. Chem. Int. Ed.* **2021**, *60*, 2304-2311. http://dx.doi.org/10.1002/anie.202009835
12. Weindl, R.; Khare, R.; Kovarik, L.; Jentys, A.; Reuter, K.; Shi, H.; Lercher, J. A., Zeolite-Stabilized Di- and Tetranuclear Molybdenum Sulfide Clusters Form Stable Catalytic Hydrogenation Sites. *Angew. Chem. Int. Ed.* **2021**, *60*, 9301-9305. http://dx.doi.org/10.1002/anie.202015769

**2022**

1. Akhade, S. A.; Lee, M.-S.; Meyer, L. C.; Yuk, S. F.; Nguyen, M.-T.; Sanyal, U.; Egbert, J. D.; Gutiérrez, O. Y.; Glezakou, V.-A.; Rousseau, R., Impact of Functional Groups on the Electrocatalytic Hydrogenation of Aromatic Carbonyls to Alcohols. *Catal. Today* **2022**, *397-399*, 63-68. http://dx.doi.org/10.1016/j.cattod.2021.11.047
2. Arpini, B. H.; Braga, A. H.; Borges, L. R.; Vidinha, P.; Gonçalves, R. V.; Szanyi, J.; Rossi, L. M., Tuning $Co_2$ Hydrogenation Selectivity by N-Doped Carbon Coating over Nickel Nanoparticles Supported on $Sio_2$. *ACS Sustain. Chem. Eng.* **2022**, *10*, 2331-2342. http://dx.doi.org/10.1021/acssuschemeng.1c05847
3. Barth, I.; Akinola, J.; Lee, J.; Gutiérrez, O. Y.; Sanyal, U.; Singh, N.; Goldsmith, B. R., Explaining the Structure Sensitivity of Pt and Rh for Aqueous-Phase Hydrogenation of Phenol. *J. Chem. Phys.* **2022**, *156*, 104703. http://dx.doi.org/10.1063/5.0085298
4. Lin, F.; Lu, Y.; Unocic, K. A.; Habas, S. E.; Griffin, M. B.; Schaidle, J. A.; Meyer, H. M.; Wang, Y.; Wang, H., Deactivation by Potassium Accumulation on a Pt/Tio2 Bifunctional Catalyst for Biomass Catalytic Fast Pyrolysis. *ACS Catal.* **2022**, *12*, 465-480. http://dx.doi.org/10.1021/acscatal.1c02368
5. Moore, C.; Zhang, D.; Rousseau, R.; Glezakou, V.-A.; McEwen, J.-S., Determining the Adsorption Energetics of 2,3-Butanediol on $Ruo_2$(110): Coupling First-Principles Calculations with Global Optimizers. *Front. Energy Res.* **2022**, *9*, Art. No. 781001. http://dx.doi.org/10.3389/fenrg.2021.781001
6. Qiu, Y.; Lopez-Ruiz, J. A.; Zhu, G. M.; Engelhard, M. H.; Gutierrez, O. Y.; Holladay, J. D., Electrocatalytic Decarboxylation of Carboxylic Acids over $Ruo_2$ and Pt Nanoparticles. *Appl. Catal. B: Environ* **2022**, *305*, 121060. http://dx.doi.org/10.1016/j.apcatb.2021.121060
7. Wiedner, E. S.; Appel, A. M.; Raugei, S.; Shaw, W. J.; Bullock, R. M., Molecular Catalysts with Diphosphine Ligands Containing Pendant Amines. *Chem. Rev.* **2022**. http://dx.doi.org/10.1021/acs.chemrev.1c01001
8. Xia, G.-J.; Lee, M.-S.; Glezakou, V.-A.; Rousseau, R.; Wang, Y.-G., Diffusion and Surface Segregation of Interstitial Ti Defects Induced by Electronic Metal–Support Interactions on a Au/$Tio_2$ Nanocatalyst. *ACS Catal.* **2022**, *12*, 4455-4464. http://dx.doi.org/10.1021/acscatal.2c00159

**2023**

1. Cardwell, N.; Hensley, A. J. R.; Wang, Y.; McEwen, J.-S., Capturing the Coverage Dependence of Aromatics' Adsorption through Mean-Field Models. *J. Phys. Chem. A* **2023**, *127*, 10693-10700. http://dx.doi.org/10.1021/acs.jpca.3c05456

2. Chaudhary, N.; Onyango, I.; Wang, Y.; McEwen, J.-S., Determining Catalytically Relevant Surfaces through Coverage-Dependent Lattice Gas Models: Carbon Adsorption on Fe(100). *J. Phys. Chem.* **2023**, *127*, 14163-14176. http://dx.doi.org/10.1021/acs.jpcc.3c01761
3. Chen, F.; Kim, S.; Barpaga, D.; Fulton, J. L.; Motkuri, R. K.; Gutiérrez, O. Y.; Camaioni, D. M.; Lercher, J. A., Activity of Brønsted Acid Sites in Uio-66 for Cyclohexanol Dehydration. *Top. Catal.* **2023**, *66*, 1196-1201. http://dx.doi.org/10.1007/s11244-023-01830-7
4. Evans, P. E., Wang, Yang, Sushko, Peter, Dohnalek, Zdenek, Understanding Palladium-Tellurium Cluster Formation on Wte2: From a Kinetically Hindered Distribution to Thermodynamically Controlled Monodispersity. *PNAS Nexus* **2023**, *2*, pgad212. http://dx.doi.org/10.1093/pnasnexus/pgad212
5. Gajardo, J.; Colmenares-Zerpa, J.; Peixoto, A. F.; Silva, D. S. A.; Silva, J. A.; Gispert-Guirado, F.; Llorca, J.; Urquieta-Gonzalez, E. A.; Santos, J. B. O.; Szanyi, J.; Sepúlveda, C.; Álvarez, M. G.; Chimentão, R. J., Revealing the Effects of High Al Loading Incorporation in the Sba-15 Silica Mesoporous Material. *J. Porous Mater.* **2023**, *30*, 1687-1707. http://dx.doi.org/10.1007/s10934-023-01453-z
6. Khivantsev, K.; Derewinski, M. A.; Szanyi, J., Novel and Emerging Concepts Related to Cationic Species in Zeolites: Characterization, Chemistry and Catalysis. *Microporous and Mesoporous Mat.* **2023**, *358*, 112378. http://dx.doi.org/10.1016/j.micromeso.2022.112378
7. Oostrom, M.; Akers, S.; Garrett, N.; Hanson, E.; Shaw, W.; Laureanti, J. A., Classifying Metal-Binding Sites with Neural Networks. *Protein Sci.* **2023**, *32*, e4591. http://dx.doi.org/10.1002/pro.4591
8. Qiu, Y.; Ray, D.; Yan, L.; Li, X.; Song, M.; Engelhard, M. H.; Sun, J.; Lee, M.-S.; Zhang, X.; Nguyen, M.-T.; Glezakou, V.-A.; Wang, Y.; Rousseau, R.; Shao, Y., Proton Relay for the Rate Enhancement of Electrochemical Hydrogen Reactions at Heterogeneous Interfaces. *J. Am. Chem. Soc.* **2023**, *145*, 26016-26027. http://dx.doi.org/10.1021/jacs.3c06398
9. Zhou, J.; Yang, P.; Kots, P. A.; Cohen, M.; Chen, Y.; Quinn, C. M.; de Mello, M. D.; Anibal Boscoboinik, J.; Shaw, W. J.; Caratzoulas, S.; Zheng, W.; Vlachos, D. G., Tuning the Reactivity of Carbon Surfaces with Oxygen-Containing Functional Groups. *Nat. Commun.* **2023**, *14*, 2293. http://dx.doi.org/10.1038/s41467-023-37962-3

**2024**

1. Han, K. S.; Lee, M.-S.; Kim, N.; Choi, D.; Chae, S.; Ryu, J.; Piccini, G.; Rousseau, R.; Thomsen, E. C., Lithium-Ion Hopping Weakens Thermal Stability of Lipf6 Carbonate Electrolytes. *Cell Rep.* **2024**, *5*, 101768. http://dx.doi.org/10.1016/j.xcrp.2023.101768
2. Lin, F.; Li, M. J.; Purdy, S. C.; Zhang, J. Y.; Wang, Y. L.; Kim, S.; Engelhard, M.; Li, Z. L.; Sutton, A. D.; Wang, Y.; Hu, J. Z.; Wang, H. M., Restructuring of the Lewis Acid Sites in Y-Modified Dealuminated Beta-Zeolite by Hydrothermal Treatment. *ACS Catal.* **2024**, *14*, 15250-15264. http://dx.doi.org/10.1021/acscatal.4c04135
3. Nelson, N. C.; Nguyen, J.; Dohnalek, Z.; Prange, M. P., Probing the Local Coordination Environment of Mononuclear Pd Ions Supported on Ceria Using Co Adsorption Infrared Vibrational Spectroscopy. *The Journal of Physical Chemistry C* **2024**. http://dx.doi.org/10.1021/acs.jpcc.4c05702
4. Onyango, I.; Collinge, G.; Wang, Y.; McEwen, J.-S., Distribution Tendencies of Noble Metals on Fe(100) Using Lattice Gas Cluster Expansions. *J. Phys. Chem. C* **2024**. http://dx.doi.org/10.1021/acs.jpcc.4c01402

5. Phipps, C. A.; Zirilli, C. D.; Duff, B. G.; Erickson, J. D.; Karki, S.; Okolocha, C.; Mashuta, M. S.; Buchanan, R. M.; Grapperhaus, C. A., Enhancing Co2 Capture Via Metal–Ligand Cooperativity: Tuning Ligand Basicity and Zn(Ii) Lewis Acidity. *lnorg. Chem.* **2024**, *63*, 9992-10000. http://dx.doi.org/10.1021/acs.inorgchem.4c01159
6. Purdy, S. C.; Collinge, G.; Zhang, J.; Borate, S. N.; Unocic, K. A.; Wu, Q.; Wegener, E. C.; Kropf, A. J.; Samad, N. R.; Yuk, S. F.; Zhang, D.; Habas, S.; Krause, T. R.; Harris, J. W.; Lee, M.-S.; Glezakou, V.-A.; Rousseau, R.; Sutton, A. D.; Li, Z., Dynamic Copper Site Redispersion through Atom Trapping in Zeolite Defects. *J. Am. Chem. Soc.* **2024**, *146*, 8280-8297. http://dx.doi.org/10.1021/jacs.3c13302
7. Resende, K. A.; Zhao, R.; Liu, Y.; Baráth, E.; Lercher, J. A., Impact of Sn Lewis Acid Sites on the Dehydration of Cyclohexanol. *ACS Catal.* **2024**, *14*, 11741-11748. http://dx.doi.org/10.1021/acscatal.4c01608
8. Tan, J. Z.; Ortega, M.; Miller, S. A.; Hullfish, C. W.; Kim, H.; Kim, S.; Hu, W.; Hu, J. Z.; Lercher, J. A.; Koel, B. E.; Sarazen, M. L., Catalytic Consequences of Hierarchical Pore Architectures within Mfi and Fau Zeolites for Polyethylene Conversion. *ACS Catal.* **2024**, *14*, 7536-7552. http://dx.doi.org/10.1021/acscatal.4c01213
9. Zhang, W.; Khare, R.; Kim, S.; Hale, L.; Hu, W.; Yuan, C.; Sheng, Y.; Zhang, P.; Wahl, L.; Mai, J.; Yang, B.; Gutiérrez, O. Y.; Ray, D.; Fulton, J.; Camaioni, D. M.; Hu, J.; Wang, H.; Lee, M.-S.; Lercher, J. A., Active Species in Chloroaluminate Ionic Liquids Catalyzing Low-Temperature Polyolefin Deconstruction. *Nat. Commun.* **2024**, *15*, 5785. http://dx.doi.org/10.1038/s41467-024-49827-4
10. Zhang, W.; Yao, H.; Khare, R.; Zhang, P.; Yang, B.; Hu, W.; Ray, D.; Hu, J.; Camaioni, D. M.; Wang, H.; Kim, S.; Lee, M.-S.; Sarazen, M. L.; Chen, J. G.; Lercher, J., Chloride and Hydride Transfer as Keys to Catalytic Upcycling of Polyethylene into Liquid Alkanes. *Angew. Chem. Int. Ed.* **2024**, e202319580. http://dx.doi.org/10.1002/anie.202319580

Thomas F. Jaramillo

# Insights into the dynamics of electrocatalysts for energy conversion reactions: In-situ and operando techniques to understand activity, selectivity, and durability

Thomas F. Jaramillo, Professor
Department of Chemical Engineering, Stanford University, School of Engineering
Department of Energy Science Engineering, Stanford Doerr School of Sustainability
Photon Science, SLAC National Accelerator Laboratory
Director, SUNCAT Center for Interface Science & Catalysis

## Presentation Abstract

Understanding how electrocatalysts evolve under reaction conditions is key to designing and developing improved systems. This contribution will focus on the dynamics of surface transformations for electrocatalysts for two key energy-conversion reactions, the oxygen reduction reaction (ORR) and the oxygen evolution reaction (OER). The focus will be on non-precious metal catalyst systems based on manganese-antimony mixed metal oxides, sulfides, and nitrides. Upon synthesizing crystalline powder catalysts systematically across a range of compositions, we evaluated their activity and selectivity performance along with durability. Two key methods that will be discussed are in-situ/operando X-ray absorption spectroscopy (XAS) and in-situ/operando inductively coupled plasma – mass spectrometry (ICP-MS). The former provides key insights into how the catalysts evolve during reaction while the latter captures catalyst corrosion and other related durability phenomena. The development of these techniques and their application to non-precious metal electrocatalysts provide new insights into understanding activity, selectivity, and durability.

**Grant or FWP Number: FWP10049**
**SUNCAT Center for Interface Science and Catalysis FWP10049**

**PI:** Thomas F. Jaramillo
**Co-PIs:** Frank Abild-Pedersen, Kirsten Winther, Simon Bare, Zhenan Bao, Michal Bajdich, Matteo Cargnello, Johannes Voss, Stacey Bent, William Tarpeh, Michaela Burke Stevens, Adam Nielander, Adam Hoffman

## RECENT PROGRESS

***Task 1: Catalysis Data Science and Computational Infrastructure***

Current catalyst search or design studies have been highly successful in finding new catalyst leads for a number of reactions based on few simulations on mostly static surfaces. However, it would be strongly desirable if we were able to accurately investigate orders of magnitude more systems in a design study than we currently and to capture the effects of the dynamic evolution of the catalyst on catalytic performance. This will allow us to investigate reaction networks of a more realistic complexity, and in particular to carry out such an analysis over many (thousands to millions) of facet structures and material compositions in parallel. It will also open for the possibility of utilizing a range of more

advanced approaches for calculating free energy contributions to the surface reaction energetics. Such a big-data revolution will soon occur in the computational catalysis field, provided we establish the enabling technologies. This will require a transformation in the way we create and manage simulations, and in the way we featurize the simulations for machine learning purposes. It will transform the way we perform analysis of data and it will deepen the scientific questions that we can address based on simulations. In this Task we aim to lay a foundation for this future - radically more data-rich - computational heterogeneous catalysis and electrocatalysis approach.

In FY2024, we have focused our efforts on model development and benchmarking for predictions on heterogeneous catalytic reactions energies and performance in general. We have developed machine learning models for the prediction of practical supported electrocatalyst performance based on an integration of computational and experimental catalysis data from our database catalysis-hub.org. In collaboration with efforts in fundamental electrocatalysis, new performant ORR catalysts suggested by the models were successfully tested. We extended our work on predicting O and OH adsorption energies on transition metal oxide interfaces from DFT-computed electronic and structural bulk oxide predictors improving predictions across transition metal oxidation states from +2 to +6. We have benchmarked advanced machine learning approaches for the performance on predicting reaction energies and bulk properties of transition metal catalysts. We have furthermore developed models for parasitic, polaron-mediated electron transport in solid-state electrolytes. As contribution to research software for the catalysis community, we have published a new microkinetic modeling code with improved numerical stability and the resulting abilities to deal with more involved reactions models including those involving adsorbate-adsorbate interactions.

***Task 2: Fundamentals of Electrochemistry***

A combined theory and experiment approach is employed to investigate the fundamentals of electrocatalysis. Theory is aimed at understanding the key properties of electrocatalysts (e.g. electronic structure, geometric structure, etc.) that govern performance, e.g. activity, selectivity, and stability. Computational efforts are also focused on the electrolyte and how factors of the solid-liquid interface influence reactivity. Experimental efforts are focused on synthesis, characterization, and evaluations of catalysts, employing a range of electrolytes and reaction conditions, strongly coupled to the theoretical tasks. Fundamental studies identifying active site motifs and mechanisms and establishing kinetics are core to the program. In situ and operando investigations play a key role in understanding the structure and properties of the catalysts under operating conditions. Novel catalyst synthesis routes are also a key feature as is the use of spectroscopy and microscopy techniques for catalyst characterization. A tightly coupled theory-experiment feedback loop for catalyst discovery is one of the main defining features of the effort.

A substantial number of studies in FY2024 were focused on carbon-based catalyst materials. Carbon offers a broad platform for catalyst design and development, both as a catalyst itself with tunable electronic structures by means of heteroatoms (e.g. boron, nitrogen, transition metals, etc.) as well as a high surface area support for transition metal-based nanoparticle catalysts. In highly collaborative efforts, we have systematically

explored computationally and experimentally two-dimensional phthalocyanine dual-site metal-organic framework catalysts for the oxygen reduction reaction (ORR) as well as Ti-based single atoms carbon-based catalysts (SAC MNCs) for Nitrate reduction ($NO_xRR$) and ORR. By synthesizing and exploiting electronic structural changes in these materials by means of single site incorporation of transition metals, we demonstrated how the activity, selectivity, and durability of these catalysts can be tuned. In parallel, we have furthered the synthesis and development of related high-surface area carbon-based materials are presenting new opportunities in catalysis. We are also developing a unified theory of boding of SAC MNCs across the period table and as function of local bonding, metal spin, and local strain effects and its effect on activity and stability.

In complementary fashion, we have also been working on more conventional transition metal alloy-based ORR catalysts: We have also been exploring new fabrication techniques based on physical vapor deposition (PVD) to achieve ultra-low loadings of reduced precious-metal systems for ORR cathodes in fuel cells, based on ionomerless designs. These fundamental studies have led to unprecedented performance in fuel cells and offer exciting opportunities to advance the technology further. Catalyzing water oxidation remains a major effort in fundamental electro catalysis. Studies have largely been directed towards non-precious metal systems, including biogenic catalysts based on manganese as well as high-entropy spinel oxides based on Fe-Ni-Co-Cr-Mn and related mixed metal oxides such as doped spinels. Computational efforts remain essential in the pursuit and understanding of such systems. We have also continued looking into oxidations of organic alternatives to water, e.g. alcohols, to understand the catalyst as a function of reaction under similar applied potentials. Importantly, we have recently integrated fundamental investigations focused on physical and chemical phenomena occurring at the device-level within water electrolyzers aimed at understanding transport processes and controlling the reaction microenvironment. Finally, we have simultaneously been developing advanced techniques and subsequently employing them to advance catalysis research. This includes collaborations with efforts in data science approaches in catalysis to combine theory and experiment to predict new materials, as well as for in-situ and operando investigations of catalysts, including ATR-FTIR, synchrotron-based techniques (e.g. GI-XRD), as well as neutron reflectometry to study key energy conversion reactions at interfaces, particularly involving nitrogen reduction to ammonia. Those insights are providing the important scientific foundations needed to approach the design and development of higher-performance nitrogen-reducing systems ahead.

***Task 3: Fundamentals of Thermal Catalysis***

An understanding of the breaking and making of chemical bonds at a solid surface is the starting point for any fundamental description of reactions at the solid-gas or solid-liquid interface. It is particularly important to understand which properties of the surface determine its chemical activity. The description and understanding of activation energies for elementary surface reactions and how it depends on the evolution of the active site and its surroundings under operation conditions is a prime focus of this task. In addition to activity of catalysts we also focus our attention on the loss of active surface area through either strong metal-support interactions or sintering. The ability to prevent such side-reactions from happening would greatly enhance catalyst lifetimes and increase the

activity/mass ratio significantly. This task is divided into three general areas: 1) Towards site-specific reactivity/selectivity trends, 2) Controlling the dynamic evolution of catalysts, 3) Designing catalysts beyond the binding site.

In FY2024 we have focused a significant effort on controlling activity beyond the local binding site on a Pt catalyst for propane dehydrogenation. This reaction is important in the efficient production of propylene and increasing its activity and selectivity requires detailed engineering of its active site. In this collaborative work between theory and experiment we studied the effect of alloying Pt and Cu using colloidal techniques, combined with characterization, testing, and density functional theory to study how Cu content enhances the activity for propane dehydrogenation at low temperatures. This work has helped further our understanding of the structure-activity relationship and improved knowledge in propane dehydrogenation catalyst development featuring reduced Pt loadings and notable thermal stability for propylene production. Ongoing work focuses on understanding $ZrO_2$ supported Cu catalysts and their inverted systems for the conversion of $CO_2$ and $H_2$. This study has provided great insight into the importance of active site mobility and how it can be manipulated by system inversion. In a purely theoretical work, we have examined the possibility of applying the spatial nature of the calculated electrostatic potential in DFT to describe reactions in heterogeneous catalysis. Because of its subatomic spatial resolution, we can analyze both directionality and confinement effects in surface adsorption. The use of the electrostatic potential when assessing the 3D nature of catalytic sites provides a new avenue in catalyst design.

***Task 4: The Consortium for Operando and Advanced Catalyst Characterization via Electronic Spectroscopy and Structure (Co-Access)***

Co-ACCESS's goals are to i) facilitate catalysis science research at the Stanford Synchrotron Radiation Lightsource (SSRL) through collaboration with user groups across the United States and internationally, ii) to develop hardware and methodologies for performing *in-situ*/*operando* catalysis X-ray experiments, and iii) to use X-ray absorption theory simulations to help understand the complex spectral changes observed due to the dynamic nature of working catalysts. Through these goals the Co-ACCESS members can assist researchers perform *in-situ/operando* thermal and electro heterogeneous catalysis X-ray absorption spectroscopy experiments. These collaborations can be as simple as supplying equipment to an established user group to helping a new experimentalist from obtaining beamtime, experimental design and data collection, to data analysis and manuscript preparation. Based upon the current performance of the Co-ACCESS program at SSRL, SSRL in collaboration with Co-ACCESS has begun the construction of a Catalysis-centric characterization beamline, 10-2ES2, to centralize the majority of *in-situ*/*operando* catalyst characterization at SSRL.

In FY24 we have participated in several novel beamtimes such as: liquid phase XAS characterization of peptide-chelated lanthanides for rare earth element recovery (Smerigan, Penn. State) vapor phase dosing of water (Cargnello, Stanford) or hydrocarbons (Roman, MIT), high pressure $CO_2$ conversion (Li, ORNL), and our first collaboration in supporting in-situ small angle X-ray scattering measurements (Accelerate Innovations FWP, SLAC). To continue engagement with our user community we host monthly office hours for

guidance and assistance on XAS analysis beyond our one-on-one meetings with specific groups. There has been an increase in overall attendance with users seeking advice on modelling the data they have collected both at SSRL and other synchrotrons. Outreach will continue in late FY24 as we host our "XAS bootcamp" a hands-on XAS short course for up to 10 collaborators/students/postdocs. In FY24 Co-ACCESS hosted a visiting professor, Dr. Alper Uzun (Koc University) on his sabbatical, and an SCGSR student, David Thompson (Univ. Arkansas).

Co-ACCESS released two pieces of software to the greater XAS community. CatMASS, a XAS sample mass calculator for complex (catalyst) samples, is available on GibHub. CatXAS, an XAS workflow for in-situ/operando measurements that allows for XAS data processing, XANES analysis, and correlation of XAS data to simultaneously measured process parameters (LabVIEW/Potentiostat) and product analysis (Mass Spectrometer) is also available on GitHub. Hoffman continues to add functionality and offers training sessions to those interested in applying it for analysis of transient data collected at the beamline. Co-ACCESS co-developed batch and flow-through electrochemical cells to meet the needs of our user community in collaboration with Adam Holewinski (CU Boulder) and Ezra Clark (Penn. State). Vila, using DFT and XANES simulations supported multiple user groups to provide an understanding of their experimental data. Rachita Rana, the graduate student at UC Davis supported by Co-ACCESS, graduated. She developed the automated EXAFS analysis protocol, QuantEXAFS. The Co-ACCESS group has designed the process gas handling system for beamline 10-2 ES2 while SSRL works on the beamlines optics upgrade to deliver a quick-scanning XAS beamline for time-resolved catalyst characterization. The quick-scanning capability will allow for XAS spectra to be collected as fast as 50 ms/spectrum. The last components of the optics hardware are planned for install late FY24 with commissioning in FY25.

**Publications Acknowledging this Grant in 2021-2024**

## *(I) Intellectually led by SUNCAT FWP*


1. Balzaretti, F.; Voss, J. Density Functional Tight-Binding Models for Band Structures of Transition-Metal Alloys and Surfaces across the d-Block. *J. Chem. Theory Comput.* **2024**, *20* (16), 7272–7286. https://doi.org/10.1021/acs.jctc.4c00345.
2. Wei, L.; Hossain, M. D.; Chen, G.; Kamat, G. A.; Kreider, M. E.; Chen, J.; Yan, K.; Bao, Z.; Bajdich, M.; Stevens, M. B.; Jaramillo, T. F. Tuning Two-Dimensional Phthalocyanine Dual Site Metal–Organic Framework Catalysts for the Oxygen Reduction Reaction. *J. Am. Chem. Soc.* **2024**, *146* (19), 13377–13390. https://doi.org/10.1021/jacs.4c02229.
3. Voss, J. Machine Learning for Accuracy in Density Functional Approximations. *Journal of Computational Chemistry* **2024**, *45* (21), 1829–1845. https://doi.org/10.1002/jcc.27366.
4. Comer, B. M.; Bothra, N.; Lunger, J. R.; Abild-Pedersen, F.; Bajdich, M.; Winther, K. T. Prediction of O and OH Adsorption on Transition Metal Oxide Surfaces from Bulk Descriptors. *ACS Catal.* **2024**, *14* (7), 5286–5296. https://doi.org/10.1021/acscatal.4c00111.

5. Deo, S.; Kreider, M. E.; Kamat, G.; Hubert, M.; Zamora Zeledón, J. A.; Wei, L.; Matthews, J.; Keyes, N.; Singh, I.; Jaramillo, T. F.; Abild-Pedersen, F.; Burke Stevens, M.; Winther, K.; Voss, J. Interpretable Machine Learning Models for Practical Antimonate Electrocatalyst Performance. *ChemPhysChem* **2024**, *25* (13), e202400010. https://doi.org/10.1002/cphc.202400010.
6. Demir, S.; Tekin, A.; Chan, Y.-T.; Scheurer, C.; Reuter, K.; Luntz, A. C.; Voss, J. Factors Affecting the Electron Conductivity in Single Crystal Li7La3Zr2O12 and Li7P3S11. *ACS Appl. Energy Mater.* **2024**, *7* (6), 2392–2404. https://doi.org/10.1021/acsaem.3c03092.
7. Halldin Stenlid, J.; Abild-Pedersen, F. Revealing Local and Directional Aspects of Catalytic Active Sites by the Nuclear and Surface Electrostatic Potential. *J. Phys. Chem. C* **2024**, *128* (11), 4544–4558. https://doi.org/10.1021/acs.jpcc.3c08512.
8. Saini, S.; Halldin Stenlid, J.; Deo, S.; Plessow, P. N.; Abild-Pedersen, F. A First-Principles Approach to Modeling Surface Site Stabilities on Multimetallic Catalysts. *ACS Catal.* **2024**, *14* (2), 874–885. https://doi.org/10.1021/acscatal.3c04337.
9. Vijay, S.; H. Heenen, H.; Singh, A. R.; Chan, K.; Voss, J. Number of Sites-Based Solver for Determining Coverages from Steady-State Mean-Field Micro-Kinetic Models. *Journal of Computational Chemistry* **2024**, *45* (9), 546–551. https://doi.org/10.1002/jcc.27263.
10. Mandal, S. C.; Abild-Pedersen, F. Classification of Adsorbed Hydrocarbons Based on Bonding Configurations of the Adsorbates and Surface Site Stabilities. *ACS Catal.* **2023**, *13* (20), 13663–13671. https://doi.org/10.1021/acscatal.3c03239.
11. Schröder, J.; Zeledón, J. A. Z.; Kamat, G. A.; Kreider, M. E.; Wei, L.; Mule, A. S.; Torres, A.; Yap, K.; Sokaras, D.; Gallo, A.; Stevens, M. B.; Jaramillo, T. F. Tracking the Dynamics of a Ag-MnOx Oxygen Reduction Catalyst Using In Situ and Operando X-Ray Absorption Near-Edge Spectroscopy. *ACS Energy Lett.* **2023**. https://doi.org/10.1021/ACSENERGYLETT.3C00823.
12. Kreider, M. E.; Burke Stevens, M. Material Changes in Electrocatalysis: An In Situ/Operando Focus on the Dynamics of Cobalt-Based Oxygen Reduction and Evolution Catalysts. *ChemElectroChem* **2023**, *10* (3), e202200958. https://doi.org/10.1002/CELC.202200958.
13. Oh, J.; Beck, A.; Goodman, E. D.; Roling, L. T.; Boucly, A.; Artiglia, L.; Abild-Pedersen, F.; van Bokhoven, J. A.; Cargnello, M. Colloidally Engineered Pd and Pt Catalysts Distinguish Surface- and Vapor-Mediated Deactivation Mechanisms. *ACS Catal.* **2023**, *13* (3), 1812–1822. https://doi.org/10.1021/ACSCATAL.2C04683
14. Wei, L.; Hossain, M. D.; Boyd, M. J.; Aviles-Acosta, J.; Kreider, M. E.; Nielander, A. C.; Stevens, M. B.; Jaramillo, T. F.; Bajdich, M.; Hahn, C. Insights into Active Sites and Mechanisms of Benzyl Alcohol Oxidation on Nickel-Iron Oxyhydroxide Electrodes. *ACS Catal.* **2023**, *13* (7), 4272–4282. https://doi.org/10.1021/ACSCATAL.2C05656
15. Craig, M. J.; Kleuker, F.; Bajdich, M.; García-Melchor, M. FEFOS: A Method to Derive Oxide Formation Energies from Oxidation States. *Catal. Sci. Technol.* **2023**, *13* (11), 3427–3435. https://doi.org/10.1039/D3CY00107E.
16. Baek, J.; Hossain, M. D.; Mukherjee, P.; Lee, J.; Winther, K. T.; Leem, J.; Jiang, Y.; Chueh, W. C.; Bajdich, M.; Zheng, X. Synergistic Effects of Mixing and Strain in

High Entropy Spinel Oxides for Oxygen Evolution Reaction. *Nat Commun* **2023**, *14* (1), 5936. https://doi.org/10.1038/s41467-023-41359-7.
17. Koshy, D. M.; Hossain, M. D.; Masuda, R.; Yoda, Y.; Gee, L. B.; Abiose, K.; Gong, H.; Davis, R.; Seto, M.; Gallo, A.; Hahn, C.; Bajdich, M.; Bao, Z.; Jaramillo, T. F. Investigation of the Structure of Atomically Dispersed NiNx Sites in Ni and N-Doped Carbon Electrocatalysts by 61Ni Mössbauer Spectroscopy and Simulations. *J. Am. Chem. Soc.* **2022**. https://doi.org/10.1021/JACS.2C09825.
18. Trepte, K.; Voss, J. Data-Driven and Constrained Optimization of Semi-Local Exchange and Non-Local Correlation Functionals for Materials and Surface Chemistry. J. Comput. Chem. **2022**, 43, 1104–1112.https://doi.org/10.1002/jcc.26872
19. Comer, B. M.; Li, J.; Abild-Pedersen, F.; Bajdich, M.; Winther, K. T. Unraveling Electronic Trends in O* and OH* Surface Adsorption in the MO2 Transition-Metal Oxide Series. J. Phys. Chem. C **2022**, 126 (18), 7903–7909. https://doi.org/10.1021/acs.jpcc.2c02381
20. Voss, J. Hubbard-Corrected Oxide Formation Enthalpies without Adjustable Parameters. J. Phys. Commun. **2022**, 6 (3), 035009. https://doi.org/10.1088/2399-6528/ac6069
21. Koshy, D. M.; Hossain, M. D.; Masuda, R.; Yoda, Y.; Gee, L. B.; Abiose, K.; Gong, H.; Davis, R.; Seto, M.; Gallo, A.; Hahn, C.; Bajdich, M.; Bao, Z.; Jaramillo, T. F. Investigation of the Structure of Atomically Dispersed NiNx Sites in Ni and N-Doped Carbon Electrocatalysts by 61Ni Mössbauer Spectroscopy and Simulations. *J. Am. Chem. Soc.* **2022**, *144* (47), 21741–21750. https://doi.org/10.1021/jacs.2c09825.
22. Zamora Zeledón, J. A.; Jackson, A.; Stevens, M.B.; Kamat, G.A.; Jaramillo, T.F. Methods—A Practical Approach to the Reversible Hydrogen Electrode Scale. *J. Electrochemical Soc.* **2022**, *169*, 066505. https://iopscience.iop.org/article/10.1149/1945-7111/ac71d1.
23. Resasco, J.; Abild-Pedersen, F.; Hahn, C.; Bao, Z.; Koper, M. T. M.; Jaramillo, T. F. Enhancing the Connection between Computation and Experiments in Electrocatalysis. *Nat Catal.* **2022**, *5* (5), 374–381. https://doi.org/10.1038/s41929-022-00789-0.
24. Lunger, J. R.; Lutz, N.; Peng, J.; Bajdich, M.; Shao-Horn, Y. Cation-Dependent Multielectron Kinetics of Metal Oxide Splitting. *Chem. Mater.* **2022**, 34, (8), 3872-3881. https://doi.org/10.1021/acs.chemmater.2c00602.
25. Kelly, S. R.; Heenen, H. H.; Govindarajan, N.; Chan, K.; Nørskov, J. K. OH Binding Energy as a Universal Descriptor of the Potential of Zero Charge on Transition Metal Surfaces. *J. Phys. Chem. C* **2022**, *126* (12), 5521-5528. https://doi.org/10.1021/acs.jpcc.1c10362.
26. Kamat, G. A.; Zamora Zeledón, J. A.; Gunasooriya, G. T. K. K.; Dull, S. M.; Perryman, J. T.; Nørskov, J. K.; Stevens, M. B.; Jaramillo, T. F. Acid Anion Electrolyte Effects on Platinum for Oxygen and Hydrogen Electrocatalysis. *Commun Chem.* **2022**, *5* (1), 1–10. https://doi.org/10.1038/s42004-022-00635-1.
27. Liu, M. J.; Guo, J.; Hoffman, A. S.; Stenlid, J. H.; Tang, M. T.; Corson, E. R.; Stone, K. H.; Abild-Pedersen, F.; Bare, S. R.; Tarpeh, W. A. Catalytic Performance and Near-Surface X-Ray Characterization of Titanium Hydride Electrodes for the

Electrochemical Nitrate Reduction Reaction. *J. Am. Chem. Soc.* **2022**, 144 (13), 5739-5744. https://doi.org/10.1021/jacs.2c01274.
28. Hubert, M. A.; King, L. A.; Jaramillo, T. F. Evaluating the Case for Reduced Precious Metal Catalysts in Proton Exchange Membrane Electrolyzers. *ACS Energy Lett.* **2022**, *7* (1), 17–23. https://doi.org/10.1021/acsenergylett.1c01869.
29. Hubert, M. A.; Gallo, A.; Liu, Y.; Valle, E.; Sanchez, J.; Sokaras, D.; Sinclair, R.; King, L. A.; Jaramillo, T. F. Characterization of a Dynamic $Y_2Ir_2O_7$ Catalyst during the Oxygen Evolution Reaction in Acid. *J. Phys. Chem. C* **2022**, *126* (4), 1751–1760. https://doi.org/10.1021/acs.jpcc.1c07760.
30. Shi, X.; Peng, H.-J.; Hersbach, T. J.; Jiang, Y.; Zeng, Y.; Baek, J.; Winther, K. T.; Sokaras, D.; Zheng, X.; Bajdich, M. Efficient and Stable Acidic Water Oxidation Enabled by Low-Concentration, High-Valence Iridium Sites. *ACS Energy Letters* **2022**, *7*, 2228–2235. https://doi.org/10.1021/acsenergylett.2c00578.
31. Saini, S.; Halldin Stenlid, J.; Abild-Pedersen, F. Electronic Structure Factors and the Importance of Adsorbate Effects in Chemisorption on Surface Alloys. npj Comput. Mater. 2022 81 2022, 8 (1), 1–12. https://doi.org/10.1038/s41524-022-00846-z.
32. Wrasman, C. J.; Zhou, C.; Aitbekova, A.; Goodman, E. D.; Cargnello, M. Recycling of Solvent Allows for Multiple Rounds of Reproducible Nanoparticle Synthesis. J. Am. Chem. Soc. 2022, 144 (26), 11646–11655. https://doi.org/10.1021/JACS.2C02837.
33. Valle, E.; Duyar, M. S.; Snider, J. L.; Regli, S. K.; Rønning, M.; Gallo, A.; Jaramillo, T. F. In Situ Studies of the Formation of MoP Catalysts and Their Structure under Reaction Conditions for Higher Alcohol Synthesis: The Role of Promoters and Mesoporous Supports. J. Phys. Chem. C **2022**, 126 (12), 5575–5583. https://doi.org/10.1021/acs.jpcc.2c00837.
34. Streibel V., Aljama H., Yang A.-C., Choksi T. S., Sánchez-Carrera R. S., Schäfer A., Li Y., Cargnello M., Abild-Pedersen F.,"Microkinetic modeling of propene combustion on a stepped, metallic palladium surface and the importance of oxygen coverage.", ACS Catalysis, **2022**, 12, 1742-1757. . https://doi.org/10.1021/acscatal.1c03699
35. Tahsini, N.; Yang, A.-C.; Streibel, V.; Werghi, B.; Goodman, E. D.; Aitbekova, A.; Bare, S. R.; Li, Y.; Abild-Pedersen, F.; Cargnello, M. Colloidal Platinum–Copper Nanocrystal Alloy Catalysts Surpass Platinum in Low-Temperature Propene Combustion. J. Am. Chem. Soc. **2022**, 144 (4), 1612–1621. https://doi.org/10.1021/jacs.1c10248.
36. Schlexer Lamoureux, P.; Choksi, T. S.; Streibel, V.; Abild-Pedersen, F. Combining Artificial Intelligence and Physics-Based Modeling to Directly Assess Atomic Site Stabilities: From Sub-Nanometer Clusters to Extended Surfaces. Phys. Chem. Chem. Phys. **2021**, 23, 22022-22034.https://doi.org/10.1039/D1CP02198B
37. Brown, K.; Maimaiti, Y.; Trepte, K.; Bligaard, T.; Voss, J. MCML: Combining Physical Constraints with Experimental Data for a Multi-Purpose Meta-Generalized Gradient Approximation. J. Comput. Chem. **2021**, 42 (28), 2004–

2013.
https://doi.org/10.1002/jcc.26732
38. Li, J.; Stenlid, J. H.; Ludwig, T.; Lamoureux, P. S.; Abild-Pedersen, F. Modeling Potential-Dependent Electrochemical Activation Barriers: Revisiting the Alkaline Hydrogen Evolution Reaction. *J. Am. Chem. Soc.* **2021**, *143* (46), 19341–19355. https://doi.org/10.1021/jacs.1c07276.
39. Ben-Naim, M.; Liu, Y.; Stevens, M. B.; Lee, K.; Wette, M. R.; Boubnov, A.; Trofimov, A. A.; Ievlev, A. V.; Belianinov, A.; Davis, R. C.; Clemens, B. M.; Bare, S. R.; Hikita, Y.; Hwang, H. Y.; Higgins, D. C.; Sinclair, R.; Jaramillo, T. F. Understanding Degradation Mechanisms in SrIrO3 Oxygen Evolution Electrocatalysts: Chemical and Structural Microscopy at the Nanoscale. *Advanced Functional Materials* **2021**, *31* (34), 2101542. https://doi.org/10.1002/adfm.202101542.
40. Koshy, D. M.; Nathan, S. S.; Asundi, A. S.; Abdellah, A. M.; Dull, S. M.; Cullen, D. A.; Higgins, D.; Bao, Z.; Bent, S. F.; Jaramillo, T. F. Bridging Thermal Catalysis and Electrocatalysis: Catalyzing CO2 Conversion with Carbon-Based Materials. *Angewandte Chemie International Edition* **2021**, *60* (32), 17472–17480. https://doi.org/10.1002/anie.202101326.
41. Lee, K.; Flores, R. A.; Liu, Y.; Wang, B. Y.; Hikita, Y.; Sinclair, R.; Bajdich, M.; Hwang, H. Y. Epitaxial Stabilization and Oxygen Evolution Reaction Activity of Metastable Columbite Iridium Oxide. *ACS Appl. Energy Mater.* **2021**, *4* (4), 3074–3082. https://doi.org/10.1021/acsaem.0c02788.
42. Zheng, X.; Tang, J.; Gallo, A.; Torres, J. A. G.; Yu, X.; Athanitis, C. J.; Been, E. M.; Ercius, P.; Mao, H.; Fakra, S. C.; Song, C.; Davis, R. C.; Reimer, J. A.; Vinson, J.; Bajdich, M.; Cui, Y. Origin of Enhanced Water Oxidation Activity in an Iridium Single Atom Anchored on NiFe Oxyhydroxide Catalyst. *PNAS* **2021**, *118* (36). https://doi.org/10.1073/pnas.2101817118.
43. Sanchez, J.; Stevens, M. B.; Young, A. R.; Gallo, A.; Zhao, M.; Liu, Y.; Ramos-Garcés, M. V.; Ben-Naim, M.; Colón, J. L.; Sinclair, R.; King, L. A.; Bajdich, M.; Jaramillo, T. F. Isolating the Electrocatalytic Activity of a Confined NiFe Motif within Zirconium Phosphate. *Advanced Energy Materials* **2021**, *11* (20), 2003545. https://doi.org/10.1002/aenm.202003545.
44. Baeumer, C.; Li, J.; Lu, Q.; Liang, A. Y.-L.; Jin, L.; Martins, H. P.; Duchoň, T.; Glöß, M.; Gericke, S. M.; Wohlgemuth, M. A.; Giesen, M.; Penn, E. E.; Dittmann, R.; Gunkel, F.; Waser, R.; Bajdich, M.; Nemšák, S.; Mefford, J. T.; Chueh, W. C. Tuning Electrochemically Driven Surface Transformation in Atomically Flat LaNiO3 Thin Films for Enhanced Water Electrolysis. *Nat. Mater.* **2021**, *20* (5), 674–682. https://doi.org/10.1038/s41563-020-00877-1.
45. Asundi, A. S.; Nathan, S. S.; Hong, J.; Hoffman, A. S.; Pennel, M.; Bare, S. R.; Bent, S. F. Identifying Higher Oxygenate Synthesis Sites in Cu Catalysts Promoted and Stabilized by Atomic Layer Deposited Fe2O3. J. Catal. **2021**, 404, 210–223. https://doi.org/10.1016/j.jcat.2021.09.015.
46. Asundi, A. S.; Hoffman, A. S.; Nathan, S. S.; Boubnov, A.; Bare, S. R.; Bent, S. F. Impurity Control in Catalyst Design: The Role of Sodium in Promoting and Stabilizing Co and Co2C for Syngas Conversion. ChemCatChem **2021**, 13 (4), 1186–1194. https://doi.org/10.1002/cctc.202001703.

47. Nathan, S. S.; Asundi, A. S.; Singh, J. A.; Hoffman, A. S.; Boubnov, A.; Hong, J.; Bare, S. R.; Bent, S. F. Understanding Support Effects of ZnO-Promoted Co Catalysts for Syngas Conversion to Alcohols Using Atomic Layer Deposition. ChemCatChem **2021**, 13 (2), 770–781. https://doi.org/10.1002/cctc.202001630.
48. Upham, D. C.; Orazov, M.; Jaramillo, T. F. Phosphate-Passivated Mordenite for Tandem-Catalytic Conversion of Syngas to Ethanol or Acetic Acid. J. Catal. **2021**, 399, 132–141. https://doi.org/10.1016/j.jcat.2021.04.029.
49. Duyar, M. S.; Gallo, A.; Regli, S. K.; Snider, J. L.; Singh, J. A.; Valle, E.; McEnaney, J.; Bent, S. F.; Rønning, M.; Jaramillo, T. F. Understanding Selectivity in CO2 Hydrogenation to Methanol for MoP Nanoparticle Catalysts Using In Situ Techniques. Catalysts **2021**, 11 (1), 143. https://doi.org/10.3390/catal11010143.
50. Goodman, E. D.; Asundi, A. S.; Hoffman, A. S.; Bustillo, K. C.; Stebbins, J. F.; Bare, S. R.; Bent, S. F.; Cargnello, M. Monolayer Support Control and Precise Colloidal Nanocrystals Demonstrate Metal–Support Interactions in Heterogeneous Catalysts. Adv. Mater. **2021**, 33 (44), 2104533. https://doi.org/10.1002/adma.202104533.
51. Wang, T.; Li, G.; Cui, X.; Abild-Pedersen, F. Identification of Earth-Abundant Materials for Selective Dehydrogenation of Light Alkanes to Olefins. Proc. Natl. Acad. Sci. **2021**, 118 (11), e2024666118. https://doi.org/10.1073/pnas.2024666118.
52. D. Goodman, E.; Z. Carlson, E.; M. Dietze, E.; Tahsini, N.; Johnson, A.; Aitbekova, A.; Taylor, T. N.; N. Plessow, P.; Cargnello, M. Size-Controlled Nanocrystals Reveal Spatial Dependence and Severity of Nanoparticle Coalescence and Ostwald Ripening in Sintering Phenomena. Nanoscale **2021**, 13 (2), 930–938. https://doi.org/10.1039/D0NR07960J.
53. Wang, T.; Cui, X.; Winther, K. T.; Abild-Pedersen, F.; Bligaard, T.; Nørskov, J. K. Theory-Aided Discovery of Metallic Catalysts for Selective Propane Dehydrogenation to Propylene. ACS Catal. **2021**, 11 (10), 6290–6297. https://doi.org/10.1021/acscatal.0c05711.
54. Wang, T.; Abild-Pedersen, F. Identifying Factors Controlling the Selective Ethane Dehydrogenation on Pt-Based Catalysts from DFT Based Micro-Kinetic Modeling. J. Energy Chem. **2021**, 58, 37–40. https://doi.org/10.1016/j.jechem.2020.09.034.
55. Stenlid, J. H.; Streibel, V.; Choksi, T. S.; Abild-Pedersen, F. Assessing Catalytic Rates of Bimetallic Nanoparticles with Active Site Specificity - A Case Study Using NO Decomposition. **2021**. https://doi.org/10.26434/chemrxiv-2021-lmlmg.
56. Yang A.-C. , Streibel V. , Choksi T. S. , Aljama H. , Werghi B. , Bare S. R. , Sánchez-Carrera R. S., Schäfer A. , Li Y. , Abild-Pedersen F. , Cargnello M., "Insights and comparison of structure–property relationships in propane and propene catalytic combustion on Pd-and Pt-based catalysts.", Journal of Catalysis, **2021**, 401, 89-101. https://doi.org/10.1016/j.jcat.2021.06.018
57. Wang, T.; Abild-Pedersen, F. Achieving Industrial Ammonia Synthesis Rates at Near-Ambient Conditions through Modified Scaling Relations on a Confined Dual Site. Proc. Natl. Acad. Sci. **2021**, 118 (30), e2106527118. https://doi.org/10.1073/pnas.2106527118.

58. R. Rana, F.D. Vila, A.R. Kulkarni, S.R. Bare, "Bridging the Gap between the X-ray Absorption Spectroscopy and the Computational Catalysis Communities in Heterogeneous Catalysis: A Perspective on the Current and Future Research Directions", *ACS Catalysis*, (2022), **12**, 13813−13830. DOI: 10.1021/acscatal.2c03863.
59. Perez-Aguilar, J. E., Caine, A., Bare, S. R. & Hoffman, A. S. "CatMass: software for calculating optimal sample masses for X-ray absorption spectroscopy experiments involving complex sample compositions", *Journal of Synchrotron Radiation* (2023), **30.** DOI:10.1107/S160057752300615X
60. A. S. Hoffman, O. Müller, J. Hong, G. A. Canning, C.-Yu Fang, J. E. Perez-Aguilar, B. C. Gates, S. R. Bare, "Observations of Ethylene-for-CO Ligand Exchanges on a Zeolite-Supported Single-Site Rh Catalyst by X-ray Absorption Spectroscopy", *J. Phys. Chem Letters*, (2023), **14**, 4591-4599. DOI: 10.1021/acs.jpclett.3c00349.
61. A. S. Hoffman, M. Greaney, J. Finzel, R. Xing, D. Covelli, V.Z. Fridman, C. Lugmair, S.R. Bare, "Elucidation of puzzling questions regarding $CrO_x/Al_2O_3$ catalyst I. X-ray absorption spectroscopy aided identification of the nature of the chromium oxide species in the $CrO_x/Al_2O_3$ dehydrogenation catalyst system." *Applied Catalysis A: General* (2023), **660**, 119187. DOI: 10.1016/j.apcata.2023.119187.
62. J. Finzel, K. Sanroman, A.S. Hoffman, J. Resasco, P. Christopher, S.R. Bare, "Limits of Detection for X-ray Absorption Spectroscopy of Heterogenous Single Atom Catalysts", *ACS Catalysis* (2023), **13**, 6462-6473. DOI: 10.1021/acscatal.3c01116.
63. B. Werghi, L. Wu, A.M. Ebrahim, M. Chi, H. Ni, M. Cargnello, S.R. Bare, "Selective catalytic behavior induced by crystal-phase transformation in well-defined bimetallic Pt-Sn nanocrystals", *Small,* (2023), 2207956. DOI: 10.1002/smll.202207956.

## *(II) Jointly funded by this grant and other grants with intellectual leadership by other funding sources*

64. Ye, R.; Ma, L.; Mao, J.; Wang, X.; Hong, X.; Gallo, A.; Ma, Y.; Luo, W.; Wang, B.; Zhang, R.; Duyar, M. S.; Jiang, Z.; Liu, J. A Ce-CuZn Catalyst with Abundant Cu/Zn-OV-Ce Active Sites for CO2 Hydrogenation to Methanol. *Nat Commun* **2024**, *15* (1), 2159. https://doi.org/10.1038/s41467-024-46513-3 .
65. Martínez-Alonso, C.; Vassilev-Galindo, V.; Comer, B. M.; Abild-Pedersen, F.; Winther, K. T.; LLorca, J. Application of Machine Learning to Discover New Intermetallic Catalysts for the Hydrogen Evolution and the Oxygen Reduction Reactions. *Catal. Sci. Technol.* **2024**, *14* (13), 3784–3799. https://doi.org/10.1039/D4CY00491D .
66. Østergaard, F. C.; Abild-Pedersen, F.; Rossmeisl, J. Coverage, Repulsion, and Reactivity of Hydrogen on High-Entropy Alloys. *Journal of Catalysis* **2024**, *435*, 115570. https://doi.org/10.1016/j.jcat.2024.115570 .
67. Li, Y.; Zheng, X.; Carlson, E. Z.; Xiao, X.; Chi, X.; Cui, Y.; Greenburg, L. C.; Zhang, G.; Zhang, E.; Liu, C.; Yang, Y.; Kim, M. S.; Feng, G.; Zhang, P.; Su, H.;

Guan, X.; Zhou, J.; Wu, Y.; Xue, Z.; Li, W.; Bajdich, M.; Cui, Y. In Situ Formation of Liquid Crystal Interphase in Electrolytes with Soft Templating Effects for Aqueous Dual-Electrode-Free Batteries. *Nat Energy* **2024**, 1–10. https://doi.org/10.1038/s41560-024-01638-z .

68. Kani, N. C.; Chauhan, R.; Olusegun, S. A.; Sharan, I.; Katiyar, A.; House, D. W.; Lee, S.-W.; Jairamsingh, A.; Bhawnani, R. R.; Choi, D.; Nielander, A. C.; Jaramillo, T. F.; Lee, H.-S.; Oroskar, A.; Srivastava, V. C.; Sinha, S.; Gauthier, J. A.; Singh, M. R. Sub-Volt Conversion of Activated Biochar and Water for H2 Production near Equilibrium via Biochar-Assisted Water Electrolysis. *Cell Reports Physical Science* **2024**, *5* (6), 102013. https://doi.org/10.1016/j.xcrp.2024.102013 .
69. Sinha, S.; Vegge, T.; Winther, K. T.; Hansen, H. A. Understanding the Electronic and Structural Effects in ORR Intermediate Binding on Anion-Substituted Zirconia Surfaces. *ChemPhysChem* **2024**, *25* (14), e202300865. https://doi.org/10.1002/cphc.202300865 .
70. Fu, X.; Niemann, V. A.; Zhou, Y.; Li, S.; Zhang, K.; Pedersen, J. B.; Saccoccio, M.; Andersen, S. Z.; Enemark-Rasmussen, K.; Benedek, P.; Xu, A.; Deissler, N. H.; Mygind, J. B. V.; Nielander, A. C.; Kibsgaard, J.; Vesborg, P. C. K.; Nørskov, J. K.; Jaramillo, T. F.; Chorkendorff, I. Calcium-Mediated Nitrogen Reduction for Electrochemical Ammonia Synthesis. *Nat. Mater.* **2024**, *23* (1), 101–107. https://doi.org/10.1038/s41563-023-01702-1.
71. Rios Amador, I.; Hannagan, R. T.; Marin, D. H.; Perryman, J. T.; Rémy, C.; Hubert, M. A.; Lindquist, G. A.; Chen, L.; Stevens, M. B.; Boettcher, S. W.; Nielander, A. C.; Jaramillo, T. F. Protocol for Assembling and Operating Bipolar Membrane Water Electrolyzers. *STAR Protocols* **2023**, *4* (4), 102606. https://doi.org/10.1016/j.xpro.2023.102606.
72. Marin, D. H.; Perryman, J. T.; Hubert, M. A.; Lindquist, G. A.; Chen, L.; Aleman, A. M.; Kamat, G. A.; Niemann, V. A.; Stevens, M. B.; Regmi, Y. N.; Boettcher, S. W.; Nielander, A. C.; Jaramillo, T. F. Hydrogen Production with Seawater-Resilient Bipolar Membrane Electrolyzers. *Joule* **2023**, *7* (4), 765–781. https://doi.org/10.1016/j.joule.2023.03.005.
73. Blair, S. J.; Doucet, M.; Niemann, V. A.; Stone, K. H.; Kreider, M. E.; Browning, J. F.; Halbert, C. E.; Wang, H.; Benedek, P.; Mcshane, E. J.; Nielander, A. C.; Gallo, A.; Jaramillo, T. F.; Stanford, D. Combined, Time-Resolved, in Situ Neutron Reflectometry and X-Ray Diffraction Analysis of Dynamic SEI Formation during Electrochemical N2 Reduction. *Energy Environ. Sci.* **2023**, *16* (8), 3391–3406. https://doi.org/10.1039/D2EE03694K.
74. Niemann, V. A.; Benedek, P.; Guo, J.; Xu, Y.; Blair, S. J.; Corson, E. R.; Nielander, A. C.; Jaramillo, T. F.; Tarpeh, W. A. Co-Designing Electrocatalytic Systems with Separations To Improve the Sustainability of Reactive Nitrogen Management. *ACS Catal.* **2023**, *13* (9), 6268–6279. https://doi.org/10.1021/ACSCATAL.3C00933.
75. Pillai, H. S.; Li, Y.; Wang, S. H.; Omidvar, N.; Mu, Q.; Achenie, L. E. K.; Abild-Pedersen, F.; Yang, J.; Wu, G.; Xin, H. Interpretable Design of Ir-Free Trimetallic Electrocatalysts for Ammonia Oxidation with Graph Neural Networks. *Nat. Commun. 2023 141* **2023**, *14* (1), 1–11. https://doi.org/10.1038/s41467-023-36322-5.

76. Zhao, W.; Xu, G.; He, Z.; Cai, C.; Abild-Pedersen, F.; Wang, T. Toward Carbon Monoxide Methanation at Mild Conditions on Dual-Site Catalysts. *J. Am. Chem. Soc.* **2023**. https://doi.org/10.1021/JACS.3C02180.
77. McShane, E. J.; Niemann, V. A.; Benedek, P.; Fu, X.; Nielander, A. C.; Chorkendorff, I.; Jaramillo, T. F.; Cargnello, M. Quantifying Influence of the Solid-Electrolyte Interphase in Ammonia Electrosynthesis. *ACS Energy Lett.* **2023**, *8* (10), 4024–4032. https://doi.org/10.1021/acsenergylett.3c01534.
78. Lee, D. U.; Joensen, B.; Jenny, J.; Ehlinger, V. M.; Lee, S.-W.; Abiose, K.; Xu, Y.; Sarkar, A.; Lin, T. Y.; Hahn, C.; Jaramillo, T. F. Controlling Mass Transport in Direct Carbon Dioxide Zero-Gap Electrolyzers via Cell Compression. *ACS Sustainable Chem. Eng.* **2023**, *11* (46), 16661–16668. https://doi.org/10.1021/acssuschemeng.3c05494.
79. Jiang, D.; Wan, G.; Halldin Stenlid, J.; García-Vargas, C. E.; Zhang, J.; Sun, C.; Li, J.; Abild-Pedersen, F.; Tassone, C. J.; Wang, Y. Dynamic and Reversible Transformations of Subnanometre-Sized Palladium on Ceria for Efficient Methane Removal. *Nat. Catal. 2023 67* **2023**, *6* (7), 618–627. https://doi.org/10.1038/S41929-023-00983-8.
80. Blair, S. J.; Nielander, A. C.; Stone, K. H.; Kreider, M. E.; Niemann, V. A.; Benedek, P.; McShane, E. J.; Gallo, A.; Jaramillo, T. F. Development of a Versatile Electrochemical Cell for in Situ Grazing-Incidence X-Ray Diffraction during Non-Aqueous Electrochemical Nitrogen Reduction. *1600-5775* **2023**, *30* (5), 917–922. https://doi.org/10.1107/S1600577523006331.
81. Kreider, M. E.; Kamat, G. A.; Zamora Zeledón, J. A.; Wei, L.; Sokaras, D.; Gallo, A.; Stevens, M.B. Jaramillo, T. F. Understanding the Stability of Manganese Chromium Antimonate Electrocatalysts through Multi-modal In Situ and Operando Measurements *JACS*. **2022**, 144,22549-22561. https://pubs.acs.org/doi/10.1021/jacs.2c08600
82. Wei, F.; Smeets, E. W. F.; Voss, J.; Kroes, G.-J.; Lin, S.; Guo, H. Assessing Density Functionals for Describing Methane Dissociative Chemisorption on Pt(110)-(2×1) Surface. Chin. J. Chem. Phys. **2021**, 34 (6), 883–895 https://doi.org/10.1063/1674-0068/cjcp2110207
83. Blair, S. J.; Doucet, M.; Browning, J. F.; Stone, K.; Wang, H.; Halbert, C.; Avilés Acosta, J.; Zamora Zeledón, J. A.; Nielander, A. C.; Gallo, A.; Jaramillo, T. F. Lithium-Mediated Electrochemical Nitrogen Reduction: Tracking Electrode–Electrolyte Interfaces via Time-Resolved Neutron Reflectometry. *ACS Energy Lett.* **2022**, *7*, (6), 1939–1946. https://doi.org/10.1021/acsenergylett.1c02833
84. Choi, S.-H.; Kreider, M. E.; Nielander, A. C.; Stevens, M. B.; Kamat, G.; Eung Koo, J.; Ho Bae, K.; Kim, H.; Young Yoon, I.; Un Yoon, B.; Hwang, K.; Un Lee, D.; Jaramillo, T. F. Origins of Wear-Induced Tungsten Corrosion Defects in Semiconductor Manufacturing during Tungsten Chemical Mechanical Polishing. *Applied Surface Science* **2022**, *598*, 153767. https://doi.org/10.1016/j.apsusc.2022.153767
85. Gunasooriya, G.T.K.K.; Kreider, M. E.; Liu, Y.; Zamora Zeledón, J. A.; Wang, Z.; Valle, E.; Yang, Y-C.; Gallo, A.; Sinclair, R.; Stevens, M.B.; Jaramillo, T.F.; Nørskov, J.K. First-row Transition Metal Antimonates for the Oxygen Reduction Reaction. *ACS Nano*, **2022**, *16*, 6334-6348. https://pubs.acs.org/doi/full/10.1021/acsnano.2c00420

86. Zeledón, J. A. Z.; Gunasooriya, G. T. K. K.; Kamat, G. A.; Kreider, M. E.; Ben-Naim, M.; Hubert, M. A.; Acosta, J. E. A.; Nørskov, J. K.; Stevens, M. B.; Jaramillo, T. F. Engineering Metal–Metal Oxide Surfaces for High-Performance Oxygen Reduction on Ag–Mn Electrocatalysts. *Energy Environ. Sci.,* **2022**, *15,* 1611-1629. https://doi.org/10.1039/D2EE00047D
87. dos Santos, E. C., Araujo, R. B., Valter, M., Salazar-Alvarez, G., Johnsson, M., Bajdich, M., Abild-Pedersen, F., & Pettersson, L. G. M. Efficient Screening of Bi-Metallic Electrocatalysts for Glycerol Valorization. *Electrochimica Acta*, **2021**, 139283. https://doi.org/10.1016/J.ELECTACTA.2021.139283
88. Zamora Zeledón, J. A.; Kamat, G. A.; Gunasooriya, G. T. K. K.; Nørskov, J. K.; Stevens, M. B.; Jaramillo, T. F. Probing the Effects of Acid Electrolyte Anions on Electrocatalyst Activity and Selectivity for the Oxygen Reduction Reaction. *ChemElectroChem* **2021**, *8* (13), 2467–2478. https://doi.org/10.1002/celc.202100500
*89.* Zamora Zeledón, J. A.; Stevens, M. B.; Gunasooriya, G. T. K. K.; Gallo, A.; Landers, A. T.; Kreider, M. E.; Hahn, C.; Nørskov, J. K.; Jaramillo, T. F. Tuning the Electronic Structure of Ag-Pd Alloys to Enhance Performance for Alkaline Oxygen Reduction. *Nat Commun* **2021**, *12* (1), 620. https://doi.org/10.1038/s41467-021-20923-z
90. Koshy, D. M., Akhade, S. A., Shugar, A., Abiose, K., Shi, J., Liang, S., Oakdale, J. S., Weitzner, S. E., Varley, J. B., Duoss, E. B., Baker, S. E., Hahn, C., Bao, Z., & Jaramillo, T. FChemical Modifications of Ag Catalyst Surfaces with Imidazolium Ionomers Modulate H2Evolution Rates during Electrochemical CO2Reduction. Journal of the American Chemical Society, **2021**, 143(36), 14712–14725. https://doi.org/10.1021/JACS.1C06212
91. Winiwarter, A.; Boyd, M.J.; Scott, S. B.; Higgins, D. C.; Seger, B.; Chorkendorff, I.; Jaramillo, T. F. CO as a Probe Molecule to Study Surface Adsorbates during Electrochemical Oxidation of Propene. *ChemElectroChem*, **2021**, *8,* 250-256. https://doi.org/10.1002/celc.202001162
92. Garcia-Esparza A. T., Park S.,Abroshan H., Paredes Mellone O. A., Vinson J., Abraham B., Kim T. R., Nordlund D., Gallo A., Alonso-Mori R., Zheng X., Sokaras D., "Local Structure of Sulfur Vacancies on the Basal Plane of Monolayer MoS2.", ACS Nano **2022**, 16, 4, 6725–6733. https://doi.org/10.1021/acsnano.2c01388
93. Ashbridge Z., Kreidt E., Pirvu L., Schaufelberger F., Halldin Stenlid J., Abild-Pedersen F., Leigh D. A., "Vernier template synthesis of molecular knots.", Science, **2022**, 375, 1035-1041. https://doi.org/10.1126/science.abm9247
94. Park S., Garcia-Esparza A. T., Abroshan H., Abraham B., Vinson J., Gallo A., Nordlund D., Park J., Kim T. R., Vallez L., Alonso-Mori R., Sokaras D., Zheng X., "Operando Study of Thermal Oxidation of Monolayer MoS2." Adv. Sci. **2021**,8, 2002768. https://doi.org/10.1002/advs.202002768
95. Y. Lu, S. Zhou, C.-T. Kuo, D. Kunwar, C. Thompson, A. S. Hoffman, A. Boubnov, S. Lin, A. K. Datye, H. Guo and A. M. Karim, "Pt/CeO2Unraveling the Intermediate Reaction Complexes and Critical Role of Support-Derived Oxygen Atoms in CO Oxidation on Single-Atom Pt/$CeO_2$", *ACS Catalysis 11,* 14, 8701-8715 (2021) DOI: 10.1021/acscatal.1c01900

96. Giannakakis, G., Kress, P., Duanmu, K., Ngan, H. T., Yan, G., Hoffman, A. S., Qi, Z., Trimpalis, A., Annamalai, L., Ouyang, M., Liu, J., Eagan, N., Biener, J., Sokaras, D., Flytzani-Stephanopoulos, M., Bare, S. R., Sautet, P., & Sykes, E. C. H. "Mechanistic and Electronic Insights into a Working NiAu Single-Atom Alloy Ethanol Dehydrogenation Catalyst" *Journal of the American Chemical Society*, ***143*** (51), 21567–21579 (2021). DOI:10.1021/jacs.1c09274.
97. Qi, M. Babucci, Y. Zhang, A. Lund, L. Liu, Y. Chen, A.S. Hoffman, S.R. Bare, Y. Han, B.C. Gates, A.T. Bell, "Propane Dehydrogenation Catalyzed by Single Pt Atoms in ZnOx Nests in Dealuminated Zeolite Beta", *Journal of the American Chemical Society*, (2021), *J. Am. Chem. Soc.* **143**, 50, 21364–21378 (2021). DOI: 10.1021/jacs.1c10261.
98. K. Groden, F.D. Vila, L. Li, S.R. Bare, S.L. Scott, J-S. McEwen, "First Principles Approach to Extracting Chemical Information from X-Ray Absorption Near-Edge Spectra of Ga-Containing Materials", *J. Phys. Chem. C* **125**, 27901–27908 (2021). DOI: 10.1021/acs.jpcc.1c07728
99. S. Samira, J. Hong, J.C. Camayang, K. Sun, A.S. Hoffman, S.R. Bare, E. Nikolla, "Dynamic Surface Reconstruction Unifies the Electrocatalytic Oxygen Evolution Performance of Nonstoichiometric Mixed Metal Oxides", *JACS Au,* **1**, 12, 2224–2241 (2021). DOI: 10.1021/jacsau.1c00359.
100. G. Canning, S. Azzam, A.S. Hoffman, A. Boubnov, F. Alshafei, R. Ghosh, B. Ko, A. Datye, S.R. Bare, D. Simonetti, "Lanthanum Induced Lattice Strain Improves Hydrogen Sulfide Capacities of Copper Oxide Adsorbents", *AIChE Journal*, **67**, e17484 (2021). DOI: 10.1002/aic.17484.
101. D. Jiang, Y. Yao; T. Li, G. Wan, X.I. Pereira-Hernández, Y. Lu, J. Tian; K. Khivantsev, M.H. Engelhard, C. Sun, Carlos E. García-Vargas, A.S. Hoffman, S.R. Bare, A.K. Datye, L. Hu, Y. Wang, "Tailoring the Local Environment of Platinum in Single-Atom Pt1/CeO2 Catalysts for Robust Low-Temperature CO Oxidation", *Angewandte Chemie Int. Ed.* **60**, 26054–26062 (2021). DOI: 10.1002/anie.202108585.
102. M. Babucci, A.S. Hoffman, Simon R. Bare, B.C. Gates, "Characterization of Metal-Organic Framework $Zr_6O_8$ Node-Supported Atomically Dispersed Iridium Catalyst for Ethylene Hydrogenation by X-ray Absorption Near Edge Structure and Infrared Spectroscopies", *J. Phys. Chem C*, **125**, 16995-17007 (2021),. DOI: 10.1021/acs.jpcc.1c03563.
103. M.C. Simons, S.D. Prinslow, M Babucci, A.S. Hoffman, J. Hong, J.G. Vitillo, S.R. Bare, B.C. Gates, C.C. Lu, L. Gagliardi, A. Bhan, "Beyond Radical-Rebound: Methane Oxidation to Methanol Catalyzed by Iron Species in Metal–Organic Framework Nodes", *J. Am. Chem. Soc.,* **143**, 12165–12174 (2021). DOI: 10.1021/jacs.1c04766.
104. L. Chen, R. Unocic, A.S. Hoffman, J. Hong, A. Braga, Z. Bao, S.R. Bare, J. Szanyi, "Unlocking the Catalytic Potential of TiO2-Supported Pt Single Atoms for the Reverse Water-Gas Shift Reaction by Altering Their Chemical Environment", *JACS Au*, **1**, 977-986 (2021). DOI: 10.1021/jacsau.1c00111.
105. J. Wang, Y. Lu, L. Liu, L. Yu, C. Yang, M. Delferro, A. S. Hoffman, S. R. Bare, A. M. Karim and H. Xin, "Catalytic CO Oxidation on $MgAl_2O_4$-supported Iridium Single

Atoms: Ligand Configuration and Site Geometry", *J. Phys. Chem. C* **125**, 11380 (2021) doi: 10.1021/acs.jpcc.1c02287
106. M. Lopez Luna, J. Timoshenko, D. Kordus, C. Rettenmaier, S. W. Chee, A. S. Hoffman, S. R. Bare, S. Shaikhutdinov and B. Roldan Cuenya, "CO2le of the Oxide Support on the Structural and Chemical Evolution of Fe Catalysts during the Hydrogenation of $CO_2$", *ACS Catal.* **11**, 6175 (2021) doi: 10.1021/acscatal.1c01549
107. M. Albrahim, C. Thompson, D. Leshchev, A. Shrotri, R. R. Unocic, J. Hong, A. S. Hoffman, M. J. Meloni, R. C. Runnebaum, S. R. Bare, E. Stavitski and A. M. Karim, "Reduction and Agglomeration of Supported Metal Clusters Induced by High-flux X-ray Absorption Spectroscopy Measurements", *J. Phys. Chem. C* **125**, 11048 (2021). doi: 10.1021/acs.jpcc.1c01823
108. N. J. Divins, D. Kordus, J. Timoshenko, I. Sinev, I. Zegkinoglou, A. Bergmann, S. W. Chee, S. Widrinna, O. Karshoglu, H. Mistry, M. Lopez Luna, J. Q. Zhong, A. S. Hoffman, A. Boubnov, J. A. Boscoboinik, M. Heggen, R. E. Dunin-Borkowski, S. R. Bare and B. Roldan Cuenya, "Operando High-pressure Investigation of Size-controlled CuZn Catalysts for the Methanol Synthesis Reaction", *Nat. Commun.* **12**, 1435 (2021) doi: 10.1038/s41467-021-21604-7
109. I. K. van Ravenhorst, A. S. Hoffman, C. Vogt, A. Boubnov, N. Patra, R. Oord, C. Akatay, F. Meirer, S. R. Bare and B. M. Weckhuysen, "On the Cobalt Carbide Formation in a Co/$TiO_2$ Fischer–Tropsch Synthesis Catalyst as Studied by High-pressure, Long-Term Operando X-ray Absorption and Diffraction", *ACS Catal.* **11**, 2956 (2021). doi: 10.1021/acscatal.0c04695
110. M. Ouyang, K. G. Papanikolaou, A. Boubnov, A. S. Hoffman, G. Giannakakis, S. R. Bare, M. Stamatakis, M. Flytzani-Stephanopoulos and E. C. H. Sykes, "Directing Reaction Pathways via In situ Control of Active Site Geometries in PdAu Single-atom Alloy Catalysts", *Nat. Commun.* **12**, 1549 (2021). doi: 10.1038/s41467-021-21555-z
111. Jeremiah Lipp, Ritubarna Banerjee, Md. Fakhruddin Patwary, Nirmalendu Patra, Anhua Dong, Frank Girgsdies, Simon R. Bare, and J. R. Regalbuto, "Extension of Rietveld Refinement for Benchtop Powder XRD Analysis of Ultrasmall Supported Nanoparticles", *Chemistry of Materials*, *34,* 18, 8091-8111 (2022). DOI: 10.1021/acs.chemmater.2c00101
112. Kurtoğlu-Öztulum, S. F., Kaan Yalçın, Zhao, Y., Pelin Çağlayan, H., Hoffman, A. S., Gates, B. C., Bare, S. R., Ünal, U., & Uzun, A. "Transformation of reduced graphene aerogel-supported atomically dispersed iridium into stable clusters approximated as Ir6 during ethylene hydrogenation catalysis", *Journal of Catalysis*, (2022), ***413***, 603–613. DOI:10.1016/j.jcat.2022.04.028.
113. Lynch, T. J., Birkner, N. R., Christian, M. S., Wrubel, J. A., Schorne-Pinto, J., Van Veelen, A., Bargar, J. R., Besmann, T. M., Brinkman, K. S., & Chiu, W. K. S. "*In Situ* Determination of Speciation and Local Structure of NaCl–$SrCl_2$ and LiF–$ZrF_4$ Molten Salts", *The Journal of Physical Chemistry B*, (2022), ***126***(7), 1539–1550. DOI:10.1021/acs.jpcb.1c07552.
114. M. Meloni, J. Hong, A.S. Hoffman, S. Holton, A. Kulkarni, S.R. Bare, R. Runnebaum, "Nano-sized metallic nickel clusters stabilized on dealuminated

beta-zeolite: a highly active and stable ethylene hydrogenation catalyst", *J. Phys. Chem C*, (2022), **50**, 21213-21222. DOI:10.1021/acs.jpcc.2c05504.
115. J. Rorrer, A. Ebrahim, Y. Questell-Santiago, J. Zhu, C. Troyano-Valls, A. Asundi, S.R. Bare, C. Tassone, G. Beckham, Y. Román-Leshkov, "The Role of Bifunctional Ru/Acid Catalysts in the Selective Hydrocracking of Polyethylene and Polypropylene Waste to Liquid Hydrocarbons", *ACS Catalysis*, (2022), **12**, 13969-13979. DOI: 10.1021/acscatal.2c03596.
116. L. Qi, Y. Zhang, M. Babucci, J. Li, C. Dun, A.S. Hoffman, J. Urban, M. Tsapatsis, S.R. Bare, Y. Han, B.C. Gates, A. Bell, "Dehydrogenation of Propane and n-Butane Catalyzed by isolated PtZn4 Sites Supported on Self-Pillared Zeolite Pentasil Nanosheets", *ACS Catalysis*, (2022), **12**, 11177–11189. DOI: 10.1021/acscatal.2c01631.
117. N. Felvey, J. Guo, R. Rana, Rachita, L. Xu, S.R. Bare, B.C. Gates, A. Katz, A. Kulkarni, R. Runnebaum, C. Kronawitter, "Interconversion of Atomically Dispersed Platinum Cations and Platinum Clusters in Zeolite ZSM-5 and Formation of Platinum gem–Dicarbonyls", *Journal of the American Chemical Society*, **144**, 13874–13887 (2022). DOI: 10.1021/jacs.2c05386.
118. S.F. Kurtoğlu-Öztulum, K. Yalçın, A.S. Hoffman, A. Jalal, Y. Zhao, B.C. Gates, S.R. Bare, U. Unal, A. Uzun, "Ionic Liquid Sheath Stabilizes Atomically Dispersed Reduced Graphene Aerogel-Supported Iridium Complexes during Ethylene Hydrogenation even at an Iridium Loading of 9.9 wt%", *ChemCatChem* (2022), e202200553. DOI: 10.1002/cctc.202200553.
119. M. Babucci, E.T. Conley, A.S. Hoffman, S.R. Bare, B.C. Gates, "Iridium pair sites anchored to Zr6O8 nodes of the metal–organic framework UiO-66 catalyze ethylene hydrogenation", *Journal of Catalysis*, **411**, 176-186 (2022). DOI: 10.1016/j.jcat.2022.04.003.
120. M. Liu, J. Guo, A.S. Hoffman, J. Stenlid, M. Tang, E. Corson, K. Stone, F. Abild-Pedersen, S.R. Bare, W. Tarpeh, "Catalytic performance and near-surface X-ray characterization of titanium hydride electrodes for the electrochemical nitrate reduction reaction", *Journal of the American Chemical Society*, **144**, 5739–5744 (2022). DOI: 10.1021/jacs.2c01274.
121. Y. Chen, R. Rana, Z. Huang, F.D. Vila, T. Sours, J.E. Perez-Aguilar, X. Zhao, J. Hong, A.S. Hoffman, X. Li, C. Shang, T. Blum, J. Zeng, M. Chi, M. Salmeron, C.X. Kronawitter, S.R. Bare, A.R. Kulkarni, B.C. Gates, "Atomically Dispersed Platinum in Surface and Sub-Surface Sites on MgO have Contrasting Catalytic Properties for CO Oxidation", *J. Phys. Chem Letters*, **13**, 3896-3903 (2022). DOI: 10.1021/acs.jpclett.2c00667.
122. C. Zhou, A.S. Asundi, E.D. Goodman, J. Hong, B. Werghi, A.S. Hoffman, S.S. Nathan, S.F. Bent, S.R. Bare, M. Cargnello, "Steering CO2 Hydrogenation Towards C-C Coupling to Hydrocarbons Using Porous Organic Polymer/Metal Interfaces", *Proc. Nat. Acad. Sci*, , **119**, e2114768119 (2022). DOI: 10.1073/pnas.21147681219.
123. N. Tahsini, A.-C. Yang, V. Streibel, B. Werghi, E. Goodman, A. Aitbekova, S.R. Bare, Y. Li, F. Abild-Pedersen, M. Cargnello, "Colloidal Platinum-Copper Nanocrystal Alloy Catalysts Surpass Platinum in Low-Temperature

Propene Combustion", *Journal of the American Chemical Society*, **144**, 1612-1621 (2022). DOI: 10.1021/jacs.1c10248.
124. L.P. Herrera, L. Freitas, J. Hong, A.S. Hoffman, S.R. Bare, E. Nikolla, J. Will Medlin, "Reactivity of Pd-MO2 inverted catalytic systems for CO oxidation", *Catalysis Science & Technology*, **12**, 1476-1486 (2022). DOI: 10.1039/d1cy01916c.
125. P. Acharya, R. Manso, A.S. Hoffman, S. Bakovic, L. Kékedy-Nagy, S.R. Bare, J. Chen, L. Greenlee, "Fe Coordination Environment, Fe-Incorporated Ni(OH)2 Phase, and Metallic Core are Key Structural Components to Active and Stable Nanoparticle Catalysts for the Oxygen Evolution Reaction", *ACS Catalysis*, **12**, 1992-2008 (2022). DOI:10.1021/acscatal.1c04881.
126. Y. Lu, C. Thompson, C.-T Kuo, X. Zhang, A.S Hoffman, A. Boubnov, S.R. Bare, L. Kovarik, H. Xin, A.M. Karim, "CO oxidation on MgAl2O4 Supported Irn: Activation of Lattice Oxygen in the Subnanometer Regime and Emergence of Nuclearity-Activity Volcano", *Journal of Materials Chemistry A,* **10**, 4266-4278 (2022). DOI: 10.1039/D1TA09740G
127. Thuy T. Le, K. Shilpa, C. Lee; S. Han, C. Weiland, S.R. Bare, P.J. Dauenhauer, J.D. Rimer, "Core-shell and Egg-shell Zeolite Catalysts for Enhanced Hydrocarbon Processing", *J. Catalysis*, **405**, 664–675 (2022). DOI: 10.1016/j.jcat.2021.11.004.
128. E. Hiennadi, F. Molajafari, R. Rana, A.S. Hoffman, S.R. Bare, J. Howe, S. Khatib, "Understanding Control of Speciation of Zeolite-Supported Metal Oxides", *Chem. Mater.* (2023), 35, 23, 9907–9923. DOI: 10.1021/acs.chemmater.3c01545.
129. M. C. Cendejas, O.A. Paredes Mellone, U. Kurumbail, Z. Zhang, J.H. Jansen, F. Ibrahim, S. Dong, J. Vinson, A.N. Alexandrova, D. Sokaras, S.R. Bare & I. Hermans, "Tracking Active Phase Behavior on Boron Nitride during the Oxidative Dehydrogenation of Propane Using Operando X-ray Raman Spectroscopy", *J. Am. Chem. Soc.,* (2023), 145, 47, 25686–25694. DOI: 10.1021/jacs.3c08679.
130. M. Stone, M. Cendejas, A. Persson, G. Liccardo, J. Smith, A. Kumar, C. Zhou, E. Gardner, A. Aitbekova, K. Bustillo, M. Chi, S.R. Bare & M. Cargnello, "Ceria incorporation in sinter-resistant platinum-based catalysts", *ACS Catalysis*, (2023), **13**, 14853-14863. DOI: 10.1021/acscatal.3c02766.
131. M. S. Hossain, G.S. Dhillon, , L. Liu, A. Sridhar, E.J. Hiennadi, J. Hong, S.R. Bare, H. Xin, T. Ericson, A. Cozzolino & S. J. Khatib, "Elucidating the role of Mo-Fe interactions in the metal oxide precursors for Fe promoted Mo/ZSM-5 catalysts in non-oxidative methane dehydroaromatization", *Chemical Engineering Journal* (2023), **475**, 14609. DOI: 10.1016/j.cej.2023.146096.
132. Ostervold, L., Smerigan, A., Liu, M., Filardi, L., Vila, F., Perez-Aguilar, J., Hong, J., Tarpeh, W., Hoffman, A., Greenlee, L., Clark, E., Janik, M. J., & Bare, S. R. "Cation Incorporation into Copper Oxide Lattice at Highly Oxidizing Potentials", *ACS Applied Materials & Interfaces* (2023), **15**, 47025–47036. DOI: 10.1021/acsami.3c10296
133. Smerigan, A., Biswas, S., Vila, F. D., Hong, J., Perez-Aguilar, J. E., Hoffman, A. S., Greenlee, L., Getman, R. B. & Bare, S. R. "Aqueous Structure of Lanthanide–EDTA Coordination Complexes Determined by a Combined

DFT/EXAFS Approach", *Inorganic Chemistry* (2023), DOI:10.1021/acs.inorgchem.3c01334.
134. Albrahim, M., Shrotri, A., Unocic, R., Hoffman, A., Bare, S., & Karim, A. M. "Size-Dependent Dispersion of Rhodium Clusters into Isolated Single Atoms at Low Temperature and the Consequences for CO Oxidation Activity", *Angewandte Chemie International Edition* (2023), e202308002. DOI:10.1002/anie.202308002.
135. Chen, L., Allec, S. I., Nguyen, M.-T., Kovarik, L., Hoffman, A. S., Hong, J., Meira, D., Shi, H., Bare, S. R., Glezakou, V.-A., Rousseau, R., & Szanyi, J. "Dynamic Evolution of Palladium Single Atoms on Anatase Titania Support Determines the Reverse Water–Gas Shift Activity", *Journal of the American Chemical Society*, (2023), ***145*** (19), 10847–10860. DOI:10.1021/jacs.3c02326.
136. Shah, S., Hong, J., Cruz, L., Wasantwisut, S., Bare, S. R., & Gilliard-Abdul Aziz, K. L. "Dynamic Tracking of NiFe Smart Catalysts using *In Situ* X-Ray Absorption Spectroscopy for the Dry Methane Reforming Reaction", *ACS Catalysis*, (2023), ***13*** (6), 3990–4002. DOI:10.1021/acscatal.2c05572.
137. C. B. Thompson, L. Liu, D.S. Leshchev, A.S. Hoffman, J. Hong, S.R. Bare, R.R. Unocic, E. Stavitski, H. Xin, A.M. Karim, "CO Oxidation on $Ir_1/TiO_2$: Resolving Ligand Dynamics and Elementary Reaction Steps", *ACS Catalysis*, (2023), **13**, 7802-7811. DOI: 10.1021/acscatal.3c01433.
138. Z. Zhang, J. Tian, Y. Lu, S. Yang, D. Jiang, W. Huang, Y. Li, J. Hong, A.S. Hoffman, S.R. Bare, M.H. Engelhard, A.K. Datye, Y. Wang, "Memory-dictated Dynamics of Single-atom Pt on CeO2 for CO Oxidation", Nature Communications (2023), **14**, 2664. DOI: 10.1038/s41467-023-37776-3.
139. P. Acharya, J. Hong, R. Manso, A.S. Hoffman, L. Kekedy-Nagy, S.R. Bare, J. Chen, L. Greenlee, "Temporal Ni K-edge Study Reveals Kinetics of Ni Redox Behavior of Iron-Nickel Oxide Bimetallic OER Catalyst", *Journal of Physical Chemistry C*, (2023), **127** (25), 11891–11901. DOI:10.1021/acs.jpcc.3c03480.
140. S. Das, U. Anjum, K.H. Lim, Q. He, A.S. Hoffman, S.R. Bare, S.M. Kozlov, B.C. Gates, S. Kawi, "Genesis of Active Pt/CeO2 Catalyst for Dry Reforming of Methane by Reduction and Aggregation of isolated Platinum Atoms into Clusters", *Small*, (2023), 202207272. DOI: 10.1002/smll.202207272.
141. L. Li, J. Chalmers, S.R. Bare, S.L. Scott, F.D. Vila, "Rigorous Oxidation State Assignments for Supported Ga-Containing Catalysts Using Theory-Informed X-Ray Absorption Spectroscopy Signatures from Well-Defined Ga(I) and Ga(III) Compounds", *ACS Catalysis* (2023), **13**, 6549-6561. DOI: 10.1021/acscatal.3c01021.
142. S. Kong, P. Singh, G. Akopov, D. Jing, R. Davis, J. Perez-Aguilar, J. Hong, S. J. Lee, G. Viswanathan, E. Soto, M. Azhan, T. Fernandes, S. Harycki, A.Gundlach-Graham, Y. V. Kolen'ko, D. D. Johnson and K. Kovnir, "Probing of the Noninnocent Role of P in Transition-Metal Phosphide Hydrogen Evolution Reaction Electrocatalysts via Replacement with Electropositive Si", *Chem. Mater.* (2023), **35**, *14*, 5300–5310. DOI: 10.1021/acs.chemmater.3c00460.
143. T.T. Le, W. Qin, N. Nikolopoulos, D. Fu, M.D. Patton, C. Weiland, S.R. Bare, B.M. Weckhuysen, J.D. Rimer, "Elemental Zoning Enhances Mass Transport in

Zeolite Catalysts", *Nature Catalysis*, (2023), **6**, 254-265. DOI: 10.1038/s41929-023-00927-2.
144. B. Yeh, S. Chheda, S.D. Prinslow, A.S. Hoffman, J. Hong, J. Perez-Aguilar, S.R. Bare, C.C. Lu, L. Gagliardi, A. Bhan, "Structure and Site Evolution of Framework Ni Species in MIL-127 MOFs for Propylene Oligomerization Catalysis", *J. Am. Chem. Soc.*, (2023), 145, 3408-3418. DOI: 10.1021/jacs.2c10551.
145. D. Thompson, A.S. Hoffman, Z. Mansley, S. York, Sarah; F. Wang, Y. Zhu, S.R. Bare, J. Chen, "Synthesis of Amorphous and Various Phase-Pure Nanoparticles of Nickel Phosphide with Uniform Sizes via a Trioctylphosphine-Mediated Pathway", *Inorganic Chemistry*, (2024), online. DOI: /10.1021/acs.inorgchem.4c03334.
146. D. Leybo, U. Etim, M. Monai, Matteo, S.R. Bare, Z. Zhong, C. Vogt, "Metal Support Interactions in Metal Oxide-Supported Atomic, Cluster, and Nanoparticle Catalysis", *Chemical Society Reviews*, (2024) online. DOI: 10.1039/D4CS00527A.
147. C. Zhou, A. Aitbekova, M. Stone, E. McShane, B. Werghi, S. Nathan, G. Liccardo, C. Song, J. Ciston, K. Bustillo, A.S, Hoffman, J. Hong, J. Perez-Aguilar, S.R. Bare, M. Cargnello, "Steam-Assisted Selective $CO_2$ hydrogenation to ethanol over Ru-In catalysts", *Angewandte Chemie Int. Ed*, (2024), **63**, e202406761. DOI: 10.1002/anie.202406761.
148. Y. Chen, R. Rana, Y. Zhang, A.S. Hoffman, Z. Huang, B. Yang, J.E. Perez-Aguilar, J. Hong, X. Li, J. Zeng, M. Chi, C.X. Kronawitter, H. Wang, S.R. Bare, A.R. Kulkarni, B.C. Gates, "Dynamic Structural Evolution of MgO-Supported Palladium Catalysts: From Metal to Metal Oxide Nanoparticles to Surface then Subsurface Atomically Dispersed Cations", *Chemical Science*, (2024), **15**, 6454-6464. DOI:10.1039/D4SC00035H.
149. S.T. Kristy, S. Svadlenak, A.S. Hoffmann, S.R. Bare, K.A. Goulas, "Site Requirements for Inhibition-free CO Oxidation over Silica-supported Bimetallic PdCu Alloys", *Catal. Sci. Technol.*, (2024), **14**, 3956-3965. DOI:10.1039/d4cy00255e.
150. C. Zhou, G. Liccardo, A.S. Hoffman, J. Oh, S.E. Holmes, A. Vailionis, S.R. Bare, M. Cargnello, "Understanding and Harnessing Nanoscale Immiscibility in Ru–In Alloys for Selective $CO_2$ Hydrogenation", *Journal of the American Chemical Society* (2024), **146**, 29, 19986-19997. DOI: 10.1021/jacs.4c03652
151. Ryan H. Manso, Jiyun Hong, Wei Wang, Prashant Acharya, Adam S. Hoffman, Xiao Tong, Feng Wang, Lauren F. Greenlee, Yimei Zhu, Simon R. Bare, and Jingyi Chen, "Revealing Structural Evolution of Nickel Phosphide-Iron Oxide Core–Shell Nanocatalysts in Alkaline Medium for the Oxygen Evolution Reaction", *Chemistry of Materials* (2024), **36**, 13, 6440-6453. DOI: 10.1021/acs.chemmater.4c00379
152. Y. Zhao, S.F. Kurtoğlu-Öztulum, A.S. Hoffman, J. Hong, J.E. Perez-Aguilar, S.R. Bare, A. Uzun, "Acetylene ligands stabilize atomically dispersed supported rhodium complexes under harsh conditions", *Chemical Engineering Journal* (2024), **485**, 149738. DOI:10.1016/j.cej.2024.149738
153. W.J. Shaw, M.K. Kidder, S.R. Bare, et al., "A US perspective on closing the carbon cycle to defossilize difficult-to-electrify segments of

our economy", *Nature Reviews Chemistry (2024)*, **8**, 376–400. DOI: 10.1038/s-41570-024-00587-1.
154. L. Ostervold, A.S. Hoffman, D. Thompson, S.R. Bare, E.L. Clark, "A Versatile Electrochemical Cell for Operando XAS", *ChemCatChem,* (2024), e202400072. DOI: 10.1002/cctc.202400072.
155. W. Zhou, N. Felvey, J. Guo, A.S. Hoffman, S.R. Bare, A. Kulkarni, R. Runnebaum, C. Kronawitter, "Reduction of co-fed carbon dioxide modifies the local coordination environment of zeolite-supported, atomically dispersed chromium to promote ethane dehydrogenation", *Journal of the American Chemical Society (2024)*, **146**, 14, 10060–10072. DOI: 10.1021/jacs.4c00995.
156. R.J. Meyer, S.R. Bare, G.A. Canning, J.G. Chen, P. Chu, R.J. Davis, J. Falkowski, A.S. Hock, A.S. Hoffman, A.M. Karim, S.D. Kelly, Y. Lei, E. Stavitski, C.J. Wrasman, "Recommendations to Standardize Reporting, Execution and Interpretation of XAS Measurements", *Journal of Catalysis (2024)*, 432, 115369. DOI: 10.1016/j.jcat.2024.115369.
157. H. Robatjazi, T. Battsengel, J. Finzel, P. Tieu, M. Xu, A.S. Hoffman, J. Qi, S.R. Bare, X. Pan, B.F. Chmelka, N.J. Halas, P. Christopher, "Dynamic behavior of Platinum atoms and clusters in the native oxide layer of Aluminum nanocrystals", *ACS Nano* (2024), 18, 8, 6638–6649. DOI:10.1021/acsnano.3c12869.
158. L.R. Filardi, F.D. Vila, J. Hong, A.S. Hoffman, J.E. Perez-Aguilar, Simon R. Bare, R.C. Runnebaum, C.X. Kronawitter, "Impact of Local Structure in Supported CaO Catalysts for Soft Oxidant-Assisted Methane Coupling Assessed through Ca K-edge X-ray Absorption Spectroscopy", *J. Phys. Chem. C* (2024), **128**, 3, 1165–1176. DOI: 10.1021/acs.jpcc.3c06527
159. Y. Zhao, O. Bozkurt, S.F. Kurtoğlu-Öztulum, M. Yordanli, A.S. Hoffman, J. Hong, J. Perez-Aguilar, A. Saltuk, D. Akgül, O. Demircan, T. Ateşin, V. Aviyente, B.C. Gates, S.R. Bare, A. Uzun, "Atomically Dispersed Zeolite-Supported Rhodium Complex: Selective and Stable Catalyst for Acetylene Semi-Hydrogenation", *Journal of Catalysis* (2024), 429, 115196. DOI: 10.1016/j.jcat.2023.115196.
160. Y. He, Y. Li, M. Lei, F. Polo-Garzon, J. Perez-Aguilar, Simon R. Bare, E. Formo, H. Kim, L. Daemen, Y. Cheng, K. Hong, M. Chi, D. Jiang, Z. Wu, "Significant Roles of Surface Hydrides in Enhancing the Performance of Cu/$BaTiO_{2.8}H_{0.2}$ Catalyst for CO2 Hydrogenation to Methanol", Angew. Chem.Int. Ed. (2024) ,**63**, e202313389. DOI: 10.1002/anie.202313389.
161. S. Kristy, S. Svadlenak, A. S. Hoffman, S. R. Bare, & K. A. Goulas, "Spectroscopic Determination of Metal Redox and Segregation Effects During CO and CO/NO Oxidation Over Silica-supported Pd and PdCu Catalysts", *Applied Catalysis B: Environmental* (2024), **342**, 123329. DOI:10.1016/j.apcatb.2023.123329.

# POSTER PRESENTATION ABSTRACTS

Frank Abild-Pedersen

# Metal Independent Site-specific Correlations for Adsorption Energies

Frank Abild-Pedersen
SUNCAT Center for Interface Science and Catalysis
SLAC National Accelerator Laboratory, 2575 Sand Hill Road, Menlo Park, CA-94025, USA

## Presentation Abstract

Establishing energy correlations among different metals can accelerate the discovery of efficient and cost-effective catalysts for complex reactions. Using a recently introduced coordination-based model, we can predict site specific metal binding energies ($\Delta E_M$) that can be used as a descriptor for chemical reactions. In this study, we have examined a range of transition metals and found linear correlations between $\Delta E_M$ which can be predicted through a simple parametrization scheme and adsorption energies of catalytically relevant intermediates at various coordination environment for all the considered metals. Interestingly, all the metals correlate with one another under specific surface site coordination, indicating that different metals are interrelated in a particular coordination environment. Furthermore, we have tested and verified for PtPd and PtIr-based alloys that they follow a similar behavior. Moreover, we have expanded the metal space by taking some early transition metals along with few s-block metals and shown a cyclic behavior of the adsorbate binding energy ($\Delta E_A$) versus $\Delta E_M$. Therefore, $\Delta E_{CH}$ and $\Delta E_O$ can be efficiently interpolated between metals, alloys and inter-metallics based on information related to one metal only. This simplifies the process of screening new metal catalyst formulations and their reaction energies.

**Grant or FWP Number: SUNCAT-FWP**

**PI:** Thomas F. Jaramillo
**Postdoc(s):** Shyama C. Mandal, Joakim Halldin Stenlid, Shikha Saini, Anshuman Goswami
**Student(s):**
**Affiliations(s):**

## RECENT PROGRESS

An understanding of the breaking and making of chemical bonds at a solid surface is the starting point for any fundamental description of reactions at the solid-gas or solid-liquid interface. It is particularly important to understand which properties of the surface

determine its chemical activity. The description and understanding of activation energies for elementary surface reactions and how it depends on the evolution of the active site and its surroundings under operation conditions is a prime focus of this task. In addition to activity of catalysts we also focus our attention on the loss of active surface area through either strong metal-support interactions or sintering. The ability to prevent such side-reactions from happening would greatly enhance catalyst lifetimes and increase the activity/mass ratio significantly. The thermal catalysis research focus has three general areas: Towards site-specific reactivity/selectivity trends, Controlling the dynamic evolution of catalysts, and Designing catalysts beyond the binding site.

***Pt alloys for active and stable propane dehydrogenation catalysts***

We have focused a significant effort on controlling activity beyond the local binding site on a Pt catalyst for propane dehydrogenation. This reaction is important in the efficient production of propylene and increasing its activity and selectivity requires detailed engineering of its active site.

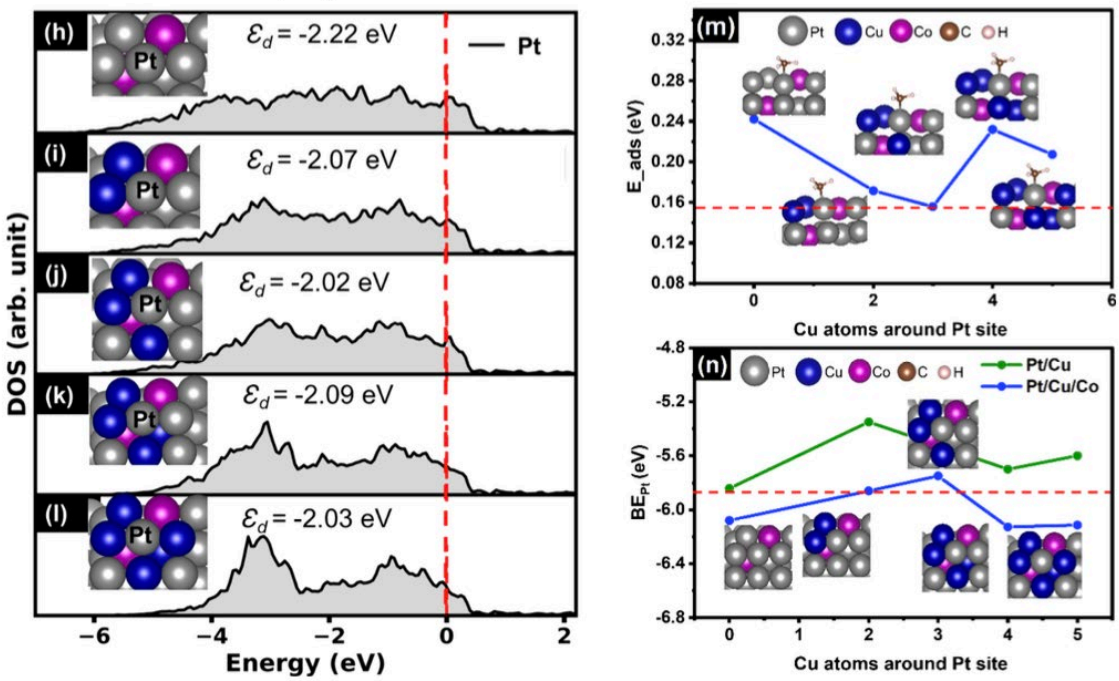


In this collaborative work between theory and experiment we studied the effect of alloying Pt and Cu using colloidal techniques, combined with characterization, testing, and density functional theory to study how Cu content enhances the activity for propane dehydrogenation at low temperatures. This work has helped further our understanding of the structure-activity relationship and improved knowledge in propane dehydrogenation

catalyst development featuring reduced Pt loadings and notable thermal stability for propylene production.[1]

Ongoing work focuses on understanding $ZrO_2$ supported Cu catalysts and their inverted systems for the conversion of $CO_2$ and $H_2$. This study has provided great insight into the importance of active site mobility and how it can be manipulated by system inversion. In a purely theoretical work.

In addition, we have examined the possibility of applying the spatial nature of the calculated electrostatic potential in DFT to describe reactions in heterogeneous catalysis. Because of its subatomic spatial resolution, we can analyse both directionality and confinement effects in surface adsorption. The use of the electrostatic potential when assessing the 3D nature of catalytic sites provides a new avenue in catalyst design.[4]

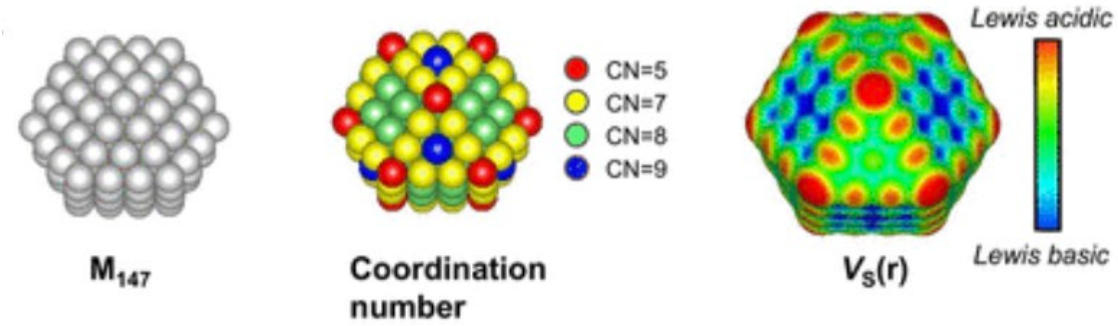


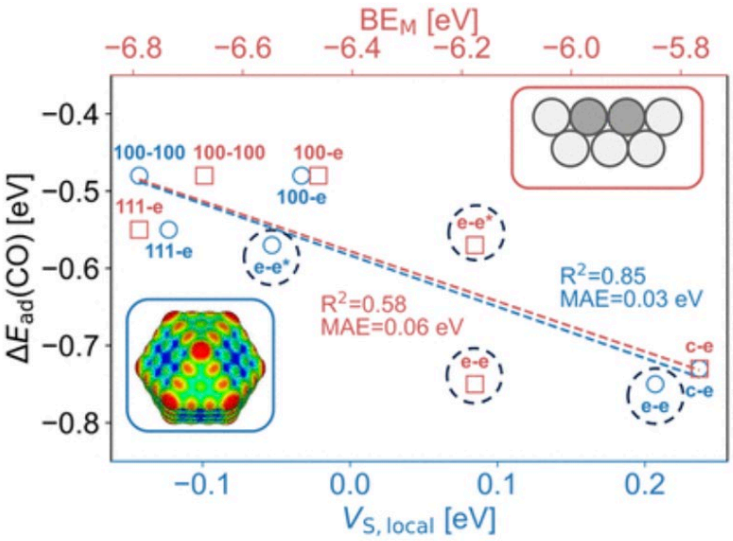

**Publications Acknowledging this Grant in 2021-2024**

*(I) Intellectually led by this grant*

1. Baraa Werghi, Shikha Saini, Pin-Hung Chung, Abinash Kumar, Amani M. Ebrahim, Kristen Abels, Miaofang Chi, Frank Abild-Pedersen, Simon R. Bare and Matteo Cargnello. Dynamic Behavior of Pt Multimetallic Alloys for Active and Stable Propane Dehydrogenation Catalysts *JACS*, **2024** (Accepted)

2. Shyam Deo, Melissa Kreider, Gaurav Kamat, McKenzie Hubert, José A. Zamora Zeledón, Lingze Wei, Jesse Matthews, Nathaniel Keyes, Ishaan Singh, Thomas Jaramillo, Frank Abild-Pedersen, Michaela Burke Stevens, Kirsten Winther, Johannes Voss. Interpretable Machine Learning Models for Practical Antimonate Electrocatalyst Performance. *ChemPhysChem*. **2024**, 25, 13 e202400010.

3. Benjamin M. Comer, Neha Bothra, Jaclyn R. Lunger, Frank Abild-Pedersen, Michal Bajdich, Kirsten T. Winther. Prediction of O and OH Adsorption on Transition Metal Oxide Surfaces from Bulk Descriptors. *ACS Catalysis*, **2024**, 14, 5286-5296.

4. Joakim Halldin Stenlid, Frank Abild-Pedersen. Revealing Local and Directional Aspects of Catalytic Active Sites by the Nuclear and Surface Electrostatic Potential. *The Journal of Physical Chemistry C*, **2024**, 128, 4544-4558.

5. Shikha Saini, Joakim Halldin Stenlid, Shyam Deo, Philipp N. Plessow, Frank Abild-Pedersen. A first principles approach to modeling surface site stabilities on multi-metallic catalysts. *ACS Catalysis*, **2024**,14, 874-885.

6. Shyama Charan Mandal, Frank Abild-Pedersen. Classification of Adsorbed Hydrocarbons Based on Bonding Configurations of the Adsorbates and Surface Site Stabilities. *ACS Catalysis*. **2023**, 13, 20, 13663–13671.

7. Joakim Halldin Stenlid, Verena Streibel, Tej Salil Choksi, Frank Abild-Pedersen. Assessing catalytic rates of bimetallic nanoparticles with active-site specificity: A case study using NO decomposition. *Chem Catalysis*, **2023**, 3, 100636.

8. Jinwon Oh, Arik Beck, Emmett D Goodman, Luke T Roling , Anthony Boucly, Luca Artiglia, Frank Abild-Pedersen, Jeroen A van Bokhoven, Matteo Cargnello. Colloidally Engineered Pd and Pt Catalysts Distinguish Surface-and Vapor-Mediated Deactivation Mechanisms. *ACS Catalysis*, **2023**, 13, 1812-1822.

9. Shikha Saini, Joakim Halldin Stenlid, Frank Abild-Pedersen. Electronic structure factors and the importance of adsorbate effects in chemisorption on surface alloys. *npj Computational Materials*, **2023**, 8, 163.

10. Benjamin M. Comer, Jiang Li, Frank Abild-Pedersen, Michal Bajdich, and Kirsten T. Winther . Unraveling Electronic Trends in O* and OH* Surface Adsorption in the MO2 Transition-Metal Oxide Series. *Journal of Physical Chemistry C*, **2022**, 126, 7903-7909.

11. Matthew J Liu, Jinyu Guo, Adam S Hoffman, Joakim Halldin Stenlid, Michael T Tang, Elizabeth R Corso, Kevin H Stone, Frank Abild-Pedersen, Simon R Bare, William A Tarpeh. Catalytic Performance and Near-Surface X-ray Characterization of Titanium Hydride Electrodes for the Electrochemical Nitrate Reduction Reaction. *Journal of the American Chemical Society*, **2022**, 144, 5739-5744.

12. Nadia Tahsini, An-Chih Yang, Verena Streibel, Baraa Werghi, Emmett D Goodman, Aisulu Aitbekova, Simon R Bare, Yuejin Li, Frank Abild-Pedersen, Matteo Cargnello. Colloidal Platinum–Copper Nanocrystal Alloy Catalysts Surpass Platinum in Low-Temperature Propene Combustion. *Journal of the American Chemical Society*, **2022**, 144, 1612-1621.

13. Verena Streibel, Hassan Aljama, An-Chih Yang, Tej S Choksi, Roel S Sánchez-Carrera, Ansgar Schäfer, Yuejin Li, Matteo Cargnello, Frank Abild-Pedersen. Microkinetic modeling of propene combustion on a stepped, metallic palladium surface and the importance of oxygen coverage. *ACS Catalysis*, **2022**, 12, 1742-1757.

14. Jiang Li, Joakim Halldin Stenlid, Thomas Ludwig, Philomena Schlexer Lamoureux, Frank Abild-Pedersen. Modeling Potential-Dependent Electrochemical Activation Barriers: Revisiting the Alkaline Hydrogen Evolution Reaction. *Journal of the American Chemical Society*, **2021**, 143, 19341-19355.

15. Philomena Schlexer Lamoureux, Verena Streibel, Tej Choksi, Frank Abild-Pedersen. Combining artificial intelligence and physics-based modeling to directly assess atomic site stabilities: from sub-nanometer clusters to extended surfaces. *Physical Chemistry Chemical Physics*, **2021**, 23, 22022-22034.

16. Tao Wang, Frank Abild-Pedersen. Achieving industrial ammonia synthesis rates at near-ambient conditions through modified scaling relations on a confined dual site. *Proceedings of the National Academy of Sciences*, **2021**, 118, e2106527118.

17. An-Chih Yang, Verena Streibel , Tej S Choksi , Hassan Aljama , Baraa Werghi , Simon R Bare , Roel S Sánchez-Carrera, Ansgar Schäfer , Yuejin Li , Frank Abild-Pedersen , Matteo Cargnello. Insights and comparison of structure–property relationships in propane and propene catalytic combustion on Pd-and Pt-based catalysts. *Journal of Catalysis*, **2021**, 401, 89-101.

18. Tao Wang, Xinjiang Cui, Kirsten T Winther, Frank Abild-Pedersen, Thomas Bligaard, Jens K Nørskov. Theory-Aided Discovery of Metallic Catalysts for Selective Propane Dehydrogenation to Propylene. *ACS Catalysis*, **2021**, 11, 6290-6297.

19. Tao Wang, Guomin Li, Xinjiang Cui, Frank Abild-Pedersen. Identification of earth-abundant materials for selective dehydrogenation of light alkanes to olefins.*Proceedings of the National Academy of Sciences*, **2021**, 118, e2024666118.

20. Tao Wang, Frank Abild-Pedersen. Identifying factors controlling the selective ethane dehydrogenation on Pt-based catalysts from DFT based micro-kinetic modeling. *Journal of Energy Chemistry*, **2021**, 58, 37-40.

*(II) Jointly funded by this grant and other grants with intellectual leadership by other funding sources*

1. Carmen Martínez-Alonso, Valentin Vassilev-Galindo, Benjamin M. Comer, Frank Abild-Pedersen, Kirsten T. Winther, Javier LLorca. Application of machine learning to discover new intermetallic catalysts for the hydrogen evolution and the oxygen reduction reactions. *Catalysis Science and Technology*, **2024**, 14, 3784-3799.

2. Frederik C Østergaard, Frank Abild-Pedersen, Jan Rossmeisl. Coverage, repulsion, and reactivity of hydrogen on High-Entropy alloys. *Journal of Catalysis*, **2024**, 435, 115570.

3. Dong Jiang, Gang Wan , Joakim Halldin Stenlid, Carlos E García-Vargas, Jianghao Zhang, Chengjun Sun, Junrui Li, Frank Abild-Pedersen, Christopher J Tassone, Yong Wang. Dynamic and reversible transformations of subnanometre-sized palladium on ceria for efficient methane removal. *Nature Catalysis*, **2023**, 6, 618-627.

4. Wanghui Zhao, Gaomou Xu, Zhaochun He, Cheng Cai, Frank Abild-Pedersen, Tao Wang. Toward Carbon Monoxide Methanation at Mild Conditions on Dual-Site Catalysts. *Journal of the American Chemical Society*, **2023**, 145, 8726-8733.

5. Hemanth Somarajan Pillai, Yi Li, Shih-Han Wang, Noushin Omidvar, Qingmin Mu, Luke EK Achenie, Frank Abild-Pedersen, Juan Yang, Gang Wu, Hongliang Xin. Interpretable design of Ir-free trimetallic electrocatalysts for ammonia oxidation with graph neural networks. *Nature Communication*, **2023**, 14, 792.

6. Joaquin Resasco, Frank Abild-Pedersen, Christopher Hahn, Zhenan Bao, Marc Koper, Thomas F Jaramillo. Enhancing the connection between computation and experiments in electrocatalysis. *Nature Catalysis*, **2022**, 5, 374-381.

7. Zoe Ashbridge, Elisabeth Kreidt, Lucian Pirvu, Fredrik Schaufelberger, Joakim Halldin Stenlid, Frank Abild-Pedersen, David A Leigh. Vernier template synthesis of molecular knots.*Science*, **2022**, 375, 1035-1041.

8. Egon Campos dos Santos, Rafael B Araujo, Mikael Valter, German Salazar-Alvarez, Mats Johnsson, Michal Bajdich, Frank Abild-Pedersen, Lars Gunnar Moody Pettersson. Efficient Screening of Bi–Metallic Electrocatalysts for Glycerol Valorization. *Electrochimica Acta*, **2021**, 398, 139283.

## Atomic-Level Modeling of Extended Environmental Effects on Catalytic Processes

Damian Duda [c], Jack Fuller, [a] Benjamin A. Jackson, [a] Carrington G. Moore, [a] Alexander D. Von Rueden, [a] Sarah Sprouse [c] David Dixon,[c] Bojana Ginovska,[a] Mal-Soon Lee,[a] Simone Raugei, [a] Greg Schenter,[a] and Líney Árnadóttir[a,b]

[a] Pacific Northwest National Laboratory, Physical and Computational Sciences Directorate and Institute for Integrated Catalysis, Richland, WA 99354, USA

[b] School of Chemical, Biological, and Environmental Engineering, Oregon State University, Corvallis, Oregon 97331, USA

[c] Department of Chemistry and Biochemistry, The University of Alabama, Tuscaloosa, AL 35487, USA

### Poster Abstract

Computational and theoretical research are a crucial part of the BES Catalysis core program at PNNL, aiming to provide detailed atomic-level understanding and predictive capabilities for catalytic processes in close collaborations with experimental efforts. To design models that better represent realistic catalytic conditions, we apply a multi-level approach tailored to the complexity of the problem. Here, recent progress in several program areas is presented, highlighting the breadth of computational methods and chemical systems studied by the computational team. 1) We developed thermodynamic and kinetic descriptors for ketone hydrogenation using hydricity and $H^-$ self-exchange rates and show how linear free energy relationships provide accuracy within 2 kcal/mol of experimentally measured barriers. 2) We developed a methodology to qualitatively capture entropic and enthalpic contributions to the kinetics and thermodynamics of CuH dimerization where ligand-ligand and ligand-solvent interactions dominate. The methodology uses coupling quantum chemical/molecular mechanics (QM/MM) and classical (MM) molecular dynamics (MD) to bridge the different timescales of phenomena affecting the reaction coordinate. 3) We studied the role of solvents in confined spaces using ab initio MD (AIMD). We showed how solvents affect the interactions between cyclohexanol and the Brønsted acid site, leading to the protonation of the cyclohexanol in a polar solvent. 4) We used a combination of AIMD structural sapling and QM geometry optimizations to build a stable model of a reconstructed $Fe_3O_4$(001) surface. This model provided mechanistic insights into the decomposition of formic acid to CO and $CO_2$ and the role of OH in the different pathways.

### FWP 47319: Advancing key catalytic reaction steps for achieving carbon neutrality

**PI:** Johannes Lercher
**Co-PI's:** Aaron M. Appel, Liney Arnadottir (Oregon State U.), David A. Dixon (U. Alabama), Zdenek Dohnalek, John L. Fulton, Bojana Ginovska, Jian Zi Hu, Abhi J. Karkamkar, Bruce D. Kay, Konstantin Khivantsev, Sungmin Kim, Greg A. Kimmel, Libor Kovarik, Thuy Thanh D. Le, Mal Soon Lee, Johannes A. Lercher, John C. Linehan, Zbynek Novotny, Simone Raugei, Udishnu Sanyal, Gregory K. Schenter, Wendy J. Shaw, Honghong Shi, Janos Szanyi, Ba L. Tran, Huamin Wang, Yong Wang, Nancy M. Washton, Eric S. Wiedner

## Integrated $CO_2$ Capture and Conversion to Methane: Understanding Ligand-Coated Nanorods for Plasmon-Enhanced Electrocatalysis

L. Robert Baker[1*], Catherine J. Murphy[2], Robert E. Warburton[3], Tomaz Neves-Garcia[1], Tithi Lai[1], Emily A. Cook[2], Amos Shi[2], and Diana Soto[2]
[1] The Ohio State University, Department of Chemistry and Biochemistry
[2] University of Illinois Urbana-Champaign, Department of Chemistry
[3] Case Western Reserve University, Department of Chemistry

### Presentation Abstract

Direct electrochemical reduction of $CO_2$ capture species, i.e. carbamate and (bi)carbonate, is promising for $CO_2$ capture and conversion, where the energetically demanding stripping step is bypassed. We have recently demonstrated that atomically dispersed Ni deposited on various electrode surfaces directly converts captured $CO_2$ to methane. A detailed study employing XPS and HAADF-STEM reveals that highly dispersed Ni atoms are uniquely active for converting capture species to methane, and the activity of single Ni atoms is further confirmed using a molecularly defined Ni phthalocyanine catalyst supported on carbon nanotubes. Comparing the kinetics of $CO_2$ capture solutions obtained from hydroxide, ammonia, primary, secondary, and tertiary amines confirm that carbamate, rather than (bi)carbonate or dissolved $CO_2$, is primarily responsible for methane production. This conclusion is supported by $^{13}C$ NMR spectroscopy as well as DFT calculations showing that single-atom Ni is more active for the reduction of carbamate compared to bulk Ni, producing methane as the primary product. To extend these findings, the Baker group at Ohio State is working closely with the Murphy group at University of Illinois to explore the role of plasmon excitation on the activation of $CO_2$ and $CO_2$ capture species using ligand-coated, multimetallic nanorods as model catalysts. This collaboration brings together the synthesis and characterization of size, shape, composition, and ligand-controlled nanorod catalysts with electrokinetic studies and advanced spectroscopy to study the mechanism of plasmon-enhanced $CO_2$ activation.

### DE-SC0024157: Multimetallic Ligand-Coated Nanoparticles for Plasmon-Enhanced Electrochemical $CO_2$ Reduction

**PI:** L. Robert Baker
**Postdoc(s):** Tomaz Neves-Garcia
**Student(s):** Tithi Lai
**Affiliations(s):** The Ohio State University

## RECENT PROGRESS

***Integrated $CO_2$ Capture and Conversion to Methane on Single-Atom Nickel***

A significant challenge associated with $CO_2$ utilization is the need to capture and sequester $CO_2$ either from the air or source production. One approach to improving the overall efficiency of $CO_2$ capture and utilization is to integrate the capture and conversion processes via the direct electrochemical reduction of the capture solution. Our group has recently discovered that single Ni atoms are highly selective for electrochemical reduction of $CO_2$ capture species to methane. Figure 1 shows results of electrochemical reduction of various capture solutions using Ni atoms finely dispersed on a Au electrode. Kinetic are shown for three different capture solutions: 1) KOH (0.5 M), 2) $NH_3$ (0.5 M), and the combination of KOH and $NH_3$ (0.5 M each). Hydroxide as well as amines capture free $CO_2$ yielding (bi)carbonate; additionally, amine solutions react with $CO_2$ to produce carbamate. Interestingly, Figure 1a shows that captured $CO_2$ is converted to methane only in the third capture solution, containing both KOH and $NH_3$.

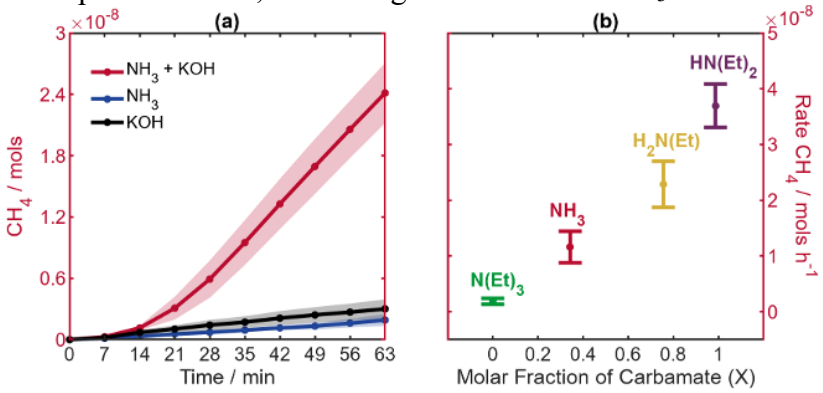


***Figure 1 (a)*** *Methane production vs time from three $CO_2$ capture solutions using a Ni catalyst deposited on a Au electrode.* ***(b)*** *Comparison of methane production rate for four amine-based capture solutions as a function of carbamate mole fraction.*

These results indicate that carbamate represents the active species for methane production. Unlike (bi)carbonate, carbamate is only formed when an amine is present in the capture solution. However, during reaction the carbamate anion is separated from the negatively charged electrode surface by the large ammonium cation. Sargent and co-workers have shown that tailoring the electric double layer (EDL) by addition of small alkali metal cations is required to bring the carbamate closer to the surface to be reduced (*Nat. Energy*, **6**, 46, 2021). Therefore, these results are explained by the fact that carbamate is only formed when $NH_3$ is present but can only be reduced at the negatively charged cathode when a small cation, such as $K^+$, is present in the EDL. This conclusion is supported by control experiments showing that similar methane yields are obtained when KOH is replaced with KCl or other alkali metal salts (not shown).

To further confirm that carbamate plays a key role in methane production, the same reaction was carried out for an additional series of amine solutions: $NH_3$, monoethylamine (MEA), diethylamine (DEA), and triethylamine (TEA), each containing KOH as a supporting electrolyte. The carbamate mole fraction, defined as the equilibrium ratio of carbamate:(bi)carbonate concentrations, is quantified using $^{13}C$ NMR (not shown). Figure 1b shows the rate of methane production as a function of carbamate mole fraction confirming a direct correlation, further suggesting that methane production

results from the reduction of carbamate. To confirm that Ni is the active species, similar results have been demonstrated for Ni deposited on Au, Cu, and C electrodes (not shown). Highly dispersed Ni is significantly more active than bulk Ni. To confirm the activity of single Ni atoms, the reaction has been performed using molecularly defined Ni phthalocyanine catalysts deposited on carbon nanotubes (not shown).

To our knowledge, this is the first example of direct conversion of carbamate to a hydrocarbon product. To understand the unique activity of Ni atoms for carbamate conversion, we collaborated with the group of Robert Warburton (Case Western) to perform DFT calculations. Figure 2 shows the free energy diagram and intermediate geometries for carbamate reduction on Ni@Au(211). Using the computational hydrogen electrode (CHE) model, the reaction pathways are calculated at 0 V and –0.83 V vs RHE (shown in black and red, respectively). Overall, the theoretical predictions are consistent with experimental observation, which show that because the C-N bond is not cleaved until the final proton-coupled electron transfer step, other possible products such as CO, formate, or methanol are not observed. Comparing the results for dispersed Ni atoms on Au with bulk Ni (not shown) indicates that carbamic acid adsorption on Ni (211) is 0.16 eV less exothermic than Ni@Au(211). Moreover, the final step of the reaction on Ni (211) is uphill at –0.83 V vs. RHE, meaning that a larger overpotential is needed to produce $NH_3$ and close the catalytic cycle, consistent with experiment. These combined experimental and theoretical results are under review for publication in the *Journal of the American Chemical Society*.

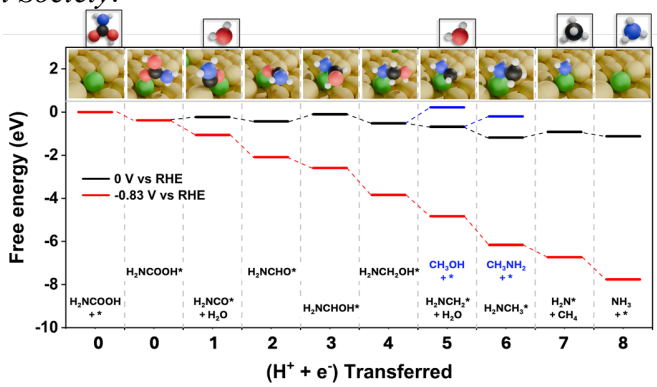


***Figure 2*** *DFT free energy diagram and intermediate geometries for carbamate reduction on single-atom Ni sites on a Au(211) electrode.*

### *Multimetallic Ligand-Coated Nanorods for Plasmon Enhanced Catalysis*

Building on these findings, the Baker group at Ohio State is working with the Murphy group at University of Illinois to explore the role of plasmon excitation on the activation of $CO_2$ and $CO_2$ capture species using ligand-coated, multimetallic nanorods as model catalysts. Au nanorods synthesized in the Murphy group, in which the aspect ratio is controlled by the addition of small amounts of impurity Ag ions, show tunable plasmon resonances in the visible and near-IR portions of the spectrum (Figure 3). The cetrimonium bromide (CTAB) bilayer on the as-synthesized rods can be ligand-exchanged to poly(ethylene glycol) monomethyl ether (mPEG) or dodecanethiol (DDT) for $CO_2$R experiments.

Measurements by the Baker group have focused on a kinetics of $CO_2$R (i.e., no capture species) on Au nanoparticles with various surface ligands (Figure 4). Results show that nanorods coated with a CTAB bilayer deactivate rapidly due to leaching of

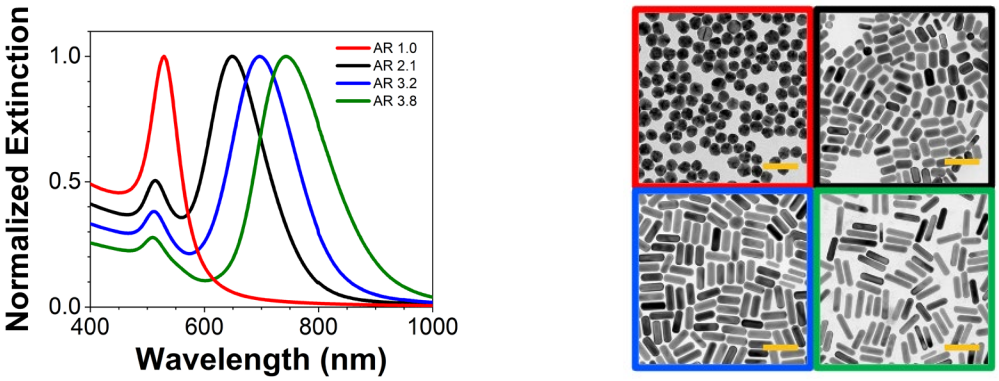


***Figure 3*** *Normalized extinction spectra of aqueous suspensions (left), and transmission electron micrographs (right) of standard gold nanorods. Scale bars represent 100 nm. Colored lines and boxes connect the optical spectrum to the micrograph of four select samples. AR = aspect ratio.*

these water-soluble particles into the aqueous electrolyte. Exchanging for mPEG surface ligands stabilizes the nanorods but shows low selectivity for $CO_2R$ compared to $H_2$ evolution. In contrast, Baker and Murphy have shown that DDT surface ligands act as a selectively permeable membrane that allows unhindered transport of $CO_2$ while blocking water and metal ions that result in $H_2$ production (*Chem. Sci.*, **11**, 12298, 2020). These results indicate that DDT is a promising surface ligand for future studies of electrochemical reduction of $CO_2$ and $CO_2$ capture species under plasmon resonant excitation.

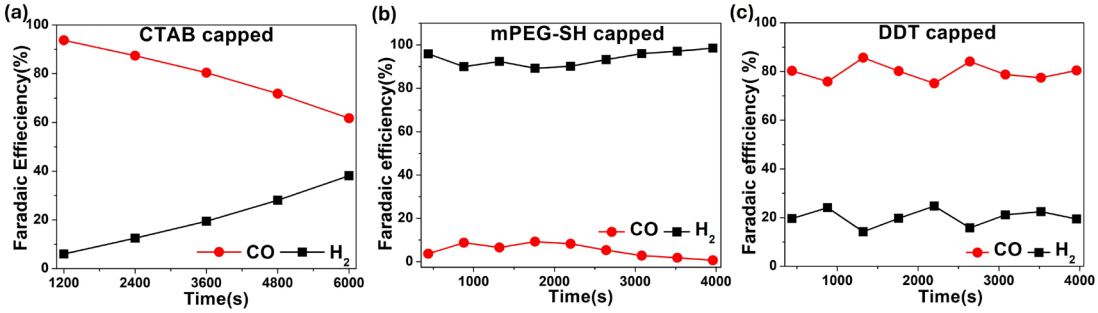


***Figure 4*** *Faradaic efficiency for CO (red) and H2 (black) vs time for Au nanoparticle catalysts containing CTAB (a), mPEG (b), and DDT (c) surface ligands.*

**Publications Acknowledging this Grant in 2021-2024**

I. Intellectually led by this grant
   1. Neves-Garcia, T.; Hasan, M.; Zhu, Q.; Li, J.; Jiang, Z.; Liang, Y.; Wang, H.; Rossi, L. M.; Warburton, R. E.; Baker, L. R. Integrated Carbon Dioxide Capture by Amines and Conversion to Methane on Single-Atom Nickel Catalysts, *J. Amer. Chem. Soc.* **2024**, *Under Review*.

II. Jointly funded by this grant and other grants with intellectual leadership by other funding sources – None

Bart M. Bartlett

# Probing Electrocatalytic Chloride Oxidation as a Redox Mediator in Water and in Ethanol

Bart M. Bartlett (PI), Jake O'Hara, Siqi Li, Ryan D. Van Daele (Graduate Students),
Katherine Morrissey (Undergraduate Student)
Department of Chemistry, University of Michigan, Ann Arbor, MI 48109-1055

## Presentation Abstract

In this past year, we have answered a key question about the mechanism of chloride ion oxidation: does the reaction proceed in an outer-sphere or inner-sphere fashion? We have answered this question on two platforms – on $WO_3$ photoelectrodes in water on glassy carbon dark electrodes in ethanol. In both instances, our prior published work shows that a hypochlorite form (hypochlorous acid in water or ethyl hypochlorite in ethanol) product is formed. This product then carries out chemical oxidation of primary alcohols like ethanol to form acetaldehyde in water, which gets further oxidized to acetic acid; or 1,1-diethoxyethane, the acetal protected form of acetaldehyde in ethanol. We find experimental evidence of inner sphere binding to the electrode on both platforms. On $WO_3$, Cl K-edge (*ligand*-based) XANES shows Cl–W covalency on films measured after chloride oxidation in water. On glassy carbon, XPS shows signatures of oxidized chloride on the surface in a Volmer step. Moreover, Koutecký-Levich analysis of glassy carbon rotating ring disk electrodes then supports overall two-electron transfer to form ethyl hypochlorite as the reaction intermediate for generating 1,1-diethoxyethane. The inner-sphere nature of the chloride oxidation reaction gives insight for exploring other chloride-mediated reactions – specifically that low chloride concentration can be effective for mediating alcohol oxidation and that controlling the defect density of Lewis acidic sites (in the case of $WO_3$) is an effective means for increasing reaction rate.

## DE-SC0006587: Tandem Electrocatalysis and Particle-based Catalysis as a Strategy for Mediated Alcohol Oxidation Reactions

## RECENT PROGRESS

### *Tungsten Oxide Photoelectrodes with Greater Surface $W^{5+}$ Ion Concentration Show Increased Photocurrent Densities for Oxidizing Covalently Bound Chloride Ion*

Tungsten oxide ($WO_3$) is an *n*-type semiconductor due to oxygen vacancies ($\square_O^{\bullet\bullet}$ in Kroger-Vink notation) or surface protonation as $H_xWO_3$. It is one of the few acid-stable oxides under large positive bias, which makes $WO_3$ ideal for interrogating the mechanism of the electrocatalytic chloride oxidation reaction (COR) to yield hypochlorous acid, a chemical oxidant. The large, positive valence band edge of ~ 3 eV provides the overpotential necessary to carry out the COR, but the reaction competes with the oxygen-evolution reaction in water. The $\square_O^{\bullet\bullet}$ defect density can be controlled by annealing temperature, so $WO_3$ films were prepared by a spin-coating method from an ammonium metatungstate

precursor annealed at 500 ºC, 585 ºC, 660 ºC, and 740 ºC. Additionally, annealing the films under an $O_2$ atmosphere hinders the formation of $\square_O^{\bullet\bullet}$. We observe higher photocurrent densities ($j_{ph}$) in films annealed at 500 ºC in air, compared to those annealed at 500 ºC in $O_2$ (0.31 mA/cm$^2$ vs. 0.27 mA/cm$^2$ at 1.5 V vs. Ag/AgCl, pH 3; before the onset of a dark reaction). In a formal oxidation sense and in the absence of other defects, each $\square_O^{\bullet\bullet}$ results in reduction of two $W^{6+}$ ions to $W^{5+}$. In films displaying the highest $j_{ph}$, we measure a high surface $W^{5+}$ concentration of 18.53 % by X-ray photoelectron spectroscopy (XPS). Finally, probing the Cl ligand K-edge by X-ray absorption near-edge spectroscopy (XANES) shows a Cl 1*s* → W 5*d* transition at 2824.5 eV, lower energy than the ligand-centered Cl 1*s* → 4*p* transition, indicating the presence of W–Cl covalent bonds. This result stands in contrast to the commonly assumed mechanistic proposal invoking outer-sphere electron transfer to a physisorbed chloride ion.

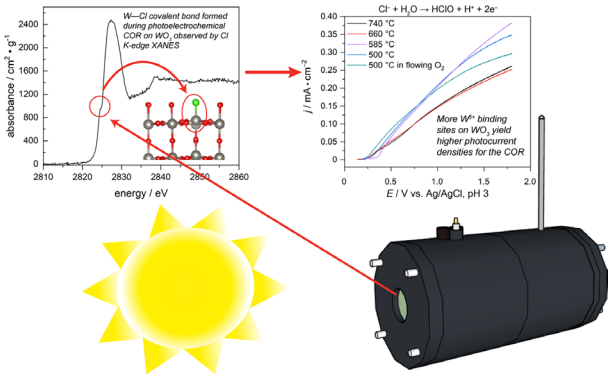


**Figure 1.** Cl K-edge XANES showing Cl–W bonding as an elementary step of electrocatalytic chloride oxidation on $WO_3$ in water. Having great $\square_O^{\bullet\bullet}$ defect concentration (measured as $W^{5+}$ by XPS) yields greater photocurrent density.

## *Insights into the Mechanism of Electrochemical Chloride Oxidation in Ethanol from Rotating Ring-Disk Electrodes and Quiescent Solution Voltammetry*

The wide availability of bio-derived alcohols provides the impetus to develop processes that convert them to valuable chemicals. Chloride ion can mediate neat ethanol oxidation to 1,1-diethoxyethane (1,1-DEE) through an ethyl hypochlorite intermediate on a glassy carbon (GC) electrode, and we have used several electrochemical methods to describe the mechanism. First, cyclic voltammetry in inert acetonitrile solvent establishes a Volmer step, where solution chloride ion adsorbs as chlorine(0) on GC. This result is corroborated by an ex-situ X-ray photoelectron spectroscopy (XPS) of the GC electrode after linear-sweep

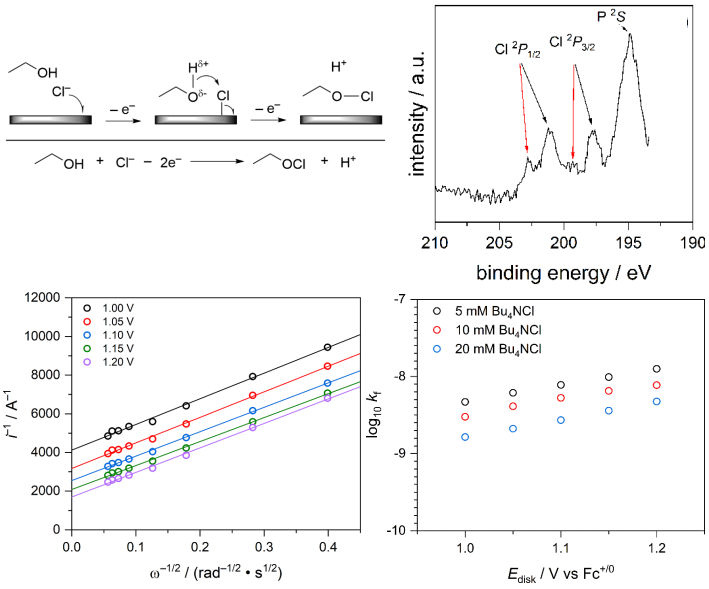


**Figure 2.** Proposed mechanism for chloride-mediated electrocatalytic ethanol oxidation. Support for the Volmer step comes from XPS data, and rate constants are determined by Koutecký-Levich analysis for RRDE data.

voltammetry (LSV). This single-electron-transfer reaction also occurs in neat ethanol, evidenced by analyzing the peak current response; we propose that the second electron transfer occurs as a chemical step with ethanol solvent. Koutecký-Levich (K-L) analysis on a rotating ring disk electrode (RRDE) shows that the kinetic rate constant of the chloride oxidation reaction (COR) is on the order of $10^{-8}$ to $10^{-9}$, which is 4 – 5 orders of magnitude faster than the direct alcohol oxidation reaction in a kinetically limited regime. This hydrodynamic approach in understanding the electrochemistry of this non-aqueous system extends the possibilities for mediated electrocatalysis in neat alcohol solvents.

**Publications Acknowledging this Grant in 2021-2024**

*Please classify your publications into two categories according to the source of support for the work published:*

*(I) Intellectually led by this grant*


1. O'Hara, J.; Thabit, N. S.; Vogt, L. I.; Penner Hahn, J. E.; Woodley, C. P.; Chrenka, H.; Bartlett, B. M.* Tungsten Oxide Photoelectrodes with Greater Surface $W^{5+}$ Ion Concentration Show Increased Photocurrent Densities for Oxidizing Covalently Bound Chloride Ion. *Submitted.*
2. Li, S.; Van Daele, R. D.; Morrissey, K. H.; Bartlett, B. M.* Insights into the Mechanism of Electrochemical Chloride Oxidation in Ethanol from Rotating Ring-Disk Electrodes and Quiescent Solution Voltammetry. *In Revision.*
3. Li, S.; Morrissey, K. H.; Bartlett, B. M.* Strategies in Photochemical Alcohol Oxidation on Noble-metal Free Nanomaterials as Heterogenous Catalysts. *Chem. Commun.* **2024**, *60*, 10295-10305.
4. Breuhaus-Alvarez, A. G.; Li, S.; Hardin, N. Z.; Bartlett, B. M.* Oxidizing Ethanol and 2-Propanol by Hypochlorous Acid Generated from Chloride Ions on $H_xWO_3$ Photoelectrodes. *J. Phys. Chem. C* **2021**, *125*, 26307-26312.
5. Li, S.; Bartlett, B. M.* Selective Chloride-Mediated Neat Ethanol Oxidation to 1,1-Diethoxyethane via an Electrochemically Generated Ethyl Hypochlorite Intermediate. *J. Am. Chem. Soc.* **2021**, *143*, 15907-15911.
6. McDonald, K. D.; Bartlett, B. M.* Microwave synthesis of Spinel $MgFe_2O_4$ Nanoparticles and the Effect of Annealing on Photocatalysis. *Inorg. Chem.* **2021**, *60*, 8704-8709.
7. DiMeglio, J. L.; Terry, B. D.; Breuhaus-Alvarez, A. G.; Whalen, M. J.; Bartlett, B. M.* Base-Assisted Nitrate Mediation as the Mechanism of Electrochemical Benzyl Alcohol Oxidation. *J. Phys. Chem. C* **2021**, *125*, 8148-8154.
8. Breuhaus-Alvarez, A. G.; Cheek, Q.; Cooper, J. J.; Maldonado, S.; Bartlett, B. M.* Chloride Oxidation as an Alternative to the Oxygen Evolution Reaction on $H_xWO_3$ Photoelectrodes. *J. Phys. Chem C.* **2021**, *125*, 8543-8550.


*(II) Jointly funded by this grant and other grants with intellectual leadership by other funding sources*

None

Wesley H. Bernskoetter

# Air Stable SPS Pincer Ligands for Catalytic $CO_2$ Hydrogenation

Wesley H. Bernskoetter and Nilay Hazari
University of Missouri and Yale University

## Presentation Abstract

Sustainable energy carriers are required to reduce our reliance on fossil fuels. The synthesis of fuels and chemical feedstocks from carbon dioxide is attractive both for environmental reasons and because carbon dioxide is inexpensive, non-toxic, and abundant. However, the production of liquid fuels from carbon dioxide requires the development of robust catalysts with improved productivity. One portion of this project undertakes the development of air and moisture tolerant pincer ligands for catalytic reversible hydrogenation of $CO_2$. Recent investigation of SPS pincer ligands on Fe and Ru have afforded new, highly active catalysts for $CO_2$ reduction to formate and provided insights into relevant catalyst deactivation pathways. These findings generate guidelines from which new catalyst are designed and elucidate productivity limiting events in the valorization of $CO_2$ by sulfur containing pincer Ru and Fe catalysts.

**DE-SC0018222: Base Metal Catalysis with Relevance to Energy Storage Applications**

**Postdoc(s):** Alex Mondragon Diaz (Missouri); Justin Wedal (Yale)
**Student(s):** Kyler Virtue (Missouri); Ayanava Ghosh (Missouri)

## RECENT PROGRESS

### *Synthesis of Fe Complexes with Air Stable SPS and SNS Pincer Ligands*

Many studies have explored the effect of varying the phosphine substituents of $^{R}PN^{R'}P$ ligands in order to understand their reactivity and generate improved catalysts. However, there are significantly fewer investigations which vary the donor atom identities in these pincer ligands. Our program has previously compared the coordination chemistry of PNP and SNS supported Ru catalysts in an effort to elucidate the steric and electronic influences of S atom incorporation into the primary ligand sphere. In addition, our program seeks to enhance the development of S-containing pincer ligands catalysts as a strategy to decrease the costs and

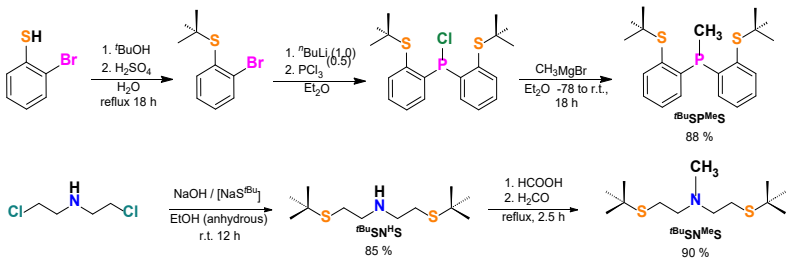


**Figure 1.** Synthetic routes to $^{tBu}SN^{H}S$, $^{tBu}SN^{Me}S$ and $^{tBu}SP^{Me}S$ pincers.

toxicity associated with ligands containing multiple alkyl phosphine groups. During this reporting period our program has extended our study of S-containing pincer ligands to the synthesis of new SNS and SPS Fe complexes. A series of $^{tBu}SN^{H}S$, $^{tBu}SN^{Me}S$ and $^{tBu}SP^{Me}S$ pincer ligands were prepared in good yields (Figure 1) and their coordination chemistry on Fe explored. ($^{tBu}SN^{H}S$)$FeX_2$ (X = Cl (**1**$^{Cl}$), Br (**1**$^{Br}$) and ($^{tBu}SN^{Me}S$)$FeX_2$ (X = Cl (**2**$^{Cl}$), Br (**2**$^{Br}$) were obtained via extended stirring of the ligands with anhydrous $FeX_2$ in THF. Analysis of select complexes using x-ray crystallography reveals a distorted trigonal bipyramidal geometry around Fe (Figure 2), and magnetic susceptibility measurements (Evans' Method) within the range expected for high spin Fe(II) compounds (4.9 – 5.2 $\mu_B$). Conducting the analogous reaction with $^{tBu}SP^{Me}S$ afforded coordination chemistry distinct from the SNS ligands (Figure 3). Metallation with $FeCl_2$ initially produced a trimetallic complex, [($^{tBu}SP^{Me}S$)Fe]$_2$($\mu$-$FeCl_4$) (**3**), in which one thioether group from each pincer ligand stabilizes the central Fe atom. Dissolving **3** in $CH_2Cl_2$ resulted in expulsion of the bridging "$FeCl_2$" unit over several hours, affording the chloride bridged dimer [($^{tBu}SP^{Me}S$)FeCl($\mu_2$-Cl)$_2$ (**4**). Monomeric dihalide Fe coordination complexes with $^{tBu}SP^{Me}S$ were only obtained from $FeBr_2$, and yielded the tetrahedral, four-coordinate species, ($\kappa^2$-$^{tBu}SP^{Me}S$)$FeBr_2$ (**5**). The coordination chemistry of the $FeX_2$ complexes of the $^{tBu}SN^{H}S$, $^{tBu}SN^{Me}S$ and $^{tBu}SP^{Me}S$ pincer ligands exhibit marked differences from the PNP ligated analogues, which typically produce monomeric, five-coordinate iron dihalide species. We anticipate that these distinctions in coordination geometry and aggregation state will also produce unique elementary reaction pathways and catalytic activity in studies of $CO_2$ reduction. Our immediate goal is to continue development of the synthetic chemistry required to convert these S-atom containing pincer iron dihalide complexes into (pre)catalyst targets bearing metal-hydride and/or stabilizing carbon monoxide ligands which will allowing direct comparison to the (PNP)Fe catalysts.

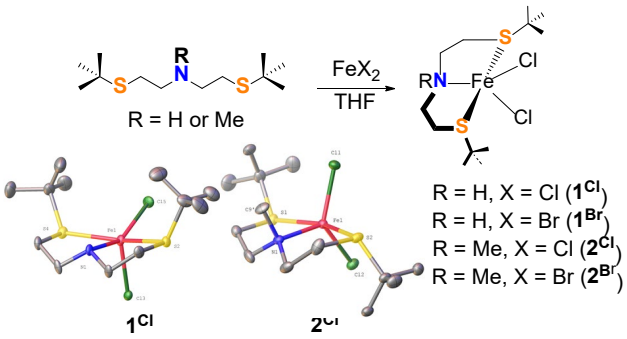


**Figure 2.** Preparation of $^{tBu}SN^{H}S$ and $^{tBu}SN^{Me}S$ ligated Fe dihalide complexes.

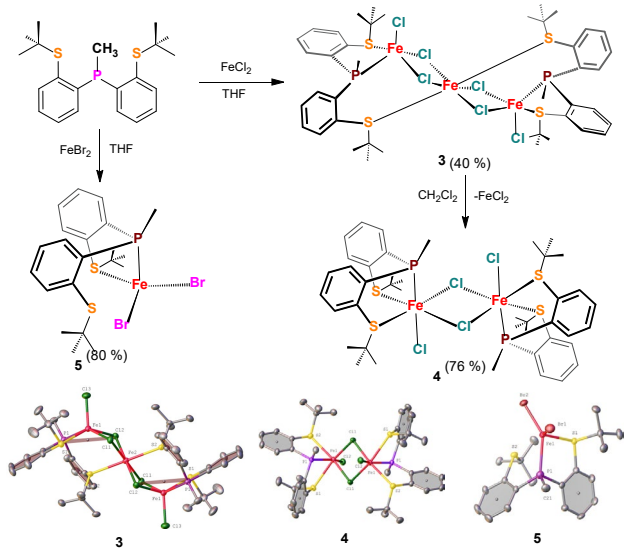


**Figure 3.** Coordination chemistry of $^{tBu}SP^{Me}S$ Fe dihalide species.

### *Synthesis of (SPS)Ru Complexes and $CO_2$ Hydrogenation Catalysis*

Our prior studies of $^{tBu}SN^{H}S$ and $^{tBu}SN^{Me}S$ ligated Ru complexes reveal significant differences in the redox properties compared to the corresponding $^{R}PNP$ complexes, in some cases SNS ligated systems are *ca* 300 mV more easily reduced. This dramatic redox shift was accompanied by numerous synthetic difficulties in isolating stable Ru(II) hydride (pre)catalysts for studying $CO_2$ reduction. Our program hypothesized that coordinating the $^{tBu}SP^{Me}S$ ligand to Ru (Figure 1) would result in complexes with electronic properties between $^{tBu}SN^{H}S$ and $^{R}PNP$ and allow us to better explore the changes in the redox properties of pincer ligated complexes containing sulfur donors and identify ligand features for $CO_2$ activation. Starting from commercially available $[Ru(PPh_3)_3]Cl_2$, the Ru dichloride complex ($^{tBu}SP^{Me}S$)$Ru(PPh_3)Cl_2$ (**6**) was prepared in nearly quantitative yield (Figure 4). Treatment of **6** with $NaBH_4$ in EtOH initially afforded a species tentatively identified as ($^{tBu}SP^{Me}S$)$Ru(PPh_3)(H)(BH_4)$, but exposure to vacuum or $NEt_3$ results in isolation of the corresponding ruthenium dihydride complex ($^{tBu}SP^{Me}S$)$Ru(PPh_3)H_2$ (**7**) (Figure 4). Complex **7** inserts $CO_2$ rapidly under 1 atm to generate the formate species, ($^{tBu}SP^{Me}S$)$Ru(PPh_3)(H)(HCO_2)$ (**8**), but extrudes the heterocumulene quickly upon exposure to vacuum. Significantly, complex **7** has proven a highly active catalyst for $CO_2$ hydrogenation to formate under basic conditions, achieving a turnover of nearly 16,000 in 1 hr (Figure 4). This ranks **7** among the most active catalysts reported for this reaction, comparing favorably to many PNP congeners, as well as a rare example of a sulfur based pincer catalyst for $CO_2$ hydrogenation. Additionally, complex **7** displays a robust tolerance to air, remaining unaffected in the solid state for more than 2 days and for hours in solution. Evidence for a possible catalyst activation route has been garnered in reactions between SPS and $[RuH_2(PPh_3)_3(CO)]$ which resulting in C-S bond cleavage of the thio substituent (Figure 4). Current investigations are exploring ligand designs which may mitigate ligand activation and well as further catalytic applications of ($^{tBu}SP^{Me}S$)$Ru(PPh_3)H_2$.

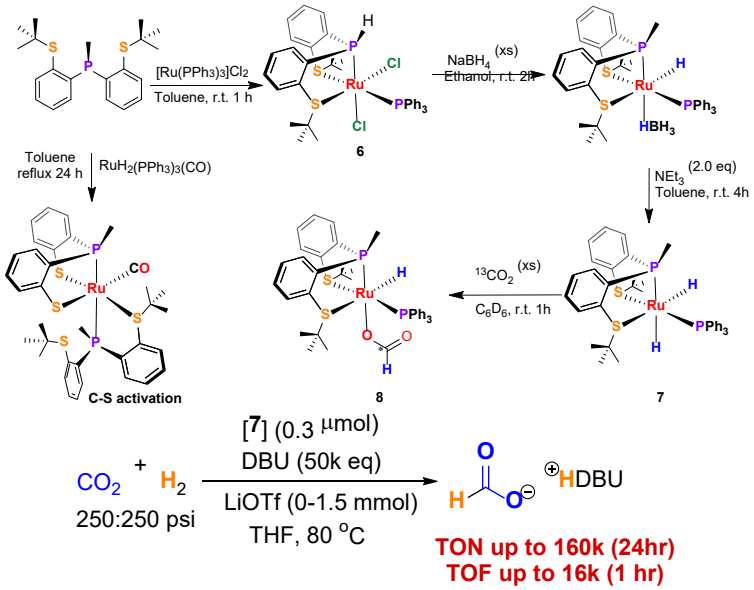


**Figure 4.** Coordination and $CO_2$ hydrogenation chemistry of of$^{tBu}SP^{Me}S$ Ru complexes.

**Publications Acknowledging this Grant in 2021-2024**

*(I) Intellectually led by this grant*

Curley, J. B.; Smith, N. E.; Bernskoetter, W. H.; Ertem, M. Z.; Hazari, N.; Mercado, B. Q.; Townsend, T. M.; Wang, X. P. "Understanding the Reactivity and Decomposition of a Highly Active Iron Pincer Catalyst for Hydrogenation and Dehydrogenation Reactions." *ACS Catal.* **2021**, *11*, 10631-10646.

Townsend, T. M.; Bernskoetter, W. H; Hazari, N.; Mercado, B. Q. "Dehydrogenative Synthesis of Carbamates from Formamides and Alcohols Using a Pincer-Supported Iron Catalyst." *ACS Catal.* **2021**, *11*, 10614-10624.

Chirdon, D. N.; Kelley, S. P.; Hazari, N.; Bernskoetter, W. H. "Comparative Coordination Chemistry of PNP and SNS Pincer Ruthenium Complexes." *Organometallics* **2021**, *40*, 4066-4076.

Curley, J. B.; Hert, C.; Bernskoetter, W. H.; Hazari, N.; Mercado, B. Q. "Control of Catalyst Isomers Using an N-Phenyl-Substituted $RN((CH_2CH_2P^iPr_2)_2$ Pincer Ligand in $CO_2$ Hydrogenation and Formic Acid Dehydrogenation." *Inorg. Chem.* **2022**, *61*, 643-656.

Curley, J. B.; Townsend, T. M.; Bernskoetter, W. H.; Hazari, N.; Mercado, B. Q. "Iron, Cobalt, and Nickel Complexes Supported by a $^{iPr}PN^{Ph}P$ Pincer Ligand." *Organometallics* **2022**, *41*, 301-312.

Hert, C. M.; Curley, J.; Kelley, S. P.; Hazari, N.; Bernskoetter, W. H. "Comparative $CO_2$ Hydrogenation Catalysis with MACHO-type Manganese Complexes." *Organometallics*, **2022**, *41*, 3332-3340.

Wedal, J. C.; Virtue, K. B.; Bernskoetter, W. H.; Hazari, N.; Mercado, B. Q. "Iron Catalysts Supported by a PNP Ligand with an Additional Hemilabile Donor for $CO_2$ Hydrogenation" *ACS Catal.* **2024**, *14*, 13903-13914.

# Metal-Metal Bonded Catalysts for Ammonia Oxidation

John F. Berry
University of Wisconsin - Madison

## Presentation Abstract

The Berry lab has recently explored the capability of metal-metal bonded dinuclear coordination complexes to serve as electrocatalysts for the oxidation of ammonia to dinitrogen. We have found that the family of $Ru_2$ catalysts supported by 6-X-2-pyridone ligands (X = F, Cl, $CH_3$) oxidize ammonia at low overpotential. We present our in-depth studies of the electronic structure and mechanism of ammonia oxidation in order to understand their unique features. In particular, the comparison between mononuclear Ru catalysts and metal-metal bonded $Ru_2$ catalysts will be described. Additional studies of next generation catalysts, including $Os_2$ complexes, will be presented.

**Grant or FWP Number: Metal-Metal Bonded Catalysts for the Ammonia Oxidation Reaction: Critical Foundational Studies for a Nitrogen Economy; DE-SC0021021**

**Student(s):** Graduate students: Milton Acosta, Patricia Armenta, Catherine Getty, and Gaby Muñoz-Sánchez. Undergraduate students Ashley Jamison, Kaleb Andersen, and Max Beardsley

## RECENT PROGRESS

***Mechanistic Studies***
We are using a combination of synthesis, spectroscopy, and computations to elucidate the mechanism of N2 formation catalyzed by metal-metal bonded compounds. We recently published a major computational paper exploring several possible mechanistic routes. Currently, we are working on kinetic studies to help discriminate the possible mechanisms.

***New Catalyst Development***
We recently published two papers in which we used computational chemistry to predict redox potentials of ammonia-bound metal-metal bonded compounds, which could relate to their overpotential as electrocatalysts for ammonia oxidation. Currently we are synthesizing osmium complexes that are predicted to have very low overpotential for ammonia oxidation, and new ruthenium catalysts supported by easily-derivitizable ligands.

## Publications Acknowledging this Grant in 2021-2024

*Please classify your publications into two categories according to the source of support for the work published:*

*(I) Intellectually led by this grant*

*1.* Trenerry, M. J.; Acosta, M.; Berry, J. F. *J. Phys. Chem. A* **2024**, *128*, 4038-4051.
Computational Analysis of Low Overpotential Ammonia Oxidation by Metal-Metal Bonded Ruthenium Catalysts, and Predictions for Related Osmium Catalysts

2. Pavelic, A. M.; Trenerry, M. J.; Berry, J. F. *Dalton Trans*. **2023**, *52*, 7239-7248.
Computational Analysis of Metal-Metal Bonded Dimetal Tetrabenzoate Redox Potentials in the Context of Ammonia Oxidation Electrocatalysis

3. Roy, M. D.; Trenerry, M. J.; Thakuri, B.; MacMillan, S. N.; Liptak, M. D.; Lancaster, K. M.; Berry, J. F. *Inorg. Chem*. **2022**, *61*, 3443-3457.
Electronic Structure of Ru26+ Complexes with Electron-Rich Anilinopyridinate Ligands

4. Park, S. V.; Corcos, A. R.; Jambor, A. N.; Yang, T.; Berry, J. F. *J. Am. Chem. Soc.*, **2022**, *144*, 3259-3268.
Formation of the N≡N Triple Bond from Reductive Coupling of a Paramagnetic Diruthenium Nitrido Compound

5. Trenerry, M. J.; Wallen, C. M.; Brown, T. R.; Park, S. V.; Berry, J. F. *Nature Chemistry*, **2021**, *13*, 1221-1227.
Spontaneous N2 formation by a diruthenium complex enables electrocatalytic and aerobic oxidation of ammonia

*(II) Jointly funded by this grant and other grants with intellectual leadership by other funding sources*

1. Gilbert, M. M.; Trenerry, M. J.; Longley, V. R.; Berry, J. F.; Weix, D. J. *ACS Catalysis* **2023**, *13*, 11277-11290.
Ligand-Metal Cooperation Enables C–C Activation Cross-Coupling Reactivity of Cyclopropyl Ketones

2. Sailer, J. K.; Sharland, J. C.; Bacsa, J.; Harris, C. F.; Berry, J. F.; Musaev, D. G.; Davies, H. M. L. *Organometallics* **2023**, *42*, 2122-2133.
Diruthenium Tetracarboxylate-Catalyzed Enantioselective Cyclopropanation with Aryldiazoacetates

3. Choi, I.; Trenerry, M.; Lee, K.; King, N.; Berry, J. F.; Schomaker, J. *ChemSusChem*, **2022**, *15*, e202201662.
Divergent C–H Aminations and Iminations by Tuning Electrochemical Reaction Potentials

Elizabeth J. Biddinger

## Electrochemical dehydrogenation of benzyl alcohol in neutral electrolyte for hydrogen storage and transportation applications

Moses D. Chilunda[1], Alexander D. von Rueden[2,3], Mal-Soon Lee[2], Juan A. Lopez-Ruiz[2, 4] and Elizabeth J. Biddinger[1]
[1]Department of Chemical Engineering, The City College of New York, CUNY, New York, New York 10031, United States
[2]Institute for Integrated Catalysis, Pacific Northwest National Laboratory, Richland, WA 99354, USA
[3]Department of Chemical and Biological Engineering, University of Wisconsin-Madison, Madison, WI 53706, USA
[4]WSU-PNNL Bioproducts Institute, Pacific Northwest National Laboratory, Richland, WA 99354, USA

### Presentation Abstract

Liquid organic hydrogen carriers (LOHCs) offer a strategic alternative for hydrogen storage and transportation over long durations and distances, respectively. Electrochemical reactions provide a direct way to store and transport hydrogen via LOHCs by integrating the process with renewable electricity. Benzyl alcohol was hereby used as a hydrogen-rich LOHC model to investigate the selective electrochemical dehydrogenation (ECD) of a primary alcohol to an aldehyde. Under neutral conditions, the limited amount of $OH^-$ ions inhibit the undesirable further electrooxidation of benzaldehyde to form benzoic acid as observed mostly in alkaline electrolytes. Furthermore, neutral electrolytes enable more materials for catalysts and reactor design avoiding corrosion concerns. Investigations for ECD of benzyl alcohol were performed on as-prepared PdO electrocatalyst in 0.5 M sodium phosphate buffer (pH 7.2). Increasing the applied half-cell potential from 1.11 to 2.11V vs reversible hydrogen electrode (RHE) enhances the reaction rates but reduces the reaction efficiency due to the occurrence of the undesirable oxygen evolution reaction (OER). Optimal benzaldehyde selectivity of 99% was achieved at 1.61 V vs RHE. Understanding the kinetics of benzyl alcohol electrooxidation will allow proper tuning of catalysts and reaction conditions to better improve the efficiency and performance of the reaction under neutral conditions.

### DE-SC0024491: Structural influences in electrochemical dehydrogenation of liquid organic hydrogen carriers

**PI:** Elizabeth J. Biddinger[1], Juan A. Lopez-Ruiz[2,3] and Mal-Soon Lee[2]
**Postdoc(s):** None
**Student(s):** Moses D. Chilunda[1] and Alexander D. von Rueden[2,4]
**Affiliations(s):** [1]Department of Chemical Engineering, The City College of New York; [2]Institute for Integrated Catalysis, Pacific Northwest National Laboratory; [3]WSU-PNNL

Bioproducts Institute, Pacific Northwest National Laboratory; [4]Department of Chemical and Biological Engineering, University of Wisconsin-Madison.

## RECENT PROGRESS

### *Investigating the kinetics of electrochemical dehydrogenation of benzyl alcohol under neutral conditions using PdO/C electrocatalyst*

Electrochemical dehydrogenation (ECD) of benzyl alcohol (BA) forms benzaldehyde (BzH) which can be further oxidized under aqueous alkaline conditions to produce benzoic acid (BzA). BzH can hydrate in aqueous solution to form a gemine-diol which is active towards further electrooxidation in the presence of $OH^-$ ions. Operating under neutral conditions reduces the $OH^-$ concentration which can inhibit further electrooxidation of benzaldehyde. Transition metal oxides (TMO) have been reported to be key in benzyl alcohol electrooxidation under alkaline conditions. Pd-based oxide catalysts have also demonstrated good performance towards electrooxidation of organic molecules. Under neutral conditions, the mechanism and kinetics of BA ECD have not been extensively studied. ECD of 20 mM BA was performed in 0.5M sodium phosphate buffer (pH 7.2) using 0.77 mg/cm$^2$ of as-prepared 4 wt% PdO/C electrocatalyst to investigate the role of applied potential.

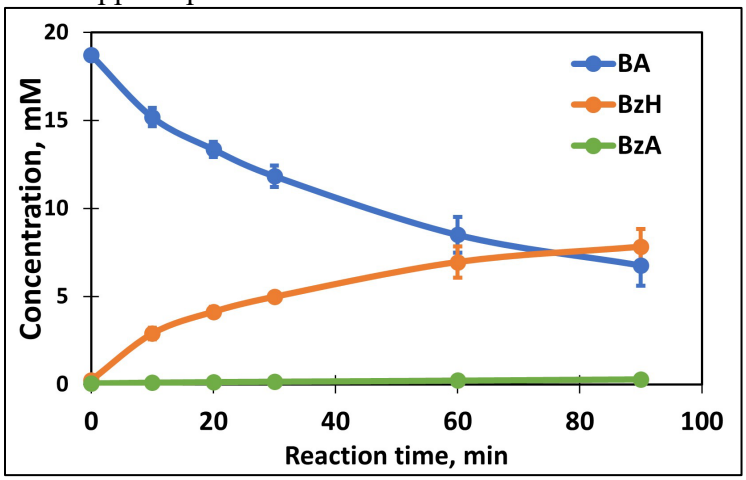


**Figure 1**: The concentrations of BA, BzH and BzA as a function of reaction time. Conditions: 20mM BA in 0.5M sodium phosphate buffer (pH 7.2), constant potential of 1.61V vs RHE and 4wt% PdO/C electrocatalyst.

Batch electrolysis was performed to observe the reaction performance as a function of reaction time. BzH was obtained as the main product with selectivity over 80% during 1.5 hr electrolysis at 1.61 V vs RHE. BzA was also observed as a minor product with selectivity around 3%. BzH concentration increased with reaction time while BzA remained constant during 1.5 hr electrolysis as shown in Figure 1.

Flow electrolysis was conducted to investigate the effect of applied potential on reaction performance and catalyst activity. Cyclic voltammetry (CV) scans were collected to provide initial insights for BA ECD. In Figure 2a, an oxidation peak at 1.6 V vs RHE associated with the electrooxidation of $Pd^{2+}$(PdO) to $Pd^{4+}$ ($PdO_2$) occurred right before the onset potential of OER. Interestingly, the addition of 20 mM BA shifted the $Pd^{2+}/Pd^{4+}$ oxidation peak 60 mV more positive. The OER current was also lowered, possibly due to fewer active sites for OER reactants and intermediates in the presence of the organic species. BA ECD was performed at 1.11, 1.61, and 2.11 V vs RHE. Steady state conditions were monitored by the current response with time and at 15-20 mins the current was stable (Figure 2b). BA conversion was negligible at 1.11 V vs RHE a (Figure 3a-d). Increasing applied potential to 1.61 V vs RHE showed an increase in conversion rate and production rate for BA and BzH, respectively (Figure 3a-b). At 1.61 V RHE, the production rate of BzA was considerably lower with a 1% selectivity and 2% FE (Figure 3b-d). Further increasing the applied potential to 2.11 V vs RHE resulted in higher BA conversion rates as seen in Figure 3b. The production rates of both BzH and BzA increased at 2.11 V vs RHE (Figure 3b) and the selectivity of BzH lowered from 99% to 88% due to its further electrooxidation to form BzA (selectivity 8.4%). The FE towards BA electrooxidation dramatically decreased to 54% at 2.11 V vs RHE. The decrease in FE is attributed to the presence of OER as a parasitic side reaction. FE towards BzA formation also increased to from 2% to 8.7% when the potential was increased from 1.61 to 2.11 V vs RHE. The mole balance of organics was consistently at 100% in both potentials suggesting that BzH and BzA were the only products formed during the reaction.

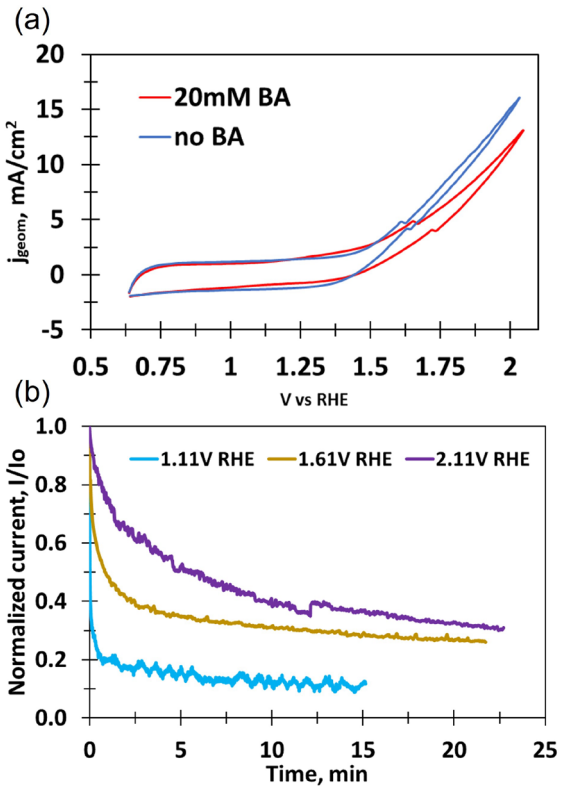


**Figure 2**:(a) CV scans of 0.5M PBS without and with addition of 20mM BA. Scan rate= 100mV/s (b) Normalized current change with time during 20mM BA ECD at different constant potentials in 0.5M sodium phosphate buffer. Experiments conducted in a continuous flow reactor and 4wt% PdO/C electrocatalyst

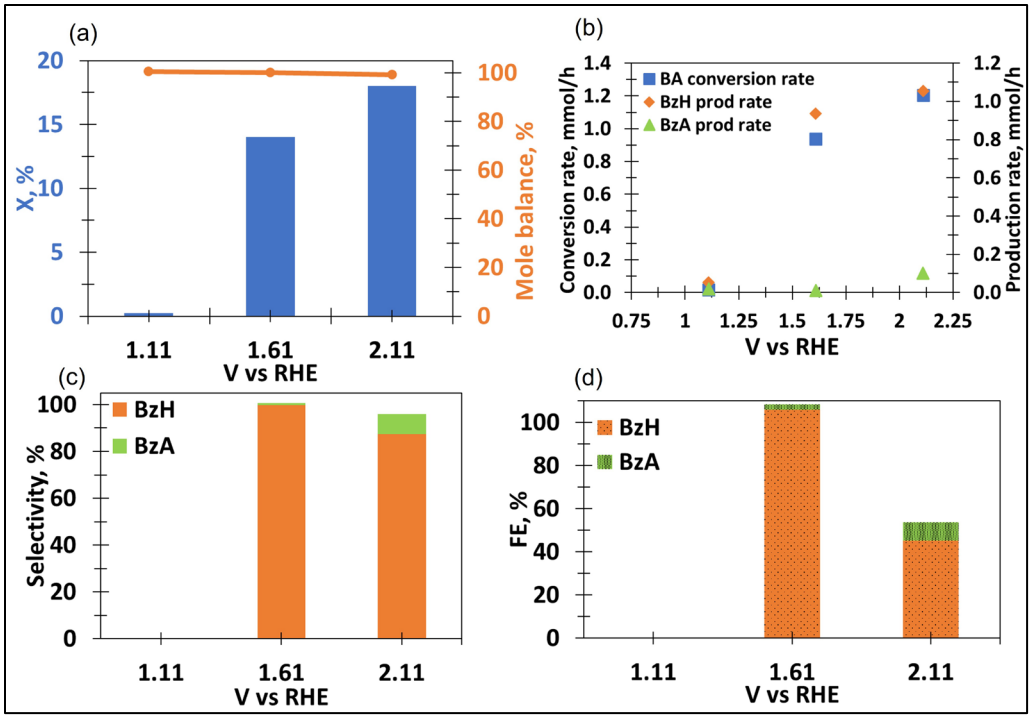


**Figure 3:** The role of applied potential on (a) Conversion and mole balance (b) BA conversion and BzH/BzA production rates (c)BzH and BzA selecitivity (d) BzH and BzA FE. Conditions: 20mM BA, 0.5M sodium phosphate buffer and 8mg of 4wt% Pd/O/C

Herein, we studied how applied potential can be tuned to selectively enhance reaction rates of BA ECD. Currently, we are working to correlate the reaction rates with the binding energies of BA, BzH, and BzA on the catalyst surface, as obtained from density functional theory (DFT) calculations. The experimental conditions (i.e., applied potential and electrolyte pH) suggest that the catalyst is in $PdO_2$ state during the electrochemical reaction based on the Pourbaix diagram. CV scans and initial surface characterization studies using X-ray photoelectron spectroscopy also indicate a $PdO_2$ state under working conditions. Guided by these observations, we have chosen $PdO_2$ for our atomistic modeling. Currently, we are evaluating the surface energy of different $PdO_2$ facets to determine appropriate $PdO_2$ surface models for representing the experimental catalyst. Once determined, we will investigate the energetics of BA ECD on these models and use the atomic-level insights gained to rationalize our experimental observations.

**Publications Acknowledging this Grant in 2021-2024**

None to date

## Interpretable Deep Learning for Advancing Field-Enhanced Catalysis

Fanglin Che
Department of Chemical Engineering, University of Massachusetts Lowell, USA, 01854

### Presentation Abstract

Electric fields can greatly impact the adsorption of polarized species, enhancing reaction rates and selectivity. These processes offer a sustainable and energy-efficient way to store renewable electricity in chemical form. However, low efficiency, high computational costs, and reliance on human-supervised calculations for field-dipole interactions have led to a trial-and-error approach in field-driven experimental processes. Deep and active learning of field-dipole interactions represents a new approach to designing high-performance catalysts with large local fields, relevant to technologies like electrostatic, electrocatalysis, and plasma catalysis. Understanding these interactions will enhance energy efficiency for decarbonization while accelerating catalyst discovery.

The aim of this presentation is to advance our understanding of field-dipole effects and promote electrostatic catalysis through a combination of multi-scale simulations, deep and active learning algorithms, and *in situ* experimental validation. We address the challenges and opportunities in field-enhanced heterogeneous catalysis, focusing on: (1) how machine learning approaches can quantify local electric fields (EF) and model the interactions between reactants and catalyst surfaces under EF conditions, (2) the role of advanced AI techniques, such as active learning and interpretable models, in guiding the design of future catalysts, (3) how field-dipole interactions can modify reaction mechanisms and lower activation energy barriers, and (4) the benefits of physics-informed machine learning in predicting reactant-surface interactions and capturing the activity of metal clusters across various surface sites, both with and without the influence of electric fields.

**Grant Number: DE-SC0024553**
**Grant Title: Interpretable Deep Learning for Advancing Field-Enhanced Catalysis**
**PI:** Fanglin Che
**Postdoc:** Qiang Li
**Students:** Mingyu Wan, Jaime Notarangelo, Yuting Xu, Charles Milhans, Runze Zhao, Pragyansh Singh, Saleh AhmatIbrahim

### RECENT PROGRESS

#### *Physics-Informed Machine Learning for Field-Dependent Adsorption Prediction*

We developed a novel physics-informed machine learning (ML) framework to map local electric fields and predict field-dependent adsorption energies on catalyst nanoparticles (NPs), as schematically illustrated in **Figure 1a**. By combining density functional theory (DFT), CO vibrational Stark effect measurements, and ML techniques, we gained efficient insights into field-enhanced catalysis. Our gradient boosting model predicts local electric fields with a mean absolute error (MAE) of 0.03 V/Å, showing excellent agreement with density functional theory (DFT)-calculated values (**Figure 1b**). Key factors, such as generalized coordination number (GCN) and nanoparticle size (nm), were identified as influencing local electric field distribution, depicted in the 3D plots showing the electric field as functions of GCN and cluster size (**Figure 1c**). Using this

information, our ML model predicts field-dependent adsorption energies with an MAE of 0.06 eV. By integrating physics-driven insights into a polynomial regression framework, we further reduced the MAE to 0.005 eV (**Figure 1e**). **Figure 1f** illustrate CO field-dependent adsorption energies can be enhanced by having smaller cluster size and GCN. The manuscript titled "*Physics-Driven Machine Learning Model for Field-Enhanced Catalysis*" by Runze Zhao; Qiang Li; Cheng Zhu; and Fanglin Che.* was submitted on September 28, 2024, and is currently under review by ***JACS Au***.

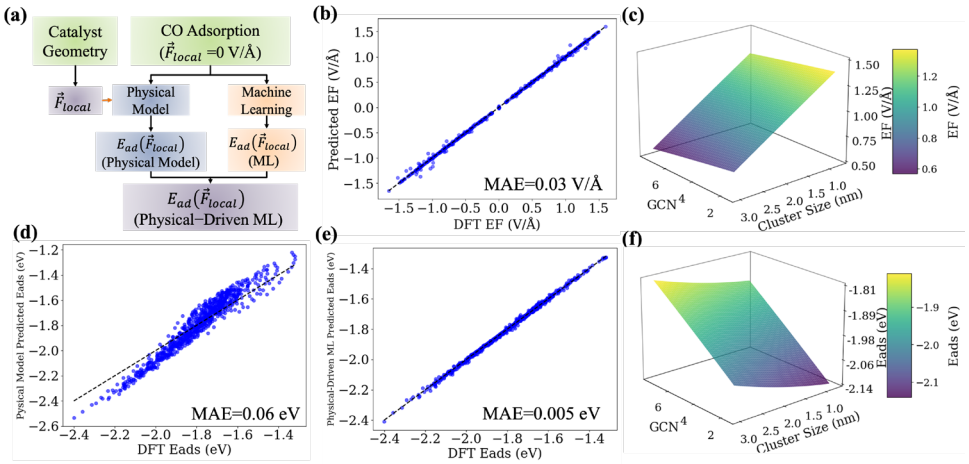


**Figure 1.** Physics-driven ML framework for field-dependent adsorption prediction. (a) Schematic of the ML approach. (b) Predicted vs. DFT-calculated local electric fields. (c) Electric field as functions of GCN and cluster size. (d) Adsorption energies using the ML model. (e) Adsorption energies using the physical-driven ML model. (f) Field-dependent adsorptions as functions of GCN and cluster size.

### *Multi-Scale Guided Interpretable Machine Learning for Ammonia Decomposition*

This study presents a novel approach to designing sustainable catalytic materials for hydrogen production, combining multiscale modeling, ML, and experimental validation. Focusing on ammonia-to-hydrogen conversion for decarbonizing the shipping industry, it addresses the limitations of traditional methods that rely on rare catalysts and produce $CO_2$ emissions. By integrating DFT-based microkinetic modeling with ML predictions, we identify optimal materials for ammonia decomposition.

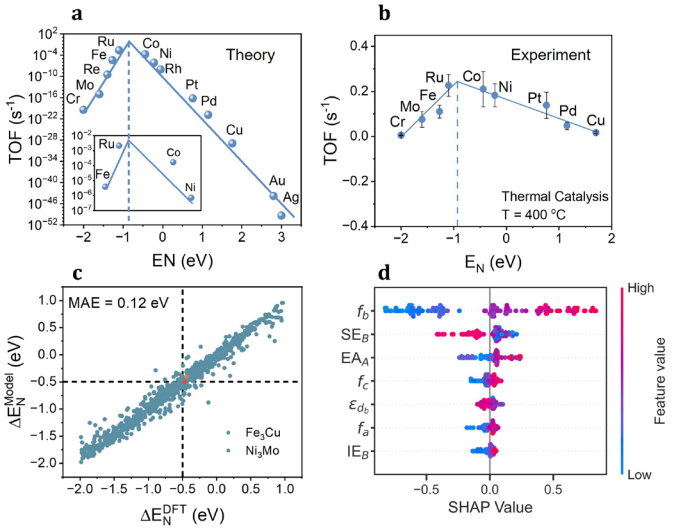


**Figure 2.** (a) and (b) Theoretical and experimental turnover frequency (TOF, $s^{-1}$) as a function of N* adsorption energy ($E_N$, eV). (c) DFT-calculated $E_N$ versus RF-predicted $E_N$ on bimetallic alloys. d) Interpretable explanation of feature importance through SHAP analysis.

Our results show Ru is the most effective catalyst (**Figure 2a**), and nitrogen binding energy ($E_N$) is a key factor influencing decomposition rates. The theoretical trend of catalytic performance on ammonia decomposition agrees well with experiment (**Figure 2b**). After comparing different ML models,

the Random Forest (RF) model (**Figure 2c**) accurately predicts $E_N$ for bimetallic alloys, and SHAP analysis (**Figure 2d**) highlights the surface atom *d*-band filling's impact. Using *d*-band filling, we can identify optimal earth-abundant bimetallic catalysts for maximizing the TOF for ammonia decomposition. The manuscript titled "*Interpretable Machine Learning Guided Plasma Catalysis for Hydrogen Economy*," authored by Saleh Ahmat Ibrahim, Shengyan Meng, Charles Milhans, Magda H. Barecka, Yilang Liu, Qiang Li, Jiaqi Yang, Yabing Sha, Yanhui Yi, and Fanglin Che, was submitted to ***Nature Chemical Engineering*** on May 31, 2024. The paper is currently undergoing its first revision.

### *Multi-Scale Simulation Guided Field-Enhanced Catalysis for Hydrogen Generation*

We investigated $NH_3$ decomposition for $H_2$ production on Ru(0001) and Ru(1013) surfaces, focusing on temperature and field effects. Our results (**Figure 3a**) show that the step-structured Ru(1013) surface, with its abundant B5 sites, significantly outperforms the flat (0001) surface, achieving full conversion at 1000 K compared to 1200 K for (0001) at zero field. The TOF increases with temperature (**Figure 3b**), reaching 0.97 $s^{-1}$ at 1000 K on Ru(1013), though it dips slightly near complete conversion due to reactant depletion.

Field-enhanced analysis (**Figure 3c**) reveals that a negative electric field reduces the kinetic barrier for dehydrogenation steps, while a positive field lowers the barrier for bond-forming steps like $N_2$ formation. The model shows that high TOF can be achieved by combining temperature with a negative electric field (**Figure 3d**). In the range of -0.5 to -1 V/Å, the highest TOF (1.25 to 1.50 $s^{-1}$) is observed between 900 and 1000 K. Sensitivity analysis (**Figure 3e**) highlights $NH_3$ dehydrogenation as the rate-limiting step at higher temperatures and negative fields due to $NH_3$ diffusion limitations.

Overall, the study demonstrates that combining electric fields with temperature can achieve high TOF efficiency under mild conditions, showing promise for enhancing catalytic performance and optimizing on-site $H_2$ production from ammonia decomposition. The manuscript titled "*Multi-scale Simulation Guided Field-Enhanced Catalysis for Hydrogen Generation*," authored by Pragyansh Singh; Qiang Li; and Fanglin Che*, is currently in preparation and is expected to be submitted by October 30, 2024.

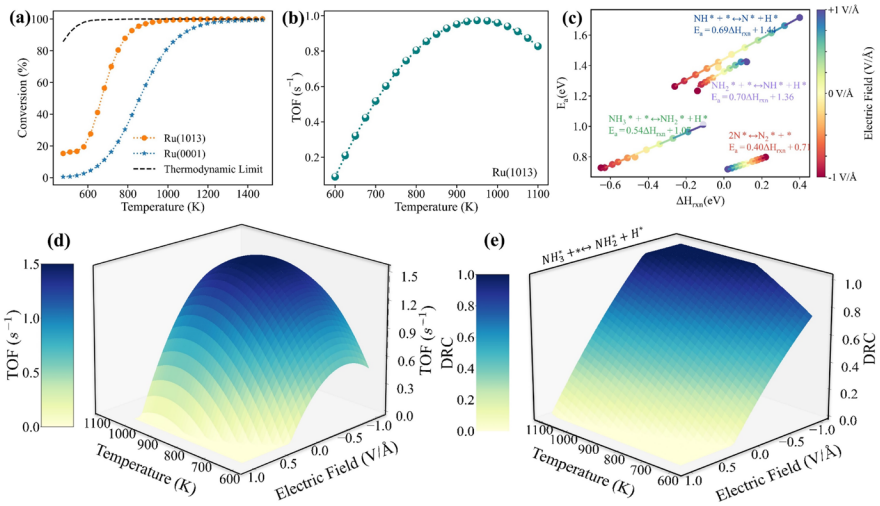


**Figure 3.** (a) Conversion over Ru(0001) and Ru(1013) surface compared with thermodynamic limit. (b) TOF over Ru(1013) in the thermal range of 600 K to 1100 K. (c) BEP correlation after field introduction. (d) Electric field enhanced TOF. (e) Field induced mechanistic shift observed for $NH_3^*$ dehydrogenation step.

### *Physical-Informed Machine Learning for Field-Enhanced Catalysis over Cluster*

We developed a coordination number-based (CN-based) group additivity (GA) framework to predict interactions between species and metal clusters in $NH_3$ decomposition. In this framework (**Figure 4a**), each surface site is represented by a central atom and its neighboring atoms, each characterized by their CNs. These CNs are encoded into a text string to uniquely define each site. Bridge and hollow sites are described using combinations of these encoded sites, allowing a comprehensive representation of multi-atom surface groups. By building a matrix of surface groups (G1, G2, G3) and their properties (e.g., binding energies), the model generalizes group contributions to predict species binding on similar sites across metal clusters of different sizes.

Our results (**Figures 4b** and **4c**) show that the CN-GA framework accurately predicts $NH_3$ physisorption and nitrogen adsorption with mean absolute errors of 0.026 and 0.048 eV, respectively, from 100 iterations of 5-fold cross-validation. We are also extending this approach to predict species-cluster interactions under electric field (EF) conditions. **Figure 4d** illustrates surface charge redistribution as the EF shifts from -1 to 1 V/Å, with edge and tip sites showing heightened sensitivity. For instance, under a 1 V/Å field, electron accumulation at edge sites strengthens nitrogen adsorption (**Figure 4e**), highlighting the importance of electrostatic effects in catalytic reactions. The manuscript titled "*Influence of Cluster Sites and Electric Field on the NH3 Decomposition Activity of Ru Catalyst*," authored by Qiang Li, Runze Zhao, and Fanglin Che*, is currently being prepared and is planned for submission by November 30, 2024.

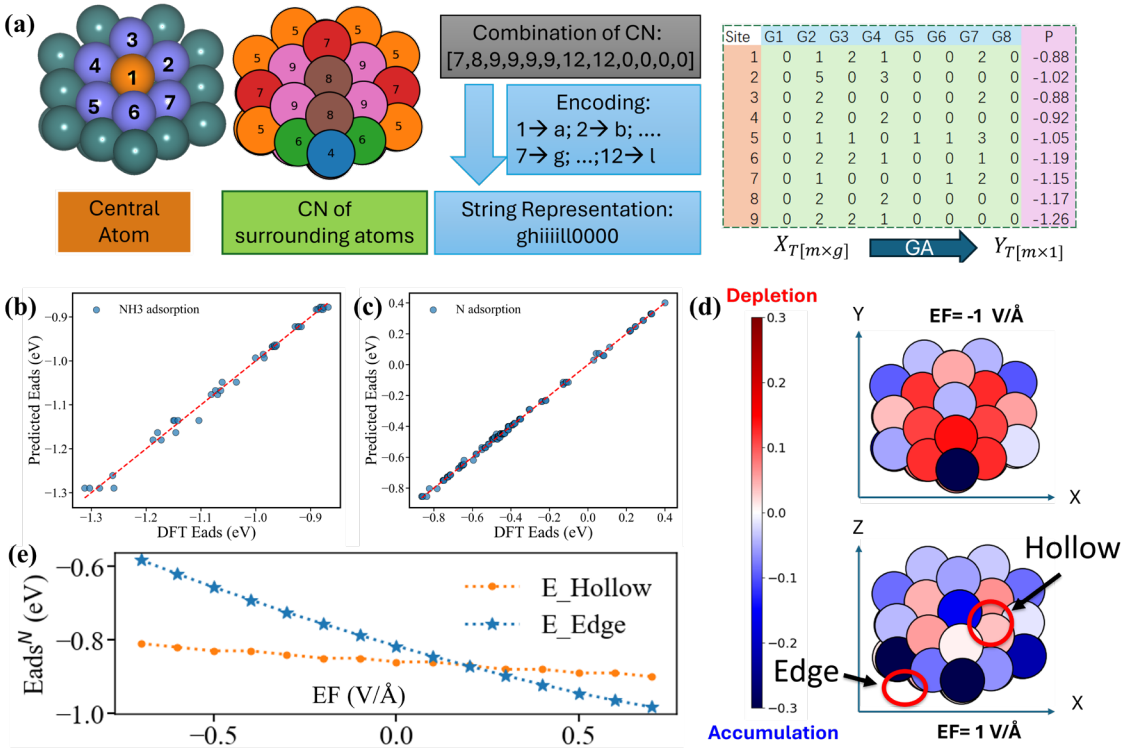


**Figure 4**. (a) Coordination number-based methodology to describe the local active sites of metal clusters via the Group Additivity concept. Performance of the CN-GA approach in predicting the (b) $NH_3$ and (c) single N adsorption on $Ru_{45}$ cluster. (d) Surface charge distribution under electric field conditions. (e) Effects of EF on the N adsorption at the hollow and edge sites of the $Ru_{45}$ cluster.

**Publications Acknowledging this Grant in 2023-2024 (PI's Grant Starting in 07/2023)**

*(I) Intellectually led by this grant*

1) Nankya, R.; Xu, Y.; Elgazzar, A.; Zhu, P.; Wi, T.-U.; Qiu, C.; Feng, Y.; **Che, F.***; Wang, H.*, Cobalt-Doped Bismuth Nanosheet Catalyst for Enhanced Electrochemical $CO_2$ Reduction to Electrolyte-Free Formic Acid. *Angew. Chem. Int. Ed.* **2024**, *63*, e202403671.

2) Garzon, A.; Wang, S.; Omoniyi, A.; Tam, L.; **Che, F.**; Hensley, A. J. R., Temperature and pressure driven functionalization of graphene with hydrogen and oxygen via ab initio phase diagrams. *Appl. Surf. Sci.* **2024**, *677*, 161053.

3) Fang, L.; Wan, M.; Liu, Y.; Reinhart, B.; Jin, Z.; Yang, M.; **Che, F.***; Li, T.*, Revealing Structural Evolution of Single Atom Catalysts during Electrochemical $CO_2$ Reduction by in Situ X-ray Absorption Spectroscopy. *ACS Mater. Lett.* **2024**, *6*, 3343-3350.

4) Wang, Y.; Zhao, R.; Rappé, K. G.; Wang, Y.; **Che, F.***; Gao, F.*, Mechanisms and site requirements for NO and $NH_3$ oxidation on Cu/SSZ-13. *Appl. Catal. B – Environ. Energy* **2024**, *346*, 123726.

5) Jin, Z.; Xu, Y.; Chhetri, M.; Wood, J.; Torreon, B.; **Che, F.***; Yang, M.*, Recent developments of single atom alloy catalysts for electrocatalytic hydrogenation reactions. *Chem. Eng. J.* **2024**, *491*, 152072.

*(II) Jointly funded by this grant and other grants with intellectual leadership by other funding sources*

6) Gerke, C. S.; Xu, Y.; Yang, Y.; Foley, G. D.; Zhang, B.; Shi, E.; Bedford, N. M.; **Che, F.***; Thoi, V. S.*, Electrochemical C–N Bond Formation within Boron Imidazolate Cages Featuring Single Copper Sites. *J. Am. Chem. Soc.* **2023**, *145*, 26144-26151.

7) Xu, Y.; Ross, M. B.; Xin, H.; **Che, F.**, Engineering bimetallic interfaces and revealing the mechanism for carbon dioxide electroreduction to $C_{3+}$ liquid chemicals. *Cell Rep. Phys. Sci.* **2023**, *4*, 101718.

8) Wan, M.; Yang, Z.; Morgan, H.; Shi, J.; Shi, F.; Liu, M.; Wong, H.-W.; Gu, Z.; **Che, F.**, Enhanced $CO_2$ Reactive Capture and Conversion Using Aminothiolate Ligand–Metal Interface. *J. Am. Chem. Soc.* **2023**, *145*, 26038-26051.

Peng Chen

# Multimodal Chemical Imaging of Cocatalyst-Induced Functional Changes in Single-Particle Photoanodes

Zhiheng Zhao, Xianwen Mao, Rocky Ye, Ming Zhao and Peng Chen*
Department of Chemistry and Chemical Biology, Cornell University

## Presentation Abstract

Using solar energy to produce clean fuels like hydrogen represents one of the most sustainable strategies to meet society's energy demands. Here photocatalytic and photoelectrocatalytic water splitting represents a promising technology, where semiconductor photocatalysts are used to harvest light to produce energetic charge carriers that react with water on their surfaces. Cocatalysts are often added onto the photocatalysts to modify the local energy levels of the semiconductor, promote charge separation, and/or provide distinct surface sites for reactant adsorption and catalytic transformation, to enhance the oxidation or reduction half reaction of the overall water splitting reaction. Many past studies have provided insights into the roles of cocatalysts; many knowledge gaps remain, however, including: how the overall performance changes are related to the local performance changes on a photocatalyst particle, especially relative to where the cocatalyst is or is not; how the overall performance change is related to the respective activity changes of holes and electrons on the surface, especially in a spatially resolved manner with regard to the location of the cocatalysts. Here we study cocatalyst-modified shaped $BiVO_4$ particles as photoanodes for photoelectrochemical water oxidation. We spatially control the deposition of single cocatalyst particles on specific facets of single $BiVO_4$ particles, exploring various combinations. We assess two types of oxidation cocatalysts: $CoO_x$, which is one of the most common high-performance oxidation cocatalysts, and $PtO_x$, which can undergo reversible transitions between semiconducting and metallic states under varying applied potentials where the semiconductor form functions as an oxidation cocatalyst and the metallic form as a reduction cocatalyst. We employ a multimodal operando imaging approach, combining sub/single-particle photoelectrochemical microscopy and super-resolution imaging of charge-carrier selective surface reactions before and after cocatalyst deposition.

**DE-SC0004911: Chemical Imaging of Single-Particle (Photo)(electro)catalysis**

**Postdoc(s):** Shasha Guo (partial), Jajung Koo (partial)
**Student(s):** Zhiheng Zhao, AnQi Chen (partial)

## RECENT PROGRESS

### *$CoO_x$ and $PtO_x$ cocatalyst modified $BiVO_4$ crystals as photoanodes*

We chose model photocatalyst $BiVO_4$ of truncated bipyramidal shapes, and $CoO_x$ and $Pt/PtO_x$ as model cocatalysts, which we were able to deposit in a spatially resolved

way on any facet of a single $BiVO_4$ particle. In the previous report, we used sub-particle photoelectrochemical current mapping and charge-carrier reaction imaging to show local and remote effects of a single $CoO_x$ cocatalyst deposition on a single $BiVO_4$ particle. Below we describe some of our progress in the last year.

***Electrochemical potential titration of sub-particle photoelectrochemical current to probe cocatalyst effects***

We observed a significant enhancement in the photoanodic current for water oxidation at the catalyst deposition site, particularly with $CoO_x$ on $BiVO_4$. This enhancement was accompanied by a unique suppression effect on remote lateral facets, especially in the case of $CoO_x$@basal — a first-of-its-kind observation. The modified Reichmann model was used to describe the photoanodic current, where the photocurrent is a function of parameters such as charge separation efficiency ($\eta$) and flat band potential ($V_{FB}$). To better understand how the observed enhancements or suppressions relate to changes in $\eta$ and $V_{FB}$ induced by cocatalyst deposition, a photocurrent applied potential titration was applied at both the deposition site and an adjacent remote facet without cocatalyst.

In all four cocatalyst deposition cases studied (**Figure 1**A-D), either at the deposition site or the remote facet, the photocurrent was found to be small at more negative applied potential. With increasing applied potential, photocurrent increased with a clear onset, continuing to rise and finally saturated at a more positive applied potential. This behavior could be well described with a modified Reichmann model, which allowed us to obtain $\eta$ and $V_{FB}$ values before and after cocatalyst deposition. At the cocatalyst deposition site, cocatalyst addition increased local charge separation efficiency, which was reflected by a larger photocurrent at very anodic applied potential. The enhancement of local charge efficiency was, on average, largest for particles with $CoO_x$ deposited on the lateral facet. $V_{FB}$ was negatively shifted as a result of cocatalyst depositions. The magnitude of the change was larger for $CoO_x$ than $PtO_x$. The changes in $\eta$ and $V_{FB}$ at the deposition site aligned with theoretical expectations, which is based on the type 2 heterojunction from the band alignment between the cocatalyst and the photocatalyst.

In the case of $CoO_x$ on $BiVO_4$, deposition on the basal or lateral facet caused larger band bending at the solid-electrolyte interface, leading to a more negative $V_{FB}$. This band bending facilitated better charge separation, which contributed to the increased $\eta$. The heterojunction effect also improved charge separation between the cocatalyst and $BiVO_4$, further enhancing the local $\eta$ (**Figure 1**E, F).

In contrast, for three of the four cases, no discernible changes in $\eta$ or $V_{FB}$ were observed at remote facets without cocatalyst deposition, consistent with a lack of change in the photocurrent. However, at the remote lateral facet in the $CoO_x$@basal case, there was a clear decrease in $\eta$, indicating a suppression of the photocurrent (Figure 1F). This remote facet suppression can be understood through the competition between the $CoO_x$/$BiVO_4$-basal junction and the intrinsic $BiVO_4$ lateral/basal junction. The latter junction typically leads to $h^+$ enrichment from basal to lateral facets, however, with $CoO_x$

deposition on the basal facet, $h^+$ enrichment shifted preferentially toward $CoO_x$ due to its higher valence band energy, which suppressed $h^+$ enrichment on the lateral facets, thereby decreasing η but not affecting $V_{FB}$.

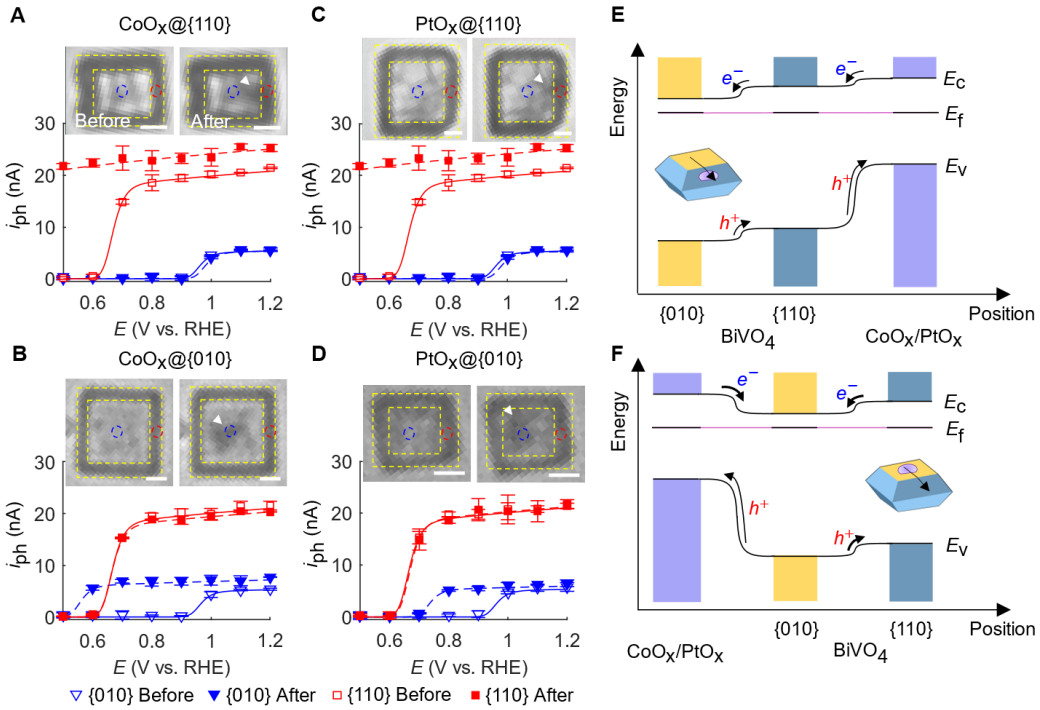


**Figure 1.** Charge separation and flat-band potential changes on local and remote facets. (**A-D**) Example data from photocurrent under different applied potential on particles from the four configurations. Inset transmission images are the corresponding particles. Yellow dashed lines indicating the boundary of {010} and {110} facets, blue and red dashed circle indicating the region illuminated by the focused laser beam during photocurrent measurements. All scale bars: 1μm. (**E, F**) Envisioned energy diagram demonstrating the interaction between introduced cocatalyst-photocatalyst junction on {110} facets (**E**) and that on {010} facets (**F**) and the intrinsic 2d junction between the two facets on a $BiVO_4$ particle.

## *CoOx cocatalyst XPS analysis*

According to the XPS data, the deposited $CoO_x$ cocatalysts are a mixture of Co(II) and Co(III). The composition of the two oxidation states also changes under different applied potential, however, all around 1:1 (**Figure 2**).

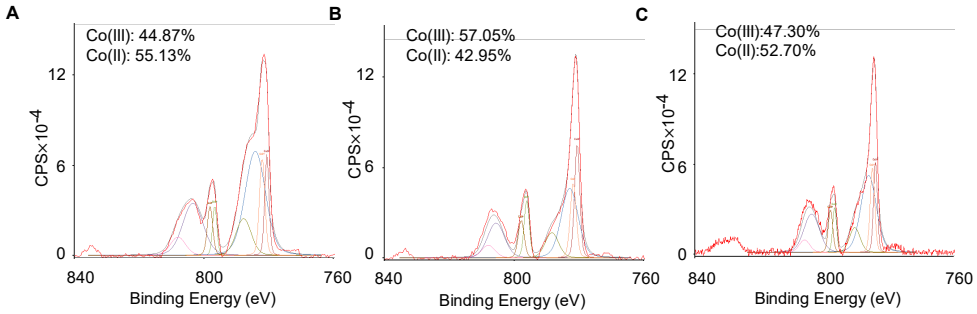


**Figure 2.** XPS in Co Region. **(A)** Right after deposition. **(B)** After applying +0.5V vs. Ag/AgCl for 2 hours. **(C)** After applying -0.5V vs. Ag/AgCl for 2 hours.

**Publications Acknowledging this Grant in 2021-2024**

*(I) Intellectually led by this grant*

1. Mao, X.; Chen, P. Inter-facet junction effects on particulate photoelectrodes. *Nature Mater.* **2022**, *21*, 331-337.
2. Mao, X.; Ye, R.; Chen, P. Fluorescence microscopy, In *Springer Handbook of Advanced Catalyst Characterization*, edited by Israel Wachs and Miguel A. Banares. pp285-294 (**2023**).
3. Zhao, M.; Li, W.; Yang, M.; Zhao, Z.; Ye, R.; Mao, X.; Padgett, P.; Chen, P. Long-range enhancement of micropollutant adsorption on metal-promoted photocatalysts. *Nature Catal.* **2024**, *7*, 912-920.

*(II) Jointly funded by this grant and other grants with intellectual leadership by other funding sources*

4. Kang, J.; Park, S. J.; Chen, P.; Sung, J. Stochastic kinetics of nanocatalytic systems. *Phys. Rev. Lett.* **2021**, *126*, 126001.
5. Sarkar, S.; Wang, X.; Hesari, M.; Chen, P.; Mirkin, M. V. Scanning electrochemical and photo-electrochemical microscopy on finder grids: toward correlative multi-technique imaging of surfaces. *Anal. Chem.* **2021**, *93*, 5377-5382.

**Zhongfang Chen**

**Theory-guided Innovation of High-performance Electrocatalysts for $CO_2$ Reduction**

Zhongfang Chen (PI), Department of Chemistry, University of Puerto Rico at Rio Piedras
William E. Mustain (Co-PI), Department of Chemical Engineering, University of South Carolina

**Presentation Abstract**

This project aims to advance the understanding and identification of single-atom catalysts (SACs), double-atom catalysts (DACs), and single-cluster catalysts (SCCs) for the electrochemical $CO_2$ reduction reaction ($CO_2RR$). We will combine theoretical (density functional theory, machine learning) and experimental (synthesis, electrochemical characterization) techniques to facilitate the development of viable $CO_2RR$ catalysts.

Our goal is to show how these catalysts can selectively produce value-added chemicals like HCOOH, CO, $CH_3OH$, $CH_3CH_2OH$, $CH_3CHO$, and $C_2H_4$. Additionally, this project offers training and education in chemistry, catalysis, and applied science for $CO_2RR$.

In this reporting period (since September 2023), we have achieved the following: i) Computational design and screening of defective graphene-based SACs, highlighting the role of weak interactions in catalyst design; ii) Computational design of DACs with an inverse sandwich structure for $CO_2$ reduction, especially the experimentally viable version: SACs with single atoms anchored on vacancy graphene loaded on Cu(111) surface; (iii) Computational design of a phosphotungstic acid-supported Os SAC for efficient purification of $CH_4$ and $H_2$ energy sources; (iv) Synthesis of Cu-based catalysts on defective carbon supports; and (v) significant progress in electrochemical analysis.

**Grant Number: DE-SC0023418**
**Grant Title: Theory-guided Innovation of High-performance Electrocatalysts for $CO_2$ Reduction**

**PI:** Zhongfang Chen (University of Puerto Rico, UPR); Co-PI: William E. Mustain (University of South Carolina, UofSC)

Postdocs: UPR, Liangliang Xu; UofSC, Venkata Sai Sriram Mosali
Graduate students
UPR, Linguo Lu; UofSC, Ian Street
Undergraduate students:
UPR: Juan Velez Reyes, Adrian Diaz Diaz; UofSC: Valerie Heimer (summer intern from Virginia Tech)
High school students:
UPR: Saleh Yassin, Jerry Chen

## RECENT PROGRESS

Computational design and screening of defective graphene-based single-atom catalysts

By density functional theory (DFT) computations, we investigated $CO_2$ reduction pathways of defective-graphene-supported single-atom catalysts (SACs) with 3d transition metals (Sc-Zn) coordinated to three carbon atoms (3C-TM, **Figure 1**). We focused on the energetic impact of hydrogen/lone pair-π interactions between $CO_2$RR intermediates and these SACs, an aspect generally overlooked previously.

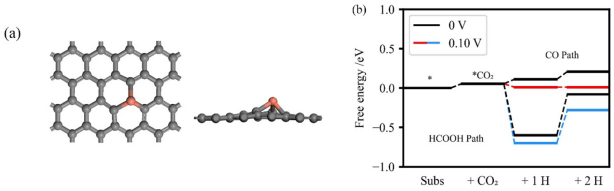


**Figure 1.** (a) The top and side views of 3C-TM, in which the carbon and metal atoms are denoted by grey and orange, respectively. (b) The free energy diagram of 3C-Co with the first 2 hydrogenation steps.

Models incorporating weak interactions reveal configurations with much lower energies, reshaping the understanding of the $CO_2$RR process. We identified a linear relationship between *COOH and *CO, challenging assumptions of poor scaling in these SACs. A new comparison method with hydrogen evolution reaction (HER) was proposed, highlighting SACs for efficient CO and $CH_4$ production. Our research introduces a modeling technique that accounts for weak interactions, enhancing large-scale screenings and ML applications and offering new insights into side reaction competition. These findings have been accepted for publication in *ChemSusChem*.

Computational design of double-atom catalysts (DACs) with an inverse sandwich structure for $CO_2$ reduction

Using a combination of DFT and machine learning (ML), we investigated DACs with an inverse sandwich structure anchored on defective graphene (gra) (**Figure 2**) for $CO_2$ reduction to $C_1$ products. We examined 5 homonuclear (M = Co, Ni, Rh, Ir, Pt) and 127 heteronuclear (M = Co, Ni, Rh, Ir, Pt; M′ = Sc ~ Au) DACs by DFT simulations. Rh⊥gra DAC excelled among its homonuclear counterparts and various Rh-based DACs. For heteronuclear DACs, 14 demonstrated strong catalytic potential. Our ML model identified 154 promising ones from 784 options. This work (*ACS Catal.* **2023**, 13, 9616) has garnered significant attention, featured on the journal cover, highlighted in science news outlets like X-mol, Nanowerk, and Advances in Engineering, and been cited 44 times.

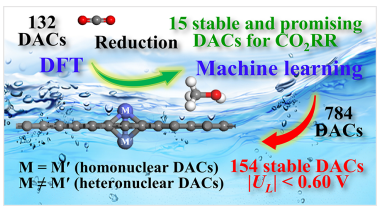



**Figure 2**. Schematic illustrating the structures, performance, and computational procedure for designing and screening of DACs, and the journal cover.

To facilitate the fabrication of inverse sandwich structures, we designed experimentally more feasible candidates: SACs with single atoms anchored on vacancy graphene loaded on Cu(111) surface, denoted as $M_1$@gra+$Cu_{slab}$ (**Figure 3**). We investigated the stability, selectivity, and activity of 27 $M_1$@gra+$Cu_{slab}$ configurations (M = Sc, Ti, V, Cr, Mn, Fe, Co, Ni, Cu, Zn, Y, Zr, Nb, Mo, Ru, Rh, Pd, Ag, Cd, Hf, Ta, W, Re, Os, Ir, Pt, and Au), and confirmed that five (M = Co, Ni, Cu, Rh, and Pd) exhibit the desired properties for electrocatalyzing $CO_2$RR. This work (*J. Phys. Chem. Lett.* **2024**, *15*, 8600) was featured as a journal cover.

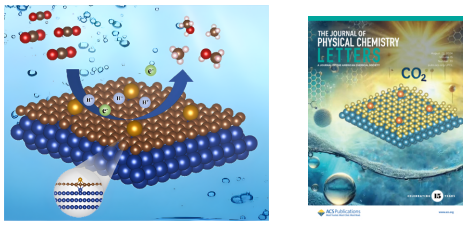


**Figure 3**. Schematic illustrating the structures, performance, and computational procedure for designing and screening of DACs, and the journal cover

Computational design of SACs for high-efficiency purification of $CH_4$ and $H_2$ energy sources

$CH_4$ and $H_2$ are promising low-carbon energy sources, but impurities like $H_2$ and CO hinder their storage and use. To tackle this, we developed a purification protocol using catalytic conversion of impurities into $CO_2$ and $H_2O$. Through DFT computations, we evaluated 11 phosphotungstic acid (PTA)-supported SACs, finding $Os_1$/PTA SACs highly effective for sequential CO, $H_2$, and $CH_4$ oxidation. These SCAs excelled in purifying $CH_4$ in solvents, such as water and MeOH, and demonstrated remarkable performance in purifying $H_2$, selectively removing CO without $H_2$ loss. This work has been published in *J. Mater. Chem. A*, **2023**,*11*, 24698-24711.

Synthesis of Cu based catalysts on defective carbon supports

The novel Switch Solvent Synthesis (SwiSS) method, developed at UofSC as a variant of incipient wetness impregnation, was used to synthesize single Cu atoms on VXC-72. SwiSS employs excess wetting solvent to improve noble metal dispersion on defective carbon supports, extending to lighter transition metals like Cu by exploring different precursor ligands to prevent aggregation during reduction. Using tetraamminecopper sulfate (TACS), ammonium tetrachlorocuprate (ATCC), and copper sulfate (CuSO4), we found that ligands on Cu affect dispersion, with attached ligands decreasing it due to higher reduction energies. X-ray diffractograms (**Figures 4A and 4B**) showed dispersion variations among precursors. A stable, 100% single-atom Cu catalyst has yet to be synthesized, explained by DFT-computed positive free energies (**Figure 4C**) due to a lack of anchoring atoms.

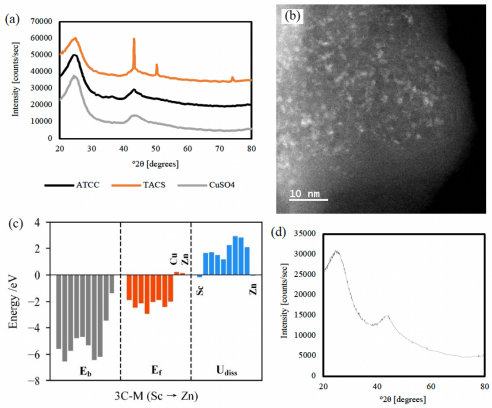


**Figure 4.** (a) XRD of TACS, ATCC, and $CuSO_4$ catalysts synthesized with SwiSS method, (b) STEM of $CuSO_4$ catalyst, (c) DFT-computed free energy of transition metal single atoms on graphitic surface, (d) XRD of Cu-N-C synthesized from Cu-ZIF-8.

To stabilize Cu single atoms on defective carbon surfaces, we are using N-functionalized graphitic planes as anchoring

sites, facilitating direct comparison with prior results. We synthesized and carbonized copper-doped zeolite imidazole frameworks (Cu-ZIF-8), removing Zn to produce a N-coordinated Cu single-atom catalyst. Post-carbonization XRD (**Figure 4D**) shows two broad peaks at ~25° and ~44° 2θ, indicating carbon planes with no crystalline Cu, confirming single-atom sites. In collaboration with Argonne National Laboratory, we will use STEM and XAS to further analyze their structure and coordination.

Electrochemical Analysis.

Extensive electrochemical testing of the synthesized catalysts involved Linear Sweep Voltammetry (LSV) in 1.0 M $KHCO_3$, under both $N_2$ and $CO_2$-saturated conditions, to assess $CO_2$ reduction activity. Catalyst performance was further evaluated using a three-electrode system in a $CO_2$-fed flow cell (**Figure 5A**). Gas products were analyzed by GC/MS, and liquid products by NMR. **Figures 5B** and **5C** compare product profiles of SwiSS nanoparticles with ligands and control SACs, showing that larger Cu particles favor hydrogen production, while smaller control particles exhibit better $CO_2$ reduction activity, though hydrogen remains dominant due to agglomeration on defective carbon. The Cu-N-C catalyst has been synthesized, with further characterization and single-atom Cu testing planned.

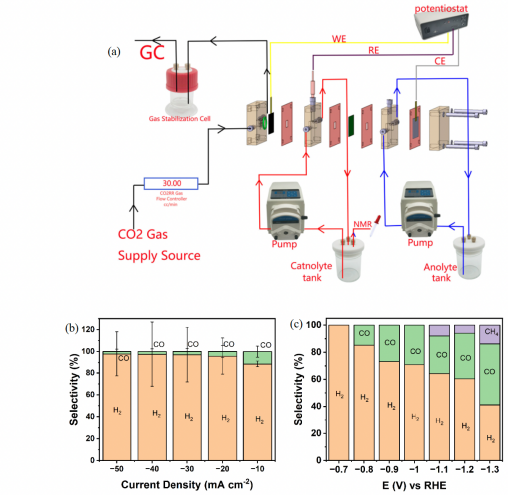


**Figure 5.** (a) Schematic of three electrode flow cells used to test the performance of synthesized catalysts, (b) Product profile of Cu nanoparticles on VXC-72 carbon, and (c) Product profile of partial single atom catalyst on VXC-72 carbon.

**Publications Acknowledging this Grant in 2022-2024**

*(I) Intellectually led by this grant*

(1) Su, J.; Yu, L.; Han, B.; Li, F.*; Chen, Z.*; Zeng, X. C. Enhanced $CO_2$ Reduction on Cu-Decorated Single Atom Catalyst *via* Inverse Sandwich M-Graphene-Cu Structure, *J. Phys. Chem. Lett.* **2024**, *15*, 8600–8607 (featured on the journal cover)

(2) Lu, L.; Huang, J.; Guerrero, A.; Street, I.; Mosali, S.; Sumpter, B. G.; Mustain, W. E.; Chen, Z. The Significance of the 'Insignificant': Non-covalent Interactions in $CO_2$ Reduction Reactions with 3C-TM (TM = Sc-Zn) Single-Atom Catalysts, *ChemSusChem* **2024**, ASAP

*(II) Jointly funded by this grant and other grants with intellectual leadership by other funding sources*

(3) Yu, L.; Li, F.; Huang, J.; Sumpter, B. G.; Mustain, W. E.; Chen, Z. Double-Atom Catalysts Featuring Inverse Sandwich Structure for $CO_2$ Reduction Reaction: A Synergetic First-Principles and Machine Learning Investigation. *ACS Catal.* **2023**, *13*, 9616–9628 (featured on the journal cover)

(4) Zhao, T.; Yan, T.; Sun, Y.; Wang, Z.; Cai, Q.; Zhao, J.; Chen, Z. Constructing the Square-Like Copper Cluster to Boost C-C Coupling for $CO_2$ Electroreduction to Ethylene, *J. Mater. Chem. A.* **2023**, *11*, 19444-19454.

(5) Rivera, J.; Soto-Pérez, J.; Sepulveda Pagán, M.; Lu, L.; Borrero, J.; Luna, A.; Trinidad, P.; Pagan, Y.; Chen, Z.; Cabrera, C.; West, W.; Jones, J.; Piñero Cruz, D. M.; New platinum complexes from a salen- and a hydroxy-substituted salpn-naphthalene ligands with $CO_2$ reduction activity. Catalysts, *Catalysts* **2023**, *13,* 911

(6) Gao, Z.; Ma, F.; Wu, H.; Ge, Y.; Zhu, Z.; Liu, Y.; Jiao, Y.; Chen, Z. Two-dimensional Ruthenium Boride: A Dirac Nodal Loop Quantum Electrocatalyst for Efficient Hydrogen Evolution Reaction. *J. Mater. Chem. A*, **2023**,*11*, 3717-3724.

(7) He, G.; Lu, L.; Zhang, N.; Liu, W.; Chen, Z.; Li, Z.; Zou, Z. Narrowing the Band Gap and Suppressing Electron–Hole Recombination in β-$Fe_2O_3$ by Chlorine Doping, *Phys. Chem. Chem. Phys.*, **2023**, *25*, 3695-3701.

(8) Zhang, L.-L.; Zheng, J.; Gu, J.; Huang, Z.; Lu, L.; Li, H.; Chen, Z.; Yang, S. High-Efficiency Purification of $CH_4$ and $H_2$ Energy Sources Enabled by a Phosphotungstic Acid-Supported Os Single-Atom Catalyst. *J. Mater. Chem. A* **2023**, *11*, 24698–24711.

(9) Zhao, T.; Yan, T.; Sun, Y.; Wang, Z.; Cai, Q.; Zhao, J.; Chen, Z. Constructing the Square-Like Copper Cluster to Boost C–C Coupling for $CO_2$ Electroreduction to Ethylene. *J. Mater. Chem. A* **2023**, *11*, 19444–19454.

Kyoung-Shin Choi

## The Impact of Electron Donating and Withdrawing Groups on Electrochemical Hydrogenolysis and Hydrogenation of Carbonyl Compounds

Jonah B. Eisenberg, Kwanpyung Lee, Xin Yuan, J. R. Schmidt, and Kyoung-Shin Choi
Department of Chemistry, University of Wisconsin-Madison

### Presentation Abstract

The hydrogenolysis or hydrodeoxygenation of a carbonyl group, where the C=O group is converted to a $CH_2$ group, is of significant interest in a variety of fields. A challenge in electrochemically achieving hydrogenolysis of a carbonyl group with high selectivity is that electrochemical hydrogenation of a carbonyl group, which converts the C=O group to an alcohol group (CH-OH), is demonstrated not to be the initial step of hydrogenolysis. Instead, hydrogenation and hydrogenolysis occur in parallel and they are competing reactions. This means that although both hydrogenolysis and hydrogenation require adding H atoms to the carbonyl group, they involve different intermediates formed on the electrode surface. Thus, revealing the difference in intermediates, transition states, and kinetic barriers for hydrogenolysis and hydrogenation pathways is the key to understanding and controlling hydrogenolysis/hydrogenation selectivity of carbonyl compounds. In this study, we aimed to identify features of reactant molecules that can affect their hydrogenolysis/hydrogenation selectivity on a Zn electrode that was previously shown to promote hydrogenolysis over hydrogenation. In particular, we examined the electrochemical reduction of *para*-substituted benzaldehyde compounds with substituent groups having different electron donating/withdrawing abilities. Our results show a strikingly systematic impact of the substituent group where a stronger electron-donating group promotes hydrogenolysis and a stronger electron-withdrawing group promotes hydrogenation. These experimental results are presented with computational results explaining the substituent effects on the thermodynamics and kinetics of electrochemical hydrogenolysis and hydrogenation pathways, which also provide critically needed information and insights for the transition states involved with these pathways.

……

**DE-SC0020983:** Mechanistic Investigation of Electrochemical Hydrogenation, Hydrogenolysis, and Dehydrogenation Pathways for Efficient and Selective Biomass Valorization

**PIs:** Kyoung-Shin Choi and J. R. Schmidt, and
**Student(s):** Jonah B. Eisenberg, Kwanpyung Lee, and Xin Yuan

## RECENT PROGRESS

### *Selective Deoxygenation of Biomass-Derived Carbonyl Compounds on Zn via Electrochemical Clemmensen Reduction*

For reductive upgrading of lignocellulosic biomass intermediates containing carbonyl groups, deoxygenation is critical to increase the energy density and storage lifetime of bio-oils. However, electrochemical reduction that cleaves the C=O bond by hydrogenolysis to form an alkane is extremely challenging because the C=O bond more readily undergoes hydrogenation to form an alcohol and the resulting alcohol C–O bond is more difficult to cleave by hydrogenolysis. Thus, hydrogenation is not an initial step of hydrogenolysis but rather a competing reaction to hydrogenolysis in electrochemical reduction of carbonyl groups (**Fig. 1a**). In traditional organic chemistry, the hydrogenolysis of aldehydes and ketones can be achieved by using zinc as a chemical reductant in strongly acidic media (e.g., concentrated HCl), which is known as the Clemmensen reduction (**Fig. 1b**). In this reaction, Zn is oxidized to $Zn^{2+}$ to provide the electrons needed for reduction and selectively promotes hydrogenolysis over hydrogenation. This led us to consider the possibility of *electrochemical* Clemmensen reduction. An *electrochemical* Clemmensen reduction reaction would use Zn as an electrocatalytic cathode with carbonyl reduction at Zn paired with some oxidation reaction at the anode (e.g., water oxidation, oxidative upgrading of biomass) (**Fig. 1c**). In contrast to the conventional Clemmensen reduction, the electrons used for carbonyl reduction would come from the oxidation reaction at the anode and not from oxidation of Zn, allowing the Zn electrode to be preserved via protection from the applied cathodic bias. If the Zn electrode in such an electrochemical cell still promotes hydrogenolysis over hydrogenation, the electrochemical Clemmensen reduction powered by electricity from renewable sources without continuously consuming Zn or other reductants can offer a sustainable

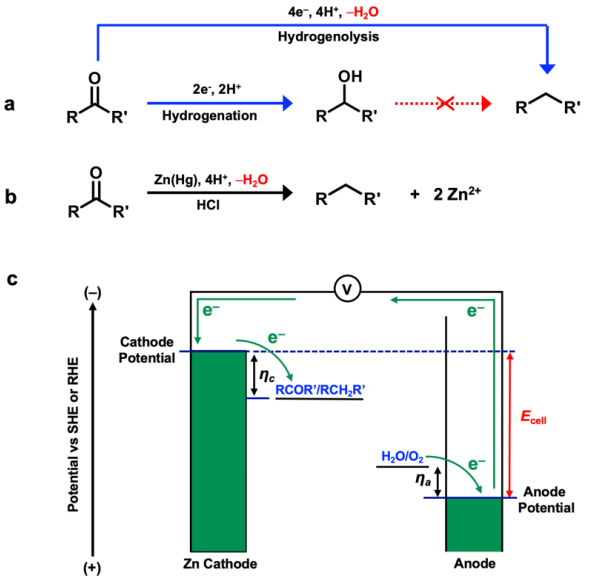


**Fig. 1.** (a) Electrochemical hydrogenation and hydrogenolysis reactions (R' = H for an aldehyde); (b) Conventional Clemmensen reduction; (c) A schematic illustration of the electrochemical Clemmensen reduction. The electrons gained by the oxidation reaction at the anode are used for the reduction of the carbonyl compounds at the Zn cathode, meaning Zn is not used as the electron source (reductant). The potential of the electrons gained at the anode becomes sufficiently negative for the carbonyl reduction by the electrical energy input. Water oxidation is used as an example anode reaction. ($\eta_a$: anodic overpotential, $\eta_c$: cathodic overpotential, $E_{cell}$: cell voltage, SHE: standard hydrogen electrode, and RHE: reversible hydrogen electrode)

route for selective hydrogenolysis. Furthermore, in the electrochemical Clemmensen reduction, we aimed to replace the strongly acidic condition used in the conventional Clemmensen reduction with the electric potential; if the concentrated acid used in the conventional Clemmensen reduction was only to increase the reaction rate (i.e., faster oxidation of Zn to $Zn^{2+}$ to increase the hydrogenolysis rate), electrifying the Clemmensen reduction will allow us to increase the reaction rate simply by increasing the overpotential. Then, the *electrochemical* Clemmensen reduction can accomplish hydrogenolysis at a desirable rate under milder and safer conditions.

During the current funding period, we successfully demonstrated *electrochemical* Clemmensen reduction of aldehydes and ketones on Zn, which resulted in remarkable hydrogenolysis selectivities compared with those attainable on Cu (**Fig. 2**). We also investigated the effects of applied potential and pH on the selectivity for hydrogenolysis of carbonyl compounds on Zn to evaluate the advantages of electrochemical Clemmensen reduction over conventional Clemmensen reduction. We also computationally examined the thermodynamics and kinetics of hydrogenolysis and hydrogenation pathways on Zn and Cu to elucidate why Zn is particularly good at hydrogenolysis. This study provided experimental and mechanistic foundations to establish electrochemical Clemmensen reduction as an effective and greener route to achieve selective hydrogenolysis.

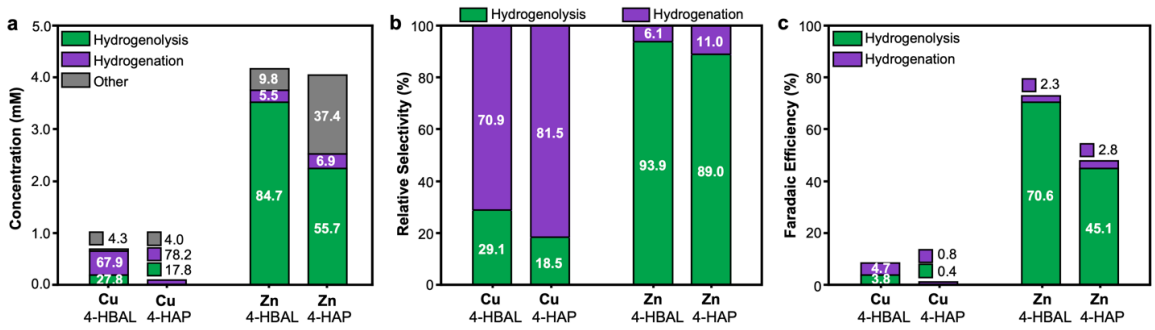


**Fig. 2.** Comparison of constant-potential reduction results for Cu and Zn at –0.8 V vs RHE in a pH 4.5 buffered solution containing 10 mM 4-hydroxybenzaldehyde (4-HBAL) or 4-hydroxyacetophenone (4-HAP). (a) Concentrations of hydrogenation, hydrogenolysis, and other products after passing an amount of charge equivalent to 2 $e^-$ per starting molecule. The white text gives the corresponding absolute selectivities (%). (b) Relative selectivities for the hydrogenation and hydrogenolysis products. (c) FEs for the hydrogenation and hydrogenolysis products.

### *The Impact of Electron Donating and Withdrawing Groups on Electrochemical Hydrogenolysis and Hydrogenation of Carbonyl Compounds.*

Most previous studies of electrochemical carbonyl reduction focused on identifying external factors (e.g., electrode type, modification of the electrode surface, solution pH) that can affect the hydrogenolysis and hydrogenation of a given carbonyl reactant molecule. For this project, we aimed to identify features of the molecules themselves that can affect their hydrogenolysis/hydrogenation selectivity. If we identify a certain electronic or structural feature of the molecule that can affect the hydrogenolysis and hydrogenation

differently, it can give us an invaluable opportunity to understand the difference in the transition states involved with the key competing hydrogenolysis and hydrogenation steps.

For this purpose, we examined the electrochemical reduction of *para*-substituted benzaldehyde compounds with substituent groups having different electron donating/withdrawing abilities (**Fig. 3**) on a Zn cathode. Benzaldehyde was chosen for this study as it is the simplest aromatic aldehyde that can make both experimental and computational studies straightforward.

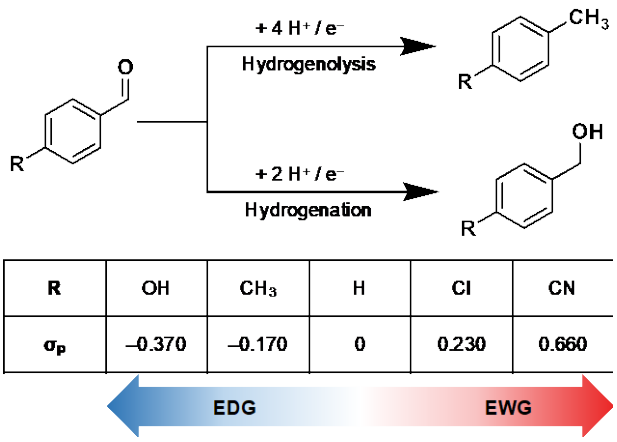


**Fig. 3.** Reactant scope with their electron donating/withdrawing ability represented by their Hammett constants.

Our results show a strikingly systematic effect on the hydrogenolysis and hydrogenation selectivity; a stronger electron-donating group (EDG) promotes hydrogenolysis and a stronger electron-withdrawing group (EWG) promotes hydrogenation (**Fig. 4**). We combined these experimental results and results obtained from a computational investigation to provide an atomic-level understanding of how EDGs and EWGs can impact the hydrogenolysis and hydrogenation pathways on Zn.

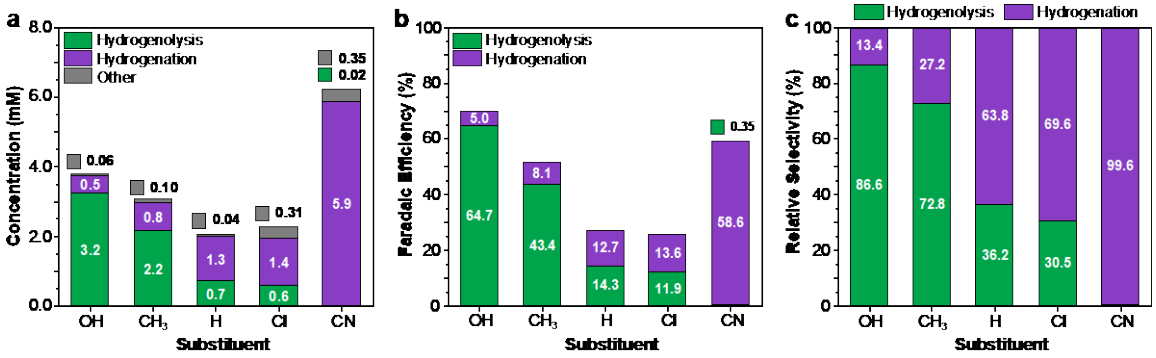


**Fig. 4.** Product distributions after passing 2 $e^-$ per reactant molecule via constant potential electrolysis at -1.46 V vs. Ag/AgCl (-0.93 V vs. RHE) in a MeCN/water (50% v/v) solution containing 0.5 M acetate buffer and 10 mM each aldehyde reactant. (a) Concentrations, (b) Faradaic efficiencies, and (c) relative selectivities. Other products in (a) are mainly composed of pinacol dimers.

**Publications Acknowledging this Grant in 2021-2024**

***(I) Intellectually led by this grant***


1. Bender, M. T.; Warburton, R.; Hammes-Schiffer, S.; Choi, K.-S. "Understanding Hydrogen Atom and Hydride Transfer Processes During Electrochemical Alcohol and Aldehyde Oxidation" *ACS Catalysis* **2021**, *11*, 15110−15124.
2. Bender, M. T.; Choi, K.-S. "Electrochemical Dehydrogenation Pathways of Amines to Nitriles on NiOOH" *JACS Au* **2022**, *2*, 1169–1180.
3. Bender, M. T.; Choi, K.-S. "Electrochemical Oxidation of HMF via Hydrogen Atom Transfer and Hydride Transfer on NiOOH and the Impact of NiOOH Composition" *ChemSusChem* **2022**, *15*, e202200675.
4. Yuan, X.; Lee, K.; Bender, M. T.; Schmidt, J. R.; Choi, K.-S. "Mechanistic Differences between Electrochemical Hydrogenation and Hydrogenolysis of 5-Hydroxymethylfurfural and Their pH Dependence" *ChemSusChem* **2022**, *15*, e202200952.
5. Goetz, M. K.; Bender, M. T.; Choi, K.-S. "Predictive Control of Selective Secondary Alcohol Oxidation of Glycerol" *Nature Commun.* **2022**, *13*:5848.
6. Bender, M. T.; Yuan, X.; Goetz, M. K. ; Choi, K.-S. "Electrochemical Hydrogenation, Hydrogenolysis, and Dehydrogenation for Reductive and Oxidative Biomass Upgrading Using 5-Hydroxymethylfurfural as a Model System" *ACS Catal.* **2022**, *12*, 12349–12368.
7. Yuan, X.; Lee, K.; Schmidt, J. R.; Choi, K.-S. "Halide Adsorption Enhances Electrochemical Hydrogenolysis of 5–Hydroxymethylfurfural by Suppressing Hydrogenation" *J. Am. Chem. Soc.* **2023**, 145, 20473–20484.
8. Goetz, M. K.; Usman, E.; Choi, K.-S. "Understanding and Suppressing C–C Cleavage during Glycerol Oxidation for C3 Chemical Production" *ACS Catal.* **2023**, *13*, 15758–15769.
9. Yuan, X.; Lee, K.; Eisenberg, J. B.; Schmidt, J. R.; Choi, K.-S. "Selective Deoxygenation of Biomass-Derived Carbonyl Compounds on Zn via Electrochemical Clemmensen Reduction" *Nat. Catal.* **2024**, *7*, 43–54.
10. Eisenberg, J. B.; Lee, K.; Yuan, X.; Schmidt, J. R.; Choi, K.-S. "The Impact of Electron Donating and Withdrawing Groups on Electrochemical Hydrogenolysis and Hydrogenation of Carbonyl Compounds" *J. Am. Chem. Soc.* **2024***, 146,* 15309–15319.
11. Yuan, X.; Lee, K.; Schmidt, J. R.; Choi, K.-S. "Diastereoselectivity Controlled by the Hydrogenation Mechanisms During Electrochemical Reduction of a Carbonyl Group" *ACS Catal.* **2024**, Under revision.


***(II) Jointly funded by this grant and other grants with intellectual leadership by other funding sources***


12. Tian, C.; Dorakhan, R.; Wicks, J.; Chen, Z.; Choi, K.-S.; Singh, N.; Schaidle, J. A.; Holewinski, A.; Vojvodic, A.; Vlachos, D. G.; Broadbelt, L. J.; Sargent, E. H. "Electro-privileged Transformations of Bio-Derived Molecules: Progress and Roadmap" *Nat. Catal.* **2024**, *7*, 350–360.

Kensha Marie Clark

# Ambiphilic C-H Bond Activation by Frustrated Lewis Pairs

Kensha Marie Clark, Pandula Archchige, Ava Callistri, Shreya Madav
Department of Chemistry and Biochemistry, University of Mississippi

## Presentation Abstract

Sterically frustrated Lewis pairs (FLPs) are composed of Lewis acids and bases containing bulky substituents that are unable to quench their respective acidities and basicities by forming acid-base adducts. As a result, FLP systems are able to induce the acute polarization and attendant activation of small molecule substrates. It was found that $Zn^{2+}$ containing FLPs can heterolytically cleave C-H bonds, forming both alkyl or hydride ligands. These reactions are reversible and yield heavier hydrocarbon products.

**Grant or FWP Number: Functionalization of Methane and Carbon Dioxide Using Earth Abundant Metal Frustrated Lewis Pair Catalysts**

**Postdoc(s):** Pandula Archchige
**Student(s):** Ava Callistri, Shreya Madav

## RECENT PROGRESS

### *Ambiphilic C-H Bond Activation*

In previous work, we found that a cationic zinc complex can form an FLP with a phosphine base. These FLPs preferentially activates weaker $sp^3$ C-H bonds, which differs from many organometallic systems. Additionally, these systems ambiphilically cleave C-H bonds to yield $H^+/H^-$ and $R^-/R^+$ fragments (R = alkyl or aryl). The generation of these components can lead to the formation of various hydrocarbon fragments.

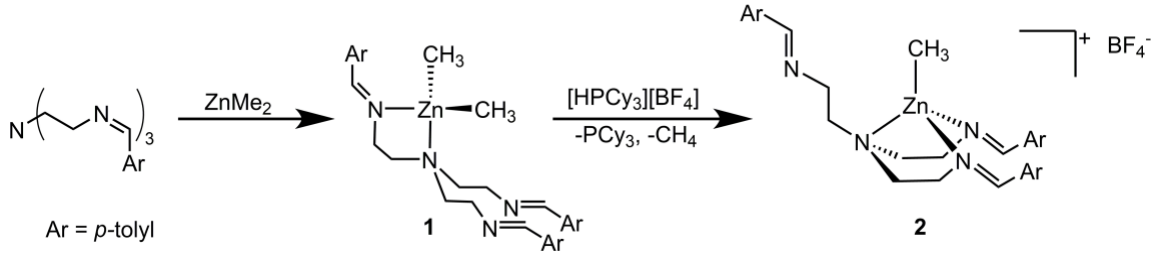


## Publications Acknowledging this Grant in 2021-2024

*(I) Intellectually led by this grant*

1. Bledsoe,K. S.; Bennett, L. K.; Gao, Y.; Byrd, J. A.; Hall, S.; Moore, C. E.; Cundari, T. R.; Clark, K.M. *Non-Oxidative Methane Activation by a Zinc-Based Frustrated Lewis Pair*, **2024,** *Under Review*.

Matthew P. Conley

# New Pathways to form $d^0$ W or Mo Alkylidenes

Matthew P. Conley
Department of Chemistry, University of California, Riverside

## Presentation Abstract

This poster will show recent organometallic chemistry developed by our group that relates to how olefin metathesis intermediates form from olefin adducts. This may relate to some of the first olefin metathesis catalysts reported in the scientific literature, which contained molybdenum or tungsten carbonyls or oxides on alumina; compositions that lack the metal carbon multiple bond required for olefin metathesis reaction chemistry. We showed that reactions of tungstacyclopentanes, which decompose to form W(IV) ethylene adducts, photochemically ring-contract to form tungstacyclobutane complexes. Transient adsorption spectroscopy and radical trapping experiments suggest that W-C bond cleavage occurs under these conditions. Reactions of W(IV) ethylene adducts with cyclohexene form substituted tungstacyclopentanes that form cyclohexylidenes in a thermal process. This poster will also show new results from reactions of $W(NR)_2R'_2$ (R = 2,6-diisopropylphenyl, adamantyl; R' = cyclohexyl, ethyl) and perfluoro-tert-butanol. When R'=cyclohexyl this reaction forms tungsten cyclohexylidenes, when R=ethyl this reaction forms ethylene adducts that can be converted to a cyclohexylidene in the presence of cyclohexene.

**Grant or FWP Number:** DE-SC0023344

**PI:** Matthew P. Conley

## RECENT PROGRESS

### *Transient Adsorption Spectroscopy of a Substituted Tungstacyclopentane*

Irradiation of the square pyramidyl $W(NCPh_3)(OSiPh_3)_2(C_7H_{12})$ (**1**)( at 450 nm in $C_6D_6$ results in the formation of the alkylidene shown in the Figure (a). Using femtosecond transient adsorption spectroscopy, we find that photoexcitation of **1** results in a band centered at ~500 nm appears and rapidly decays over the course of 9 ps as the major signal centered at

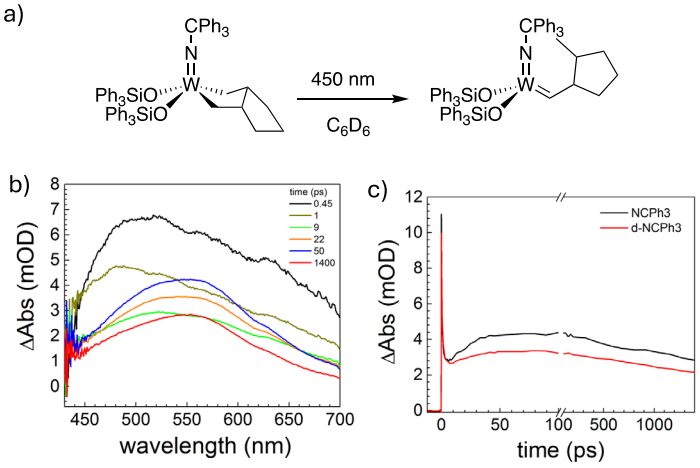

540 nm appears (b). This intermediate has a lifetime on at least the ns time regime (c). Neither the rate of formation of the W(V) intermediate nor the lifetime are affected by deuteration at the α-positions of the $WC_4$. Kinetic isotope studies show that $k_H/k_D = 1.3$, indicating that H-abstraction is likely not rate limiting. Photolysis of **1** in the presence of 5,5-Dimethyl-1-pyrroline-*N*-oxide (DMPO), a common radical trapping reagent, forms a species consistent with cleavage of a W–C bond. Taken together, these results suggest that the data in Figure are related to interconversion of the square pyramidal **1** to the trigonal bipyramid that undergoes rate limiting W–C bond cleavage, followed by fast H-abstraction to form the product alkylidene.

**Publications Acknowledging this Grant in 2021-2024**

*Please classify your publications into two categories according to the source of support for the work published:*

*(I) Intellectually led by this grant*

Rodriguez, J.; Boudjelel, M.; Schrock, R. R.; Conley, M. P. A Tungsten Oxo Alkylidene Supported on Sulfated Zirconium Oxide for Olefin Metathesis. *Organometallics* **2023**, *42*, 1286-1290.

Maji, M.; Sousa-Silva, A.; Solans-Monfort, X.; Schrock, R. R.; Conley, M. P.; Farias, P.; Carta, V. Thermal Formation of Metathesis-Active Tungsten Alkylidene Complexes from Cyclohexene. *J. Am. Chem. Soc.* **2024**, *146*, 18661-18671.

Maji, M.; Riedel, R.; Schrock, R. R.; Conley, M. P.; Carta, V. Syntheses of Tungsten Imido Cyclohexylidene Complexes Using Perfluoro-*t*-butanol or Hexafluoro-*t*-butanol as Acids. *Angew. Chem. Int. Ed. In Press.*

*(II) Jointly funded by this grant and other grants with intellectual leadership by other funding sources*

Lakliang, Y.; Kolganov, A.; Groves, M. C.; Pidko, E. A.; Sydora, O. L.; Conley, M. P. C-H Bond Activation by Sulfated Zirconium Oxide is Mediated by a Sulfur-Centered Lewis Superacid, *Submitted*.

Steven P Crossley

**Catalyst evolution and kinetics of stable catalytic methane pyrolysis**

Steven Crossley,[1] Daniel Resasco,[1] Bin Wang,[1] Anibal Boscoboinik[2]
1) University of Oklahoma, Department of Sustainable Chemical, Biological and Materials Engineering
2) Brookhaven National Laboratory, Center for Functional Nanomaterials

**Presentation Abstract**

Catalytic methane pyrolysis is a promising approach toward hydrogen production without $CO_2$ formation. Improving overall energy efficiency and potential of such systems requires improved fundamental understanding of mechanisms of methane activation, carbon flux, as well as catalyst stability. Regardless of the activity of the catalyst, if the active metal component separates from the support during reaction, often referred to as tip growth, the catalyst is not capable of separation and reuse. Here we study a highly promising family of catalyst exhibits each of these desired properties while also preserving base growth. We report through in-situ XPS, Raman, TEM, and XRD the evolution of the catalyst among various growth phases, leading to the exsolution of a carbide phase from the underlying support, and subsequent active metal particle exsolution from the carbide to create highly stable active centers. We further evaluate steady state kinetics coupled with DFT calculations to illustrate the critical role of carbon scavenging co-feeds that retain activity of the most active sites and profound impacts that result in terms of measured activation barriers. In addition, we show how sensitive both the particle evolution during initial carburization stages and deactivation at longer reaction times are to reaction conditions, which explains the wide range of reported activation barriers often reported in literature.

**DE‐SC0023497: Interrogating complex and dynamic interfaces during carbon‐free H2 production**

**Postdoc(s):** Laura Alejandra Gomez (8 months)
**Student(s):** Caleb Bavlnka (3 months), Israel Solomon (7 months)

**RECENT PROGRESS**

***Evolution of Active Catalyst during growth stages***

Through a combination of in-situ XPS, XRD, Raman, and same spot TEM, we have studied the journey of a NiMoMgO catalyst, one we had previously identified as exhibiting base growth while showing remarkable catalyst stability when compared with other combinations. We first studied the impact of pre-reduction step on this chemistry,

revealing that a modest initial reduction leads to the creation of small Ni particles, with size controlled by the Ni loading and pre-reduction temperature as shown in Figure 1.

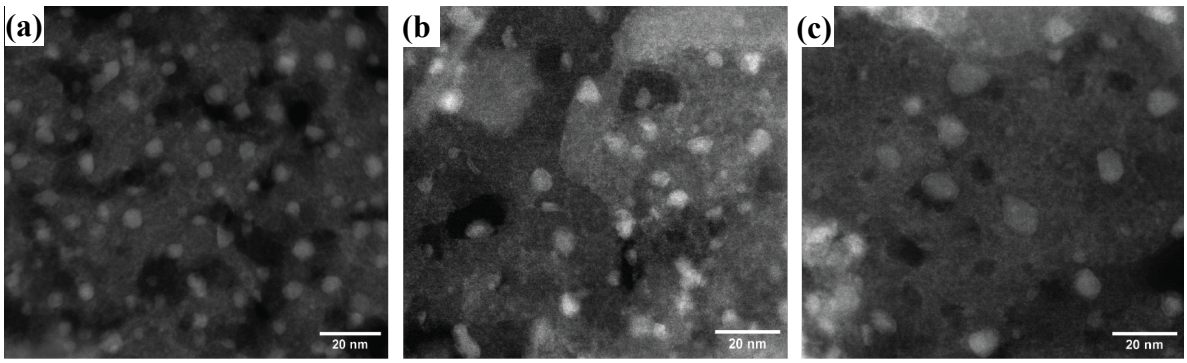


**Figure 1.) HAADF-STEM characterization of Ni particles. (a)** 5% Ni-25% Mo/MgO, **(b)** 10% Ni-25% Mo/MgO, and **(c)** 20% Ni-25% Mo/MgO.(1)

We then show that the absence of this pre-reduction step leads to remarkably lower methane conversion rates, which we presume is due to limited initial exsolution of the Ni particles that ultimately activate CH4 and promote carbide formation.

XRD and XPS analysis reveals a mixed oxide of MgMoOx that partially decomposes after this pre-reduction step to form a NiMoO4 surface layer. Subsequent introduction of a carbon source reveals the formation of sheets of Mo2C with intercolated Ni which slowly exsolves along the Mo2C sheets as revealed both with Raman, XPS, and TEM images with elemental mapping. These Ni particles then nucleate carbon nanotubes and exhibit remarkable stability with time on stream which allows us to assess steady state kinetic behavior as will be discussed next.

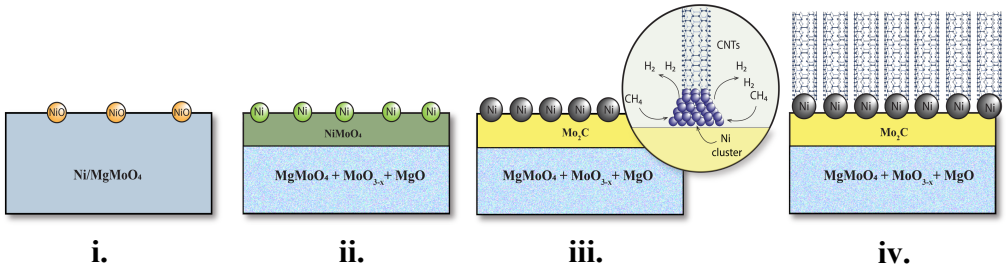


**Scheme 1.** Proposed catalyst evolution and CNTs growth: **(i)** fresh catalyst, **(ii)** reduced catalyst, **(iii)** catalyst carburization initial state (<5 min), and **(iv)** carbon nanotube growth.(1)

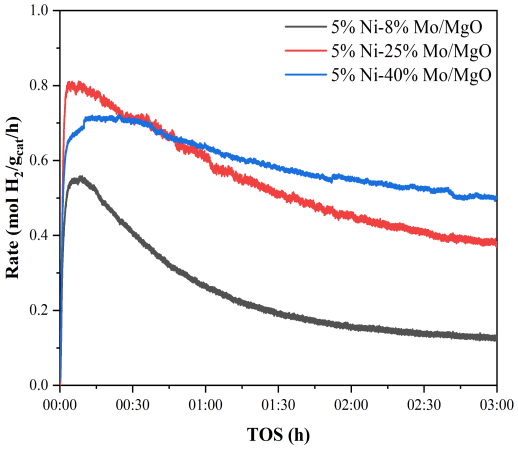


**Figure 2.** $H_2$ production rates as a function of Mo loading over Ni-Mo/MgO **(b)** $H_2$ production rates as a function of Ni loading over Ni-Mo/MgO (1)

Reaction kinetics experiments were carried out at steady state to reveal activation barriers and learned several new intriguing things. First, we studied the kinetics of the reaction, revealing that the hydrogen generated in the reaction exhibits positive rate behavior. Given the fact that methane activation is often presumed as rate-controlling, this is intriguing. Replacing the carbon source with a more active phase, such as plasma activate methane, ethylene, or acetylene even at the same hydrogen to carbon ratios during in-situ XPS treatments reveal significantly different rates of carbon conversion with more readily activated species, implying that methane activation is a kinetically relevant step. This does not align well with the positive hydrogen order dependence as the activation should be inversely proportional to hydrogen partial pressure. We then carried out steady state kinetic runs to reveal profound impacts on observed activation barriers spanning well over 100kJ/mol even at very low conversions of methane (~1-3%). We hypothesized that this was due to a dynamic shift in the number of active sites present at steady state under reaction conditions, which is more pronounced at lower hydrogen pressures as the small pressures generated in-situ corrupt activation barriers if not properly accounted for. We then incorporated these into a kinetic model to explain the intriguing behavior as well as the important role of the underlying carbide, which can readily mobilize H and C species as well, leading to apparent reversible deactivation behavior at different conditions. We believe these findings help to explain some of the contrasting behavior in the literature regarding intrinsic reported activation energies while also providing clear pathways to markedly enhance reaction rates.

## Publications Acknowledging this Grant in 2021-2024

1. Gomez, L.A.; Bavlnka, C.Q.; Nguyen,[1] P.T.; Alalq, I.; Sabisch, J.E.C.; Boscoboinik,[3] J.A.; Resasco,D. E.; Crossley S.P. Dynamic exsolution of Ni-Mo/MgO catalysts for base nanotube growth during methane conversion *Under minor revision 2024*

Lisandro F. Cunci

## Catalysts Research in Oxygen Reduction and Oxidation Reactions to Increase Representation in Energy Science in Puerto Rico

Dr. Lisandro Cunci
Department of Chemistry, School of Natural Sciences, University of Puerto Rico – Rio Piedras Campus

### Presentation Abstract

Dr. Cunci's lab works in the development and understanding of non-platinum group metal (non-PGM) and non-metal catalysts for the oxygen reduction reaction (ORR) and oxygen evolution reaction (OER), which are essential for the mass production and use of alkaline membrane fuel cell and green hydrogen production.

Catalysts for the ORR: Despite advancements in fuel cell technologies for power production, there is still limited insight into the characteristics of bimetallic transition metal catalysts that enhance energy conversion processes. These catalytic materials have not been extensively investigated to identify the factors influencing reaction mechanisms and efficiency. Highly controlled electrodeposition methods can control the size and shape of nanoparticles, enabling detailed structural and morphological analysis. Graduate student Laura Cruz is dedicated to synthesizing Fe and Co nanoparticles using controlled techniques to maintain a uniform composition during particle growth. Atomic force microscopy is used to observe catalyst degradation.

Catalysts for the OER: Graduate student Ambar Maldonado aims to understand how the structural template of nickel and iron layered double hydroxides (NiFe-LDH) is enhanced for the OER under an alkaline environment. To conceptualize this enhancement, catalyst electronic structures and physicochemical properties by heteroatom doping with high-valence transition metals will be correlated.

Dr. Cunci is the Lead PI of the BES RENEW project titled ***"Partnership to Increase Representation in Energy Research in Puerto Rico"***. Three graduate student and 14 undergraduate students were recruited from underrepresented populations and 59% are women. We just had the second co-organized Electrochemistry Hands-On (ECHO) Workshop at the National Renewable Energy Laboratory with Dr. Bryan Pivovar following by the second Summer Internship for 10 weeks.

### DE-SC0023686: Partnership to Increase Representation in Energy Research in Puerto Rico

**PI:** Dr. Lisandro F Cunci
**Co-PIs:** Dr. Jorge Colon, Dr. Lymari Fuentes Claudio, Dr. Mitk'El Santiago, Dr. Miguel Goenaga, and Dr. Juan Santana.
**Student(s):** Ambar Maldonado Santos (Graduate Student); Alannisse Santos, Daniella Gibson Colon, Hector Gonzalez Velez, Alejandra Rodriguez Nazario, Kevin Torres, and Yaneiska Ruiz Torres (Undergraduate Students).
**Affiliations(s):** University of Puerto Rico – Rio Piedras, Humacao, and Cayey Campus; Universidad Ana G. Mendez – Cupey and Gurabo Campus.

## RECENT PROGRESS

***Summer Electrochemistry Hands-On Workshop (ECHO) at the National Renewable Energy Laboratory (NREL)***

Our project **Partnership to Increase Representation in Energy Research in Puerto Rico (PIRES-PR)** is dedicated to increase the number of Hispanic students working in basic energy research. We were able to recruit three (3) graduate students and fourteen (14) undergraduate students with **59% of them women** starting in the right direction toward one of our main objectives of increase the number of women in energy science in Puerto Rico. During the Summer Internship 2024 at NREL, the graduate student and three undergraduate students (100% women!) did research under the mentorship of four researchers and under the supervision of Dr. Bryan Pivovar (Co-PI of PIRES-PR) and Dr. Shaun Alia, two experts in hydrogen research. Figure 1 shows a picture of the final poster presentation at NREL on 2023 and Figure 2 in 2024 (this year).

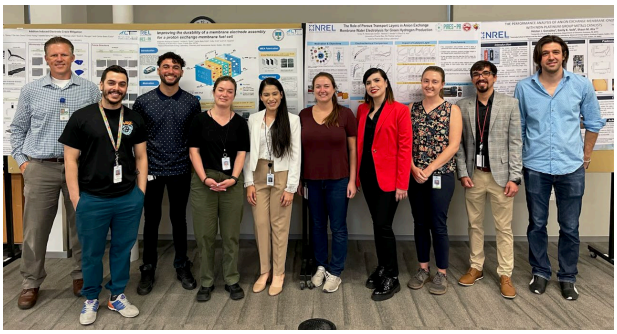

Figure 1 – Final presentation in 1st Sumer Internship at NREL (2023).

Figure 2 – Final presentation in 2nd Sumer Internship at NREL (2024).

***Oregano biomass as a support for the biosynthesis of non-precious metal catalysts (Dr. Lymari Fuentes-Claudio, Universidad Ana G Mendez – Cupey)***

Titania particles were synthesized using the biotemplation method. Oregano biomass was used as a biotemplate to control particle growth and enhance metal doping. The titania network was doped with different non-precious metals, including iron, copper, and cobalt. X-ray Photoemission Spectroscopy spectra show characteristic peaks of calcium and magnesium that are though to be a contribution of the biotemplate. Doping of the samples was confirmed by Diffuse reflectance spectroscopy where characteristic bands of the metals are observed.

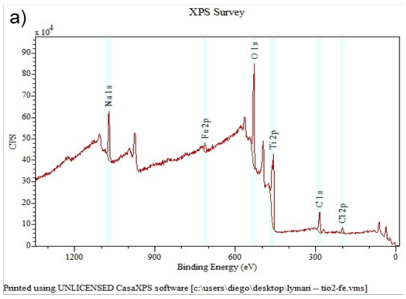


b) Measured DLS Particule Distribution

| Sample | Size (d.nm) | St Dev (d.nm) |
|---|---|---|
| $TiO_2$ Control | 186.7 | 71.3 |
| $TiO_2$ Fe Control | 179.2 | 75.8 |
| Bio $TiO_2$ Control | 82.4 | 5.6 |
| Bio $TiO_2$ Fe | 157.8 | 10.6 |

Figure 3 – a) XPS of Bio$TiO_2$ Fe. b) Dynamic light scattering shows different size intensities for biotemplated and non-biotemplated sample.

***OER Catalysts Supported on Zirconium Phosphate Nanomaterials***
***(Dr. Jorge Colón, University of Puerto Rico, Rio Piedras)***

CoFe OER electrocatalyst supported on layered zirconium phosphate (ZrP) nanomaterials show slightly higher activity in an anion exchange membrane electrolyzer (AEMEL) compared to a commercial Co catalyst. Commercial NiFe oxide OER catalysts have higher activity and stability than a commercial NiO catalyst. CoFe@ZrP catalysts performed better that the commercial Co catalyst with lower kinetic losses despite of lower anode loading (0.04-0.18 mg/cm$^2$ vs 3 mg/cm$^2$). Lessons learn in stability studies of commercial NiFe catalysts will be used for optimizing NiFe@ZrP catalysts.

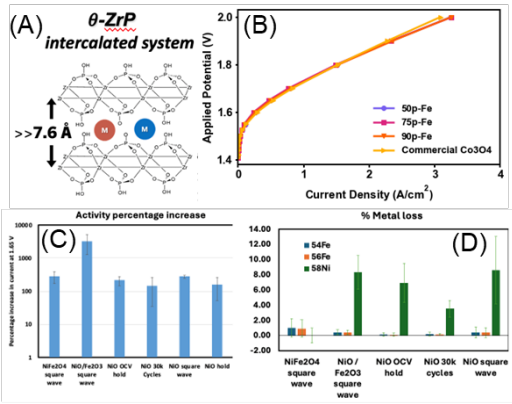


Figure 4 – A. Schematic of intercalated ZrP; B. Polarization curves for CoFe@ZrP and commercial Co OER electrocatalyst in AEMEL; C. Activity comparison of NiFe and NiO catalysts; D. % Metal loss of NiFe and NiO catalysts after various experiments.

***Process of coating the electrodes with catalytic material***
***(Dr. Miguel Goenaga, Universidad Ana G Mendez – Gurabo)***

The gun and the servomotor were assembled on the head of the 3D printer. A base for the magnetic stirrer device was created. The code was developed in Python for the gun's movement, in G-code for the gun's operation, and in C++ for the activation of the servo. The students developed the ability to communicate and collaborate effectively with others. They gained skills in computer-aided design and in modifying 3D printers. They acquired experience in programming and process automation, essential skills in the industrial sector. They learned to face challenges and find creative solutions to technical problems in the project.

Figure 5 – First prototype of automated coating sprayer.

***Synergistic Activities between Energy-based Research Efforts in Puerto Rico***

We have devised a training program during the academic year for the students to take advantage of synergistic activities with other energy research projects in Puerto Rico. We have joined four research efforts together supported by DOE and NSF in energy materials. The students that are part of these three research efforts in energy meet every other Friday to participate of research seminars, professional development workshops, presentation practice, and networking with other researchers in Energy Science.

**Publications Acknowledging this Grant in 2021-2024**

Lopez-Astacio, H., Vargas-Perez, B. L., Del Valle-Perez, A., Pollock, C. J. & Cunci, L. (2024). Open-source electrochemical cell for in situ X-ray absorption spectroscopy in transmission and fluorescence modes. *J. Synchrotron Rad.* **2024**, 31, 322-327.

**Abhaya K. Datye**

# Sub Nanometer Sized Clusters for Heterogeneous Catalysis

Abhaya Datye[1] and Yong Wang[2]
[1]University of New Mexico and [2]Washington State University

## Presentation Abstract

The size regime from isolated metal atoms to clusters containing about 30 atoms (~1 nm) is of great interest since most of the metal atoms are at the surface, hence accessible for catalytic reactions. A major challenge in the industrial application of these sub-nm catalysts is that atoms are mobile and can cause changes in the catalyst structure, often leading to a loss of reactivity and selectivity. The objective of this project is to develop a fundamental understanding of the stability of single atoms, and to use this understanding to improve the thermal stability of sub-nm clusters. Our goal is to design catalysts that can continue to catalyze reactions over extended time periods. We bring to bear the method of atom trapping, where we learnt how to stabilize individual atoms on an oxide support, preventing their agglomeration to form large particles. We make use of such strongly bound atoms to control the nucleation and growth of clusters that are deposited on such strongly bound atoms. This helps elucidate the roles of surface sites on generating stable sub-nm clusters. While trapping atoms allows us to prevent growth of large particles, the strongly bound atoms may not be as catalytically active as nanoclusters. Hence, we also explore a novel approach to generate self-healing catalysts, where mobile atoms are trapped and restored to active nanoparticles, generating a thermodynamically stable structure. Single atoms on oxides are not static. One of the aims of this research is to investigate the dynamics of single atoms, and understand on how they can be tuned to achieve the highest catalytic reactivity. Since most industrial catalysts use rare and expensive metals (platinum group metals) as catalysts, there is a need to investigate whether earth abundant metals (EAMs) could perform similar chemistry. This will address looming shortages in critical materials needed for the chemical industry. We will therefore extend the learning from generating self-healing catalysts and mechanistic insight on the dynamics of single atoms mentioned above to control the reactivity and stability of EAM based catalysts, for reactions of interest to the DOE mission.

**DOE grant # DE-FG02-05ER15712**
**Sub Nanometer Sized Clusters for Heterogeneous Catalysis**

Post-docs: Andrew DeLaRiva (UNM) and Junming Sun, Dong Jiang and Hao Xu (WSU)
Graduate Students: Stephen Porter and Brandon Burnside (UNM), Carlos Eduardo Garcia-Vargas, Jianghao Zhang and Zhiyu Qi (WSU)

## RECENT PROGRESS

### *Controlling the nucleation and growth of sub-nm clusters*

The underlying hypothesis of this project is that the proper design of trapping sites will allow us to control the nucleation and growth of sub-nm clusters. These trapping sites may be on the

surface of oxide supports, as in the case of step edge sites on ceria, which allow trapping of transition metals such as Pt, Pd or Rh, or they may involve incorporation of the single atoms into substitutional sites such as in the case of Ni doped into ceria. The study of $Pd/CeO_2$ best illustrates how we can control the formation of sub-nm clusters and their transformation back into single atoms (Jiang et al., *Nature Catalysis*, 2023). In this work, we reported the reaction-environment-modulated transformations of subnanometer-sized Pd on $CeO_2$ for efficient methane removal, leveraging the reaction environments at different stages of automotive exhaust aftertreatment. During the cold start of vehicles, inactive Pd1 single atoms are readily transformed into PdOx subnanometer clusters by CO even at room temperature with excess $O_2$, resulting in boosted low-temperature $CH_4$ oxidation. At elevated temperatures, dispersion of PdOx cluster into $Pd_1$ against metal sintering renders outstanding hydrothermal stability to the catalyst, to be activated during the next vehicle start. Combined experimental and computational studies elucidate the dynamically evolved Pd speciation on $CeO_2$ at an atomic level. Modulating the reversible nature of supported metals helps overcome the long-existing trade-off between low-temperature activity and high-temperature stability, also providing a new paradigm for designing intelligent catalysts that brings single-atom/cluster catalysts closer to real applications. This work was also submitted as a highlight to the DOE Catalysis Science program.

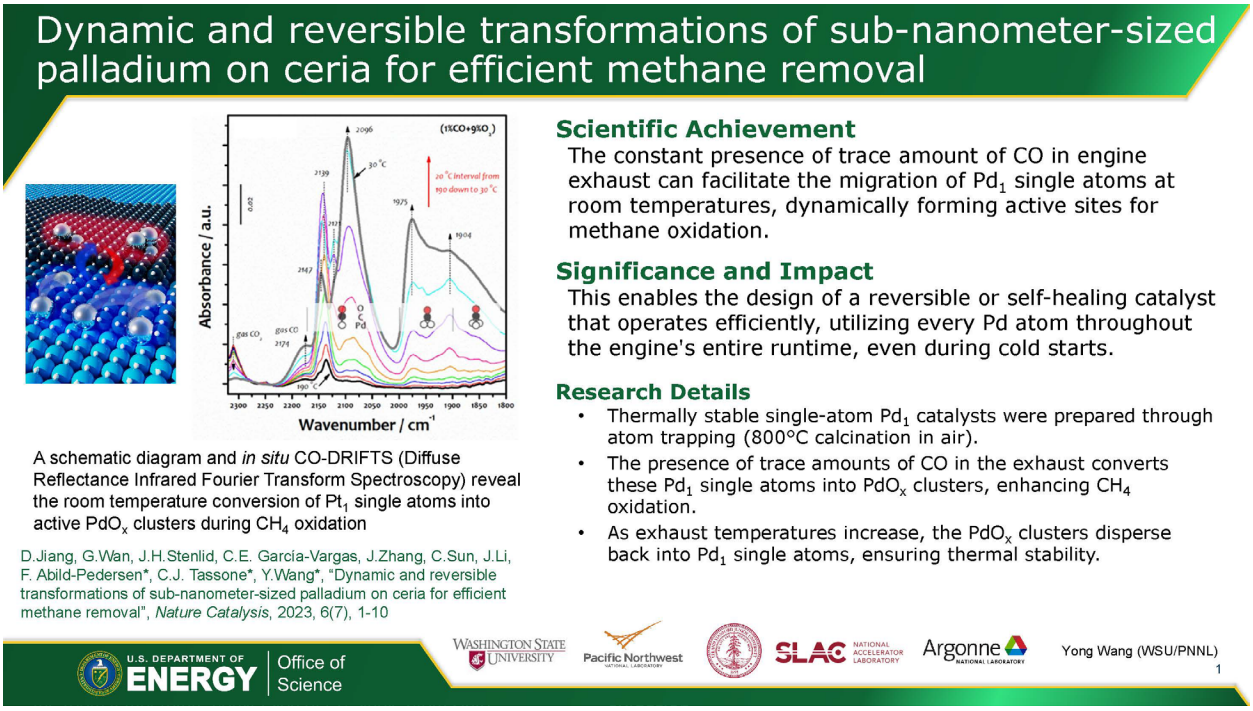


***Developing the science of self-healing catalysts***

Catalyst regeneration is well developed in industrial practice, for example, in reforming reactions where the use of halides and oxidative treatments allow restoration of the initial dispersion of Pt and Ir catalysts. To achieve similar results without halides, we need suitable supports that provide sites for trapping atoms. Our previous work focused on $CeO_2$ supports, where we can stabilize high metal loadings of single atom species (3wt% Pt). Reduction of the single atom $Pt/CeO_2$ catalyst transforms it into nanoparticles yielding excellent low temperature CO

oxidation reactivity. Therefore, $CeO_2$ represents a prototypical regenerable catalyst where the mobile atoms emitted from a nanoparticle can be trapped on the ceria support, regenerating the Pt single atom catalyst. But regeneration of the single atom sites is only possible with an oxidizing environment, and a subsequent reduction step is needed to form nanoparticles which may be the active sites for certain reactions. Our concept of a self-healing catalyst is one that heals itself and continues to operate without the need for periodic regeneration. As described in this work (Porter et al., *ACS Catal*, 2023) we consider the Pt-Pd catalyst as a protypical self-healing catalyst. The addition of Pd to Pt-based diesel oxidation catalysts is known to enhance performance and restrict the anomalous growth of Pt nanoparticles when subjected to aging at high temperatures in oxidative environments. Our study of this catalyst illustrates some of the key principles involved in a self-healing catalyst. We learned that the PdO helps to trap mobile $PtO_2$, impeding the transport of Pt to the vapor phase and preventing the growth of abnormally large particles. Besides lowering the vapor pressure of Pt oxides, we learned that Pt allows Pd to remain metallic, making it possible to retain both metal and oxide functionality for catalysis. The regeneration of deactivated catalysts in industrial practice typically requires an external input, such as a change in the working environment from reducing to oxidizing, or vice-versa. Here we find that the mobile species which are primary contributors to catalyst sintering are effectively returned to the active site, hence our use of the term 'self-healing'. Detailed insights into the inner workings of the Pt-Pd diesel oxidation catalysts can help provide clues to the design of robust and durable heterogeneous catalysts. This work was submitted as a highlight to the BES Catalysis Science program.

## Self Healing Catalysts for Clean Air

### Scientific Achievement

**Electron microscopy, along with other characterization techniques, helped to establish the self-healing nature of Pt-Pd nanoparticles in diesel emission exhaust catalysts.**

### Significance and Impact

**Designing catalysts that can heal themselves, without requiring any external stimulus, is the dream of every catalyst designer. This work shows how this concept is realized in industrial catalysts used for diesel oxidation.**

### Research Details

- Pt sinters at high temperatures in air due to formation of volatile Pt oxides which lead to formation of anomalously large Pt particles.
- Pd is added to Pt to improve long-term performance, but the underlying mechanisms are not understood.
- The critical finding in this work was that Pt-Pd catalysts under working conditions are biphasic, with an oxide and metal phase conjoined via a coherent interface.
- Volatile species emitted from the metal phase are captured by the oxide, via atom trapping, effectively returning the metal atoms back to the active sites without the need for catalyst regeneration.

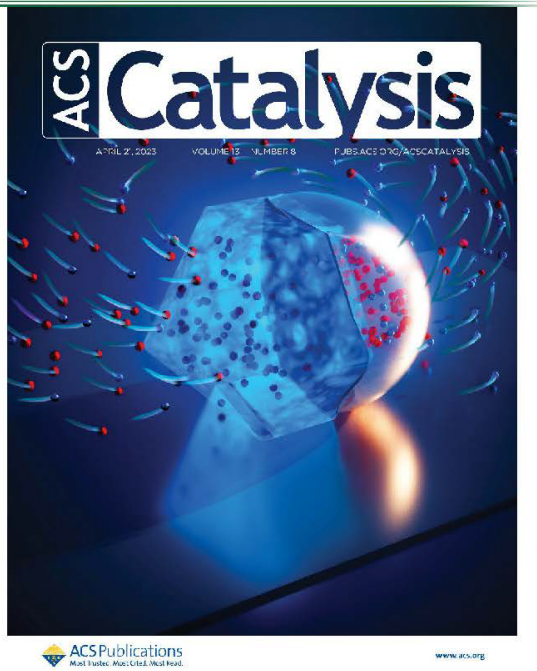


Porter, S., Ghosh, A., Liu, C.H., Kunwar, D., Thompson, C., Alcala, R., Dean, D.P., Miller, J.T., DeLaRiva, A., Pham, H., Peterson, E., Brearley, A., Watt, J., Kyriakidou, E.A., and Datye, A.K., Biphasic Janus Particles Explain Self-Healing in Pt–Pd Diesel Oxidation Catalysts. ACS Catalysis, 2023. 13(8): p. 5456-5471. 10.1021/acscatal.3c00360

The cover art is courtesy of Ella Maru Studios, illustrating how atoms emitted from the metal phase are captured by the oxide.

U.S. DEPARTMENT OF ENERGY | Office of Science
The Advanced Photon Source
National Synchrotron Light Source II
THE UNIVERSITY OF NEW MEXICO

### *Unraveling the dynamics of single atom catalysts*

Pt single atom catalysts prepared by atom trapping have been extensively studied in CO oxidation where we see a positive reaction rate dependence on CO partial pressure. However, we also found negative reaction order on CO depending on the initial partial pressure of CO and partial pressure ratio of $CO/O_2$. These findings suggest single atoms are dynamic under reaction conditions, depending on reactant adsorbent and coordination environment. Single atoms of platinum group metals on $CeO_2$ represent a potential approach to lower precious metal requirements for automobile exhaust treatment catalysts. In this work we demonstrated the dynamic evolution of two types of single-atom Pt ($Pt_1$) on $CeO_2$, i.e., adsorbed $Pt_1$ in $Pt/CeO_2$ and square planar $Pt_1$ in $Pt_{AT}CeO_2$, fabricated respectively at 500 °C and by the atom-trapping method at 800 °C. Adsorbed $Pt_1$ in $Pt/CeO_2$ is mobile with the in-situ formation of few-atom Pt clusters during CO oxidation, contributing to high reactivity with near-zero reaction order in CO. In contrast, square planar $Pt_1$ in $Pt_{AT}CeO_2$ is strongly anchored to the support during CO oxidation leading to relatively low reactivity with a positive reaction order in CO. Reduction of both $Pt/CeO_2$ and $Pt_{AT}CeO_2$ in CO transforms $Pt_1$ to Pt nanoparticles. However, both catalysts retain the memory of their initial $Pt_1$ state after subsequent oxidative treatments, which illustrates the importance of the initial single-atom structure in practical applications. This work was published in *Nature Communications*, 2023.

### *Tuning the reactivity of earth abundant metals (EAMs)*

Metallic Ni is a well-known catalyst for reactions such as dry reforming, or hydrogenation, but not for reactions such as CO oxidation, methane oxidation or for selective hydrogenation of acetylene. Also, Ni catalysts are known to suffer from challenges such as coke formation, which leads to formation of carbon filaments and plugging of the reactor, or from difficulties in handling reduced Ni catalysts due to their pyrophoric nature. In our preliminary work, we have found that when Ni is present in the cerium oxide lattice, the single atom Ni catalysts are active for a broad range of reactions such as hydrogenation as well as oxidation. Over the past year, we have focused on a study of Ni catalysts in ceria focusing on the role of dopants in the ceria lattice. In this work we have developed single atom Ni catalysts that perform a range of reactions, under oxidizing and reducing conditions, without needing any activation. By stabilizing Ni in ceria, we can generate Ni in ionic form that is not pyrophoric and can perform reduction and oxidation reactions without the need for any activation. We have used XAS, TEM and other characterization methods to ensure that the catalyst contains exclusively single atom Ni species, and the reactivity can be attributed to the ionic form of Ni. The results are surprising, in view of the expectation that it is metallic Ni that is active as a catalyst, and not ionic, single atom Ni. These catalysts have been tested for selective acetylene hydrogenation, for CO and $CH_4$ oxidation and for dry reforming of methane. This work is being written up for publication and will demonstrate how the reactivity of earth abundant metals can be tuned by stabilizing the single atoms in suitable supports.

## Publications Acknowledging this Grant in 2021-2024

*(I) Intellectually led by this grant (19);*


1. D.Jiang, Y. Yao, T. Li, G.Wan, X.Pereira-Hernández, Y.Lu, J.Tian, K.Khivantsev, M.H. Engelhard, C.Sun, C.E. García-Vargas, A,S. Hoffman, S. R. Bare, A.K. Datye, L.Hu, Y.Wang, "Tailoring the Local Environment of Pt in Single-Atom Pt1/$CeO_2$ Catalysts for Robust Low-Temperature CO Oxidation", Angewandte Chemie.Int.Ed**, 2021**, 60, 26054-26062, DOI: 10.1002/anie.202108585
2. H.Xiong, D.Kunwar, D.Jiang, C.E. García-Vargas, H.Li, C.Du, G.Canning, X.I.Pereira-Hernandez, Q.Wan, S.Lin, S.C.Purdy, J.T.Miller, K.Leung, S.S.Chou, H.H.Brongersma, Rik ter Veen, J.Huang, H.Guo*, Y.Wang*, A.K.Datye*, "Engineering catalyst supports to stabilize PdOx two-dimensional rafts for water-tolerant methane oxidation", Nature Catalysis, **2021**, doi: 10.1038/s41929-021-00680-4.
3. J.Zhang, B.Sudduth, J.Sun, L.Kovarik, M.H.Engelhard, Y.Wang, "Elucidating the Active Site and the Role of Alkali Metals in Selective Hydrodeoxygenation of Phenols over Iron-carbide-based Catalyst", ChemSusChem, **2021**, doi: 10.1002/cssc.202101382.
4. S. Porter, and A. Datye, Identifying Individual Atoms in Single Atom Pt/$CeO_2$ Catalysts. Microscopy and Microanalysis, **2021**. 27(S1): p. 2608-2610. Doi: 10.1017/S1431927621009260
5. C.E. García-Vargas, X.I.Pereira-Hernández, D.Jiang, R.Alcala, A.T. DeLaRiva, A.Datye, Y.Wang, "Highly active and stable single atom Rh1/CeO2 catalyst for CO Oxidation during redox cycling", *ChemCatChem*, **2022**, DOI:10.1002/cctc.202201210.
6. C.García-Vargas, G.Collinge, D.Yun, M. Lee, V.Muravev, Y.Su, X.I.Pereira Hernandez, D.Jiang, V.Glezakou, E.Hensen, R.Rousseau, A.Datye, Y.Wang, "Activation of Lattice and Adatom Oxygen by Highly Stable Ceria-supported Cu Single Atoms", *ACS Catalysis*, **2022**, https://doi.org/10.1021/acscatal.2c04001 (cover).
7. J.Zhang, J.Li, B.Sudduth, J.Sun, C.Zhang, H.He, Y.Wang, "Enhanced Selective Hydrogenolysis of Phenolic C-O Bond over Graphene-covered Fe-Co Alloy Catalysts", *ACS Sus.Chem.Eng*., **2022**, 10.1021/acssuschemeng.2c02075.
8. Porter, S., Liu, C., Pham, H., Ghosh, A., Watt, J., Kyriakidou, E., & Datye, A. (2022). Epitaxy of the Metal and Oxide Phases in Pt-Pd 'Janus' Particles in 800 °C Air-aged Diesel Oxidation Catalysts. *Microscopy and Microanalysis*, **2022**, 28(S1), 2482-2484. doi:10.1017/S1431927622009497
9. J. R. Regalbuto and A. K. Datye, All the lonely atoms, where do they all belong? *Nat Nanotechnol*, **2022**. 17(2): p. 110-111, doi: 10.1038/s41565-021-01047-3
10. Jiang, D., Wan, G., Halldin Stenlid, J., García-Vargas, C.E., Zhang, J., Sun, C., Li, J., Abild-Pedersen, F., Tassone, C.J., and Wang, Y., Dynamic and reversible transformations of subnanometre-sized palladium on ceria for efficient methane removal. *Nature Catalysis*, **2023**. 6(7): p. 618-627. DOI: 10.1038/s41929-023-00983-8.
11. Zhang, R., Wang, Y., Gaspard, P., and Kruse, N., The oscillating Fischer-Tropsch reaction. *Science*, **2023**. 382(6666): p. 99-103, DOI:10.1126/science.adh8463.
12. Porter, S., Ghosh, A., Liu, C.H., Kunwar, D., Thompson, C., Alcala, R., Dean, D.P., Miller, J.T., DeLaRiva, A., Pham, H., Peterson, E., Brearley, A., Watt, J., Kyriakidou, E.A., and Datye, A.K., Biphasic Janus Particles Explain Self-Healing in Pt–Pd Diesel Oxidation Catalysts. *ACS Catalysis*, **2023**. 13(8): p. 5456-5471. 10.1021/acscatal.3c00360
13. Zhang, Z., Tian, J., Lu, Y., Yang, S., Jiang, D., Huang, W., Li, Y., Hong, J., Hoffman, A.S., Bare, S.R., Engelhard, M.H., Datye, A.K., and Wang, Y., Memory-dictated dynamics of single-atom Pt on CeO2 for CO oxidation. *Nature Communications*, **2023**. 14(1): p. 2664. DOI: 10.1038/s41467-023-37776-3
14. Liu, C.-H., Porter, S., Chen, J., Pham, H., Peterson, E.J., Khatri, P., Toops, T.J., Datye, A., and Kyriakidou, E.A., Enhanced low temperature performance of bimetallic Pd/Pt/SiO2 (core)@ Zr

(shell) diesel oxidation catalysts. *Applied Catalysis B: Environmental*, 2023. 327: p. 122436. 10.1016/j.apcatb.2023.122436
15. García‐Vargas, C.E., Pereira‐Hernández, X.I., Jiang, D., Alcala, R., DeLaRiva, A.T., Datye, A., and Wang, Y., Highly Active and Stable Single Atom Rh1/CeO2 Catalyst for CO Oxidation during Redox Cycling. *ChemCatChem*, **2023**. 15(1): p. e202201210. 10.1002/cctc.202201210
16. Porter, S., Liu, C.H., Pham, H., DeLaRiva, A., Peterson, E., House, S., Watt, J., Kyriakidou, E.A., and Datye, A.K., Formation of Pt-Pd 'Janus' Biphasic Particles During High-Temperature Aging of Diesel Oxidation Catalysts. *Microscopy and Microanalysis*, **2023**. 29(Supplement_1): p. 1599-1601. DOI:10.1093/micmic/ozad067.821
17. Hansen, T.W., DeLaRiva, A., and Datye, A.K., Nanoparticle Mobility and Coalescence During Sintering of a Ni/MgAl2O4 Methane Steam Reforming Catalyst. *Microscopy and Microanalysis*, **2023**. 29(Supplement_1): p. 1618-1619. DOI:10.1093/micmic/ozad067.831
18. Porter, S. and Datye, A.K., Imaging of single atom catalysts, in Heterogeneous Inorganic Catalysts, R.A. van Santen and E. Hensen, Editors. **2023**, Elsevier: Oxford. p. 222-243. B978-0-12-823144-9.00135-7
19. Datye, A. and DeLaRiva, A., Scanning Electron Microscopy (SEM), in Springer Handbook of Advanced Catalyst Characterization, I.E. Wachs and M.A. Bañares, Editors. **2023**, Springer International Publishing: Cham. p. 359-380. 10.1007/978-3-031-07125-6_18

*(II) Jointly funded by this grant and other grants with intellectual leadership by other funding sources (11);*

1. R. Alcala, A. DeLaRiva, E.J. Peterson, A. Benavidez, C.E. Garcia-Vargas, D. Jiang, X.I. Pereira-Hernández, H.H. Brongersma, R.t. Veen, J. Staněk, J.T. Miller, Y. Wang, and A. Datye, Atomically Dispersed Dopants for Stabilizing Ceria Surface Area. Applied Catalysis B: Environmental, **2021**. 284: p. 119722.
2. B.Qian, J.Zhang, S.Zhou, J.Lu, Y.Liu, B.Dai, C.Liu, Y.Wang, H.Wang, L.Zhang, "Synthesis of (111) facet-engineered MgO nanosheet from coal fly ash and its superior catalytic performance for high-temperature water gas shift reaction", *Appl.Catal.A, General*, **2021**, doi: 10.1016/j.apcata.2021.118132.
3. A.J.R.Hensley, G.Collinge, Y.Wang, J.S.McEwen, "Guiding the design of oxidation-resistant Fe-based single atom alloy catalysts with insights from configurational space", *J.Chem.Phy.*, **2021**, doi:10.1063/5.00048698.
4. H. Xiong, A.K. Datye, and Y. Wang, Thermally Stable Single-Atom Heterogeneous Catalysts. *Advanced Materials*, **2021**: p. 2004319. Doi: 10.1002/adma.202004319.
5. Y. B. Lu, S. L. Zhou, C. T. Kuo, D. Kunwar, C. Thompson, A. S. Hoffman, A. Boubnov, S. Lin, A. K. Datye, A.K., H. Guo, and A. M. Karim, Unraveling the Intermediate Reaction Complexes and Critical Role of Support-Derived Oxygen Atoms in CO Oxidation on Single-Atom Pt/$CeO_2$. *ACS Catalysis*, **2021**. 11(14): p. 8701-8715, 10.1021/acscatal.1c01900.
6. H. N. Pham, A. DeLaRiva, E. J. Peterson, R. Alcala, K. Khivantsev, J. Szanyi, X. S. Li, D. Jiang, W. Huang, Y. Sun, P. Tran, Q. Do, C. L. DiMaggio, Y. Wang and A. K. Datye, Designing Ceria/Alumina for Efficient Trapping of Platinum Single Atoms, *ACS Sus. Chem. & Engr.*, **2022**, doi: 10.1021/acssuschemeng.2c01380.
7. Li, H., Wan, Q., Du, C., Liu, Q., Qi, J., Ding, X., Wang, S., Wan, S., Lin, J., Tian, C., Li, L., Peng, T., Zhao, W., Zhang, K.H.L., Huang, J., Zhang, X., Gu, Q., Yang, B., Guo, H., Lin, S., Datye, A.K., Wang, Y., and Xiong, H., Vapor-phase self-assembly for generating thermally stable single-atom catalysts. *Chem*, **2022**. 8(3): p. 731-748.Doi: 10.1016/j.chempr.2021.11.002
8. X. Li, X. I. P. Hernandez, Y. Chen, J. Xu, J. Zhao, C. Pao, C.-Y. Fang, J. Zeng*, Y. Wang*, B. C. Gates*, J. Liu*, "Functional CeOx Nanoglues for Robust Atomically Dispersed Catalysts", *Nature*, **2022**, doi: 10.1038/s41586-022-05251-6.

9. Chen, J., Pham, H.N., Mon, T., Toops, T.J., Datye, A.K., Li, Z., and Kyriakidou, E.A., Ni/CeO2 nanocatalysts with optimized CeO2 support morphologies for CH4 oxidation. *ACS Applied Nano Materials*, **2023**. 6(6): p. 4544-4553. 10.1021/acsanm.2c05496
10. Riley, C., Valdez, N., Smyth, C.M., Grant, R., Burnside, B., Park, J.E., Meserole, S., Benavidez, A., Craig, R., Porter, S., DeLaRiva, A., Datye, A., Rodriguez, M. and Chou, S.S. Vacancy-Driven Stabilization of Sub-Stoichiometric Aluminate Spinel High Entropy Oxides. *The Journal of Physical Chemistry C,* **2023**. 127(23): p. 11249-11259. 10.1021/acs.jpcc.3c01499
11. Tian, J., Kong, R., Wang, Z., Fang, L., He, T., Jiang, D., Peng, H., Sun, T., Zhu, Y., and Wang, Y., Enhancing Methane Combustion Activity by Modulating the Local Environment of Pd Single Atoms in Pd1/CeO2 Catalysts. *ACS Catalysis*, **2024**. 14(1): p. 183-191.DOI: 10.1021/acscatal.3c02167.

# Modeling and Design of Main-Group Metal Catalyzed Alkane C-H Functionalization Reactions

Daniel H. Ess
Department of Chemistry and Biochemistry, Brigham Young University, Provo, UT 84604

## Presentation Abstract

This poster will describe our efforts using quantum-mechanical calculations and experiments to develop and understand alkane and arene C-H activation and functionalization reactions with main-group metal complexes. This poster will also describe new software tools and computational approaches that aid in the prediction of new catalysts.

**Grant or FWP Number: DE-SC0018329**

**PI:** Daniel H. Ess
**Postdoc(s):** Anjaneyulu Koppaka, Jyothish Joy, and Shusen Chen
**Student(s):** Zack Meyer (undergraduate), Drew Hartsfield (undergraduate), Alex Kraus (undergraduate), Sanaz Koumleh (graduate student), and Dongdong Yang (graduate student),

## RECENT PROGRESS

### *Mechanism and Reactivity of $Sb^V$ C-H Activation and Functionalization*

Direct and selective oxidative functionalization of unactivated aromatic $sp^2$ C-H bonds to ester (or alcohol) functional groups is a surprisingly difficult transformation. There are only a few examples where this transformation is promoted by transition metal complexes, such as Pd and Cu. In most of these reactions it was proposed that Pd and Cu induce functionalization through a two-step reaction mechanism that first involves C-H activation/metalation to generate an organometallic metal-aryl intermediate and a second step that involves reductive functionalization to generate the new C-O bond.

Because of the lack of transition metal-based complexes that directly induce oxidative functionalization of aromatic C-H bonds we examined if p-block main-group metals might be an advantageous alternative for this type of transformation. The major results are: 1) Experimental and theoretical studies that show that at lower temperatures (~60 °C) $Sb^V$ induces innersphere metal-mediated chemoselective *para* C-H activation of toluene followed by disproportionation to give a *para* bis-tolyl $Sb^V$ intermediate without functionalization. 2) Experiments at elevated temperatures (170 °C for 3 hours) generated the aryl esters with good yields and with selectivity switched to *ortho*-substituted and *meta*-substituted esters. 3) Our calculations indicate that the *para* to *ortho*/*meta* selectivity change occurs because at the higher temperatures there is a Curtin-Hammet

type equilibrium with rate limiting functionalization from the more electron deficient mono-tolyl $Sb^V$ intermediate.

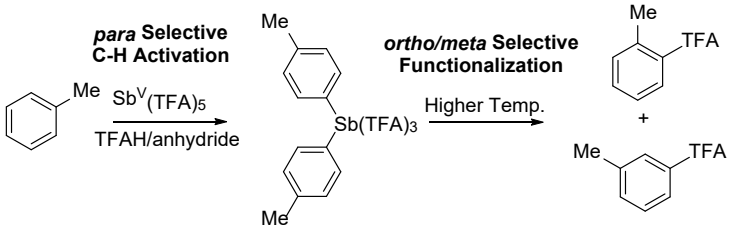


## Mechanism and Selectivity of Model Bi(V)-Aryl Oxy-Functionalization in Trifluoroacetic Acid Solvent

Previous examination of main-group metal reactions indicates that while C-H metalation can be kinetically fast it is generally kinetically slow to generate oxy-functionalization products. Kinetically slow functionalization is a potential problem if functionalization is carried out in relatively strong acid where protonation has the potential to outcompete and prevent oxy-functionalization. Therefore, we examined model main-group metal aryl complexes that would be especially susceptible to protonation and determine if oxy-functionalization is possible.

We decided to experimentally and computationally analyze the oxy-functionalization reaction of $Bi^V$-aryl complexes in strong trifluoroacetic acid (TFAH) solvent. $Bi^V$-aryl complexes were selected because they are both a model for a metal-aryl intermediate that could be potentially generated from Bi C-H activation (or C-H activation at a lower oxidation followed by oxidation) and Bi-C bonds are generally highly polar and susceptible to protonation. We were encouraged by the previous work of Mukaiyama, Barton, Ball, and Cornella who have shown some functionalization of Bi-aryl complexes in non-acid solvent.

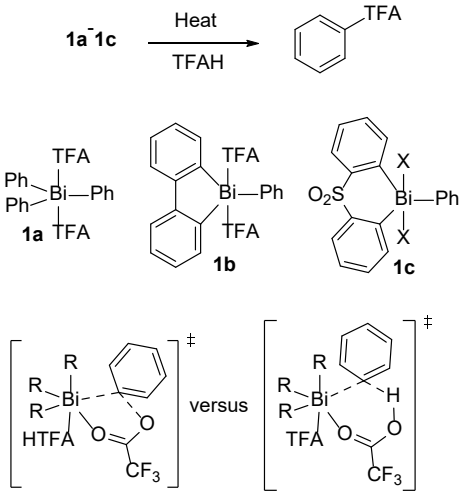


We first synthesized the $(Ph)_3Bi^V(TFA)_2$ (TFA = trifluoroacetate) complex and examined its reactivity in trifluoroacetic acid (TFAH) solvent, which gave clean formation of a single oxy-functionalization product phenyl trifluoroacetate (PhTFA) and two equivalents of benzene. We also used DFT calculations with explicit/continuum solvent to extensively examine possible oxy-functionalization reaction mechanisms and selectivity versus protonation, which revealed that oxy-functionalization occurs through a direct

intramolecular reductive functionalization pathway rather than ion pair or radical pair pathways. Surprisingly this reductive functionalization pathway is kinetically faster than protonation. We also experimentally synthesized and examined the oxy-functionalization of Bi-Ph with biphenyl and biphenyl sulfone ligands.

**Mechanism and Selectivity of Main-Group Metal Oxides for Methane C-H Functionalization**

With evidence that $Bi^V$ has the potential for oxy-functionalization reactions and preliminary calculations that show low barriers for C-H activation with $Bi^V$, we experimentally examined Bi oxide in sulfuric acid for reaction with methane. Perhaps surprisingly, $NaBiO_3$ dissolved in sulfuric acid provides nearly quantitative conversion of methane to methyl bisulfate when reacted with methane at 180 °C. Background experiments show very little methyl bisulfate formed without Bi, which indicates oleum-based reactivity is not occurring. However, test experiments showed that at lower temperatures (e.g. <90 °C) methane sulfonic acid is first formed, which is then converted to methyl bisulfate. This result is significant because normally it is assumed that methane sulfonic acid is formed from radical initiators and provides a mixture of several products. Therefore, we have undertaken a general experimental and computational study to examine possible C-H activation versus solvent oxidation/radical reaction mechanisms for the series of main-group metals (MG) and solvents ($H_2SO_4$, TfOH, TFAH, and AcOH).

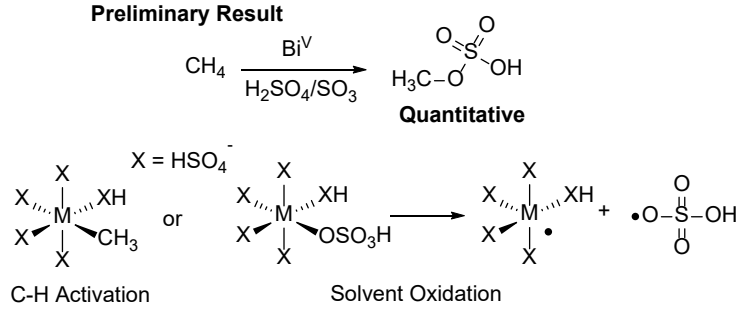


***Software, Ligand Libraries, and Machine Learning for Catalyst Design***

The key to successful computational homogeneous catalyst design is identification of a specific ligand framework mounted on a transition metal that will result in the desired reaction reactivity and/or selectivity. Our approach to computationally design catalysts is to directly evaluate reactivity and selectivity of possible catalyst ligands through optimization of transition-state structures and intermediates. This can now be done in a semi-automated manner using programs such as the AARON toolkit, Kulik's molSimplify, or our Mason program (https://github.com/DanielEss-lab/Mason).

However, a major limitation of this catalyst design approach is the lack of ligand libraries that would be ideal to begin searching chemical space and that would directly translate to a plausible experimental system that can be straightforwardly synthesized. Therefore, we developed an experimentally based library of >30,000 monodentate, bidentate (didentate), tridentate, and larger ligands cultivated by dismantling experimentally reported crystal structures. The library is called ReaLigands (https://github.com/DanielEss-lab/ReaLigands). Individual ligands from mononuclear crystal structures were identified using a modified depth-first search algorithm and charge

was assigned using a machine learning model based on quantum-chemical calculated features. In the library ligands were sorted based on direct ligand-to-metal atomic connections and on denticity. Representative principal component analysis (PCA) and uniform manifold approximation and projection (UMAP) analyses were used to analyze several tridentate ligand categories, which revealed both the diversity of ligands and connections between ligand categories. We also demonstrated the utility of this library by implementing it with our building and optimization tools, which resulted in the very rapid generation of barriers for 750 bidentate ligands for Rh-hydride ethylene migratory insertion.

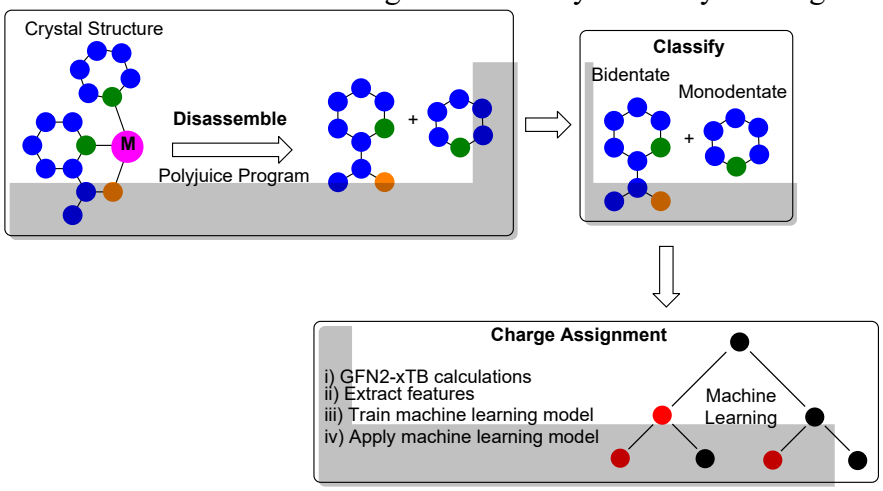


**Publications Acknowledging this Grant in 2021-2024**


(I) a) Chen, S-S.; Koppaka, Anjaneyulu, Periana, R. A.; Ess, D. H. Theory and Experiment Demonstrate that Sb(V)-Promoted Methane C-H Activation and Functionalization Outcompetes Superacid Protonolysis in Sulfuric Acid. *J. Am. Chem. Soc.* **2021**, *143*, 18242-18250.

b) Chen, S.; Nielson, T.; Zalit, E.; Skjelstad, B. B.; Borough, B.; Hirschi, W. J.; Yu, S.; Balcells, D. Ess, D. H. Automated Construction and Optimization Combined with Machine Learning to Generate Pt(II) Methane C–H Activation Transition States. *Topics in Catalysis* **2022**, 65, 312-324.

c) Chen, S-S.; Meyer, Z.; Jensen, B.; Kraus, A.; Lambert, A.; Ess, D. H. ReaLigands: A Ligand Library Cultivated from Experiment and Intended for Molecular Computational Catalyst Design. *J. Chem. Inf. Model.* **2023**, *63*, 7412-7422.

d) Gunsalus, N.; Koppaka, A.; Chen, S.-S.; Park, S. H. Hashiguchi, B. G.; Ess, D. H.; Periana, R. A. Reactivity and Mechanisms of Methane, Ethane, and Benzene C-H Amination with an Iodine(III) Bistriflimide Complex. *Organometallics,* **2023**, *42*, 1505-1512.

*(II)* a) Koppaka, A.; Kirkland, J. T.; Periana, R. A.; Ess, D. H. Experimental Demonstration and Density Functional Theory Mechanistic Analysis of Arene C–H Bond Oxidation and Product Protection by Osmium Tetroxide in a Strongly Basic/Nucleophilic Solvent. *J. Org. Chem.* **2022**, *J. Org. Chem.* **2022**, *87*, 13573-13582.

Alison Fout

# Exploring Ligand Dynamics in Oxyanion Reduction

J. M. Moore,[a] K. L. Gullett,[b] T. J. Miller,[b] H.-L. Cho [a] and A. R. Fout[a*]
[a]Texas A&M University
[b]University of Illinois at Urbana-Champaign

## Presentation Abstract

The global nitrogen cycle represents a variety of pathways for the conversion of nitrogen containing substrates. This study presents advancements in the selective reduction of nitrogen-containing oxyanions. Building on previous work that demonstrated the reduction of $NO_3^-$ to NO using the $[N(afaCy)_3Fe]OTf_2$ complex, we have developed a new ligand framework to look for intermediates in the reaction. A new ttrapodal ligand on iron has allowed us to now see intermediates in the reaction for the conversion of nitrate to nitric oxide, including the formation of a nitrite-bound iron species and a reactive iron(III)-hydroxide. This reduction to NO from nitrate or nitrite relies on a bimetallic mechanism to form an iron-nitrosyl species and water.

We have also been targeting the reduction of NO to $NH_3$ or $N_2$. The conversion of NO to $NH_3$ is achieved with a 29% yield, confirmed via $^{15}N$ labeling studies. Hydroxylamine ($NH_2OH$) is identified as a key intermediate in this process, supported by computational and experimental findings. Additionally, an alternative reduction pathway of $NO_2^-$ to $N_2$ is proposed, where NO generated from $NO_2^-$ is converted to $N_2O$ by $PPh_3$, and subsequently reduced to $N_2$ by the iron complex. These mechanisms provide insights into natural enzymatic processes that reduce nitrogen-containing oxyanions.

Finally, the versatile binding behavior of a tetrapodal ligand framework with nickel is explored. The ligand fluxionality enables interconversion between octahedral and square planar geometries, influenced by solvent coordination. UV-vis and NMR kinetic studies suggest that solvent binding initiates dynamic changes, shedding light on how water binding could drive coordination mode changes in metalloenzymes. A reverse-dative Ni → Ag interaction, triggered by the addition of silver triflate, provides further insight into altering nickel geometry. These findings advance the understanding of dynamic processes in metalloenzymes and metal-ligand systems.

**Grant or FWP Number:** Aspatial Oxyanion Reduction DE-SC0025026.

## RECENT PROGRESS

### Publications Acknowledging this Grant in 2021-2024

*(I) Intellectually led by this grant*

1. Moore, J.M.; Fout, A. R. "Tetrapodal Iron Complexes Invoke Observable Intermediates in Nitrate and Nitrite Reduction." **2024** Manuscript under review.
2. Moore, J. M.; Miller, T. J.; Mu, M.; Peñas-Defrutos, M. N.; Gullett, K. L.; Elford, L. S.; Qunitero, S.; García-Melchor, M.; Fout, A. R. "Selective and Stepwise Reduction of Nitrate and Nitrite to Ammonia and Dinitrogen" **2024** Manuscript submitted.
3. Cho, H.-L.; Gullett, L. K.; Fout, A. R. *Chem. Commun.*, **2024**, *60*, 10564-10567.
4. Gullett, K.L.; Ford, C.L.; Garvey, I.J.; Miller, T.J.; Leahy, C.A.; Awaitey, L. N.; Hofmann, D.M.; Woods, T.J.; Fout, A.R. *J. Am. Chem. Soc.* **2023**, *145*, 20868–20873.
5. Park, Y. J.; Peñas-Defrutos, M. N.; Drummond, M.J.; Gordon, Z.; Kelly, O.R.; Garvey, I.J.; Gullett, K. L.; M. N.; García-Melchor, M.; Fout, A.R. *Inorg. Chem.* **2022**, *61*, 8182–8192.
6. Leahy, C. A.; Drummond, M. J.; Vura-Weis, J.; Fout, A. R. *Dalton Trans*. **2021** 50, 12088–12092.

**Lewis acid and redox reactivity of antimony compounds and application to catalysis**

François Gabbaï
Department of Chemistry, Texas A&M University

**Presentation Abstract**

Pentavalent antimony compounds have been extensively explored as Lewis acids. Because the trivalent state of this heavy group 15 element is also readily accessible, these compounds can engage in two-electron chemistry, offering unique opportunities in the area of small molecule activation and catalysis. This presentation will cover the recent progress that we have made while exploring such concepts. We will begin by describing our results on the synthesis of transition metal catalysts whose reactivity is modulated by a neighboring antimony center. In the second part of this presentation, we will discuss unpublished results concerning the interaction of $SbCl_3$ and *o*-chloranil, which results in the formation of pentavalent antimony species when in the presence of a Lewis basic or electron-rich substrate. Our results show that access to such pentavalent antimony species can be exploited for the activation of strong bonds, including C-F bonds, for the polymerization of cyclic ethers, and for the cis-functionalization of olefins.

**Grant or FWP Number: Electrophilic catalysts featuring antimony Lewis acids**

**Student(s):** Shantabh Bedajna, Paula Castro Castro, Benyu Zhou

## RECENT PROGRESS

***Transition metal catalyst containing antimony-based ligands***

Our interest in the design of ambiphilic ligands and their coordination to late transition metals has led us to synthesize several complexes featuring a donor functionality such as a phosphine and an *N*-heterocyclic carbene positioned next with an antimony functionality. These efforts have allowed us to isolate three examples of transition metal complexes featuring such ligands. These include an indazol-3-ylidene gold chloride complex functionalized at the 4-position of the indazole backbone by a stibine functionality which cleanly reacts with o-chloranil to afford the corresponding stiborane derivative **1**. Structural analysis indicates that the stiborane coordination environment is best described as a distorted square pyramid whose open face is oriented toward the gold center, allowing for the formation of a long donor-acceptor, or pnictogen, Au → Sb bonding interaction. The presence of this interaction, which has been probed computationally, is also manifested in the enhanced catalytic activity of this complex in the cyclization of N-propargyl-4-fluorobenzamide. The other two examples are also gold chloride complexes in which a phosphine gold-chloride unit is connected to a stiborane by a dimethylxanthene (**2**) or ferrocene (**3**) backbone. Evaluation of these systems in propargyl amide cyclization reactions reveals two important aspects. The first one pertains to the rigidity and of the backbone which needs to be sufficient to old the two functionalities next to each other as a prerequisite for catalysis. Indeed, the dimethylxanthene system is significantly more active than its ferrocene counterpart, a difference that we assign to the rotational flexibility of the ferrocene backbone. The second important outcome of this work is the finding that the antimony must be in the pentavalent state in order to enhance the reactivity of the adjacent phosphine gold-chloride uinit, a process which we propose based on compoatui result for the formation of an Au-Cl → Sb(v) interaction which leave the gold exposed to the reaction substrates

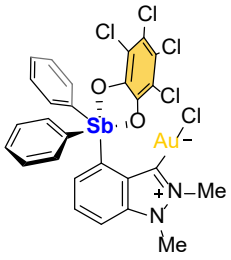


**1**

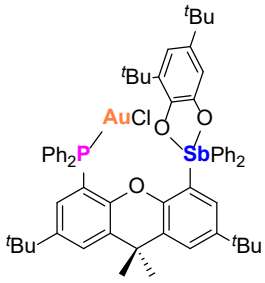


**2**

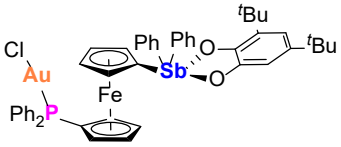


**3**

***Transition metal catalyst containing antimony-based ligands***

Our efforts to diversify the type of donor functionalities that we include in such systems have led us to consider the incorporation of nitrogen donors instead of phosphines or carbenes. This approach has led us to prepare tris(8-quinolyl)stibine and tris(6-methyl-8-quinolyl)stibine which could be easily obtained from the lithiated ligands and $SbCl_3$. The coordination behavior of these new ligands has been tested using rhodium as a metal. We found that both ligands react with $(MeCN)_3RhCl_3$. The resulting complexes **4** and **5** feature an unusual $[RhSb]^{VI}$ core and show the migration of one of the chloride ligands to the

antimony center, which shows it valence increased by two. Computational analysis using density functional theory reveals that the resulting Rh-Sb $\sigma$ bond is polarized toward the Rh atom, suggesting a description of this linkage as a Rh → Sb Z-type interaction. Evaluation of the complexes as catalysts are ongoing.

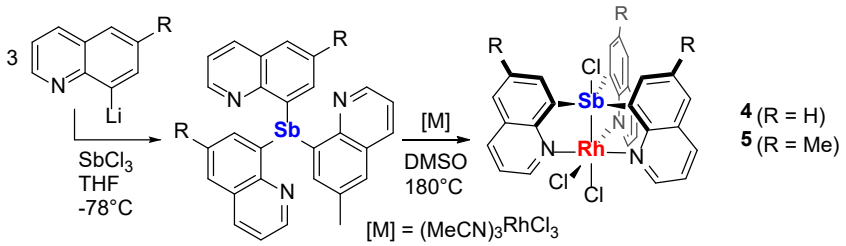


***Redox chemistry of the $SbCl_3$ and o-chloranil system***

We have been intrigued by the possibility of accessing Lewis acidic antimony(V) derivatives starting for $SbCl_3$ and ortho-quinones. To begin this investigation, we first computed the structure of $SbCl_3$(cat) (cat$^{2-}$ = [*o*-$C_6Cl_4O_2$]$^{2-}$), the target Lewis acid. The structure of this derivative was optimized and found to adopt a square pyramidal geometry about the Sb center. A thermodynamic analysis indicated the formation of $SbCl_3$(cat) from $SbCl_3$ and *o*-chloranil is endergonic by 3.0 kcal/mol. This prediction is consistent with our observation that $SbCl_3$ and *o*-chloranil do not react with one another. However, this situation can be altered by addition of a base such as triphenylphosphine oxide which traps the pentavalent complex in the form of the ocathedral complex $Ph_3PO \rightarrow SbCl_3$(cat). Access to pentavalent $SbCl_3$(cat) from $SbCl_3$ and *o*-chloranil can also be used to activate the C-F bond of fluoroalkanes, leading to the generation of carbocations readily trapped by Friedel-Crafts reactions. We also found that $SbCl_3$ catalyzes the addition of *o*-chloranil to olefins, a process that we also speculate involves the intermediacy of $SbCl_3$(cat). These results will soon be submitted for publication.

**Publications Acknowledging this Grant in 2021-2024**

*(I) Intellectually led by this grant*


1. Castro Castro, P.; Gabbaï, F. P. Pnictogen Bonding at the Core of a Carbene-Stiborane-Gold Complex: Impact on Structure and Reactivity. *Organometallics* **2024**, *43*, 2334-2341.
2. Zhou, B.; Bedajna, S.; Gabbaï, F. P. Pnictogen bonding at the service of gold catalysis: the case of a phosphinostiborane gold complex. *Chem. Commun.* **2024**, *60*, 192-195.
3. Wade, C. R.; Murphy, B. L.; Bedajna, S.; Gabbaï, F. P. Rh → Sb Interactions Supported by Tris(8-quinolyl)antimony Ligands. *Organometallics* **2024**, *43*, 1785-1788.
4. Zhou, B.; Gabbaï, F. P. Four-Electron Reduction of $O_2$ Using Distibines in the Presence of *ortho*-Quinones. *J. Am. Chem. Soc.* **2023**, *145*, 13758-13767.


*(II) Jointly funded by this grant and other grants with intellectual leadership by other funding sources*

Nilay Hazari

# First-Row Transition Metal Catalysts Supported by PNP Ligands with an Additional Hemilabile Donor for $CO_2$ Hydrogenation

Nilay Hazari,[a,*] Justin C. Wedal,[a] Kyler B. Virtue,[b] & Wesley H. Bernskoetter[b,*]

[a]The Department of Chemistry, Yale University, P. O. Box 208107, New Haven, Connecticut, 06520, USA.

[b]The Department of Chemistry, The University of Missouri, Columbia, Missouri, 65211, USA.

## Presentation Abstract

First-row transition metal complexes supported by pincer ligands of the type R'N($CH_2CH_2PR_2$)$_2$ ($^{R}$PN$^{R'}$P) are highly active catalysts for a range of hydrogenation and dehydrogenation reactions but are prone to catalyst deactivation. Here, we describe the synthesis of the ligands (E$CH_2CH_2$)N($CH_2CH_2P^iPr_2$)$_2$ (E = OMe, $^{iPr}$PN$^{OMe}$P; & $NMe_2$) and (OMe$CH_2CH_2CH_2$)N($CH_2CH_2P^iPr_2$)$_2$, which are $^{R}$PN$^{R'}$P-type ligands containing a pendant hemilabile ether or amine donor. We describe the preparation and characterization of a series of iron and manganese complexes supported by these ligands and assess their performance for catalytic $CO_2$ hydrogenation to formate. It is demonstrated that iron hydride species supported by $^{iPr}$PN$^{OMe}$P give comparable turnover numbers for catalytic $CO_2$ hydrogenation to formate as the state-of-the-art iron system ligated by MeN($CH_2CH_2P^iPr_2$)$_2$ ($^{iPr}$PN$^{Me}$P). Further, $^{iPr}$PN$^{OMe}$P ligated iron catalysts show improved catalytic lifetimes compared to $^{iPr}$PN$^{Me}$P supported systems, albeit with lower turnover frequencies. Experimental and theoretical studies indicate that the pendant hemilabile ether donor aids in stabilizing the catalyst by binding to the iron center but impedes catalytic turnover by forming an off-cycle cationic complex, which is the catalyst resting state. Overall, this work provides rare examples of pincer ligands with additional hemilabile donors and demonstrates that the incorporation of an additional donor is a viable strategy for optimizing the catalytic performance of systems supported by $^{R}$PN$^{R'}$P ligands.

**Grant or FWP Number: DE-SC0018222 - Base Metal Catalysis with Relevance to Energy Storage Applications**

**PI:** Wesley H. Bernskoetter & Nilay Hazari
**Postdoc(s):** Justin C. Wedal
**Graduate Student(s):** Kyler B. Virtue

## RECENT PROGRESS

### *Synthesis of PNP Ligands with an Additional Hemilabile Donor*

In previous DOE funded work, we demonstrated that the presence of exogenous phosphine ligands, such as PM e$_3$, can improve the catalytic performance of $^{iPr}$PN$^{R'}$P-ligated iron catalysts in formic acid dehydrogenation (Figure 1a). We propose that this is because reversible coordination of $PMe_3$ slows bimolecular catalyst decomposition, while still providing access to the coordinatively unsaturated species required for productive catalysis. Although intermolecular stabilization of the active species provides evidence that catalytic performance improves when another coordinating ligand is present, *we hypothesized that introducing an intramolecular hemilabile pendant group, such as an ether, on the $^{iPr}$PN$^{R'}$P*

*pincer scaffold is a better method to impart enhanced stability to the resulting iron complexes*. We also proposed that we could extend this strategy to stabilize catalysts based on other first-row transition metal catalysts.

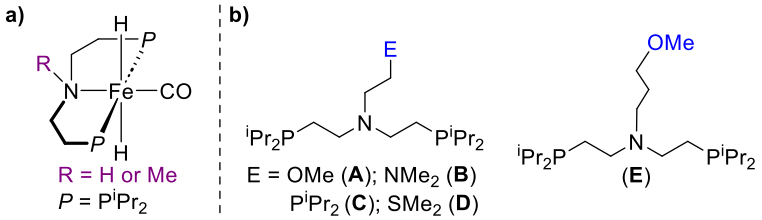


**Figure 1: a)** Structure of $^{iPr}PN^{R'}P$-ligated iron catalysts that are highly active for dehydrogenation and hydrogenation reactions. **b)** Pincer ligands with pendant donors synthesized as part of this work.

Over the last year, we synthesized a family of $^{iPr}PN^{R}P$ ligands with pendant amine, ether, phosphine, and thiol donors (**A-E**) (Figure 1b). For brevity, only the synthesis of **A** is described (Figure 2). The three-step synthesis starts with an $S_N2$ reaction between two inexpensive commercially available reagents, diethanolamine and 1-chloro-2-methoxyethane, to generate intermediate **i**. Treatment of **i** with $SOCl_2$ generates the salt **ii**, which can be treated with $^{n}$BuLi and then two equivalents of $LiP^{i}Pr_2$ to generate **A**. Although the yield of step one is low (~10%), the subsequent two steps proceed in good yield (59 & 80%, respectively) and it is possible to synthesize **A** on a gram scale. Using similar procedures, we have synthesized ligands **B**-**E**.

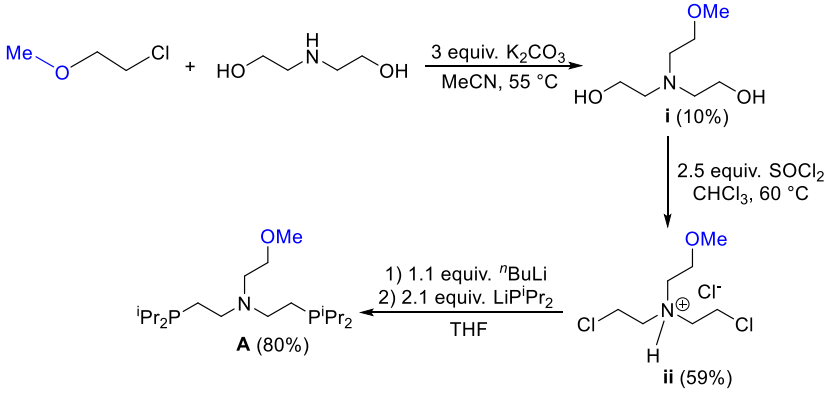


**Figure 2:** Synthesis of ligand **A**.

***Iron Complexes Supported by $^{iPr}PN^{R'}P$ Ligands with an Additional Hemilabile Donor***

We initially targeted the synthesis of iron catalysts ligated by **A-D** to test our hypothesis that the pendant arm would lead to more stable catalysts. Our goal was to access an iron hydride that could be used as a precatalyst for formic acid dehydrogenation and/or $CO_2$ hydrogenation. To access the iron hydrides, we first coordinated the free ligand to $FeCl_2$, as

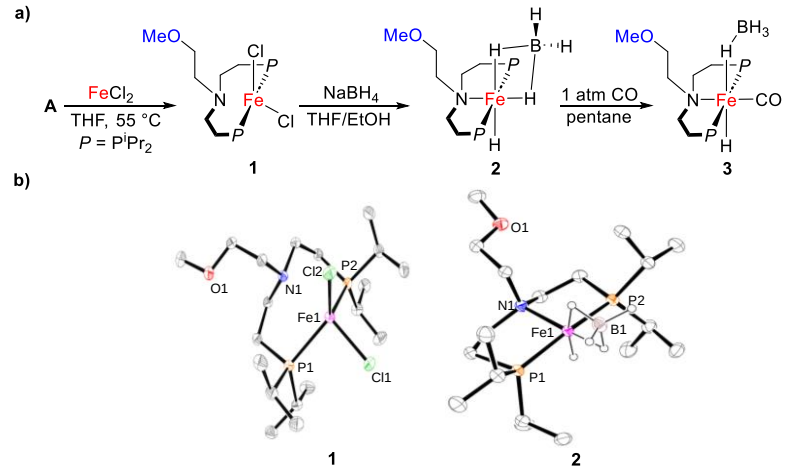


**Figure 3: a)** Synthesis of iron complexes **1-3** and **b)** solid-state structures of **1** & **2**.

shown in Figure 3 for **A**. This generated a tetrahedral Fe(II) complex **1**, where neither the tertiary amine of the pincer ligand or the pendant methoxy arm were bound. Subsequent treatment of **1** with $NaBH_4$ generated the diamagnetic octahedral compound **2**, containing a $\kappa^2$-$BH_4$ ligand. Exposure of **2** to 1 atm of CO formed compound **3**, which has a $\kappa^1$-$BH_4$ ligand. Compounds **1** and **2** were characterized by x-ray crystallography. Attempts to coordinate ligands **B**-**D** to $FeCl_2$ were successful and resulted in the formation of analogues of **1**. However, treatment of the resulting complexes with $NaBH_4$ generated complexes in which the pendant ligand arm was bound to $BH_3$.

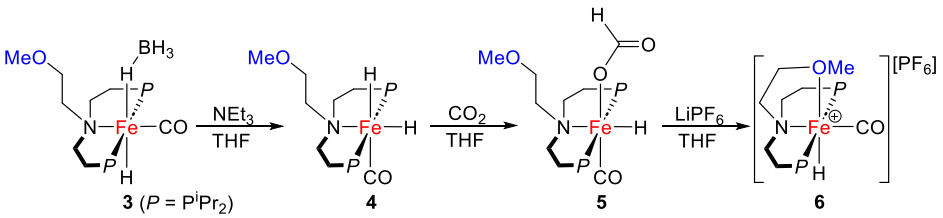


3 ($P$ = P$^i$Pr$_2$) 4 5 6

**Figure 4:** Reactions of iron complexes ligated by **A** relevant to $CO_2$ hydrogenation.

The reaction of **3** with $NEt_3$ generates the dihydride **4**, which upon exposure to $CO_2$ forms the formate complex **5** (Figure 4). Interestingly, exposure of **5** to $LiPF_6$ results in the loss of the formate ligand and the generation of complex **6**, in which the pendant OMe group is coordinated to the Fe center. This validates our hypothesis that the pendant OMe group can coordinate to the metal center. It is also possible to convert **6** back to **4** through a reaction with $H_2$ in the presence of DBU. This is important because it demonstrates that starting from **4** it is possible to perform all the elementary steps that are proposed in $CO_2$ hydrogenation using $^{iPr}PN^{Me}P$ -ligated Fe catalysts. Complexes **4** and **6** were characterized by x-ray crystallography.

### *$CO_2$ Hydrogenation with $^{iPr}PN^{OMe}P$ Ligated Iron Complexes*

We evaluated the catalytic activity of **3**, **4**, and **6** for $CO_2$ hydrogenation using conditions we had previously developed (Table 1). They are all active for $CO_2$ hydrogenation and give approximately the same number of TONs, which is consistent with each operating through the same catalytic cycle. Their overall productivity is comparable to the state-of-the-art iron catalyst ligated by $^{iPr}PN^{Me}P$. However, the TOFs are consistently lower by approximately a factor of 2 compared with $^{iPr}PN^{Me}P$ ligated systems. We interpret this difference as indicating that complexes with a pendant methoxy donor are more stable but less active catalysts. This is likely because the pendant methoxy donor can coordinate to the iron center and create an off-cycle species that is stable but less catalytically active. Theoretical calculations support that displacement of the pendant

**Table 1:** Catalytic performance of complexes **3**, **4**, and **6** in $CO_2$ hydrogenation.

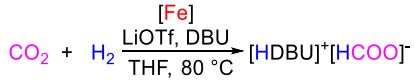


| Entry | [Fe] | Loading | TOF (1 h) | TON (time) | Yield (%) |
|---|---|---|---|---|---|
| 1 | **3** | 0.3 $\mu$mol | 9800 ± 1500 | 39,000 ± 3800 (24 h) | 49 |
| 2 | **3** | 0.3 $\mu$mol | | 37,000 ± 2000 (72 h) | 46 |
| 3 | **4** | 0.3 $\mu$mol | | 34,500 ± 2500 (24 h) | 43 |
| 4 | **6** | 0.3 $\mu$mol | 10,700 ± 300 | 37,000 ± 3400 (24 h) | 46 |
| 5 | **3** | 0.6 $\mu$mol | | 27,000 ± 4000 | 68 |

Reaction conditions: 500 psi $CO_2$, 500 psi $H_2$, [Fe], 24 mmol DBU, 3.2 mmol LiOTf, 10 mL THF, 80 °C.

arm in **6** with $H_2$ is thermodynamically uphill. Overall, these results demonstrate that the incorporation of an additional donor is a viable strategy for optimizing the catalytic performance of systems supported by $^{R}PN^{R'}P$ ligands. However, due to the limited range of iron hydride complexes we could synthesize, we were unable to evaluate the catalytic performance of all the new ligands we had prepared.

***Manganese Complexes Supported by $^{iPr}PN^{R'}P$ Ligands with an Additional Hemilabile Donor***

In previous work, we demonstrated that manganese complexes of the form $(^{iPr}PN^{Me}P)Mn(CO)_2H$ are active for $CO_2$ hydrogenation to formate, albeit with lower activity and stability than related iron complexes. To assess the catalytic activity of our full series of ligands (Figure 1), we coordinated them to manganese (Figure 5). Initially, the free ligands, **A**-**C** and **E**, were heated with $Mn(CO)_5Br$ in toluene. This generated complexes of the type $(^{iPr}PN^{R'}P)Mn(CO)_2(Br)$, which were fully characterized, including by x-ray crystallography. Subsequent treatment of $(^{iPr}PN^{R'}P)Mn(CO)_2(Br)$ with a hydride source generated the corresponding manganese hydrides. Different hydride sources, for example $NaBH_4$ *vs* $LiEt_3BH$, were required to ensure that $BH_3$ did not coordinate to the pendant group on the pincer ligand. Additionally, in some cases when $BH_3$ was coordinated to the pendant group it was possible to use an amine, such as $NEt_3$, to remove the $BH_3$.

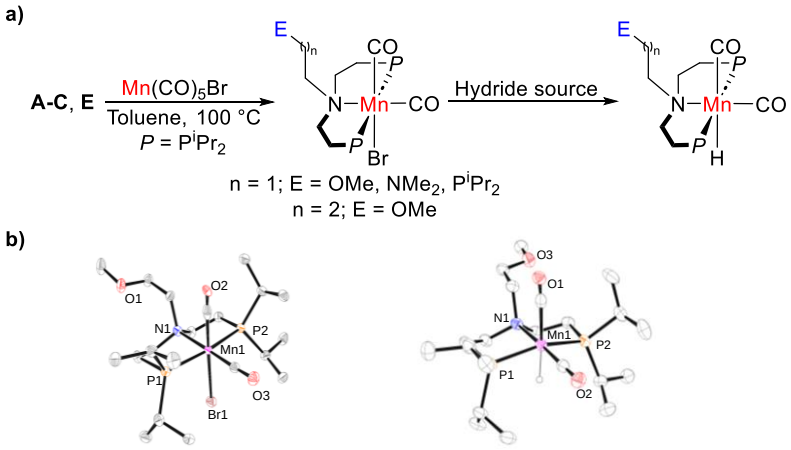


**Figure 5: a) a)** Synthesis of manganese complexes supported by ligands **A**-**C** and **E** and **b)** solid-state structures of $PN^{OMe}P$-ligated complexes.

The synthesis of manganese hydrides with four different ligands has positioned us to perform studies that correlate the performance of the different catalysts for $CO_2$ hydrogenation with the binding constant for the coordination of the pendant arm. We will establish the binding constant for the pendant arm using both theoretical methods and equilibrium exchange reactions with ligands, such as $PMe_3$ and MeCN. We expect that if the pendant donor binds too tightly, the catalyst will be highly stable but give low activity for $CO_2$ hydrogenation, whereas if the pendant donor binds weakly, the catalyst will be unstable but give high activity. We hypothesize that in a similar fashion to a heterogeneous volcano plot, there will be an optimal binding constant that gives good activity and stability.

***Future Work***

We will focus on three areas: (i) evaluating the new complexes we have already prepared in different catalytic reactions, for example methanol dehydrogenation, amide hydrogenation, and amine formylation with $CO_2$ and $H_2$, (ii) coordinating the $^{iPr}PN^{R'}P$ ligands we have already prepared to metals, such as ruthenium and cobalt, and (iii) synthesizing pincer ligands with new hemilabile donors with specific binding strengths.

**Publications Acknowledging this Grant in 2021-2024**

*(I) Intellectually led by this grant*


1. Wedal, J. C.; Virtue, K. B.; Bernskoetter, W. H.; Hazari, N.; Mercado, B. Q. Iron Catalysts Supported by a PNP Ligand with an Additional Hemilabile Donor for $CO_2$ Hydrogenation. *ACS. Catal.* **2024**, *14*, 13903-13914.
2. Hert, C. M.; Curley, J. B.; Kelley, S. P.; Hazari, N.; Bernskoetter, W. H. Comparative $CO_2$ Hydrogenation Catalysis with MACHO-type Manganese Complexes. *Organometallics*, **2022**, *41*, 3332-3340.
3. Curley, J. B.; Townsend, T. M.; Bernskoetter, W. H.; Hazari, N.; Mercado, B. Q. 'Iron, Cobalt, and Nickel Complexes Supported by a $^{iPr}PN^{Ph}P$ Pincer Ligand.' *Organometallics*, **2022**, *41*, 301-312.
4. Curley, J. B.; Hert, C.; Bernskoetter, W. H.; Hazari, N.; Mercado, B. Q. 'Control of Catalyst Isomers Using an N-Phenyl Substituted $RN(CH_2CH_2P^iPr_2)_2$ Pincer Ligand in $CO_2$ Hydrogenation and Formic Acid Dehydrogenation.' *Inorg. Chem.* **2022**, *61*, 643-656.
5. Chirdon, D. N.; Kelley, S. P.; Hazari, N.; Bernskoetter, W. H. 'Comparative Coordination Chemistry of PNP and SNS Pincer Ruthenium Complexes.' *Organometallics*, **2021**, *40*, 4066-4076.
6. Curley, J. B.; Smith, N. E.; Bernskoetter, W. H.; Ertem, M. Z.; Hazari, N.; Mercado, B. Q.; Townsend, T. M.; Wang, X. 'Understanding the Properties and Decomposition of Highly Active Iron Pincer Complexes for Hydrogenation and Dehydrogenation Reactions.' *ACS Catal.* **2021**, *11*, 10631-10646.
7. Townsend, T. M.; Bernskoetter, W. H.; Hazari, N.; Mercado, B. Q. 'Dehydrogenative Synthesis of Carbamates from Formamides and Alcohols using a Pincer-Supported Iron Catalyst.' *ACS Catal.* **2021**, *11*, 10614-10624.


*(II) Jointly funded by this grant and other grants with intellectual leadership by other funding sources*

Nothing to report.

# Theoretical Investigation of Heterogeneous Catalysis at the Solid-Liquid Interface for the Conversion of Lignocellulosic Biomass Model Molecules

Andreas Heyden
University of South Carolina, Department of Chemical Engineering

## Presentation Abstract

The objectives of this research program are to develop and validate a hierarchy of multi-scale methods for computing reaction and activation free energies of elementary processes occurring at metal surface-liquid and porous media-liquid interfaces and to apply these methods to the rational design of novel heterogeneous catalysts with exceptional activity, selectivity, and stability for the liquid-phase conversion of lignocellulosic biomass into transportation fuels or commodity and specialty chemicals. An overarching theme of our method developments is rapid applicability. We aim to limit the computational cost of our novel methods for computing free energies of elementary processes at solid-liquid interfaces to a cost of only two orders of magnitude higher than that of similar calculations at solid-gas interfaces. To achieve at the same time high accuracy in our free energy calculations, we rely on adapting and optimizing previously developed computational tools in the enzyme and homogeneous catalysis communities, such as hybrid quantum mechanical and molecular mechanical (QM/MM) methods. By adapting already parameterized and validated methods and force fields from these communities, we reap the benefits of the experience of many decades of computational studies in liquid-phase environments. Specifically, in this presentation, we will report recent progress on the development of a hybrid quantum mechanical, molecular mechanical, and machine learning potential for computing aqueous-phase adsorption free energies on metal surfaces and its application to the carbonyl group hydrogenation over Ru and Pt catalysts. Also, we report on an extension of our QM/MM explicit solvation method to porous zeolite systems and butane cracking in the presence of condensed water.

**DE-SC0007167: Theoretical Investigation of Heterogeneous Catalysis at the Solid-Liquid Interface for the Conversion of Lignocellulosic Biomass Model Molecules**

**Postdoc(s):** Dr. Mehdi Zare, Dr. Dia Sahsah, Dr. Wenqiang Yang
**Student(s):** Paratee Komen, Muhammad Zeeshan

## RECENT PROGRESS

***Liquid phase effects on adsorption processes in heterogeneous catalysis***
Performing reliable computer simulations of elementary processes occurring at metal–water interfaces is pivotal for novel catalyst design in sustainable energy applications. Computational catalyst design hinges on the ability to reliably and efficiently compute the potential energy surface (PES) of the system. Due to the large system sizes needed for studying processes at liquid water–metal interfaces, these systems can currently not be

described using density functional theory (DFT). In this work, we used a hybrid quantum mechanical, molecular mechanical, and machine learning potential for studying the adsorption behavior of phenol, atomic hydrogen, 2-butanol, and 2-butanone on the (0001) facet of Ru under reducing conditions when Ru is not oxidized. Specifically, we describe the adsorbate and the surrounding metal atoms at the DFT level of theory. Here, we also considered the electrostatic field effect of the water molecules on adsorbate–metal interactions. Next, for the water–water and water–adsorbate interactions, we used established classical force fields. Finally, for the water–Ru surface interaction, for which no reliable force fields have been published, we used Behler–Parrinello high-dimensional neural network potentials (HDNNPs). Employing this setup, we used our explicit solvation for metal surface (eSMS) approach to compute the aqueous-phase effect on the low-coverage adsorption of selected molecules and atoms on the (0001) facet of Ru. In agreement with previous experimental and computational studies of oxygenated molecules over transition metal facets, we found that liquid water destabilizes the tested adsorbates on Ru(0001). Interestingly, our findings indicate that adsorbates on Ru are less affected by the presence of an aqueous phase than on other transition metals (e.g., Pt), highlighting the necessity of experimental investigations of Ru-based catalytic systems in liquid water.

***Machine learning accelerated first-principles studies of biomass model molecules***

The complex reaction network of catalytic biomass conversions often involves hundreds of surface intermediates and thousands of reaction steps, greatly hindering the rational design of metal catalysts for these conversions. Here, we present a framework of machine learning (ML)-accelerated first-principles studies for the hydrodeoxygenation (HDO) of propanoic acid over transition metal surfaces. The microkinetic model (MKM) is initially parametrized by ML-predicted energies and iteratively improved by identifying the rate-determining species and steps (RDS), computing their energies by density functional theory (DFT), and reparameterizing the MKM until all the RDS are computed by DFT. The Gaussian process (GP) model performs significantly better than the linear ridge regression model for predicting both the adsorption free energies and transition state free energies. Parameterized with energies from the GP model, only 5–20% of the full reaction network has to be computed by DFT for the MKM to possess DFT-level accuracy for the TOF and dominant reaction pathway. While the linear ridge regression model performs worse than the GP model, its performance is greatly improved when only transition states are predicted by the regression model and adsorption energies are computed by DFT. Overall, we find that a high accuracy in adsorption free energies is more important for a reliable MKM than a high accuracy in TS free energies. Finally, based on the GP model with $G_{OH}$ and $G_{CHCHCO}$ as catalyst descriptors, we build two-dimensional volcano plots in activity and selectivity that can help design promising alloy catalysts for HDO reactions of organic acids.

**Publications Acknowledging this Grant in 2021-2024**

*(I) Intellectually led by this grant*

1) Zare, M.; Sahsah, D.; Saleheen, M.; Behler, J.; Heyden,* A. Hybrid quantum mechanical, molecular mechanical, and machine learning potential for computing aqueous-phase adsorption free energies on metal

surfaces. *J. Chem. Theory Comput.* **2024**, 20, 8247-8260. https://doi.org/10.1021/acs.jctc.4c00869

2) Yang, W.; Abdelfatah, K. E.; Kundu, S. K.; Rajbanshi, B.; Terejanu,* G. A.; Heyden,* A. Machine learning accelerated first-principles study of the hydrodeoxygenation of propanoic acid. *ACS Catal.* **2024**, 14, 13, 10148-10163. https://doi.org/10.1021/acscatal.4c01419
3) Saleheen, M.; Mamun, O.; Verma, A. M.; Sahsah, D.; Heyden,* A. Understanding the influence of solvents on the Pt-catalyzed hydrodeoxygenation of guaiacol. *J. Catal.* **2023**, 425, 212-232. https://doi.org/10.1016/j.jcat.2023.06.009
4) Zare, M.; Saleheen, M.; Singh, N.; Uline, M.; Faheem, M.; Heyden,* A. Liquid-phase effects on adsorption processes in heterogeneous catalysis. *JACS Au* **2022**, 2, 9, 2129-2134. https://doi.org/10.1021/jacsau.2c00389
5) Greydanus, B., Saleheen, M., Wu, H., Heyden, A., Medlin, J.W., Schwartz,* D.K. Probing surface-adsorbate interactions through active particle dynamics. *J. Colloid Interface Sci.* **2022**, 614, 425-435. https://doi.org/10.1016/j.jcis.2022.01.053
6) Zare, M., Saleheen, M., Mamun, O., Heyden,* A. Aqueous-phase effects on ethanol decomposition over Ru-based catalysts. *Catal. Sci. Tech.* **2021**, 11, 6695-6707. https://doi.org/10.1039/d1cy01057c
7) Rajbanshi, B., Yang, W., Yonge, A., Kundu, S.K., Fricke, C., Heyden*, A. Computational investigation of the catalytic hydrodeoxygenation of propanoic acid over a Cu(111) surface. *J. Phys. Chem. C* **2021**, 125, 19276-19293. https://doi.org/10.1021/acs.jpcc.1c05240

*(II) Jointly funded by this grant and other grants with intellectual leadership by other funding sources*

1. Zare, M.; Sahsah, D.; Bamidele, O. H.; Heyden,* A. Polyolefin melt-phase effects on alkane hydrogenolysis over Pt catalysts. *Chem Catal.* **2024**, 4, 101093. https://doi.org/10.1016/j.checat.2024.101093

# Coupling Dinitrogen and Hydrocarbons with Iron Complexes

Patrick L. Holland
Yale University, Department of Chemistry

## Presentation Abstract

A challenging frontier in cross-coupling is to couple abundant molecules like hydrocarbons and atmospheric $N_2$ which have strong bonds. We have discovered a low-coordinate iron system that mediates the one-pot conversion of petroleum-derived arenes and $N_2$ into aniline derivatives, a net formation of C–N bonds from hydrocarbons and $N_2$. The reaction uses a mixture of sodium powder, crown ether, and trimethylsilyl bromide, and silylated anilines are isolated. Numerous iron complexes along the cyclic reaction pathway have been isolated and crystallographically characterized, and their stoichiometric reactivity outlines a mechanism for sequential C–H activation and $N_2$ functionalization. This presentation will describe new insights on several of these steps. In the C–H activation step, there is a marked dependence of the equilibrium constant and the rate upon the presence and choice of alkali metal, and a system without crown can activate the C–H bond much more rapidly. In the next step, "hydride deletion" from the phenyl hydride complex, silyl halides can play an important facilitating role. Next is the reduction of the phenyl complex, which we have begun to study electrochemically. Finally, $N_2$ silylation has yielded isolable disilylhydrazido complexes that are formally iron(IV) but are dominated by an iron(II)-nitrene resonance structure. This makes them electrophilic enough at N to enable migration of the phenyl group to form the N–C bond. The N–C bond formation occurs rapidly with small alkyl substituents as well, but not with large alkyls or with alkynyls. The mechanistic detail on these various steps helps to elucidate the requirements for a catalytic reaction that incorporates abundant atmospheric $N_2$ into organic molecules.

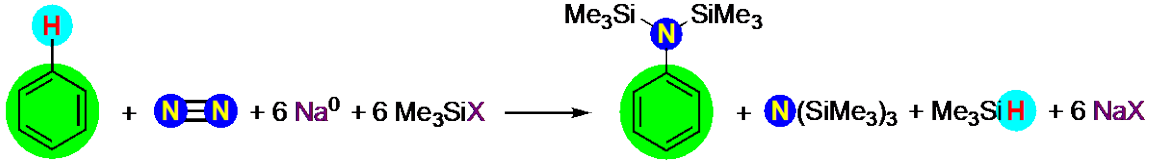


**DE-SC0020315: Tandem Catalytic C-H Activation and $N_2$ Activation Using Iron Complexes**

**Postdoctoral:** Erik J. T. Phipps, Conner V. Wilson, Nereida Hidalgo, Ryan Walser-Kuntz
**Students:** Samuel M. Bhutto, Reagan X. Hooper, Ryan S. Donnelly

## RECENT PROGRESS

### *Introduction*

This project aims at mechanistic understanding of the following transformation:

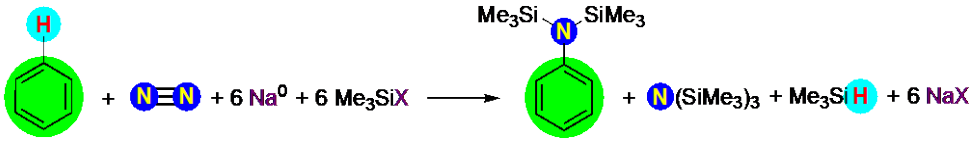


The cyclic mechanism shown in the illustration below is based on isolable iron compounds **A** through **H**. Starting from the lower left, it begins with binding of benzene (green) and C–H bond activation to form a phenyl fragment along the top. After $N_2$ binding, silylation gives a disilylhydrazido species, and the phenyl group migrates to it to form a C–N bond in silylated aniline products along the bottom. Our mechanistic efforts have focused on the distinctive steps of the reaction, namely (1) C–H activation (**C** to **D**), (2) deposition of H (**D** to **E**), and (3) migration of a hydrocarbyl group from Fe to $N_2$ (**G** to **H**).

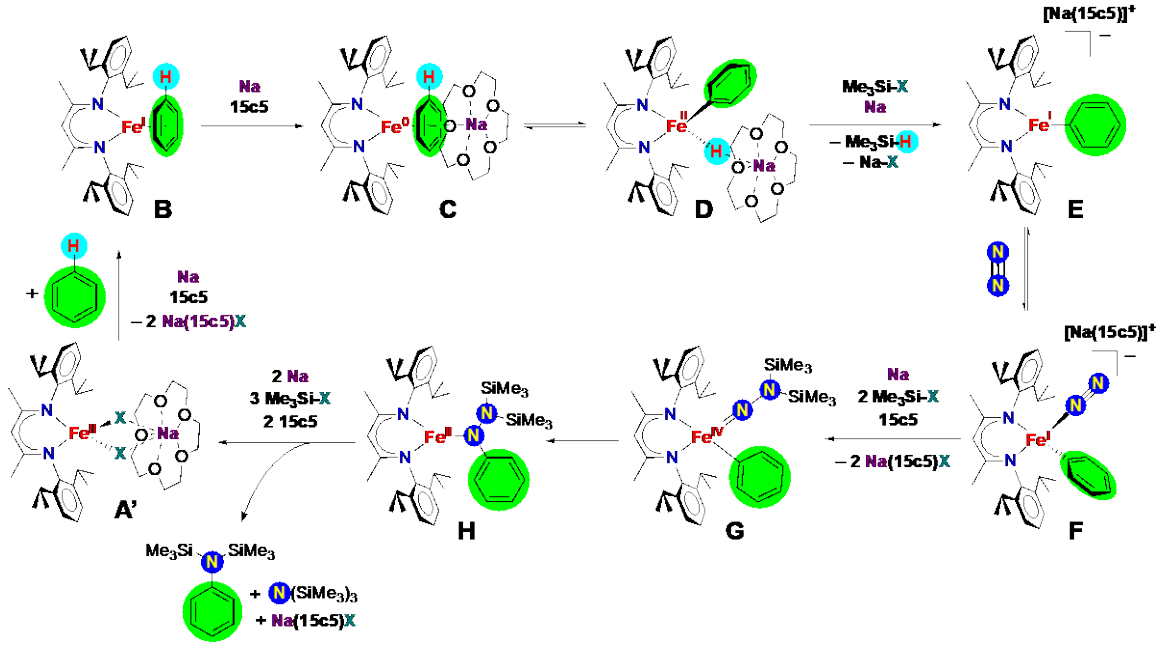


### *Alkali-metal dependence on C–H activation*

We collaborated with Hui Chen, an expert on coupled-cluster calculations, for an experimental/computational paper that is nearing completion. We probed the C–H activation, which involves a spin state crossover from **C** ($S = 1$) to **D** ($S = 2$). The lowest-energy transition state for the concerted oxidative addition is on the $S = 1$ surface. The equilibrium constant is calculated to be >1 for the Na system, but <1 for K, Rb, and Cs, in agreement with experiments. The energetics derive from a balance of alkali-metal binding to the arene in **C** and the hydride in **D**.

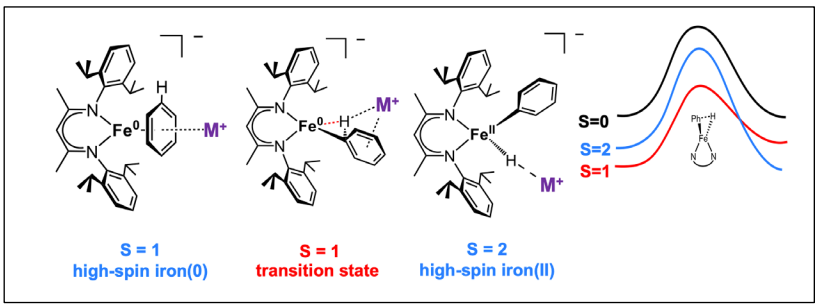

***Removal of alkali metal can speed C–H activation***

In an effort to disentangle the effects of the alkali metal choice and the crown ether, we have now reduced **B** with K/Rb/Cs in the *absence* of crown ether. Surprisingly, even at low temperature, the products have oxidatively added the C–H bonds with each alkali metal. The phenyl hydride complexes **[LFe(Ph)(H)(AM)]$_2$** (**AM** = K, Rb, Cs) dimerize through cation-π interactions as shown by X-ray crystallography (illustration shows the complex with AM = Cs).

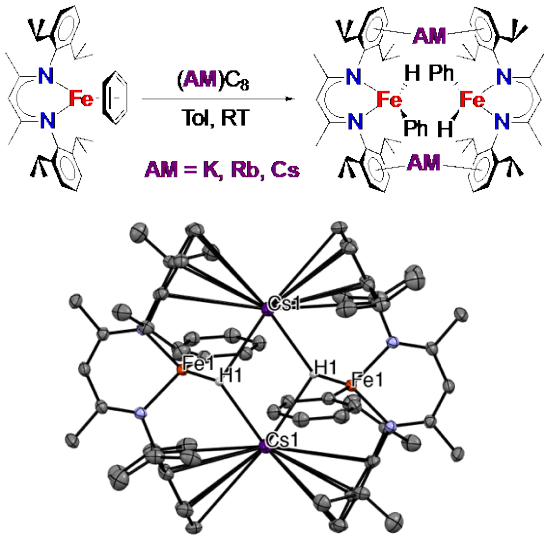


This has two important implications: (1) *C–H activation can be much more rapid than previously thought.* Therefore, if conditions can be controlled appropriately, C–H activation should not be the turnover-limiting step. (2) the presence of the crown ether has a large effect on the equilibrium constant for C–H activation, as K and Rb favor the iron(0) arene complex in the presence of 18-crown-6 but the iron(II) phenyl hydride without crown. We are varying the choice of solvent to further explore the possibilities for controlling the rate of C–H activation.

***Hydride deletion by delivery to silane***

In our initial paper (*Nature* **2020**), we assumed that the hydrogen atom that is lost from **D** to **E** ended up as (insoluble) sodium hydride, because this balances the reaction. However, the low solubility of sodium hydride hindered our ability to determine whether it is actually present. We have developed several tests for NaH, which show that *it is not present.* In order to provide an alternative explanation, we added $Et_3SiX$ (X = OTf or Br) to **D**, and it forms **E** (plus $Et_3SiH$ byproduct) in >60% yield. In the cyclic reaction sequence, this hydride deletion can explain the formation of the iron-phenyl complex which ultimately migrates to the silylated $N_2$ ligand. As a result, we now have a complete cycle with verification of each stoichiometric step. In addition, this discovery leads us into the future by providing a method for hydride deletion through capture by silyl groups.

***Electrochemical conditions for reduction***

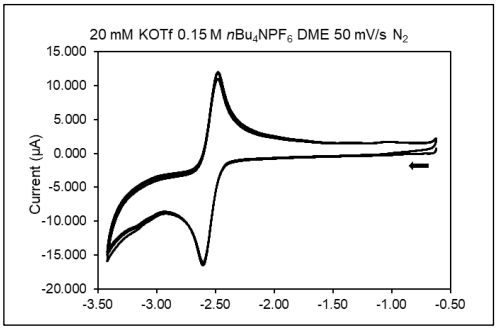


Elemental alkali metal reductants are inconvenient, because they are harsh and have variable surface area that limits reproducibility. The most energy-efficient alternative would be electrochemical reduction. However, this is challenging due to the need for a compatible solvent and electrolyte under the strongly reducing conditions. We have now discovered that dimethoxyethane/$NBu_4PF_6$ is a suitable medium for cyclic voltammetry of LFePh, and reproducibly observe a reversible wave at –2.5 V vs. $Fc^{+/0}$. We are currently testing the effect of alkali metal additives on this and other reduction waves, which should yield mechanistic information about the role of alkali metal cations, as well as practical guidance on how to achieve electrochemical N–C bond formation from arenes and $N_2$.

***Scope of N–C bond formation from migration to disilylhydrazido ligands***

The coupling of an organoiron complex with a silylhydrazido ligand (derived from $N_2$) is a new fundamental reaction in organometallic chemistry, and we explored the scope of this reaction. Aryl migration seems to be general, as phenyl, tolyl, and mesityl groups all migrate smoothly and rapidly. Kinetic studies and DFT studies have shown the nature of the transition state. Alkynyl migration is not observed, despite the accessibility of the formally iron(IV) disilylhydrazido analogue of **G**. Alkyl migration is observed in some cases, namely with a methyl group. However, larger alkyl groups suffer a number of side reactions: with trimethylsilylmethyl, no migration of the alkyl ligand is observed; with benzyl, the Fe–C bond homolyzes to give a three-coordinate hydrazido(2−) complex, which is likely due to the greater stability of a benzyl radical.

**Publications Acknowledging this Grant in 2021-2024**

*(I) Intellectually led by this grant*


1. Weber, J. E.; Bhutto, S. M.; Genoux, A. T.-Y.; Holland, P. L. Dinitrogen Binding and Functionalization. In *Comprehensive Organometallic Chemistry IV* (O'Hare, Parkin, Meyer, Eds.), Elsevier, 2022, Vol. I, pp 521-554.
2. Bhutto, S. M.; Hooper, R. X.; Mercado, B. Q.; Holland, P. L. Mechanism of Nitrogen-Carbon Bond Formation from Iron(IV) Disilylhydrazido Intermediates during $N_2$ Reduction. *J. Am. Chem. Soc.* **2023,** *145*, 4626-4637.
3. Bhutto, S. M.; Mercado, B. Q.; Holland, P. L. Dinitrogen Binding and Functionalization from a Low-Coordinate Alkynyliron Complex. *Inorg. Chem.* **2023,** *62*, 9335-9342.
4. Bhutto, S. M.; Hooper, R. X.; McWilliams, S. F.; Mercado, B. Q.; Holland, P. L. Iron(IV) alkyl complexes: electronic structure contributions to Fe–C bond homolysis and migration reactions that form N–C bonds from $N_2$. *Chem. Sci.* **2024,** *15*, 3485-3494.

Friederike C. Jentoft

# Spectrokinetics of Hydrocarbon Pool Transformations – Role of Framework Topology and Acid Strength

Friederike C. Jentoft, Dipti Bhave and R. Morgan Whitfield III
University of Massachusetts Amherst, Amherst, MA, USA

## Presentation Abstract

Proposed cycles for methanol-to-olefins catalysis consist of complex multistep reactions around the long-lived intermediates known as hydrocarbon pool, making it difficult to extract adsorption and rate constants for each step. Our approach is to focus on specific transformations, by adsorbing and reacting suitable test molecules and measuring heats of adsorption and activation energies. We report on ring contraction, which appears in the proposed cycles, and on cyclization, which is required to form the hydrocarbon pool. UV-vis and IR spectra were recorded to observe the kinetics of cation transformations in the pores. Ring contraction of tetramethylcyclohexenyl cations produces two types of cyclopentenyl cations in a network of parallel and sequential reactions. Cyclization of dimethyloctatrienyl cations occurs more easily in large pores (MOR) than in medium pores (MFI). Among metal cations as origin of acid sites in MFI, a clear distinction emerges among Al, Ga and B in heats of base adsorption and cyclization barriers, while Fe is difficult to place.

**Grant or FWP Number: DE-SC0021041 Acid Catalysis Design Guided by Spectroscopic Analysis of Reaction Networks**
**Student(s):** Dipti Bhave, R. Morgan Whitfield III, Isaac Ogabiela

## RECENT PROGRESS

***Brief description of scientific problem, objectives, prior findings and current thrusts***

Methanol-to-hydrocarbons (MTH) conversion is emerging as a sustainable route to small olefins (MTO) such as the monomers ethene and propene, and to jet fuel (MTJ). Catalysts in use for MTO conversion are microporous solid acids, that is, zeolites and zeotypes, with HZSM-5 and SAPO-34 as the key materials. While the MTO process is commercialized, selectivity control is limited, and deactivation by carbonaceous deposits is a problem. At the core of these issues is the unique mechanism, which requires long-lived species (“hydrocarbon pool”) inside the catalyst pores that cyclically grow and cleave to give the products. The objective of this project is to better understand this mechanism and its dependency on catalyst properties, and to use the gained knowledge to improve catalyst and process.

In the first phase of this project, we established correlations between the nature of surface species and their spectroscopic signatures (UV-vis, IR), which allows us to distinguish cyclic and acyclic enylic cations as well as determine their size with an accuracy of +/- one carbon and their degree of unsaturation. Further, we observed reaction sequences of individual species such as cyclization, rearrangement, cleavage, and aromatization.

With the transformations qualitatively established, we are now measuring surface kinetics and surface thermochemistry, focusing on specific steps and adsorbates. In parallel, we

are expanding the catalysts that we investigate to isomorphously substituted MFI and BEA frameworks (B, Ga, Fe instead of Al) and to SAPO-34. Varying the framework metal cation that creates the Brønsted site alters the acid strength of the site. The large-pore materials allow us to adsorb precursors that would not fit into the MFI or CHA framework of HZSM-5 and SAPO-34.

### *Kinetics of MTO-relevant steps: Approach*

To deconstruct the complex multistep cycles proposed for methanol-to-olefins conversion, we monitor the transformations of individual species. Further, we first create a surface species, *viz.* a carbocation, and then track its chemical reaction inside the zeolite pore spectroscopically. Both reactant and product states are therefore adsorbates, which avoids obfuscation by transport limitations or by adsorption and protonation equilibria, as illustrated in Figure 1. Measurements at different temperature and Arrhenius analysis then deliver true activation energies (rather than apparent ones that are altered by the heat of adsorption).

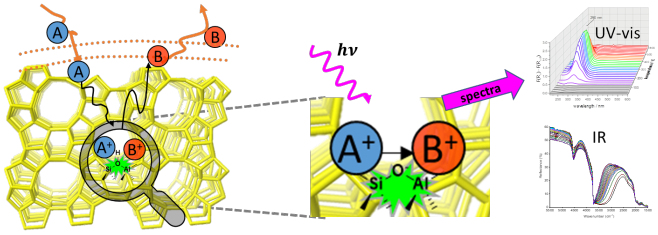


**Figure 1: Approach to kinetics analysis**

### *Kinetics results I: Ring contraction*

Prompted by reports and own observations of five-membered and six-membered rings in zeolite pores during methanol conversion, the ring contraction of a cyclohexenyl species was investigated. The precursor diene can only be adsorbed into zeolites characterized by large pores, restricting the frameworks that could be used. The MOR framework was found to be best for kinetics, as it permitted far fewer side reactions than the FAU or BEA framework with their spacious cavities, in which oligomerizations occurred. Diffuse reflectance IR spectroscopy was used to monitor the kinetics (Figure 2, top), and after transformation into the Kubelka-Munk function, the band height was analyzed. Fit of overlapping bands and use of the areas confirmed the results while not improving precision. At low temperatures (80 °C to 110 °C), the ring contraction reaction network in MOR could be reasonably described by parallel reactions to two cyclopentenyl species, which were distinguished by the substitution pattern at their allylic system (1,2- or 1,2,3-substitution). At higher temperatures,

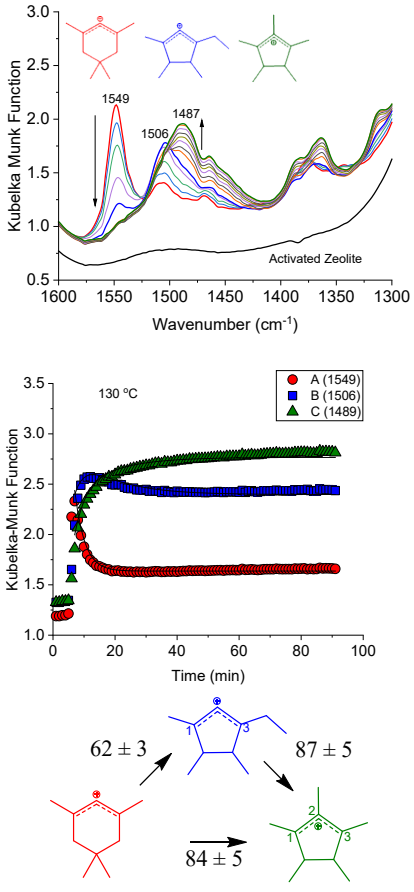


**Figure 2: Time-resolved IR spectra of the ring contraction of the tetra-methylcyclohexenyl cation (top), example kinetics (middle), and network with associated activation energies in MOR in kJ/mol (bottom).**

isomerization of the 1,2-substituted allylic system to the 1,2,3- substituted allylic system had to be included (Figure 2, middle). Formation of this bulky ion was associated with a more than 20 kJ/mol higher activation energy than formation of an 1,3-substituted system (Figure 2, bottom).

### *Kinetics results II: Cyclization*

**Table 1: Activation energies for cyclization in MFI framework**

| Zeolites (Si/E) | $OCT^+$ to $HCP^+$ / kJ $mol^{-1}$ |
|---|---|
| Al-MFI (15) | 68 ± 5 |
| Al-MFI (40) | 58 ± 6 |
| Al-MFI (140) | 61 ± 5 |
| Ga-MFI (50) | 87 ± 6 |
| Ga-MFI (100) | 88 ± 8 |

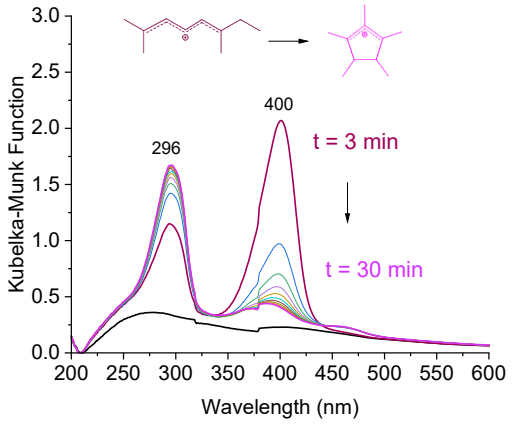


**Figure 3: Time-resolved diffuse reflectance UV-vis spectra of the cyclization of the dimethyloctadienyl cation at a temperature of 100 °C in the pores of zeolite MOR with Si/Al= 10.**

The second investigated transformation was a cyclization, which is a necessary step en route from methanol to any cyclic hydrocarbon pool species. The reactant was 2,6-dimethyl-2,4,6-octatriene. This molecule can be adsorbed into the medium-pore MFI framework, which is the basis for one of the commercial MTO catalysts.

In MFI, the 2,6-dimethyl-2,4,6-octadienyl cation ($OCT^+$ in Table 2) cyclized to an 1,3-substituted cyclopentenyl cation ($HCP^+$). We tested Si/Al contents ranging from 15 to 140, but there was no influence of the Si/Al ratio on the activation energy for the cyclization within the precision of the measurement. However, gallium substitution (instead of aluminum) resulted in a significantly higher activation energy (Table 1). Experiments with boron and iron substitution in MFI were not conclusive, for lack of protonation and slow reaction.

In the large-pore MOR framework, the cyclization produced a 1,2,3-substituted species (Figure 3) at an activation energy of only 47 kJ/mol.

### *Establishing calorimetry for measurement of heats of adsorption*

Our ultimate objective of the calorimetry experiments is to measure the enthalpies of adsorption of MTO-relevant hydrocarbon species, to complement our measurements of activation energies for surface steps in the MTO cycle and construct energy profiles for various intermediates and their adsorption, protonation and transformation on MTO catalysts.

To first establish the method in our laboratory, we started with the adsorption of nitrogen bases. Some literature data are available for the heats of adsorption of pyridine or amines on zeolites. We note that values reported by different groups do not necessarily agree. The methodology is illustrated in Figure 4 (left). An inert gas stream is used to carry a pulse of the sorptive vapor to the activated sample. For each adsorption step, the weight gain and the evolved heat are measured by gravimetry and differential scanning calorimetry, respectively. Coverage and total adsorbed amount are determined through cumulative weight gain and total weight gain at saturation. After achieving consistency

with the literature for pyridine adsorption on HZSM-5, we embarked on characterizing isomorphously substituted MFI samples obtained from our collaborator Dr. Nataliya Shcherban. Adsorption calorimetry provides the site distribution, that is, the number of each type of site and their strength. Boron substitution did not elicit very strong sites, and the heat of adsorption was lower than seen for the other samples. Aluminum substitution produced the strongest sites, followed by gallium and iron. The acid strength sequence Al > Ga > B is consistent with the trend observed in the activation energies for cyclization. Calorimety suggests that iron substitution in the MFI framework also produces strong acid sites, and we will continue to collect kinetics data to rank the performance of these sites in hydrocarbon transformations.

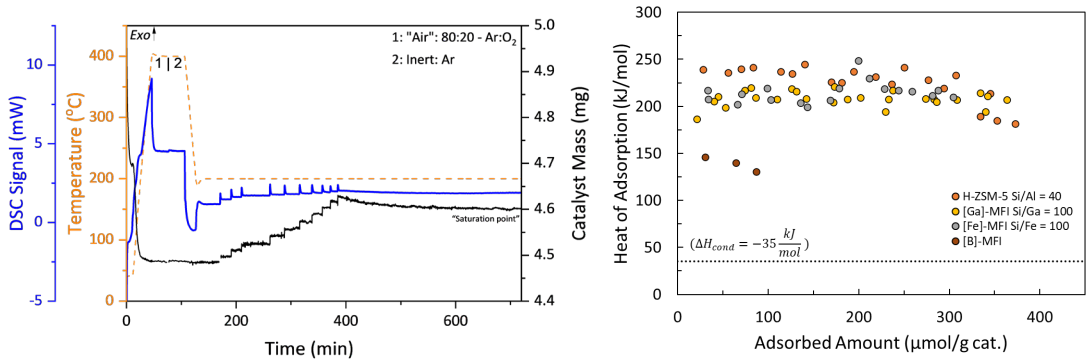


**Figure 4: Measurement of enthalpies of adsorption by pulse chemisorption in a thermobalance with differential scanning calorimetry. Illustration of thermogravimetric and differential scanning calorimetry data (left) and heats of adsorption of isopropylamine on MFI samples with different metal cations (right).**

### *Characterization of isomorphously substituted zeotypes by catalytic behavior*

Acid-catalyzed aldol reactions present an interesting route to olefins, with the best-known example perhaps the production of isobutylene from acetone. With suitable substrates and catalysts, the fission of the intermediate aldol (in competition to the dehydration to the normal aldol condensation product) can become the dominant pathway. Since we found zeolites to be excellent fission catalysts, this catalytic chemistry presents an opportunity to probe the acid strength of isomorphously substituted frameworks while exploring the role of acid strength for the fission rate. We normalized first order rate constants to the number of acid sites as determined thermogravimetrically through amine adsorption and found a clear ranking of the fission activity in the order of Al > Ga >> Fe, B (Table 2). Except for Fe, this ranking is expected from reported deprotonation energies.

**Table 2: Comparison of catalysts in aldol-fission reaction of benzaldehyde and 3-pentanone at a temperature of 140 °C**

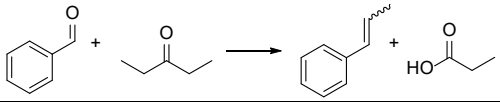


| Sample (Si/E) | Site-normalized fission first-order rate constant / $mol^{-1}\ s^{-1}$ |
|---|---|
| B-BEA (200) | n.d. |
| Fe-BEA (200) | n.d. |
| Ga-BEA (200) | 42±10 |
| Al-BEA (150) | 80±6 |

### *Ongoing work*

We have received a family of SAPO-34 samples prepared with the help of different organic structure-directing agents from our collaborator Dr. Nataliya Scherban and are in the process of testing them in methanol-to-olefins conversion.

**Publications Acknowledging this Grant in 2021-2024**

*(I) Intellectually led by this grant*

1. *(peer-reviewed article)* Hernandez, E. D.; Manookian, B.; Auerbach, S. M.; Jentoft, F. C., Shape-selective Synthesis of Alkylcyclopentenyl Cations in Zeolites and Spectroscopic Distinction of Constitutional Isomers *ACS Catal.* **2021**, *11*, 12893−12914.
2. *(invited lecture)* Jentoft, F. C. Spectroscopic Tracking of Methanol-To-Hydrocarbons Chemistry in Zeolite Pores *Seminar at ExxonMobil Research*, Virtual: Clinton, NJ - Baytown, TX - Machelen, Belgium, Nov. 17, **2023**.
3. *(invited lecture)* Jentoft, F. C. Direct Observation of Transformations and Their Kinetics in Zeolite Pores *Monthly Meeting of the Catalysis Society of Metropolitan New York*, Somerset, NJ, USA, Sept. 20, **2023**.
4. *(invited lecture)* Jentoft F. C. Nature and Dynamics of Catalytically Active Centers: Insights from In Situ Spectroscopy *Seminar of the Department of Chemical and Biological Engineering, Princeton University*, Princeton, NJ, USA, Sept. 13, **2023**.
5. *(invited lecture)* Jentoft F. C. Spectroscopic Analysis of Reactions in Zeolite Pores *Webinar of the Great Plains Catalysis Society*, Jan. 20, **2023**.
6. *(keynote lecture)* Jentoft F. C. Spectroscopic Analysis of Transformations in Zeolite Pores, *Winter Meeting of the New England Catalysis Society*, Worcester Polytechnic Institute, Worcester, MA, USA, Jan. 6, **2023**.
7. *(invited oral presentation)* Hernandez, E. D.; Manookian, B.; Auerbach, S. M.; Jentoft, F. C., Analogies in Acid Catalysis: Unsaturated Carbenium Ions in Liquid, Solid and Gas Phase Environments *American Chemical Society Spring Meeting*, San Diego, CA, USA, March 20-24, **2022**.
8. *(contributed oral presentation)* Bhave, D.; Shvets, O. V.; Kurmach, M. M.; Shcherban, N.; Jentoft, F. C. True Activation Energies as Anchor Points in Hydrocarbon Pool Kinetics *2024 AIChE Annual Meeting, San Diego*, CA, USA, Oct. 27-31, **2024**.
9. *(contributed oral presentation)* Bhave, D.; Jentoft, F. C. Spectroscopic Analysis of Ring Contraction Kinetics Relevant to Methanol-to-Olefins Conversion *ACS Fall Meeting*, San Francisco, CA, USA, Aug. 13-17, **2023**.
10. *(contributed oral presentation)* Hernandez, E. D.; Jentoft, F. C. Role of Brønsted and Lewis Acid Sites in Zeolites for Hydride Transfer, *27th North American Catalysis Society Meeting*, New York City, NY, USA, May 22-27, **2022**.
11. *(contributed poster presentation)* Bhave, D.; Jentoft, F. C. Spectro-kinetics of Carbocation Transformations in Zeolite Pores, *18th International Congress on Catalysis*, Lyon, France, July 14-19, **2024**.
12. *(contributed poster presentation)* Whitfield III, R. M.; Bhave, D.; Shvets, O. V.; Kurmach, M. M.; Shcherban, N.; Jentoft F. C. Evaluation of Acidic Characteristics of Isomorphously Substituted MFI Type Zeolites by Various Techniques, *18th International Congress on Catalysis*, Lyon, France, July 14-19, **2024**.

13. *(contributed poster presentation)* Bhave, D.; Jentoft F. C. Kinetics of Hydrocarbon Transformations in Zeolite Pores, *2023 AIChE Annual Meeting*, Orlando, FL, USA, Nov. 5-10, **2023**.
14. *(contributed poster presentation)* Bhave, D.; Jentoft F. C., Understanding the Nature and Transformation Kinetics of Surface Intermediates in Methanol-to-Olefins Conversion *New England Catalysis Society Symposium in Honor of Maria Flytzani Stephanopoulos*, Tufts University, Medford, MA, June 3, **2022**.

*(II) Jointly funded by this grant and other grants with intellectual leadership by other funding sources*

15. *(peer-reviewed article)* Araujo-Barahona, G.; Shcherban, N.; Eränen, K.; Kopa, I.; Bezverkhyy, I.; Martínez-Klimov, M.; Vajglová, Z.; Aho, A.; García-Serna, J.; Salmi, T.; Murzin, D. Yu. Ruthenium Supported on Silicate and Aluminosilicate Mesoporous Materials Applied to Selective Sugar Hydrogenation: Xylose to Xylitol *Chemical Engineering Journal* **2024**, *485*, 150019.
16. *(peer-reviewed article)* Kopa, I.; Yevdokimova, O.; Martínez-Klimov, M. E.; Kurmach, M.; Yu. Murzin, D.; Shcherban, N. Furfural Acetalization with Ethanol over Hierarchical vs. Conventional Beta Zeolites *ChemistrySelect* **2024**, *9* (15), e202304754.
17. *(peer-reviewed article)* Shvets, O. V.; Kurmach, M. M.; Konysheva, K. M.; Lozovytska, O. I.; Shcherban, N. D. Evaluation of Acidity of Hierarchical Zeolites Using a Potentiometric Titration Method *Materials Today Chemistry* **2024**, *36*, 101921.
18. (*contributed oral presentation*) Ogabiela, I. O., Shvets, O. V.; Kurmach, M. M.; Shcherban, N.; Jentoft, F. C. Effect of Strength of Soluble and Solid Acid Catalysts on Selectivity in Cross Aldol Reactions *2024 AIChE Annual Meeting, San Diego*, CA, USA, Oct. 27-Oct. 31, **2024**.
19. (*contributed oral presentation*) Shcherban, N.; Martinez-Klimov, Yevdokimova, O.; Kurmach, M.; Mäki-Arvela, P.; Murzin, D. Yu. Solvent-free hydrocracking of oleic acid over zeolite-supported Pd catalysts International Symposium on Zeolites and Microporous Crystals 2024, Osaka, Japan, July 21- July 25, **2024**.
20. (*contributed poster presentation*) Shcherban, N.; Martinez-Klimov, Yevdokimova, O.; Kopa, I; Mäki-Arvela, P; Murzin D. Ru Nanoparticles Deposited on Amorphous Aluminosilicates as Effective Low-Temperature Catalysts for Hydrocracking of *n*-Hexadecane *18$^{th}$ International Congress on Catalysis*, Lyon, France, July 14-19, **2024**.

# Catalytic Activation of C-H and O-H Bonds for the Upgrading of Alcohols

William D. Jones
Department of Chemistry, University of Rochester, Rochester, NY 14627

## Presentation Abstract

This project is directed towards fundamental investigations of the reactions of homogeneous transition metal complexes with C-H and O-H bonds for the upgrading of alcohols via the Guerbet reaction. The Guerbet reaction combines two alcohols to produce a larger alcohol plus water. Our studies will provide fundamental information about the mechanisms and energetics of reactions of metal complexes with alcohols and related substrates in the aldol reaction. We will also examine new tandem catalyst systems for the upgrading of alcohols to higher products. We have synthesized several bulky trispyrazolylborate complexes of first row metal hydroxides and are examining these for aldol condensation catalysis. Another goal of our proposed work relates to our discovery of new bis-fused oxazolidine (FOX) ligands and their complexation to first row transition metals. One copper-FOX complex has been found to be a catalyst for alcohol dehydration, converting phenylethanol into styrene plus water. A rhenium-FOX complex has been prepared and examined for electrochemical $CO_2$ reduction. A series of complexes (Mn, Fe, Co, Ni Cu) has been prepared with a quinoline-substituted FOX ligand and these have been explored for alcohol dehydration. Further exploration of catalysis with these complexes is planned. We are also continuing a collaboration with a theory group at UTRGV (with Prof. Tulay Atesin) and an experimental group at the Free University of Berlin (with Prof. Christian Müller) looking at DFT calculations of aryl-CN cleavage and the effects of ortho-fluorine and related substituents.

## DE-SC0020230: Catalytic Activation of C-H and O-H Bonds for the Upgrading of Alcohols

**Student(s):** Aurodeep Panda (G), Ryan Pohorenec (G), Ruilin Zhang (UG), Caz Wood (UG)[+]
**Affiliations(s):** [+]SUNY New Paltz (REU)

## RECENT PROGRESS

***Accomplishments During Year One.***

We targeted these specific areas: (1) the evaluation of transition metal complexes that have been found to have high reactivity for alcohol dehydration in aqueous solution, (2) the synthesis of new catalysts with geometrically constrained bis-fused oxazolidine (FOX) ligands that can be used for the dehydration/hydration catalysis, (3) the synthesis of bulky tris-pyrazolylborate metal hydroxide complexes for aldol condensation, and (4) DFT studies of the effect of *ortho* substituents on the C-CN cleavage of benzonitriles.

The specific accomplishments of the current grant period include:

(1) We have co-published an article describing the conversion of ethanol to butanol using a ruthenium catalyst in air.[9]

(2) We have synthesized a rhenium-FOX complex and deprotonated the hydroxymethyl group. This compound was electrochemically active for $CO_2$ reduction to CO.[11]

(3) We have investigated reactions of FOX transition metal complexes of copper and zinc as bases for the dehydration of phenylethanol.[14]

(4) We have synthesized a series of new quinoline-FOX complexes with Mn, Fe, Co, Ni, and Zn. This ligand affords a very constrained geometry to the metal center, which we are systematically investigating for alcohol dehydration.

(5) We have synthesized a series of bulky tris-pyrazolylborate transition metal complexes (Mn, Fe, Co, Ni, Zu, Zn) and made several metal hydroxide derivatives. These are being examined for aldol condensation chemistry. The nickel hydroxide catalyzes the formation of crotonaldehyde from acetaldehyde.

(6) Through a collaboration sponsored by the Alexander von Humboldt Foundation the PI has collaborated with Prof. Christian Müller at the Free University of Berlin on C-CP bond cleavage.[6,13]

(7) Through a collaboration with Prof. Tulay Atesin at U. Texas Rio Grande Valley the PI has used DFT to examine substituent effects on C-CN and C-CP cleavage.[10,12,13]

### *1. Synthesis of fused-Bisoxazolidine Ligands and Metal Complexes*

We have developed methodology to synthesize specifically the *meso*-FOX isomer (eq 1) which can act as a tetradentate toward metals. As we reported previously, $AlCl_3$ is the best catalyst for conversion of the *rac* to the *meso* isomer.[5]

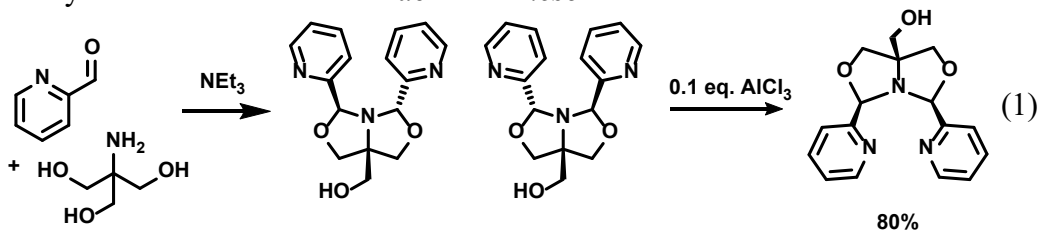


(1)

**Aurodeep Panda** has made complexes of the meso-FOX ligand with other $MCl_2$ where M = Mn, Fe, Co, Ni, and Cu. Further reaction with AgOTf allows for isolation of the $(FOX)M(OTf)_2$ complexes. X-ray structures have been obtained for most of these compounds. They all feature an intact OH group. Specifically, the Mn triflate has been isolated as the $\kappa^4$-FOX bis-triflate, the aquo-triflate, and the bromo-triflate complexes. The cobalt complex is obtained as a bis-μ-Br complex with external triflate. The nickel triflate has been isolated as the $\kappa^4$-FOX acetonitrile-triflate and bis-aquo complexes. The copper(II) complexes were isolated as the $\kappa^4$-FOX acetonitrile, $\kappa^4$-FOX aquo-triflate and $\kappa^4$-FOX bromo complex (Fig. 1).

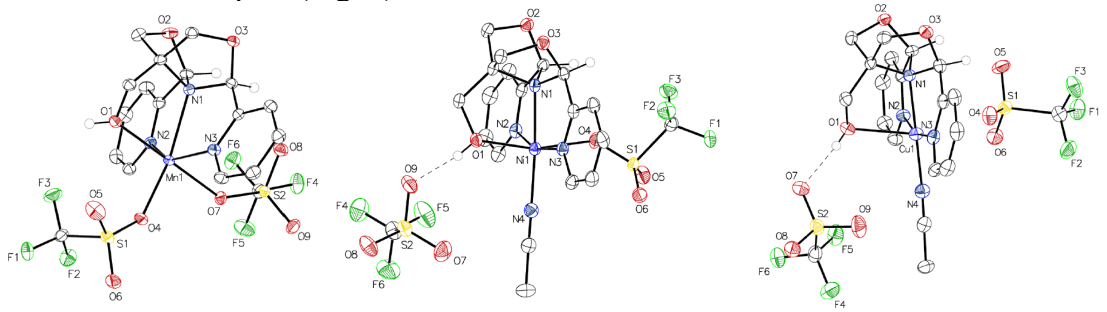

**Fig. 1.** X-ray structures of $Mn(FOX)(OTf)_2$, $[Ni(FOX)(CH_3CN)(OTf)]^+[OTf]^-$, & $[Cu(FOX)(CH_3CN)]^{2+}[OTf]^-_2$

A summer REU student, **Caz Wood**, synthesized a series of zinc-FOX complexes for comparison. They prepared the $\kappa^3$-FOX dichloride and dibromides (with dangling $CH_2OH$), a $\kappa^4$-FOX monochloride cation, and a $\kappa^4$-FOX aquo-triflate complex. They also prepared derivatives with ortho-Me and MeO groups on the FOX pyridine ligand. Notice that the parent FOX dichloride is square pyramidal, whereas the $^{Me}$FOX dibromide is a trigonal bipyramid, showing the steric influence of the pyridyl methyl groups. We have also synthesized several derivatives with a quinoline group replacing the pyridine group in the FOX ligand ($^{Q}$FOX) (undergraduate **Ruilin Zhang**). The goal was to produce catalysts that have a steric pocket surrounding the metal center.

## 2. Dehydration of Phenylethanol using fused-Bisoxazolidine Metal Complexes

With all of these complexes in hand, we have initiated studies of their reactivity as alcohol dehydration catalysts. The $Cu^{II}$ complexes proved particularly active, and there were peculiarities noticed about the reaction. Using $Cu(FOX)(CH_3CN)]^+[OTf]^-$ as catalyst, it was observed that dehydration of phenylethanol proceeded to give styrene in >95% yield if toluene was used as solvent (eq 2).[14] The reaction was much slower (or didn't go at all) in other solvents. In addition, it was noted that the catalyst did not dissolve in toluene, but that the solution became cloudy once it was heated. At the end of the reaction, there was a small droplet of water that was bright blue, indicating the catalyst was dissolved in the water. It appears that as the reaction proceeds and water is produced, the water separates from solution and drives the reaction to completion. Since the catalyst partitions into the water phase, the dehydration either occurs in the aqueous phase, or perhaps at the interface of the water and the toluene solvent.

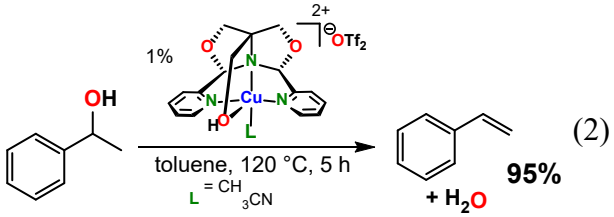

(2)

The rate of the reaction was observed to be variable, perhaps due to the heterogeneous nature of the system. We just recently discovered that water content is a crucial variable. If both solvent and substrate are rigorously dried (<5 ppm $H_2O$), the reaction does not proceed at all. However, if water is introduced into dry phenylethanol at a level of 300 ppm (3 μL/10mL), the reaction proceeds quickly ($t_{1/2}$ = 1.5 h). Large amounts of water inhibit the reaction. We are currently trying to find conditions to make the reaction homogeneous, whereby greater control might be obtained.

### Publications Acknowledging this Grant in 2021-2024


1. Vetter, A. J.; DiBenedetto, T. A.; Ritz, M.D.; Jones, W. D. The Functionalization of Benzene by Boranes using Trispyrazolylborate Complexes. *Polyhedron*, **2021**, *197*, 115042. (DOE, NSF) DOI: 10.1016/j.poly.2021.115042 *(I)*
2. Nachtigall, O.; VanderWeide, A. I.; Brennessel, W. W.; Jones, W. D. First-Row Transition Metals Complexes with Fused Oxazolidine (FOX) Ligands. *Z. Anorg. Alleg. Chem.* **2021**, *647*, 1442-1448. DOI: 10.1002/zaac.202100056 (DOE, Humboldt) *(I)*

3. DiBenedetto, T. A.; Jones, W. D. Upgrading of Ethanol to n-Butanol via a Ruthenium Catalyst in Aqueous Solution. *Organometallics.* **2021**, *40*, 1884-1888. DOI: 10.1021/acs.organomet.1c00217 (DOE) *(I)*
4. Reshma G., Kumar, M.; Kulkarni, N. V.; Jones, W. D. Dehydrogenation of 1-Phenylethanol Catalyzed by Nickel (II)-Diphosphine Complexes. *Acta Chim. Slov.* **2021**, *68*, 955-960. (DOE, NSF) DOI: http://dx.doi.org/10.17344/acsi.2021.6920 *(II)*
5. Nachtigall, O.; VanderWeide, A. I.; Brennessel, W. W.; Jones, W. D. Iron-Based Dehydration Catalyst for Selective Formation of Styrene. *ACS Catal.* **2021**, *11*, 10885-10891. (DOE) *Editor's Choice* DOI: 10.1021/acscatal.1c03037 *(I)*
6. Görlich, T.; Frost, D. S.; Boback, N.; Coles, N. T.; Dittrich, B.;; Müller, P.; Jones, W. D.; Müller, C. Photochemical C(*sp*)-C($sp^2$) Bond Activation in Phosphaalkynes: a New Route to Reactive Terminal Cyaphido Complexes $L_nM$-C≡P. *J. Am. Chem. Soc.* **2021**, *143*, 19365-19373. (DOE, DFG) DOI: 10.1021/jacs.1c07370 *(II)*
7. Jones, W. D. Selectivity in the Activation of C–H Bonds by Rhodium and Iridium Complexes. *Adv. Orgmet. Chem.* **2022**, *78*, 1-34. (DOE) DOI: 10.1016/bs.adomc.2022.03.001 *(I)*
8. Shanahan, J. P.; Vicic, D. A.; Brennessel, W. W.; Jones, W. D. Trapping of a Late Metal Terminal Sulfido Intermediate with Phenyl Isothiocyanate. *Organometallics*, **2022**, *41*, 3448-3453. DOI: 10.1021/acs.organomet.2c00435 (DOE) *(I)*
9. Mahitha, P. M., Nakul, S., Kulkarni, N. V., Jagirdar, B. R.; Jones, W. D., Guerbet Upgrading of Ethanol to n-Butanol using Ru(III) Catalysts under Air. *New J. Chem.* **2023**, *47*, 7470-7475. (DOE, CENTC) DOI: 10.1039/D3NJ00535F *(II)*
10. Lachaize, S.; Gallegos, D. C.; Antonio, J. J.; Atesin, A. C.; Ateşin, T. A.; Jones, W. D. *Ortho*-Fluoro Effect on the C—C Bond Activation of Benzonitrile Using Zerovalent Nickel. *Organometallics* **2023**, *42*, 2134-2147. (DOE, Welch) DOI: 10.1021/acs.organomet.3c00275 *(I)*
11. Pohorenec, R. A.; Brennessel, W. W.; Jones, W. D. Synthesis, Characterization, and Structure Determination of Bis-oxazolidine Complexes of Rhenium. *New J. Chem.* **2023**, *47*, 16872-16878. DOI: 10.1039/D3NJ02181E (DOE) *(I)*
12. Ateşin, T. A.; Jones, W. D.; Atesin, A. C. *Ortho*-Fluoro or *Ortho* Effect? Oxidative Addition of Zerovalent Nickel into the C—CN Bond of Substituted Benzonitriles. *Inorg. Chem.***2023**, *62*, 19698-19705. DOI: 10.1021/acs.inorgchem.3c03065 (DOE, Welch) *(II)*
13. Escobar, R.; Meza, J. Pena, J.; Atesin, A. C.; Jones, W. D.; Müller, C.;Ateşin, T. A. A DFT Comparison of C—C Reductive Coupling from Terminal Cyanido and Cyaphido Complexes of Nickel. *Inorg. Chem.* **2024**, *63*, 16622-16630. DOI: 10.1021/acs.inorgchem.4c01194. (DOE, DFG, Welch) *(II)*
14. Panda, A.; Wood, C. R.; Jones, W. D. Efficient Dehydration of 1-Phenylethanol to Styrene by Copper(II) and Zinc(II) Fused-bisoxazolidine Catalysts. *ACS Catal.*, **2024**, in revision. (DOE) *(II)*

*(I) Intellectually led by this grant*
*(II) Jointly funded by this grant and other grants with intellectual leadership by other funding sources.* Green implies deposited in DOE E-Link

**Shyam Kattel (PI), Xiaofeng Feng (Co-PI)**

## Electrochemical nitrate reduction to ammonia on single-atom catalysts

Shyam Kattel[1,2], Adyasa Priyadarsini[2], Zhen Meng,[3] Xiaofeng Feng[1]

[1]Department of Physics, University of Central Florida, Orlando, FL 32816
[2]Department of Physics, Florida A&M University, Tallahassee, FL 32307
[3]Department of Chemistry, University of Central Florida, Orlando, FL 32816

### Presentation Abstract

Sustainable production of fuels/chemicals using renewable energy is essential to reduce the energy dependence on fossil fuels and to mitigate the negative environmental impacts of greenhouse gas emissions. Ambient electrochemical processes that convert wastes/pollutants to valuable chemicals using the electricity generated from renewable sources are ideal in this regard. Ammonia, one of the widely used chemicals in agriculture and industries, is currently produced via the energy- and carbon-intensive Haber-Bosch process, while the increasing use of nitrogen fertilizers has caused nitrate contamination of water resources. Therefore, the electrochemical nitrate ($NO_3$) reduction ($NO_3RR$) to ammonia presents an attractive approach for a low-carbon and convergent ammonia manufacturing technology that concurrently remediates nitrate-polluted water systems. Here we have carried out density functional theory (DFT) calculations and experimental electrochemical measurements to obtain a mechanistic understanding of $NO_3RR$ on Fe-$N_x$ single-atom catalysts supported on graphene. Our combined DFT and experimental results have identified the active sites and energetically most favorable pathways of the $NO_3RR$. The results show that Fe-$N_4$ atomic sites embedded in a graphene plane are thermodynamically stable and selectively promote the $NO_3RR$ to ammonia with greater than 80% Faradic efficiency in acidic, neutral, and alkaline media.

**Grant or FWP Number:** DE-SC0024485
**Grant Title:** Electrochemical nitrate reduction to ammonia on single-atom alloy catalysts

**Postdoc(s):** Adyasa Priyadarsini
**Student(s):** Zhen Meng, Debit Subedi*
**Affiliations(s):** *Department of Physics, Florida A&M University, Tallahassee, FL 32307

### RECENT PROGRESS

***Theoretical study of $NO_3RR$ on Fe single-atom catalyst***

Density functional theory (DFT) calculations were performed to compute the free energy diagrams using the optimized binding energies/geometries of the reaction intermediates to gain a deeper insight into the structure-activity-selectivity relationship of nitrate reduction reaction ($NO_3RR$) to ammonia on Fe single atom catalysts modeled as Fe-$N_4$ sites embedded in graphene. Two other competing reactions to $NO_3RR$, are nitrite ($NO_2^-$) desorption and hydrogen evolution reaction (HER). The free energy diagrams of $NO_3RR$ along all possible pathways are shown in Figure 1.

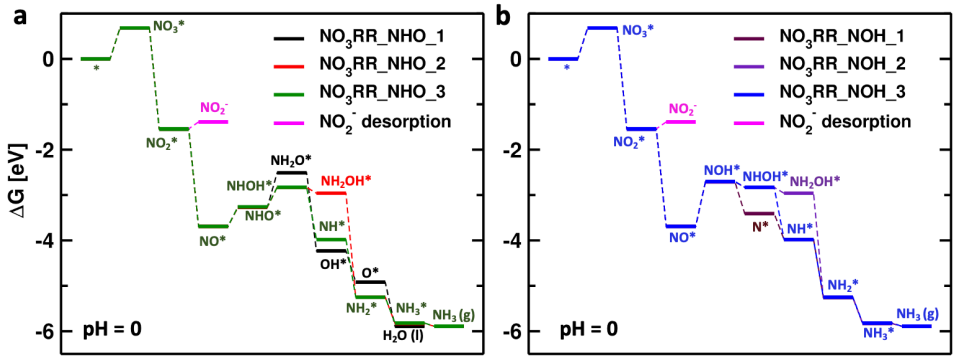


**Figure 1.** The free energy diagrams of $NO_3RR$ along the 6 different pathways mediated by (a) NHO* and (b) NOH* formation at pH = 0.

The free energy change of the reaction involving $NO_2^-$ is calculated using the reaction $NO_2^* + H^+ + e^- \rightarrow HNO_2^*$. $NO_2^*$ to NO* formation can involve a deoxygenation step or two protonation steps. Independent of protonation or deoxygenation pathway, $NO_3^*$ to NO* formation steps remain the same for all six pathways as listed in Figure 1. The next proton-coupled electron transfer step after the formation of NO* splits into two major pathways, namely NOH* through protonation at O* of *NO and NHO* through protonation at N of *NO. The stepwise reaction free energy values calculated for NHO*-mediated pathways are depicted in Figure 1a and NOH*-mediated pathways are depicted in Figure 1b. Considering the NHO*-mediated pathways, there are again two distinct ways for ($H^+ + e^-$) transfer to NHO* leading to the formation of NHOH* or $NH_2O^*$. The final product $NH_3^*$ formation and its desorption from $NH_2O^*$ proceeds through O* formation, which makes the $NO_3RR$_NHO_1 pathway a unique case. If the reduction proceeds through NHOH* formation, then the reaction again splits into two channels, i.e., $NH_2OH^*$ formation by protonation, along the $NO_3RR$_NHO_2 pathway, or NH* formation by deoxygenation, along the $NO_3RR$_NHO_3 pathway. Similarly for NOH-mediated pathways, the reaction channel initially splits into two, leading to the formation of N* through deoxygenation and the formation of NHOH* through protonation, named $NO_3RR$_NOH_1 and $NO_3RR$_NOH_2 pathways, respectively. The next ($H^+ + e^-$) transfer to NHOH* again leads to two pathways, namely $NO_3RR$_NOH_2, via $NH_2OH^*$ intermediate and $NO_3RR$_NOH_3, NH* via deoxygenation step.

The DFT calculated free energy diagrams (Figure 1) show that the NHO* formation is more favorable than the NOH* formation by 0.54 eV on the Fe-$N_4$ sites. Therefore, the subsequent discussion is focused on the NHO* facilitated pathways (Figure 1(a)). Along the NHO*-mediated pathways, it is observed that $NH_2O^*$ formation is more energy-demanding than the NHOH* formation by 0.32 eV. Hence, NHOH* is the intermediate that will likely form due to NHO* protonation. Next, NHOH* decomposition to form $NH^* + H_2O$ is not only exothermic but also energetically more favorable than the formation of $NH_2OH^*$, which is an endothermic process. Thus, our free energy diagrams show that the $NO_3RR$_NHO_3 pathway is the most favorable pathway of $NO_3RR$ to $NH_3$.

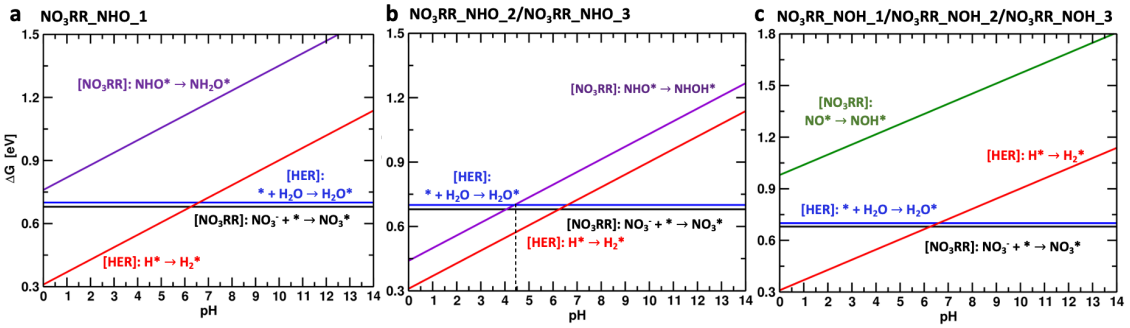


**Figure 2.** The pH-dependent free energy barrier of the PDS of HER and $NO_3RR$ mediated by (a) $NO_3RR\_NHO\_1$, (b) $NO_3RR\_NHO\_2$/ $NO_3RR\_NHO\_3$, and (c) $NO_3RR\_NOH\_1$/ $NO_3RR\_NOH\_2$/ $NO_3RR\_NOH\_3$ pathways. $NO_3RR\_NHO\_3$ is the most favorable pathway and the crossing point of the pH-dependent PDS of $NO_3RR$ and HER is depicted by a vertical dotted line. $NO_3RR$ is favorable in the acidic media, i.e. till pH = 4.5, after which the $NO_3RR$ pathway becomes more energy-demanding, and the catalyst favors HER.

To gain further insight into the pH dependence of HER and $NO_3RR$, we have plotted the free energy change of the endothermic steps of $NO_3RR$ and HER in Figure 2. Depending upon the potential determining step (PDS), we have segregated the pH-dependence of $NO_3RR$ pathways into 3 sections, pictorially depicted in Figures 2a-c. From Figures 2a and 2c, it is evident that $NO_3RR$ is not favorable since the PDS of $NO_3RR$ is more endothermic compared to that of HER throughout the pH range. For HER step 1, $H_2O^*$ formation, and step 3, $H_2^*$ formation, are endothermic at pH = 0. Along the $NO_3RR\_NHO\_3$ pathway, step 1, i.e., the $NO_3^*$ formation, and step 7, i.e., the NHOH* formation are the most energy demanding elementary steps. As the pH value changes from acidic to alkaline $H_2O^*$ barrier remains the same and is more endothermic than the PDS of $NO_3RR$, i.e., $NO_3^*$ formation.

***Experimental study of $NO_3RR$ on Fe single-atom catalyst***

Experimentally, we first synthesized and characterized Fe-$N_x$ single-atom catalysts, and then investigated them for the $NO_3RR$ under different conditions. The Fe-$N_x$ catalysts were prepared as follows: $Zn(NO_3)_2.6H_2O$ and $Fe(acac)_2$ were dispersed in methanol, and another solution with 2-methylimidazole dispersed in methanol was added to the solution. After sufficient stirring and reaction, the mixed solution was washed and dried to derive the MOF precursor, which was subsequently transferred to a tube furnace and pyrolyzed at 950 °C for 2 h in $Ar/H_2$ gas flow. The leaching of possible Fe particles was further carried out using HCl solution. Typical characterizations were performed to examine the prepared sample. The transmission electron microscopy (TEM) image and X-ray diffraction (XRD) pattern of the sample did not show the presence of Fe nanoparticles, indicating that the Fe species should be mainly in the isolated atom state. The single-atom structure of the Fe-$N_x$-C sample was verified using X-ray absorption spectroscopy (XAS) at the Beamline 9-3 of the Stanford Synchrotron Radiation Lightsource with a modified H-cell and a Germanium detector. X-ray absorption near edge structure (XANES) and Fourier-transformed extended X-ray absorption fine structure (FT-EXAFS) spectra of the Fe K-edge were collected for the Fe-$N_x$ sample, while the dominant Fe−N peak and the absence of Fe−Fe peak in the FT-EXAFS confirmed the single-atom structure of Fe in the sample.

The Fe-$N_x$ catalyst was deposited on a carbon substrate to form an electrode, which was then assembled into a two-compartment electrochemical cell (H-cell) for the $NO_3RR$ tests. Two products, $NH_3$ and $NO_2^-$, were quantified by the indophenol blue method and the Griess method, respectively. The quantification of $NH_3$ production was further verified by $^1H$ nuclear magnetic resonance (NMR) spectroscopy, and the N source of the detected ammonia was confirmed to be nitrate using $^{15}N$ isotope labeling experiment. Linear sweep voltammetry (LSV) was first performed to evaluate the electrocatalytic activity, and bulk electrolysis was carried out at selected potentials to quantify the activity (current density) and selectivity (Faradaic efficiency) of $NO_3RR$. We thus evaluated the Fe-$N_x$ catalyst for $NO_3RR$ in three electrolytes containing 0.1 M $NO_3^-$ but different pH values (pH = 2, 7, and 14), respectively, which showed excellent stability under different conditions such as acidic or alkaline electrolytes as compared to other metal catalysts. As shown in Figure 3, the Fe-$N_x$ catalyst achieved a great performance for the $NO_3RR$ with >80% Faradaic efficiency for $NH_3$ production in the electrolytes, making it a stable and versatile electrocatalyst for the conversion of $NO_3^-$ to $NH_3$ under various conditions. The experimental results have verified the above computational results to elucidate the $NO_3RR$ mechanism on the single-atom catalyst as well as the competition between the HER and $NO_3RR$.

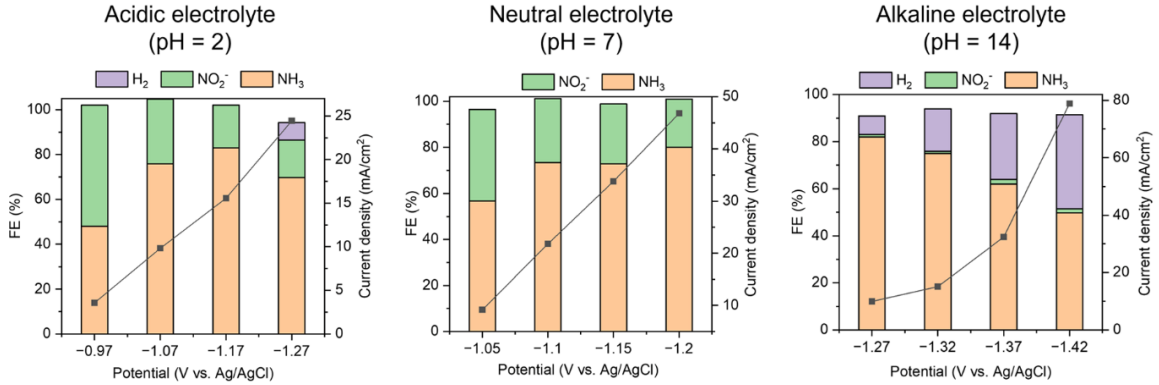


**Figure 3.** Electrocatalytic performance of Fe-N-C catalysts for $NO_3RR$ in different media, showing the current density and Faradaic efficiency (FE) for the $NO_3RR$ in the electrolytes with 0.1 M $NO_3^-$ but different pH values (pH = 2, 7, and 14), respectively.

**Publications Acknowledging this Grant in 2021-2024**

Two manuscripts are under preparation for submission.

Sheima J. Khatib

# Insights into Bimetallic Active Sites for Methane Dehydroaromatization

Sheima J. Khatib, Md Sifat Hossain, Emanuele J. Hiennadi

Department of Chemical Engineering, Virginia Tech, Blacksburg, VA 24061, USA

## Presentation Abstract

Literature indicates that adding Fe in oxidic or metallic form as a separate phase to Mo/ZSM-5 catalysts can improve benzene selectivity in the methane dehydroaromatization reaction (MDA), but only when added in a small quantity. The low Fe loadings make it difficult to properly characterize the state of Fe in the catalyst to understand the possible role of Fe-Mo interactions on the catalytic properties. Here, we present a systematic approach where we aim to control the relative location of the Mo and Fe species in the pre-catalysts in order to explore how the nature of the Mo-Fe interactions influence catalytic activity in MDA. We have tested catalysts where both Mo and Fe are located on the external surface of the zeolite and contrasted the behavior of the metal sites to ones where both Mo and Fe are located within the zeolite channels. Our results indicate that Fe tends to trap Mo sites and that the nature of the Mo-Fe interaction in the precatalyst plays a crucial role on how the two metals evolve during reaction, impacting the rate of formation of benzene.

**PI:** Sheima J. Khatib
**Student(s):** Md Sifat Hossain, Emanuele J. Hiennadi

## RECENT PROGRESS

***How the location of metals in the precatalysts affects the structural evolution and the catalytic activity in methane dehydroaromatization.***

We are currently establishing a systematic study where we are prepare model catalysts where we control the relative location of Mo and Fe in the starting catalysts in their oxidic form. In particular, we are targeting starting catalysts where Mo and Fe are (1) both located on the external surface of the zeolite, (2) both located within the zeolite channels, (3) Mo located within the zeolite channels, and Fe in the external surface (Figure 1).

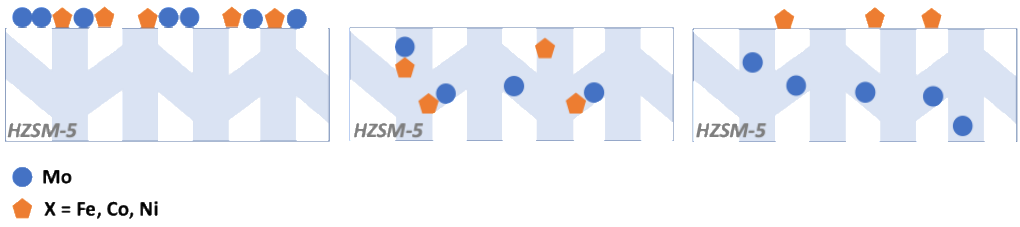


**Figure 1. Schematic of the three model catalysts with controlled location of metal sites.**

For the first case, where both Mo and Fe start on the external surface of the zeolite, we prepared a catalyst consisting of $Fe_2(MoO_4)_3$ physically mixed with H-ZSM-5, and we determined that during catalyst pretreatment the $Fe_2(MoO_4)_3$ phase segregates to form $Fe_2O_3$ species that remain on the external surface of the zeolite, while $MoO_x$ species migrate into the ZSM-5 channels conferring the catalyst with the ability to selectively form benzene in MDA. A similar speciation is observed with a starting catalyst consisting of a physical mixture of $MoO_3$ and $Fe_2O_3$ with H-ZSM-5, however, DFT calculations and activity results indicate that the presence of pre-existing $Fe_2O_3$ phases tend to trap $MoO_x$ species reducing their likelihood of anchoring inside the zeolite channels and thus reducing selectivity to benzene formation. Concurrent segregation of $Fe_2O_3$ and $MoO_x$ in a preexisiting $Fe_2(MoO_4)_3$ phase increases likelihood of $MoO_x$ to avoid entrapment by $Fe_2O_3$ and anchor within the channels to a greater extent, leading to a more stable and selective catalyst.

Recently we prepared model catalysts where both Mo and Fe are located within the zeolite channels. This was achieved by employing lower metal loadings and employing the incipient wetness impregnation technique. Activity data (Figure 2) indicate that coexistence of Mo and Fe leads to higher rates of formation of benzene compared to a monometallic Mo catalyst containing the same Mo loading.

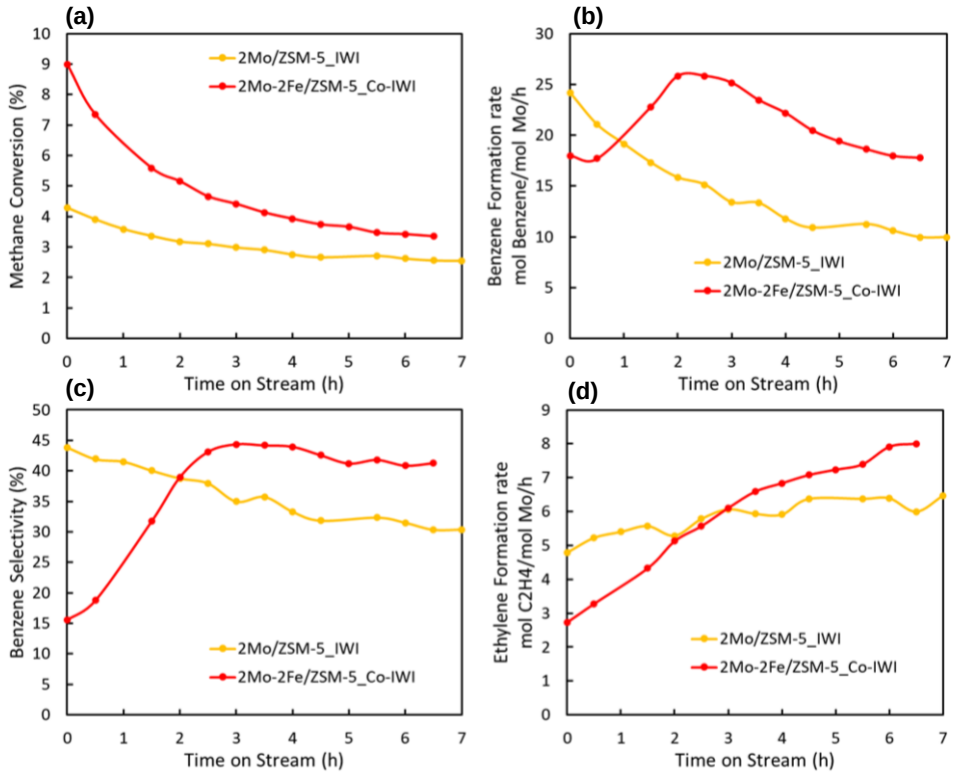


**Figure 2. Activity as a function of time on stream over 2Mo/ZSM-5, and 2Mo-2Fe/ZSM-5 catalysts. (a) methane conversion over time on stream, (b) benzene formation rate over time on stream, (c) benzene selectivity over time on stream, (d) ethylene formation rate over time on stream.**

The higher benzene selectivity could be indicative of a synergistic relation between Mo and Fe when they are co-located within the zeolite channels. We performed structural characterization of the catalysts to better understand the Mo-Fe interactions. In particular we have performed temperature programmed reduction (TPR) measurements (Figure 3 (a)), Raman (Figure 3 (b)) and UV-Vis spectroscopy (Figure 3 (c)), XPS, and XRD. Interpretation of the structural characterization data is currently under progress, but so far, we can confirm via XRD, Raman and UV-Vis spectroscopy that in both Mo and Mo-Fe catalysts, both metal species are well dispersed and do not form crystalline phases, reinforcing that they both co-exist within the zeolite channels. TPR profiles point to an unusual reduction peak when both metals coexist that could be suggesting that Mo affects the reducibility of Fe, indicating that the two metals are probably in close proximity to each other. Further analysis of the results and additional characterization by X-Ray absorption are planned for future work.

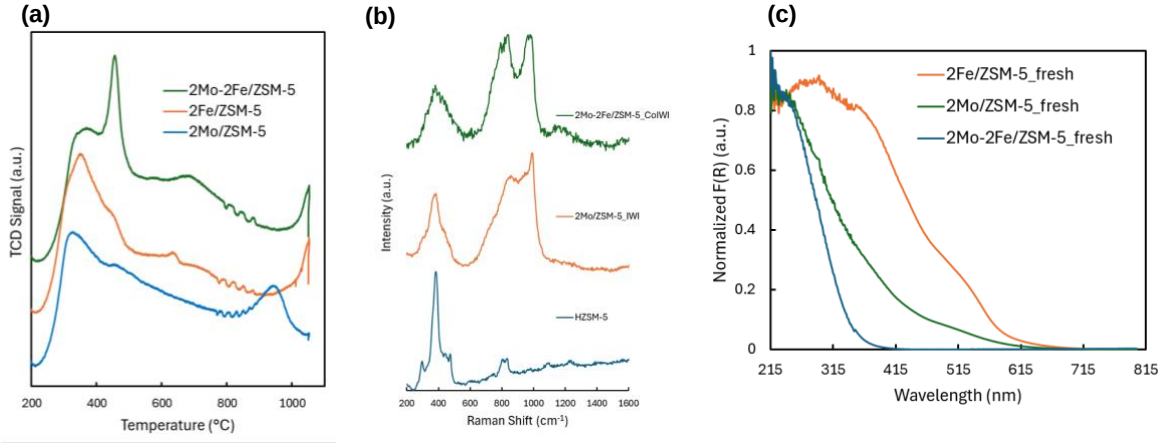


**Figure 3. (a) TPR profiles; (b) Raman spectra; (c) UV-Vis spectra of bimetallic and monometallic catalysts.**

## Publications Acknowledging this Grant in 2021-2024

*(I) Intellectually led by this grant*

(1) Hossain, M.S.; Dhillon, G.S.; Liu, L.; Sridhar, A.; Hiennadi, E.J.; Hong, J.,; Bare, S.R.; Xin, H.; Ericson, T.; Cozzolino, A.; Khatib*, S.J. Elucidating the role of Fe-Mo interactions in the metal oxide precursors for Fe promoted Mo/ZSM-5 catalysts in non-oxidative methane dehydroaromatization, *CEJ*, **2023** , *146096*.

(2) Hossain, M.S.; Hiennadi, E.J.; Liu, L.; Xin, H.; Khatib*, S.J. Investigating Methane Activation on Mo-Fe/ZSM-5: Insights into Bimetallic Active Sites for Aromatization, *in preparation*.

Sungmin Kim

## Manipulating active sites and molecular environments in zeolite micropores for hydrogen activation and C-O elimination

Sungmin Kim, Jian Zhi Hu, Mal-Soon Lee, Huamin Wang, and Johannes Lercher
Pacific Northwest National Laboratory, Physical and Computational Sciences Directorate and Institute for Integrated Catalysis

### Poster Abstract

Zeolites are crystalline microporous aluminosilicates with well-defined Brønsted acid sites (BAS) and Lewis acid sites (LAS), resulting from the substitution of $Si^{4+}$ by $Al^{3+}$ at tetrahedral positions in the framework. Tailoring the molecular environment and catalytically active sites in zeolite micropores enhances the catalytic reactivity. In the presented work, we modulate transition metal sulfide clusters in NaY for hydrogen activation and quantitatively describe the impact of the molecular environment in the presence of water on C-O elimination.

We synthesized $Mo_xS_y$ clusters encapsulated in faujasite-type NaY zeolite with precisely defined nuclearity, geometry, and atomic connectivity. The thermal treatment in sulfiding and reducing atmosphere stabilized two different molecular cluster structures of dimeric $Mo_2S_4$ and $Mo_4S_4$. Those catalysts exhibited remarkable stability and reactivity for ethene hydrogenation compared to classic, layered $MoS_2$ catalysts.

Controlling the molecular environment of zeolite micropores, where the reacting molecules interact in liquid solvents, has been a formidable challenge. The environment in the micropores of acidic zeolites is determined by the ordering and partitioning of the solvents and the reactive substrates in the zeolite pores. In addition, the interactions with the substrates involve hydrogen bonding or interactions with surface functionalities. Water in zeolite micropores forms hydronium ions. Hydronium ions and a negatively charged zeolite framework create a high local ionic strength. The work presented here demonstrates how the ionic environment in the zeolite pore (de)stabilizes the initial and transition states for C-O elimination, leading to two orders of magnitude higher reaction rates compared to an unconfined aqueous acid solution.

**FWP 47319: Advancing key catalytic reaction steps for achieving carbon neutrality**

**PI:** Johannes Lercher
**Co-PIs:** Aaron M. Appel, Liney Arnadottir (Oregon State U.), David A. Dixon (U. Alabama), Zdenek Dohnalek, John L. Fulton, Bojana Ginovska, Jian Zi Hu, Abhi J. Karkamkar, Bruce D. Kay, Konstantin Khivantsev, Sungmin Kim, Greg A. Kimmel, Libor Kovarik, ThuyThanh D. Le, Mal Soon Lee, Johannes A. Lercher, John C. Linehan, Zbynek Novotny, Simone Raugei, Udishnu Sanyal, Gregory K. Schenter, Wendy J. Shaw, Honghong Shi, Janos Szanyi, Ba L. Tran, Huamin Wang, Yong Wang, Nancy M. Washton, Eric S. Wiedner

Kyle M. Lancaster

# Electronic Structure/Function Relationships in Heterobimetallic *d*-block/*p*-block Catalysts

Kyle M. Lancaster
Department of Chemistry and Chemical Biology, Baker Laboratory, Cornell University
Ithaca NY USA 14850

## Presentation Abstract

This project leverages the Lancaster group's expertise in physical inorganic chemistry and coordination/organometallic synthesis to unravel how bonding between main group and transition metals contributes to and tunes catalysis. Central to the studies is a versatile ligand platform that can not only accommodate a large range of transition metals, but also can support main group metals through a range of bonding configurations. Initial studies are focused on the reactivity of low-valent Sn(II) centers whose electronics are tuned by interactions with transition metals X-ray spectroscopic methods will be developed to facilitate electronic structure investigations. Kinetics studies will be undertaken to reveal how Sn electronics influence elementary steps of hydroboration catalysis. Synthesis campaigns are being pursued towards expanding the library of Sn(II)-TM heterobimetallics to obtain systems that can leverage the cooperativity between Sn-hydride catalysis and transition metal redox reactivity. Insights gleaned are expected to be generally applicable to tetrylene catalysis.

## DE-SC0024172: Electronic Structure/Function Relationships in Heterobimetallic *d*-block/*p*-block Catalysts

**Postdoc(s):** Dr. Richard Y. Kong, Dr. Benyu Zhou
**Student(s):** Mr. Guy R. Anello (undergraduate), Mr. Jinwoo Jung (undergraduate)

## RECENT PROGRESS

### *Accelerating σ-bond Metathesis at Sn(II) Centers*

Using the binucleating scaffold CarbPy$_2^{iPr2}$P$_2$ (**Figure 1**), we synthesized a series of formally Sn$^{II}$–Ni$^0$ heterobimetallic complexes differentiated by monodentate ligands L = CO, PMe$_3$, PPh$_3$, P$^n$Bu$_3$, CNTripp (CNTripp = bis-2,6-[2,4,6-tri-isopropylphenyl]phenylisocyanide), and IMe$_4$ (IMe$_4$ = 1,3,4,5-tetramethylimidazol-2-ylidene). These complexes are generated by the formal insertion of Ni$^0$ (delivered as Ni(COD)$_2$) into a Sn$^{II}$–Cl bond to yield the corresponding Sn–NiCl species, which can then be converted to the SnCl–NiL species

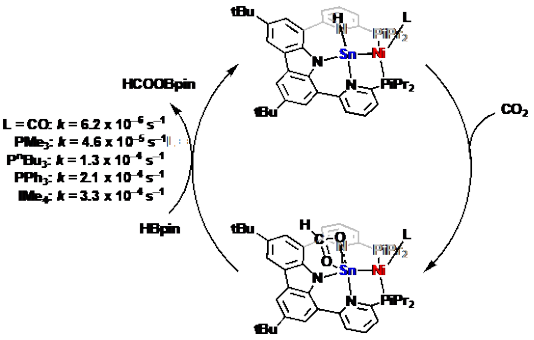


**Figure 1.** $CO_2$ hydroboration catalysis effected by CarbPy$_2^{iPr2}$P$_2$-supported Sn$^{II}$–Ni$^0$ complexes.

following treatment with L. Substitution of Cl for *tert*-butoxide furnishes a precursor to SnH–NiL species that are competent for selective hydroboration of $CO_2$ to monopinacolboratoformate. Catalysis rates are modulated by the nature of the ligand coordinated to the formal $Ni^0$ center. Fastest rates are obtained when L is a strong σ-donor, while the most sluggish catalysis occurs when L is a π-acceptor. This is due to the Ni center acting as an electron donor to Sn; Sn electronic structure was probed using Sn $L_1$ X-ray absorption spectroscopy, which showed that strong σ-donation to Ni was communicated to Sn via the Sn–Ni bond. This lowers the barrier to product (formate) release, accelerating the overall σ-bond metathesis catalysis. Additional acceleration can be obtained via dispersion interactions stabilizing the incoming pinacolborane. This work, which was published in *J. Am. Chem. Soc.*, was largely carried out by a former postdoc (Richard Kong, now at U. Edinburgh) and a current undergraduate, Guy Anello.

### *Catalytic Hydroboration of Aryl and Alkyl Nitro Groups*

Undergraduate Guy Anello, working with postdoc Benyu Zhou, has extended the substrate scope of hydroboration by the $Sn^{II}$–$Ni^0$ platform to include both aryl and alkyl nitro functional groups. This includes a convenient hydroboration of nitromethane to the corresponding borylated methylamine. Mr. Anello has carried out optimization studies including NMR kinetics. A preliminary substrate table including NMR yields is given in Figure 2. Catalysis is quite efficient, with many substrates consumed in under 2 hours with low (1%) catalyst loadings at room temperature.A manuscript describing this work is nearing completion for submission to *Organometallics*.

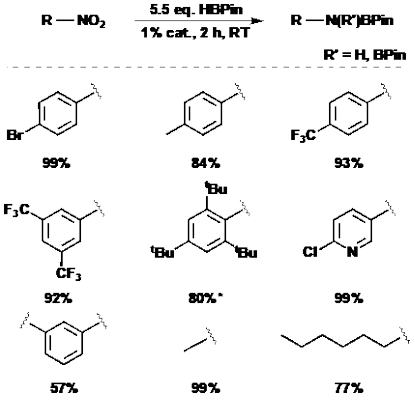


**Figure 2.** Substrate scope and NMR yields for nitro group hydroboration by $CarbPy_2^{iPr2}P_2$-supported $Sn^{II}$–$Ni^0$ complexes.

### *Expanding the Library of Sn–TM Heterobimetallics*

A principal goal of the current funding period is to extend our library of Sn–TM heterobimetallics to include transition metals that can participate in substrate activation and thus enable cooperative two-site catalysis. Postdoc Dr. Benyu Zhou has targeted $Sn^{II}$–$Fe^0$, $Sn^{II}$–$Co^0$, and $Sn^{II}$–$Co^I$ complexes. Thus far, we have been unable to unambiguously characterize the products of $Fe^0$ metalations, which have been carried out using a number of different Fe starting materials. Similarly, Co metalations either lead to intractable product mixtures or to ligand decomposition via P–C bond activation leading to bridging phosphide complexes.

Dr. Zhou has successfully synthesized $Sn^{II}$–$Rh^I$ and $Sn^{II}$–$Pd^{II}$ heterobimetallics. We have been using the $Sn^{II}$–$Rh^I$ species as a platform to assess the viability of $H_2$ activation at the transition metal center for subsequent transfer to Sn for Sn–H catalysis (**Figure 3**). We acknowledge that $Rh^I$ centers by themselves form the basis for excellent hydrogenation catalysts— this work has been entirely a proof-of-concept study carried out in parallel with attempts to synthesize the 3d metal containing heterobimetallics. Thus far, we have

demonstrated that, unsurprisingly, $H_2$ is readily activated at the Rh centers to generate a σ-complex between $Sn^{II}$ and the Rh–H. A similar motif is encountered when the *tert*-butoxy-Sn-Rh species is treated with HBpin, indicating that oxidative addition of Sn–H to the Rh center is favored over $H^-$ migration to Sn. This work is currently being compiled into a manuscript.

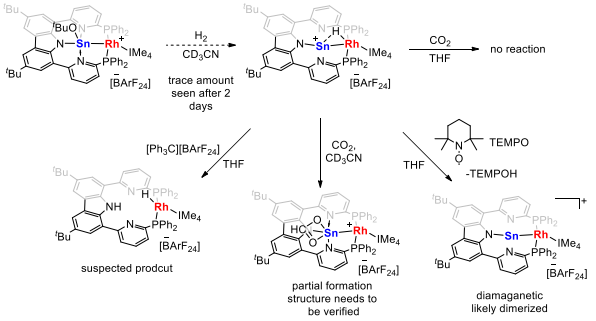


**Figure 3.** Summary of reactions carried out using $CarbPy_2^{iPr2}P_2$-supported $Sn^{II}$–$Rh^{I}$.

### *Electronic Structure of Sn(II)–TM Hydroboration Catalysts*

In our initial paper reporting the $Sn^{II}$–$Ni^0$ complexes and their use in catalysis, we quantified electron density at Sn using Sn $L_1$-edge XAS calibrated to $^{119}$Sn Mössbauer data. To elaborate on this work, we have obtained additional Sn XAS data as well as Ni $L_{2,3}$-edge XAS. The latter data report on the degree of vacancy in the Ni 3d orbitals, providing complementary information correlating Sn electron density to Sn–Ni bonding. These data thus far show substantial d-vacancy in the Ni 3d orbitals, indicating that the oxidation state at Ni *physically* is closer to $Ni^I$. To complement these studies, we are obtaining additional Sn XAS and TM XAS data for the large array of Sn–TM heterobimetallics that we have accessed. Our aim here is to quantify the limits to which a TM center can donate electron density to Sn and thus to understand the limits to which a TM center can enhance the reactivity of Sn in hydrogenation catalysis.

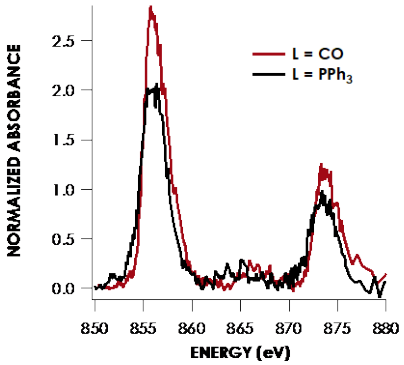


**Figure 4.** Ni $L_{2,3}$-edge XAS of $CarbPy_2^{iPr2}P_2$-supported $Sn^{II}$–$Ni^0L$ complexes where L = CO and $PPh_3$. The more intense features of the CO species show a greater degree of vacancy in Ni 3d relative to the $PPh_3$, but in both cases substantial 3d vacancy is present indicating that the Ni centers are better described as physically $Ni^I$. In the case of the $PPh_3$, this depletion is principally due to donation from Ni to Sn.

## Publications Acknowledging this Grant in 2021-2024

*Class I: Intellectually Led by this Grant*


1. Kong, R. Y.; Parry, J. B.; Anello, G. R.; Ong, M. E.; Lancaster, K. M. Accelerating σ-bond Metathesis at Sn(II) Centers. *J. Am. Chem. Soc.* **2023**, *145*, 24136–24144.

# Experimental and Modeling Studies of the Role of Chemical Promoters in Ethylene Epoxidation over Silver (Ag) Catalysts

Suljo Linic
Department of Chemical Engineering, University of Michigan, Ann Arbor, MI, 48109

## Presentation Abstract

Heterogeneous catalysts are in general solid nanostructures (nanoparticles or zeolite frameworks) that are often richly promoted with various additives. These additives (promoters) are usually introduced in very small amounts (mmol per gram of catalyst) covering a fraction of the catalytically active surface. While these chemical promoters have a dramatic impact on the performance of many solid catalysts, in terms of enhancing rates of reactions or improving the selectivity towards the desired products, our understanding of the underlying mechanisms of promotion is rather limited. The central objective of this project is to investigate the role of chemical promoters in catalytic reactions on metal surfaces. We will focus on ethylene epoxidation on promoted silver (Ag) nanoparticle catalysts, one of the largest commercial catalytic processes, as a case study. This process employs Ag nanoparticle catalysts supported on alumina and promoted with Cesium (Cs), Rhenium (Re), Chlorine (Cl) and Molybdenum (Mo). The addition of these promoters significantly enhances the selectivity of the process towards the desired products. In the absence of promoters, ethylene oxide (EO) selectivity is limited to ~50% (with $CO_2$ being the unselective product). With chlorine, alkali (*e.g.,* Cs, K), and other promoters, 90% selectivity is achievable. Despite widespread adoption of these promoters, the exact mechanism by which these promoters work is still unknown.

In this work, we deployed a range of experimental (SERS, IR and XPS spectroscopies along with state-of-the-art microscopy and kinetic measurements) and modeling techniques (density functional theory (DFT) calculations, microkinetic and ab-initio thermodynamic modelling) to analyze the mechanisms behind chemical promotion in heterogeneous ethylene epoxidation over $Ag/Al_2O_3$ catalysts. Based on these studies we concluded that: (i) The structural (atomistic organization), physical and chemical properties of the promoted metal surfaces are fundamentally different than those of an unpromoted surface under a given set of external reaction conditions (i.e. temperature and pressure), (ii) The presence of promoters enhances the surface concentration (and the rate of formation) of particular surface intermediates that are critical for the selective outcome of a reaction. In the case of ethylene epoxidation reaction, this surface intermediate is a special kind of “selective” oxygen surface species that has a specific electronic structure and that exists in a specific geometric arrangement on the metal surface. We measure the concentration of this intermediate using SERS and correlate it to the product selectivity.

**DE-SC0021008:** Experimental and modeling studies of the role of chemical promoters in heterogeneous catalysis

**Student(s):** Shiuan-Bai Ann, Shawn Lu

## RECENT PROGRESS

### *Computational studies of ethylene epoxidation on unpromoted and promoted Ag surface*

We developed an approach based on first-principles density functional theory (DFT) augmented with Machine Learnt Artificial Neural Network Potential (ANNP) coupled with Grand Canonical Monte Carlo (GCMC) simulations approach to study the process of oxygen adsorption on promoted and unpromoted Ag surfaces with first principles Density Functional Theory (DFT) accuracy. We note that the adsorption and activation of oxygen is a critical elementary process involved in various reactions on metal surfaces, including the epoxidation of ethylene on Ag. The GCMC approach employs trained neural network potentials that allow for rapid evaluation of the energy of various surface structures. The main conclusions of these studies are that under ethylene epoxidation reaction conditions, there are multiple Ag-Ox structures (surface motifs) that are sufficiently thermodynamically stable to be present and relevant, i.e., it is likely that chemical transformations are taking place on all these sites. This was published in ACS Catalysis journal in 2023.[3]

In addition, we used DFT calculations to study the kinetics of the elementary steps that govern the selectivity in ethylene epoxidation of Ag on these different Ag-Ox surfaces that were identified as stable in the GCMC simulations. These studies have led to a compete mapping of different reaction pathways by which ethylene and oxygen react to form ethylene oxide. The main conclusions were that, surprisingly, there are different molecular pathways by which the reaction can proceed under reaction conditions. For example, at low oxygen surface coverages, the main pathway includes a surface oxametallacycle, while at higher coverages (Ag surface oxide) additional pathways that include a direct attachment of gas-phase ethylene to atomic oxygen also became viable. The results point to a complexity of chemistry that governs the reaction outcome. It is our view that this level of complexity is not an exception but rather a rule in catalysis on metals.. This work was included in the publications in ACS Catalysis journal in 2023.[3]

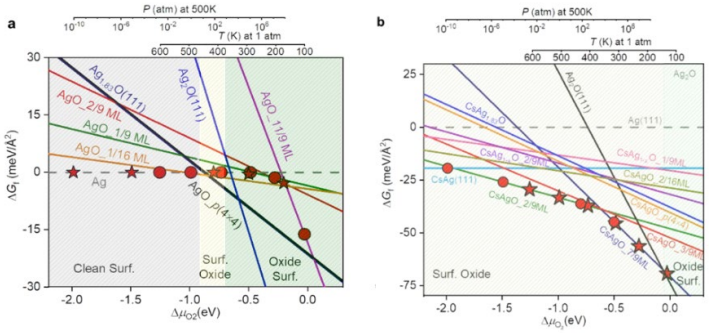


***Figure 1***. (a) Phase diagram of AgOx structures in equilibrium with gas phase $O_2$ for an unpromoted Ag surface. Gibbs formation energies of AgOx structures searched by GCMC-ANNP simulations at different temperatures and pressures are shown by dots and stars, respectively. (b) Phase diagram for Cs-promoted AgOx structures.

We performed similar GCMC DFT studies for Cs-promoted Ag surfaces. These efforts suggested that there were some very significant differences in the behavior of unpromoted and Cs-promoted surfaces with oxygen surface concentration being dramatically impacted by the presence of and Cs-promoted Ag surfaces at industrially relevant temperatures and pressures (see ***Figure 1***). The data revealed that Cs-promoted

surface is generally more oxidized than an unpromoted Ag surface at the same set of external conditions and that it is kinetically easier to activate $O_2$ on the Cs-promoted surface.

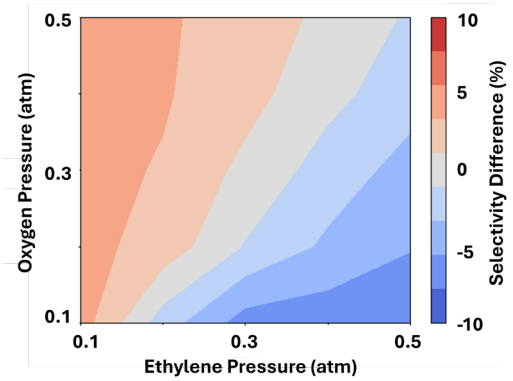


**Figure 2**. Heatmap showing the difference in EO selectivity between 1000 ppm Cs-promoted and unpromoted $Ag/Al_2O_3$ catalysts. Reaction temperature: 180°C.

### *Experimental studies of ethylene epoxidation on unpromoted and promoted Ag surface*

On the experimental front, we have established experimental procedures for the synthesis of $Ag/Al_2O_3$ catalysts that are promoted by various additives. The synthesis procedure was inspired by patent literature, so that our catalysts are mimicking the commercially used materials as much as possible. In general, our results are consistent with the previous literature reports in terms of the measured reaction rates values and the conversion/selectivity curves for promoted and unpromoted catalysts. In addition, we find that Cs enhances the rates of reaction and impacts the EO selectivity in a way that is very dependent on the reactions conditions (see Figure 2). On the other hand, we found that Cl suppresses the reaction rate and dramatically enhances the EO selectivity (see Figure 3).

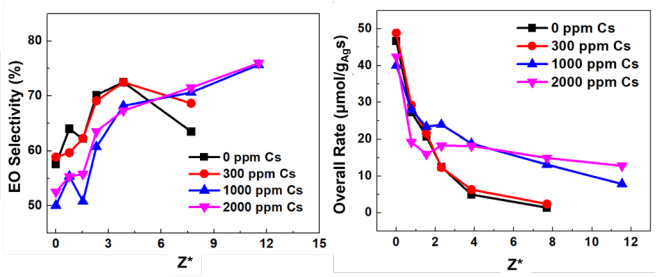


**Figure 3**. EO selectivity and overall activity (ethylene consumption rate) between $Ag/Al_2O_3$ catalysts with different Cs loading amounts as a function of Z*. Reaction condition: 0.3 atm $C_2H_4$, 0.1 atm $O_2$, cofed with $C_2H_6$ and EtCl. Z* is a proportional to the Cl coverage and it is calculated using:

$$Z^* = \frac{C_2H_5Cl\ (ppmv)}{0.01 * C_2H_4\ (mol\%) + C_2H_6\ (mol\%)}$$

### *Spectroscopic studies of ethylene epoxidation over unpromoted Ag/α-$Al_2O_3$*

We also sought to spectroscopically characterize the factors driving EO selectivity over unpromoted and promoted $Ag/Al_2O_3$ catalysts using Surface Enhanced Raman Spectroscopy (SERS). In one of these efforts, we used SERS to simultaneously measure surface oxygen intermediates at various conditions and correlate these with the EO selectivity (one of the data sets is shown in Figure 4). Our measurements revealed that, under reaction conditions, the Ag surface contains a complex mixture of atomic (with Raman fingerprints in the 300 – 600 $cm^{-1}$ range), molecular oxygens (800 – 1200 $cm^{-1}$) and surface oxides (600 – 800 $cm^{-1}$). By systematically varying reaction conditions, we built a

structure-selectivity database that correlates the oxygen species SERS signals and the EO selectivity for a wide range of conditions.

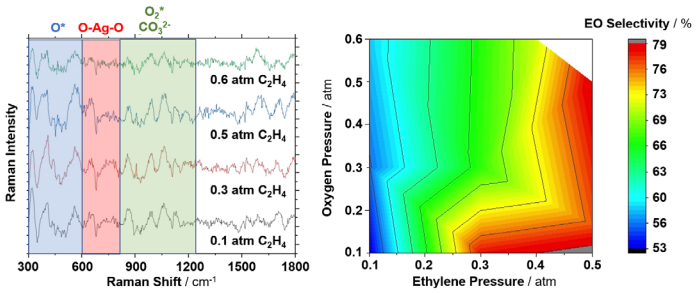


Figure 4: SERS spectra under EO reaction conditions

An analysis of this data showed that on unpromoted Ag surfaces most oxygen species that we measured experimentally correlate negatively with EO selectivity, i.e., a higher concentration of these oxygen species is linked to lower EO selectivity. We are currently examining how promotion impacts the surface concentration of the oxygen species.

### *Microkinetic Modeling Analysis of Cs Promoter Effects in Ethylene Epoxidation over Ag Catalysts*

Since the above-described studies generated a large amount of data related to conversion and selectivity to different reaction conditions for different levels of promotion by Cs and Cl, we used this data in parallel to develop an experimentally informed (*i.e.*, using experiments to fit kinetic parameters) microkinetic model for ethylene epoxidation. In combination with the above-described spectroscopic studies, the microkinetic mode is helping us understand how reaction conditions and chemical promotion impact catalyst performance. For example, the model showed that Cs acts to increase the reaction rate by decreasing the activation barrier for the $O_2$ dissociation which is the kinetically controlling elementary step. This also results in a Cs-induced increase in the concentration of atomic oxygen species on Ag, with a side effect of a slightly lower EO selectivity (Figure 5).

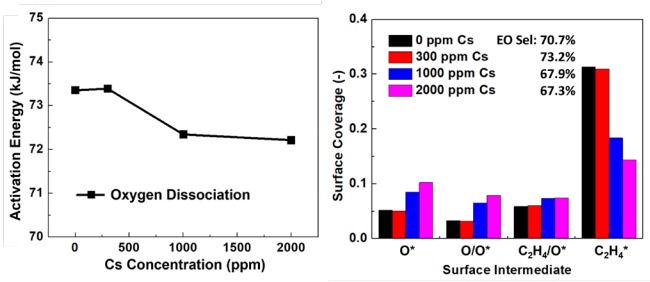


**Figure 5**. Microkinetic modeling simulated results of (left) comparison of oxygen dissociation activation energy as a function of Cs concentration over $Ag/Al_2O_3$ catalysts and (right) surface coverage comparison between highlighted surface intermediates between catalysts. Reaction condition: 500K, 0.1 atm $O_2$, 0.5 atm $C_2H_4$.

## Publications Acknowledging this Grant in 2021-2024

**The publications intellectually driven by this DOE award are:**


1. Almallahi, R.; Wortman, J.; Linic, S. Overcoming limitations in propane dehydrogenation by codesigning catalyst-membrane systems. ***Science***, 2024. 383, 1325-1331. https://doi.org/10.1126/science.adh3712
2. Wortman, J.; Igenegbai, V. O.; Almallahi, R.; Motagamwala, A. H.; Linic, S. Optimizing hierarchical membrane/catalyst systems for oxidative coupling of

methane using additive manufacturing. ***Nature Materials*****,** 2023, 22, 1523-1530. https://doi.org/10.1038/s41563-023-01687-x
3. Liu, J.-X.; Lu, S.; Ann, S.-B.; Linic, S. Mechanisms of Ethylene Epoxidation over Silver from Machine Learning-Accelerated First-Principles Modeling and Microkinetic Simulations. ***ACS Catalysis*****,** 2023, *13*, 8955-8962. https://doi.org/10.1021/acscatal.3c00410
4. Esterhuizen, J. A.; Goldsmith, B. R.; Linic, S. Interpretable Machine Learning for Knowledge Generation in Heterogeneous Catalysis. ***Nature Catalysis***, 2022, 5 (3), 175–184. https://doi.org/10.1038/s41929-022-00744-z.
5. Motagamwala, A. H.; Almallahi, R.; Wortman, J.; Igenegbai, V. O.; Linic, S. Stable and Selective Catalysts for Propane Dehydrogenation Operating at Thermodynamic Limit. ***Science*****,** 2021, 373 (6551), 217–222. https://doi.org/10.1126/science.abg7894.
6. Esterhuizen, J. A.; Goldsmith, B. R.; Linic, S. Uncovering Electronic and Geometric Descriptors of Chemical Activity for Metal Alloys and Oxides Using Unsupervised Machine Learning. ***Chem Catalysis***, 2021, 1 (4), 923–940. https://doi.org/10.1016/j.checat.2021.07.014.
7. Baz, A.; Dix, S. T.; Holewinski, A.; Linic, S. Microkinetic Modeling in Electrocatalysis: Applications, Limitations, and Recommendations for Reliable Mechanistic Insights. ***Journal of Catalysis***, 2021, 404, 864–872. https://doi.org/10.1016/j.jcat.2021.08.043.
8. Dix, S. T.; Linic, S. In-Operando Surface-Sensitive Probing of Electrochemical Reactions on Nanoparticle Electrocatalysts: Spectroscopic Characterization of Reaction Intermediates and Elementary Steps of Oxygen Reduction Reaction on Pt. ***Journal of Catalysis*****,** 2021, 396, 32– 39. https://doi.org/10.1016/j.jcat.2021.02.009.

**Publications jointly funded by the DOE award and other grants but not intellectually driven by the DOE award:**

9. Elias, R.; Yan, B.; Linic, S. Probing Spatial Energy Flow in Plasmonic Catalysts from Charge Excitation to Heating: Nonhomogeneous Energy Distribution as a Fundamental Feature of Plasmonic Chemistry. ***Journal of the American Chemical Society*****,** 2024**.** https://doi.org/10.1021/jacs.4c10395
10. Lee, D.; Chen, H.T.; Linic, S. Plasma-Induced Selective Propylene Epoxidation Using Water as the Oxygen Source. ***JACS Au*****,** 2023. 3 (4). https://doi.org/10.1021/jacsau.3c00030
11. Elias, R.; Linic, S. Elucidating the Roles of Local and Nonlocal Rate Enhancement Mechanisms in Plasmonic Catalysis, ***Journal of the American Chemical Society***, 2022, 144, 43, 19990–19998, https://pubs.acs.org/doi/full/10.1021/jacs.2c08561
12. Linic, S.; Chavez, S.; Elias, R. Flow and Extraction of Energy and Charge Carriers in Hybrid Plasmonic Nanostructures. ***Nature Materials***, 2021, 1–9. https://doi.org/10.1038/s41563-020-00858-4.

Ping Liu

# Catalyst Optimization Driven by Insights into Catalytic Behavior under Reaction Conditions

Ping Liu, Hong Zhang, Erwei Huang and Josè A. Rodriguez
Chemistry Division, Brookhaven National Laboratory

## Presentation Abstract

Capturing catalytic behaviors under operational conditions is pivotal to gain mechanistic understanding and promoting the design of robust catalysts. The challenge lies in the difficulty of monitoring real-time surface dynamics driven by catalyst-environment interaction. This poster introduces a framework based on density functional calculations and kinetic modeling [1]. This framework significantly improves the accuracy of theoretical models in description of experimental observations by quantifying environmental impacts on surface phases, active sites and catalytic activity and selectivity. It not only deepens the comprehension of dynamics of active sites under active chemical conditions but also effectively promotes establishment of structure-catalytic performance relationship and optimization of catalysts. Here, carbon dioxide reduction over palladium-based catalysts and methane partial oxidation over Cu-based catalysts were presented as showcase [1-3].

References:
[1] H. Zhang, P. Liu, "Fine-tuning catalytic selectivity by modulating catalyst-environment interaction: $CO_2$ hydrogenation over Pd-based catalysts", *Chem Catalysis*, accepted.
[2] E. Huang, P. Liu, "Screening of Cu-based catalysts for selective methane to methanol conversion", *Journal of Physical Chemistry C* 128 (2024) 7876–7883.
[3] A. Islam, E. Huang, Y. Tian, P. J. Ramírez, P. R. Kasala, H. Lim, N. White, A. Hunt, I. Waluyo, P. Liu, J. A. Rodriguez, "Low temperature activation and coupling of methane on MgO nanostructures embedded in $Cu_2O$/Cu(111)", *ACS Nano* 18 (2024) 28371-28381.

**Karthish Manthiram**

## Electrocatalytic epoxidation via water activation

Karthish Manthiram
California Institute of Technology, Division of Chemistry and Chemical Engineering

Oxygen-atom functionalization of chemical intermediates to generate epoxides is critical for the production of diverse textiles, plastics, and pharmaceuticals. The wet chemical and thermochemical routes used today suffer from large carbon dioxide footprints, stoichiometric waste products, and hazardous reagents. In this poster, we will present methods by which water can be used as the oxygen source in functionalization reactions, such as epoxidation, with tailored metal and metal oxide nanoparticle anodic electrocatalysts. At the cathode, hydrogen is selectively generated, reflecting that this reaction can be thought of as a derivative of water splitting, in which the oxidizing equivalents go towards generating a valuable product rather than generating molecular oxygen. Our group has demonstrated that oxidized palladium platinum catalysts are effective for oxygen atom transfer, with high rates and Faradaic efficiencies for converting olefins into epoxides. We have developed mechanistic understanding of how water is activated, providing means by which the selectivity for oxygen-atom functionalization can be rationally improved. In recent work, we have understood how catalyst oxidation and supporting electrolyte identity impact the mechanism of epoxidation. This understanding has provided means of stabilizing the catalyst for long-term operation, further facilitating mechanistic studies of the catalyst.

**DE- SC0023207: Electrocatalytic alkene epoxidation at disrupted metal ensembles in blended electrolytes**

**Postdoc(s):** Jason Adams, Kalipada Koner

## RECENT PROGRESS

Our recent research activities investigated the relationship between the structure of PdPtOx and its performance and stability during electrochemical epoxidation reactions in organic-aqueous mixtures and purely aqueous electrolyte solvents. Additional work has also focused on operating these systems in flow and for extended periods while identifying the causes of deactivation in this material.

### Catalytic performance and mechanism of propylene epoxidation on PdPtOx

Electrochemical kinetic studies were conducted on $PdPtO_x$ by chronoamperometry, in which 10 C of charge was typically passed, and the resulting products were analyzed by $^1H$

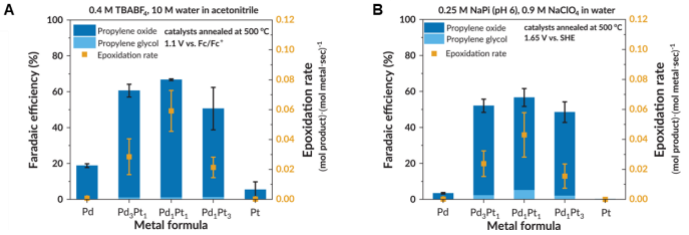


**Figure 1.** Faradaic efficiencies and propylene epoxidation rates with different Pd and Pt compositions in (**A**) water-acetonitrile blended electrolyte and (**B**) aqueous electrolyte. Potentials in this figure were 100% iR-compensated (i, current; R, resistance). The error bars show standard deviations from the mean of multiple replicate measurements ($n$ = 3) of the same condition and material.

NMR. The $PdPtO_x$ (1:1 Pd to Pt) shows the highest rates and Faradaic efficiency of electrochemical propylene epoxidation compared to other alloy compositions (i.e., 3:1 or 1:3 Pd to Pt) or pure $PdO_x$ and $PtO_x$ nanoparticle catalysts in both organic and aqueous electrolytes (**Figure 1**). Moreover, PdPtOx annealed at 500°C also showed the highest rates and Faradaic efficiency of electrochemical propylene epoxidation compared to other annealing temperatures (**Figure 2**), consistent with it having the greatest extent of Pt-O coordination and the highest concentration of $Pt^{2+}$ species. Thus, we hypothesize that oxygen species on $Pt^{2+}$ surface sites are likely responsible for propylene epoxidation.

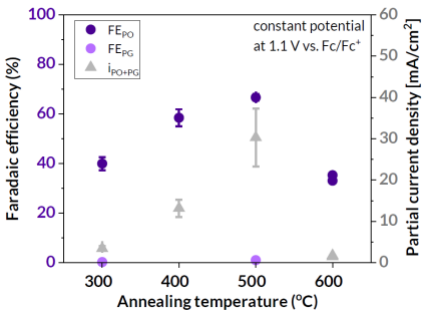


**Figure 2.** Faradaic efficiencies and partial current densities of propylene epoxidation with different Pd and Pt annealing temperatures within the water-acetonitrile blended electrolyte. Potentials in this figure were 100% iR-compensated (i, current; R, resistance). The error bars show standard deviations from the mean of multiple replicate measurements ($n$ = 3) of the same condition and material.

With this understanding of the active site, we sought to understand the reaction mechanism by measuring partial current densities at varying potentials and substrate concentrations and fitting these data to analytical models. These data show a measured Tafel slope of 119 ± 5 mV decade$^{-1}$ (**Figure 3A**), consistent with a rate-limiting step involving a single electron transfer step and no pre-equilibrated electron transfer steps occurring between the most abundant reactive intermediate and kinetically relevant step. The rate also shows an approximately 2$^{nd}$-order dependence on the concentration of water that approaches a near 1$^{st}$-order dependence at higher water concentrations (**Figure 3B**). By comparison, the rate shows a nearly linear dependence on the pressure of propylene that approaches 0$^{th}$-order behaviors at the greatest pressures of propylene (**Figure 3C**), consistent with significant changes in the coverage of water and propylene-derived species on the surface of $PdPtO_x$. Kinetic modeling of these data combined with kinetic isotope effect measurements ($k_H/k_D$ = 1.8) are most consistent with a rate-limiting step involving the formation of

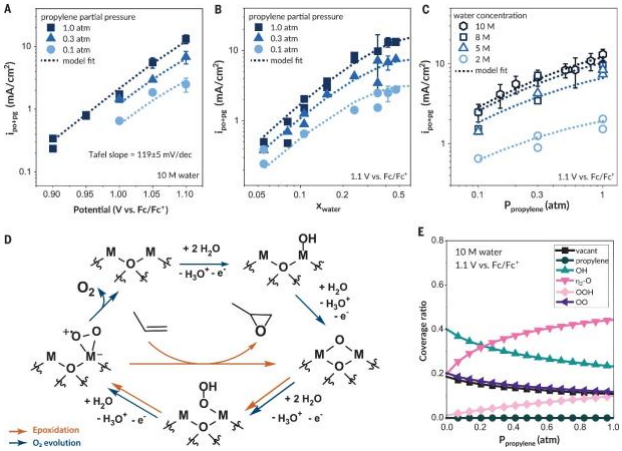


**Figure 3.** Dependence of anodic partial current densities of the combined formation of propylene oxide (PO) and propylene glycol (PG) as a function of (**A**) applied potential at 0.1-1.0 atm of propylene with 10 M water (**B**) water mole fraction at 0.1-1.0 atm of propylene at 1.1 V vs. Fc/Fc$^+$ (**C**) propylene partial pressure at 2-10 M water at 1.1 V vs. Fc/Fc$^+$. All measurements were conducted using a solution of 0.4 M tetrabutylammonium tetrafluoroborate ($TBABF_4$) in acetonitrile, in which the reported potentials were 100% iR-compensated (i, current; R, resistance). These data were used to postulate (**D**) a putative reaction mechanism for direct epoxidation of propylene and evolution of oxygen on the anodic catalyst surface. These proposed elementary steps were used to develop an analytical model fit to these data to (**E**) simulate the propylene partial-pressure dependences of intermediate species coverage at 10 M water and 1.1 V versus Fc/Fc$^+$. Vertical error bars represent standard deviations from the mean of multiple replicates ($n$ = 3) of the same experiment.

hydroperoxy species (OOH*) from monoatomic oxygen (O*) and $H_2O$ (**Figure 3D**). Still, the kinetic modeling and measurements using stilbene suggest that the selectivity of epoxide formation likely depends on the relative rate of reacting OO* species with propylene versus the rate that OO* desorbs from the surface as molecular oxygen ($O_2$). With this plausible mechanism, these data also provide predictions for the coverage of reactive surface species as a function of reactant concentrations (**Figure 3E**). Ultimately, this mechanistic understanding provides a basis for designing more effective epoxidation catalysts by tuning the electrophilic character of oxygen ligands formed upon mixed metal oxide surfaces.

### *Role of electrolyte composition on catalytic performance and stability*

With the development of highly selective catalysts with industrially relevant current densities, we next sought to understand the role of the electrolyte on the performance and long-term stability of $PdPtO_x$, particularly within aqueous electrolytes. First, we investigated the role of the supporting electrolyte in aqueous media, in which we found that the greatest faradaic efficiency to epoxidation and glycol formation (~55% ± 2%) was achieved during chronopotentiometry measurements (50 mA) at neutral pH conditions (5-8) using electrolyte solutions buffered by phosphate salts (i.e., $NaH_2PO_4$, $Na_2HPO_4$). Notably, the dependence of Faradaic efficiency on pH was weak between values of 1-12. Still, highly acidic conditions (pH < 4) led to significant propylene glycol formation from acid-catalyzed hydrolysis of the epoxide. We also screened 13 different supporting electrolytes, including halides (NaCl, NaBr, NaI, NaF) and inorganic salts ($Na_xH_yPO_4$, $NaSO_4$, $NaNO_3$, $NaClO_4$, NaOH, etc.). Generally, the use of halides led to the in situ generation of halogen compounds that were sometimes beneficial for epoxidation (e.g., $Cl_2$, $Br_2$). For the inorganic salts, the highest performance of epoxidation was achieved using phosphate buffers ($Na_xH_yPO_4$) and perchlorate ($NaClO_4$) at neutral pH conditions at an ionic strength of 1.2 M.

Next, we considered the long-term stability of PdPtOx in blended and aqueous electrolyte media to maintain performance for extended reaction periods. First, we constructed a recirculating batch reactor to measure the continuous accumulation of propylene oxide (**Figure 4A**) over 3 hours within a blended electrolyte (**Figure 4B**) during chronopotentiometry measurements (50 mA). The rate and Faradaic efficiency remained mostly constant during chronopotentiometry measurements. By comparison, the aqueous electrolyte systems deactivate far more rapidly, in which Faradaic efficiency declines from ~55% to <10% during the first hour of operation during chronopotentiometry measurements (50 mA). This loss of reactivity can result from physical changes in the system (e.g., flooding, degradation of electrodes), but further development of the electrode architectures now suggests that catalyst restructuring is the primary means of deactivation within the aqueous electrolyte media. Overall, our preliminary findings show that blended electrolytes may inhibit the restructuring of PdPtOx, which is greatly accelerated within

aqueous electrolyte solutions with high concentrations of salt (>1.2 M) at high current densities (50 mA). Furthermore, these efforts to understand and eliminate the deactivation of the PdPtOx in aqueous media will enable the use of more economical and environmentally benign solvents for later commercial applications of this technology.

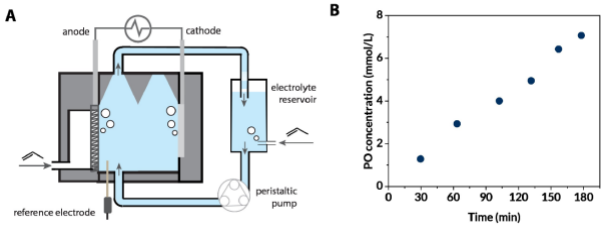


**Figure 4. (A)** A process flow diagram for a recirculating batch reactor, in which propylene is sparged through a gas diffusion electrode with flowing electrolyte that pumps from a reservoir. **(B)** Accumulation of propylene oxide within the electrolyte reservoir during recirculating batch measurements over 3 hours within an electrolyte of 0.4 M TBABF4 and 10 M water in acetonitrile at a constant current density of 50 mA/cm$^2$.

### *Key Outcomes*

In summary, we synthesized PdPtOx materials and studied their electronic and geometric structures for the electrochemical epoxidation of propylene using XPS and *operando* XAS. The 1:1 Pd to Pt alloy prepared at 500°C showed the greatest rates and selectivities of propylene epoxidation. We also determined the mechanism of epoxidation on this material, providing evidence that $Pt^{2+}$ species stabilize highly reactive OO* species that are highly electrophilic and implicated in the selective and reactive formation of propylene oxide. We then investigated the role of the electrolyte on catalytic performance and stability, in which neutral pH conditions with phosphate and perchlorate salts show the highest faradaic efficiencies of epoxidation in aqueous solutions but lead to much greater rates of deactivation compared to blended electrolytes. Overall, our findings highlight the design of materials that achieve industrially relevant current densities and selectivities for producing hydrogen and epoxides.

### Publications Acknowledging this Grant in 2021-2024

*(I) Intellectually led by this grant:*


1. Chung, M.; Jin, K.; Zeng, J. S.; Ton, T.; Manthiram, K. Tuning single atom dopants on manganese oxide for selective electrocatalytic cyclooctene epoxidation. *Journal of the American Chemical Society* **2022**, 144, 17416-17422.
2. Chung, M.; Maalouf, J. H.; Adams, J. S.; Jiang, C.; Román-Leshkov, Y.; K. Manthiram. Direct propylene epoxidation via water activation over Pd-Pt electrocatalysts. *Science* **2024**, 383, 49-55.

# Well-Defined Molecule-Based Heterogeneous Catalysts for Challenging Reactions

Tobin Marks and Michael Bedzyk
Northwestern University

## Presentation Abstract

The goal of this hypothesis-driven effort is to create, understand, and intelligently implement the molecule-support complex as a unique catalytic entity. We focus on two closely related SSHC (Single Site Heterogeneous Catalyst) systems having in common: earth-abundant high oxidation state transition metals tightly bound to earth-abundant supports, unusual reactivity patterns, shared catalyst evaluation methodologies, high percentages of catalytically significant sites, characterization conventional and emerging physical techniques, and closely interfaced theorical analysis of both systems. The goal is to understand catalyst-support structure-function-mechanism relationships in systems lying between homogeneous and heterogeneous catalysis. These are:

- *Electrophilic early transition metal alkyl and hydride cations electrostatically bound to highly Brønsted acidic functionalized oxides.* How can Zr $d^0$ catalysts rapidly polymerize olefins, hydrogenate arenes with high chemo- and facial-selectivity, and rapidly, selectively hydrogenolyze diverse polyolefins at unprecedented rates under very mild conditions?
- *Earth-abundant high-valent early transition metal-oxo complexes covalently bound to a variety of carbons, ranging from activated carbons to graphenes to carbon nanohorns.* How do these Mo $d^0$ complexes catalyze rapid alcohol dehydration and dehydrogenation, ester transesterification, N-oxide and sulfoxide reduction, alcohol dehydrogenation, as well as solventless and selective polyethylene terephthalate deconstruction under very mild conditions?

This effort is strengthened by leveraging close collaborations with U.S. National Laboratories and US industry, as well as specialists abroad.

**Award Number DOE DE-SC0024448.** "**Well-Defined Molecule-Based Heterogeneous Catalysts for Challenging Reactions"**

**Postdoc(s):** Yosi Kratish, Qingheng Lai
**Student(s):** Alex Mason, Carter Edenfield, Amol Agarwal

## RECENT PROGRESS

### *Electrophilic early transition metal alkyl and hydride cations electrostatically bound to highly Brønsted acidic functionalized oxide supports*

***Group 4 Complexes.*** A homologous series of cationic electrophilic group IV metal hydrides (M = Ti, Zr, Hf) created by chemisorption of the corresponding $MNp_4$ precursors on highly Brønsted acidic sulfated alumina (AlS) to yield loosely coordinated surface AlS/$MNp_2$ (Np = neopentyl) species (**Fig. 1**) are systematically characterized by ICP, EXAFS/XANES, DRIFTS, and solid-state high-resolution multi-dimensional NMR spectroscopy (SSNMR), as well as by energy span DFT computation. With effective stirring, these complexes readily undergo reaction with $H_2$ to yield AlS/M(alkyl)H species which are highly active for the hydrogenolysis of diverse commercial polyethylenes, α-olefin-ethylene copolymers, isotactic polypropylene, and post-consumer polyolefins including high-density polyethylenes, yielding medium and small linear and branched hydrocarbons at turnover frequencies as high as 36,300 $h^{-1}$ at 200 °C/17 atm $H_2$ for M = Zr. For a given polyolefin and reaction conditions, turnover frequencies scale approximately as M = Zr > Hf > Ti, while catalyst thermal stability scales approximately as M = Hf ≈ Zr > Ti, and these trends are qualitatively

understandable from the DFT analysis. These catalytic results reveal that the AlS/Hf(R)H-mediated hydrogenolysis favors wax-like and liquid products while the AlS/Zr(R)H-mediated hydrogen-olysis can be tuned between gases and liquids. DFT analysis identifies β-alkyl elimination as the turnover-limiting C-C scission process, which is particularly facile in these cationic $d^0$ complexes, but not so in the neutrally charged analogues. The relative activity trend of Zr >> Hf > Ti, is consistent with the relative DFT computed energy barriers. The AlS/$MNp_2$ thermal stability trend is Hf ≈ Zr > Ti, which is consistent with the approximate thermal stability of the $MNp_4$ precursors. The energy span DFT analysis implicates β-alkyl elimination as the turnover-limiting C-C scission step which is extremely facile in these cationic $d^0$ complexes.

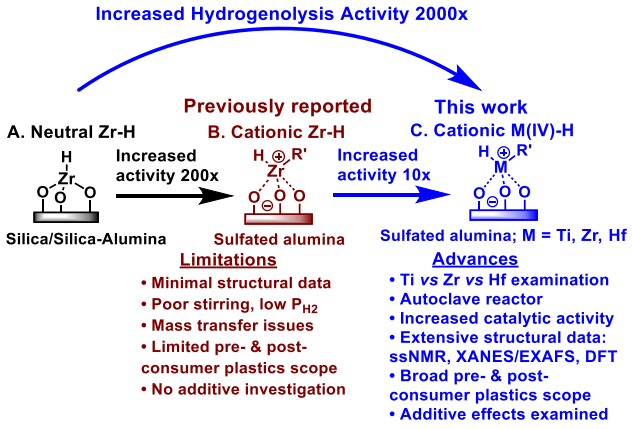


**Figure 1**. Catalytic properties of single-site heterogeneous organo-group IV catalysts **A**. Neutrally charged Zr hydrocarbyl adsorbate on a weak Brønsted acid surface[28], **B.** Previously reported cationic AlS/Zr(R)H on a very strong sulfated alumina (AlS) Brønsted acidic surface and limitations, **C.** Generalized cationic AlS/M(R)H catalysts on sulfated alumina (M = Ti, Zr, Hf), and advances reported in this work.

***Group 5 Complexes.*** Formally neutrally charged surface organo-tantalum species chemisorbed on silica were first studied and characterized by this Laboratory and Basset nearly 20 years ago. However, catalysis of polyolefin hydrogenolysis was sparsely examined in the 1990s, with the main focus being alkane metathesis Furthermore, the reported qualitatively higher thermal stability of the supported organo-Ta over the organo-Zr adsorbates motivated us to address the intriguing question of whether the AlS support might yield a formally isoelectronic cationic $d^0$ Ta adsorbate, whether and to what degree, it might be active for efficient and broad-scope polyolefin hydrogenolysis, and whether the presence of potentially alternative established reaction pathways, such as α-alkyl transfer (carbene extrusion), alkane metathesis, and α-hydride elimination followed by olefin metathesis might alter polyolefin hydrogenolysis pathways. In this work we achieved the synthesis of highly active cationic surface organo-Ta complex(es) prepared by chemisorbing the well-defined alkylidene $Np_3Ta{=}CH^tBu$ "super acidic" sulfated alumina (AlS). The resulting catalyst (**1**), which surprisingly contains two different surface cationic Ta species, was characterized by ICP, DRIFTS, multinuclear/multi-dimensional solid-state NMR (SSNMR) spectroscopy, XANES/EXAFS, and the resulting structural formulation is in good agreement with the DFT-derived structure (**Fig. 2**). This supported Ta catalyst has very high thermal stability and exceptionally high polyolefin hydrogenolysis activity-- as high as 9800 $(CH_2$ units)·mol(Ta)$^{-1}$·h$^{-1}$ at 200 °C/17 atm $H_2$. Moreover, AlS/$TaNp_x$ is effective in hydrogenolysis of pristine, pre-, and post-consumer polyethylenes and α-olefin-polyethylene copolymers, including water bottle caps, sandwich bags, milk jugs, and mixed plastics with commercial additives.

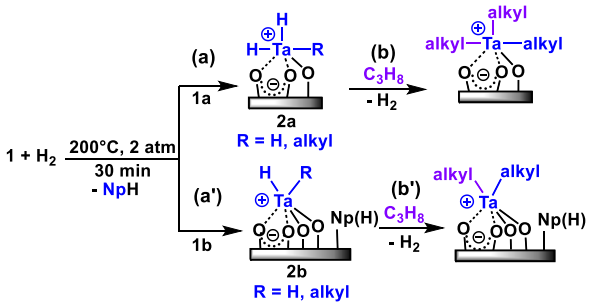


**Fig. 2.** Synthesis of cationic single-site tantalum hydrides and their reaction with propane .

To the best of our knowledge, catalyst **1** exhibits one of the highest polyolefin hydrogenolysis activities reported to date in the peer-reviewed literature. Unlike the AlS/$ZrNp_2$ analog, the Ta catalyst is more thermally robust and offers multiple potential reaction pathways for C-C scission. Catalyst **1** is also compatible with a wide variety of pre-and post-consumer plastics and is not extensively deactivated in the presence of standard commercial polymer additives under the present reaction conditions.

***Demystifying Group-4 Polyolefin Hydrogenolysis Catalysis. Gaseous Propane Hydrogenolysis Mechanism over the Same Catalysts.*** Catalytic hydrogenolysis is promising for converting waste polyolefins into useful products. A heterogeneous catalyst class AlS/$MNp_2$ (M = Zr, Hf; AlS = sulfated alumina; Np = neopentyl) prepared from well-defined molecular precursors is active for efficient solvent-free hydrogenolysis. Nevertheless, mechanistic studies are challenged by a reaction medium complexity having polymers and hydrogenolysis products of widely time-varying viscosity, complex stirring/mixing characteristics, and unknown catalyst thermal stability. Here the analysis is simplified using a model small alkane reactant and heterogeneous reactor techniques.

A kinetic/mechanistic investigation of gaseous propane hydrogenolysis over the single-site heterogeneous polyolefin depolymerization catalysts AlS/$ZrNp_2$ and AlS/$HfNp_2$ (AlS = sulfated alumina, Np = neopentyl), is used to probe intrinsic catalyst properties without the complexities introduced by time- and viscosity-dependent polymer medium effects. In a polymer-free automated plug-flow catalytic reactor, propane hydrogenolysis turnover frequencies approach 3000 $h^{-1}$ at 150°C. Both catalysts exhibit approximately linear relationships between rate and [$H_2$] at substoichiometric [H2] with rate law orders of 0.66 ± 0.09 and 0.48 ± 0.07 for Hf and Zr, respectively; at higher [$H_2$], the rates approach zero-order in [$H_2$]. Reaction orders in [$C_3H_8$] and [catalyst] are essentially zero-order under all conditions, with the former implying rapid, irreversible alkane binding/activation. This rate law, activation parameter, and DFT energy span analysis support a scenario in which [$H_2$] is pivotal in one of two plausible and competing rate-determining transition states -- bimolecular metal-alkyl bond hydrogenolysis versus unimolecular β-alkyl elimination. That is, the e law and DFT analyses indicate competition between bimolecular metal-alkyl bond hydrogenolysis and unimolecular β-alkyl elimination as rate-determining transition states. The Zr and Hf catalyst activation parameters, $\Delta H^{\ddagger}$ = 16.8 ± 0.2 kcal·$mol^{-1}$ and 18.2 ± 0.6 kcal·$mol^{-1}$, respectively, track the relative turnover frequencies, while $\Delta S^{\ddagger}$ = -19.1 ± 0.8 and -16.7 ± 1.4 cal·$mol^{-1}$·$K^{-1}$, respectively, imply highly organized transition states. These catalysts maintain activity up to 200°C, while time-on-stream data indicate multi-day activities with an extrapolated turnover number ~92,000 at 150°C for the Zr catalyst.

***Synthesis and Characterization of a Single-Site Mo(=O)$_2$ Catalytic Functionality Anchored on Reduced Graphene Oxide.*** A single-site molybdenum dioxo catalyst, rGO/$MoO_2$ is prepared via direct grafting of (dme)$MoO_2Cl_2$ onto reduced graphene oxide (rGO). The physiochemical and chemical properties of the (dme)$MoO_2Cl_2$ precursor, the rGO support (**Fig. 3**), and the supported catalyst were extensively characterized by NMR spectroscopy, ICP-OES, single-crystal XRD, XPS, DRIFTS and Raman spectroscopy, PXRD, $N_2$ physisorption, $NH_3$-TPD, advancing aqueous contact angle analysis, EXAFS, and DFT computation. The precise cis-$MoO_2$ geometry of the (dme)$MoO_2Cl_2$ complex was assessed by single-crystal XRD and DRIFTS. XPS shows that rGO has sufficient surface hydroxyl coverage to function as a support, adsorbing 0.28 $MoO_2$/$nm^2$. The contact angle data show that the rGO/$MoO_2$ surface is more hydrophobic than that of rGO, likely reflecting surface hydroxyl consumption on $MoO_2$ chemisorption. The DRIFTS data are in EXAFS structural data align well with those of model compounds, other Carbon/$MoO_2$ catalysts, and DFT computation, providing an atomic-level description of the active site structure and agreement with those for cis-$MoO_2$ model complexes and DFT computation. The rGO/$MoO_2$ catalyst shows good catalytic activity for

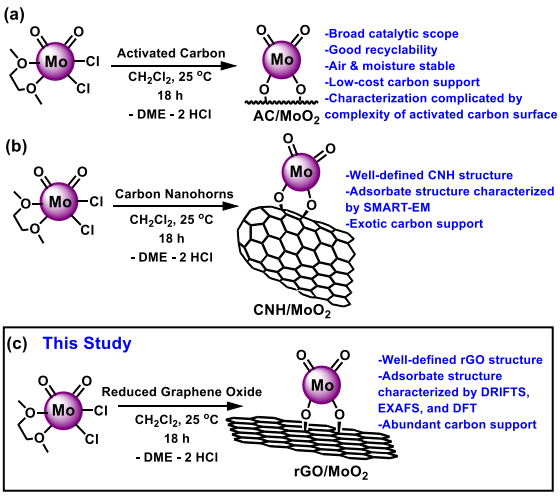


**Fig. 3.** Synthesis of (**a**) AC/$MoO_2$. (b) CNH/$MoO_2$. (**c**) rGO/$MoO_2$ single-site heterogeneous catalysts**.**

reductive carbonyl coupling and N-oxide reductions, rendering it a well-defined and efficient single-site heterogeneous catalytic system.

**Publications Acknowledging this Grant in 2021-2024.** All intellectually led by this Grant


1. Edenfield, W.C.; Mason, A.H.; Lai, Q.; Agarwal, A.; Kobayashi, T.; Kratish, Y.; Marks; T.J.; Rapid Polyolefin Plastics Hydrogenolysis Mediated by Single-Site Heterogeneous Electrophilic/Cationic Organo-Group IV Catalysts, ACS Catalysis, 2024, 14, 554–565. DOI: 10.1021/acscatal.3c05161.

2. Agarwal, A.; Liu, Y.; Kraevaya, O.A.; Troshin, P.A.; Kratish, Y.; Marks, T.J.; Creation and Structure-Function Characterization of a Single-Site MoO2 Epoxidation Catalyst Supported on a Fullerene Scaffold, ChemCatChem, 2024, in press. DOI:10.1002/cctc.202401259.

3. Mason, A.H.; Motta, A.; Kratish, Y.; Marks, T.J.; Demystifying Group-4 Polyolefin Hydrogenolysis Catalysis. Gaseous Propane Hydrogenolysis Mechanism over the Same Catalysts, 2024, PNAS, 121, e2406133121. DOI: 10.1073/pnas.2406133121.

4. Liu, Y.; Agarwal, A.; Kratish, Y.; Marks, T.J.; Aldehyde and Ketone Hydroboration Mediated by a Heterogeneous Single-Site Molybdenum-Dioxo Catalyst: Scope and Mechanistic Implications, ChemCatChem, 2024, 16, DOI: 10.1002/cctc.202301417.

5. Lai, Q.; Mason, A.H.; Agarwal, A.; Edenfield, W.C.; Zhang, X.; Kobayashi T.; Kratish, Y.; Marks, T.C.; Rapid Polyolefin Hydrogenolysis by a Single-Site Organo-Tantalum Catalyst on a Super-Acidic Support. Structure and Mechanism., Angew Chemie., 2023, 62, e202312546. DOI: 10.1002/anie.202312546.

6. Kratish, Y.; Marks, T.J.; Efficient Polyester Hydrogenolytic Deconstruction via Tandem Catalysis, Angew. Chem. Int. Ed. 2021, 61, e202112576. DOI: 10.1002/anie.202112576.

7. Zhang, J.; Mason, A.; Motta, A.; Cesar, L.; Kratish, Y.; Lohr, T.; Miller, J.; Gao, Y.; Marks, T.J.; Surface vs Homogeneous Organo-Hafnium Catalyst Ion-Pairing and Ligand Effects on Ethylene Homo- and Copolymerizations, ACS Catalysis 2021, 11, 3239-3250. DOI: 10.1021/acscatal.0c

8. Liu, Y.; Agarwal, A.; Kratish, Y.; Marks, T.J.; Aldehyde and Ketone Hydroboration Mediated by a Heterogeneous Single-Site Molybdenum-Dioxo Catalyst: Scope and Mechanistic Implications, ChemCatChem, 2024, 16, DOI: 10.1002/cctc.202301417.

9. Mason, A. H.; Motta, A.; Das, A.; Ma, Q.; Bedzyk, M. J.; Kratish, Y.; Marks, T. J., Rapid Atom-Efficient Polyolefin Plastics Hydrogenolysis Mediated by a Well-Defined Single-Site Electrophilic/Cationic
Organo-Zirconium Catalyst, Nature Commun, 2022, 13, 7187-7199. DOI:10.1038/s41467-022-34707-6.

10. Li, J.; Das, A.; Ma, Q.; Bedzyk, M.J.; Kratish, Y.; Marks, T.J.; Diverse Mechanistic Pathways in Single-Site Heterogeneous Catalysis. Alcohol Conversions Mediated by a High-Valent Carbon-Supported Molybdenum-Dioxo Catalyst, ACS Catalysis, 2022, 12, 1247–1257. DOI: 10.1021/acscatal.1c04319.

11. Zhang, J.; Mason, A.H.; Wang, Y.; Motta, A.; Kobayashi, T.; Pruski, M.; Gao, Y.; Marks, T.J.; Beyond the Active Site. Cp*$ZrMe_3$/Sulfated Alumina-Catalyzed Olefin Polymerization Tacticity via Catalyst···Surface Ion-Pairing, ChemCatChem, 2021, 13, 2564-2569. DOI: 10.1002/cctc.202100406.

12. Liu, Y.; Li, J.; Das, A.; Kim, H.; Jones, L.O.; Ma, Q.; Bedzyk, M.J.; Schatz, G.C.; Kratish, Y.; Marks, T.J.; Synthesis and Structure–Activity Characterization of a Single-Site MoO2 Catalytic Center Anchored on Reduced Graphene Oxide, J. Amer. Chem. Soc. 2021, 143, 21532–21540. DOI: 10.1021/jacs.1c07236.

13. Kratish, Y.; Nakamuro, T.; Liu, Y.; Li, J.; Tomotsuka, I.; Harano, K.; Nakamura, E.; Marks, T.J.; Synthesis and Characterization of a Well-Defined Carbon Nanohorn-Supported Molybdenum Dioxo Catalyst by SMART-EM Imaging. Surface Structure at the Atomic Level: A contribution to the “Frontiers of Molecular Science, Diamond Collection”, Bull. Chem. Soc. Japan, 2021, 94, 427-432. DOI:10.1246/bcsj20.2020299.

# Atomic-scale Design of Metal and Alloy Catalysts: A Combined Theoretical and Experimental Approach

Manos Mavrikakis,[†] Younan Xia[‡]
[†] Department of Chemical & Biological Engineering, University of Wisconsin–Madison
[‡] School of Chemistry & Biochemistry, Georgia Institute of Technology

## Presentation Abstract

The main objective of this combined theoretical and experimental project is to: *i) design* from first-principles, *ii) synthesize* using advanced *nanosynthesis* techniques, and *iii)* experimentally evaluate *new metal* and *alloy catalysts*, with unique *catalytic* properties for industrially relevant chemical reactions. Measurable impact can be found in several applications, including low-temperature fuel cells, hydrogen production and purification, and production of fuels and chemicals. The importance of the atomic-scale architecture of these new, theoretically designed catalysts, to their unique properties is driving the development of *new inorganic materials synthesis* approaches, which can synthesize the theoretically determined optimal, and in some cases, metastable, nanoscale catalytic architectures.

**Grant or FWP Number: DOE Grant No. DE-FG02-05ER15731** (Atomic-scale Design of Metal and Alloy Catalysts: A Combined Theoretical and Experimental Approach)

**Postdocs** (partially supported by this grant)**:** Lance Kavalsky (UW), Lang Xu (UW)
**Students** (partially supported by this grant)**:** Michael Rebarchik (UW), Jacob Jeskey (GIT)

## RECENT PROGRESS

### *Formation of Active Sites on Metals through Reaction-Driven Migration of Surface Atoms*[1–4]

Elucidating the nature of the active sites on catalytic surfaces *under reaction conditions* is an enormously challenging task. Recent advanced microscopic studies demonstrated adsorbate-induced formation of sub-nanometer clusters on several single-crystal surfaces at near-ambient temperatures and pressures,[5–7] revealing the complex and dynamic nature of metal catalytic surfaces under *reactive* environments. To this end, we performed density functional theory (DFT) and Kinetic Monte Carlo (KMC) calculations to elucidate the conditions that lead to reaction-driven migration of surface atoms on metal catalysts and show how adatom formation energies enable efficient screening of catalytic systems where adsorbate-induced cluster formation may occur. Together with our experimental collaborators (Salmeron/Somorjai group at UC-Berkeley/LBNL) who performed high-pressure scanning tunning microscopy (HP-STM) studies, we showed that the reaction-driven metal-metal bond breaking and surface atom migration on metal surfaces occur

more broadly than previously perceived and could have dramatic consequences on the catalytic properties of the metal nanoparticles.

We established a theoretical framework for predicting adsorbate-induced cluster formation behavior utilizing the DFT-computed adatom formation energy as a single energetic descriptor. We demonstrated that such a framework allowed for proper prediction of the experimental observations that CO induced cluster formation on Cu,[5] but not on Rh[8] and Pt[9] surfaces.

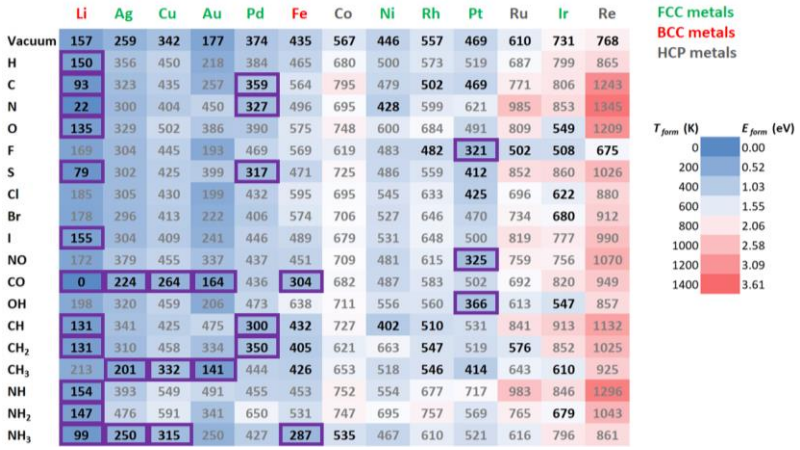


| | Li | Ag | Cu | Au | Pd | Fe | Co | Ni | Rh | Pt | Ru | Ir | Re |
|---|---|---|---|---|---|---|---|---|---|---|---|---|---|
| Vacuum | 157 | 259 | 342 | 177 | 374 | 435 | 567 | 446 | 557 | 469 | 610 | 731 | 768 |
| H | 150 | 356 | 450 | 218 | 384 | 465 | 680 | 500 | 573 | 519 | 687 | 799 | 865 |
| C | 93 | 323 | 435 | 257 | 359 | 564 | 795 | 479 | 502 | 469 | 771 | 806 | 1243 |
| N | 22 | 300 | 404 | 450 | 327 | 496 | 695 | 428 | 599 | 621 | 985 | 853 | 1345 |
| O | 135 | 329 | 502 | 386 | 390 | 575 | 748 | 600 | 684 | 491 | 809 | 549 | 1209 |
| F | 169 | 304 | 445 | 193 | 469 | 569 | 619 | 483 | 482 | 321 | 502 | 508 | 675 |
| S | 79 | 302 | 425 | 399 | 317 | 471 | 725 | 486 | 559 | 412 | 852 | 860 | 1026 |
| Cl | 185 | 305 | 430 | 199 | 432 | 595 | 695 | 545 | 633 | 425 | 696 | 622 | 880 |
| Br | 178 | 296 | 413 | 222 | 406 | 574 | 706 | 527 | 646 | 470 | 734 | 680 | 912 |
| I | 155 | 304 | 409 | 241 | 446 | 489 | 679 | 531 | 648 | 500 | 819 | 777 | 990 |
| NO | 172 | 379 | 455 | 337 | 437 | 451 | 709 | 481 | 615 | 325 | 759 | 756 | 1070 |
| CO | 0 | 224 | 264 | 164 | 436 | 304 | 682 | 487 | 583 | 502 | 692 | 820 | 949 |
| OH | 198 | 320 | 459 | 206 | 473 | 638 | 711 | 556 | 560 | 366 | 613 | 547 | 857 |
| CH | 131 | 341 | 425 | 475 | 300 | 432 | 727 | 402 | 510 | 531 | 841 | 913 | 1132 |
| $CH_2$ | 131 | 310 | 458 | 334 | 350 | 405 | 621 | 663 | 547 | 519 | 576 | 852 | 1025 |
| $CH_3$ | 213 | 201 | 332 | 141 | 444 | 426 | 653 | 518 | 546 | 414 | 643 | 610 | 925 |
| NH | 154 | 393 | 549 | 491 | 455 | 453 | 752 | 554 | 677 | 717 | 983 | 846 | 1296 |
| $NH_2$ | 147 | 476 | 591 | 341 | 650 | 531 | 747 | 695 | 757 | 569 | 765 | 679 | 1043 |
| $NH_3$ | 99 | 250 | 315 | 250 | 427 | 287 | 535 | 467 | 610 | 521 | 616 | 796 | 861 |

**Figure 1.** Heatmap of estimated adsorbate-induced adatom formation temperatures on the close-packed surfaces of FCC, BCC, and HCP metals. In general, kink or step-edge defect is the preferred atom ejection source. Gray-faded numbers indicate systems in which the adsorbate hinders adatom formation. Systems with both a favorable adsorbate effect for adatom formation and adatom formation temperature < 373 K are marked with purple boxes. Metals are listed from left to right in ascending order of experimental bulk cohesive energy. Adapted from data in Refs. 1 and 2.

We then extended this framework to a wide range of metals (face-centered cubic (FCC), body-centered cubic (BCC), and hexagonal close-packed (HCP)) and adsorbates commonly involved in catalytic reactions (Figure 1). Many adsorbate-metal pairs with potential clustering behavior under conditions relevant to industrial catalytic applications were identified, e.g., CO oxidation, water-gas shift, methanol synthesis, ammonia synthesis and oxidation, NO reduction by $H_2$, methane oxidation, Fischer-Tropsch synthesis, and methane steam reforming. For the CO-Cu system, we performed KMC simulations for surface atom migration on Cu(111) under CO exposure and predicted CO-decorated Cu cluster structures similar to those observed in HP-STM experiments.[5] Specifically, Cu trimers, predicted by our DFT calculations to be highly active for CO oxidation, were shown to be present on Cu(111) even after extended periods of simulation time. Additionally, through a combination of HP-STM experiments and DFT calculations, we showed that local dislocation defects could lead to CO-induced cluster formation on Ni(111) at unexpectedly low temperatures (77 K). This can be attributed to combined effects of high CO coverage and large local strain at these defect sites, which drastically reduces the adatom formation energy, demonstrating the rich structure sensitivity in such cluster formation processes.

Our discovery in this series of studies also elucidates a unique "bottom-up" route toward the formation of metal nanoclusters as active catalytic centers. This bottom-up approach is expected to outperform the commonly adopted "top-down" approach of size-selected nanocluster synthesis. The stability of the latter synthesized metal nanoclusters under realistic reaction conditions is often challenged, which is a serious drawback for the top-down approach, while not present in the case of *in-situ* formed clusters.

**A Coverage Self-Consistent Microkinetic Model for Vapor-Phase Formic Acid Decomposition over Pd/C Catalysts**[10]

Formic acid (FA), which can be formed from biomass reforming processes,[11] is a promising hydrogen storage vector due to its low toxicity, low flammability, and high volumetric carrying capacity.[12,13] An efficient catalyst is required for FA decomposition to produce $CO_2$ and extractable $H_2$. Carbon-supported palladium (Pd/C) has been identified as one of the most active catalysts for FA decomposition.[14,15] To further elucidate the mechanism and catalytically active sites for this reaction, we employed DFT calculations and reaction kinetics experiments to develop a *coverage-cognizant* microkinetic model to better understand FA decomposition on Pd/C catalysts.

DFT energetics for FA decomposition were developed on both Pd(111) and Pd(100) as possible active site models for the Pd/C catalyst. In our microkinetic model, we considered a comprehensive reaction network (26 elementary steps in total) including both the dehydrogenation path (forming $CO_2$* as an adsorbed intermediate) and the dehydration path (forming CO* as an adsorbed intermediate). Parameter fitting of DFT-calculated energetics on Pd(111) and Pd(100) to reaction kinetics measurements was conducted until an agreement was reached between experiments and theory in terms of both reaction rates and surface coverages. The microkinetic models formulated using DFT energetics on clean Pd(111) and Pd(100) predicted FA decomposition rates several orders of magnitude lower than the experimental rates. The extremely low reaction rates were caused by high surface coverages of CO* (~0.99 and ~0.90 monolayer (ML) for Pd(100) and Pd(111), respectively) predicted by the microkinetic models, which contradict the assumption of a clean surface used in the original DFT calculations. Consequently, the microkinetic models were reformulated using DFT energetics calculated on CO-decorated (0.55 ML) Pd(111) and Pd(100). On the 0.55 ML CO-decorated Pd(100) model only a subset of the experimental turnover frequencies (TOFs) for the dehydrogenation path could be rationalized, and the observed selectivity towards FA decomposition through the dehydration path could not be explained. In contrast, the CO-decorated Pd(111) model (Figure 2) was able to explain the entire experimental dataset, including reactions proceeding through both the dehydrogenation and dehydration paths. These results demonstrate that CO-decorated Pd(111) can be used to represent the active site for FA decomposition on Pd/C catalysts with minimal parameter adjustments.

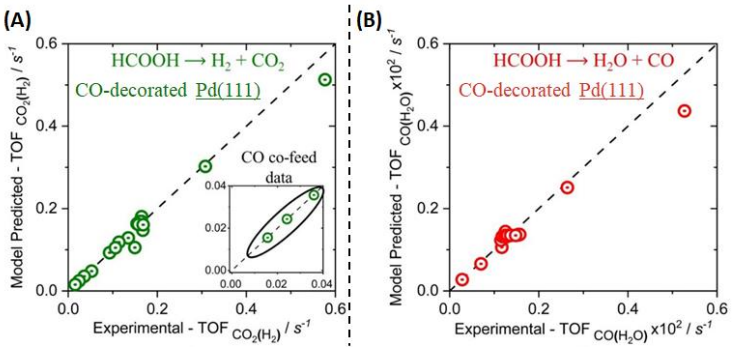


**Figure 2.** Parity plot of the CO*-coverage-cognizant Pd(111) model predicted vs experimental TOFs for **(A)** dehydrogenation and **(B)** dehydration pathways. The CO-decorated Pd(111) model yielded high parity for both experimental datasets, indicating that this model can represent the active site in Pd/C catalysts under realistic reaction conditions. From Ref. [23].

This work further highlights the utility of our combined experimental and computational modeling approach towards elucidating reaction mechanisms and the nature of catalytically active sites, particularly under *in-operando* conditions.

## The Role of Coverage Effects on the Structure–Sensitivity of Formic Acid Electrooxidation on Pd Surfaces[16]

In addition to thermal decomposition of FA, direct formic acid fuel cells (DFAFCs) serve as another promising candidate for the employment of FA as a highly efficient and portable energy carrier. Compared to Pt, Pd catalysts are less prone to CO* poisoning and have been demonstrated to outperform Pt catalysts in FA electrooxidation (FAO) activity.[17] FAO on Pd catalysts is, however, experimentally shown to be highly structure-sensitive[18,19] and prone to notable CO accumulation.[20] To study the effects of CO* coverage and the structure-sensitivity of Pd FAO electrocatalysts, we performed DFT calculations for the Gibbs Free Energy of FAO using realistic CO* coverages on four Pd facets: (111), (100), (110), and (211), and under relevant conditions (0.00 V – 0.40 V vs. the reversible hydrogen electrode (RHE)).

Our results predicted saturation coverages of CO* of 0.11-0.55 ML for Pd(111) and Pd(211), 0.11-0.66 ML for Pd(100), and 0.33-1.00 ML for Pd(110) over the range of applied potentials considered. The large and variable saturation coverages on each of the considered facets provides strong evidence that CO* coverage effects may prove considerable factors in determining the activity of Pd electrocatalysts for FAO. We then generated CO*-*coverage-cognizant* Gibbs free energy diagrams for applied potentials of 0.00 V, 0.20 V, and 0.40 V vs. RHE for Pd(111), (100), (110), and (211) through two FAO paths, namely a direct route proceeding through COOH* or HCOO* intermediates, and an indirect route proceeding exclusively via COOH* to yield CO* and $H_2O$. Using the DFT-derived energetics, we assessed the performance descriptors for FAO over Pd surfaces, which include difference in Gibbs free energies between COOH* and HCOO* ($\Delta G_{COOH-HCOO}$) and the $H_2O$ activation potential for Pd(111), Pd(100), and Pd(211) (Figure 3; Pd(110) were excluded due to strong CO* surface poisoning). Pd(100) emerged as the most promising facet at intermediate applied potentials (0.20 V vs. RHE) due to a low onset potential required for the HCOO*-mediated pathway and its ability to destabilize COOH* intermediates (thus preventing CO* formation). As the next most promising facet, Pd(211) stabilized COOH* relatively stronger compared to HCOO*, yet retained a smaller $H_2O$ activation potential at 0.20 V vs. RHE compared to both Pd(111) and Pd(100) (Figure 3B). The lower $H_2O$ activation potential translated to an easier CO* removal from the surface through its oxidation to $CO_2$, thereby reducing surface poisoning by CO*. Overall, we predicted the order of FAO activity on Pd surfaces to follow Pd(100) > Pd(211) > Pd(111) > Pd(110), in accord with past experimental results involving single crystal electrodes and nanocrystals.[18,21,22]

This work provides an accurate description of Pd surfaces under realistic FAO reaction conditions and highlights opportunities for developing improved FAO electrocatalysts through facet engineering.

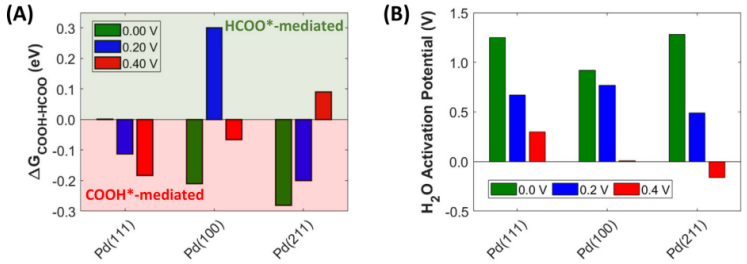


**Figure 3.** CO*-coverage-cognizant **(A)** difference in Gibbs free energies between COOH* and HCOO* ($\Delta G_{COOH-HCOO}$) and **(B)** the $H_2O$ activation potential for Pd(111), Pd(100), and Pd(211). From Ref. [24].

## References


(1) Xu, L.; Papanikolaou, K. G.; Lechner, B. A. J.; Je, L.; Somorjai, G. A.; Salmeron, M.; Mavrikakis, M. Formation of Active Sites on Transition Metals through Reaction-Driven Migration of Surface Atoms. *Science* **2023**, *380*, 70–76.

(2) Xu, L.; Mavrikakis, M. Adsorbate-Induced Adatom Formation on Lithium, Iron, Cobalt, Ruthenium, and Rhenium Surfaces. *JACS Au* **2023**, *3*, 2216–2225.

(3) Xu, L.; Rebarchik, M.; Bhandari, S.; Mavrikakis, M. Adsorbate-Induced Adatom Formation on Au-Cu Bimetallic Alloys and Its Possible Consequences for $CO_2$ Electroreduction. *Surf. Sci.* **2024**, 122613.

(4) Xu, L.; Mavrikakis, M. Structure Sensitivity in Adsorbate-Induced Adatom Formation on FCC Transition-Metal Surfaces. *J. Catal.* **2024**, *431*, 115373.

(5) Eren, B.; Zherebetskyy, D.; Patera, L. L.; Wu, C. H.; Bluhm, H.; Africh, C.; Wang, L.-W.; Somorjai, G. A.; Salmeron, M. Activation of Cu(111) Surface by Decomposition into Nanoclusters Driven by CO Adsorption. *Science* **2016**, *351*, 475–478.

(6) Eren, B.; Torres, D.; Karslıoğlu, O.; Liu, Z.; Wu, C. H.; Stacchiola, D.; Bluhm, H.; Somorjai, G. A.; Salmeron, M. Structure of Copper–Cobalt Surface Alloys in Equilibrium with Carbon Monoxide Gas. *J. Am. Chem. Soc.* **2018**, *140*, 6575–6581.

(7) Roiaz, M.; Falivene, L.; Rameshan, C.; Cavallo, L.; Kozlov, S. M.; Rupprechter, G. Roughening of Copper (100) at Elevated CO Pressure: Cu Adatom and Cluster Formation Enable CO Dissociation. *J. Phys. Chem. C* **2019**, *123*, 8112–8121.

(8) Cernota, P.; Rider, K.; Yoon, H. A.; Salmeron, M.; Somorjai, G. Dense Structures Formed by CO on Rh(111) Studied by Scanning Tunneling Microscopy. *Surf. Sci.* **2000**, *445*, 249–255.

(9) Longwitz, S. R.; Schnadt, J.; Vestergaard, E. K.; Vang, R. T.; Lægsgaard, E.; Stensgaard, I.; Brune, H.; Besenbacher, F. High-Coverage Structures of Carbon Monoxide Adsorbed on Pt(111) Studied by High-Pressure Scanning Tunneling Microscopy. *J. Phys. Chem. B* **2004**, *108*, 14497–14502.

(10) Bhandari, S.; Rangarajan, S.; Li, S.; Scaranto, J.; Singh, S.; Maravelias, C. T.; Dumesic, J. A.; Mavrikakis, M. A Coverage Self-Consistent Microkinetic Model for Vapor-Phase Formic Acid Decomposition over Pd/C Catalysts. *ACS Catal.* **2023**, *13*, 3655–3667.

(11) Alonso, D. M.; Bond, J. Q.; Dumesic, J. A. Catalytic Conversion of Biomass to Biofuels. *Green Chem.* **2010**, *12*, 1493–1513.

(12) Mellmann, D.; Sponholz, P.; Junge, H.; Beller, M. Formic Acid as a Hydrogen Storage Material – Development of Homogeneous Catalysts for Selective Hydrogen Release. *Chem. Soc. Rev.* **2016**, *45*, 3954–3988.

(13) Grasemann, M.; Laurenczy, G. Formic Acid as a Hydrogen Source – Recent Developments and Future Trends. *Energy Environ. Sci.* **2012**, *5*, 8171–8181.

(14) Bulushev, D. A.; Jia, L.; Beloshapkin, S.; Ross, J. R. H. Improved Hydrogen Production from Formic Acid on a Pd/C Catalyst Doped by Potassium. *Chem. Commun.* **2012**, *48*, 4184.

(15) Zacharska, M.; Bulusheva, L. G.; Lisitsyn, A. S.; Beloshapkin, S.; Guo, Y.; Chuvilin, A. L.; Shlyakhova, E. V.; Podyacheva, O. Y.; Leahy, J. J.; Okotrub, A. V.; Bulushev, D. A. Factors Influencing the Performance of Pd/C Catalysts in the Green Production of Hydrogen from Formic Acid. *ChemSusChem* **2017**, *10*, 720–730.

(16) Papanikolaou, K. G.; Shi, Y.; Schimmenti, R.; Xia, Y.; Mavrikakis, M. The Role of Coverage Effects on the Structure–Sensitivity of Formic Acid Electrooxidation on Pd Surfaces. *J. Catal.* **2023**, *417*, 408–420.
(17) Capon, A.; Parsons, R. The Oxidation of Formic Acid on Noble Metal Electrodes. *J. Electroanal. Chem. Interfacial Electrochem.* **1973**, *44*, 239–254.
(18) Hoshi, N.; Kida, K.; Nakamura, M.; Nakada, M.; Osada, K. Structural Effects of Electrochemical Oxidation of Formic Acid on Single Crystal Electrodes of Palladium. *J. Phys. Chem. B* **2006**, *110*, 12480–12484.
(19) Jin, M.; Zhang, H.; Xie, Z.; Xia, Y. Palladium Nanocrystals Enclosed by {100} and {111} Facets in Controlled Proportions and Their Catalytic Activities for Formic Acid Oxidation. *Energy Environ. Sci.* **2012**, *5*, 6352–6357.
(20) Miyake, H.; Okada, T.; Samjeské, G.; Osawa, M. Formic Acid Electrooxidation on Pd in Acidic Solutions Studied by Surface-Enhanced Infrared Absorption Spectroscopy. *Phys. Chem. Chem. Phys.* **2008**, *10*, 3662.
(21) Vidal-Iglesias, F. J.; Arán-Ais, R. M.; Solla-Gullón, J.; Garnier, E.; Herrero, E.; Aldaz, A.; Feliu, J. M. Shape-Dependent Electrocatalysis: Formic Acid Electrooxidation on Cubic Pd Nanoparticles. *Phys. Chem. Chem. Phys.* **2012**, *14*, 10258.
(22) Pu, H.; Zhang, T.; Dong, K.; Dai, H.; Zhou, L.; Wang, K.; Bai, S.; Wang, Y.; Deng, Y. Twinned and Single-Crystal Palladium Nanocrystals for the Electrooxidation of HCOOH. *ACS Appl. Nano Mater.* **2021**, *4*, 10185–10193.
(23) Bhandari, S.; Rangarajan, S.; Li, S.; Scaranto, J.; Singh, S.; Maravelias, C. T.; Dumesic, J. A.; Mavrikakis, M. A Coverage Self-Consistent Microkinetic Model for Vapor-Phase Formic Acid Decomposition over Pd/C Catalysts. *ACS Catal.* **2023**, *13* (6), 3655–3667.
(24) Papanikolaou, K. G.; Shi, Y.; Schimmenti, R.; Xia, Y.; Mavrikakis, M. The Role of Coverage Effects on the Structure–Sensitivity of Formic Acid Electrooxidation on Pd Surfaces. *J. Catal.* **2023**, *417*, 408–420.

**Publications Acknowledging this Grant in 2021-2024**

**Intellectually led by this grant**

**2024**

1. Xu, L.; Rebarchik, M.; Bhandari, S.; Mavrikakis, M. Adsorbate-Induced Adatom Formation on Au-Cu Bimetallic Alloys and Its Possible Consequences for $CO_2$ Electroreduction. *Surf. Sci.* **2025**, *751*, 122613.
2. Xu, L.; Mavrikakis, M. Adsorption Properties of Au−Ni Surface Alloys with a Nonstoichiometric Moiré Structure: A Density Functional Theory Study. *J. Phys. Chem. C* **2024**, *128*, 9973–9980.
3. Xu, L.; Mavrikakis, M. Structure Sensitivity in Adsorbate-Induced Adatom Formation on FCC Transition-Metal Surfaces. *J. Catal.* **2024**, *431*, 115373.

**2023**

4. Xu, L.; Papanikolaou, K. G.; Lechner, B. A. J.; Je, L.; Somorjai, G. A.; Salmeron, M.; Mavrikakis, M. Formation of Active Sites on Transition Metals through Reaction-Driven Migration of Surface Atoms. *Science* **2023**, *380*, 70–76.
5. Xu, L.; Mavrikakis, M. Adsorbate-Induced Adatom Formation on Lithium, Iron, Cobalt, Ruthenium, and Rhenium Surfaces. *JACS Au* **2023**, *3*, 2216–2225.
6. Rebarchik, M.; Bhandari, S.; Kropp, T.; Mavrikakis, M. Insights into the Oxygen Evolution Reaction on Graphene-Based Single-Atom Catalysts from First-Principles-Informed Microkinetic Modeling. *ACS Catal.* **2023**, *13*, 5225–5235.
7. Bhandari, S.; Rangarajan, S.; Li, S.; Scaranto, J.; Singh, S.; Maravelias, C. T.; Dumesic, J. A.; Mavrikakis, M. A Coverage Self-Consistent Microkinetic Model for Vapor-Phase Formic Acid Decomposition over Pd/C Catalysts. *ACS Catal.* **2023**, *13*, 3655–3667.
8. Papanikolaou, K. G.; Shi, Y.; Schimmenti, R.; Xia, Y.; Mavrikakis, M. The Role of Coverage Effects on the Structure–Sensitivity of Formic Acid Electrooxidation on Pd Surfaces. *J. Catal.* **2023**, *417*, 408–420.
9. Jeskey, J.; Chen, Y.; Kim, S.; Xia, Y. EDTA-Assisted Synthesis of Nitrogen-Doped Carbon Nanospheres with Uniform Sizes for Photonic and Electrocatalytic Applications. *Chem. Mater.* **2023**, *35*, 3024–3032.
10. Rangarajan, S.; Mavrikakis, M. A comparative analysis of different van der Waals treatments for molecular adsorption on the basal plane of 2H-$MoS_2$. *Surf. Sci.* **2023**, *729*, 122226.

**2022**

11. Shi, Y.; Elnabawy, A. O.; Gilroy, K. D.; Hood, Z. D.; Chen, R.; Wang, C.; Mavrikakis, M.; Xia, Y. Decomposition Kinetics of $H_2O_2$ on Pd Nanocrystals with Different Shapes and Surface Strains. *ChemCatChem* **2022**, *14*, e202200475.
12. Elnabawy, A. O.; Murray, E. A.; Mavrikakis, M. Trends in Formic Acid Electro-Oxidation on Transition Metals Alloyed with Platinum and Palladium. *J. Phys. Chem. C* **2022**, *126*, 4374–4390.
13. Shi, Y.; Schimmenti, R.; Zhu, S.; Venkatraman, K.; Chen, R.; Chi, M.; Shao, M.; Mavrikakis, M.; Xia, Y. Solution-Phase Synthesis of $PdH_{0.706}$ Nanocubes with Enhanced Stability and Activity toward Formic Acid Oxidation, *J. Amer. Chem. Soc.* **2022**, *144*, 2556–2568.
14. Xu, L.; Stangland, E.; Dumesic, J. A.; Mavrikakis, M. Mechanistic Study of 1,2-Dichloroethane Hydrodechlorination on Cu-Rich Pt-Cu Alloys: Combining Reaction Kinetics Experiments with DFT Calculations and Microkinetic Modeling. *ACS Sustainable Chem. Eng.* **2022**, *10*, 1509–1523.

**2021**

15. Huang, W.; Johnston-Peck, A. C.; Wolter, T.; Yang, W. D.; Xu, L.; Oh, J.; Reeves, B. A.; Zhou, C.; Holtz, M. E.; Herzing, A. A.; Lindenberg, A. M.; Mavrikakis, M.;

Cargnello, M. Steam-Created Grain Boundaries for Methane C–H Activation in Palladium Catalysts**.** *Science* **2021**, *373*, 1518–1523.
16. Gao, W.; Elnabawy, A. O.; Hood, Z. D.; Shi, Y.; Wang, X.; Roling, L. T.; Pan, X.; Mavrikakis, M.; Xia, Y.; Chi, M. Atomistic Insights into the Nucleation and Growth of Platinum on Palladium Nanocrystals. *Nat. Commun.* **2021**, ***12***, 3215.
17. Peng, G.; Xu, L.; Glezakou, V.; Mavrikakis, M. Mechanism of Methanol Synthesis on Ni(110). *Catal. Sci. Technol.* **2021**, *11*, 3279–3294.
18. Elnabawy, A. O.; Herron, J. A.; Liang, Z.; Adzic, R. R.; Mavrikakis, M. Formic Acid Electrooxidation on Pt or Pd Monolayer on Transition-Metal Single Crystals: A First-Principles Structure Sensitivity Analysis. *ACS Catal.* **2021**, *11*, 5294–5309.
19. Li, S.; Rangarajan, S.; Scaranto, J.; Mavrikakis, M. On the Structure Sensitivity of and CO Coverage Effects on Formic Acid Decomposition on Pd Surfaces. *Surface Science* **2021**, *709*, 121846.
20. Chen, B. W. J.; Bhandari, S.; Mavrikakis, M. Role of Hydrogen-Bonded Bimolecular Formic Acid–Formate Complexes for Formic Acid Decomposition on Copper: A Combined First-Principles and Microkinetic Modeling Study. *ACS Catal.* **2021**, *11*, 4349–4361.
21. Zhu, J.; Xu, L.; Lyu, Z.; Xie, M.; Chen, R.; Jin, W.; Mavrikakis, M.; Xia, Y. Janus Nanocages of Platinum-Group Metals and Their Use as Effective Dual-Electrocatalysts. *Angew. Chem. Int. Ed.* **2021**, *60*, 10384–10392.
22. Chen, B. W. J.; Xu, L.; Mavrikakis, M. Computational Methods in Heterogeneous Catalysis. *Chem. Rev.* **2021**, *121*, 1007–1048.
23. Tacey, S. A.; Chen, B. W. J.; Szilávsi, T.; Mavrikakis, M. An Automated Cluster Surface Scanning Method for Exploring Reaction Paths on Metal-Cluster Surfaces. *Comput. Mater. Sci.* **2021**, *186*, 110010.
24. Schimmenti, R.; Mavrikakis, M. HCOOH Decomposition on Sub-Nanometer $Pd_6$ Cluster Catalysts: The Effect of Defective Boron Nitride Supports through First Principles. *Appl. Catal. B Environ.* **2021**, *280*, 119392.

**Jointly funded by this grant and other grants with intellectual leadership by other funding sources**

**2023**

25. Xu, L.; Ye, R.; Mavrikakis, M.; Chen, P. Molecular-Scale Insights into Cooperativity Switching of *x*TAB Adsorption on Gold Nanoparticles. *ACS Cent. Sci.* **2024**, *10*, 65–76.
26. Bao, N.; Liu, Q.; Reynolds, M. F.; Figueras, M.; Smith, E.; Wang, W.; Cao, M. C.; Muller, D. A.; Mavrikakis, M.; Cohen, I.; McEuen, P. L.; Abbott, N. L. Gas-Phase Microactuation Using Kinetically Controlled Surface States of Ultrathin Catalytic Sheets. *Proc. Natl. Acad. Sci. U. S. A.* **2023**, *120*, e2221740120.
27. Ma, J.; Rebarchik, M.; Bhandari, S.; Mavrikakis, M.; Huber, G. W.; Zavala, V. M. Exploiting Electricity Market Dynamics Using Flexible Electrolysis Units for Retrofitting Methanol Synthesis. *Energy Environ. Sci.* **2023**, *16*, 2346–2357.

**2022**

28. Lyu, Z.; Shang, Y.; Xia, Y. Shape-Controlled Synthesis of Copper Nanocrystals for Plasmonic, Biomedical, and Electrocatalytic Applications. *Acc. Mater. Res.* **2022**, *3*, 1137–1148.

**2021**

29. Cai, H.; Schimmenti, R.; Gradiski, M. V.; Morris, R. H.; Mavrikakis, M.; Chin, Y. C. Mechanistic Similarities and Differences for Hydrogenation of Aromatic Heterocycles and Aliphatic Carbonyls on Sulfided Ru Nanoparticles. *ACS Catal.* **2021**, *11*, 12585–12608.
30. Demir, B.; Kropp, T.; Gilcher, E. B.; Mavrikakis, M.; Dumesic, J. A. Effects of Water on the Kinetics of Acetone Hydrogenation over Pt and Ru Catalysts. *J. Catal.* **2021**, *403*, 215–227.
31. Xu, L.; Stangland, E. E.; Dumesic, J. A.; Mavrikakis, M. Hydrodechlorination of 1,2-Dichloroethane on Platinum Catalysts: Insights from Reaction Kinetics Experiments, Density Functional Theory, and Microkinetic Modeling. *ACS Catal.* **2021**, *11*, 7890–7905.

Charles C. L. McCrory

## Building from Molecular Catalyst to Multimetallic Assemblies: The Effects of Charge Delocalization on Electrocatalytic Activity for the $CO_2$ Reduction Reaction

Charles C. L. McCrory, Jukai Zhou, MD. Waseem Hussain, Faridat Agboola, Weixuan Nie, and Drew Tarnopol
Department of Chemistry and Macromolecular Science & Engineering Program, University of Michigan, Ann Arbor, MI, 48109

Our work focuses on determining how the interrelated effects of charge delocalization, electronic coupling, and intramolecular electrostatics influence catalytic activity and selectivity from discrete, molecular systems to extended multidimensional catalyst architectures. We have adopted a bottom-up approach to study these effects as we build in structural complexity: from simple molecular catalysts, to multimetallic assemblies, and finally towards macromolecular extended structures. In previous studies, we have studied how charge delocalization and intramolecular electrostatics influence $CO_2R$ activity and reaction selectivity by molecular catalysts. We will present some of our new studies exploring the role of all three effects on $CO_2R$ activity in multimetallic assemblies. For example, by systematically modifying the structure of multimetallic assemblies, we have demonstrated that electrostatic effects are the most influential intramolecular interactions on per-site activity in multimetallic systems. We will also present our work exploring whether intramolecular electrostatic effects are best described as through-space electric field effects or through-bond effects when considering cationic substituents incorporated onto redox-active ligands. Finally, we will present our work successfully incorporating Co-based molecular building units with redox-active ligands into larger 1D and 2D coordination polymers.

**DE-SC0022019: Building from Discrete Molecular Electrocatalysts to Multidimensional Catalyst Architectures: The Effects of Charge Delocalization and Electronic Coupling on Electrocatalytic Activity**

**Postdoc(s):** Md. Waseem Hussain
**Student(s):** Jukai Zhou, Faridat Agboola, Weixuan Nie, Drew Tarnopol

### RECENT PROGRESS

#### *Bimetallic Complexes for Electrocatalytic $CO_2$ Reduction: The Role of Intramolecular Interactions on Activity*

One of the key knowledge gaps in designing multimetallic architectures for electrochemical $CO_2$ reduction is understanding how the various interrelated intramolecular electronic effects between active sites influence catalytic activity. We synthesized a model system of homo- and hetero-bimetallic catalysts to study the role of intramolecular electrostatics and electronic coupling between active sites on $CO_2$ reduction ability. Our bimetallic Co-Co complex, [Co (PDI)-(PDI)Co], reduced $CO_2$ with higher activity and selectivity compared to our monometallic Co analogue, [Co(PDI)]. The Co-Co complex shows both electronic coupling between the Co sites and putative electrostatic interactions between the cationic $Co^+$ metal ions in the catalytically active species of the

complex and reduced $CO_2$ intermediates. We then modulated these effects by incorporating a redox-inactive $Zn^{2+}$ cation into the structure. The resulting heterobimetallic Co-Zn complex, [Zn(PDI)-(PDI)Co], has no electronic coupling between the metal sites and increased electrostatic effects due to higher total positive charge of the $Zn^{2+}$ metal ion in the catalytically active species compared to the Co-Co complex. The Co-Zn complex has the highest $CO_2$ reduction activity measured, and this higher activity is attributed to the increased electrostatic stabilization of reduced intermediates. Our studies with these model complexes demonstrate that maximizing intramolecular electrostatics is a crucial consideration in designing larger multimetallic architectures for $CO_2$ reduction and provide a design strategy to boost catalytic activity through incorporation of redox-inactive metal ions in multimetallic assemblies. This work was published in *Chem Catalysis*.

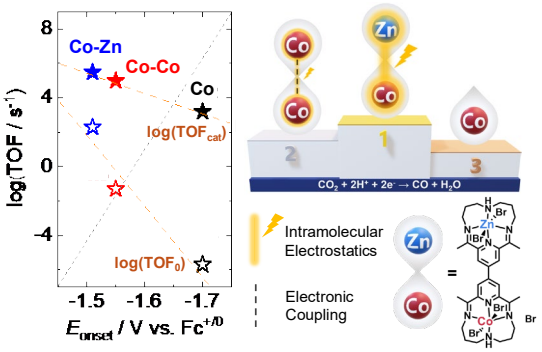


**Figure 1.** A plot of the log of the activity as a function of the onset potential ($E_{onset}$) shows an inverse scaling relationship where the bimetallic Co-Zn has the highest activity and most positive potential, followed by Co-Co and the monometallic Co complex. $TOF_{cat}$ (maximum catalyst turnover frequency) and $TOF_0$ (intrinsic activity) are the primary metrics for comparing activity of homogeneous electrocatalysts.

***Intramolecular Electrostatic Effects in Electrocatalysis: Through-Space vs Through-Bond Substituent Effects***

Numerous studies, including our own work, have shown that incorporating cationic species into catalyst frameworks leads to an increase in catalytic activity for electrochemical $CO_2$ reduction. This increase in catalytic activity is typically attributed to a through-space electric field effect—electrostatic stabilization of reduced $CO_2$ adducts at the binding site by the electric field exerted by the cationic substituents. However, for complexes in which the cationic moieties are incorporated into redox-active ligands, this simple description of through-space

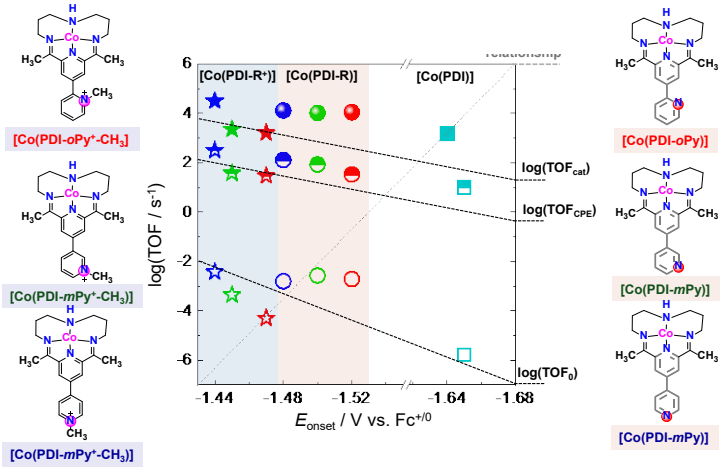


**Figure 2.** Activity measurements for the [Co(PDI-$R^+$)] and [Co(PDI-R)] catalyst investigated calculated from controlled potential electrolysis experiments ($TOF_{CPE}$) and scan-rate dependent cyclic voltammograms ($TOF_{cat}$ and $TOF_0$) plotted as a function of $E_{onset}$. The catalyst system shows a complicated inverse scaling relationships—the black lines are guides to the eye to show general trends, and the gray dashed line shows a typical scaling relationship.

electrostatic effects may become more complicated due to charge delocalization throughout the conjugated ligand. To test this, we synthesized a series of regioisomers of cobalt complexes with redox-active pyridyldiimine ligands substituted with cationic pyridinium moieties *ortho*-, *meta*-, and *para*- to the rest of the complex. We hypothesized that a through-space electrostatic effect should show increasing activity with proximity of the cationic site to the Co site: *ortho* > *meta* > *para.* However, we saw a complicated activity profile with *para* >> *ortho* > *meta*. Moreover, when compared to the analogous complexes with uncharged pyridyl moieties, the *ortho* and *meta* pyridinium complexes show lower $CO_2$ reduction activity compared to their pyridyl analogues. Computational studies conducted with collaborator Prof. Paul M. Zimmerman suggest that these trends in activity cannot be explained by simple $CO_2$ binding affinities or stabilization of reduced intermediates, but instead may be related to charge stabilization of $CO_2$ adducts through charge delocalization—an inherently through-bond effect. This study highlights not only the hidden complexity of electrostatic interactions in electrocatalysis, but also highlights the importance of understanding the influence of extended conjugation in driving catalytic activity as researchers increasingly move to incorporate molecular catalysts into larger macromolecular structures. This work is currently in preparation for publication.

### *1D Polymeric Catalysts for Electrocatalytic $CO_2$ Reduction*

Our original goal was to incorporate [Co(PDI-R)] catalysts into conductive polymer structures to explore the role of backbone conjugation on catalytic activity. However, in initial studies, we found that background polymer charging of conductive polymers led to undesirable polymer degradation and other side reactions. Instead, we have successfully synthesized poly-[Co(VinylPDI)] polymer catalysts with non-conductive polymer backbones. By modulating the extent of crosslinking in the systems, we are exploring how charge density (e.g. through-space electrostatics) influences catalytic activity. Our hypothesis is that the polymer with increased crosslinking will force the cationic charges closer together, increasing charge density and therefore stabilize reduced $CO_2$ adducts via through-space electrostatic effects. Both poly-[Co(VinylPDI)] and the crosslinked version poly-crossl-[Co(VinylPDI)] have been characterized using NMR, XPS, and FTIR. Both polymers are soluble in polar solvents, including acetonitrile and water, and providing the unique opportunity to conduct $CO_2$ reduction experiments with the polymers as homogeneous catalysts. The poly-crossl-[Co(VinylPDI) system is more active than the poly-[Co(VinylPDI)] system according to cyclic voltammetry experiments, consistent with our hypothesis. However, controlled potential electrolysis

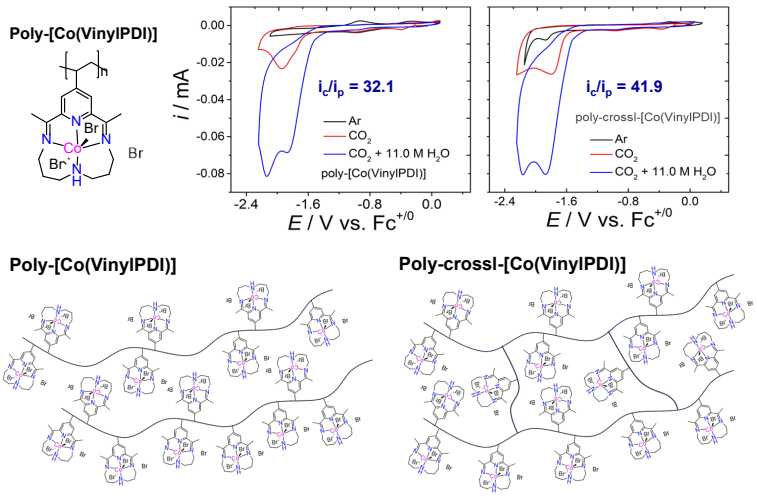


**Figure 3.** The Poly-[Co(VinlyPDI)] and Poly-crossl-[Co(VinylPDI)] polymers are active for the $CO_2$ reduction reaction in acetonitrile with 11 M $H_2O$ as a proton source.

measurements show only ~25% CO generation with significant loss of charge due to nonproductive interchain coupling. We are currently exploring copolymerization strategies to decrease extent of this interchain coupling reaction, and polymerizing the [Co(VinylPDI)] catalyst into hydrogels to form a heterogeneous catalyst for aqueous $CO_2$ reduction studies.

***2D Macromolecular Cobalt Catalysts for $CO_2$ Reduction to Methanol***

We have previously shown that that the complex cobalt bis-pyridylmonoimine, is active for the reduction of $CO_2$ to CO. However, we found that if we perturbed the flexibility of the BPMI ligand we would perturb the molecular geometry of the Co center from square planar, increasing its nucleophilicity and CO binding affinity. The net result was that increased ligand flexibility ultimately led to increased product inhibition by CO, and lower overall $CO_2$ to CO activity. We hypothesized that we could take advantage of this effect by incorporating the [Co(BPMI)] complex into a conjugated macromolecular structure. If the curvature of the 2D structure elicited an appropriate amount of strain on the [Co(BPMI)] building units, it may distort the geometry of the Co center just enough to retain the CO for further activation and reduction without being poisoned by CO. To test this, we synthesized a 2D porous material Co@COF-BTAP-AA. The material has been characterized by scanning electron microscopy, inductively-coupled plasma mass spectrometry, elemental analysis, FTIR, X-ray photoelectron spectroscopy, gas-adsorption surface area measurements, and solid-state NMR. The material forms densely-packed spherical nanoparticles with low surface area that show relatively low activity for $CO_2$ reduction compared to other heterogeneous catalysts. However, the material shows promising selectivity for the 6-$e^-$ reduction of $CO_2$ to $CH_3OH$. Further studies are focused on $^{13}CO_2$ isotopic labeling experiments, understanding the mechanism of $CO_2$ reduction, and introducing perturbations to modulate pore size and catalyst loading.

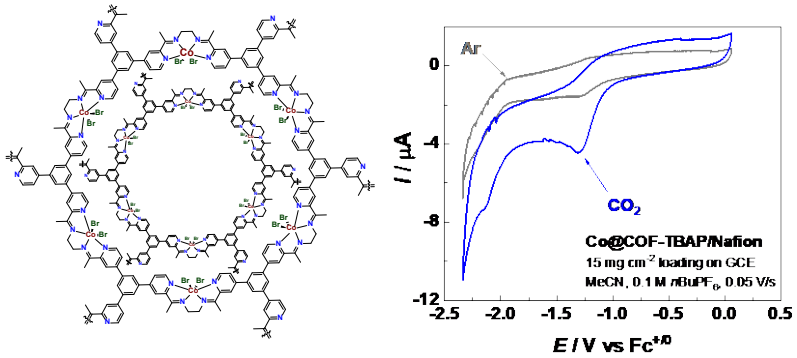


**Figure 4.** The Co@COF-BTAP-AA material is constructed of cobalt bispyridylmonoimine complexes as building units with conjugated linkers. The material shows modest activity for $CO_2$ reduction to methanol in acetonitrile solutions.

**Publications Acknowledging this Grant in 2021-2024**

*Intellectually Led by this Grant:*


1. Nie, W-X.; McCrory, C. C. L. Strategies for Breaking Molecular Scaling Relationships for the Electrochemical $CO_2$ Reduction Reaction. *Dalton Trans.*, **2022**, *51*, 6993-7010.
2. Zhou, J.; Nie, W-X.; Tarnopol, D. E.; McCrory, C. C. L. Co-Co and Co-Zn Bimetallic Complexes for Electrocatalytic $CO_2$ Reduction: the Role of Interrelated Intramolecular Effects on Activity. *Chem Catal.*, **2024**, *4*, 101006.

## Multimetallic Ligand-Coated Nanoparticles for Plasmon-Enhanced Electrochemical $CO_2$ Reduction: Synthesis and Characterization of the Nanoparticles

Catherine J. Murphy[1]*, L. Robert Baker[2], Emily A. Cook[1], Amos Shiau[1], Siyu Zhou[1], Diana Soto[1], Tomaz Neves-Garcia[2], Tithi Lai[2]
[1] University of Illinois Urbana-Champaign, Department of Chemistry
[2] The Ohio State University, Department of Chemistry & Biochemistry

### Presentation Abstract

The electrochemical reduction of $CO_2$ into valuable hydrocarbon products presents a promising approach to mitigate greenhouse gas emissions, but the reaction is generally slow. Recent research has highlighted the potential of plasmonic materials as the catalysts in $CO_2$ electroreduction. Upon illumination, these materials generate localized electric fields, which can accelerate the rate of $CO_2$ reduction and allow for more controlled selectivity than achieved with current methods. Among plasmonic materials, gold nanorods are particularly effective due to their tunable optical properties. By adjusting their size and aspect ratio, the absorption wavelength can be controlled (in the 520 nm – 1200 nm range) to optimize the performance of $CO_2$ reduction. This work aims to synthesize gold nanorod-based catalysts with enhanced performance toward $CO_2$ reduction. The first step in achieving this goal is to synthesize and characterize gold-silver-copper nanomaterials that are large enough (smallest dimension >5 nm) to exhibit plasmons. The addition of copper (also plasmonic on its own, around 600 nm) is designed to promote the formation of C-C bonds in $CO_2$ reduction products. The synthesis and characterization of two sizes of the trimetallic nanorods, with varying ratios of copper/gold, is described. Second, we coat the nanorods with a protective ligand shell (i.e., PEO groups), which, as our recent findings suggest, not only maintains catalytic activity but also shields the surface from contamination, improving the durability of the catalysts.

### DE-SC00243-18: Multimetallic Ligand-Coated Nanoparticles for Plasmon-Enhanced Electrochemical $CO_2$ Reduction

**PI:** Catherine J. Murphy
**Postdoc(s):** Siyu Zhou
**Student(s):** Emily A. Cook, Amos Shiau, Diana Soto (undergrad)
**Affiliations(s):** University of Illinois Urbana-Champaign

## RECENT PROGRESS

### *Synthesis of Gold-Silver-Copper Nanorods in Colloidal Solution*

The synthetic protocol of gold-silver-copper nanorods was developed by modifying the seed-mediated synthesis of gold nanorods. Gold nanorods, in which the aspect ratio (length/width) is controlled by the addition of small amounts of impurity silver ions, show tunable plasmon resonances in the visible and near-IR portions of the spectrum (Figure 1). The seed-mediated growth approach to control crystal formation on the nanoscale relies on two steps: in the first step, $H^+[AuCl_4]^-$ is reduced in water with borohydride to create metastable gold "seeds" that are 1-2 nm in diameter. These seed are added to a fresh pot of $HAuCl_4$, a surfactant (cetyltrimethylammonium bromide, CTAB), a weak reducing agent such as ascorbic acid, and a small quantity of silver nitrate (about 1/1000 of the gold salt); the exact concentrations as well as pH dictate final nanorod dimensions. "Standard" rods are 10-15 nm in diameter, with lengths tunable from 20-80 nm based on the silver concentration. "Mini" rods are 5-8 nm diameter, with lengths tunable from 10-40 nm based on the silver concentration. In the case of creating nanorods containing copper, the amount of $AuCl_4^-$ is reduced, and is compensated by the addition of $[CuCl_4]^{2-}$. Gold, silver, and copper are miscible in all proportions in the bulk; but this is not necessarily true on the nanoscale. Indeed, the initial syntheses produced only gold nanoparticles with no copper whatsoever.

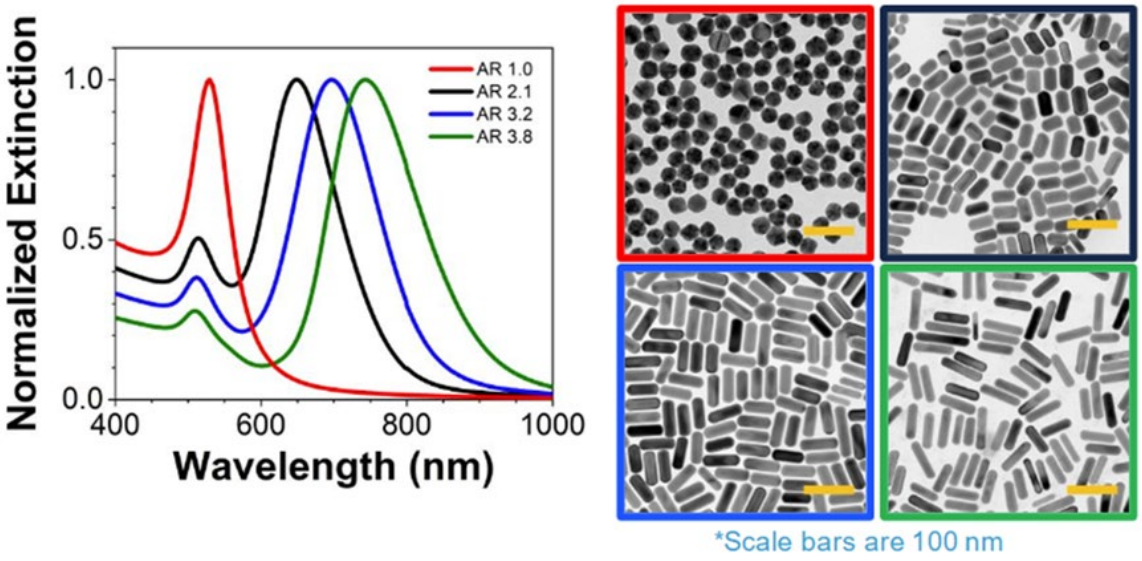


***Figure 1. Normalized extinction spectra of aqueous suspensions (left), and transmission electron micrographs (right) of standard gold nanorods. The colored lines and boxes connect the optical spectrum to the micrograph of four select samples. AR = aspect ratio.***

Eventually, using design-of-experiment optimization techniques, samples of gold nanorods, both "standard" and "mini" with similar sizes to the gold nanorods without copper, were obtained from initial feedstocks in the growth step that contained a molar ratio of 5:1 Au:Cu, 3:1 Au:Cu, and 1:1 Au:Cu. The general observation is that the extinction spectra of rods that contain copper are similar, but do not extend into the red as much, as the rods that are copper-free (Figure 2). Transmission

electron microscopy of the rods shows good monodispersity (not shown).

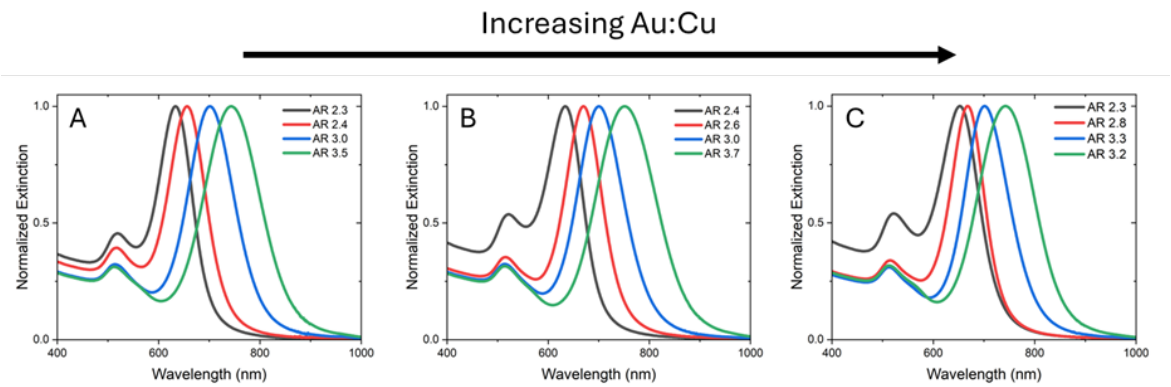


***Figure 2. Extinction spectra of standard gold nanorods containing copper for (a) 1:1 Au:Cu initial ratios, (b) 3:1 Au:Cu initial ratios, and (c) 5:1 Au:Cu initial ratios. The nanorods diameters are between 10 to 14 nm. The tunable plasmons arise from differing silver concentrations, similar to copper-free rods. AR = aspect ratio.***

### *Quantification of Metal Content in Trimetallic Nanorods*

Two methods were employed to quantify the metal content in the copper-containing nanorods: ICP-MS, inductively-coupled plasma mass spectrometry, which is an accurate but destructive method; and EDS, energy-dispersive x-ray spectroscopy, which can be done in imaging mode in an electron microscope but is less accurate.

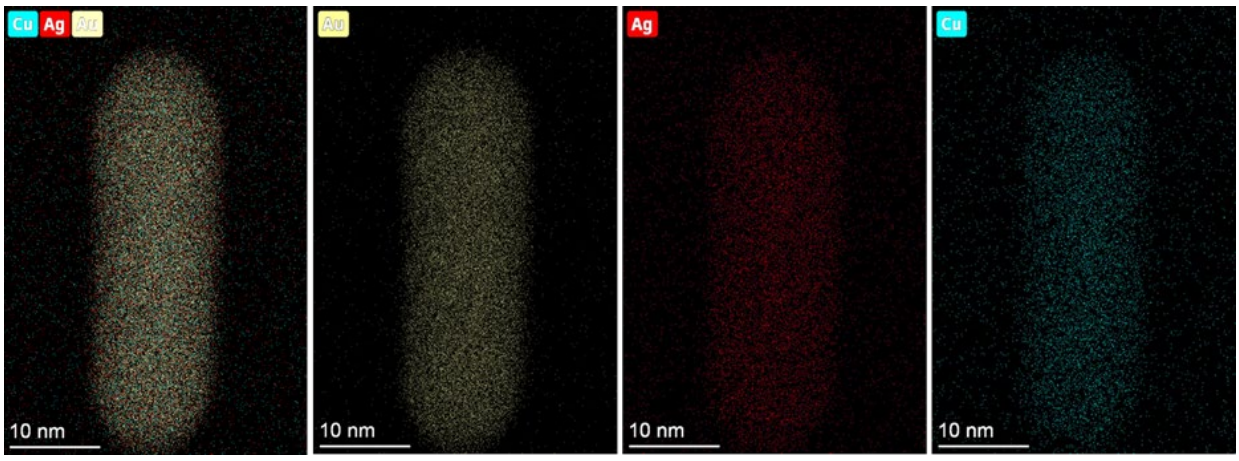


***Figure 3. EDS mapping of copper, silver and gold in a nominal 3:1 Au:Cu standard nanorod with an aspect ratio of 2.6 shows the elements dispersed throughout the nanorod.***

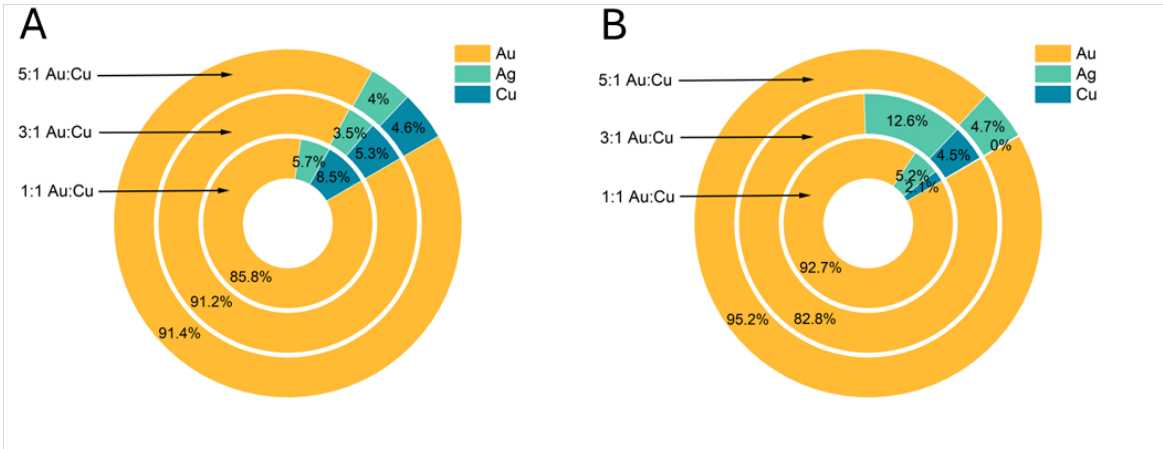


***Figure 4. Elemental analysis data for the indicated nominal Au:Cu composition of standard nanorods with an aspect ratio 2.8 +/- 0.2 as measured by (a) EDS and (b) ICP-MS. Compositions from the EDS data are an average of 10 nanorods.***

In spite of the large amount of copper added to the synthesis, only a few percent of copper at most makes it into the isolated nanorods. The agreement between the ICP-MS and EDS data is acceptable for many samples, but the variability is still a cause for concern in some samples. Extinction coefficients for all particles (multiple aspect ratios, standard and mini, with different nominal copper content) are now obtained. Copper does appear to be found throughout the nanorods, including the surface, a positive sign for its potential to serve as catalytic sites for $CO_2$ electroreduction. The CTAB bilayer on the rods was ligand-exchanged to present PEO groups, terminating in methoxy, as an example of a "non-fouling" surface for catalysis experiments in the Baker lab. Given the Baker lab's recent intriguing results with single-atom Ni on gold as a catalyst, trimetallic nanorods containing Ni are a clear next target.

**Publications Acknowledging this Grant in 2021-2024:** none yet

Oleg V. Ozerov

# Highly Reactive Main Group Cations and C-F Activation

Oleg V. Ozerov*, Derek W. Leong, Joshua Daum, Jack Raker, Jovanny J. Contreras, Nattamai Bhuvanesh
Department of Chemistry, Texas A&M University, College Station, TX 77842

## Presentation Abstract

Our group is exploring advanced strategies for hydrodefluorination of perfluoroalkyl substances (PFAS) utilizing highly Lewis acidic main group cations (e.g., $X_3Si^+$) as catalysts. We have determined that in order to target fully fluorinated alkanes (such as $CF_4$, $C_2F_6$, etc.) in hydrodefluorination, silylium cations more reactive (Lewis acidic) than trialkylsilylium (X= alkyl) are necessary, possible with X = halogen instead of X = alkyl. Silylium cations are typically generated by hydride abstraction from an $X_3Si$-H silane with a carbocation, most commonly $Ph_3C^+$. However, the hydride affinity of $Ph_3C^+$ is insufficient for abstraction of a hydride from $X_3Si$-H with X groups more electron-withdrawing than an alkyl. To this end, we have devised syntheses of fluorinated trityl salts [(*m,m*-$F_2C_6H_3)_3C$][$HCB_{11}Cl_{11}$] (**$F_6Tr^+$**) and [$(C_6F_5)_3C$][$HCB_{11}Cl_{11}$] (**$F_{15}Tr^+$**). This presentation will highlight the remarkably high hydride affinities for these "bottlable" **$F_6Tr^+$** and **$F_{15}Tr^+$** in reactions with silanes, hydrocarbons, and other relevant small molecules. The presentation will explore how the increased hydride affinity of **$F_{15}Tr^+$** permits much more effective hydrodefluorination reactions.

**Grant or FWP Number:** **New Challenges for C-F Activation with Cationic Main Group Electrophiles, *DE-SC0023280***

**Students:** Derek W. Leong, Jovanny J. Contreras, Jack Raker, Joshua Daum

## RECENT PROGRESS

***New carborane anion syntheses***. Work on this project relies heavily on the use of robust weakly coordinating anions,[1] with the halogenated carboranes such as $[HCB_{11}Cl_{11}]^-$ being the anions of choice. $[HCB_{11}Cl_{11}]^-$ itself is a great choice based on its inertness and low basicity, but the solubility of its derivatives is not very high. The work with the most reactive cations requires least basic solvents and that means that most common polar solvents are not appropriate. In addition, our work on the perfluorotrityl cation (vide infra) places even more stringent requirements on the solvent or on the substituents on the carborane cage because the perfluorotrityl cation readily reacts with most C-H bonds in alkyl or aryl moieties. To this end, we prepared carborane derivatives shown in Figure 2. In particular, the $-SC_6F_5$ substituted carborane anion is an option that provides notably higher solubility in solvents such as $C_6F_5Br$ while remaining resistant to the perfluorotrityl or the silylium cations.

**Figure 1**. Chlorination of $[HCB_{11}Cl_{11}]^-$ with refluxing $SbCl_3/SbCl_5$ mixtures.

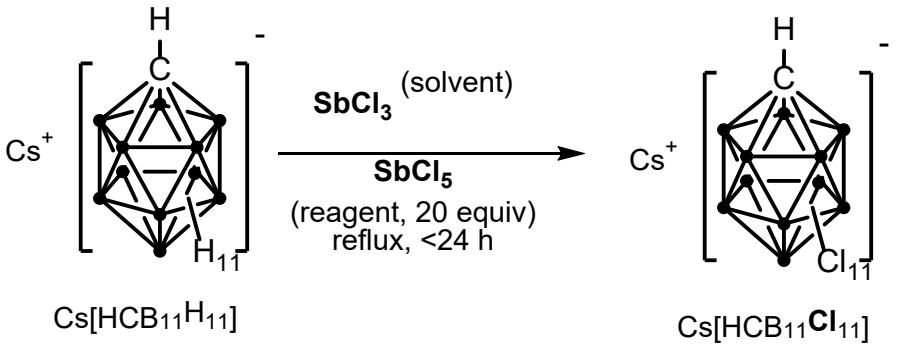


*Each unlabeled vertex is a boron atom*

***Reactivity of the perfluorotrityl cation***. A part of our proposal focuses on the synthesis of silylium (and other main group) cations that are more reactive than trialkylsilylium cations. We view this as necessary for lowering the barrier for reactions with highly electron-poor perfluoroalkanes and perfluoroalkyl chains. In order to access the more reactive silylium cations, we need more reactive but isolable carbocations, to be able to abstract the hydride from more electron-deficient silanes. To this end, we recently reported the preparation of a hexafluorotrityl cation $F_6Tr^+$ as a $[HCB_{11}Cl_{11}]^-$ salt.[2] It possesses ca. 15-20% higher hydride affinity than its parent $Tr^+ = [(C_6H_5)_3C^+]$. An even higher hydride affinity is predicted[3] for the perfluorotrityl $F_{15}Tr^+$. An additional advantage of $F_{15}Tr^+$ as an activator is that $F_{15}Tr$-H, the product of hydride abstraction, is resistant to Friedel-Crafts substitution reactions. Friedel-Crafts alkylation can lead to alkylarenes with benzylic positions which can give rise to carbocations that are too stable for the desired improvement in HDF reactivity.

Riedel and coworkers recently reported the preparation of $F_{15}Tr^+$ partnered with a $[Al(OTeF_5)_4]^-$ anion.[4] Unfortunately, this anion is not compatible with hydrodefluorination strategies. In addition, the Riedel work largely handled $F_{15}Tr^+$ in solution at low temperature and did not isolate bulk solid samples. We were able to prepare $F_{15}Tr^+$ with the $[HCB_{11}Cl_{11}]$ and $[C_6F_5SCB_{11}Cl_{11}]$ counteranions (Figure XXX). Analytically pure solid samples of $F_{15}Tr[HCB_{11}Cl_{11}]$ and $F_{15}Tr[C_6F_5SCB_{11}Cl_{11}]$ can be isolated at ambient temperature.

**Figure 2**. Synthesis of the perfluorotrityl cation salts.

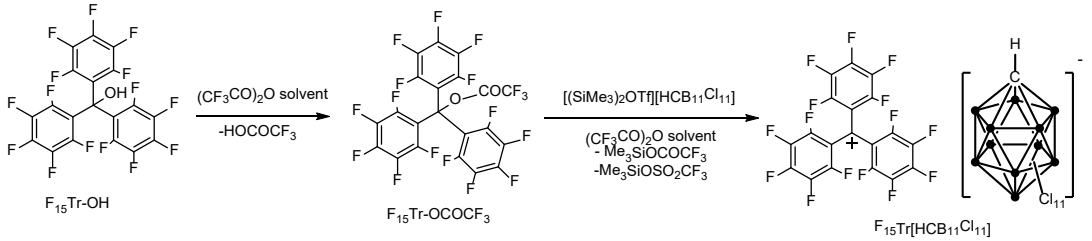


$F_{15}Tr^+$ is extremely reactive towards aliphatic C-H bonds (abstracts hydride) and aromatic compounds with C-H bonds (likely engages in Friedel-Crafts with subsequent rearrangements). Because of this, choosing solvents for solution characterization and reactivity was quite challenging. After some screening, we determined that $F_{15}Tr^+$ is compatible with $SO_2Cl_2$, $C_6F_5Br$, and $CH_2Br_2$ as solvents. However, some reactions of

$F_{15}Tr^+$ we wish to study generate new cations (silylium or carbocations) that are not necessarily compatible with $SO_2Cl_2$ and $CH_2Br_2$. $C_6F_5Br$ is clearly the solvent most chemically inert, but the solubility of $F_{15}Tr[HCB_{11}Cl_{11}]$ in it is very poor. On the other hand, $F_{15}Tr[C_6F_5SCB_{11}Cl_{11}]$ dissolves in $C_6F_5Br$ well enough to be observed by NMR spectroscopy. $SO_2Cl_2$ brings the most solubility to $F_{15}Tr^+$ salts, but we found that $F_{15}TrH$ in $SO_2Cl_2$ under highly acidic conditions may undergo F/Cl exchange – that greatly complicates the analysis of the fate of $F_{15}Tr^+$-derived products.

**Figure 3**. Hydride-abstracting reactions of $F_{15}Tr^+$.

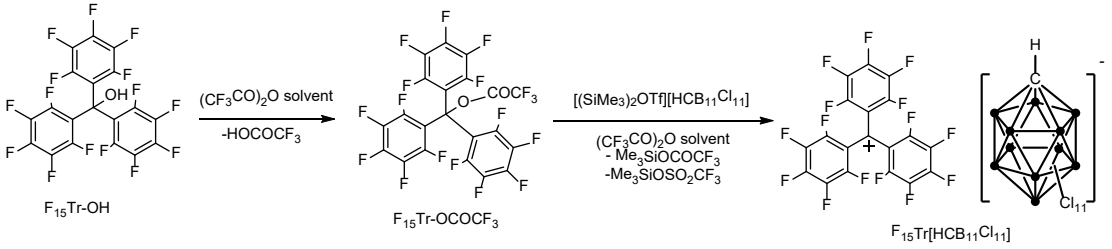


We found that $F_{15}Tr^+$ readily abstracts a hydride from sterically unencumbered alkanes containing -$CH_2$- groups, such as cyclohexane and pentane. This far exceeds the hydride abstracting power of $F_6Tr^+$ we reported earlier, which only reacts with alkaned containing tertiary CH sites, and rather slowly. Interestingly, $F_{15}Tr^+$ did not react with alkanes where the $CH_2$ site was attached to a $Me_3C$- substituent. This suggests that there is a steric component to the hydride abstraction activation barrier. We also attempted to use $F_{15}Tr^+$ to abstract a hydride from $CH_4$ and $C_2H_6$ (1 atm in a J. Young tube). However, it did not appear to react, at least no more than a few percent after days of heating at 70 °C. It appears that the hydride abstracting power of $F_{15}Tr^+$ peters out at the primary $CH_3$ sites (or methane).

In another unusual reaction, we determined that $F_{15}Tr[C_6F_5SCB_{11}Cl_{11}]$ abstracts a hydride from $H_2$ (or a deuteride from $D_2$) in $C_6F_5Br$ solvent (1 atm hydrogen). The reaction reached ~50% conversion after about 24 h at 70 °C, and reached 70-90% conversion after several days. This can be viewed as an extreme version of an FLP splitting of $H_2$, where the acid is extremely "hydridophilic" while the base is essentially absent.


[1] "Taming the Cationic Beast: Novel Developments in the Synthesis and Application of Weakly Coordinating Anions", Riddlestone, I. M.; Kraft, A.; Schaefer, J.; Krossing, I. *Angew. Chem. Int. Ed*. **2018**, *57*, 13982-14024.

[2] "Isolable fluorinated triphenylmethyl cation salts of $[HCB_{11}Cl_{11}]^-$: demonstration of remarkable hydride affinity", Gunther, S. O.; Lee, C.-I; Song, E.; Bhuvanesh, N.; Ozerov, O. V. *Chem. Sci*. **2022**, *13*, 4972-4976.

[3] "Is the Perfluorinated Trityl Cation Worth a Revisit? A Theoretical Study on the Lewis Acidities and Stabilities of Highly Halogenated Trityl Derivatives", Couchman, S. A.; Wilson, D. J. D.; Dutton, J, L. *Eur. J. Org. Chem*. **2014**, 3902-3908.

[4] "The Tris(pentafluorophenyl)methylium Cation: Isolation and Reactivity", Hoffmann, K. F.; Battke, D.; Golz, P.; Rupf, S. M.; Malischewski, M.; Riedel, S. *Angew. Chem. Intl. Ed*. **2022**, *61*, e202203777.

**Publications Acknowledging this Grant in 2021-2024**

*I. Publications with DOE grant being the lead:*

1. Davidson, J. J.; Gunther, S. O.; Leong, D. W.; Ozerov, O. V. Synthesis of Fluorinated Aminium Cations Coupled with Carborane Anions For Use as Strong One-Electron Oxidants, submitted to *Dalton Trans*. **2023**, *52*, 16027-16031.

Joshua J. Pak

## Gamma-Ray Induced Deconstruction of Urea Model Compounds: An Exploratory Study for Polymer Upcycling

Courtney L. Jenkins and Joshua J. Pak
Idaho State University, Department of Chemistry, Pocatello, ID 83209

### Presentation Abstract

The primary goal of this project is to develop strategies to better design future materials and transform polymer waste into industrially relevant raw chemicals, thereby reducing the amounts of plastics that wind up in landfills, incinerators, or the environment. We set out to examine the deconstruction and modification of condensation polymers upon exposure to gamma irradiation. The strategy is to prepare small model compounds that resemble key segments of common condensation polymers which can be irradiated by gamma-ray which may produce predictable degradation products based upon the polymer backbone and presence of additives. This project is mainly carried out by several undergraduates and MS students with assistance by a postdoctoral associate. The irradiation of samples was conducted using the gamma-irradiator user facility at the Idaho National Laboratory. In this presentation, we discovered that urea functional group containing model compounds can undergo selective deconstruction to form their original starting materials, isocyanate, when irradiated with gamma-ray in dichloromethane. The reaction proceeds through radiolysis of dichloromethane which produces a mixture of radical species followed by radical proton abstraction of phenyl urea model compounds that results in formation of phenyl isocyanates. In addition to mechanistic description of the reaction, we will present the scope and limitations of the deconstruction reaction of urea model compounds. Finally, we will discuss irradiation reactions of model compounds containing carbonates, urethanes, esters and amides.

**DE-SC0023413: Mechanistic and Kinetic Analysis of Polymer Deconstruction and Modification by Irradiation for Polymer Upcycling**

**PI:** Lead PI(s) Name(s) (*include only if different from above*)
**Postdoc(s):** Samjhana Pradhan

**Student(s):** Lauren E. Jager, Mikaela L. Spafford, Kendal P. Olson, Carlyn C. Osterhout, Raiden H. Hunter
**Affiliations(s):** (*include only if different from above*)

## RECENT PROGRESS

### *Training*

The project hired one postdoctoral associate who has been working on the project for about 1 year. The project hired and trained two MS students, three undergraduates and two high school summer interns. Of those students, one MS student and one undergraduate with BS.

### *Collaboration*

The project has a collaborative relationship with two scientists from the Idaho National Lab where the samples are irradiated with gamma-ray.

### *Research Progress*

We are in process of preparing our first paper to be submitted.

## Publications Acknowledging this Grant in 2021-2024

*Please classify your publications into two categories according to the source of support for the work published:*

*(I) Intellectually led by this grant - None*

*(II) Jointly funded by this grant and other grants with intellectual leadership by other funding sources*

1. Sayer, K. B.; Miller, V. L.; Merrill, Z.; Davis, A. E.; **Jenkins, C. L.*** Allyl Sulfides in Garlic Oil Initiate the Formation of Renewable Adhesives. *Polymer Chemistry*. **2023**. 14(26) 3091-3098.

2. Davis, A. E.; Sayer, K. B.; **Jenkins, C. L.*** A Comparison of Adhesive Polysulfides Initiated by Garlic Essential Oil and Elemental Sulfur to Create Recyclable Adhesives. *Polymer Chemistry*. **2022**. 13(32), 4634-4640.

3. Eder, M. L.; Call, C. B.; **Jenkins, C. L.*** Utilizing Reclaimed Petroleum Waste to Synthesize Water-soluble Polysulfides for Selective Heavy Metal Binding and Detection. *ACS Applied Polymer Materials*. **2022**. 4(2), 1110–1116.

Gerard Parkin

# Magnesium and Zinc Compounds for Transformations Involving $CO_2$ and C–C Bond Formation

David Vaccaro, Ran Yan, Aaron Loo, Gonzalo Fernandez de la Mora and Gerard Parkin
Columbia University, Department of Chemistry

## Presentation Abstract

The reactivity of unsaturated molecules with compounds that have M–H and M–R bonds provides an important means for functionalizing organic compounds. In this regard, we have investigated the reactivity of terminal Mg–H and Mg–Me bonds in well-defined monomeric compounds towards carbonyl compounds. For example, both [Tism$^{Pr^iBenz}$]MgH and [Tism$^{Pr^iBenz}$]MgMe react with methyl formate $HCO_2Me$ to afford the methoxy derivative [Tism$^{Pr^iBenz}$]MgOMe *via* a sequence that is proposed to involve the insertion of the carbonyl group to afford [Tism$^{Pr^iBenz}$]MgOC{(OMe)(H)X} (X = H, Me) which undergoes a formal β-methoxide elimination to afford [Tism$^{Pr^iBenz}$]MgOMe. The hydride complex [Tism$^{Pr^iBenz}$]MgH reacts similarly with ethyl acetate $MeCO_2Et$ to afford the ethoxide complex, [Tism$^{Pr^iBenz}$]MgOEt. In contrast, while the methyl complex [Tism$^{Pr^iBenz}$]MgMe likewise reacts with $MeCO_2Et$ to form [Tism$^{Pr^iBenz}$]MgOEt, a notable difference is that the β-keto ester derivative, [Tism$^{Pr^iBenz}$]Mg($\kappa^2$-etac) [$\kappa^2$-etac = Me(O)CHC(O)OEt], is also obtained as a result of C–C bond forming reaction. Metal formate compounds are of considerable relevance to transformations that involve the reduction of $CO_2$ and we have employed 2,2':6',2"-terpyridine (terpy) and 2,2'-bipyridine (bipy) to investigate the bonding and reactivity of zinc formate compounds.

## DE-SC0019204: Metal Catalyzed Transformations involving C–X bonds for the Conversions of Carbon Dioxide and Organic Chemicals

**Students:** David Vaccaro, Aaron Loo, Ran Yan, Eshe Hummingbird, Gonzalo Fernandez de la Mora

## RECENT PROGRESS

### 1. Reactivity of Mg–H and Mg–Me Bonds Towards Esters: C–C bond Forming reactions

We recently reported that the Mg–H and Mg–Me bonds of the *tris*[(1-isopropylbenzimidazol-2-yl)dimethylsilyl]methyl atrane compounds [Tism$^{Pr^iBenz}$]MgH and [Tism$^{Pr^iBenz}$]MgMe undergo insertion of the carbonyl moieties of $CO_2$, PhCHO and $Ph_2CO$ to afford [Tism$^{Pr^iBenz}$]Mg$O_2$CX, [Tism$^{Pr^iBenz}$]MgOCH(X)Ph and [Tism$^{Pr^iBenz}$]MgOCX$Ph_2$ (X = H, Me). In contrast, the corresponding reactions with enolizable ketones, namely $Me_2CO$ and PhC(O)Me, afford the enolate derivatives [Tism$^{Pr^iBenz}$]OC(Me)=$CH_2$ and [Tism$^{Pr^iBenz}$]OC(Ph)=$CH_2$. To develop further the chemistry of Mg–H and Mg–Me bonds with respect to carbonyl compounds, we have investigated the reactivity of [Tism$^{Pr^iBenz}$]MgH and [Tism$^{Pr^iBenz}$]MgMe towards esters. Interestingly, and in marked contrast to the aforementioned reactions, an additional pathway ensues, which leads to C–C bond formation.

Both [Tism$^{Pr^iBenz}$]MgH and [Tism$^{Pr^iBenz}$]MgMe react with methyl formate $HCO_2Me$ to afford the methoxy derivative [Tism$^{Pr^iBenz}$]MgOMe. A plausible mechanism for the formation of [Tism$^{Pr^iBenz}$]MgOMe upon reactions of [Tism$^{Pr^iBenz}$]MgH and [Tism$^{Pr^iBenz}$]MgMe with the ester $HCO_2Me$ involves the insertion of the carbonyl group to afford [Tism$^{Pr^iBenz}$]MgOC{(OMe)(H)X} which undergoes a formal β-methoxide elimination to afford [Tism$^{Pr^iBenz}$]MgOMe, as illustrated in Figure 1. The formation of the methoxide [Tism$^{Pr^iBenz}$]MgOMe from

$HCO_2Me$ is noteworthy because there are few examples of the formation of metal alkoxide compounds *via* reactions of metal-hydride and alkyl compounds with esters. The molecular structure of [Tism$^{Pr^iBenz}$]MgOMe has been determined by X-ray diffraction and is of interest because *(i)* there are no other monomeric magnesium methoxide compounds and *(ii)* the Mg–OMe moiety is ***linear*** with a short Mg–OMe bond.

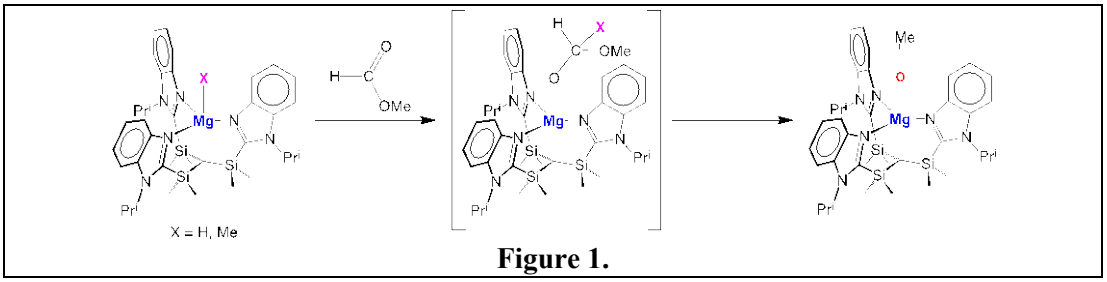


**Figure 1.**

The hydride complex [Tism$^{Pr^iBenz}$]MgH reacts similarly with ethyl acetate $MeCO_2Et$ to afford the ethoxide complex, [Tism$^{Pr^iBenz}$]MgOEt. The methyl complex [Tism$^{Pr^iBenz}$]MgMe likewise reacts with $MeCO_2Et$ to form [Tism$^{Pr^iBenz}$]MgOEt, but a notable difference is that the β-keto ester derivative, [Tism$^{Pr^iBenz}$]Mg($\kappa^2$-etac) [$\kappa^2$-etac = Me(O)CHC(O)OEt], is also obtained (Figure 2) and has been structurally characterized by X-ray diffraction. The different reactivity of [Tism$^{Pr^iBenz}$]MgH and [Tism$^{Pr^iBenz}$]MgMe towards $MeCO_2Et$ is of considerable interest, especially because the formation of [Tism$^{Pr^iBenz}$]Mg($\kappa^2$-etac) in the latter reaction involves the formation of a C–C bond. A plausible mechanism for the formation of [Tism$^{Pr^iBenz}$]Mg($\kappa^2$-etac) involves the initial formation of an enolate derivative, [Tism$^{Pr^iBenz}$]MgOC(OEt)=$CH_2$, which provides a means to form the C–C bond.

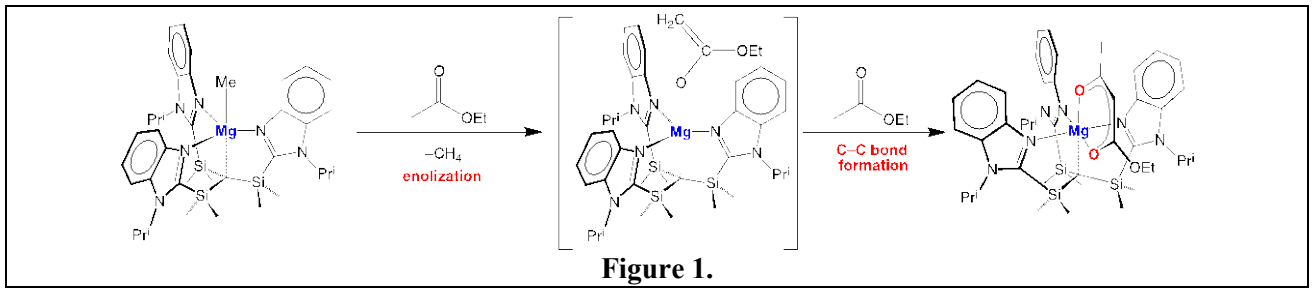


**Figure 1.**

**2. Catalytic Reactivity Mediated by a Tetrahedral Magnesium Methyl Compound**

Our previous studies have disclosed the reactivity of the *tris*[(1-isopropylbenzimidazol-2-yl)dimethylsilyl]methyl magnesium hydride and methyl compounds, [Tism$^{Pr^iBenz}$]MgH and [Tism$^{Pr^iBenz}$]MgMe, towards unsaturated substrates such as $CO_2$ and carbonyl compounds and so we have sought to extend this chemistry to related compounds that do not bear the atrane motif. Specifically, we have investigated the *tris*(pyrazolyl)hydroborato compound, [Tp$^{Bu^t,Me}$]MgMe, that features three nitrogen donors akin to [Tism$^{Pr^iBenz}$]MgMe but is devoid of the transannular Mg•••C interaction. Significantly, [Tp$^{Bu^t,Me}$]MgMe reacts with methyl ketones, RC(O)Me (R = Me, Bu$^t$, Ph), to afford enolate derivatives, [Tp$^{Bu^t,Me}$]MgOC(R)=$CH_2$ (Figure 3). The ability of [Tp$^{Bu^t,Me}$]MgMe to serve as a catalyst precursor has also been examined and we have demonstrated that it is very effective for achieving the hydroboration of ketones and aldehydes by pinacolborane (HBpin), as illustrated in Figure 3. In addition to hydroboration, [Tp$^{Bu^t,Me}$]MgMe also provides a catalyst system for dehydrocoupling of aniline and HBpin to form PhN(H)Bpin (Figure 3).

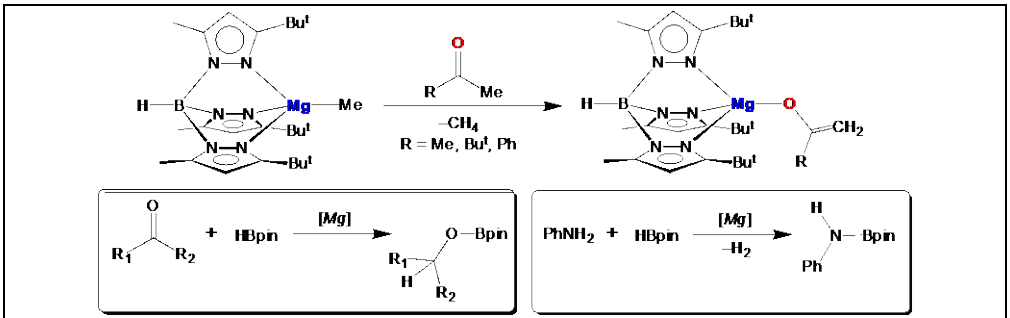


**Figure 3.**

### 3. Zinc Formate Complexes Supported by 2,2':6',2"-Terpyridine (terpy) and 2,2'-Bipyridine (bipy) for Reduction of $CO_2$ and Carbonyl Compounds

Metal formate compounds are of considerable relevance to both *(i)* the use of formic acid as a storage medium for $H_2$ *via* decarboxylation and *(ii)* transformations that involve the reduction of $CO_2$ and carbon capture and utilization. In this regard, we have previously described the roles of zinc formate compounds in the reduction of $CO_2$. To expand the role of zinc formate compounds, we have employed 2,2':6',2"-terpyridine (terpy) to afford (terpy)Zn$(O_2CH)_2$ (Figure 4). In addition, we have also employed 2,2'-bipyridine (bipy) to afford (bipy)Zn$(O_2CH)_2$, which has been synthesized in an analogous manner to that of (terpy)Zn$(O_2CH)_2$ *via* the reaction of Zn$(O_2CH)_2$ with bipy, but has also been obtained from $ZnH_2$. Specifically, (bipy)Zn$(O_2CH)_2$ can also be obtained directly from $CO_2$ by treatment of $ZnH_2$ with bipy followed by addition of $CO_2$. The insertion of $CO_2$ into the Zn–H bond is a critical step in the zinc-catalyzed reduction of $CO_2$ and has been directly observed for a variety of complexes but there are few examples that employ $ZnH_2$ to form zinc formate compounds.

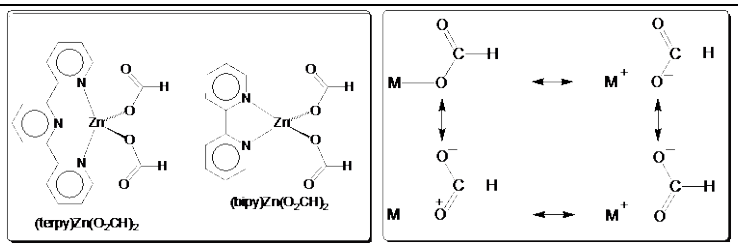


**Figure 4.**

While a large variety of zinc formate compounds are known, there are few examples of discrete mononuclear bis(formate) derivatives of the type $L_nZn(O_2CH)_2$ that feature pyridine donors. The structure of (bipy)Zn$(O_2CH)_2$ is also of interest because although there are structurally characterized examples of formate compounds of other metals supported by bipy, there no examples with the composition (bipy)M$(O_2CH)_2$. A noteworthy feature of (terpy)Zn$(O_2CH)_2$ and (bipy)Zn$(O_2CH)_2$ pertains to the C–O bond lengths within the formate moiety. For example, the ZnO–C(O)H bond [1.233(2) Å] of (bipy)Zn$(O_2CH)_2$ is only slightly longer than the C=O bond [1.220(2) Å], a difference (0.013 Å) that is significantly smaller than that expected (0.14 Å) on the basis of the sum of the respective single and double bond covalent radii of carbon and oxygen. Although the difference in C–O and C=O bond lengths, Δ(C–O), for (bipy)Zn$(O_2CH)_2$ is smaller than that anticipated on the basis of covalent radii, it is comparable to the values for other zinc formate compounds. In contrast to these small values of Δ(C–O) for metal formates, nonmetal derivatives have large values. For example, formate esters have an average Δ(C–O) value of 0.145 Å, while other nonmetal formates have an average value of 0.089 Å. These data indicate that the bonding within metal formates is significantly different to that in nonmetal derivatives. In particular, it suggests that the M–O–C(=O)H resonance structure that is typically used to represent a metal formate may not be the most appropriate and that ionic resonance structures may play a significant role (Figure 4).

The solid state structures of metal formate compounds are also of interest, as illustrated by the fact that formate is often a structural component of metal-organic frameworks. In this regard, hydrogen-bonding is known to be a structure directing element in solid state chemistry and we have observed that the aqua adduct (terpy)Zn($O_2CH$)$_2$•$H_2O$ exists in two polymorphic forms that exhibit distinctly different hydrogen bonding motifs. Specifically, while one polymorph forms chains in which water molecules link adjacent (terpy)Zn($O_2CH$)$_2$ molecules (Figure 5, right), the other polymorph consists of discrete tetranuclear [(terpy)Zn($O_2CH$)$_2$•$H_2O$]$_4$ moieties (Figure 5, left).

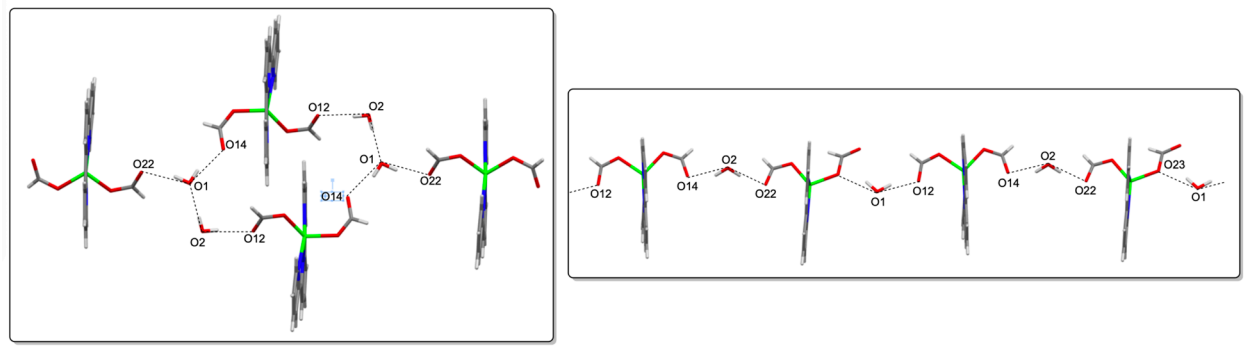


**Figure 5.**

In terms of reactivity, (terpy)Zn($O_2CH$)$_2$ participates in catalytic transformations involving $CO_2$ and carbonyl compounds *via* hydrosilylation and hydroboration reactions. For example, (terpy)Zn($O_2CH$)$_2$ achieves hydroboration of $Me_2CO$ and $Ph_2CO$ by HBpin to afford $R_2C(H)OBpin$, and a competition experiment indicates that insertion of $Me_2CO$ is more favored than that of $Ph_2CO$ by a factor of *ca.* 3. Similar reactivity is also observed for Si–H bonds, as illustrated by the triple insertion of $Ph_2CO$, PhC(O)Me, $Me_2CO$ and PhCHO into the Si–H bonds of $PhSiH_3$ to afford PhSi[OCH(R)R']$_3$ *via* $PhSiH_2$[OCH(R)R'] and PhSiH[OCH(R)R']$_2$. A competition experiment, nevertheless, indicates that hydrosilylation is less favored than hydroboration. Specifically, addition of $Ph_2CO$ to a mixture of HBpin and $PhSiH_3$ in the presence of (terpy)Zn($O_2CH$)$_2$ results in the quantitative formation of $Ph_2CH(OBpin)$ and none of $PhSi(OCHPh_2)_xH_{3-x}$. In addition to RC(O)R' carbonyl compounds, $CO_2$ also undergoes hydroboration and hydrosilylation by HBpin and $(MeO)_3SiH$. Thus, $CO_2$ reacts with HBpin in the presence of (terpy)Zn($O_2CH$)$_2$ to afford the formate compound $HCO_2Bpin$ and also undergoes hydrosilylation by $(MeO)_3SiH$ to afford $HCO_2Si(OMe)_3$.

**4. An Anionic Zinc Hydride Compound for Reduction of Carbonyl Compounds**

While a variety of molecular zinc hydride compounds are now known, anionic variants are rare. Nevertheless, we recently synthesized and structurally characterized the anionic complex, $[HZn(pz^{Me2})_3ZnH]^-$ by the reaction of $ZnH_2$ with 2 equivalents of 3,5-dimethylpyrazole ($Hpz^{Me2}$) in the presence of Li($pz^{Me2}$) and have observed that it is effective for the room temperature hydrosilylation of $Me_2CO$, PhC(O)Me and $Ph_2CO$ with $PhSiH_3$ to afford $PhSiH_x$[OCHRR']$_{3-x}$ derivatives.

**Publications Acknowledging this Grant in 2021-2024**

*(I) Intellectually led by this grant*

1. Vaccaro, D.; Yan, R.; Parkin, G. Reactivity of [Tism$^{Pr^iBenz}$]MgH and [Tism$^{Pr^iBenz}$]MgMe towards Carbonyl Compounds: Access to Terminal Alkoxide and Enolate Complexes *Organometallics* **2024**, 43, 746−763.
2. Loo, A.; Fernandez de la Mora, G.; Parkin, G. Synthesis and Structural Characterization of 2,2':6',2"-Terpyridine Zinc Formate: Hydroboration and Hydrosilylation of $CO_2$ and Carbonyl Compounds" *Polyhedron* **2024** (DOI: 10.1016/j.poly.2024.117235).
3. Shlian, D. G.; Amemiya, E.; Parkin, G. Synthesis and Structural Characterization of *Bis*(2-pyridylthio)methyl Zinc Hydride and the Catalytic Hydrosilylation and Hydroboration of $CO_2$ *Chem. Commun.* **2022**, 58, 4188-4191.
4. Ruccolo, S.; Sambade, D.; Shlian, D. G.; Amemiya, E.; Parkin, G. Catalytic Reduction of Carbon Dioxide by a Zinc Hydride Compound, [Tptm]ZnH, and Conversion to the Methanol Level *Dalton Trans.* **2022**, 51, 5868–5877
5. Sambade, D.; Collins, C.; Parkin, G. Structure and Bonding of 1,2,4-Triazole Thiones Derived from Nitron *J. Mol. Struct.* **2021**, *1231*, 129682.
6. Ruccolo, S.; Amemiya, E.; Shlian, D. G.; Parkin, G. Hydrosilyation of $CO_2$ Using a Silatrane Hydride: Structural Characterization of a Silyl Formate Compound *Can. J. Chem.* **2021**, *99*, 259-267.
7. Quinlivan, P. J.; Loo, A.; Shlian, D. G.; Martinez, J.; Parkin, G. *N*-heterocyclic Carbene Complexes of Nickel, Palladium and Iridium Derived from Nitron: Synthesis, Structures and Catalytic Properties *Organometallics* **2021**, *40*, 166-183.
8. Rauch, M.; Strater, Z.; Parkin, G. Methods for Preparing Formaldehyde from Carbon Dioxide US Patent # 11,111,199 (September 7, 2021).
9. Sattler, W.; Shlian, D. G.; Sambade, D.; Parkin, G. Synthesis and Structural Characterization of *Bis*(2-pyridylthio)(*p*-tolylthio)methyl Zinc Complexes and the Catalytic Hydrosilylation of $CO_2$ *Polyhedron* **2020**, *187*, 114542.
10. Amemiya, E.; Loo, A.; Shlian, D. G.; Parkin, G. Rhenium versus Cadmium: An Alternative Structure for a Thermally Stable Cadmium Carbonyl Compound *Chem. Sci.* **2020**, *11*, 11763-11776.

*(II) Jointly funded by this grant and other grants with intellectual leadership by other funding sources*

1. Parkin, G. Impact of the Coordination of Multiple Lewis Acid Functions on the Electronic Structure and $v^n$ Configuration of a Metal Center *Dalton Trans.* **2022**, *51*, 411-427.

# Solidification of, and Catalysis with, Transient Metallophosphidenes

David C. Powers
Texas A&M University, Department of Chemistry

## Presentation Abstract

Terminal metal–phosphorous (M–P) complexes are of significant contemporary interest as potential platforms for P-atom transfer (PAT) catalysis. Decarbonylation of metal-phosphaethynolate (M–PCO) complexes is often carried out to generate terminal M–P complexes and observation of transition-metal diphosphorous complexes (*i.e.*, M–P–P–M species), following thermolysis or photolysis of M–PCO precursors, is frequently advanced as evidence for the intermediacy of unobserved, transient M–P species. Here, we demonstrate that while diphosphorous complexes can arise from reactive M–P species, P–P coupling can also proceed directly from M–PCO species without the intermediacy of M–P complexes. Photochemical extrusion of CO from a pincer-supported Ni(II)–PCO complex at 77 K affords an observable Ni–P species, which is best described as a triplet, Ni(II)-metallophosphinidene with two unpaired electrons localized on the atomic phosphorous ligand. Thermal annealing of this transient Ni–P complex results in rapid dimerization to afford the corresponding $P_2^{2-}$-bridged dinickel complex. Unexpectedly, the same $P_2^{2-}$-bridged dinickel complex can be accessed via a heretofore unknown thermal pathway initiated by [2+2] cycloaddition between two equivalents of the Ni–PCO to afford an isolable 1,3-diphosphacyclobutadione-bridged dinickel complex. These observations provide critical mechanistic understanding of the activation modes relevant to PCO activation of P-atom transfer.

## DE-SC0024121: Solidifying Reactive Intermediates to Advance Hydrocarbon Upgrading Catalysis

**Postdoc(s):** Rick Thompson, Duleeka Wannipurage
**Student(s):** Aishanee Sure, Matthew Figgins, Arpan Paikar

## RECENT PROGRESS

### *Synthesis, Characterization, and Photochemistry of $Ru_2$(II,III) Complexes of Chalcogen Oxides*

We developed the synthesis, characterization, and photochemistry of a pair of $Ru_2$(II,III) complexes featuring dibenzochalogen oxide ligands in order to interrogate potential $Ru_2$ oxo photochemistry. These studies were further motivated by an ongoing interest in the program to develop photolabile ligands without gaseous leaving groups in order to access solid-state photochemistry without intracrystalline pressure that we hypothesize often leads to loss of crystallinity. Here, we described that treatment of $[Ru_2(chp)_4H_2O]BF_4$ with either dibenzo[*b*,*d*]thiophene 5-oxide (DBTO) or dibenzo[*b*,*d*]selenophene 5-oxide (DBSeO) affords $[Ru_2(chp)_4DBTO]BF_4$ or $[Ru_2(chp)_4DBSeO]BF_4$, respectively, in which the dibenzochalcogen oxide ligands display coordination through oxygen (chp = 6-chloro-2-oxypyridinate). Both

dibenzochalcogen oxide complexes are characterized by NMR, UV-vis, and IR spectroscopies as well as X-ray crystallography. Photolysis (λ = 300 nm) of $[Ru_2(chp)_4DBTO]BF_4$ and $[Ru_2(chp)_4DBSeO]BF_4$ effects cleavage of the chalcogen–oxygen bond and oxygen atom transfer to phosphine additives is observed. These results expand the family of potential metal–oxo photoprecursors and demonstrate new opportunities in the photochemical synthesis of reactive metal-oxygen complexes.

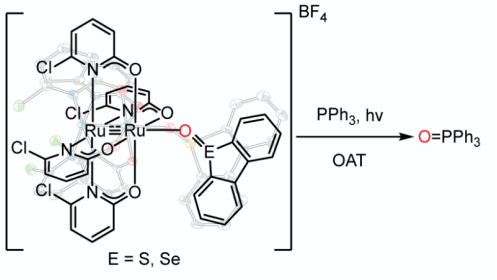


**Figure.** Oxo photochemistry of dibenzochalcogen oxide complexes.

## Probing Aerobic Oxidation Catalysis with TAM-3, a MOF with Accessible Co(II) Sites and Large Pore Channels

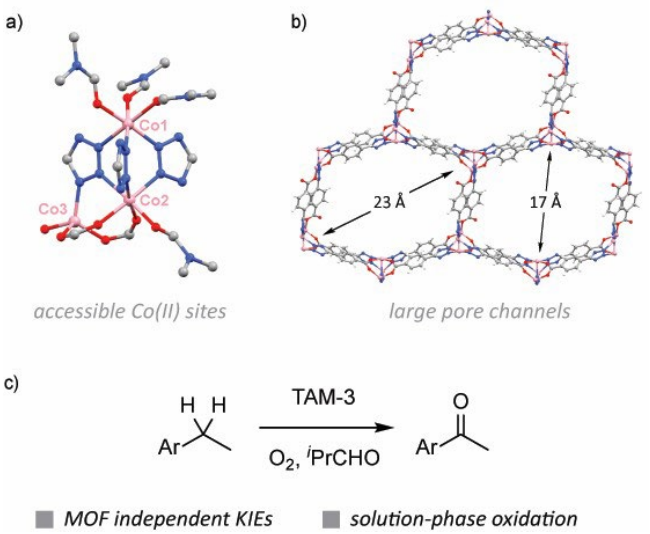


**Figure.** (a) Accessible octahedral and tetrahedral Co(II) centers in TAM-3. (b) Large pseudohexagonal pore channels of TAM-3 allow for easy substrate diffusion. (c) Kinetic studies suggest solution phase oxidation instead of MOF-centered catalysis.

Application of microporous MOF-based materials as catalysts for C–H functionalization continues to garner significant attention, however tools to understand then impact of material structure an reaction kinetics are largely not available due to challenges deconvoluting the impact of mass transport barriers. We have prepared a new MOF, TAM-3, which features Co(II) sites housed within a large-pore lattice. Single crystal X-ray diffraction and other spectroscopic analyses show distinct octahedral and tetrahedral Co(II) sites formed by diverse coordination modes of the tetrazolyl linker. These Co(II) centers are found to be readily react with peracids, resulting in the formation of Co(III). Substrate oxidation was demonstrated in the presence of TAM-3 under aerobic oxidation conditions. Further investigations employing kinetic isotope effect (KIE) and diastereoselectivity analyses revealed that the oxidation process primarily occurs via aldehyde autoxidation intermediates in the solution phase, rather than direct involvement of TAM-3. This study highlights the importance of conducting kinetic experiments to assess the true catalytic potential of MOFs, despite their apparent reactivity and significantly expands earlier work from the group by demonstrating that even large-pore materials face considerable mass-transport barriers to interstitial catalysis.

**Publications Acknowledging this Grant in 2021-2024**

*Intellectually led by this grant*

*Pre-Prints*

Deegan, M. M.; Antonio, A. M.; Korman, K. J.; Ezazi, A. A.; Yap, G. P. A.; Powers, D. C.*; Bloch, E. D.* Manipulation of Charged Porous Cages as Tunable Platforms for Selective Gas Adsorption. **2024**, *submitted. ChemRXiv* **2023**, DOI: 10.26434/chemrxiv-2023-mvsps.

*Peer-Reviewed Publications*

Paikar, A.; Martinez, E.; Powers, D. C.* Synthesis, Characterization, and Photochemistry of $Ru_2$(II,III) Complexes of Chalcogen Oxides. *Polyhedron* **2024**, *250*, 116798. DOI: 10.1016/j.poly.2023.116798

*Student Dissertations*

Ezazi, A. A. *New Materials for the Immobilization, Generation, and Characterization of Reactive Intermediates.* Texas A&M University, 2023.

Talat S Rahman

## Profound effect of ammonium-based cations on $CO_2$ electrolysis: insights from theory and experiments

Kaige Shi, Duy Le, Theodoros Panagiotakopoulos, John Janisch, Xiaofeng Feng, and Talat S. Rahman

Department of Physics and Renewable Energy and Chemical Transformations (REACT) Cluster, University of Central Florida, Orlando, FL 32816, USA.

### Presentation Abstract

Electrolyte cations play a critical role in the electrochemical $CO_2$ reduction reaction ($CO_2RR$), as indicated by recent studies using alkali metal cations. Through an intertwined computational and experimental effort, we show that non-metal ammonium-based cations can have an even more profound effect on the $CO_2$ adsorption characteristics and $CO_2RR$ activity than the popular metal cation $Na^+$. *Ab initio* calculations based on grand canonical density functional theory (GC-DFT) find both $NH_4^+$ and $CH_3NH_3^+$ to help bind $CO_2$ to a Bi electrode (chosen for its propensity to lead to both formate and CO production) more strongly than $Na^+$ and track the difference to the electrostatic interaction between the cations and adsorbed $CO_2$, benefiting from the charge distribution and hydration shell of the cations. These results are validated by experimental studies which find a much stronger promotional effect of $CH_3NH_3^+$ cation on the $CO_2RR$ than $Na^+$, and further reveal a significant impact of the cation identity and concentration on CO production activity but a minor one on formate. Interestingly, we find the most facile pathway for formate formation to be with $CO_2$ in the solvent in the vicinity of H adsorbed on the Bi electrode, while $CO_2$ adsorption is an essential step for CO production which proceeds via proton shuttling. Furthermore, for the hydrogen evolution reaction (HER) which generally competes with CO2RR, we also establish the efficacy of nonmetal cations over that of $Na^+$, as summarized by the trend $(CH_3)_4N^+ < Na^+ < CH_3NH_3^+ < (CH_3)_2NH_2^+ < (CH_3)_3NH^+ < NH_4^+$. These comparative in-depth analyses of reaction mechanisms for CO2RR and HER provide insights into processes that could serve as descriptors to accelerate the discovery of cost effective electrodes for CO2RR.

**Grant: DE-SC0024083**
**Grant Title: Theoretical and experimental investigations of the electrocatalytic environment for sustainable fuel production**

**Co-PI:** Xiaofeng Feng
**Senior Personnel**: Duy Le
**Student(s):** Kaige Shi, Theodoros Panagiotakopoulos, John Janisch, Zhuanghe Ren

### *Effect of quaternary ammonium cations on $CO_2$ electroreduction*

In Fig. 1, we compare our findings for $CO_2$ adsorption characteristics and the propensity for formate and CO formation in the presence Na+ and three quarternary ammonium cations. In Fig 1b, GC-DFT calculations find that both $NH_4^+$ and $CH_3NH_3^+$ help bind $CO_2$ to a Bi electrode more strongly than $Na^+$. At the same time experimental data in Fig. 1c, show that while formate production is insensitive to the nature of the cation, the non-metal cations are much more effective than Na+ for CO formation. These results are in qualitative agreement with our finding for the reaction pathways for both processes. Our calculations of the reaction mechanism of CO2RR with the presence of $NH_4^+$ cation, as shown in Fig. 2, reveal that the reduction of $CO_2$ to formate is driven by the direct hydrogenation of aqueous $CO_2$ with a hydrogen atom adsorbed on the electrode (H*), i.e., $CO_{2(aq)}$ + H* → $HCOO^-$, reaction (1)→(3) in Fig. 2a. We find that the formation of CO requires $CO_2$ to adsorb on the electrode before forming the adsorbed intermediate COOH*, via a proton shuttling process, i.e., H* moves from the Bi(111) electrode to an $H_2O$ molecule one of its H atom is then transfer to a $CO_2$*, as shown in Fig. 2b. The CO is formed via the dissociation of the COOH* with the help of a proton donated from $NH_4^+$ cation. Such a proton donation is not possible with $Na^+$ as the cation explaining the improvement of CO formation with ammonium-based cation as shown in Fig. 1d. We also found that the rate-

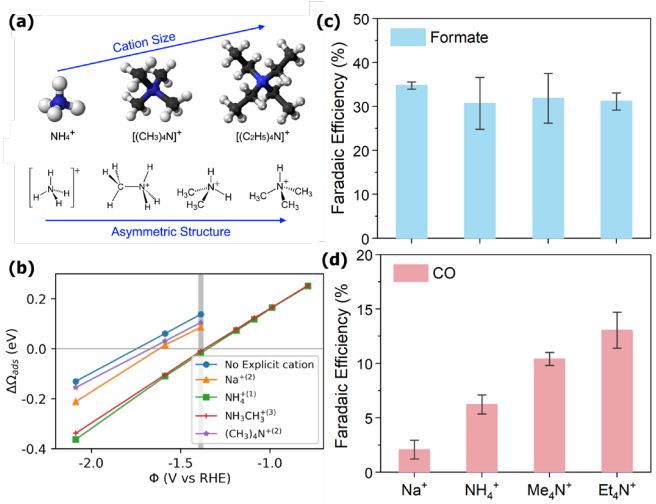


***Figure 1 (a)*** *Tunability of non-metal cation.* ***(b)*** *Dependence of the grand canonical adsorption energy of $CO_2$ on Bi electrode with the presence of metal and non-metal cation. Dependent on cation of Faraday efficiency towards format (c) and CO (d) formation measured for $CO_2$ reduction on Bi electrode.*

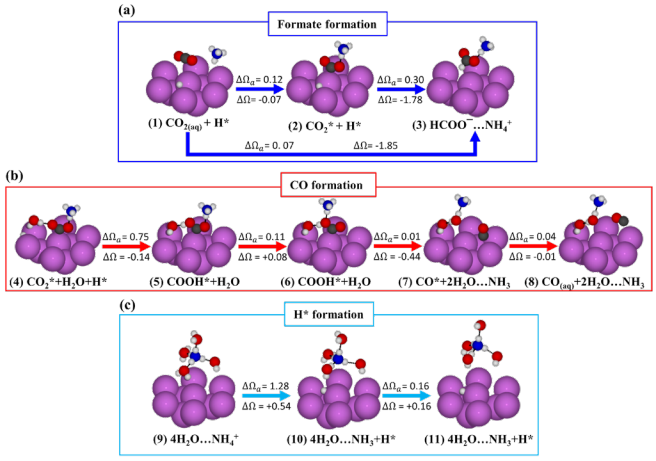


***Figure 2*** *Mechanism of $CO_2$ reduction on Bi(111) in the presence of $NH_4^+$. Calculated grand-canonical activation barrier ($\Delta\Omega_a$) and grand-canonical reaction energy ($\Delta\Omega$) at −1.4 V vs RHE for elementary steps of the proposed mechanism for the $CO_2$RR on Bi(111) in the presence of $NH_4^+$. Magenta, black, red, blue, and white balls represent Bi, C, O, N, and H atoms. Only 10 Bi atoms surrounding the reaction site are shown for clarity.*

limiting step for the formation of both products is the water dissociation to form H* (Volmer process) as shown in Fig. 2c.

### *Hydrogen evolution reaction enhanced by ammonium cations*

We have investigated the effect of cations on the hydrogen evolution reaction (HER), which is a competing reaction in the $CO_2$ electrolysis but holds great promise for the sustainable production of hydrogen as a clean fuel and energy carrier. We observe a general trend of HER activity depending on cations: $(CH_3)_4N^+$ < $Na^+$ < $CH_3NH_3^+$ < $(CH_3)_2NH_2^+$ < $(CH_3)_3NH^+$< $NH_4^+$, as shown in Figure 3a-b. The Tafel plots and Electrochemical Impedance Spectroscopy further confirm a lower energy barrier for the HER in the presence of the substituted ammonium cations: $CH_3NH_3^+$, $(CH_3)_2NH_2^+$, and $(CH_3)_3NH^+$, consisting with the measured HER activities. We performed grand canonical ab initio molecular dynamics (GC-AIMD) of the $H_2O$ and cation structures on Pt electrode to understand the effect of cations on HER. In the presence of $Na^+$, the grand canonical activation free energy ($\Delta\Omega^\dagger$) is found to be 1.07 eV (Fig. 3c1-c3). Moreover, after the Volmer step, $H_2O$ dissociation (**c1**→**c2**), the proton transfer within $H_2O$ network (**c2**→**c3**) helps to transport the $OH^-$ group away from the electrode. With the presence of $NH_4^+$ cation, the activation barrier of the Volmer step reduces to 0.66 eV (Fig. 3d1-d3). This reduction of barrier is attributed to the proton shuttling from $NH_4^+$ to $OH^-$ to form $NH_3$…$H_2O$ complex. In addition, $NH_4^+$ cation can also act as a direct proton donor for the *H formation on metal electrodes, shown in Fig. 3e1-e3. The activation barrier of this process is found to be 0.81 eV. The lower activation energy of Volmer step and the direct proton donation to electrode of ammonium cation helps improve HER, as shown in experiment.

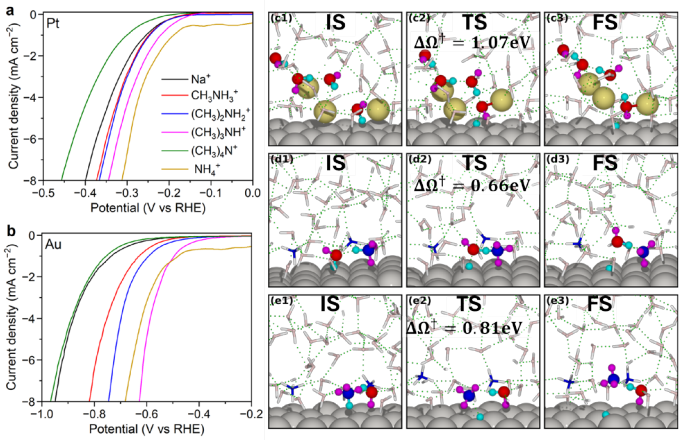


***Figure 3.*** *Comparison of the HER activities in the presence of $Na^+$ and ammonium cations. Linear sweep voltammetry (LSV) curves recorded on (a) Pt and (b) Au electrodes in 0.1 M $H_2$-saturated NaCl, $NH_4Cl$, $CH_3NH_3Cl$, $(CH_3)_2NH_2Cl$, $(CH_3)_3NHCl$, and $(CH_3)_4NHCl$ electrolytes, respectively. Scan rate: 10 mV $s^{-1}$. GC-AIMD simulations to compute activation barrier of the Volmer step in the presence of $Na^+$ cation **(c1-c3)** and $NH_4^+$ cation **(d1-d3)** and of the direct proton donation from $NH_4^+$ cation to Pt electrode **(e1-e3)**. The calculations were done with electrode potential kept constant at -0.5 V vs RHE.*

### *Ammonium-cation-enhanced acidic $CO_2$ electrolysis on Au*

Taking cues from the above studies that ammonium-based cations selectively enhance the $CO_2$RR to CO on Bi, we further investigate the cation effect on acidic $CO_2$ electrolysis with Au nanocatalyst using selected cations including $NH_4^+$, $CH_3NH_3^+$ and $(CH_3)_4N^+$, with $Na^+$ as a reference. A comparison of the cations is performed for acidic $CO_2$RR with 5-nm sized Au nanoparticles in a gas-diffusion electrode (GDE) flow cell. As shown in Figure 4, both $NH_4^+$ and $CH_3NH_3^+$ cations show a more significant promotion of the $CO_2$RR than $Na^+$, achieving a CO production activity that is around three times that with $Na^+$ (Figure

4d). Detailed analyses of the cation concentration dependence, pH dependence, and kinetic isotope effect attribute the stronger promotional effect of $NH_4^+$ and $CH_3NH_3^+$ to the electrostatic stabilization of $*CO_2$ adsorption, which is the rate-limiting step for $CO_2$RR on Au. In addition, the lower p$K_a$ of $NH_4^+$ helps buffer the local pH in the vicinity of the electrode, thus allowing more $CO_2$ to react at the interface. A further comparison of the cation effect on Au catalysts of different sizes ranging from 3.5 to 8.5 nm reveals a similar promotional effect, *leading to the conclusion that the cation effect is independent of the nature and population of active sites.* Our work further advances the understanding of the cation effect on $CO_2$RR using ammonium-based cations, and suggests a cation strategy to enhance acidic $CO_2$ electrolysis.

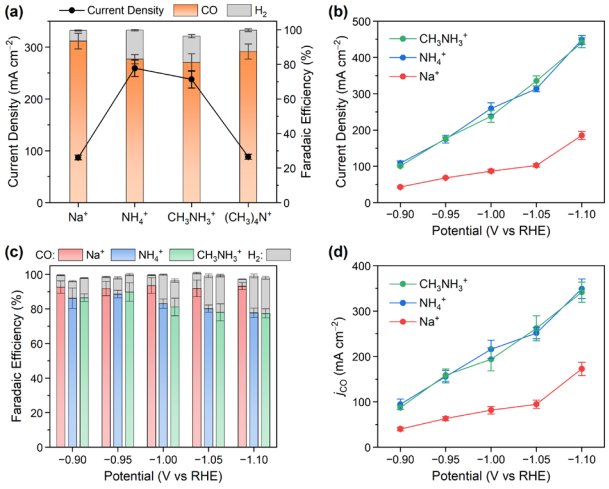


***Figure 4.*** *Effects of different cations on the $CO_2$RR with Au catalyst in a GDE flow cell. (a) Total current densities and Faradaic efficiencies for $CO_2$RR at −1.0 V vs RHE in acidic electrolytes (pH = 2) containing 1.0 M cations. (b−d) Potential-dependent performance for the $CO_2$RR in acidic electrolytes with 1.0 M cations: (b) total current densities; (c) Faradaic efficiencies; (d) partial current densities for CO production.*

### *Method development for simulations of electrochemical environments*

We have developed an efficient computational method that enables **grand-canonical (GC) *ab initio* molecular dynamics (AIMD) simulations** of the electrochemical system for tracking the dynamics of explicit solvent molecules in the presence a constant electrode potential. In addition, we have developed a **SOLHYBRID** model that can simulate the inner Helmholtz plane (IHP) and outer Helmholtz plane (OHP) of the electric double layer explicitly while treating the diffuse layer implicitly. More importantly, to make application of the self-consistent grand canonical DFT (GC-DFT) feasible for systems with few hundred atoms, we have proposed the **TPOT** (**T**arget **POT**ential) routine that was implemented locally to the popular Vienna Ab initio Simulation Package (VASP). **Fig. 5** shows an example of constant electrode potential AIMD simulation of the $CO_2$ adsorption on Au(110) with the presence of $K^+$ cation at a constant electrode potential of -1V vs RHE.

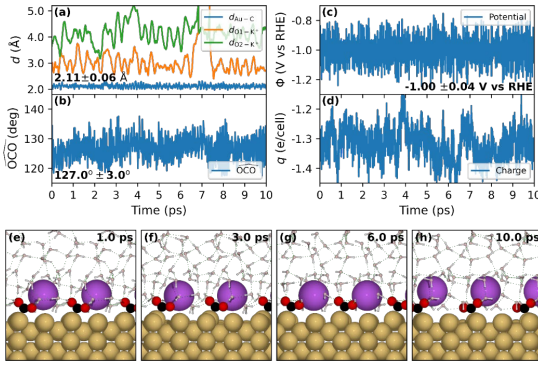


***Figure 5***. *Grand-canonical AIMD simulation in an electrochemical environment. Evolution of **(a)** distance from Au and C atom of $CO_2$ molecule ($d_{Au-C}$), distance from $K^+$ to two O atoms of $CO_2$ molecule ($d_{O1-K^+}$ and $d_{O2-K^+}$), **(b)** the bending angle of the $CO_2$ molecule ($\widehat{OCO}$), **(c)** potential of Au(110) electrode ($\Phi$), and **(d)** charge in the supercell (q) during the GC-AIMD simulation of $CO_2$-$K^+$/Au(111) with SOLHYBRID model at TPOT algorithm at -1 V vs RHE. Snapshots of the simulations are shown in **(e-h)**. Yellow, black, red, and purple balls represent Au, C, O, and K atoms.*

**Publications Acknowledging this Grant in 2023-2024**

*Please classify your publications into two categories according to the source of support for the work published:*

*(I) Intellectually led by this grant*

- D. Le, "An Explicit-Implicit Hybrid Solvent Model for Grand Canonical Simulations of the Electrochemical Environment," *Submitted* (preprint ChemRvix DOI:10.26434/chemrxiv-2023-z2n4n)
- K. Shi, D. Le, T. Panagiotakopoulos, T. S. Rahman, and X. Feng, "Effect of Ammonium-Based Cations on $CO_2$ Electroreduction," *Submitted*.
- Z. Ren, K. Shi, Z. Meng, T. Egan, D. Le, T. S. Rahman, and X. Feng, "Cation-enhanced acidic CO2 electrolysis on a molecular catalyst," *Submitted*.

*(II) Jointly funded by this grant and other grants with intellectual leadership by other funding sources*

Daniel K. Schwartz

## Biocatalytic Nanoparticles that Enable Supra-biological Cascade Reactions

Daniel K. Schwartz and Joel L. Kaar
University of Colorado Boulder

### Presentation Abstract

In this project, we are developing biohybrid catalytic materials that expand the performance limits of enzymes far beyond what can be achieved through conventional enzyme engineering approaches. These biocatalysts exhibit greatly enhanced catalytic activity, enabling one-pot multi-step cascade reactions that are relevant to fuel production and polymer upcycling applications. In the process, we are developing insights into the mechanisms by which abiotic materials interact with enzymes to stabilize and/or "heal" them. These biocatalysts also serve as highly tunable systems to test fundamental questions about how the efficiency of one-pot cascade reactions depends on the selectivity and activity of catalysts for independent steps. The catalysts comprise complex materials as enzyme supports, including random copolymer brushes and mixed lipid bilayers. A critical requirement for this research involves the need to understand complex, dynamic, and heterogeneous environments, where biomolecules interact with material interfaces via both covalent and non-covalent interactions. In particular, to understand the mechanisms by which abiotic materials enhance the performance of biocatalysts, it is necessary to directly probe the relevant dynamic behavior of enzymes, in particular the conformational changes that reflective catalytic activity. Notably, we are employing single-molecule FRET methods that are uniquely capable of this type of analysis, which is performed in a highly multiplexed manner, resulting in large datasets that are analyzed using statistical methods and machine learning algorithms to provide insights into the mechanisms that underlie complex behavior.

**DE-SC0023449**
**Biocatalytic Nanoparticles that Enable Supra-biological Cascade Reactions**
**PI:** Daniel K. Schwartz and Joel L. Kaar
**Student(s):** David Kelaita and Evan Bissiri
**Affiliations(s):** University of Colorado Boulder

## RECENT PROGRESS

### *Aim 1: Catalyst Design, Preparation, and Activity Screening*

We have prepared biohybrid catalytic nanoparticles by incorporating enzymes of interest into tunable complex support materials, and we are functionally screening these chimeric materials, by measuring catalytic activity under harsh conditions, to identify promising candidates, that demonstrate strong (or weak) performance-enhancing effects. Parameters of particular interest for use in cascade reactions, are thermal and pH denaturation resistance. Earlier in this grant period, we found that incorporation of small amounts of aromatic monomers into polymer brush supports greatly enhanced the thermal stability and activity of LipA lipase, which has a particularly high fraction of surface exposed aromatic residues. We hypothesize that this remarkable stabilization is related to aromatic pi-stacking interactions between support and enzyme surface moieties. More recently, to impart supra-biological performance in the context of extreme pH, we have employed a high throughput screening approach to discover new supports that incorporate anionic / cationic monomers into polymer brush supports to shift the local pH while maintaining or enhancing enzyme stability and activity. Interestingly, this resulted in the discovery of a new three-component anionic polymer brush support that resulted in the highest ever activity of LipA at low pH and high temperature.

We have developed a protocol for making supported lipid bilayers (SLBs) using silica-coated magnetic nanoparticles as the support, enhancing our ability to purify nanoparticle catalyst without the needs for centrifugation and/or vortexing for re-suspension. Successful coating of these particles has been confirmed using dynamic light scattering and zeta potential measurements. We have successfully used these SLBs to immobilize LipA, one of the proposed cascade components. We have screened a variety of mixed lipid supports to test their ability to enhance immobilized enzyme performance (activity and stability) under extremes of pH and temperature. Specific support compositions were identified that greatly enhanced the performance of LipA, while the performance of benzaldehyde lyase (which exhibits strong stability in the native soluble state) was only modestly improved by immobilization to lipid bilayer supports.

### *Aim 2: Mechanistic Information from SM-FRET*

Here we are studying and understanding the mechanisms of biocatalytic performance enhancement using highly multiplexed single-molecule Förster Resonance Energy Transfer characterization of enzyme conformational dynamics, distinguishing between chemical stabilization of the native state, rescue of inactivated biocatalytic sites, and physical stabilization through nanoconfinement. We have developed a dual labeled Lipase A construct for use in single molecule FRET experiments to interrogate the mechanisms of enzyme stabilization on surface grafted polymer brushes, and supported lipid bilayers.

In this period, we used this method to understand the mechanisms by which polymer brush supports containing aromatic monomers enhance the thermal stability and activity of LipA. SM-FRET microscopy experiments revealed that these supports maintained catalytic LipA activity in thermally denaturing environments by preserving the folded and catalytically-active state of LipA. A Markov chain analysis demonstrated that this effect was achieved via simultaneous stabilization of the folded state and chaperone-like acceleration of refolding, both due to interactions with aromatic moieties. SM-FRET also revealed that optimally composed supports restricted LipA's unfolded state to a constrained partially unfolded conformation, resulting in the effective acceleration of enzyme refolding. Experiments are currently underway to explore the mechanistic basis for the stabilization of LipA on anionic polymer supports at low pH.

***Aim 3: and Biocatalytic Cascade Reactions***

Here we are employing the knowledge from Aims 1 and 2 to create biocatalytic systems that perform selective and efficient one-pot multi-step enzymatic reactions. The systems describe above are used to develop knowledge about the connections between biocatalyst and process design and cascade reaction efficiency. The performance of biohybrid catalytic nanoparticles are compared to soluble enzymes in cascade reactions under extreme conditions. Moreover, we are comparing the effects of employing multi-enzyme nanoparticles (where each particle catalyzes the full cascade reaction) vs. mixing multiple types of single-enzyme nanoparticles (where each particle catalyzes a single reaction step). We have developed an activity assay for the lipase + lyase cascade reaction using high performance liquid chromatography (HPLC) and are comparing the performance of cascade reactions using soluble vs. immobilized enzyme catalysts.

In particular, supports that enhance activity and stability of LipA at low pH are of particular interest because the cascade reaction produces an acid side-product, gradually deactivating LipA. We have determined that immobilization on optimized lipid bilayer supports can improve the yield by as much as 50% over 24h.

**Publications Acknowledging this Grant in 2021-2024**

*(I) Intellectually led by this grant*

1. Bisirri, E.A.; Kaar, J.L.; Schwartz, D.K. High Throughput Screening Identifies Unexpected Polymer Supports to Improve Enzyme Performance at Low pH. (under review)
2. Kelaita, D.; Kaar, J.L.; Schwartz, D.K. Enhancement of an Enzymatic Cascade using Lipid Bilayers (under preparation)

Christo S. Sevov

# Electrocatalytic Grafting of PVC Plastics

The Ohio State University

## Presentation Abstract

The presented poster will detail our efforts towards electrocatalytic functionalization of polyvinyl chloride (PVC) to covalently graft plasticizing additives directly to the polymer backbone. Despite the wide-ranging uses of polyvinyl chloride (PVC) plastics, it is the high loadings of plasticizers and additives that give PVC many of the bulk properties desired by consumers. However, those non-covalent additives can leach from formulated PVC plastics to deteriorate the function of the original plastic and cause environmental hazards.

PVC modification reactions have long been sought after, but known methodologies suffer from limited fragments that can be grafted, elimination reactions, or chain fragmentation. Here, mechanistic insights guided the design of electrocatalysts capable of modifying the C-Cl bonds of PVC under mild conditions with high selectivity and suppress side reactions that plague known methods. Functional groups that mimic common PVC plasticizers can be covalently installed into the backbone of PVC to create new materials with distinct bulk properties from the original PVC. The degree of polymer grafting – and therefore the bulk material property – is easily controlled by simply changing the grafting agent and the redox capacity that is passed during electrolysis. This strategy is directly applied to mixtures of consumer PVC products to create chemically- and leach-resistant PVC materials.

**DE-SC0021961: Electrocatalytic Modification and Upcycling of Polyvinylchloride and Chloroparaffins**
**Grant Title Second Line if Necessary**

**PI:** Christo Sevov
**Student(s):** Jordan Zackasee, Samir Al Zubaydi, Immaculata Onuigbo

## RECENT PROGRESS

### Publications Acknowledging this Grant in 2021-2024

*(I) Intellectually led by this grant*

1. Al Zubaydi, S.; Onuigbo, I. O.; Truesdell, B. L.; Sevov, C. S. Cobalt-Catalyzed Electroreductive Alkylation of Unactivated Alkyl Chlorides with Conjugated Olefins. *Angew. Chemie - Int. Ed.* **2024**, *63* (1), e202313830. https://doi.org/10.1002/anie.202313830

2. Zackasee, J. L. S.; Srivardhan, V.; Truesdell, B. L.; Vrana, E. J.; Sevov, C. S. Electrocatalytic Grafting of Polyvinyl Chloride Plastics. *Chem* **2024**. https://doi.org/https://doi.org/10.1016/j.chempr.2024.08.021

Natalia B. Shustova

## Catalytically active Site Mapping Realized through Energy Transfer Modeling

Natalia B. Shustova,[a] Jeffery A. Byers,[b] Buddhima K. P. Maldeni Kankanamalage,[a] Jia Niu,[b] William J. Thompson,[b] Corey R. Martin,[a] and Kyoung Chul Park,[a]

[a]Department of Chemistry and Biochemistry, University of South Carolina Columbia, SC 29208
[b]Department of Chemistry, Boston College, Chestnut Hill, MA 02467

The demands of a sustainable chemical industry are a driving force for the development of heterogeneous catalytic platforms exhibiting facile catalyst recovery, recycling, and resilience to diverse reaction conditions. Homogeneous-to-heterogeneous catalyst transitions can be realized through the integration of efficient homogeneous catalysts within porous matrices. Herein, we offer a versatile approach to understanding how guest distribution and evolution impact the catalytic performance of heterogeneous host-guest catalytic platforms by implementing the resonance energy transfer (RET) concept using fluorescent model systems mimicking the steric constraints of targeted catalysts. Using the RET-based methodology, we mapped condition-dependent guest (re)distribution within a porous support on the example of modular matrices such as metal-organic frameworks. Furthermore, we correlate RET results performed on the model systems with the catalytic performance of two MOF-encapsulated catalysts used to promote $CO_2$ hydrogenation and ring-closing metathesis. Guests are incorporated using aperture-opening encapsulation, and catalyst redistribution is not observed under practical reaction conditions, showcasing a pathway to advance catalyst recyclability in the case of host-guest platforms. These studies represent the first generalizable approach for mapping the guest distribution in heterogeneous host-guest catalytic systems, providing a foundation for predicting and tailoring the performance of catalysts integrated into various porous supports.

**DE-SC0023182: Organometallic Catalysis from Molecular Catalysts Non-Covalently Confined in Metal-Organic Frameworks**

***Mapping catalytically active sites within the porous scaffold***

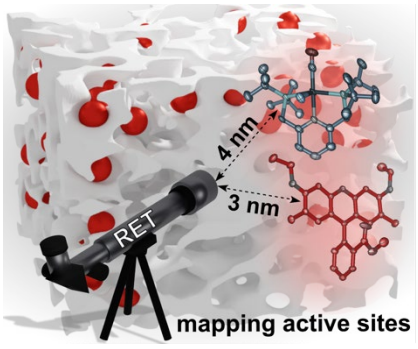

**Publications**

Maldeni Kankanamalage, B. K. P.; Thompson, W. J.; Thaggard, G. C.; Park, K. C.; Martin, C. R.; Niu, J.; Byers, J.A.; Shustova, N. B. *Angew. Chem. Int. Ed.* **2024**, e202416695 (*intellectually led by this grant*)

Jeremy M. Smith

# A Nucleophilic Imido Ligand Enables New Catalytic Transformations of an Iron Complex

Bin Feng, Arya Sree Ajay, Maren Pink, Nobuyuki Yamamoto, and Jeremy Smith
Department of Chemistry, Indiana University

## Presentation Abstract

Reduction of a three-coordinate iron(III) imido complex affords the corresponding iron(II) imido complex. The high spin ($S = 2$) state of the iron(II) complex attenuates the iron-nitrogen multiple bond character. Combined with the anionic nature of the complex, this helps create an electrophilic imido ligand that has reactivity patterns akin to those of early transition metals. Notably, the iron(II) imido complex catalyzes bond rearrangement and H/D exchange reactions, including selective alkyne and nitrile α-deuteration and p$K_a$-dictated alkene transposition. Mechanistic studies reveal the critical role of metal-ligand cooperativity in facilitating these unusual transformations, which extend beyond classical nitrene transfer reactivity of late metal imido complexes.

**DE-SC0019466: Harnessing Spin as a Design Element in Low Valent Iron Catalysis**

**Postdoc(s):** Bin Feng
**Student:** Arya Sree Ajay

## RECENT PROGRESS

***Selectivity of H/D Exchange is Dictated by the Counterion.*** The Fe(II) imido complex [K(18-c-6)][$Ph_2B(^tBuIm)_2Fe{=}NDipp$] reacts with pyridine to afford the structurally characterized complex [K(18-c-6)$(THF)_2$][$Ph_2B(^tBuIm)_2Fe$(2-py)(N(H)Dipp)]. In the presence of $D_2N^tBu$, the iron complex catalyzes H/D exchange in pyridines, with the counterion dictating the regioselectivity of the reaction. No H/D exchange occurs for $K(crypt)^+$, selective 3,4,5-exchange is observed for $K(18\text{-}c\text{-}6)^+$ and all positions are exchanged for $K^+$. Experimental and computational investigations provide insight into th origin of this selectivity. The presence of $Li^+$ transforms the iron imido to a bis(2-pyridyl) complex that is selective for 2,6-H/D exchange in pyridine.

***Towards C-H Amination without Nitrene Transfer Reagents.*** A directed C-H insertion reaction between 2-picoline and the Fe(III) imido complex [$Ph_2B(^tBuIm)_2Fe{=}N$(terph)] affords the iron(II) amido complexes [$Ph_2B(^tBuIm)_2Fe$–N(H)(terph)] and [$Ph_2B(^tBuIm)_2Fe(\kappa^2\text{-}C_5H_4CH_2N$(terph)]. The former complex can be oxidized to the imido complex using 1,4-quinone, providing the first steps towards catalytic amination reactions that do not require nitrene transfer reagents.

**Publications Acknowledging this Grant in 2021-2024**

*Intellectually led by this grant*

1. Gao, Y.; Smith, J.M. "Enabling Nucleophilic Reactivity in High-Spin Fe(II) Imido Complexes: From Elementary Steps to Cooperative Catalysis" *Acc. Chem. Res.* **2023**, *56*, 3392-3403
2. Gao, Y.; Li, X.; Stevens, J.E.; Tang, H.; Smith, J.M. Catalytic 1,3-Proton Transfer in Alkenes Enabled by Fe═NR Bond Cooperativity: A Strategy for p$K_a$-Dictated Regioselective Transposition of C═C Double Bonds *J. Am. Chem. Soc.* **2023**, *145*, 11978-11987.
3. Gao, Y.; Lee, W.-T..; Carta, V.; Chen, C.-H.; Telser, J.; Smith, J.M. Heteroleptic Square Planar Cobalt(I/II) Complexes, *Eur. J. Inorg. Chem.* **2023**, e202200675.
4. Gao, Y.; Pink, M.; Carta, V.; Smith, J.M., Ene Reactivity of an Fe=NR Bond Enables the Catalytic α-Deuteration of Nitriles and Alkynes, *J. Am. Chem. Soc.* **2022***, 144*, 17165-17172.
5. Gao, Y.; Pink, M.; Smith, J.M., Alkali Metal Ions Dictate the Structure and Reactivity of an Iron(II) Imido Complex, *J. Am. Chem. Soc.* **2022**, *144*, 1789-1794.
6. Gao, Y.; Carta, V.; Pink, M.; Smith, J.M., Catalytic Carbodiimide Guanylation by a Nucleophilic, High Spin Iron(II) Imido Complex, *J. Am. Chem. Soc.* **2021**, *143*, 5324-5329.

Dario J. Stacchiola

## Synthesis and Hydrogenation of Cu(111) Supported Borophene

Dario J. Stacchiola,[1] Kevin Sutherland,[2] Abdullah Al-Mahboob,[1] Jennifer Sanchez, and Fang Xu[2]
[1]Center for Functional Nanomaterials, Brookhaven National Laboratory, Upon, NY 11973, United States
[2]Department of Chemistry, the University of Texas at San Antonio, San Antonio, TX 78249, United States

### Presentation Abstract

The 2D boron materials, or borophene, have been theoretically predicted and synthesized over multiple metallic substrates in the past 10 years. However, due to the polymorphism of boron, multiple structures tend to co-exist during synthesis. Chemically, borophene could be an excellent support for single atom catalysts, but the chemical stability of the material needs improvement. This poster will discuss two parts: (1) the synthesis of borophene over Cu(111) by physical vapor deposition and a film growth strategy of using temperature to control the subsurface-surface migration of boron atoms; (2) hydrogenation of multiple borophene surfaces, such as B/Cu(111) and B/Ru(0001), as a chemical treatment to stabilize the borophene layers. Through collaborations between the University of Texas at San Antonio (UTSA) and Brookhaven National Laboratory (BNL), low energy electron diffraction/microscopy (LEED/LEEM), X-ray photoelectron spectroscopy (XPS), scanning tunneling microscopy (STM), and Auger electron spectroscopy (AES) were used to achieve an understanding of the pressure and temperature dependence on borophene structure and chemical identity. The results provide fundamental insights into the growth mode of 2D materials, as well as hydrogenation induced structural changes on borophene.

### DE-SC0024228: Atomic Level Structure-activity Relationship of Small Molecule Activation on Single Atom Catalysts Supported on 2D Boron-based Materials

**PI:** Fang Xu
**Student(s):** Kevin Sutherland; Jennifer Sanchez

### RECENT PROGRESS

***Temperature Dependent Migration Cycles of Subsurface Boron Atoms***

The synthesis of borophene on Cu(111) is temperature sensitive. The typically in-situ preparation temperature during physical vapor deposition is to hold the Cu(111) around 500 °C. During the process, some boron atoms will migrate into the subsurface layers in a reversible process. According to in-situ LEEM, no borophene islands were observed at 700 °C (Figure 1a), but as the sample is cooled down to 500 - 600 °C, the borophene islands re-appear on the surface (Figure 1b). The process can be repeated a few cycles

without losing significant amount of borophene on the surface (Figure 1c-1f). This process can be used as a strategy to synthesize borophene. More detailed analysis on the kinetics and corresponding STM images of the atomic structure of borophene during these cycles will be collected.

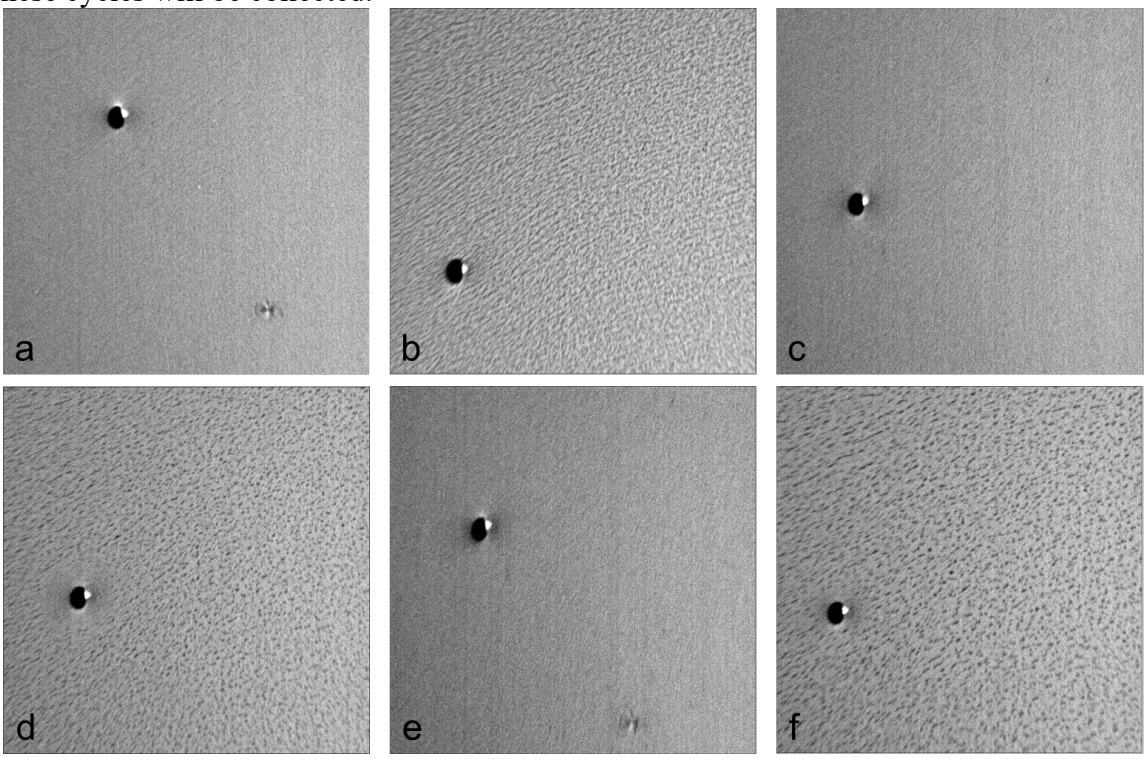


Figure 1. LEEM (50×50μm) images showing the migration of B from Cu(111) subsurface to surface in a few cycles. Borophene is first grown from a clean surface (a) at 500°C, followed by several cycles of annealing to 700°C (c and e) and cooling to 600°C (d and f). The first cycle of annealing and cooling is shown in c and d while the second cycle is shown in e and f.

***Atomic Structures of Borophene on Cu(111) Resolved by STM***

Multiple borophene structures on Cu(111) were obtained by LEED/LEEM at BNL. We succeeded in preparing a defined monolayer of crystalline borophene, and transfer the recipe to synthesize the same structure based on its LEED pattern at UTSA (Fig. 2a and 2b), indicating the same borophene structure was synthesized. The atomic resolution shows a quasi-hexagonal pattern that covers the whole surface (Fig. 2c).

***Hydrogenation of Borophene on Cu(111)***

Exposure of both 2D borophene or Cu(111) to air results in their immediate oxidation. The surface chemistry of oxidized copper is an active topic of research due to its wide use in catalysis [1]. Controlling the degree of oxidation on both 2D borophne and Cu(111) is one of the main goals of our project. Upon hydrogenation of 2D borophene, the resulting 2D material can be stabilized for days in air without oxidation. We will present preliminary results on the hydrogenation and characterization of 2D borophene on Cu(111).

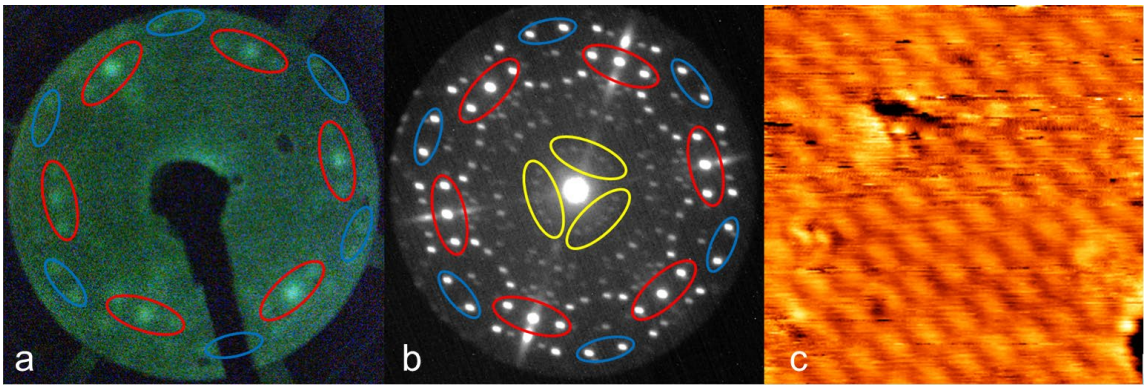


Figure 2. Comparison of LEED taken at UTSA (a) and corresponding LEED taken at BNL (b). The red and blue circles indicate the matching patterns in both LEEDs. STM image of borophene (c, 20×20 $nm^2$) was taken at 6 nA tunneling current and 2.00 V. The measured spacing of the borophene spots in (c) is 1.7 nm, while the measured spacing of the internal spots (yellow) of the borophene structure shown in (b) is 1.604 nm.

**Publications Acknowledging this Grant in 2021-2024**

*Jointly funded by this grant and other grants with intellectual leadership by other funding sources*

1. Hu, T.; Karagoz, B.; Xu, F.; Head, A. R.; Weissenrieder, J.; Stacchiola, D. The surface chemistry of cuprous oxide. *Surf. Sci.* **2025**, *751*, 122622.

## Shannon S. Stahl

### Aerobic Oxidation Reactions with M-N-C Heterogenous Catalysts

Shannon S. Stahl
University of Wisconsin-Madison

Materials composed of metal ions integrated within nitrogen-doped carbon (M-N-Cs) are a class of "single-atom" catalysts that have received extensive attention for the electrochemical oxygen reduction reaction (ORR) in fuel cells. The ability M-N-C catalysts to support $O_2$ reduction at low overpotential prompted us to begin exploring the same materials as thermal catalysts for aerobic oxidation of organic molecules. Our work focuses on elucidating the mechanisms by which M-N-C catalysts mediate oxidation of organic molecules and leveraging the insights to guide the synthesis and characterization of new M-N-C materials that support more effective catalysis. The results of these efforts are beginning to show similarities and differences between the thermal and electrochemical reactions of $O_2$ on these materials.

### Oxidation of O-H and N-H Bonds with Non-Precious-Metal Catalysts
### DE-FG02-05ER15690

**PI:** Shannon S. Stahl
**Postdoc(s):** Qiang Gao, Fatemeh Khamespanah, Jack Twilton, Jason Bates, Patrick Kelly
**Student(s):** Melissa N. Hall, Jesse Martinez, Philip Zhou, Shannon L. Goes, Jordan E. Nutting, Ian Garvey, Madeline MacDonnell
**Affiliations(s):** Department of Chemistry, University of Wisconsin - Madison, Madison, WI 53706

## RECENT PROGRESS

***Mechanism of M-N-C-catalyzed aerobic oxidation of hydroxylamines***

One primary focus of our research seeks to characterize the mechanism(s) of aerobic oxidation reactions catalyzed by metalated nitrogen-doped carbon (M-N-C) materials. Two different mechanisms have been proposed: “independent half reactions” in which the ORR and substrate oxidation redox have reactions occur as independent redox half reactions at different sites on the catalyst surface or “inner-sphere reaction” in which the ORR and substrate oxidation reaction involve direct reaction between the two substrates on the catalyst surface. Both mechanisms have been proposed for M-N-C-catalyzed oxidation reactions. To examine these mechanisms further, we have been investigating the aerobic oxidation of a hydroxylamine, TEMPOH (1-hydroxy-2,2,6,6-tetramethylpiperidine), to the corresponding oxoammonium, $TEMPO^+$, in aqueous media using a commercial Fe-N-C catalyst

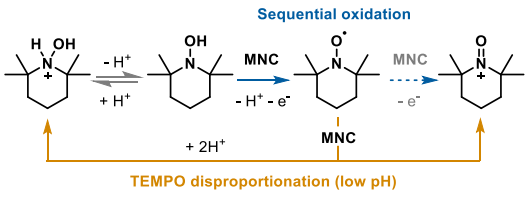


Two possible pathways for oxidation of $TEMPOH_2^+$ to $TEMPO^+$, catalyzed by M-N-C catalysts: sequential oxidations (blue pathway) or an oxidation/disproportionation (orange pathway).

from “Pajarito Powder” (PAJ). This reactivity is of interest because oxoammonium species are effective co-catalysts in various aerobic oxidation reactions. Experimental kinetic data that we have obtained provide clear support for an inner-sphere reaction pathway. M-N-C catalyzed oxidation of $TEMPOH_2^+$ is initiated by pre-equilibrium deprotonation to form TEMPOH, followed by inner-sphere proton-coupled oxidation of TEMPOH to TEMPO. TEMPO can then either be further oxidized directly by PAJ or undergo disproportionation (a step found to be catalyzed by PAJ) to generate 0.5 equiv of $TEMPO^+$ and 0.5 equiv of the original $TEMPOH_2^+$. Disproportionation is found to be the major pathway. Progression through this mechanism ultimately generates high yields of $TEMPO^+$. Key to elucidation of this mechanism was kinetic modeling of the various redox processes that are occurring simultaneously on the M-N-C surface, including the oxygen reduction reaction (ORR), TEMPOH oxidation, TEMPO oxidation, and disproportionation. This fundamental understanding of the mechanisms of aerobic generation of oxoammonium species with the PAJ catalyst has been leveraged for successful co-catalysis of PAJ and nitroxyl compounds to oxidize alcohols in aqueous media under both low and high pH conditions.

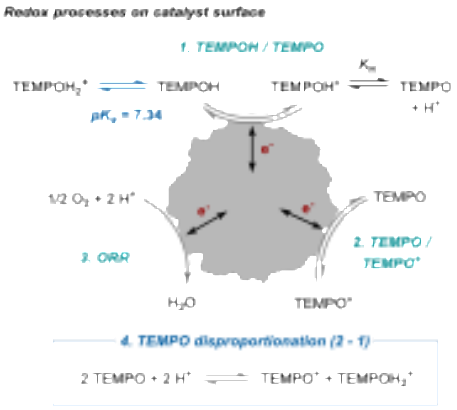


***M-N-C-catalyzed hydrazone oxidation***

We are interested in exploring a range of oxidation reactions of substrates with O–H and N–H. Recently, we showed that Fe-N-Cs support aerobic oxidation of hydrazones to form diazo compounds. The reactions proceed readily at room temperature using $O_2$ (1 atm) as the oxidant. Aryl diazoesters, ketones, and amides are accessible, in addition to less stable diaryl diazo compounds. Initial-rate data show that the Fe-N-C catalyst achieves faster rates than a heterogeneous Pt/C catalyst, in addition to higher yields, highlighting the effectiveness of M-N-C catalysts for mediating these aerobic oxidation reactions. We have also been studying the mechanism of M-N-C catalyzed aerobic hydrazone oxidation as a model system to interrogate the preference for inner sphere reactions (ISR, $O_2$ and substrate at the same active site) or independent half reactions (IHR, $O_2$ and substrate at separate active sites). These mechanistic models will be evaluated using kinetic data measured for hydrazone oxidation. The mechanistic analysis is being supported by exploring alternative applications where the system is biased to operate via IHR by decoupling proton and electron transfer, enabling mediated electrochemical oxidation of hydrazones with oxidant and base pairs through proton-coupled electron transfer (PCET). In addition to the successful oxidation of hydrazones, we hypothesize that this reactivity may be general and will explore the use of tailored reagents to promote PCET for reactions such as alcohol oxidation, *N*-heterocycle dehydrogenation, or alkane dehydrogenation.

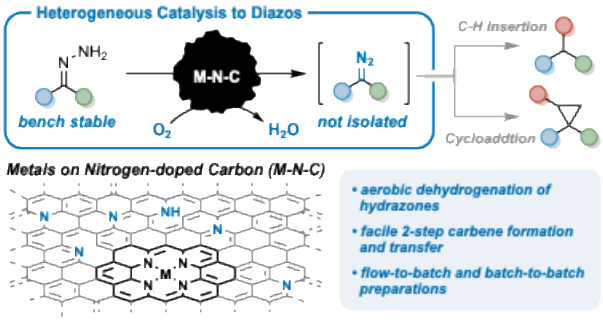

***Development of a kinetic probe to quantify M-N-C active site densities***

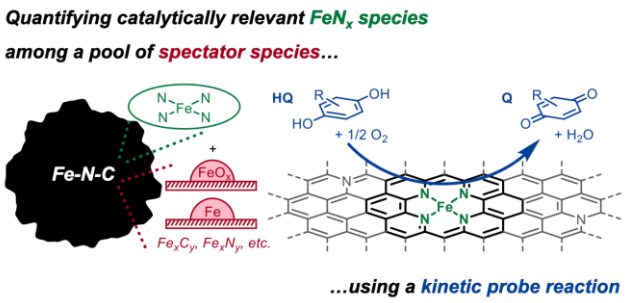


Traditionally, improvements to M-N-C catalysts have been made empirically by observing increases or decreases in catalytic activity. From this work, $FeN_x$ single-atom sites have been identified as the active sites in electrochemical and thermochemical ORR. Methods for quantifying the number of $FeN_x$ sites are varied and often require specialized equipment. We have developed a straightforward *kinetic probe* to quantify the $FeN_x$ active site densities on the surface of M-N-Cs. The kinetic probe involves measuring rates of aerobic oxidation of a hydroquinone derivative under conditions relevant to the ORR and using those rates to quantify the number of accessible active sites. Initial rates of hydroquinone oxidation were determined for a wide range of materials, including samples made in-house and sent by collaborators, which were used to give $FeN_x$ active site densities. The kinetic probe $FeN_x$ site densities were correlated with active site densities determined by other techniques, including CO pulse chemisorption, low temperature Mössbauer spectroscopy, and electrochemical reductive stripping of NO derived from $NO_2^-$. Our kinetic probe gave the best correlation with CO pulse chemisorption, followed by low temperature Mössbauer spectroscopy. For every quantification method, outliers are present, indicating that different site quantification methods may be more appropriate for M-N-Cs synthesized by certain protocols. Our study encompassed materials synthesized through various methods and displayed robust correlations with literature methods, indicating the broad applicability of our kinetic assay for active site density measurements. The kinetic probe technique that we have developed requires no specialty equipment other than an appropriate reaction vessel and a standard NMR spectrometer.

***New structure activity relationships to explain M-N-C activity in organic media***

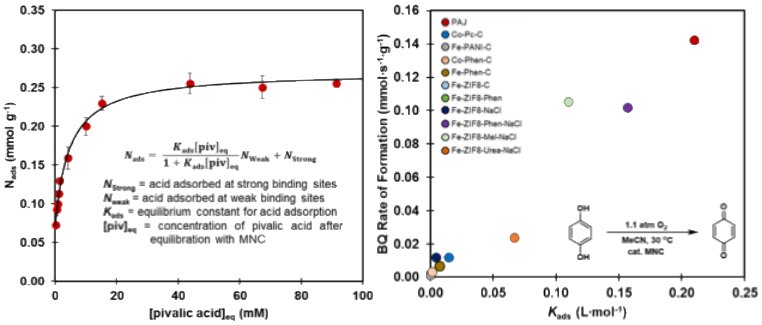


Previous structure-activity relationships for M-N-C catalysts have implicated the number of $FeN_x$ active sites as the most important structural feature for increasing ORR activity. Specifically, higher $FeN_x$ site count leads to a more active material). Recent work in our lab has been exploring factors that improve the performance of M-N-C catalysts for aerobic oxidation reactions of organic molecules, such as the oxidation of hydroquinone to quinone. These aerobic oxidation reactions are performed under neutral-to-basic conditions in organic solvent rather than the aqueous acidic conditions typically used for ORR studies. The results show that in organic solvent catalyst activity has little correlation with the conventional "active site counts" (e.g., $FeN_x$ site density). We hypothesized that differences in surface basicity arising from varying nitrogenous functionality play a key role in enabling organic aerobic oxidation. We have

probed the surface basicity of a variety of M-N-Cs by recording the solvent-phase adsorption isotherms for acid titrants onto each M-N-C surface. This experiment provides an equilibrium acid binding constant, $K_{ads}$, for each M-N-C as a quantitative measure of surface basicity. In direct contrast to $FeN_x$ site density, $K_{ads}$ correlates very well with rates of aerobic oxidation in organic solvent, for both hydroquinone and other organic oxidation reactions. We believe this role of surface basicity effect is relevant for many aerobic oxidations, as observed from improved rates and yields for heterocycle dehydrogenation and co-catalyzed alcohol oxidation, where more basic M-N-Cs give higher product yields. This work identifies a new structure-activity relationship for M-N-Cs used as organic aerobic oxidation catalysts, where surface basicity is the primary predictor of activity, rather than $FeN_x$ site density. This understanding provides a route for targeted synthesis of improved M-N-Cs for aerobic oxidation and has been leveraged in our lab to develop a new class of M-N-C materials that outperform the leading M-N-C catalyst shown in the figure above.

**Publications Acknowledging this Grant in 2021-2024**

*Intellectually led by this grant*


1. Hall, M. N.; Lee, M.; Root, T. W.; Davies, H. M. L.; Stahl, S. S. Heterogeneous Fe-N-C Catalyst for Aerobic Dehydrogenation of Hydrazones to Diazo Compounds Used for Carbene Transfer. *J. Am. Chem. Soc*. **2024**, *146*, 13741-13747. DOI: 10.1021/jacs.4c04430

2. Gerken, J. B.; Stamoulis, A.; MacDonnell, M. L.; Stahl, S. S. Rate Equations for Reversible Disproportionation Reactions and Fitting to Time-Course Data. *J. Phys. Chem. A*. **2024**, *128*, 328-332. DOI: 10.1021/acs.jpca.3c05232

3. King, D. S.; Wang, F.; Gerken, J. B.; Gaggioli, C. A.; Guzei, I. A.; Kim, Y. J.; Stahl, S. S.; Gagliardi, L. Divergent Bimetallic Mechanism in Copper(II)-Mediated C-C, N-N, and O-O Oxidative Coupling Reactions. *J. Am. Chem. Soc*. **2024**, *146*, 3521-3530. DOI: 10.1021/jacs.3c13649\

4. Bates, J. S.; Martinez, J. J.; Hall, M. N.; Al-Omari, A. A.; Murphy, E.; Zeng, Y.; Luo, F.; Primbs, M.; Menga, D.; Bibent, N.; Sougrati, M.T.; Wagner, F. E.; Atanassov, P.; Wu, G.; Strasser, P.; Fellinger, T-P.; Jaouen, F.; Root, T. W.; Stahl, S. S. Chemical Kinetic Method for Active-Site Quantification in Fe-N-C Catalysts and Correlation with Molecular Probe and Spectroscopic Site-Counting Methods. *J. Am. Chem. Soc*. **2023**, *145*, 26222-26237. DOI: 10.1021/jacs.3c08790

5. Stamoulis, A.G.; Bruns, D. L.; Stahl S.S. Optimizing the Synthetic Potential of $O_2$: Implications of Overpotential in Homogeneous Aerobic Oxidation Catalysis. *J. Am. Chem. Soc.* **2023**, *145*, 17515-17526. DOI: 10.1021/jacs.3c02887

6. Bates, J. S.; Johnson, M. R.; Khamespanah, F.; Root, T. W.; Stahl, S. S. Heterogeneous M-N-C Catalysts for Aerobic Oxidation Reactions: Lessons from

Oxygen Reduction Electrocatalysts. *Chem. Rev*. **2023**, *123*, 6233-6256. DOI: 10.1021/acs.chemrev.2c00424

7. Bates, J. S.; Khamespanah, F.; Cullen, D. A.; Al-Omari, A. A.; Hopkins, M. N.; Martinez, J. J.; Root, T. W.; Stahl, S. S. Molecular Catalyst Synthesis Strategies to Prepare Atomically Dispersed Fe-N-C Heterogeneous Catalysts. *J. Am. Chem. Soc*. **2022**, *144*, 18797-18802. DOI: 10.1021/jacs.2c08884

8. Nutting, J. E.; Gerken, J. B.; Stamoulis, A. G.; Bruns, D. L.; Stahl, S. S. "How Should I Think About Voltage? What is Overpotential?": Establishing an Organic Chemistry Intuition for Electrochemistry. *J. Org. Chem*. **2021**, *86*, 15875-15885. DOI: 10.1021/acs.joc.1c01520

9. Nutting, J. E.; Mao, K.; Stahl, S. S. Iron(III) Nitrate/TEMPO-Catalyzed Aerobic Alcohol Oxidation: Distinguishing between Serial versus Integrated Redox Cooperativity. *J. Am. Chem. Soc*. **2021**, *143*, 10565-10570 DOI: 10.1021/jacs.1c05224

10. Salazar, C. A.; Thompson, B. J.; Knapp, S. M. M.; Myers, S. R.; Stahl, S. S. Multichannel Gas-Uptake/Evolution Reactor for Monitoring Liquid-Phase Chemical Reactions. *Rev. Sci. Instrum*. **2021**, *92*, 044103. DOI: 10.1063/5.0043007

11. Liu, W.; Twilton, J.; Wei, B.; Lee, M.; Hopkins, M. N.; Bacsa, J.; Stahl, S. S.; Davies, H. M. L. Copper-Catalyzed Oxidation of Hydrazones to Diazo Compounds Using Oxygen as the Terminal Oxidant. *ACS Catal*. **2021**, *11*, 2676-2683 DOI: 10.1021/acscatal.1c00264

*Jointly funded by this grant and other grants with intellectual leadership by other funding sources*

12. Palumbo, C. T.; Ouellette, E. T.; Zhu, J.; Roman-Leshkov, Y.; Stahl, S. S.; Beckham, G. T. Accessing Monomers from Lignin Through Carbon-Carbon Bond Cleavage. *Nat. Rev. Chem*. **2024**. DOI: 10.1038/s41570-024-00652-9

13. Palumbo, C. T.; Gu, N. X.; Bleem, A. C.; Sullivan, K. P.; Katahira, R.; Stanley, L. M.; Kenny, J. K.; Ingraham, M. A.; Ramirez, K. J.; Haugen, S. J.; Amendola, C. R.; Stahl, S. S.; Beckham, G. T. Catalytic carbon-carbon bond cleavage in lignin via manganese-zirconium-mediated autoxidation. *Nat. Commun*. **2024**, *15*, 862. DOI: 10.1038/s41467-024-45038-z

14. Gu, N. X.; Palumbo, C. T.; Bleem, A. C.; Sullivan, K. P.; Haugen S. J.; Woodworth, S. P.; Ramirez, K. J.; Kenny, J. K.; Stanley, L. D.; Katahira, R.; Stahl, S. S.; Beckham, G. T. Autoxidation Catalysis for Carbon-Carbon Bond Cleavage in Lignin. *ACS. Cent. Sci*. **2023**, *9*, 2277-2285. DOI: 10.1021/acscentsci.3c00813

15. Carroll, G. M. Gebbie, M. A.; Stahl, S. S.; Johnson, M. R.; Luca, O. R.; Peterson, H. A.; Bomble, Y. J.; Neale, N. R.; Cortright, R. D. Alternative Energy Carriers: Unique Interfaces for Electrochemical Hydrogenic Transformations. *Adv. Energy Mater*. **2023**, 2203751 DOI: 10.1002/aenm.202203751

16. Sullivan, K. P.; Werner, A. Z.; Ramirez, K. J.; Ellis, L. D.; Bussard, J.; Black, B. A.; Brandner, D. G.; Bratti, F.; Buss, B. L.; Dong, X.; Haugen, S. J.; Ingraham, M. A.; Konev, M. O.; Michener, W. E.; Miscall, J.; Pardo, I.; Woodworth, S. P.; Guss, A. M.; Román-Leshkov, Y.; Stahl, S. S.; Beckham, G. T. Mixed Plastics Waste Valorization Through Tandem Chemical Oxidation and Biological Funneling. *Science* **2022**, *378*, 207-211. DOI: 10.1126/science.abo4626

## Electrocatalytic reduction of nitrate: manipulating the solid/liquid interface

Kelsey A. Stoerzinger
University of Minnesota, Chemical Engineering and Materials Science

### Presentation Abstract

Nitrate electroreduction can help close the nitrogen cycle and convert waste to value added products. On abundant first-row transition metal surfaces, however, this process occurs at conditions where the surface can also bind hydrogen species (H*). The potential-dependent adsorption of H* takes up sites otherwise available for nitrate adsorption, but H* could also be involved in the reaction mechanism (i.e. hydrogen addition) and tailor product distribution. We develop a microkinetic model to better understand this competitive adsorption landscape and compare the findings to potential-dependent measurement of nitrate reaction rate order. Metals that bind H* relatively strongly have low Faradaic efficiency for nitrate electroreduction but favor more reduced products (ammonium), whereas surfaces that bind nitrate relatively strongly have higher Faradaic efficiency but favor nitrite as a primary product. More reducing conditions where surfaces have higher ratios of adsorbed H* to nitrate shift product distribution to ammonium over nitrite. These findings suggest bimetallic surfaces might offer avenues to access both high Faradaic efficiency and ammonium selectivity. Understanding the reactive electrode/electrolyte interface is complicated by the negative surface charge present under conditions where these catalyze the electrocatalytic reduction of the anion nitrate. We find the identity of cations in the electrolyte can influence numerous aspects of the reaction: Faradaic efficiency (with the hydrogen evolution reaction competing for electrons), observed reaction rates, and product distribution—the extent to which depends on the metal catalyst considered. The origin of cation effects are multifold, including manipulating transport to the electrode surface, impacting local pH, and likely modifying the interaction of nitrate with the electrode itself. Understanding these contributions can shed light on the complex reaction mechanism of NO3RR and provide insight into feedstocks most amenable for green ammonia production.

**DE-SC0024865: Electrocatalytic nitrate reduction: controlling adsorbate affinity to tailor reaction products**

**Postdoc(s):** Sri Krishna Murthy Padavala, Devesh Pathak
**Student(s):** Ruth E Bello, Kaavya Nimmakayala, Jorin Dawidowicz,[1] O. Quinn Carvalho[1]
**Affiliations(s):** [1]Oregon State University, School of Chemical, Biological, and Environmental Engineering

## RECENT PROGRESS

This proposal seeks a mechanistic understanding of nitrate reduction reaction (NO3RR) Faradaic efficiency (FE) and product selectivity based on catalyst electronic structure, spectroscopic insight into competitive adsorption, and distribution of charge at the electrode‐electrolyte interface. We hypothesize that inverse coupling between FE and $NH_3/NH_4^+$ selectivity can be disrupted by alloying catalyst elements with distinct $NO_3$* and H* affinities, and that the rate limiting reduction of $NO_3$* can be facilitated by modifying the local charge both on the surface via oxide co‐catalysts and in the double layer by ion‐pairing. The resulting insight will develop design strategies not only for NO3RR but also generally for electroreduction reactions (e.g. $CO_2$, organics) in competition with HER.

One of our primary objectives was to experimentally assess NO3RR FE and product selectivity across 3d and 4d transition metals, as well as select alloys, to develop electronic structure metrics for catalyst design. Metrics including the d-band center, validated by collaborators with computational approaches, will be used to understand competition between $NO_3$* and H* adsorption but also propensity of surfaces to form N-O and N-H bonds. We have found that the relative coverage of $NO_3$* and H*, manipulated via electronic structure and electrochemical potential, will tailor not only selectivity to $NH_3/NH_4^+$ but also its route of formation (via direct N-H bond formation vs a $NH_2OH$ intermediate). We have considered an experimental assessment of NO adsorption and dissociation via ambient pressure XPS, coupled with theoretical modeling of adsorption in relation to electronic structure. We have found that NO prefers oxidation to nitrite and desorption of nitrogen suboxides on metals with nearly or completely filled d-bands (e.g. Cu and Ni) and stabilization of dissociation products (N*) on metals with increasingly empty d bands (e.g. Ni, Co, and Fe). These findings are important in understanding NO3RR on such surfaces, as Ni, Co, and Fe all are selective to $NH_3/NH_4^+$ products and this likely occurs via N* protonation/hydrogenation (as opposed to NO* protonation in a hydroxylamine pathway. This work was recently accepted at JPCC.

We have recently been investigating whether select alloy formation can circumvent scaling relations in adsorption and promote dual active sites with individually tailored affinities for reaction intermediates. Based on our investigations of elemental metals, we have recently assessed of the role of dual active sites/alloying in NiFe. We were motivated by these elements having d-band centers on either side of Co (which we've observed has the best FE and $NH_4^+$ selectivity). Ni binds H relatively strongly compared to Fe, where Fe binds $NO_3^-$ relatively strongly. We observed that a large number of NiFe alloy compositions all demonstrate higher FE and $NH_4^+$ selectivity compared to the Ni and Fe end members, but similar regardless of Ni/Fe ratio. XPS illustrates alloys are enriched in Fe, but DFT calculations suggest a mixed termination with some Ni remains favorable compared to a complete Fe skin. Efforts are ongoing to establish whether surface decorated foils demonstrate similar Fe and selectivity that trend with Ni-Fe interfacial area in the low coverage limit – which would indicate a dual-active site mechanism – or whether electronic structure changes from bulk alloy formation play an appreciable role. A manuscript is in preparation concerning this work.

Another primary objective is to better understand the electrical double layer, including its relation to surface charge and electrolyte composition. This is intricately linked to the consumption of protons (or hydroxide production) and nitrate during the reaction. We have assessed local pH in neutral media and the role of pH gradients on rates and mechanism. We have measured the local pH under forced convection measurements, finding for Cu in 100 mM phosphate buffer at pH 7 that the buffering capacity is exceeded by the high rates of NO3RR and $H^+$ consumption, leading to a local pH exceeding 13. This allows us to better understand the driving force at the surface and the nature of the proton donor and mechanism. We are currently investigating whether the gradient in $OH^-$ at the surface may impact the electric field and migration in unique ways compared to a bulk solution with the same pH.

We have also assessed cation effects on FE and selectivity. In neutral phosphate buffer media, we have seen that different cations ($Li^+$, $Na^+$, $K^+$) lead to distinct impacts on different metals. For example, Cu has changes in FE, selectivity, and activity, whereas Co maintains high FE and $NH_4^+$ selectivity but demonstrates differences in rates. We have used forced convection approaches to understand the relative roles of diffusion and migration in NO3RR, observing differences in mass transport limited current ~4x comparing $Li^+$ and $K^+$. We are preparing a publication on these findings. There is an additional impact of cations on kinetics that is isolated from transport effects using forced convection approaches (~100 mV shift to lower overpotential with $K^+$) that we are investigating with in situ FTIR and collaborations with theory.

**Publications Acknowledging this Grant in 2021-2024**

*(I) Intellectually led by this grant*

Carvalho, O.Q.; Nguyen, H.K.K.; Padavala, S.K.M.; Árnadóttir, L.; Crumlin, E.J.; Stoerzinger, K.A. Interaction of nitric oxide with late 3d transition metals: Dissociation and metal oxidation. *J. Phys. Chem. C.* **2024**, accepted.

Pathak D.K.; Jana R.; Bello R.; White K.; Stoerzinger K.A. Robust catalyst assessment for the electrocatalytic nitrate reduction reaction. *Under Review.*

*(II) Jointly funded by this grant and other grants with intellectual leadership by other funding sources*

Barton, D.J.; Nguyen, D.-T.; Perea, D.E.; Stoerzinger, K.A.; Lumagui, R.M.; Lambeets, S.V.; Wirth, M.G.; Devaraj, A.; Towards Quantitative Analysis of Deuterium absorption in Ferrite and Austenite during Electrochemical Charging by Comparing Cyclic Voltammetry and Cryogenic Transfer Atom Probe Tomography *Int. J. Hydrogen Energy* **2024**, *50*, 30-40.

Jin Suntivich

## Dynamics at Solid-Liquid Interfaces: Water Dehydrogenation on $RuO_2$(110)

Austin Reese[1], Chia-Yi Lin[1], Abigail Nason[2], Jin Suntivich[2]
[1]Smith School of Chemical and Biomolecular Engineering, Cornell University, NY
[2]Department of Materials Science and Engineering, Cornell University, Ithaca NY

### Presentation Abstract

Green hydrogen is essential to the decarbonization of chemical and materials manufacturing. Yet, the mechanistic understanding of hydrogen production from water on catalytic surfaces is elusive. This research investigates the formation mechanism of the intermediates in water splitting, particularly of the oxygen evolution reaction (OER). The goal is to track the formation dynamics of the OER intermediates and their dependence on environmental factors such as pH. Our approach harnesses well-defined single-crystalline transition-metal-oxide surfaces to interrogate the intermediate formation. The model systems are rutile-oxide thin films ($RuO_2$, $IrO_2$, etc.) grown using molecular beam epitaxy (MBE). Our methodology assesses the $O_{ad}$ formation rate by measuring how the pre-equilibrium isotherm varies with the sweeping rate of applied potential. We present a strategy for converting these experimental results into the $O_{ad}$ formation rates and rate constants. In parallel, we have developed electrochemical atomic force microscopy (EC-AFM) to image solid-liquid interfaces with atomic resolution. We demonstrate this capability on graphite-water interfaces and show that our image analysis can resolve the dynamics of graphite corrosion under oxidative potential. We will discuss a preliminary result on how this capability can track the OER intermediate formation in water splitting. Finally, while we worked on creating an algorithm to analyze carbon corrosion images, we found that the same analysis tool was useful for quantifying the depolymerization rates of polyethylene terephthalate (PET) fibers (as both require tracking the morphology of materials as a function of time.) We have applied this advance to quantify single-fiber PET hydrolysis to understand chemical variations in post-consumer plastic materials.

**Grant or FWP Number: Rate and Mechanism of Water Activation on Transition Metal Oxides (DE-SC0023896)**

**PI:** Suntivich, Jin
**Postdoc(s):** n/a
**Student(s):** Austin Reese, Chia-Yi Lin, Abigail Nason
**Affiliations(s):** Cornell University

## RECENT PROGRESS

### *Measurement of $O_{ad}$ formation kinetics on $RuO_2$(110) surfaces*

On the MBE-grown $RuO_2$(110) films, we observe the reversible formation of $OH_{ad}$ and $O_{ad}$ (via $H_2O_{ad} \rightarrow OH_{ad} + H^+ + e^-$ and $OH_{ad} \rightarrow O_{ad} + H^+ + e^-$), two critical intermediates to the OER cycle. **Figure 1A** shows the cyclic voltammetry (CV) with the $OH_{ad}$ and $O_{ad}$ formation regions. We determine the dynamics of this pre-equilibrium formation and formulate the formation mechanism by quantifying how their rate constant depends on environmental factors such as pH and the donor/acceptor chemistry.

Our methodology for quantifying the $O_{ad}$ formation rate builds on the idea that when the scan rate is "too slow", the $O_{ad}$ formation has enough time to equilibrate to the equilibrium isotherm; however, when the scan rate becomes comparable to the formation kinetics, the isotherm will deviate from equilibrium adsorption. We have applied this methodology to characterize the $O_{ad}$ formation. **Figure 1B** shows the CV of $RuO_2$(110) at different scan rates. At "slow" scan rates, for example, <1 V/s, the adsorption features are reversible (**Figure 1B.**) As a result, the $O_{ad}$ formation follows the equilibrium isotherm (**Figure 1C.**) However, as the scan rates ramp up (>1 V/s), the observed isotherms start deviating from equilibrium (**Figure 1B-C**). We quantify the $O_{ad}$ formation rates from the current measured on these non-equilibrium isotherms. Then, we extract the driving force from the equilibrium deviation (as it is the force to restore equilibrium adsorption.) From this analysis, we can construct the relationship between the $O_{ad}$ formation rates and the driving force to determine the rate constant. The results of the rate constant analysis are shown in **Figure 2,** shown at three $O_{ad}$ coverages to demonstrate the consistency.

We characterize the $O_{ad}$ formation rate constants as a function of pH to identify the $O_{ad}$ formation mechanism. As shown in **Figure 2,** the $O_{ad}$ formation rate constants were the fastest in acidic and basic media, but slow at neutral pH. When pH < 3, the reaction order was ~0.8. Between pH 10 and 12, we observed a unity reaction order before plateauing (zero reaction order) at pH > 12. A unity reaction order describes a classical proton-coupled electron transfer (PCET) process. We propose that the $O_{ad}$ formation between pH 10 and 12 obeys this framework, *i.e.,* the $O_{ad}$ forms via the $OH_{ad}$ dehydrogenation, where the electron and proton transfers are coupled at the oxide-water interface. We propose that this situation is similar when pH < 3, even though the observed reaction order was (slightly) below 1. This observation could be due to possible anion adsorption. We plan to evaluate this possibility using EC-AFM, which we will discuss in the next section. We also plan to study why the reaction order plateaued at pH > 12 by characterizing the $O_{ad}$ formation with different alkali cations and temperatures to determine why the reaction order turned zero at this alkaline pH.

### *Development of EC-AFM for monitoring surface structures at high potentials*

EC-AFM provides unique insights into the microstructure of electrode-electrolyte interfaces. However, quantifying solid-liquid structures in the middle of electrocatalysis is challenging. We attribute this challenge to the fact that (i) most electrocatalytic reactions require extreme pH where conventional Si probes are unstable, (ii) existing cell design uses metal-based references (*e.g.,* Ag/AgCl) which create impurities, and (iii) the profile of the conventional AFM cell is set up for large volume, causing mechanical drift. Over the past year, we have redesigned our EC-AFM setup by extensively studying the in-situ cell design

literature. In our latest design, we adopted a low-profile setup. Furthermore, we moved the sample near the mounting post to minimize drift and integrated a reversible hydrogen electrode (RHE) to eliminate the need for metal-based references. In parallel, we have fabricated an oxide-coated tip using materials that do not corrode in acid/base media.

**Figure 3** shows an EC-AFM imaging of graphite (HOPG) in 0.1M $HClO_4$ using the EC-AFM setup in our laboratory**.** The observed periodic pattern and symmetry match well with the graphite structure, suggesting that we have successfully performed a scanning probe microscopy on the surface of a solid in electrolyte liquids at **atomic resolutions**. Most excitingly, the observed images were stable throughout the experimental duration (hours), suggesting that we have addressed the tip's stability concern. We have started applying this capability to image $IrO_2(110)$. **Figure 4** illustrates example EC-AFM images of $IrO_2(110)$ in pH 13 electrolyte (0.1M KOH), showing the atomic structure of $IrO_2(110)$ during the $OH_{ad} \rightarrow O_{ad}$ transition. We are currently working on an image analysis algorithm to retrieve the details of the adsorbed water. Even though our image analysis algorithm work is not yet completed, it has already yielded an unexpected side benefit. Specifically, we found that we could use the image-analysis algorithm to quantify the morphological evolution of plastics during depolymerization at a single-particle level. We have already submitted this work for publication and plan to submit a paper on the EC-AFM design at the year's end.

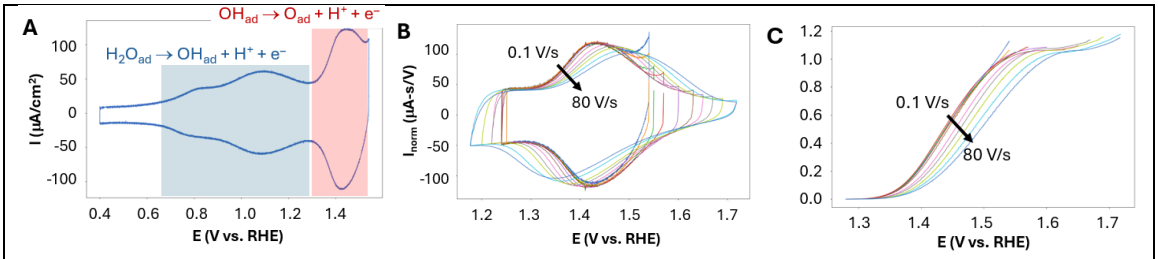


**Figure 1. Measurement of the rate constants of the $O_{ad}$ formation. (A)** CV of a $RuO_2(110)$ film on $TiO_2(110)$ single crystal. The $O_{ad}$ formation region is colored red. **(B)** $RuO_2(110)$ CV as a function of scan rate. All CVs were corrected using active feedback compensation at 85%. **(C)** Integrated $O_{ad}$ isotherm from CV data in **(B).**

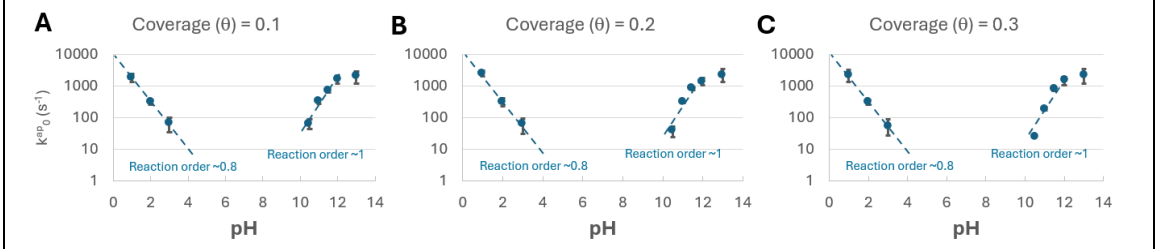


**Figure 2. pH dependence of the rate constants of the $O_{ad}$ formation at $O_{ad}$ coverage at (A) 0.1, (B) 0.2, and (C) 0.3.** In acidic pH (pH < 3), the reaction order was ~0.8, while in alkaline pH (>10), the reaction order was ~1 before reaching the plateau at pH 14. We hypothesize that the reaction order in pH <3 (~0.8) could be due to surface blocking by anions, while the reaction order plateauing (at pH 14) could be due to a switch in the mechanism (currently under investigation.)

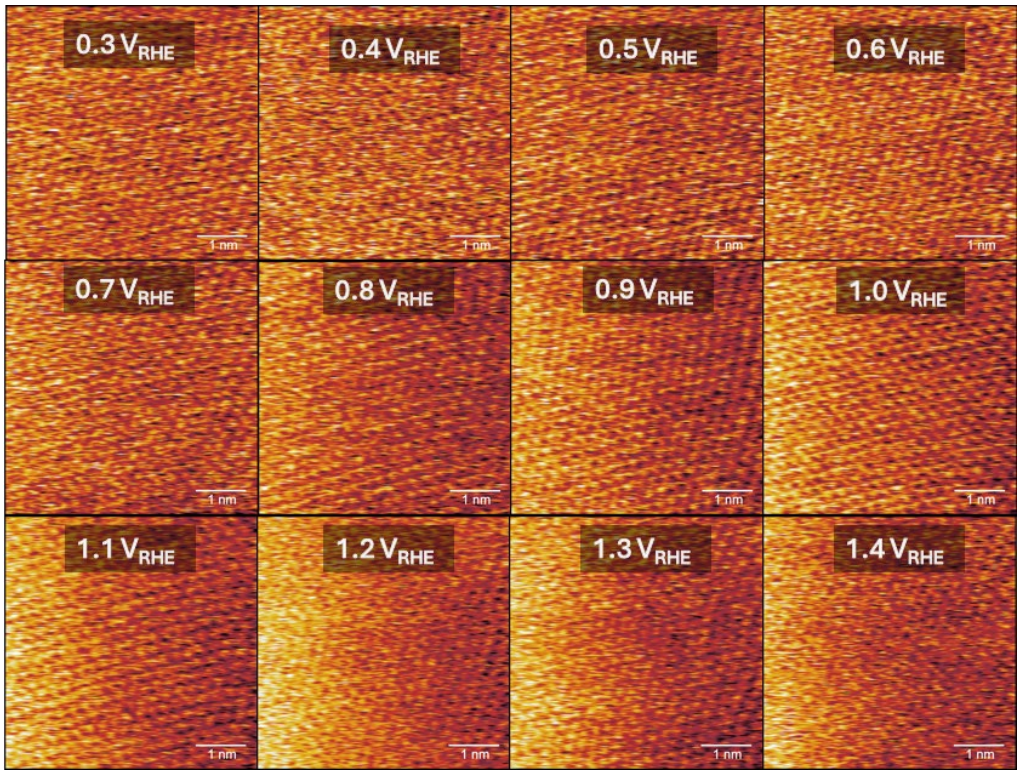


**Figure 4. EC-AFM imaging of graphites as a function of potential in 0.1 M $HClO_4$ solution.** From 0.3V vs. RHE to 1.4 V vs. RHE, we were able to image the graphite lattice, suggesting the atomic resolution capability as a function of potential.

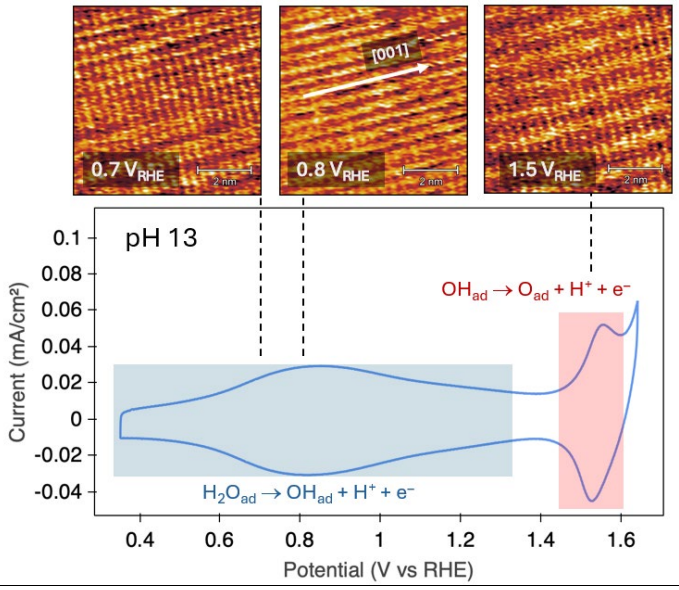


**Figure 5. EC-AFM imaging of an $IrO_2$(110) film grown on $TiO_2$(110) single crystal as a function of potential in pH 13 and the corresponding CV in the same electrolyte.** Images were taken at 0.7, 0.8, and 0.9 V vs. RHE. The observed lattice parameter and symmetry agree well with the $IrO_2$(110) structure. We are working on analyzing the image pattern, *i.e.,* why the shapes of the adsorbates are not spherical and potential-dependent.

**Publications Acknowledging this Grant in 2021-2024**

*(I) Intellectually led by this grant*

- Xu, P. T.; Suntivich, J., Time-Resolved Monitoring of Electrochemical Reactions Using In Situ Stimulated Raman Spectroscopy. *ACS Sustain. Chem. Eng.* **2023,** *11* (1), 13-17.
- Wan, G.; Freeland, J. W.; Kloppenburg, J.; Petretto, G.; Nelson, J. N.; Kuo, D. Y.; Sun, C. J.; Wen, J. G.; Diulus, J. T.; Herman, G. S.; Dong, Y. Q.; Kou, R. H.; Sun, J. Y.; Chen, S.; Shen, K. M.; Schlom, D. G.; Rignanese, G. M.; Hautier, G.; Fong, D. D.; Feng, Z. X.; Zhou, H.; Suntivich, J., Amorphization mechanism of $SrIrO_3$ electrocatalyst: How oxygen redox initiates ionic diffusion and structural reorganization. *Sci. Adv.* **2021,** *7* (2), eabc7323.

*(II) Jointly funded by this grant and other grants with intellectual leadership by other funding sources*

n/a

# Metal-ligand Single Atom Heterogeneous Catalysts

Steven L. Tait
Indiana University

## Presentation Abstract

Single atom catalysis has evolved as a promising strategy to enhance atom utilization efficiency, lower reaction temperatures, and control reaction pathways in heterogeneous catalytic reactions. An important challenge using supported single atom catalysts is the stability of metal single atoms during reactions. Our group has developed a metal-ligand coordination strategy to stabilize single transition metal atoms on high surface area powder oxide supports. We characterize these catalysts using a range of techniques to demonstration the single atom character and well-defined chemical properties of the metal centers. Flow reactor experiments demonstrate the efficacy of these catalysts for small molecule reactions at moderate temperatures with high reaction selectivity and excellent stability. This presentation will highlight several recent results from our work.

**Grant or FWP Number:** DE-SC0021390
**Grant Title: Rational Design of Metal-ligand Single Atom Heterogeneous Catalysts**

**PI:** Steven L. Tait
**Postdoc(s):** Nicholas A. Maciulis, Wondemagegn Wanna, Xuemei Zhou
**Student(s):** Iyad S. Ali, Linxiao Chen, Ayanna Culmer-Gilbert, Fereshteh Rezvani, Eman Wasim, Bobby Woodburn
**Affiliations(s):** Indiana University

## RECENT PROGRESS

Our research group has been developing novel strategies to create single-atom catalysts (SACs) from metal-ligand single-sites on high surface area oxide supports. The metal-ligand approach results in high metal loading, exhibits an ultimate dispersion of metal species, and maximizes atom efficiency. We characterize the structural and chemical properties of the resulting catalysts using a variety of techniques. We use a flow reactor to evaluation catalytic reaction performance of the novel catalysts for a variety of small molecule reactions that require a high level of reaction selectivity. After rational design and optimization of the catalysts, several of these are highly effective and exhibit excellent activity, selectivity, and stability.

### *Ligand-coordinated Pt single-atom catalyst facilitates support-assisted water-gas shift reaction*

The water-gas shift (WGS) reaction ($CO + H_2O \rightarrow CO_2 + H_2, \Delta H = -41.1\ kJ/mol$) is an essential process in the production of hydrogen and has grown significantly in usage

over time. We developed metal-ligand supported catalysts for highly selective WGS reactions. 1,10-phenanthroline-5,6-dione (PDO) was chosen as the ligand for its oxidative potential for stabilizing Pt metal cations via two different binding pockets. The single-atom nature of the Pt-ligand is characterized with extended X-ray absorption fine structure (EXAFS), X-ray photoelectron spectroscopy (XPS), X-ray diffraction (XRD), diffuse reflectance infrared Fourier transform spectroscopy (DRIFTS), and transmission electron microscopy (TEM) techniques. The catalytic activity is evaluated for the WGS reaction, revealing that Pt-ligand SACs supported on defective $TiO_2$ show higher inherent catalytic activity than Pt NPs and a significantly lower activation energy. This characteristic is generally desirable for the redox mechanism. Density functional theory (DFT) calculations reveal that metal-ligand SACs allow CO interaction with oxygen atoms from the $TiO_2$ surface. The redox mechanism of the WGS reaction demonstrates a lower effective activation barrier than the associative mechanism for Pt-ligand SAC. Moreover, the metal-ligand strategy, according to DFT results, facilitates the reaction redox mechanism by reducing the CO binding energy and promoting $CO_2$ and $H_2$ formation process.

***CO oxidation over ligand-coordinated single-site Rh catalyst: Identification of active complex***

Our group developed an approach to stabilize single rhodium atoms on high surface area titania powder supports via a metal-ligand coordination strategy. We examined the reaction activity and mechanism of CO oxidation, as well as the stability in oxidative reaction conditions. Kinetic studies suggest that, with an excess of oxygen in the feed gas, oxygen activation is more facile on defective titania surfaces than on pristine titania surfaces. *In situ* diffuse reflectance infrared Fourier transform spectroscopy (DRIFTS) analysis shows that on the pristine titania surface, the 1,10-Phenanthroline-5,6-dione (PDO) coordinated Rh catalyst (Rh-PDO/$TiO_2$) catalyzes CO oxidation via the formation of carbonate-like species, which is similar to what occurs on Rh nanoparticle catalysts. However, on the defective titania surface, no carbonate species form for Rh-PDO/def-$TiO_2$. The supported Rh-ligand catalysts are also shown to be very stable in such a reaction environment at elevated temperatures, potentially allowing for wide applications.

***Carboxylic acid ligand substituent impacts hydrosilylation activity of platinum single atom catalysts on ceria***

Current industrially employed hydrosilylation catalysts rely on homogeneous platinum catalysts which are not recovered after the reaction. To eliminate this issue, our group has optimized recyclability of heterogeneous platinum single atom catalysts (SACs) on ceria via 1,10-phenanthroline-5,6-dione ligands (PDO), which incorporates mono (PDO-C) and dicarboxylic acid (PDO-C2) groups in the 2- and 9-position of PDO ligand to increase metal–surface interaction. DRIFTS results confirm carboxylic acid coordination to the terminal hydroxy groups of the ceria surface. New catalyst synthesis conditions wherein PDO was combined with the metal prior to exposure to the surface allow control of Pt oxidation state on the surface. The highest metal loading was observed for PDO and PDO-C, correlating with improved catalytic recyclability compared to the PDO-C2 ligand. It is proposed that the location of the carboxylic acid groups and the steric effects can explain the lower activity and metal loading for PDO-C2 ligands. Post-reaction XPS

and DRIFTS spectra show the appearance of new Si and O species on the catalyst during the hydrosilylation reaction, indicating the silane reagent is depositing on the surface. The silane coverage and leaching of catalyst from the surface can cause reduced catalytic activity.

***Tuning coordinated supported catalysts: Carboxylic acid-based ligands to improve ceria-supported Pt catalysts for hydrosilylation***

Ligand-coordinated supported catalysts (LCSCs) with highly-dispersed metal centers are of growing interest to bring the high selectivity and metal utilization efficiency of isolated, well-defined metal centers to a solid support for recyclability and stability. Pt LCSCs with bidentate N-based ligands have shown high activity, selectivity, and stability in hydrosilylation catalysis. We tuned Pt LCSCs with carboxylic acid-based ligands as "anchoring ligands" with bidentate N-based ligands as "coordination ligands." XPS and inductively coupled plasma mass spectrometry were performed after the test reaction, hydrosilylation of 1-octene, to evaluate the leaching of Pt. Using trimesic acid (TMA) as the "anchoring ligand" reduced Pt leaching from 34% after only 1 batch to ~25% after 4 batches. Using TMA as the "coordination ligand" creates a catalyst with 7 times higher turnover number than previous LCSCs. Two other carboxylic acid-based ligands were explored, both creating active and selective Pt hydrosilylation LCSCs.

***Ligand-coordination effects on the selective hydrogenation of acetylene in single-site Pd-ligand supported catalysts***

The selective hydrogenation of acetylene to ethylene is a critical step in the synthesis of polyethylenes. Achieving high conversion to ethylene without over-hydrogenation to ethane is a challenge that requires control of the transition metal site, which we achieved through an LCSC strategy. Using Pd catalysts coordinated to 1,10-phenanthroline-5,6-dione (PDO) ligands on $CeO_2$ supports, we discovered that the reaction selectivity depends strongly on the ligand:metal ratio with higher selectivity when more ligand is present in the catalyst. Catalyst structure was examined by EXAFS, transmission electron microscopy, and CO adsorption, which indicate single-atom character of the Pd. The ligand:metal ratio is determined by XPS measurements and correlated with hydrogenation reactions under steady-state flow conditions to examine trends in hydrogenation activity and selectivity. Those trends can be better understood by DFT calculations that indicate hydrogen binding on the ligand to guide reaction selectivity toward the desired ethylene hydrogenation product. These results demonstrate the importance of considering the dynamic character of LCSCs and inform the design of future single-site heterogeneous catalysts.

***Tuning ligand-coordinated single metal atoms on $TiO_2$ and their dynamic response during hydrogenation catalysis***

We investigated the effect of the organic ligand choice on the activity and stability of $TiO_2$-supported single-atom Pt-ligand catalysts for ethylene hydrogenation. The activity of these catalysts showed a significant dependence on the choice of ligand and also correlated with coordination number for Pt−ligand and Pt−$Cl^-$. Of the three ligands examined in this study, the one with the lowest Pt coordination number, 1,10-phenanthroline-5,6-dione (PDO), showed the lowest reaction temperature and highest

reaction rate, likely due to those metal sites being more accessible to reactant adsorption. In-situ X-ray absorption spectroscopy (XAS) experiments showed that the activity also correlated with good heterolytic dissociation of hydrogen, which was supported by OH/OD exchange experiments and was the rate-determining step of the hydrogenation reaction. In these in-situ XAS experiments up to 190 °C, the supported Pt-ligand catalyst showed excellent stability against structural and chemical change. Instead of Pt, the PDO ligand could be coordinated with Ir on $TiO_2$ to form Ir LCSCs that showed slow activation by loss of Ir−Cl bonds, then excellent stability in the hydrogenation of ethylene. These results provide the chance to engineer ligand-coordinated supported catalysts at the single-atom catalyst level by the choice of ligand and enable new applications at relatively high temperature.

***Ligand-coordinated Ir single-atom catalysts stabilized on oxide supports for ethylene hydrogenation and their evolution under a reductive atmosphere***

In this work, we present a novel series of oxide-supported Ir-ligand single-atom catalysts (SACs) for ethylene hydrogenation. The SACs were created by metal–ligand self-assembly using one of two ligands, either 1,10-phenanthroline-5,6-dione (PDO) or 3,6-Di-2-pyridyl- 1,2,4,5-tetrazine (DPTZ), on powder supports of either $CeO_2$ or MgO. Characterization by XAS, XPS, and CO adsorption proved that Ir exist principally as highly uniform, cationic single-atoms. Ir SACs show significantly higher durability and metal utilization efficiency than Ir nanoparticle (NP) catalysts during ethylene hydrogenation at 100 °C, as well as excellent stability, as no Ir aggregates were detected after >10 h reaction. The activity can be tuned by ligand and support effects: PDO and $CeO_2$ are superior to DPTZ and MgO, respectively. This tunability is attributed to differences in $H_2$ activation capability, which results from differences in support reducibility, electron density on Ir, and, potentially, the local coordination environment of Ir. The Ir SACs lose $H_2$ activation activity either under inert gas or under $H_2$. Through XPS and in situ XAS studies, we attributed the former to the reversible loss of Ir hydride, which is the active species for $H_2$ activation, and the latter to irreversible over-hydrogenation and loss of Ir–O/N coordination. This work presents a new type of Ir hydrogenation SACs that are more durable, efficient, and tunable than supported Ir NPs, while more stable than homogeneous Ir complexes. It also offers fundamental understanding regarding ligand and support effects, as well as the evolution of Ir single-atoms under $H_2$, instructing future design of stable, effective hydrogenation SACs.

**Publications Acknowledging this Grant in 2021-2024**

*Please classify your publications into two categories according to the source of support for the work published:*

*(I) Intellectually led by this grant*

1. Fereshteh Rezvani,† Dave Austin, Duy Le, Talat S. Rahman,* Steven L. Tait,* "Ligand-Coordinated Pt Single-Atom Catalyst Facilitates Support-Assisted Water-Gas Shift Reaction," *Journal of Catalysis*, **438**, 115723 (2024). DOI: 10.1016/j.jcat.2024.115723
2. Fereshteh Rezvani,† Xuemei Zhou,† Debora Motta Meira, George E. Sterbinsky, and Steven L. Tait,* "CO Oxidation over a Ligand Coordinated Single Site Rh Catalyst: Identification of the Active Complex," *Catalysis Science & Technology*, **14**, 5266-5277 (2024). DOI: 10.1039/d4cy00507d
3. Nicholas A. Maciulis,† Eman Wasim,† Fereshteh Rezvani,† Maren Pink, George E. Sterbinsky, Kenneth G. Caulton, and Steven L. Tait,* "Carboxylic Acid Ligand Substituent Impacts Hydrosilylation Activity of Platinum Single Atom Catalysts on Ceria," *Catalysis Science & Technology*, **12**, 7349-7360 (2022). DOI: 10.1039/D2CY01017H
4. Eman Wasim,† Naseem Ud Din, Duy Le, Xuemei Zhou,† Michael S. Pape, George E. Sterbinsky, Talat S. Rahman,* Steven L. Tait,* "Ligand-Coordination Effects on the Selective Hydrogenation of Acetylene in Single-site Pd-Ligand Supported Catalysts," *Journal of Catalysis,* **413**, 81-92 (2022). DOI: 10.1016/j.jcat.2022.06.010
5. Iyad S. Ali,‡ Linxiao Chen,† Fereshteh Rezvani,† Xuemei Zhou,† and Steven L. Tait,* "Tuning Coordinated Supported Catalysts: Carboxylic Acid-Based Ligands to Improve Ceria-Supported Pt Catalysts for Hydrosilylation," *Applied Catalysis A: General* **639**, 118634 (2022). DOI: 10.1016/j.apcata.2022.118634
6. Xuemei Zhou,† George E. Sterbinsky, Eman Wasim,† Linxiao Chen,† and Steven L. Tait,* "Tuning Ligand-coordinated Single Metal Atoms on $TiO_2$ and their Dynamic Response during Hydrogenation Catalysis," *ChemSusChem* **14**, 3825-3837 (2021). DOI: 10.1002/cssc.202100208
7. Linxiao Chen,† Iyad S. Ali,‡ George E. Sterbinsky, Xuemei Zhou,† Eman Wasim,† and Steven L. Tait,* "Ligand-coordinated Ir Single-atom Catalysts Stabilized on Oxide Supports for Ethylene Hydrogenation and Their Evolution under a Reductive Atmosphere," *Catalysis Science & Technology* **11**, 2081-2093 (2021). DOI: 10.1039/D0CY01132K

*(II) Jointly funded by this grant and other grants with intellectual leadership by other funding sources*

N/A

V. Sara Thoi

# Developing Electrocatalytic Systems for the Conversion of Nitrogen Species to Value-added Products

V. Sara Thoi
Johns Hopkins University, Department of Chemistry

## Presentation Abstract

We present our results in developing electrochemical systems for C-N coupling using waste products to form urea, an important fertilizer for agriculture. Herein, we report a series of AuCu alloys that can achieve up to 70% selectivity for urea from carbon dioxide and nitrate at a current density of up to 400 μA $cm^{-2}$ upon optimization. We also discovered a molecular metal-organic cage with six isolated Cu sites for simultaneous carbon dioxide and nitrate activation to convergently produce urea. Utilizing a suite of *in situ* electrochemical, spectroscopic, and computational techniques, we postulate a catalytic cycle involving a Cu-CO species that is subsequently attacked by $NH_2OH$, a reduced product of nitrate.

## RECENT PROGRESS

### *Electrochemical C-N Coupling*

Motivated by this our prior studies on Au-catalyzed C-N electrocoupling, we focused on tuning the reactivity of Au by introducing Cu sites. Three different AuCu alloys was electrochemically deposited with a Au:Cu ratio of approximately 75:25, 50:50, and 25:75. Phase purity was achieved only for $Au_{75}Cu_{25}$ and $Au_{50}Cu_{50}$, as shown by X-ray diffraction (**Figure 2a**). Of the three alloys, $Au_{75}Cu_{25}$ was determined to be the most active catalyst, achieving nearly 70% selectivity for urea and up to 400 μA $cm^{-2}$ (**Figure 2b, c**). This study, which shows AuCu alloys exhibiting a significant performance enhancement over Au alone, illustrates a path towards more abundant metal catalysts.

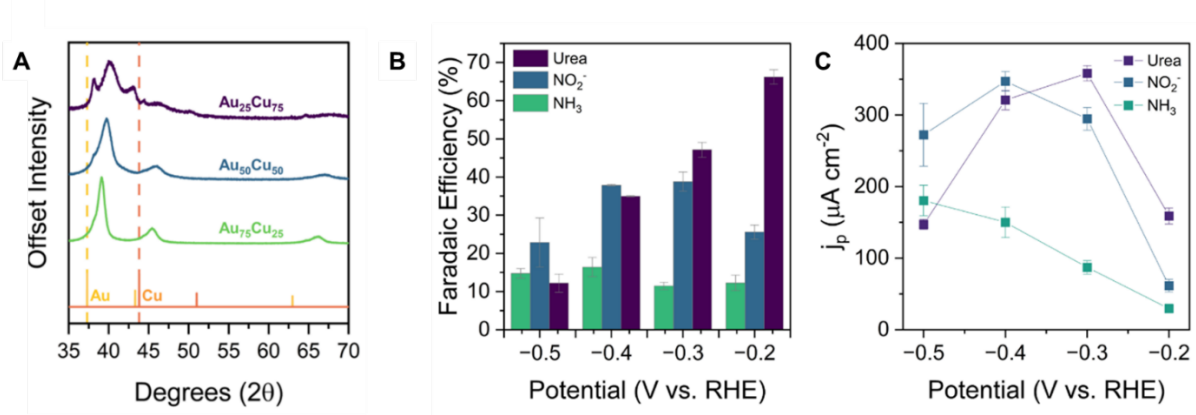


**Figure 2.** (a) Powder X-ray diffraction of three AuCu alloys, and (b) Faradaic efficiency and (c) activity for C-N coupling of $CO_2$ and $NO_3^-$.

We also have developed a molecular Cu-based cage, BIF-29(Cu), that is a competent catalyst for the co-reduction of $CO_2$ and $NO_3^-$ (**Figure 3a**). At the mild cathodic potential of -0.3 V vs RHE,

we saw a remarkable urea selectivity of nearly 70% and a high activity of 400 uA $cm^{-2}$ (**Figure 3b**). Since each of the six Cu sites is isolated, we hypothesized that a cascade reaction occurs where an electrochemically generated $NH_2OH$ from nitrate reduction attacks an experimentally observed Cu-CO species. Significantly, we conducted in situ X-ray absorption spectroscopy (XAS) to determine if BIF-29(Cu) remains molecularly intact during electrocatalytic conditions. Surprisingly, we found that BIF-29(Cu) forms a Cu aggregate reversibly under no substrate conditions (HER, **Figure 4a**) and nitrate reduction ($NO_3RR$, **Figure 4b**), as seen by a decrease in the Cu-N band and an increase Cu-Cu band in the extended X-ray fine structure (EXAFS) range. However, upon exposure to $CO_2$, no Cu-Cu band appears suggesting that the Cu-CO intermediate stabilizes the molecular cage and prevents Cu aggregation (**Figure 4c)**. Under the relevant C-N coupling conditions where $CO_2$ and $NO_3^-$ are both present, we see negligible changes in the EXAFS (**Figure 4d**), suggesting that the molecular cage remains intact during catalysis. DFT calculations suggest that $NH_2OH$ from $NO_3RR$ can react with the Cu-CO intermediate (**Figure 5**, with Dr. Fanglin Che).

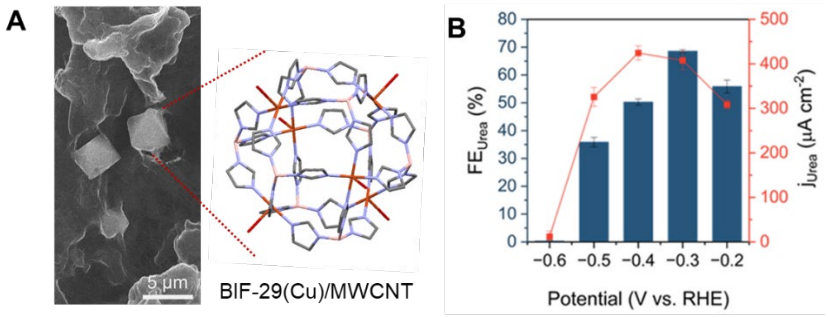


**Figure 3**. (a) Scanning electron microscopy image of BIF-29 on top of multiwalled carbon nanotubes (MWCNTs) and (b) urea selectivity and activity as a function of cathodic potential.

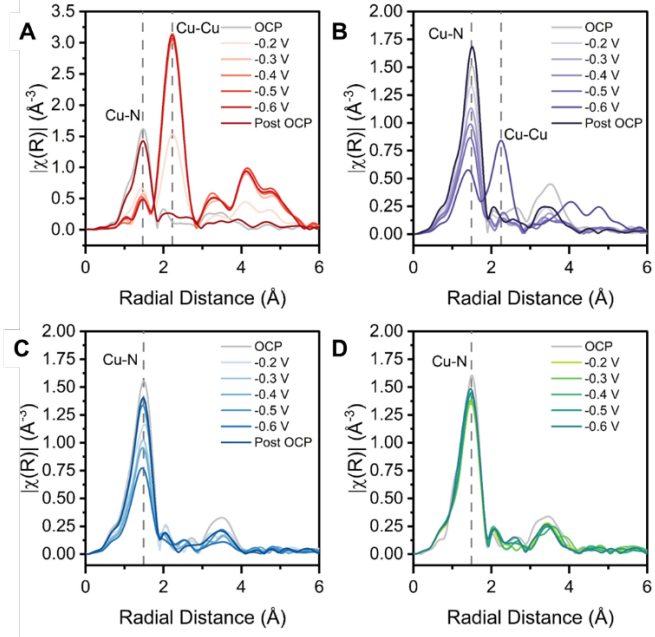


**Figure 4**. Extended X-ray absorption fine structure (EXAFS) of BIF-29(Cu) at different potentials in (a) 0.1M $KHCO_3$ ($N_2$ purged), (b) 0.1M $KHCO_3$ and 0.1M $KNO_3$ ($N_2$ purged), (c) 0.1M $KHCO_3$ ($CO_2$ purged), and (d) 0.1M $KHCO_3$ and 0.1M $KNO_3$ ($CO_2$ purged).

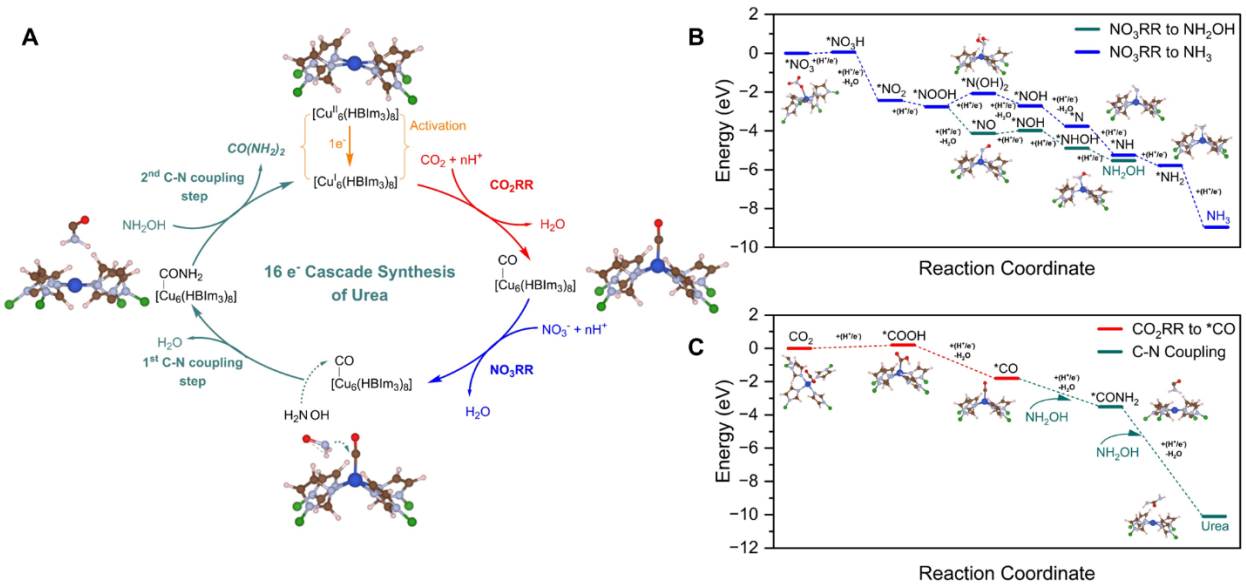


**Figure 5.** (a) The proposed mechanism for urea production from $CO_2$ and $NO_3^-$ within the BIF-29(Cu) cage and (b) Gibbs free energy diagrams for $NO_3RR$ to hydroxylamine or ammonia, and (c) Gibbs free energy diagram of $CO_2RR$-to-CO and hydroxylamine over the single Cu atom site within the structure of BIF-29(Cu) with applied potential of -0.20 V vs. RHE and pH set as 6.8.

**Publications Acknowledging this Grant in 2020-2023**

*Intellectually led by this grant*

- Banerjee, S.,[#] Gorham, J. M.,Beccar-Varela, P., Hackbarth, H. G., Siegler, M. A., Drichko, N., Write, J. T., Bedford, N. M.,* Thoi, V. S.* Atomically Dispersed $CuN_x$ Sites from Thermal Activation of Boron Imidazolate Cages for Electrocatalytic Methane Generation, *ACS Appl. Energy Mater.*, **2022**, *in press*. **DOI: 10.1021/acsaem.2c01174**
- Davis, J., Banerjee, S., Beccar-Varela, P., Thoi, V. S., Drichko, N.* Raman Scattering Spectra of Boron Imidazolate Frameworks Containing Paramagnetic Ions, **2023,** *158*, 214707. **DOI: 10.1063/5.0152070**
- Gerke, C. S.,[‡] Xu, Y.,[‡] Foley, G. D., Zhang, B., Shi, E., Bedford, N. M., Che, F.,* **Thoi, V. S.*** Electrochemical C-N Bond Formation Within Boron Imidazolate Cages Featuring Single Copper Sites, *J. Am, Soc. Chem.*, **2023,** *145*, 26144-26151. DOI: 10.1021/jacs.3c08359
- Gerke, C. S., Klenk, M., Zapol, P.**, Thoi, V. S.*** Electrochemical Heteroatom Coupling of $CO_2$ and $NO_3^-$ to Urea over a Polycrystalline Gold Electrode, *ACS. Catal.,* **2023**, *13,* 14540-14547. DOI: 10.1021/acscatal.3c03027
- Singh, K. K.,[‡] Gerke, C. S.,[‡] Saund, S. S., Zito, A. M., Siegler, M. A., **Thoi, V. S.*** $CO_2$ Activation with Manganese Tricarbonyl Complexes via an H-Atom Responsive Benzimidazole Ligand, *Chem. Eur. J.,* **2023**, *29*, e202300796. Invited to a special issue on "Manganese Homogeneous Catalysis." DOI: 10.1002/chem.202300796

Christine M. Thomas

## Coordination-Induced Element-Hydrogen Bond Weakening and $N_2$ Activation by Phosphinoamide-Bridged Heterobimetallic Zr/Co Complexes

Christine M. Thomas, Julia Feresin, Brett A. Barden, Seth M. Barrett, and Adwitiya Singh
Department of Chemistry and Biochemistry, The Ohio State University

### Presentation Abstract

The formation and cleavage of chemical bonds in catalytic reactions often relies on accessible two-electron processes that are challenging for base metals such as first row and early transition metals. Metal-metal cooperativity provides a potential solution to this challenge by facilitating redox processes and providing access to cooperative bond activation mechanisms. Dinucleating phosphinoamide ligands have been used to link early and late transition metals into a single heterobimetallic framework, supporting metal-metal multiple bonds across a broad range of metal-metal combinations. The resulting complexes have been shown to activate small molecules, cleave strong bonds, and catalyze organic transformations. This presentation will focus on (1) the effect of a pendent redox-active Co center on the weakening of O-H and N-H bonds of substrates bound to a neighboring $d^0$ $Zr^{IV}$ site in a tris(phosphinoamide) framework, and (2) the use of coordinatively unsaturated bis(phosphinoamide) $Zr^{IV}/Co^{-I}$ compounds to activate and functionalize dinitrogen.

## DE-SC0019179: A Multimetallic Approach to Dinitrogen Reduction, Ammonia Oxidation, and C-N Bond Formation

**PI:** Christine M. Thomas
**Postdoc(s):** Preshit C. Abyhankar
**Student(s):** Nathanael H. Hunter, Julia Feresin, Adwitiya Singh, Jose A. Sanabria-Gracia, Brett A. Barden, Sean M. Morrison, Joshua A. Shoopman, David R. Ullery, R. Maya Kumar
**Affiliations(s):** Department of Chemistry and Biochemistry, The Ohio State University

## RECENT PROGRESS

***N-N bond activation and functionalization by bis(phosphinoamide) Zr/Co compounds***

In the absence of exogenous ligands, arenes, or coordinating solvents, two-electron reduction of the bis(phosphinoamide) $Zr^{IV}/Co^{I}$ complex **1** under a $N_2$ atmosphere results in formation of the tetrametallic, side-on bound, dinitrogen complex **2** (Figure 1)**.** Although the N-N distance in the solid-state structure of **2** is 1.40 Å and suggests a highly activated N-N bond, $N_2$ is readily displaced by coordinating solvents, arenes, and donor ligands. Moreover, while THF does not displace $N_2$, it does coordinate to Zr and break up the tetrametallic cluster into the end-on-bridged $N_2$ complex **3**. Compounds **2** and **3** can be reproducibly crystallized independently, as confirmed through single crystal X-ray diffraction. Solid-state Raman spectroscopy of **2** reveals an ν(N-N) stretching frequency of 1106 $cm^{-1}$, consistent with the long N-N distance observed in the solid-state structure. The solution-state Raman spectrum of the same sample of **2** indicates that it exists as an equilibrium mixture with **3** (ν(N-N) = 1878 $cm^{-1}$) in solution.

**Figure 1.**

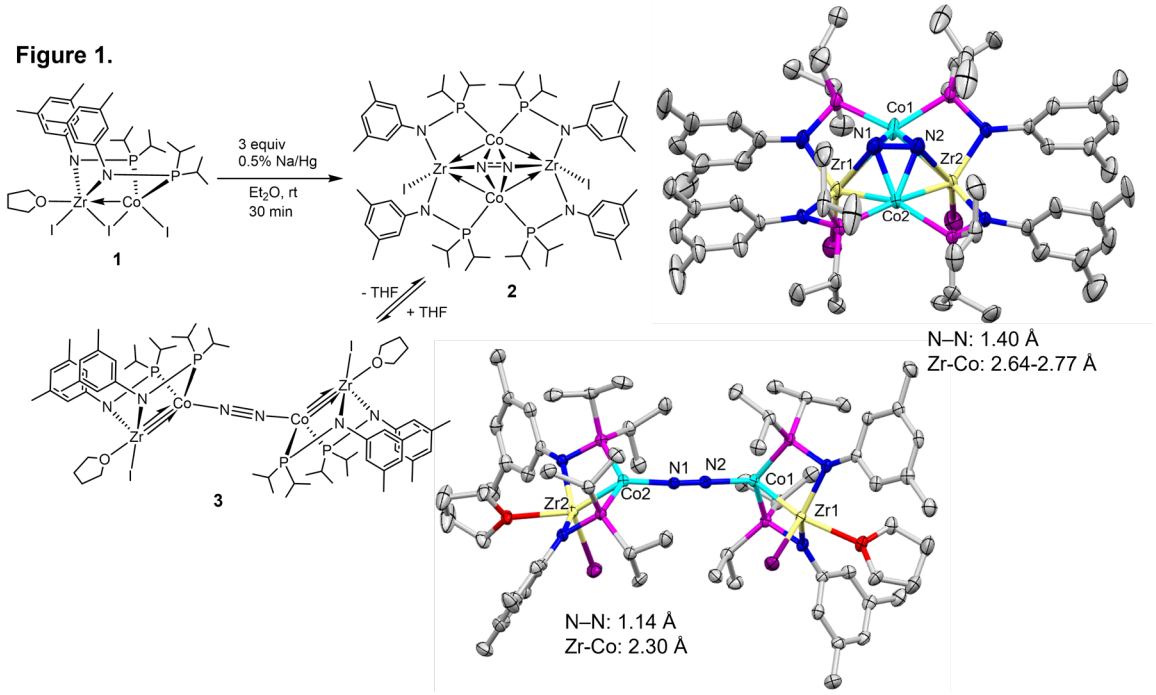


In addition to this stoichiometric reactivity, we have established that **1** is an effective precatalyst for the reduction of $N_2$ to $N(TMS)_3$ in the presence of 4000 equiv KC8 and 4000 equiv TMSCl, reaching a maximum of 543 turnovers in 18 hours at room temperature. Dinitrogen complex **2** can also be used as a catalyst for this $N_2$ silylation reaction, albeit with fewer turnovers (TON = 188) as a result of the increased reactivity/sensitivity of this compound.

**Scheme 1.**

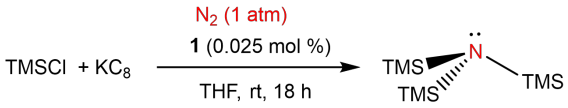


In addition to direct reactions with $N_2$, the role of the two metals centers has been investigated using stoichiometric reactions to model the N-N bond cleavage process and analogues of intermediates in the hypothetical $N_2$ reduction cycle have been synthesized.

The $Zr^{IV}/Co^{-I}$ arene complex **4** reacts immediately with 0.5 equiv diazene ($Ph_2N_2$) to cleave the N=N bond and generate the tetrametallic imido-bridged species **5** (Figure 2). The imido ligands in **5** are triply bridging between two Zr and one Co center, potentially modelling one of the first intermediates in $N_2$ cleavage and functionalization. The imido fragments can be effectively silylated with TMSCl to release $PhN(TMS)_2$ and regenerate a chloride analogue of **1**, modelling the final step in $N_2$ silylation.

**Figure 2.**

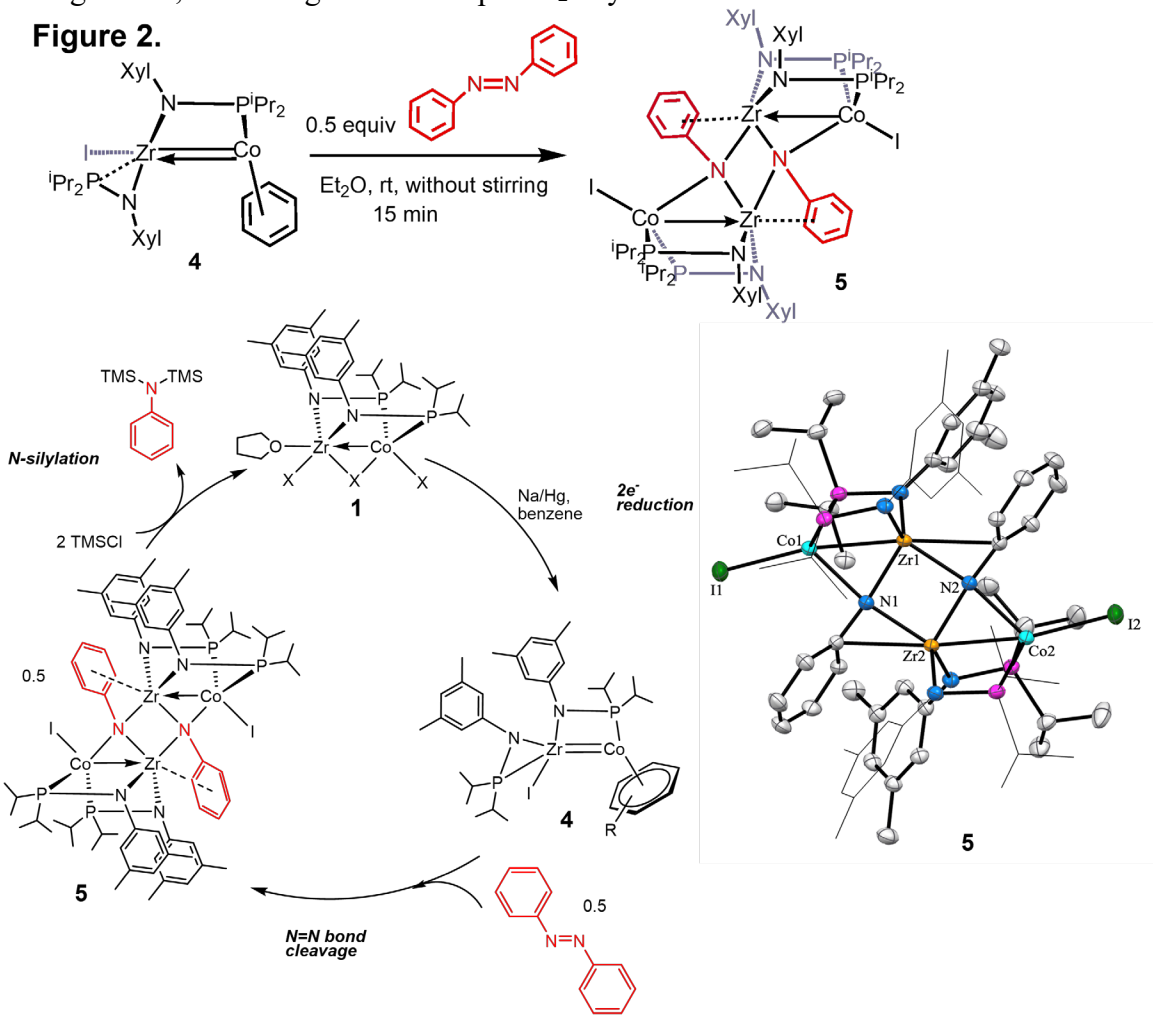


***Coordination-induced bond weakening in early/late heterobimetallics***

The focus of this study is to explore ammonia oxidation steps by tris(phosphinoamide) Zr/Co compounds, but as an initial proof-of-principle model, the square scheme for conversion between the previously reported $Co^0/Zr^{IV}$-oxo (**6**) and $Co^I/Zr^{IV}$-hydroxo (**7**) compounds was investigated to probe the impact of the pendent redox-active Co center on the element-hydrogen BDFE of substrates bound to Zr (Figure 3). The open circuit potential (OCP) of a lutidine/lutidinium buffer solution containing a 1:1 mixture of **6** and **7** was used to determine that the BDFE of the O-H bond in **7** is roughly 63 kcal/mol using eq 2. This very low value indicates that the presence of an appended redox-active metal center (Co) provides a similar weakening of the O-H bond as would be expected if the hydroxide ligand were bound directly to a redox-active metal. Inputting the $BDFE_{OH}$ value into eq 1, which relates the known **8**/**7** and **6**/**9** redox potentials to the BDFE of **7** and $pK_a$s of **7** and **8**, we can estimate that the $pK_a$ of **7** is 30.9 and the $pK_a$ of **8** is 21.1.

**Figure 3.**

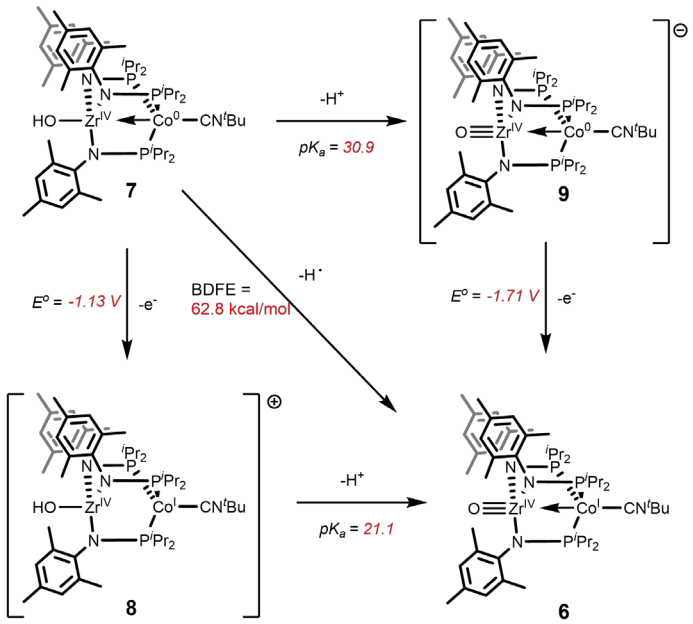


$$BDFE_{sol(X\text{-}H)} = 1.37pK_a + 23.06E^o + C_{G,sol} \quad (eq\ 1)$$

$$BDFE_{sol(X\text{-}H)} = 23.06E^o(X/XH\ V\ vs\ H_2) + \Delta G(0.5H_{2(g)}/H^{\bullet}{}_{1M}) \quad (eq\ 2)$$

The $BDFE_{OH}$ and $pK_a$ values have been experimentally corroborated through a series of reactions with H-atom abstraction reagents with known BDFEs and with acids and bases with known $pK_a/pK_b$ values.

With these proof-of-concept results in hand, current attention is focused on determining the impact of bimetallic frameworks on the N-H BDFEs of bound substrates. For simplicity, this study began with $PhNH_2$ as a model substrate surrogates for $NH_3$ in efforts to initially avoid complications from unwanted dimerization processes. The $PhNH_2$ adduct **11** was synthesized via addition of $PhNH_2$ to $Zr^{IV}/Co^{-I}$ species **10**.

Successive addition of equivalents of 2,4,6-tri-*tert*-butylphenoxyl radical resulted in H-atom abstraction to form the $Zr^{IV}/Co^{0}$ amide complex **12** and the $Zr^{IV}/Co^{I}$ imide complex **13** (Figure 4). With compounds **11**-**13** in hand, we are poised to determine the N-H BDFEs of **11** and **12**, fill in the redox potential and $pK_a$ values in square schemes analogous to that in Figure 3, and determine to what extent the coordination-induced bond weakening effects imparted by the pendent Co center can be generalized for substrates with element-hydrogen bonds.

**Figure 4.**

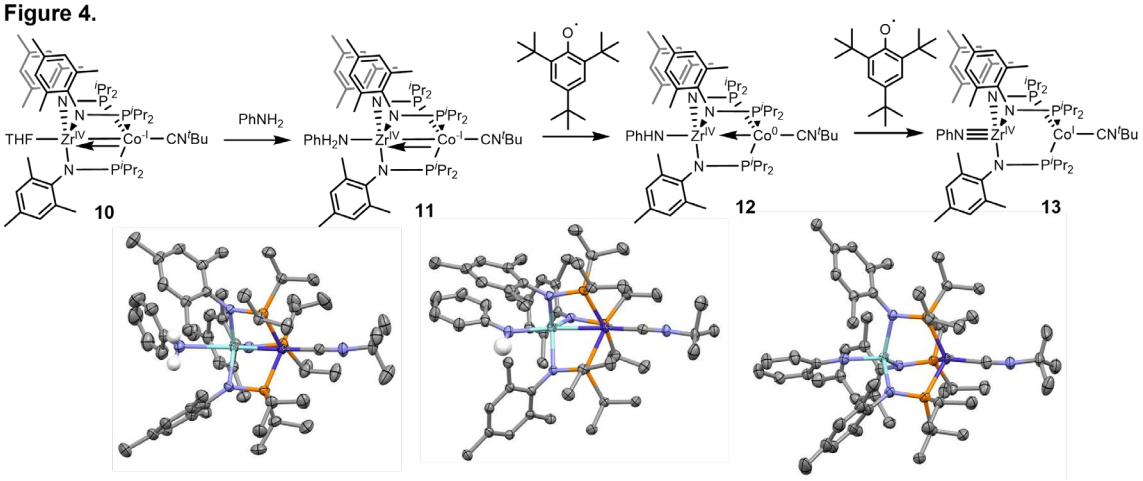

**Publications Acknowledging this Grant in 2021-2024**

*(I) Intellectually led by this grant*

1. Abhyankar, P. C.; Thomas. C. M. Hydrogenation Reactions with Heterobimetallic Complexes. *Angew Chem. Int. Ed.* **2024**, e202416100.
2. Hunter, N. H.; Thomas, C. M. Polarized Metal-Metal Multiple Bonding and Reactivity of Phosphinoamide-Bridged Heterobimetallic Group IV/Cobalt Compounds. *Dalton Trans.* **2024**, *53*, 15764-15781.
3. Abhyankar, P. C.; Morrison, S. M.; Shoopman, J. A.; Kumar, R. M.; Singh, A.; Moore, C. E.; Thomas, C. M. $M^{IV}/Co^{-I}$ (M = Zr, Hf) Bis(phosphinoamide) Complexes with $\eta^6$- and $\eta^4$-Arenes. *Organometallics* **2024**, *43*, 1837-1851.
4. Hunter, N. H.; Stevens, J. E.; Moore, C. E.; Thomas, C. M. One Bridge, Three Bonds: A Frontier in Multiple Bonding in Heterobimetallic Complexes. *Inorg. Chem.* **2023**, *62*, 659-663.
5. Hunter, N. H.; Lane, E. M.; Gramigna, K. M.; Moore, C. E.; Thomas, C. M. C-H Bond Activation Facilitated by Bis(phosphinoamide) Heterobimetallic Zr/Co Complexes. *Organometallics* **2021**, *40*, 3689-3696.
6. Ullery, D. R.; Moore, C. E.; Thomas, C. M. Two Polymorphs of $[Rh(\mu\text{-}I)(COD)]_2$ *Acta Crys.* **2021**, *E77*, 871-874.

*(II) Jointly funded by this grant and other grants with intellectual leadership by other funding sources*

none

## Reductive Transformations of Nitrite and Nitrosyl at a Dicopper Center

Jose Martinez Fernandez,[†] Alireza Haji Seyed Javadi,[‡] Simon J. Teat,[‖] Thomas R. Cundari,[‡] and T. Don Tilley[†]

[†]Chemical Sciences Division, Lawrence Berkeley National Laboratory, Berkeley, California 94720
[‡]Department of Chemistry, Center for Advanced Scientific Computing and Modeling (CASCaM), University of North Texas, Denton, Texas 76203
[‖]Advanced Light Source, Lawrence Berkeley National Laboratory, Berkeley, CA 94720

### Presentation Abstract

Nitrite $(NO_2)^-$ and nitric oxide $(NO)^\cdot$ are essential signaling molecules in biological neurotransmission and vasodilation, and their interconversion is key to transition metal-catalyzed denitrification carried out by nitrogen fixing bacteria. With the goal of studying nitrite reduction on a dicopper platform, a robust dinucleating ligand, DPFN [2,7-bis(fluoro-di(2-pyridyl)methyl)-1,8-naphthyridine], was employed to facilitate metal-metal cooperativity. A mono-cationic dicopper(I,I) nitrite complex, $[Cu_2(\mu{-}\kappa^1{:}\kappa^1\text{-}O_2N)DPFN][NTf_2]$ ($NTf_2^- = N(SO_2CF_3)_2^-$), was synthesized by treatment of a dicopper acetonitrile complex, $[Cu_2(\mu\text{-MeCN})DPFN][NTf_2]_2$, with tetrabutylammonium nitrite ($[nBu_4N][NO_2]$). Notably, the reaction of the dicopper nitrite complex with $HNTf_2$ results in N−O bond cleavage in the putative, HONO-ligated complex to form the more thermodynamically favorable nitrosyl-bridged dicopper complex $[Cu_2(\mu\text{-NO})(\mu\text{-OH})DPFN][NTf_2]_2$. This scission can be reversed *via* deprotonation of the hydroxy ligand with $KO^tBu$. The $\mu{-}\kappa^1{:}\kappa^1\text{-}O_2N$ complex was also found to be a potent nucleophile, a quality that can be leveraged towards reactions with nitriles at ambient temperatures to produce the corresponding dicopper(I,I) carboxylate complex and dinitrogen as the byproduct in very good yields. This synthetic pathway is amenable to a wide range of nitriles with R groups of varying size, only suffering slower reaction times with very sterically demanding nitriles such as *tert*-butyl nitrile or 1-adamantanecarbonitrile. The synthesis, reactivity, and characterization of these complexes through IR and NMR spectroscopies, and X-ray crystallography, will be presented.

**Program in Catalysis and Chemical Transformations -**
**Harnessing Complexity for Catalytic Efficiency - FWP CH030201**

**PI:** T. Don Tilley
**Student:** Jose Martinez Fernandez

## RECENT PROGRESS

***Nitrite Activation at Dicopper***

Mononuclear copper coordination compounds have been extensively studied in the context of biomimetic nitrite reduction. Meanwhile, nitrite bond activation at dicopper cores has only recently garnered attention, despite the valuable information these systems can offer. These results demonstrate that two copper(I) centers in proximity can work in concert to stabilize what historically has been an unstable linkage for mononuclear complexes. Moreover, this cooperativity allows the nitrito ligand to be reversibly cleaved by a proton, a process permitted by nitrosyl retention at the dicopper core. To our knowledge, this is the first instance of a stoichiometric cycle reminiscent of the CuNiR's pH-dependent, bidirectional catalysis occurring on a dicopper platform. Computational and spectroscopic methods were used to describe a rare antiferromagnetically coupled dicopper(II,II) nitrosyl hydroxy complex that possesses unusual thermal stability. The lability of the nitrosyl ligand provides a new avenue for the formation and study of other reactive bimetallic species and possesses relevance towards the study of NO-releasing systems.

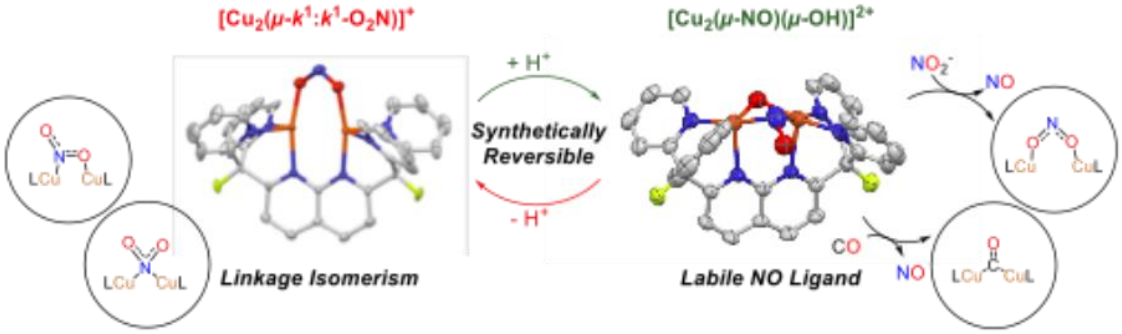


**Publications Acknowledging this Grant in 2021-2024**

*(I) Intellectually led by this grant*


1. Dombrowski, J. P.; Ziegler, M. S.; Phadke, N. M.; Mansoor, E.; Levine, D. S.; Witzke, R. J.; Head-Gordon, M.; Bell, A T.; Tilley, T. D. Siloxyaluminate and Siloxygallate Complexes as Models for Framework and Partially Hydrolyzed Framework Sites in Zeolites and Zeotypes. *Chem. Eur. J.* **2021**, *27*, 307-315.
2. Desnoyer, A. N.; Nicolay, A.; Ziegler, M. S.; Lakshmi, K. V.; Cundari, T. R.; Tilley, T. D. A Dicopper Nitrenoid by Oxidation of a $Cu^{I}Cu^{I}$ Core: Synthesis, Electronic Structure and Reactivity. *J. Am. Chem. Soc.* **2021**, *143*, 7135–7143.
3. Nicolay, A.; Heron, J.; Shin, C.; Kuramarohit, S.; Balcells, D.; Tilley, T. D. Unsymmetrical Naphthyridine-Based Dicopper(I) Complexes: Synthesis, Stability and Carbon-Hydrogen Bond Activations. *Organometallics* **2021**, *40*, 1866-1873.
4. Amtawong, J.; Skjelstad, B. B.; Handford, R. C.; Suslick, B. A.; Balcells, D.; Tilley, T. D. C−H Activation by $RuCo_3O_4$ Oxo Cubanes: Effects of Oxyl

Radical Character and Metal-Metal Cooperativity. *J. Am. Chem. Soc.* **2021**, *143*, 12108-12119.

5. Amtawong, J.; Nguyen, A. I.; Tilley, T. D. Mechanistic Aspects of Cobalt Oxo Cubane Clusters in Oxidation Chemistry." J. Amtawong, A. I. Nguyen and T. D. Tilley, *J. Am. Chem. Soc.* **2022**, *144*, 1475–1492.
6. Piesch, M.; Nicolay, A.; Haimerl, M.; Seidl, M.; Balázs, G.; Tilley, T. D. Binding, Release and Functionalization of Intact Pnictogen Tetrahedra Coordinated to Dicopper Complexes. *Chem. Eur. J.* **2022**, e202201144.
7. Rios, P.; See, M. S.; Handford, R. C.; Teat, S. J.; Tilley, T. D. Robust dicopper(I) μ-boryl complexes supported by a dinucleating naphthyridine-based ligand. *Chem. Sci.* **2022**, *13*, 6619–6625.
8. Kynman, A. E.; Elghanayan, L. K.; Deesnoyer, A. N.; Yang, Y.; Severy, L.; Di Giuseppe, A.; Tilley, T. D.; Maron, L.; Arnold, P. L. Controlled monodefluorination and alkylation of C($sp^3$)-F bonds by lanthanide photocatalysts: importance of metal – ligand cooperativity. *Chem. Sci*. **2022**, *13*, 14090-14100.
9. Ríos, P.; See, M. S.; Handford, R. C.; Cooper, J. K.; Tilley, T. D. Tetracopper $\sigma$-Bound $\mu$-Acetylide and -Diyne Units Stabilized by a Naphthyridine-based Dinucleating Ligand. *Angew. Chem. Int. Ed.* **2023**, e202310307.
10. Ríos, P.; See, M. S.; Gonzalez, O.; Handford, R. C.; Nicolay, A.; Rao, G.; Britt, R. D.; Bediako, D. K; Tilley, T. D., Iron Homo- and Heterobimetallic Complexes Supported by a Symmetrical Dinucleating Ligand. *Chem. Commun.* **2024**, 60, 8912-8915.
11. See, M. S.; Ríos, P.; Tilley, T. D., Diborane Reductions of $CO_2$ and $CS_2$ Mediated by Dicopper μ-Boryl Complexes of a Robust Bis(Phosphino)-1,8-Napthyridine Ligand. *Organometallics* **2024**, *43*, 1180-1189.
12. Dombrowski, J. P.; Kalendra, V.; Ziegler, M. S.; Lakshmi, K. V.; Bell, A. T.; Tilley, T. D. M–Ge–Si Thermolytic Molecular Precursors and Models for Germanium-Doped Transition Metal Sites on Silica. *Dalton Trans.* **2024**, *53*, 7340-7349.
13. Wheeler, T. A.; Tilley, T. D. Metal-Metal Redox Exchange to Produce Heterometallic Manganese-Cobalt Oxo Cubanes *via* a "Dangler" Intermediate. *J. Am. Chem. Soc.* **2024**, *146*, 20279-20290.
14. Ríos, P.; See, M. S.; Gonzales, O.; Handford, R. C.; Nicolay, A.; Rao, G.; Britt, R. D.; Bediako, D. K.; Tilley, T. D. Iron Homo- and Hetero-bimetallic Complexes Supported by a Symmetrical Dinucleating Ligand. *ChemComm.* **2024**, *60*, 8912-8915.
15. Fernandez, J. M.; Hajiseyedjavadi, A.; Teat, S.; Cundari, T.; Tilley, T. D. Synthetically Reversible, Proton-Mediated Nitrite N–O Bond Cleavage at a Dicopper Site. submitted.

*(II) Jointly funded by this grant and other grants with intellectual leadership by other funding sources*

1. Kanbur, U.; Witzke, R. J.; Xu, J.; Ferrandon, M. S.; Goetjen, T. A. Kropf, A. J.; Perras, F. A.; Liu, C.; Tilley, T. D.; Kaphan, D. M.; Delferro, M. Supported Electrophilic Organoruthenium Catalyst for the Hydrosilylation of Olefins. *ACS Catal.* **2023**, *13*, 13383-13394.

Ba Tran

## Experimental and Computational Studies on $H_2$ Activation, β-Elimination, and Catalytic Hydrogenation Reactions at Cu(I) Centers

Evan A. Patrick, Jack T. Fuller III, Bojana Ginovska, Simone Raugei, R. Morris Bullock, Ba L. Tran
Pacific Northwest National Laboratory, Physical and Computational Sciences Directorate and Institute for Integrated Catalysis

### Poster Abstract

The elucidation of mechanisms to understand the controlling factors for reactions catalyzed by Earth abundant metals is critical to the development of sustainable organotransition chemistry. The promotion of new or enhanced reactivity at metal complexes by controlling their coordination geometries with ancillary ligands is a hallmark of organometallic chemistry. $d^{10}$ Cu(I) complexes can adopt a variety of geometries, with linear, trigonal planar and tetrahedral environments being common. Through experimental and computational studies, we demonstrate the significant contrast between linear and trigonal planar geometries at Cu(I) centers supported by monodentate N-heterocyclic carbene (NHC), dicarbene and diphosphine ligands on $H_2$ activation, catalytic olefin hydrogenation, and β-elimination reactions of alkyl and alkoxide Cu(I) complexes.

**FWP 47319: Advancing key catalytic reaction steps for achieving carbon neutrality**

**PI:** Johannes Lercher
**Co-PIs:** Aaron M. Appel, Liney Arnadottir (Oregon State U.), David A. Dixon (U. Alabama), Zdenek Dohnalek, John L. Fulton, Bojana Ginovska, Jian Zi Hu, Abhi J. Karkamkar, Bruce D. Kay, Konstantin Khivantsev, Sungmin Kim, Greg A. Kimmel, Libor Kovarik, ThuyThanh D. Le, Mal Soon Lee, Johannes A. Lercher, John C. Linehan, Zbynek Novotny, Simone Raugei, Udishnu Sanyal, Gregory K. Schenter, Wendy J. Shaw, Honghong Shi, Janos Szanyi, Ba L. Tran, Huamin Wang, Yong Wang, Nancy M. Washton, Eric S. Wiedner

Christopher Uyeda

# Catalytic N=N Coupling Reactions

Department of Chemistry, Purdue University, West Lafayette IN 47907

## Presentation Abstract

Azo compounds have numerous applications in emerging energy and sustainability technologies, including organic photovoltaic devices, batteries, electrochromic windows, and advanced displays. Most of the current approaches to the synthesis of azo compounds require the use of harsh redox reagents to induce N=N bond formation. Consequently, there are significant limitations in substrate scope, and low yields are often observed for highly functionalized or hindered aryl azides.

The overarching goal of this project is to develop catalytic redox-neutral N=N coupling reactions using organic azides as starting materials. These reactions do not require the use of any redox reagents and produce only gaseous $N_2$ as a byproduct. We recently demonstrated that dinickel catalysts promote efficient N=N coupling reactions to form azoarenes. The reaction exhibits broad substrate scope and uses a catalyst comprising earth abundant elements. The dinuclear nature of the active site is critical to the mechanism of catalysis and avoids the problem of strong product inhibition. This project provides fundamental insight into the unique catalytic properties of metal–metal bonds through a combination of experimental studies and computational models. These mechanistic studies will inform the development of new catalysts for the coupling of hindered aryl azides and for enantioselective N=N coupling reactions.

**DE-SC0022086: Catalytic N=N Coupling Reactions for the Synthesis of Azomaterials**

**PI:** Christopher Uyeda, Jianguo Mei (co-PI)
**Student(s):** Kyle B. Brook, Christopher J. Rybak, Sumeet R. Sahoo, Parijat Sharma
**Affiliations(s):** Department of Chemistry, Purdue University, West Lafayette, IN 47907

## RECENT PROGRESS

### *Dicobalt-Catalyzed N=N Coupling Reactions of Tertiary Alkyl Azides to form Azoalkanes*

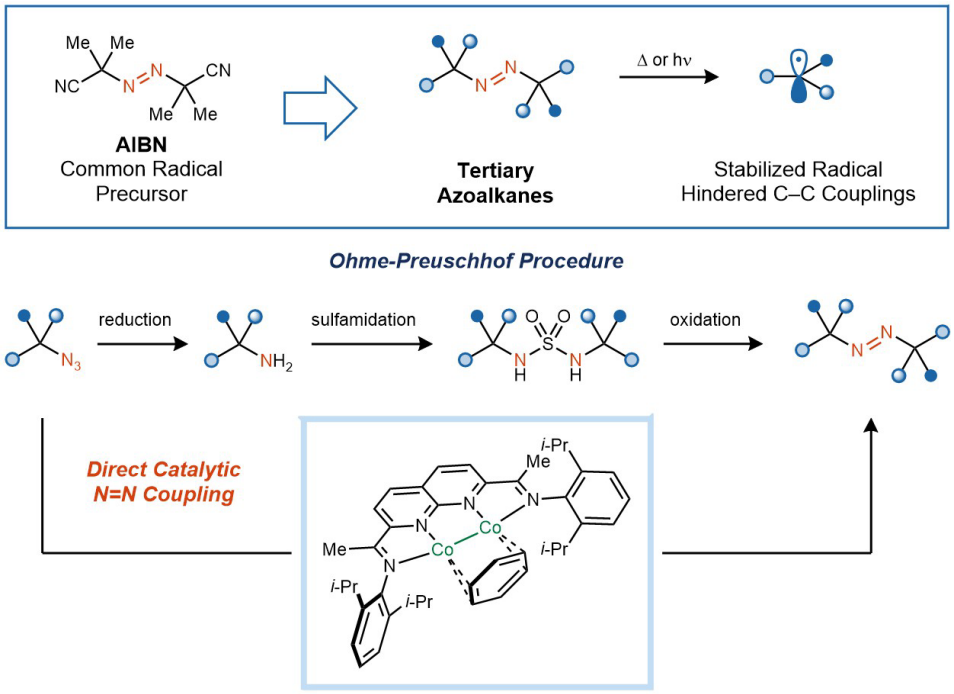


Azoalkanes can serve as radical precursors for various catalytic and stoichiometric C–C bond-forming reactions. However, their use in these processes is hampered by the complexity of their synthesis, which often requires multiple steps and strong oxidants. We developed a direct denitrogenative dimerization of tertiary alkyl azides to form azoalkanes. The reaction uses a dicobalt catalyst, which is uniquely effective in this transformation relative to analogous monocobalt catalysts and an isostructural dinickel catalyst. Critical to the N=N coupling reactivity is the formation of a dicobalt imido intermediate that is resistant to undergoing competing H-atom abstraction. The catalytic N=N coupling provides access to a broad scope of tertiary azoalkanes, and the resulting products can be used to form congested C–C bonds between quaternary carbon centers.

### *Dinickel-Catalyzed N=N Coupling Reactions for the Synthesis of Hindered Azoarenes*

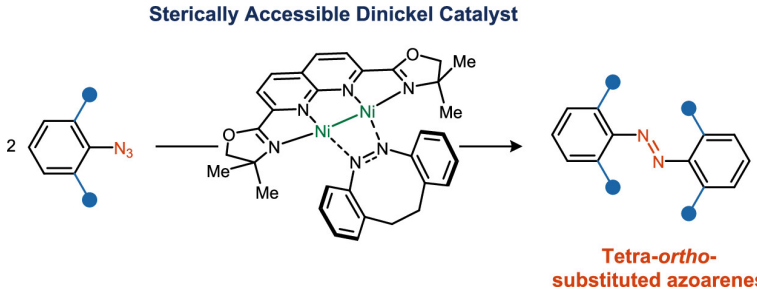

Azoarenes are the largest class of photoswitching molecules, and they have a broad range of applications in photopharmacology and materials science. Azoarenes possessing ortho-substitution often display improved properties, including isomerization under visible light irradiation, near-quantitative switching, and long thermal half-lives in the cis form. The synthesis of hindered ortho-substituted azoarenes is often low-yielding using established oxidative or reductive coupling methods. We designed and synthesized a new dinickel complex that catalyzes the dimerization of ortho-substituted aryl azides in high yield. This method was applied to the synthesis of high-performance photoswitches, photoactive peptide cross-linkers, hindered diazocines, and main-chain azoarene polymers.

***Black-to-Transmissive dual polymer complementary electrochromics with high coloration efficiency***

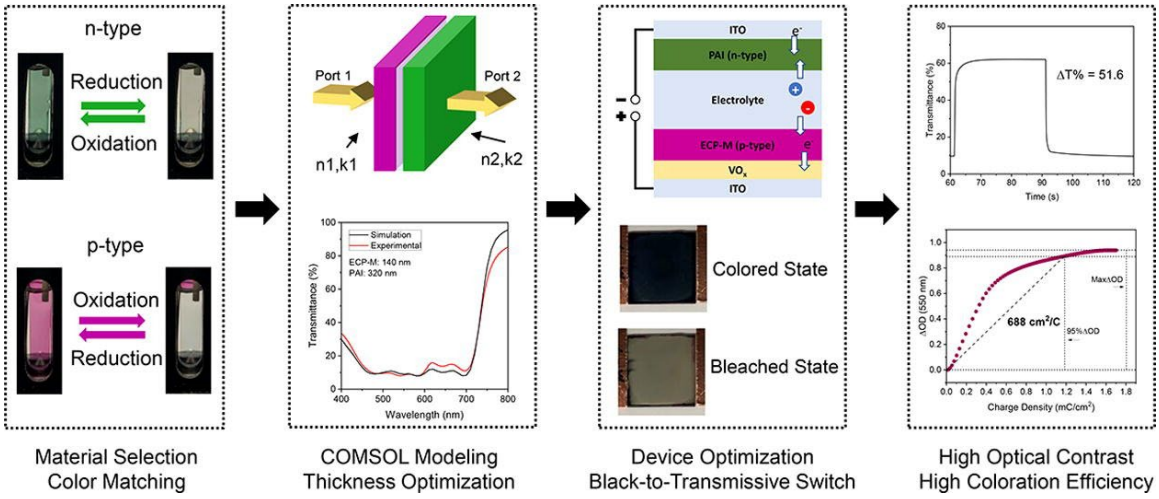


In a complementary electrochromic device (ECD), both the anode and the cathode can synergistically change color in response to an electrical bias, allowing for a high coloration efficiency. Complementary ECD that can switch from black to transmissive state is rare, due to the difficulty of pairing two electrochromic electrodes. We constructed high coloration efficiency complementary ECDs by pairing polyazoisoindigo (PAI), an n-type electrochromic polymer that undergoes green-to-transmissive switching, with p-type magenta (ECP-M) and red (ECP-R) electrochromic polymers to obtain black-to-transmissive ECD. Physical modeling tool, COMSOL, is introduced for complementary color matching. Through balancing the charge densities of two electrochromic electrodes, black-to-transmissive ECDs with record-high coloration efficiencies of 688 cm2/C and 437 cm2/C have been achieved for PAI|ECP-M and PAI|ECP-R, respectively.

***Dinickel-Catalyzed N═N Bond Rotation***

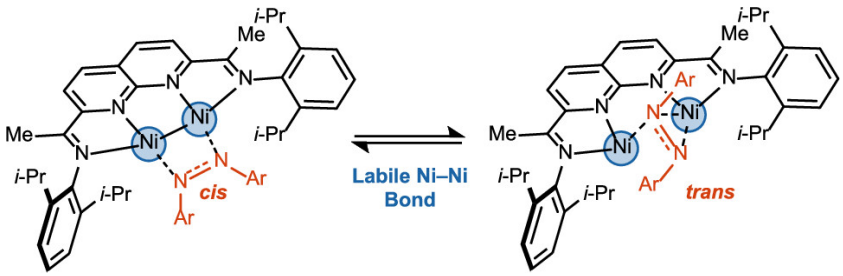


Azoarenes function as molecular switches that can be triggered by external stimuli, such as heat, light, and electrochemical potential. We showed that a dinickel catalyst can induce cis/trans isomerization in azoarenes through a N═N bond rotation mechanism. Catalytic intermediates containing azoarenes bound in both the *cis* and *trans* forms are characterized. Solid-state structures reveal the importance of π-back-bonding interactions from the dinickel active site in lowering the N═N bond order and accelerating bond rotation. The scope of the catalytic isomerization includes high-performance acyclic, cyclic, and polymeric azoarene switches.

**Publications Acknowledging this Grant in 2021-2024**

*(I) Intellectually led by this grant*

(1) Rybak, C. J.; Fan, C.; Sharma, P.; Uyeda, C. "Dinickel-Catalyzed N=N Coupling Reactions for the Synthesis of Hindered Azoarenes" *J. Am. Chem. Soc.* **2024**, *146*, 29720–29727.

(2) Rybak, C. J.; Andjaba, J. M.; Fan, C.; Zeller, M.; Uyeda, C. "Dinickel-Catalyzed N═N Bond Rotation" *Inorg. Chem.* **2023**, *62*, 5886–5891.

(3) Wang, Z.; Andjaba, J. M.; Rybak, C.; You, L.; Uyeda, C.; Mei, J. "Black-to-Transmissive dual polymer complementary electrochromics with high coloration efficiency" *Chem. Eng. J.* **2023**, *456*, 141013–141019.

(4) Brook, K. B.; Sahoo, S. R.; Uyeda, C. “Dicobalt-Catalyzed N=N Coupling Reactions of Tertiary Alkyl Azides to form Azoalkanes.” *In Review* **2024**

Johannes Voss

# Probing of energy and charge transfer and adsorbate dynamics in heterogeneous catalysis

Johannes Voss, Hirohito Ogasawara, Ralph Page, Anders Nilsson,* Alan Luntz, Frank Abild-Pedersen, Tony Heinz
SLAC National Accelerator Laboratory
*Collaborator at Stockholm University

## Presentation Abstract

Discriminating competing reaction pathways is crucial for developing a deeper understanding of selectivity in heterogeneous catalysis. Due to the rare occurrence of corresponding reaction intermediates along these paths, intense optical laser pumps and subsequent substrate electron and phonon heating can be used to dramatically increase the population of reaction intermediates. We benefit from revolutionary advances in x-ray free electron lasers, allowing us to follow induced adsorbate dynamics in real time with fs resolution. Electronic structure simulations are essential to deduce atomic motion and thus reaction coordinates from the observed x-ray spectral evolution. In our combined experimental and theoretical studies, we probe energy and charge transfer from the catalyst substrate to the adsorbates and induced adsorbate dynamics.
Probing the K-edge of carbon species in a number of adsorbate systems, we show how excited adsorbate vibrational and electronic degrees of freedom can be identified in the x-ray spectral evolution. We find that a vibrational mode-resolved understanding of adsorbate and catalyst substrate coupling is necessary to predict the evolution of energy transfer to the adsorbate and the resulting adsorbate dynamics.

## FWP Number 100435: Following ultrafast reaction dynamics and capturing rare intermediates

**PI:** Tony Heinz
**Postdoc(s):** Elias Diesen (former), Han Wang (former), Xixi Qin, Monique Tie

## RECENT PROGRESS

### Probing ultrafast surface dynamics

In recent work, we studied adsorbate-substrate dynamics and the behavior of heterogeneous catalytic reactions in which competing reaction pathways were present. Our experimental approach made use of x-ray spectroscopy techniques, particularly in the form of femtosecond x-ray absorption spectroscopy as implemented using X-ray free-electron lasers. We briefly summarize experimental progress below.

The mechanism for the important low temperature water gas shift reaction ($CO + H_2O \rightarrow CO_2 + H_2$) on copper catalysts has remained elusive and controversial under relevant catalytic conditions. The principal candidates are a redox mechanism ($CO^* + O^* + 2H^* \rightarrow CO_2 + H_2$), a carboxy mechanism ($CO^* + OH^* + H^* \rightarrow COOH^* + H^* \rightarrow CO_2 + H_2$) and even possibly a formate mechanism ($CO^* + O^* + 2H^* \rightarrow HCO^* + O^* + H^* \rightarrow HCOO^* + H^* \rightarrow CO_2 + H_2$), with * referring to adsorbed species. We have used ambient pressure K edge O and C XPS studies at DESY to study the adsorbate species, O*, OH* and a C containing intermediate (possibly formate). These have been studied in a flow system at high pressures somewhat similar to the typical catalytic reactor as a function of $H_2O$ to CO ratios and surface temperature. A small fraction of the studies is shown in Figure 1. Analysis of the results and their implications for the mechanism and its variation with temperature are not yet completed, but involves microkinetic modeling of the coverages of all species under the given reaction conditions with all individual coverage dependent rates predicted by DFT calculations.

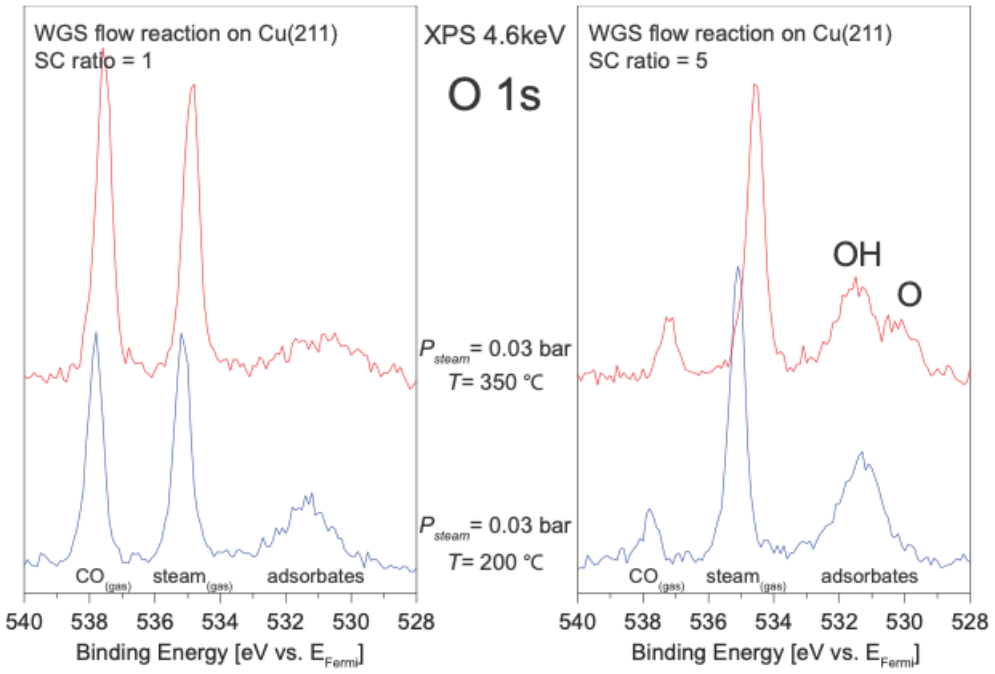


Figure 1: XPS of Cu(211) taken under WGS flow reaction conditions (SC ration = 1, 4, temperature = 200, 350 °C)
SC ratio = steam to carbon ratio

We are extending our investigations of graphene/Cu to examine nitrogen-doped graphene. This system is a promising earth-abundant catalyst for the oxygen reduction reaction (ORR) for both two-electron (2e-) ORR and four-electron (4e-) ORR. It has been suggested that 4e- versus 2e- ORR selectivity is governed by the material's electrical conductivity and, hence, the degree of nitrogenation. The electrochemistry depends upon how electrons are injected into the N-graphene electrode and transported to active catalytic sites. Using static X-ray spectroscopy at SLAC's SSRL beamline 10-1, we investigated the role of the N dopant configuration on the electrochemical activity of nitrogen-doped graphene toward the ORR. X-ray absorption spectroscopy (XAS) and resonant inelastic x-ray scattering (RIXS) results showed a finite density of states near

the Fermi level assigned to either graphitic or pyridinic nitrogen species, in which pyridinic nitrogen-rich graphene exhibited ORR activity superior to graphitic nitrogen-rich graphene. Using femtosecond optical pumping of a metal substrate that the N-graphene is supported on, we investigated the ultrafast dynamics of electron injection, migration, and trapping with element specificity using C 1s and N 1s X-ray absorption spectroscopy (XAS) at Pohang Accelerator Laboratory (PAL) X-ray Free Electron Laser facility in South Korea. We are evaluating the role played by the different types of nitrogen dopant sites as there has been much disagreement as to the identity of the catalytically active sites.

Reducible oxides, such $CoO_x$ , exhibit superior activity in many chemical reactions, but the origin of the increased activity is not well understood. We studied the active phase of $CoO_x$ on the Au(111) surface as related to the CO oxidation reaction. We found multiple active catalyst phases depending on the reactant gas phase $CO/O_2$ stoichiometry, from oxygen-lean to oxygen-rich, and temperature. Resonant photoemission spectroscopy revealed the unique role of $Co^{3+}$ sites in catalyzing CO oxidation. These findings show different active phases of the catalyst present in response to reaction conditions. Future studies are planned using LCLS-II at SLAC to explore how the reaction pathway varies between active phases.

**Preparation of x-ray free-electron laser measurements at LCLS-II**

A user-supplied endstation has been developed and authorized for installation in the Near-Experimental Hall at SLAC's LCLS free electron laser and will support research under this FWP. The existing standard LCLS endstations in their prescribed configurations are not suitable to support the planned investigations of heterogeneous catalysis. The custom-designed ultrahigh vacuum (UHV) system in this endstation will permit us to study the dynamics and pathways of model catalytic reactions under highly controlled surface and dosing conditions. To achieve the desired femtosecond time resolution we rely on a pump-probe approach. Both the ultrafast optical/infrared pump and x-ray probe pulses are provided by LCLS and excite / probe sample surfaces in our endstation. The ultrafast measurements will be based on time-resolved x-ray absorption spectroscopy (XAS), x-ray emission spectroscopy/resonant inelastic x-ray scattering (XES/RIXS), and x-ray photoelectron spectroscopy (XPS). We have also developed a complementary laboratory-based instrument to examine adsorbates on catalyst surfaces using mass spectrometry using temperature-programmed thermal desorption measurements or ultrafast-laser-excited reactions. This will serve to prepare for measurements using the free-electron laser.

During FY24, we have conducted scientific and technical commissioning studies for time-resolved XAS and XES/RIXS of adsorbed molecules and atoms. The first step was improving the surface sensitivity of XAS and XES/RIXS measurement by optimizing the angle of incidence. We have obtained optimized surface-sensitive conditions from the incident angle-dependent XAS and XES/RIXS of monolayer adsorbate on a metal surface using beamline 13-2 of SLAC's SSRL synchrotron. To improve X-ray detection performance from the monolayer adsorbate, we have explored the application of a transition edge sensor-based X-ray detector, which is a microcalorimeter based on

superconductivity. In complementary measurements in the SLAC Building 40 laser laboratory, we have performed further experiments to optimize conditions for both dosing the sample and driving recombinative desorption by ultrafast laser pulses. These synchrotron- and laboratory-based studies prepare us for scientific commissioning and time-resolved experiments at LCLS in the coming fiscal year.

**Theoretical capabilities for and research on ultrafast surface dynamics**

We benchmarked different methods (time-dependent density functional theory, density functional tight binding, pseudopotential and numerical atomic-orbital basis set density functional theory) for simulating non-adiabatic molecular dynamics on transition metal surfaces, which are crucial to simulate for an under-standing of energy and charge transfer in catalytic surface reactions. We found that the optimal method for simulation is here numerical atomic-orbital basis set density functional theory, which allows for efficient but sufficiently accurate calculation of electron-vibrational mode coupling matrix elements required for beyond Born-Oppenheimer dynamics. Specific area of interest: simulations of supported nitrogen-doped graphene as an ORR catalyst in conjunction with experimental investigations of this system in this project. We have furthermore performed simulations modeled dynamics and energetics of OH on stepped Cu(211) surfaces in support the analysis of our recent water-gas-shift reaction experiments presented above.

**Publications Acknowledging this Grant in 2021-2024**

(I) Publications intellectually led by this grant


1. Ogasawara, H.; Wang ,H.; Gladh, J.; Gallo, A.; Page, R. H.; Voss, J.; Luntz, A. C. ; Diesen, E.; Abild-Pedersen, F.; Nilsson, A.; Soldemo, M.; Zajac, M.; Attar, A.; Chen, M. E.; Cho, S. W.; Katoch, A.; Kim, K.-J.; Kim, K. H.; Kim, M.; Kwon, S.; Park, S. H.; Ribeiro, H.; Sainio, S.; Wang, H.-Y.; Yang, C.; Heinz, T. F. X-ray free electron laser studies of electron and phonon dynamics of graphene adsorbed on copper. *Phys. Rev. Lett*. **2023**, *7*, 024005. https://doi.org/10.1103/PhysRevMaterials.7.024005.
2. Schreck, S.; Diesen, E., Dell'Angela, M., C. Liu, M. Weston, M.; Capotondi, F.; H. Ogasawara; LaRue, J.; Costantini, R.; Beye, M.; Miedema, P. S.; Halldin, J. H.; Gladh, J.; Liu, B.; Wang, H-Y.; Perakis, F.; Cavalca, F.; Koroidov, S.; Amann, P.; Pedersoli, E.; Naumenko, D.; Nikolov, I.; Raimondi, L.; Abild-Pedersen, F.; Heinz, T. F.; Voss, J.; Luntz, A. C.; Nilsson, A. Atom-Specific Probing of Electron Dynamics in an Atomic Adsorbate by Time-Resolved X-ray Spectroscopy. *Phys. Rev. Lett.* **2022**, *129*, 276001. https://doi.org/10.1103/PhysRevLett.129.276001.
3. Rodrigues, G. L. S.; Diesen E.; Voss J.; Norman P., Pettersson L. G. M. Simulations of x-ray absorption spectra for CO desorbing from Ru(0001) with transition-potential and time-dependent density functional theory approaches, *Struct. Dyn.* **2022,** *9*, 014101. https://doi.org/10.1063/4.0000135.

4. LaRue, J.; Liu, B.; Rodrigues, G. L. S.; Liu, C.; Torres, J. A. G.; Schreck, S.; Diesen, E.; Weston, M.; Ogasawara, H.; Perakis, F.; Dell'Angela M.; Capotondi, F.; Ball, D.; Carnahan, C.; Zeri, G.; Giannessi, L.; Pedersoli, E.; Naumenko, D.; Amann, P.; Nikolov, I.; Raimondi, L.; Spezzani, C.; Beye, M.; Voss, J.; Wang, H.-Y.; Cavalca, F.; Gladh, J.; Koroidov, S.; Abild-Pedersen, F.; Kolb, M.; Miedema, P. S.; Costantini, R.; Heinz, T. F.; Luntz, A. C.; Pettersson, L. G. M.; Nilsson, A. Symmetry-resolved CO desorption and oxidation dynamics on O/Ru(0001) probed at the C K-edge by ultrafast X-ray spectroscopy. *J. Chem. Phys*. **2022**, *157*, 164705. https://doi.org/10.1063/5.0114399.

5. Diesen, E.; Wang, H.-Y.; Schreck, S.; Weston, M.; Ogasawara, H.; LaRue, J.; Perakis, F.; Dell'Angela, M.; Capotondi, F.; Giannessi, L.; Pedersoli, E.; Naumenko, D.; Nikolov, I.; Raimondi, L.; Spezzani, C.; Beye, M.; Cavalca, F.; Liu, B.; Gladh, J.; Koroidov, S.; Mediema, P. S.; Costantini, R.; Heinz, T.F.; Abild-Pedersen, F.; Voss, J.; Luntz, A. C.; Nilsson, A. Ultrafast adsorbate excitation probed with subpicosecond-resolution x-ray absorption spectroscopy. *Phys. Rev. Lett*. **2021**, *127*, 016802. https://doi.org/10.1103/PhysRevLett.127.016802.

(II) Publications jointly funded by this grant and other grants with intellectual leadership by other funding sources

6. Chen, H.; Falling, L.J.; Kersekk, H.; Yan, G.; Zhao X.; Oliver-Meseguer, J.; Jaugstetter, M.; Nemsak, S.; Hunt, A.; Waluyo, I.; Ogasawara, H.; Bell, A. T.; Sautet, P.; Salmeron, M. Elucidating the active phases of $CoO_x$ films on Au(111) in the CO oxidation reaction. *Nat. Commun.* 2023, 14, 6889. https://doi.org/10.1038/s41467-023-42301-7.

7. Reinhard, M.; Gallo. A.; Guo, M; Garcia-Esparza, A. T.; Biasin, E.; Qureshi, M.; Britz, A.; Ledbetter, K.; Kunnus K.; Weninger C.; van Driel, T.; Robinson, J.; Glownia, J. M.; Gaffney, K. J.; Kroll, T.; Weng, T.-C.; Alonso-Mori, R.; Sokaras D. Ferricyanide photo-aquation pathway revealed by combined femtosecond Kβ main line and valence-to-core x-ray emission spectroscopy. *Nat. Commun.* **2023**, *14*, 2443. https://doi.org/10.1038/s41467-023-37922-x.

8. Singh S. K.; Takeyasu K.; Homma K., Ito S.: Morinaga T.; Endo Y.; Furukawa M.; Mori T., Ogasawara H.; Nakamura J.; Activating nitrogen-doped graphene oxygen reduction electrocatalysts in acidic electrolytes using hydrophobic cavities and proton-conductive particles. *Angew. Chem. Int. Ed.* e202212506 (2022). https://doi.org/10.1002/anie.202212506.

9. Britz, A.; Attar, A. R.; Zhang, X.; Chang, H.-T.; Nyby C.; Krishnamoorthy, A.; Park, S. H.; Kwon, S.; Kim, M.; Nordlund, D.; Sainio, S.; Heinz, T. F.; Leone, S. R.; Lindenberg, A. M..; Nakano, A.; Ajayan, P.; Vashishta, P.; Fritz, D.; Lin, M.-F.; Bergmann, U. Carrier-specific dynamics in 2H-$MoTe_2$ observed by femtosecond soft x-ray absorption spectroscopy using an x-ray free-electron laser. *Struct. Dyn.* **2021,** *8*, 014501. https://doi.org/10.1063/4.0000048.

Bin Wang

# Dynamics of Water Structures and Active Sites for Aqueous-Phase Hydrogenation

Bin Wang, Daniel Resasco
School of Sustainable Chemical, Biological and Materials Engineering
University of Oklahoma, Norman

## Presentation Abstract

The presence of water has been shown to enhance hydrogenation of polar chemical functional groups, such as C=O and N=O bonds, through proton shuttling. To demonstrate such rather sophisticated reaction pathways, explicit solvent models with dynamic change of local solvent structures should be considered. Beyond what we reported previously for water-promoted C=O hydrogenation in furfural, in this presentation, we will highlight how the dynamics of the local water structures within the first solvation shell may affect the hydrogenation kinetics. Specifically, we find that the activation barriers correlate well with some collective variables that determine the local configuration and relative positions of surface hydrogen and water. In addition, very recently we show that the proton shuttling can also be applied to C=C hydrogenation at solid-liquid interfaces in the presence of bifunctional metal-acid sites containing boric acid adsorbed on Ni. Our recent calculations show that the dynamic transformation of this metal-acid interface can promote hydrogenation of the C=C bond in cyclohexene. In experiments, a rate enhancement by more than 100 times has been observed when adding small amount of water into an organic solvent. According to our atomic models, dynamic formation of a $B(OH)_3$-$H_2O$ complex is crucial for lowering the activation barrier of the first hydrogenation. Our findings thus provide fundamental insights of this dynamic transformation at the solid-liquid interface and its impact on catalytic activity and selectivity.

**Grant Number:** DE-SC0018284
**Grant Title:** Hydrophobic enclosures in bio-inspired nanoreactors for enhanced phase selectivity. A combined experimental/theoretical approach

**Postdoc(s):** Shoutian Sun, Tien Le
**Student(s):** Thomas Salas

## RECENT PROGRESS

### Conceptual development

Under finite temperatures, the water-catalyst interfaces explore dynamic configurations in a multi-dimensional space. We show that the catalytic thermodynamics and kinetics at the interfaces are very sensitive to the local configuration (e.g., H-bonding) and global environment (e.g. electrostatic interaction that changes the work function of catalysts). We have developed fundamental understanding, using hydrogenation of aldehyde as an example, of the correlation between water dynamics and reaction kinetics. This allows us to conclude that, while water explores the dynamic configurations, only certain configurations can lead to enhanced kinetics through a couple of different scenarios, which are further determined by the local water-metal-reactant configuration.

**Solvent effects at bifunctional sites for promoting C=C and C=O hydrogenation.**
We investigated the role of water in the selective hydrogenation in cinnamaldehyde on cobalt boride catalysts. The boron species, during thermal treatments, exsolved from the bulk phase and become enriched on the surface, forming acidic species that enhance the activity and selectivity of carbonyl bond hydrogenation by three and two times, respectively, due to enhanced water-catalyst interaction and proton shuttling to the C=O bonds shown in DFT calculations. [Li et al. *Cell Rep. Phys. Chem.* 2023]

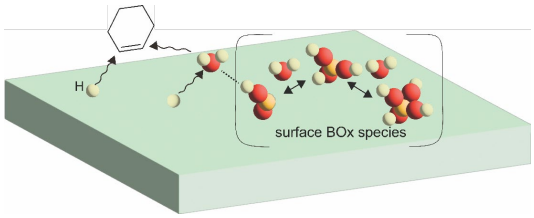

Fig. 1. Water-mediated proton shuttling promotes hydrogenation of C=C at a bifunctional metal-acid site.

Surprisingly, we observed > 100 rate increase for C=C hydrogenation in cyclohexene when a small amount of water was introduced over nickel boride catalysts. [Li et al. *J. Catal.* 2024] This observation was not anticipated as it is generally believed that water cannot promote the C=C hydrogenation due to the lack of H-bonds between cyclohexene and water; in fact, water suppresses C=C hydrogenation over pure Ni. Our metadynamics simulations and DFT calculations show that water transforms the boric acid sites to a hydrated configuration, which is stabilized by the metal, and that the new configuration can shuttle protons for the first hydrogenation step (Figure 1), which is also the rate-determining step, due to moderate cation-$\pi$ interaction. [Sun et al. to be submitted]

**Confined water and enhanced proton shuttling**
We previously published a work showing that in metal-catalyzed nitrite reduction the presence of protons is essential to complete the reaction in the aqueous phase. By coupling rigorous kinetics studies of nitrite hydrogenation on Pd with kinetic isotope studies and theoretical calculations we have shown that in aqueous environments the reaction proceeds via H-shuttling in which protons move via the aqueous environment while the electrons reach the NO* through the metal in a concerted fashion. This mechanism flattens the energy landscape, which leads to the same apparent activation energy barrier (0.6 eV) for the formation of two intermediate species, HNO* and HNOH*. These results are consistent with the hydrogen reaction orders, kinetic isotopic experiments, and micro-kinetic modeling including co-limiting reaction steps for NO* hydrogenation to HNO* and HNOH*. [Huang et al. *J. Catal.* 2022]

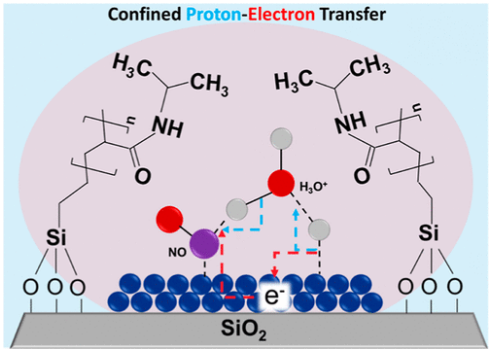

Fig. 2. Water confined at the interface further promote hydrogenation through a more structured H-bond network.

Following this work, we explored different approaches to constrain the water dynamics and narrow its distribution. One approach is to introduce surface functionalization either

by surfactants [Li et al. *ACS Catal.* 2022] or polymers [Huang et al. *JACS Au* 2024]. We investigated nitrite reduction over Pd decorated with temperature-sensitive polymers. We suggest that water can be confined at the polymer-metal interface and that this confinement perturbs the water interaction with the metal, reducing the barrier for the proton– electron transfer reduction of nitrite. This can thus explain the experimentally observed reduced activation enthalpy but increased activation entropy. The latter is caused by the more structured water due to the confinement effect.

**Publications Acknowledging this Grant in 2021-2024**

***(I) Intellectually led by this grant***


1. Li, G. N.; Salas, T.; Sun, S. T.; Wang, B.; Komarneni, M. R.; Resasco, D. E. Bifunctional metal-acid sites on nickel boride catalysts: Phenol hydrodeoxygenation and water-promoted C = C hydrogenation. *Journal of Catalysis* **2024**, *431*, 115384. DOI: 10.1016/j.jcat.2024.115384.
2. Duong, N. N.; Teles, C. A.; Noronha, F. B.; Resasco, D. E. Non-Linear Arrhenius Behavior of m-Cresol Hydrogenation over Platinum. *Catalysis Letters* **2024**, 6123–6132. DOI: 10.1007/s10562-024-04776-x.
3. Huang, P. C.; Yan, Y.; Martinho, R. P.; Lefferts, L.; Wang, B.; Albanese, J. F. Water Confinement on Polymer Coatings Dictates Proton-Electron Transfer on Metal-Catalyzed Hydrogenation of Nitrite. *JACS Au* **2024**, *4* (7), 2656-2665. DOI: 10.1021/jacsau.4c00389.
4. Li, G. N.; Komarneni, M. R.; Wang, B.; Marinkovic, N.; Resasco, D. E. Cooperative roles of water and metal-support interfaces in the selective hydrogenation of cinnamaldehyde over cobalt boride catalysts. *Cell Reports Physical Science* **2023**, *4* (4), 101367. DOI: 10.1016/j.xcrp.2023.101367.
5. Yan, Y.; Masood, Z.; Wang, B. Lanthanum-Doped Graphene for Electrocatalytic Reduction of Nitrogen Monoxide. *Journal of Physical Chemistry C* **2023**, *127* (27), 12967-12975. DOI: 10.1021/acs.jpcc.3c01366.
6. Crouch, J.; Mou, T.; Li, G. N.; Resasco, D.; Wang, B. How van der Waals Approximation Methods Affect Activation Barriers of Cyclohexene Hydrogenation over a Pd Surface. *ACS Engineering Au* **2022**, *2* (6), 547-552. DOI: 10.1021/acsengineeringau.2c00031.
7. Li, G. N.; Marinkovic, N.; Wang, B.; Komarneni, M. R.; Resasco, D. E. Manipulating the Microenvironment of Surfactant-Encapsulated Pt Nanoparticles to Promote Activity and Selectivity. *ACS Catalysis* **2022**, *12* (22), 13930-13940. DOI: 10.1021/acscatal.2c03780.
8. Huang, P. C.; Yan, Y.; Banerjee, A.; Lefferts, L.; Wang, B.; Albanese, J. A. F. Proton shuttling flattens the energy landscape of nitrite catalytic reduction. *Journal of Catalysis* **2022**, *413*, 252-263. DOI: 10.1016/j.jcat.2022.06.007.
9. Bababrik, R.; Santhanaraj, D.; Resasco, D. E.; Wang, B. A comparative study of thermal- and electrocatalytic conversion of furfural: methylfuran as a primary and major product. *Journal of Applied Electrochemistry* **2021**, *51* (1), 19-26. DOI: 10.1007/s10800-020-01427-y.
10. Li, G. N.; Wang, B.; Resasco, D. E. Solvent effects on catalytic reactions and related phenomena at liquid-solid interfaces. *Surface Science Reports* **2021**, *76* (4), 100541. DOI: 10.1016/j.surfrep.2021.100541.

11. Resasco, D. E.; Crossley, S. P.; Wang, B.; White, J. L. Interaction of water with zeolites: a review. *Catalysis Reviews-Science and Engineering* **2021**, *63* (2), 302-362. DOI: 10.1080/01614940.2021.1948301.
12. Li, G. N.; Zhao, Z.; Mou, T.; Tan, Q. H.; Wang, B.; Resasco, D. Experimental and computational kinetics study of the liquid-phase hydrogenation of C=C and C=O bonds. *Journal of Catalysis* **2021**, *404*, 771-785. DOI: 10.1016/j.jcat.2021.09.002.
13. Li, G. N.; Wang, B.; Kobayashi, T.; Pruski, M.; Resasco, D. E. Optimizing the surface distribution of acid sites for cooperative catalysis in condensation reactions promoted by water. *Chem Catalysis* **2021**, *1* (5), 1065-1087. DOI: 10.1016/j.checat.2021.08.005.
14. Yang, F. F.; Komarneni, M. R.; Libretto, N. J.; Li, L. W.; Zhou, W.; Miller, J. T.; Ge, Q. F.; Zhu, X. L.; Resasco, D. E. Elucidating the Structure of Bimetallic NiW/SiO2 Catalysts and Its Consequences on Selective Deoxygenation of m-Cresol to Toluene. *Acs Catalysis* **2021**, *11* (5), 2935-2948. DOI: 10.1021/acscatal.0c05560.

***(II) Jointly funded by this grant and other grants with intellectual leadership by other funding sources***

15. Wrasman, C. J.; Bell, A. T.; Chandler, B. D.; Harris, J. W.; Kwon, S.; Ball, M. R.; Krishna, S. H.; Khatib, S. J.; Bollini, P.; Román-Leshkov, Y.; et al. Recommendations for improving rigor and reproducibility in site specific characterization. *Journal of Catalysis* **2024**, *433*, 115451. DOI: 10.1016/j.jcat.2024.115451.
16. Phan, V. T. T.; Nguyen, Q. P.; Wang, B.; Burgess, I. J. Oxygen Vacancies Alter Methanol Oxidation Pathways on NiOOH. *Journal of the American Chemical Society* **2024**, *146* (7), 4830-4841. DOI: 10.1021/jacs.3c13222.
17. Le, V. T. C.; Nguyen, Q. P.; Mai, H. D.; Wang, B.; Bui, N. T. An Adsorptive Membrane Platform for Precision Ion Separation: Membrane Design and First-Principles Studies. *Small Structures* **2024**, *5* (8), 2400067. DOI: 10.1002/sstr.202400067.
18. Yu, J. Q.; Yan, Y.; Lin, Y. M.; Liu, H. Z.; Li, Y. T.; Xie, S. H.; Sun, S. M.; Liu, F. D.; Zhang, Z. G.; Li, W. Z.; et al. Improved high-current-density hydrogen evolution reaction kinetics on single-atom Co embedded in an order pore-structured nitrogen assembly carbon support. *Nanoscale Horizons* **2024**. DOI: 10.1039/d4nh00299g.
19. Chau, H. K.; Nguyen, Q. P.; Jerdy, A. C.; Bui, D. P.; Lobban, L. L.; Wang, B.; Crossley, S. P. Role of Water on Zeolite-Catalyzed Dehydration of Polyalcohols and EVOH Polymer. *ACS Catalysis* **2023**, 1503-1512. DOI: 10.1021/acscatal.2c05303.
20. Luo, Z. C.; Yin, Z. Y.; Yu, J. Q.; Yan, Y.; Hu, B.; Nie, R. F.; Kolln, A. F.; Wu, X.; Behera, R. K.; Chen, M. D.; et al. General Synthetic Strategy to Ordered Mesoporous Carbon Catalysts with Single-Atom Metal Sites for Electrochemical CO2 Reduction. *Small* **2022**, *18* (16), 2107799. DOI: 10.1002/smll.202107799.
21. Chen, M. D.; Yan, Y.; Gebre, M.; Ordonez, C.; Liu, F. D.; Qi, L.; Lamkins, A.; Jing, D. P.; Dolge, K.; Zhang, B. Y.; et al. Thermal Unequilibrium of PdSn Intermetallic Nanocatalysts: From In Situ Tailored Synthesis to Unexpected Hydrogenation Selectivity. *Angewandte Chemie-International Edition* **2021**, *60* (33), 18309-18317. DOI: 10.1002/anie.202106515

Timothy H. Warren

## Conversion of Ammonia to Its Elements via Earth Abundant Metal Complexes

Md Estak Ahmed, Josalyne A. M. Beringer, Daya Shylendran and
Timothy H. Warren*

Department of Chemistry, Michigan State University, East Lansing, MI 48824, United States

### Presentation Abstract

Molecular catalysts for ammonia oxidation to dinitrogen represent enabling components to utilize ammonia as a fuel and/or source of hydrogen. Ammonia oxidation requires not only the breaking of multiple strong N-H bonds, but also controlled N-N bond formation. Owing to its high energy density and established global production and distribution networks, ammonia ($NH_3$) is an appealing fuel, particularly when synthesized by green methods. On a per-hydrogen atom basis, ammonia contains nearly the same chemical energy as hydrogen ($H_2$). Thus, sustainable catalysts that electrocatalytically oxidize ammonia for fuel cells or on-demand hydrogen production with only nitrogen ($N_2$) as a byproduct are highly desirable.

We describe three systems based on the Earth abundant metals iron and copper for the conversion of ammonia to its elements. In electrocatalytic ammonia oxidation employing molecular iron- and copper-based catalysts, a key step is the conversion of $NH_3$ to masked forms of the amidyl radical $\bullet NH_2$ via PCET. Pendant pyridine bases covalently attached to ferrocenium engage in H-bonding to ammonia that facilitates PCET of the H-bonded ammonia molecules to give an amidyl radical ($\bullet NH_2$) stabilized by a protonated pyridinium base en route to hydrazine ($H_2N\text{-}NH_2$) that undergoes facile oxidation to nitrogen ($N_2$). Based on this success, we have appended a pyridine base to our successful copper β-diketiminate system for ammonia oxidation. We seek to encourage H-bonding and deprotonation of resulting $\{[Cu^{II}]\text{-}NH_3\}^+$ intermediates to simultaneously lower the overpotential and increase the rate of N-N formation via reactive $[Cu^{II}]\text{-}NH_2$ intermediates. Finally, we illustrate a dinuclear copper system that enables direct conversion to $[Cu_2](\mu\text{-}NH_2)$ and $[Cu_2](\mu\text{-}NH)$ species through stepwise loss of $H_2$ induced by the high stability of these dicopper amido and nitrene intermediates.

**Grant or FWP Number: Grant or FWP Number:** DE-SC0025575
Catalytic Interconversion of Ammonia and Dinitrogen at Base Metals

**Student(s):** Josalyne A. M. Beringer, Daya Shylendran

**Postdoc(s):** Dr. Md Estak Ahmed

## RECENT PROGRESS

### *Ammonia oxidation via ferrocenes with pendant amine arms*

H-bonding of ammonia to pyridine (py···H-$NH_2$) followed by 1-electron oxidation leads to proton movement to the pyridine to form the pyridinium-stabilized amidyl radical cation $[pyH\cdots NH_2]^{+/\bullet}$ susceptible to amidyl radical coupling to form $H_2N$-$NH_2$. We hypothesized that fast electron transfer would take place from ferrocenium, provided that that pyridine arm is covalently teathered.

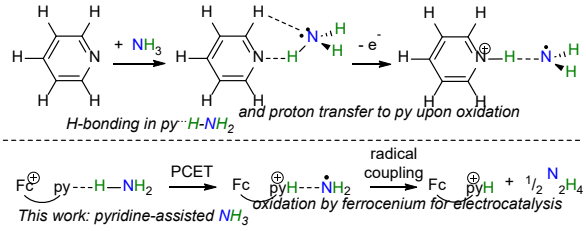


Synthesis of a small family of ferrocenes with pyridine arms reveals that the rate of electrocatalytic ammonia oxidation in 2.4 M $NH_3$ DMSO actually increases with decreasing overpotential. Analysis by cyclic voltammetry in DMSO indicates that the reaction is both first order $^{py}$Fc and $NH_3$ to give a rate law: rate = $k[^{py}Fc][NH_3]$. Moreover, we observe a primary kinetic isotope effect $k_H/k_D$ = 2.05(1) in electrocatalysis of $NH_3$ and $ND_3$. Curiously, the observed KIE decreases as the pyridine becomes more electron-rich.

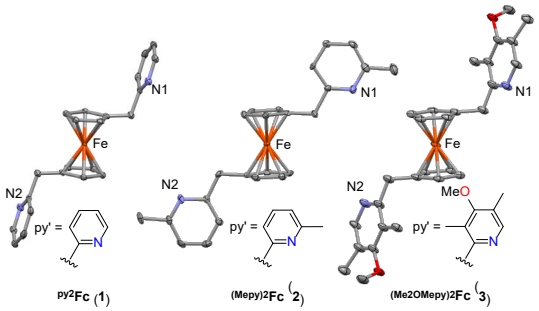


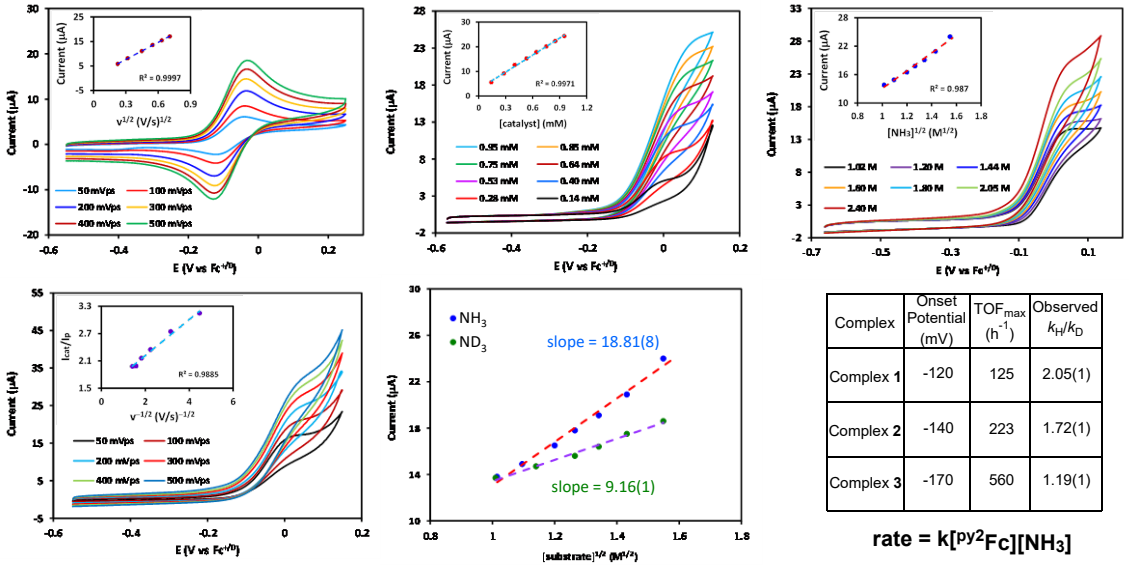


| Complex | Onset Potential (mV) | $TOF_{max}$ ($h^{-1}$) | Observed $k_H/k_D$ |
|---|---|---|---|
| Complex 1 | -120 | 125 | 2.05(1) |
| Complex 2 | -140 | 223 | 1.72(1) |
| Complex 3 | -170 | 560 | 1.19(1) |

**rate = k[$^{py2}$Fc][$NH_3$]**

The slight electronic influence the electron-rich pyridine arms lowers the reduction potential of the $Fe^{III}/Fe^{II}$ couple while stronger H-bonding enabled by electron-rich pyridines also lowers the barrier for PCET of $\{Fc^{III}\text{---}py\cdots H\text{-}NH_2\}^+$ species to $\{Fe^{II}\text{---}pyH\cdots NH_2\}^+$. DFT studies reveal how electron-rich pyridine arms lower the barrier for PCET which enhances turnover frequency.

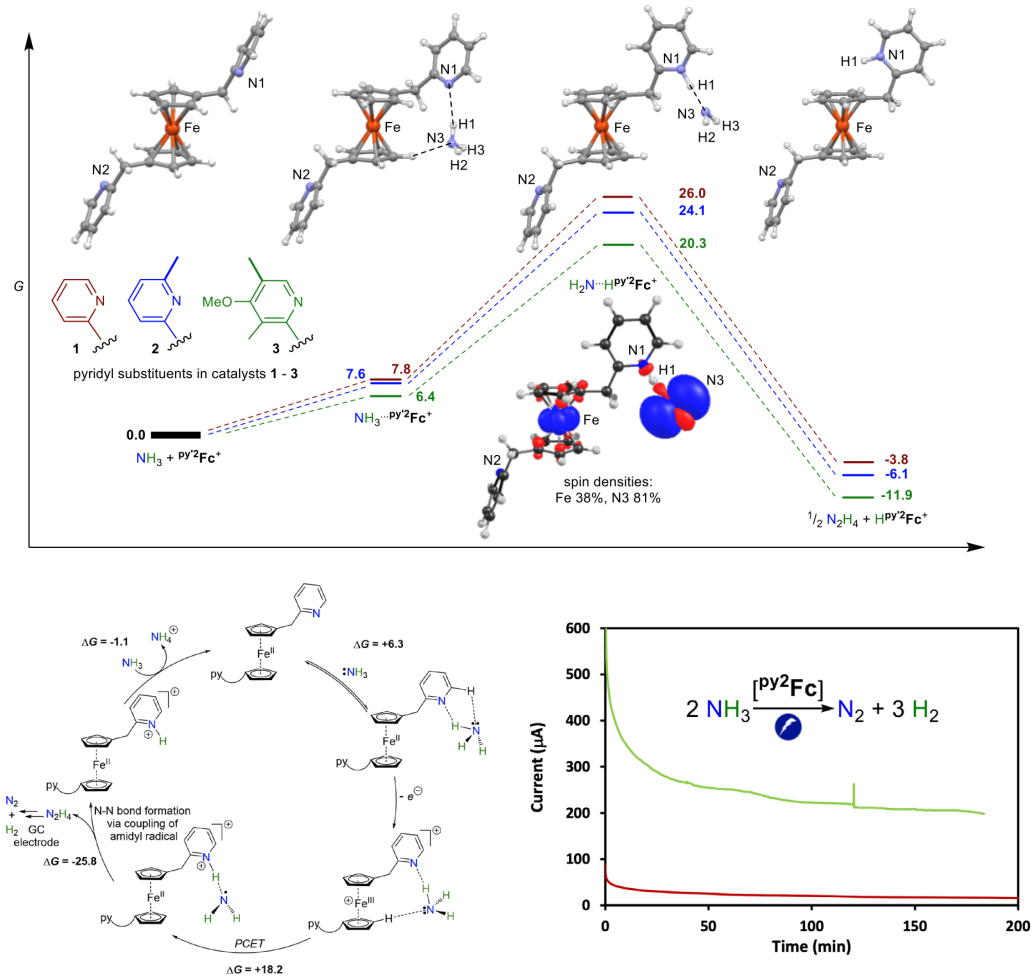


A combination of experimental and theoretical studies outline the catalytic mechanism for ammonia oxidation that directly generates hydrazine and ammonium. The result is long-lived generation $N_2$ and $H_2$ from ammonia: hydrazine is easily oxidized by the anode (and likely the catalyst) to $N_2$ while reduction of $NH_4^+$ at the cathode produces $H_2$.

### *Electrocatalytic ammonia oxidation by copper β-diketiminates: pendant pyridine arms*

We recently reported use of the copper β-diketiminate catalyst [$^i$Pr$_2$NN$_{F6}$]Cu as an electrocatalyst for ammonia oxidation at modest overpoentials in MeCN (η = 700 mV). Based on the catalytic cycle that was validated by cyclic voltammetry, synthetic studies, and theory, we hypothesized that both the 1-electron oxidation and deprotonation steps could be encouraged by use of a pendant base that engages in H-bonding with copper-bound ammonia in [Cu$^I$]-NH$_3$ species. We have synthesized a copper complex which exists as a py-bridged dimer

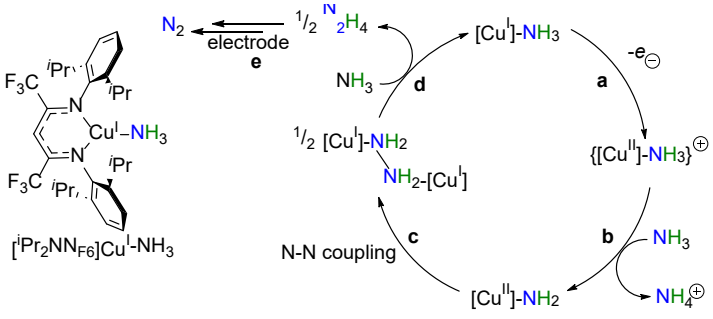

in the solid state, yet binds HN=$CMe_2$ (the imine derived from $NH_3$ in acetone) and DFT studies indicate that H-bonding to Cu-bound ammonia is favorable.

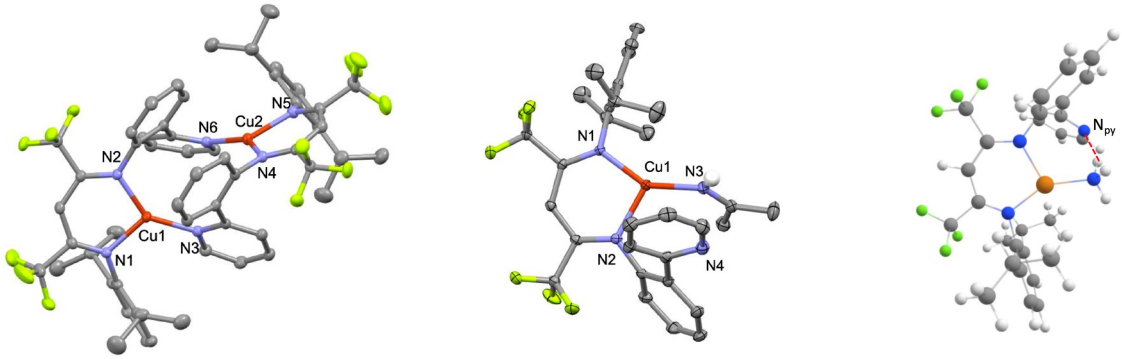


***Conversion of ammonia to dicopper stabilized μ-$NH_2$ and μ-NH intermediates***

Through the use of a novel bis-β-diketiminate ligand joined by a flexible N,N-biphenyl linker that accommodates a range of metal-metal distances, we find that reaction of $NH_3$ with the dicopper species [$Cu_2$] spontaneously generates the crystallographically characterized [$Cu_2$](μ-$NH_2$). Addition of pyridine to transiently abstract a H-atom via a pyridinium radical $pyH^{0/\bullet}$ results in converstion to the unprecedented dicopper parent nitrene [$Cu_2$](μ-NH). We hypothesize that the loss of ½ equiv. $H_2$ accompanies each step; we are vigorously pursuing this tantalizing transformation.

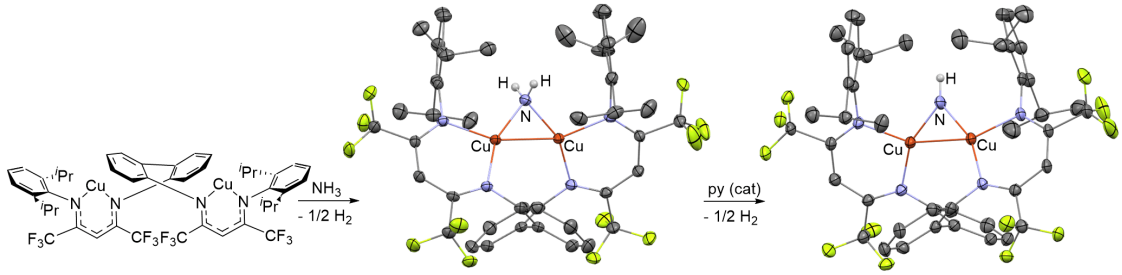


**Publications Acknowledging this Grant in 2021-2024**

*(I) Intellectually led by this grant*


Gardner, E. J.; Marguet, S. C.; Cobb, C. R.; Pham, D. M.; Beringer, J. A. M.; Bertke, J. A.; Shafaat, H. S.*; Warren, T. H.* Uncovering Redox Non-Innocent H-Bonding in Cu(I)-Diazene Complexes. *J. Am. Chem. Soc.* **2021**, *143*, 15960-15974.

Ahmed, M. E.; Boroujeni, M. R.; Ghosh, P.; Greene, C.; Kundu, S.; Bertke, J. A.; Warren, T. H.* Electrocatalytic Ammonia Oxidation by a Low Coordinate Copper Complex. *J. Am. Chem. Soc.* **2022**, *144*, 21136-21145.

Boroujeni, M. R.; Greene, C.; Bertke, J. A.; Cundari, T. R.; Warren, T. H.* Chemical and Electrocatalytic Ammonia Oxidation by Ferrocenium, *ChemRxiv* **2023**, doi: 10.26434/chemrxiv-2023-l1dtg-v2.

Ahmed M. E.; Staples, R. J.; Cundari, T. R.; Warren, T. H. "Electrocatalytic Ammonia Oxidation by Pyridyl Substituted Ferrocenes" *ChemRxiv* **2024**, doi: 10.26434/chemrxiv-2024-29hgx

Aleksandr V. Zhukhovitskiy

# Deconstruction of Diene Rubber via C–H Amination and Aza-Cope Rearrangement

Aleksandr V. Zhukhovitskiy, Sydney E. Towell, Maxim Ratushnyy, Fu-Sheng Wang, and Lauren Cooke
Department of Chemistry, University of North Carolina at Chapel Hill

## Presentation Abstract

Limited strategies exist for chemical recycling of diene rubber waste, a major sustainability challenge at present. I will discuss our approach, utilizing C–H amination and skeletal editing of polymer backbones, to deconstruct diene rubber into precursors for epoxy resins. Specifically, I will discuss our advances in selenium-catalyzed C–H amination, as well as the application of phospholene catalysis to prepare novel C–H amination reagents. I will also cover how acid-catalyzed cationic 2-aza-Cope rearrangement (ACR) can enable deconstruction of aminated diene polymers. Lastly, I will discuss the cross-linking of the aminated polymer fragments that results from the deconstruction to form epoxy resins.

**DE-SC0022898: Upcycling of all-carbon polymer backbones into value-added amines via skeletal rearrangement**
**Postdoc(s):** Maxim Ratushnyy, Fu-Sheng Wang
**Student(s):** Sydney E. Towell, Lauren Cooke

## RECENT PROGRESS

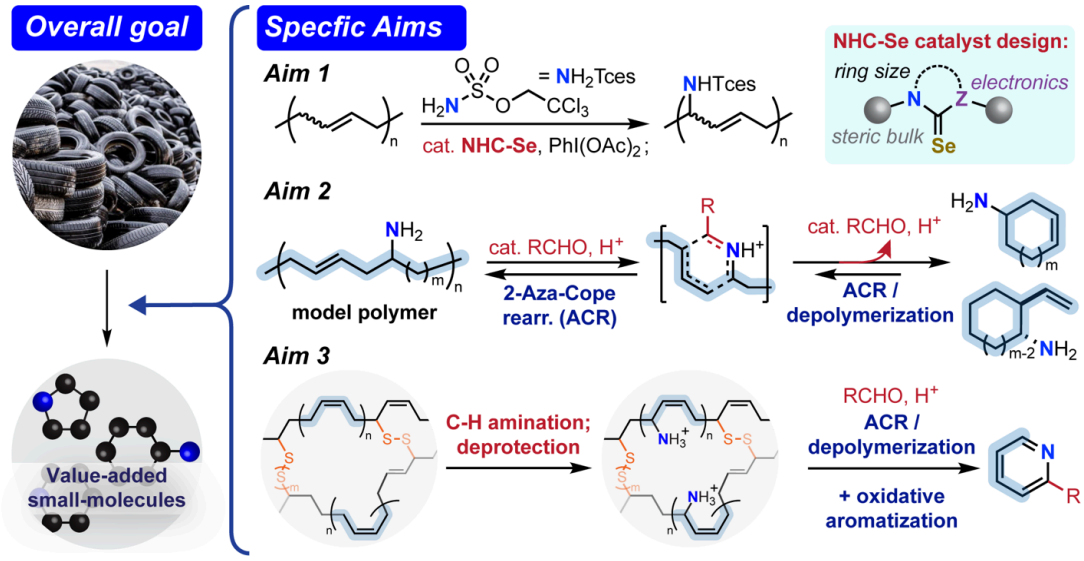


**Figure 1.** Summary of the proposal aims.
The major goals of the project are to (1) develop allylic C-H amination of diene polymers via selenium catalysis, (2) develop 2-aza-Cope rearrangement (ACR) of model substrates, and (3) adapt the developed C-H amination and ACR to convert diene polymers and rubber into value-added nitrogen-containing small molecules.

**Aim 1:**

Last year, we discovered that 1,3-dimethylimidazolidine-2-selenone is ~20 times more active as a catalyst for allylic C-H amination compared to established amination reported by Michael and coworkers (*J. Am. Chem. Soc.* **2020**, *142* (39), 16716–16722). We have begun to explore the substrate scope of this amination, focusing specifically on substrates that were challenging (i.e., afforded low yields of product) for the previously reported catalysis (Figure 1). In parallel, we are working on the synthesis of a diamidoselenourea, which is expected to be considerably more reactive and attempting to isolate intermediates of the selenourea catalysis.

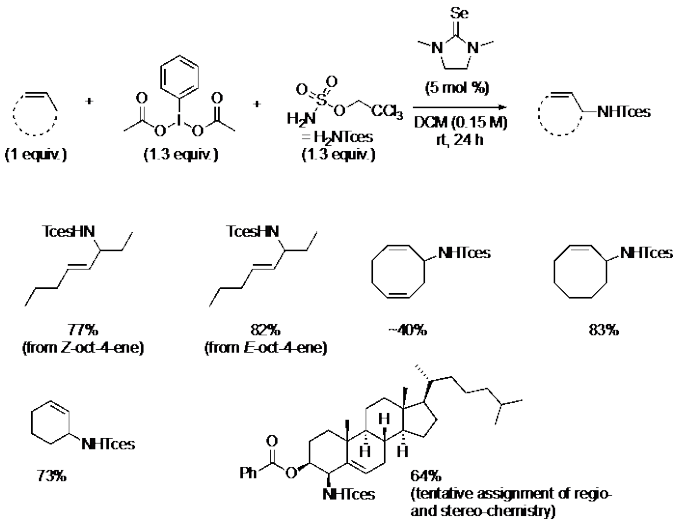


**Figure 2.** Current substrate scope of amination.

**Aim 2:**

This aim has been completed and the work is incorporated in both a manuscript currently in revision in *Nature*, as well as in an International Patent Application No. PCT/US24/19903 filed based on U.S. Provisional Application No. 63/454,452. Since last time, the aza-Cope rearrangement (ACR) chemistry has now been not fully optimized on model substrates, with some of the products separated, isolated, and fully characterized. Under the optimized ACR reaction conditions, based on $^1$H NMR spectroscopy, the homoallylic amine repeat units were consumed with multi-step equilibrium kinetics, reaching a plateau of 85% conversion in 48 h. Aliquots withdrawn at different time points were also subjected to global Boc-protection of amine functional groups with di-tert-butyl decarbonate ($Boc_2O$), which enabled analysis of the samples by gel permeation chromatography (GPC). Notably, universal calibration proved most convenient for the extraction of molecular weights from crude aliquots. Based on GPC, after just one hour of deconstruction, a factor of 20 reduction in viscosity-average molecular weight ($M_v$) was observed, and after 48 h, the starting polymer 21 with $M_v$ = 58.1 kg/mol was converted to oligomers with $M_v$ of ~400 g/mol (Fig. 3). Our universal calibration curve only extends to 1,000 g/mol, so these final timepoints are extrapolated. Nonetheless, this final molecular weight aligns well with the one calculated via end group analysis of the corresponding $^1$H NMR spectrum after Boc- protection: via this analysis we calculate 3 alkene units per amine end group which gives a product mass of 307 g/mol. Additionally, the observed precipitous drop in the molecular weights with conversion is consistent with a deconstruction mechanism that is the reverse of "step-growth."

Combination of preparative GPC, column chromatography, and high-resolution mass spectrometry enabled us to isolate and characterize several deconstruction products, albeit in small quantities. Namely, we identified aminoaldehydes **23b** and **24b** and bis-amines **25b**, **26b**, and **27b**, which were isolated in ~0.5, 0.2, 3, 6, and 1.5 % yields respectively.

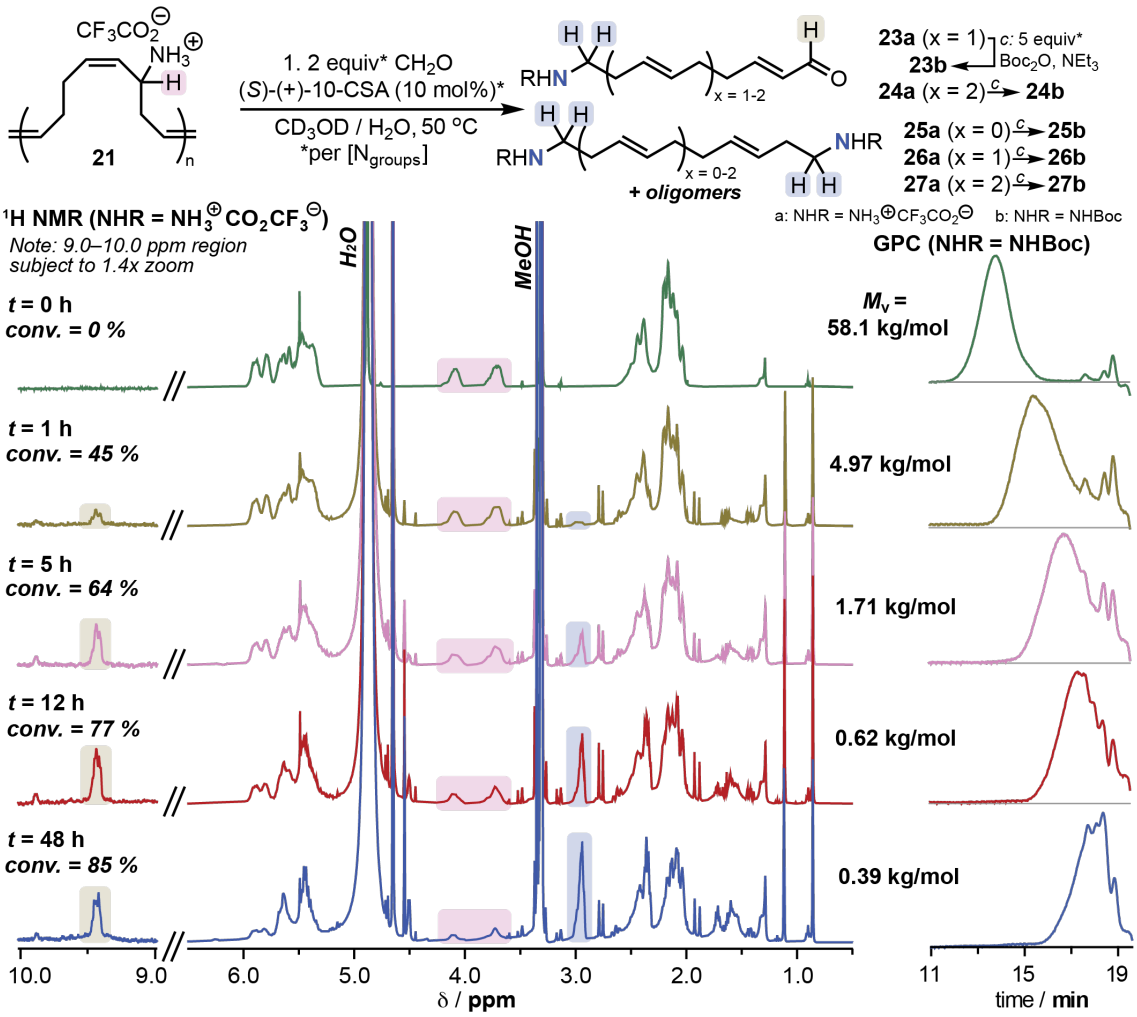


**Fig 3: Results from ACR deconstruction studies.** Deconstruction reaction of **21** showing deconstruction products **23a**–**27a**. (Left) $^{1}$H NMR spectra of deconstruction of **21** at various time points; (Right) Associated GPC differential refractive index (dRI) traces of $^{1}$H NMR samples after *c*.

Formation of these products is expected through a sequence of two or more ACR steps from polymer **21**, which features both sequence isomerism (i.e., head/tail-to-head/tail) and regioisomerism due to ring-opening at one alkene or the other in the cyclooctadiene monomer. While ROMP of 3-substituted cyclooctenes is known to be regioselective, as this is a substituted cyclooctadiene, we observe isomerism more consistent with 5-substituted cyclooctene ROMP.

## Aim 3:

This aim has been largely completed and the work is incorporated in both a manuscript currently in revision in *Nature*, as well as in an International Patent Application No. PCT/US24/19903 filed based on U.S. Provisional Application No. 63/454,452. However, we pivoted to utilized sulfur diimide reagents for allylic C–H amination of the diene polymers and rubber, rather than selenourea catalysis. This work is incorporated in a manuscript currently in revision in *Nature*. In short, we discovered that a commercially

available phospholene oxide enabled the synthesis of a novel sulfur diimide reagent *N,N'*-di-*tert*-butoxycarbonyl sulfur diimide (**DTSD**), which in turn was particularly well-suited for our amination goals because it afforded Boc-protected amines, which we could readily deprotect when needed. Amination of model substrate **1** with **DTSD** cleanly afforded the mono-aminated product (**2**) in 59% $^{1}$H NMR yield after 24 h, which was subsequently cleanly deprotected (Figure 4A). Having established a protocol for amination and deprotection of **1**, we further demonstrated that it was successful in the context of linear 1,4-polybutadiene (Figure 4B) and vulcanized polybutadiene (Figure 4C). Notably, this amination-deprotection sequence can also be performed under greener conditions. Amination of **1** using DTSD proceeds to 51% conversion in 2-MeTHF over 48 hours at 50 °C. Additionally, in the Boc- deprotection, we can substitute excess TFA in DCM with 1.1 equivalents of HCl in 200:1 MeOH/$H_2O$ at 50 °C.

We then applied the Sharpless-Kresze amination sequence to post-consumer waste rubber, which we determined to be vulcanized polyisoprene with various proprietary additives. Notably,

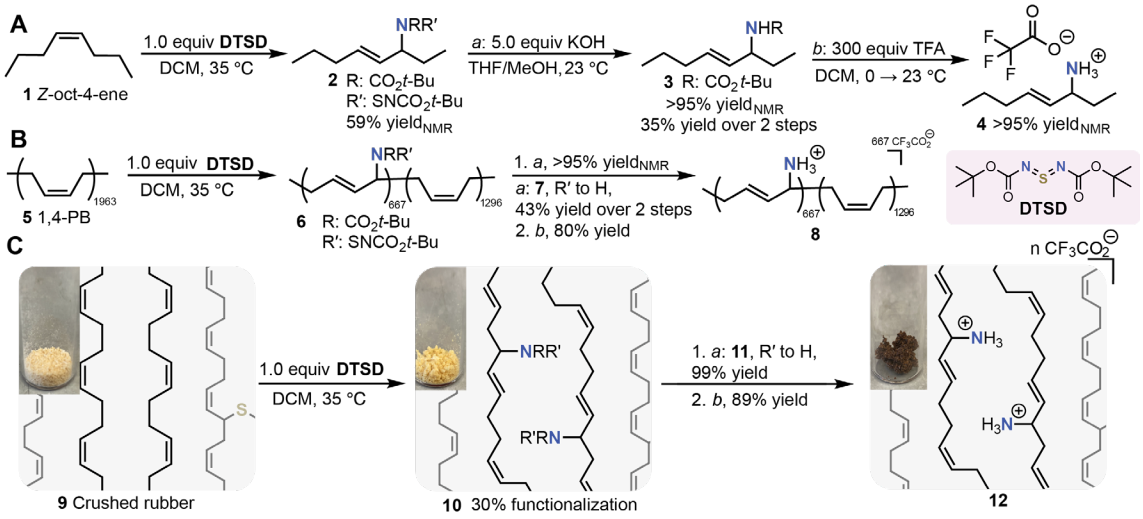


**Fig. 3: Allylic amination on model substrates 1, 5, and 9. A**, **B**, **C**, Amination of *Z*-oct-4-ene, 1,4-PB, and crushed rubber, respectively.

in contrast to polybutadiene, polyisoprene has three chemically distinct allylic sites per repeat unit: one methyl and two methylenes. In our system, achieving amination at the methylene allylic hydrogens, as opposed to the methyl ones, is necessary for the aza-Cope rearrangement step to proceed. To probe the likelihood of methyl versus methylene amination, we tested amination of squalene, and found that its exposure to 6 equivalents of DTSD led to installation of an average of 4.6 amines per molecule. After cleaving the N–S bond to give 15 and purifying via recycling preparative GPC (prepGPC), NMR analysis allowed us to estimate a 3:1 ratio of methyl/methylene amination. Base on these results, we expected that the desired amination of methylene positions would take place, albeit unselectively, in the post-consumer waste rubber.

When we applied the Sharpless-Kresze amination to post-consumer ground rubber, we observed amination as confirmed by FTIR, $^{13}$C MAS-NMR, and elemental analysis. By elemental analysis, we estimate 35% amination in this post-consumer system, although an exact percent amination is challenging to determine due to the presence of unidentified

additives. Deprotections using KOH followed by TFA gave the final ammonium functionalized product.

ACR enabled the deconstruction of the aminated crushed rubber into aminated cleaved polymeric products (Figure 4A–B). We applied the optimized ACR reaction conditions to aminated vulcanized 1,4-polybutadiene and observed after 3 hours complete dissolution of the crosslinked material and formation of aminated polymeric products detected by $^{1}$H NMR spectroscopy and GPC (after global Boc-protection). Applying similar conditions to non-aminated yielded no soluble polymeric products with 94% of the mass recovered. Application of these ACR conditions to aminated post-consumer rubber also yielded soluble aminated polymeric products.

These aminated polyisoprene fragments can be utilized as curing agents to make epoxy resins—materials with numerous high-value applications: from adhesives, paints and coatings to aerospace materials. Indeed, when our polymeric products are mixed with Bisphenol A

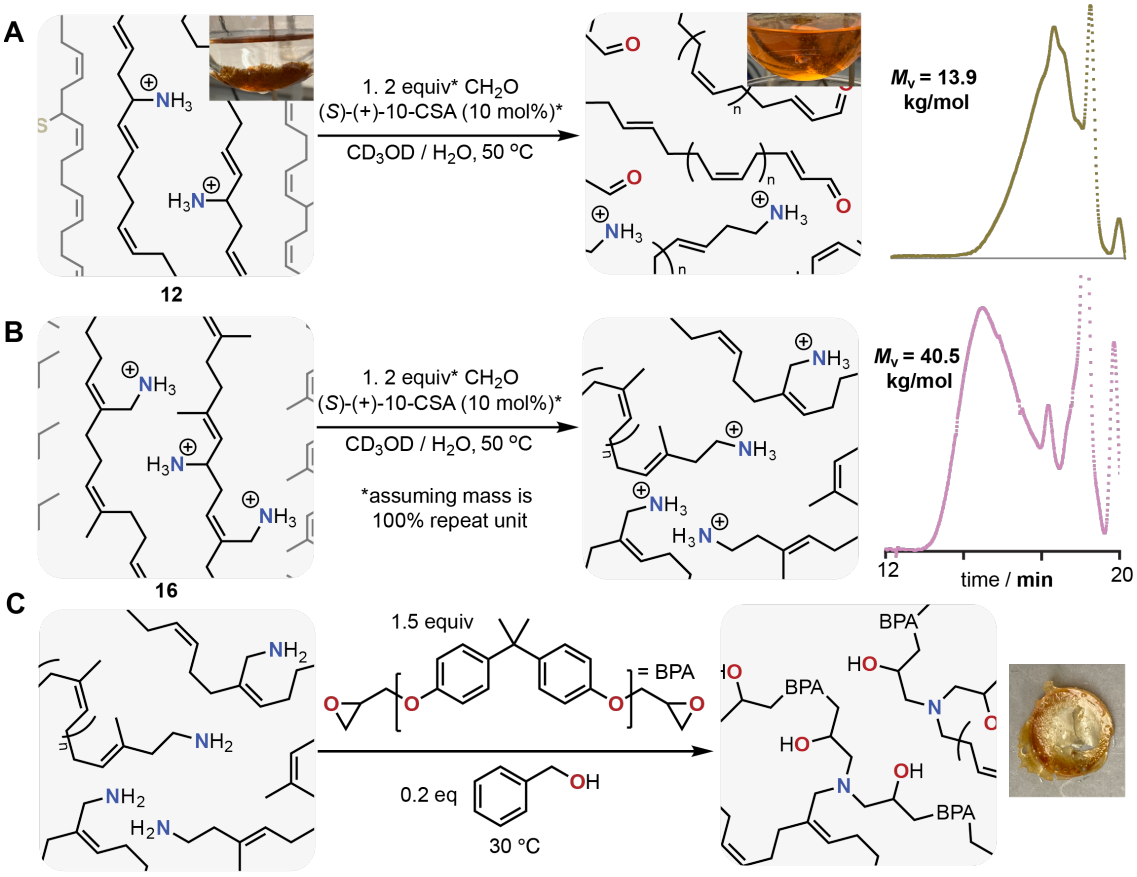


**Fig 4: Deconstruction of crosslinked materials and application of products. A**, (Left) ACR deconstruction of aminated polybutadiene rubber **12** with (crosslinks and counterions omitted for clarity); (Right) GPC dRI trace of Boc-protected deconstruction products after 48 h. **B**, (Left) ACR deconstruction of **16** (crosslinks and counterions omitted for clarity); (Right) GPC dRI trace of Boc-protected deconstruction products after 48 h. **C**, Crosslinking reaction between polymeric products and DGEBA with photo of crosslinked final epoxy resin product.

diglycidyl ether (DGEBA) and benzyl alcohol as an accelerant, we observe solid cross-linked material form overnight after heating to 30 °C (Figure 4C). This finding demonstrates that waste rubber could serve as a convenient feedstock material for epoxy thermosets.

**Publications Acknowledging this Grant in 2020-2024**


1. Towell, S. E.[#]; Ratushnyy, M.[#]; Satkowiak, L. C.; **Zhukhovitskiy, A. V.*** Deconstruction of Rubber via C–H Amination and Aza-Cope Rearrangement. *Nature* **2024**, *In revision*.

# LIST OF PARTICIPANTS

| First Name | Last Name | E-mail Address |
|---|---|---|
| Frank | Abild-Pedersen | abild@slac.stanford.edu |
| Lipi | Acharya | lipi.acharya@hq.doe.gov |
| Anastassia | Alexandrova | ana@chem.ucla.edu |
| Liney | Arnadottir | liney.arnadottir@oregonstate.edu |
| Polly | Arnold | pla@lbl.gov |
| Robert | Baker | baker.2364@osu.edu |
| Simon | Bare | srbare@slac.stanford.edu |
| Bart | Bartlett | bartmb@umich.edu |
| Wesley | Bernskoetter | bernskoetterwh@missouri.edu |
| John | Berry | berry@chem.wisc.edu |
| Aditya | Bhan | abhan@umn.edu |
| Elizabeth | Biddinger | ebiddinger@ccny.cuny.edu |
| Suzanne | Blum | blums@uci.edu |
| Jesse | Bond | jqbond@syr.edu |
| Chris | Bradley | chris.bradley@science.doe.gov |
| Charles | Campbell | charliec@uw.edu |
| Matthew | Chambers | chambers@lsu.edu |
| Bert | Chandler | bert.chandler@psu.edu |
| Fanglin | Che | fanglin_che@uml.edu |
| Donna | Chen | dachen@sc.edu |
| Jingguang | Chen | jgchen@columbia.edu |
| Zhongfang | Chen | zhongfang.chen1@upr.edu |
| Peng | Chen | pc252@cornell.edu |
| Chris | Chervin | christopher.chervin@science.doe.gov |
| Kyoung-Shin | Choi | kschoi@chem.wisc.edu |
| Phillip | Christopher | pchristopher@ucsb.edu |
| Kensha | Clark | Kmclark8@olemiss.edu |
| Geoffrey | Coates | gc39@cornell.edu |
| Matthew | Conley | mconley@ucr.edu |
| Steven | Crossley | stevencrossley@ou.edu |
| Damien | Culver | culver@ameslab.gov |

| | | |
|---|---|---|
| Lisandro | Cunci | cuncil1@uagm.edu |
| Thomas | Cundari | t@unt.edu |
| Abhaya | Datye | datye@unm.edu |
| Olafs | Daugulis | olafs@uh.edu |
| Max | Delferro | delferro@anl.gov |
| Zdenek | Dohnalek | zdenek.dohnalek@pnnl.gov |
| James | Dorman | james.dorman@science.doe.gov |
| Keary | Engle | keary@scripps.edu |
| Daniel | Ess | dhe@byu.edu |
| Carrie | Farberow | carrie.farberow@nrel.gov |
| Byron | Farnum | farnum@auburn.edu |
| Chris | Fecko | Christopher.Fecko@science.doe.gov |
| David | Flaherty | dflaherty3@gatech.edu |
| Alison | Fout | fout@tamu.edu |
| Francois | Gabbai | francois@tamu.edu |
| Rachel | Getman | getman.11@osu.edu |
| Aura | Gimm | aura.gimm@science.doe.gov |
| Vassiliki-Alexandra | Glezakou | glezakouva@ornl.gov |
| Karen | Goldberg | kig@sas.upenn.edu |
| Alan | Goldman | alan.goldman@rutgers.edu |
| Chris | Goldsmith | crgoldsmith@auburn.edu |
| John | Gordon | jgordon1@bnl.gov |
| Rajamani | Gounder | rgounder@purdue.edu |
| Jeffrey | Greeley | jgreeley@purdue.edu |
| Thomas | Gunnoe | tbg7h@virginia.edu |
| Robbie | Hable | robert.hable@hq.doe.gov |
| Amanda | Haes | amanda.haes@science.doe.gov |
| John | Hartwig | jhartwig@berkeley.edu |
| Nilay | Hazari | nilay.hazari@yale.edu |
| Gregory | Herman | gherman@anl.gov |
| Andreas | Heyden | heyden@cec.sc.edu |
| Adam | Hoffman | ashoff@slac.stanford.edu |
| Patrick | Holland | patrick.holland@yale.edu |
| Jiyun | Hong | jiyun.hong@slac.stanford.edu |
| Paul | Hudson | paul.hudson@orau.org |

| | | |
|---|---|---|
| Simon | Humphrey | smh@cm.utexas.edu |
| Thomas | Jaramillo | jaramillo@stanford.edu |
| Friederike | Jentoft | fcjentoft@umass.edu |
| William | Jones | jones@chem.rochester.edu |
| David | Kaphan | kaphand@anl.gov |
| Ayman | Karim | amkarim@vt.edu |
| Shyam | Kattel | shyam.kattel@ucf.edu |
| Alexander | Katz | askatz@berkeley.edu |
| Sheima | Khatib | sheimajk@vt.edu |
| Timothy | Kidd | timothy.kidd@science.doe.gov |
| Sungmin | Kim | sungmin.kim@pnnl.gov |
| Takeshi | Kobayashi | takeshi@ameslab.gov |
| Clemens | Krempner | clemens.krempner@ttu.edu |
| Kyle | Lancaster | kml236@cornell.edu |
| Johannes | Lercher | Johannes.Lercher@pnnl.gov |
| Yuting (Emily) | Li | yutingli@ameslab.gov |
| Yuanyuan | Li | liy4@ornl.gov |
| Suljo | Linic | linic@umich.edu |
| Cong | Liu | congliu@anl.gov |
| Ping | Liu | pingliu3@bnl.gov |
| Charles | Machan | machan@virginia.edu |
| Neal | Mankad | npm@uic.edu |
| Karthish | Manthiram | karthish@caltech.edu |
| Smaranda | Marinescu | smarines@usc.edu |
| Tobin J. | Marks | t-marks@northwestern.edu |
| Manos | Mavrikakis | emavrikakis@wisc.edu |
| James | Mayer | james.mayer@yale.edu |
| Charles | McCrory | cmccrory@umich.edu |
| Jean-Sabin | McEwen | js.mcewen@wsu.edu |
| James | McKone | jmckone@pitt.edu |
| Gail | McLean | gail.mclean@science.doe.gov |
| Will | Medlin | medlin@colorado.edu |
| Phillip | Milner | pjm347@cornell.edu |
| Raul | Miranda | raul.miranda@science.doe.gov |
| Liviu | Mirica | mirica@illinois.edu |
| Karl | Mueller | karl.mueller@pnnl.gov |

| | | |
|---|---|---|
| Catherine | Murphy | murphycj@illinois.edu |
| Bindu | Nair | Bindu.Nair@science.doe.gov |
| Andy | Nguyen | andyn@uic.edu |
| Eranda | Nikolla | erandan@umich.edu |
| Jack | Norton | jrn11@columbia.edu |
| Oleg | Ozerov | ozerov@chem.tamu.edu |
| Umit | Ozkan | ozkan.1@osu.edu |
| Joshua | Pak | pakjosh@isu.edu |
| Barratt | Park | barratt.park@gmail.com |
| Gerard | Parkin | parkin@columbia.edu |
| Frederic | Perras | fperras@ameslab.gov |
| Jonas | Peters | jonas.peters@gmail.com |
| Cory | Phillips | cory.phillips@hq.doe.gov |
| Craig | Plaisance | plaisance@lsu.edu |
| David | Powers | powers@chem.tamu.edu |
| Long | Qi | lqi@ameslab.gov |
| Talat S | Rahman | talat@ucf.edu |
| Robert | Rallo | robert.rallo@pnnl.gov |
| Jeffrey | Rimer | jrimer@central.uh.edu |
| Robert | Rioux | rmr189@psu.edu |
| Jennifer | Roizen | jennifer.roizen@science.doe.gov |
| Roger | Rousseau | rousseaur@ornl.gov |
| Aaron | Sadow | sadow@iastate.edu |
| Caroline | Saouma | csaouma@vt.edu |
| Philippe | Sautet | sautet@ucla.edu |
| J.R. | Schmidt | schmidt@chem.wisc.edu |
| Viviane | Schwartz | viviane.schwartz@science.doe.gov |
| Daniel | Schwartz | daniel.schwartz@colorado.edu |
| Natalia | Shustova | shustova@sc.edu |
| Carsten | Sievers | carsten.sievers@chbe.gatech.edu |
| Emily | Smith | esmith1@ameslab.gov |
| Jeremy | Smith | smith962@indiana.edu |
| Dario | Stacchiola | djs@bnl.gov |
| Erin | Stache | estache@princeton.edu |
| Shannon | Stahl | ssstahl@wisc.edu |
| Corey | Stephenson | stephenson@chem.ubc.ca |

| | | |
|---|---|---|
| Kelsey | Stoerzinger | zinger@umn.edu |
| Jin | Suntivich | jsuntivich@cornell.edu |
| Yogesh | Surendranath | yogi@mit.edu |
| Charles | Sykes | charles.sykes@tufts.edu |
| Nathaniel | Szymczak | nszym@umich.edu |
| Brian | Tackett | bmtacket@purdue.edu |
| Steven | Tait | tait@iu.edu |
| V. Sara | Thoi | sarathoi@jhu.edu |
| Christine | Thomas | thomas.3877@osu.edu |
| Don | Tilley | tdtilley@berkeley.edu |
| Ian | Tonks | itonks@umn.edu |
| Ba | Tran | ba.tran@pnnl.gov |
| Christopher | Uyeda | cuyeda@purdue.edu |
| Fernando | Vila | fdv@uw.edu |
| Dionisios | Vlachos | vlachos@udel.edu |
| Aleksandra | Vojvodic | alevoj@seas.upenn.edu |
| Johannes | Voss | vossj@slac.stanford.edu |
| Josh | Vura-Weis | vuraweis@illinois.edu |
| Israel E. | Wachs | iew0@lehigh.edu |
| Bin | Wang | wang_cbme@ou.edu |
| Timothy | Warren | warre155@msu.edu |
| Ross | Widenhoefer | rwidenho@chem.duke.edu |
| Eric | Wiedner | eric.wiedner@pnnl.gov |
| Lea | Winter | lea.winter@yale.edu |
| Kirsten | Winther | winther@slac.stanford.edu |
| Zili | Wu | wuz1@ornl.gov |
| Hongliang | Xin | hxin@vt.edu |
| Fang | Xu | fang.xu@utsa.edu |
| Jenny | Yang | j.yang@uci.edu |
| Francisco | Zaera | zaera@ucr.edu |
| Sen | Zhang | sz3t@virginia.edu |
| Aleksandr | Zhukhovitskiy | alexzhuk@email.unc.edu |

Cover images courtesy of: Zili Wu (ORNL), Christine Thomas (The Ohio State University), Friederike Jentoft (University of Massachusetts Amherst), Charles McCrory (University of Michigan), Frank Abild-Pedersen (SLAC), David Powers (Texas A&M University), Steven Crossley (University of Oklahoma).

U.S. DEPARTMENT OF ENERGY | Office of Science